Developments in Mineral Processing
D.W. Fuerstenau/advisory editor

1 A.J. Lynch
Mineral Crushing and Grinding Circuits.
Their Simulation, Optimisation, Design and Control

2 J. Laskowski (editor)
Mineral Processing.
Proceedings of the 13th International Mineral Processing Congress.
Warsaw, June 4–9, 1979

3 A.J. Lynch, N.W. Johnson, E.V. Manlapig and C.G. Thorne
Mineral and Coal Flotation Circuits.
Their Simulation and Control

4 H.J. Schulze
Physico-chemical Elementary Processes in Flotation.
An Analysis from the Point of View of Colloid Science
including Process Engineering Considerations

5 R.O. Burt
Gravity Concentration Technology.

6 K.S.E. Forssberg (editor)
Flotation of Sulphide Minerals.

7 J. Srb and Z. Růžičková
Pelletization of Fines.

8 J. Svoboda
Magnetic Methods for the Treatment of Minerals.

9 S.H. Castro and J. Alvarez (editors)
Froth Flotation.
Proceedings of the 2nd Latin-American Congress on Froth Flotation, Concepción,
Chile, 19–23 August 1985

10 K.S.E. Forssberg (editor)
Proceedings of the XVI International Mineral Processing Congress, Stockholm,
Sweden, June 5–10, 1988.

11 K. Tkáčová
Mechanical Activation of Minerals

12 J.S. Laskowski and J. Ralston (editors)
Colloid Chemistry in Mineral Processing

Developments in Mineral Processing, 12

Colloid Chemistry in Mineral Processing

Edited by

J. S. Laskowski

The University of British Columbia, Department of Mining and Mineral Process Engineering, 517-6350 Stores Road, Vancouver, B.C. V6T 1W5, Canada

and

J. Ralston

School of Chemical Technology, University of South Australia, The Levels, S.A. 5095, Australia

ELSEVIER
Amsterdam — London — New York — Tokyo 1992

ELSEVIER SCIENCE PUBLISHERS B.V.
Sara Burgerhartstraat 25
P.O. Box 211, 1000 AE Amsterdam, The Netherlands

Distributors for the United States and Canada:

ELSEVIER SCIENCE PUBLISHING COMPANY INC.
655, Avenue of the Americas
New York, NY 10010, U.S.A.

ISBN 0-444-88284-7

This book is printed on acid-free paper.

Printed in The Netherlands

Foreword

"Colloid Chemistry in Mineral Processing" was born out of our strong desire to recognise the excellent scientific studies of Dr. Joseph A. Kitchener in a tangible and constructive manner.

Joe Kitchener influenced, guided and educated many scientists and engineers during his impeccable career. We therefore approached distinguished researchers, all of whom had either worked directly with Joe or came from research groups with which he had a long association, and asked them to contribute specific chapters to the book.

Since the size of the particles which are currently processed is rapidly approaching colloidal range, mineral processing is, of necessity, becoming more and more an applied colloid chemistry. Colloid chemistry is inevitably involved in all aspects of

Joseph and Phyllis Kitchener at home in Tewin Wood, Hertfordshire, England (September 1989).

mineral processing, ranging from rheological phenomena in grinding, selective adsorption of various chemical additives (flotation collectors, flocculants, dispersants, etc.) onto mineral surfaces, and analysing the forces which control the stability of dispersions as well as the wettability of mineral surfaces. Colloid chemistry also plays an equally important role in influencing the stability and viscosity of magnetite dense media. Surface phenomena control both the dewatering of "fines" and are involved in dust suppression. Joe Kitchener worked in these and related areas, and it is pertinent to recall aspects of his career, for this will serve the dual purpose of informing readers who have not had the privilege of working with him as well as developing some historical perspective of the subject of the book.

Joe Kitchener was born in London in 1916 and attended an excellent council grammar school from 1926 to 1934. At the conclusion of his secondary education, Joe won an open scholarship to University College, were he skipped the first year of the Bachelor's degree and obtained first class honours in Chemistry in 1936. His Ph.D. was completed by June 1938, just three years and nine months after leaving secondary school, a truly remarkable feat from the editors' viewpoint, although would demur on this issue! His Ph.D. topic was "Photosensitization" by Titanium Dioxide", undertaken under the energetic direction of C.F. Goodeve, a notable physical chemist in the Department of Chemistry headed by Professor F.G. Donnan. The research environment was very stimulating for G.S. Hartley, N.K. Adams and H. Freundlich had all been recruited by Donnan, thus there was a rich colloid and surface chemistry milieu for a young doctoral student to develop in.

At the conclusion of his doctoral studies Joe was appointed as a Demonstrator in Physical Chemistry at Imperial College, enabling him to combine teaching and independent scientific research. By 1956 he was Reader in Physical Chemistry and was awarded the D.Sc. in 1958 for his eminent contributions, exceeding fifty in number, to the scientific literature. In 1961 the Department of Mining and Mineral Technology, led by the perceptive Professor M.G. Fleming, lured Joe away from Chemistry and conferred upon him the unique title of "Reader in the Science of Mineral Processing". Joe completed forty years on the staff of Imperial College in 1978 at which point the College, coaxed by Fleming, bestowed the coveted title of Senior Research Fellow upon him. Joe enjoyed this role for the next seven years, finally leaving Imperial College in 1985. He now lives in Tewin Wood, near Welwyn in Hertfordshire with his gracious wife Phyllis. Joe and Phyllis have two daughters and a son. Since his departure from Imperial College, Joe and Phyllis travel widely in the United Kingdom and involve themselves in a myriad of activities, with Joe still indulging in the occasional scientific foray.

More than one hundred and fifty scientific publications flowed from Joe's scientific work. Many of these are noted in this book, both in the body of the text, as well as in the bibliographies at the end of each chapter. However it is worth mentioning a few highlights here. With A.P. Prosser, Joe made the first correct measurements in the West of long-range van der Waals forces between macroscopic bodies (Proceed-

ings of the Royal Society of London (1957) A 242, p. 403). This work was carried out in parallel with Derjaguin and his group in Russia and, as a result, a strong bond was forged between the two men. Their mutual fascination with each other's work continues until this day, with Joe Kitchener assuming editorship of Derjaguin, Churaev and Muller's book on "Surface Forces" (Consultants Bureau, New York and London, 1987).

There was a long-term interest in thin liquid films, encompassing surface forces, film thickness measurements and structural effects. Collaborators in this work included A.D. Read, J.S. Laskowski, T.D. Blake and R.M. Pashley. Surfactant adsorption at solid–water interfaces was performed in conjunction with R. Tolun and T.Z. Saleeb. "Mechanisms of Adsorption from Aqueous Solutions: Some Basic Problems", a review by Joe which was published in the Journal of Photographic Science in 1965 (13, p. 152), to this day remains an excellent introduction for a newcomer to this field. Pioneering selective flocculation studies were carried out with J.P. Friend, B. Yarar, J. Rubio and Y.A. Attia whilst the phenomenon of selective coagulation in mixed colloidal suspensions was confirmed with R.J. Pugh. Sulphide mineral surface chemistry and flotation were investigated with R. Tolun, M.G. Fleming and B. Yarar whilst the surface properties of silicates were studied with J. Ralston and L.J. Warren. Quebracho and the mechanism of its action as a depressant was investigated with J. Iskra and C. Gutierrez. Adsorption investigations were carried out with O. Mellgren and H. Shergold whilst joint studies into dissolved air flotation were performed with R. Gochin and J. Solari. Fine particle and fundamental flotation studies were performed with J.F. Anfruns, S. Sobieraj, H. Wright and M. Urban. Although Phil Parsonage and Luuk Koopal were never directly associated with Joe Kitchener, they rapidly accepted our invitation to write their respective chapters, without which the book would be incomplete. Joe's scientific work is characterized by brilliant diagnostic experiments, lucid, perceptive interpretations and a remarkable clear exposition. We cannot do justice to his work by a few mere lines here — the reader is urged to consult the original literature for the full flavour.

The book is divided into two sections, the first of which commences with an analytical overview by Joe Kitchener. Each chapter is couched in the form of a review, but is written with the prospective student in mind. We therefore hope that it will be a useful teaching book. The editors have attempted to give coherence to the entire volume. We thank our contributors and Elsevier, particularly Jacques Kiebert, for their support and our families for their tolerance. The blame for any errors or omissions rests with us. We trust, however, that our readers will find this book to be a valuable contribution to the "science of mineral processing".

May, 1991

J.S. LASKOWSKI, Vancouver
J. RALSTON, Adelaide

List of Contributors

Y.A. ATTIA	*Department of Materials Science and Engineering, The Ohio State University, 116 West 19th Avenue, Columbus, OH 43210, U.S.A.*
R.J. GOCHIN	*Department of Mineral Resources Engineering, Imperial College of Science, Technology and Medicine, London SW7 2BP, England*
J.A. KITCHENER	*2A Purcell Close, Tewin Wood, Welwyn, Hertfordshire AL6 0NN, England*
L.K. KOOPAL	*Department of Physical and Colloid Chemistry, Wageningen Agricultural University, Dreijenplein 6, 6703 HB Wageningen, The Netherlands*
J.S. LASKOWSKI	*Department of Mining and Mineral Process Engineering, The University of British Columbia, Vancouver, B.C., V6T 1W5 Canada*
G. NEWCOMBE	*School of Chemical Technology, University of South Australia, The Levels, S.A. 5095, Australia.*
P. PARSONAGE	*Biological Treatment Department, Warren Spring Laboratory, Stevenage, Hertfordshire SG1 2BX, England*
R.M. PASHLEY	*Department of Chemistry, Faculty of Science, Australian National University, G.P.O. Box 4, Canberra, ACT, 2601, Australia*
R.J. PUGH	*Mineral Section, Institute for Surface Chemistry, Box 5607, S-114 86 Stockholm, Sweden and the Division of Mineral Processing, Luleå University of Technology, S-951 87 Luleå, Sweden*
J. RALSTON	*School of Chemical Technology, University of South Australia, The Levels, S.A. 5095, Australia.*
J.A. SOLARI	*Departamento de Ingeniería de Minas, Facultad de Ciencias Físicas y Matemáticas, Universidad de Chile Casilla 2777, Santiago, Chile*
L.J. WARREN	*CSIRO, Division of Mineral Products, c/o Curtin University, Box U1987, W.A. 6001, Australia*

Chapter 1

Minerals and surfaces

J.A. KITCHENER

Foreword

About this article

Ideally, Technology is simply Applied Science and science is a unity. But that is not how students meet it! Academic science has long been rigidly packaged into physics, chemistry, geology, biology, etc. Within each department are many sub-departments — labelled, for example, inorganic, organic, physical, etc. In turn, each sub-department guards its own sub-sub-specialities. One of these, under the wing of physical chemistry, is *surface chemistry*, and this, along with surface physics and surface mineralogy (to coin a term for a new field of study), provides the basic science for the present book.

In the conventional scheme, *colloid science*, which is the study of dispersed materials, has no home. It is dismissed as "interdisciplinary" ("multidisciplinary" would be more accurate). Consequently, its rating for lecture time in departments of chemistry or physics is negligible. Thousands of science graduates emerge from our universities and colleges totally ignorant of a tremendously important area of knowledge — important for technology and biology. Quite apart from the industrial applications (mineral processing being just one of them) the colloidal state of matter includes all living creatures, all natural products, foods and soils. Colloids are emphatically important in the real world, if not in the class-room! Shakespeare put it most aptly (in a very different context) in King Henry V, Act 5, Scene 2:

"... [we]... do not learn for want of time
The sciences which should become our country"

("become" means suit, improve).

As colloids are unfamiliar to many young scientists, it may be useful to explain briefly some of the key ideas and technical terms of our subject before proceeding

to the main theme of the book — namely, the processing of nearly-colloidal minerals. Of course, readers already familiar with the basic concepts of colloid science can go directly to the specialist articles that follow. I hope, however, that mineral technologists and others will find this preview helpful — notably, research chemists and chemical engineers who find themselves faced with problems involving colloidal materials with no previous acquaintance with the science.

This short introduction to a huge subject must necessarily be both selective and sketchy. Students who want a more systematic introductory course are recommended to read a short recent textbook by Everett [1], which includes references to some standard monographs. Be warned, however, that the *research literature* of colloid science, although fascinating, is nothing short of overwhelming in volume and often confusing in significance. Students will find difficulty in distinguishing between established, accepted, principles and unproven, tentative, ideas that researchers are perhaps "trying out"! Here I have endeavoured to summarize only accepted concepts; so it would be ridiculous to quote original publications. Where names and dates are mentioned, they are simply to set the science in its historical context.

Although surface and colloid science are not as widely taught as their importance deserves, research work is progressing vigorously on many topics and in many laboratories, both academic and industrial. The reader will gain some idea of a small selection of these activities from the specialist articles in this book, and should realise that many parallel books are appearing on other aspects of the subject.

Colloids and surfaces

Introducing colloids

The concept and the name of "colloid" are credited to Thomas Graham (1861). (Incidently, the first professor of chemistry at my alma mater, University College, London). His two criteria were: (a) restricted diffusivity (colloids being held back by a membrane), and (b) optical turbidity (light scattering). Both indicate the presence of particles much larger than ordinary molecules such as sucrose. It turned out to be rather unfortunate that two distinctly different classes of material qualified as colloids — for example, gold sols and gelatin solutions. Nowadays it is clear that the former typify *dispersions* of optically sub-microscopic particles, while the latter consist of stable *solutions* of very large molecules. The first class is now referred to as "lyophobic" colloids (i.e. disliking their environment, and hence potentially unstable) and the second as "lyophilic" (liking and spontaneously soluble in their liquid).

Graham can hardly be blamed for the confusion that followed. Techniques for investigating the structure of colloids were entirely lacking and it needed more than half a century to establish the simple principle stated above. For many years colloids

were treated as somehow peculiar by comparison with familiar "crystalloids" such as sucrose solution. Colloids seemed not to fit the standard laws of the classical physical chemists, and were simply disregarded by many of them.

It was not until the 1930's, with the advent of new techniques such as the ultramicroscope, the electron microscope, precision osmometry, X-ray powder diffraction and the simultaneous rise of a new science of high molecular weight polymers that the distinction between lyophobic and lyophilic colloids became obvious. Much of the mystery of what had been wittily dubbed "the cloudy science" was thereby dissipated. However, there still remained a puzzling theoretical problem: how to explain the stability (actually metastability) of lyophobic colloidal dispersions? They were long known to be susceptible to slow or rapid coagulation on addition of particular electrolytes, and Smoluchowski developed the kinetic theory of coagulation as early as 1917. But the forces keeping the particles apart in stable dispersion could not be quantitatively accounted for.

Qualitative ideas about "electrical charges" on colloidal particles were around long before 1930. However, calculating the repulsion forces between particles as a function of the distance between them is not a simple matter of applying Coulomb's law. A start on the problem was made around 1938. By then it was realised that all colloidal particles have an influence on the liquid around them. Lyophobic particles, when "charged", exert an effect on the ionic environment; lyophilic particles interact with their solvent medium in the same way that sucrose does.

Already in the 1920's the great classical colloid chemist H. Freundlich realised that the key to colloid science was to be found in the special phenomena associated with *surfaces*. To understand colloids requires a knowledge of basic surface science. Today that is a very extensive chapter in physical chemistry and chemical physics.

For our present purposes, bearing in mind new-comers to the subject, it is only necessary to recapitulate certain relevant principles, starting with the classical concepts of surface physics and then progressing to modern discoveries.

In what follows, for "surface" henceforth read "interface". Much muddled thinking has confused this simple concept. It needs to be defined; is it a mathematical plane, a monolayer, or a "skin" we are talking about?

The classical interface model

An interface is a boundary between two phases (such as GAS/LIQUID, L/S, L_1/L_2; Figure 1). To the eye it appears perfectly sharp. The very fact that the phases do not intermingle shows that there is a drastic difference in the molecular environment on the opposite sides. The difference may lie in the packing (as for a solid at its m.p.) or molecular kind (as for oil/water). Long before it became possible to analyze intermolecular forces at interfaces, valuable understanding was achieved through the thermodynamic approach — a method which, within limits, is still valid and useful.

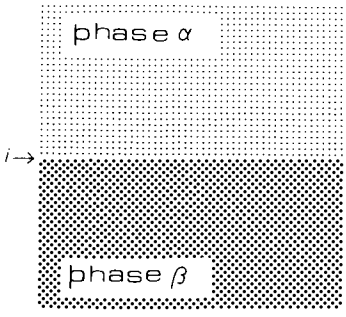

Fig. 1. The interface, *i*, is formally defined as a boundary between phases; but what is its physical structure?

Capillary phenomena indicate that a force is required to extend a liquid meniscus — the classical model of surface tension. Experiment shows that the "tension" (γ) does not change with extension of area (A) and does not depend on the size or form of the liquid surface, but does depend on the substance. It follows that an interface of area A and tension γ requires work γA to form it (at constant temperature and pressure) and this work must somehow be stored by the molecules, for it is recoverable and is therefore surface *free* energy. For pure liquids the surface free energy per unit area (measured nowadays in mJ m^{-2}) in numerically equal to its surface tension (mN m^{-1}). (Incidently, there is also surface enthalpy and entropy.) All the phenomena of capillarity can be perfectly explained by the surface tension model — provided the system is macroscopic. The model must fail eventually with exceedingly *small* bodies — actually for any which are small compared with "the range of action of intermolecular forces". The apparent surface tension then becomes a function of size. However, the bodies must certainly be sub-microscopic for that regime to be encountered. For example, Israelachvili and Fisher (1979) validated the classical Kelvin equation for the influence of curvature on vapour pressure down to a mean radius of 4 nm.

Surface energies may seem small quantities, but they do provide all the driving force for a whole set of processes, such as those listed below. As many of these involve *solids* (as in capillary rise) the question of the surface free energy of solids needs consideration. The rigidity of solids precludes the direct measurement of a surface tension. The fact that work is required to cleave a crystal does not necessarily mean that all the work expended gets stored in the new surface; some of it must go into elastic or plastic deformation and some may go into electrostatic charging. However, there are a few favourable crystals, such as muscovite (mica), on which the cleavage experiment can be performed in a practically reversible manner and the proper corrections can be applied for elastic deformation. It turns out that the surface free energy term is large. Other evidence indicates that hard solids generally

TABLE 1

A short list of some surface tensions of pure liquids, interfacial tensions and approximate surface free energies of solids at 20°C (in mN m^{-1} or mJ m^{-2})

Pure liquids		Interfacial		Solids	
diethyl ether	17.0	water/ether	10.7	paraffin wax	45
n-hexane	18.4	water/hexane	56.1	polyethylene	55
ethanol	22.3	water/mercury	375	NaCl (halite)	400
benzene	28.9			mica (cleavage)	300
glycerol	63.4			CaF_2 (fluorite)	500
water	72.7			MgO (periclase)	1200
mercury	465			C (diamond)	4–9 $\times 10^3$ (theor.)

have higher surface energies than soft ones. Molecular theory shows that different crystal faces are likely to have different surface energies per unit area.

One piece of evidence for surface energy of solids is the spontaneous growth of larger crystals at the expense of smaller, either through the vapour (sublimation) or through a saturated solution. Attempts have been made to determine the surface energies of crystals from differences of vapour pressure or solubility but they have generally failed because of the experimental difficulty of obtaining strictly comparable, stable, crystals of truly microscopic sizes.

Finally, the familiar phenomena of rise (with water in *clean* glass) or fall (mercury) of liquids in capillary tubes can be regarded as proof enough of the reality of surface free energy of solids. Water can be made to stand level by coating the glass with an invisible film of silicone or to fall by a thin coating of paraffin wax, thus demonstrating the role of the solid as well as the liquid. Capillarity can be satisfactorily explained by presumed changes in the net sum of γA terms — although the individual γ_s and and γ_{sl} quantities cannot be evaluated (see below).

Several lines of evidence indicate that the surface free energies of various solids, like those of liquids, can be very different. It is often convenient to differentiate (loosely) between "low energy solids" and "high energy solids". In molecular terms the former are mostly soft solids held together by Van der Waals forces while the latter are ionic, covalent or metallic crystals. Some approximate published values are included in Table 1 (the data should not be taken as precise).

The concept of surface energy provides a satisfactory basis for explaining a wide range of "capillary phenomena", *many of which are pertinent to the flotation process.* For example:

(1) The shapes of liquid drops, bubbles, or menisci at equilibrium, either with or without deformation by gravity.

(2) The internal pressure difference across curved interfaces, as given by the Laplace equation.

(3) The vapour pressure over curved interfaces of droplets or small particles, as given by the Kelvin equation.

(4) The growth of particles (or bubbles) at the expense of smaller ones, either through the vapour phase or via a solvent (as in the "Ostwald ripening" of precipitates). Thermodynamic activity is related to curvature by an equation similar to that of Kelvin.

(5) The creepage or retraction of a film of liquid over another liquid or solid.

(6) The establishment of an equilibrium angle of contact of a liquid on a solid substrate — as governed by Young's equation (see below).

(7) The accumulation of one or more components at an interface — adsorption.

In all these physical processes, the system moves towards an equilibrium which corresponds to a net minimum of surface energy, $\Sigma \gamma A$, plus gravitational energy where significant. In cases (1)–(6) only areas change; in (7) A remains constant while γ decreases during adsorption. Cases (1)–(4) do not call for further comment here; but (5), (6) and (7) are highly relevant to the theme of this book and merit closer attention. The important flotation process depends on them.

Creepage of liquids: wetting and de-wetting

Liquid-on-liquid

If a small quantity of a certain liquid (α) is placed on the surface of another (β) in which it is insoluble, will it spread spontaneously? With pure liquids experiment shows three types of behaviour — complete spreading, or immediate shrinkage into a drop, or initial spreading followed by shrinkage into several droplets. No chemical change is involved. The movements are driven by the relative values of the surface tensions of the two liquids, γ_α and γ_β and their interfacial tension, $\gamma_{\alpha\beta}$. Spontaneous spreading occurs if there is a net decrease of $\Sigma \gamma A$ which means that $(\gamma_\alpha + \gamma_{\alpha\beta} - \gamma_\beta) < 0$ (see Figure 2A). Conversely, shrinkage is the spontaneous process if the inequality sign is reversed. This simple principle is readily verified by measuring the surface and interfacial tensions of the phases.

The third type of behaviour mentioned occurs when the spreading liquid affects the surface tension of the substrate considerably. A classic example is benzene on water. Initially $\gamma_\alpha = 28.9$, $\gamma_\beta = 72.8$, $\gamma_{\alpha\beta} = 35.0$; but after mutual saturation in a closed vessel, γ_α becomes 28.8, γ_β falls to 62.2, while $\gamma_{\alpha\beta}$ of course is the same being an equilibrium value. The sharp fall in the surface tension of the water is due to an invisible film of adsorbed benzene vapour. This type of behaviour is even more marked with slightly polar liquids such as oleic acid. After such liquids have rapidly spread out as a visible layer, they quickly produce a series of micro-droplets, which actually are separated by a *monolayer* of spread oil. The droplets are said to exert a "film pressure", π, defined simply as the lowering of the surface tension of the water produced by the film. In fact, a film can push small floating objects; π acts like a two-dimensional pressure. An attenuated unsaturated film exerts a lesser pressure. The study of force-area graphs of spread monolayers forms a special branch of surface chemistry, but not one of immediate importance for the present subject, except for

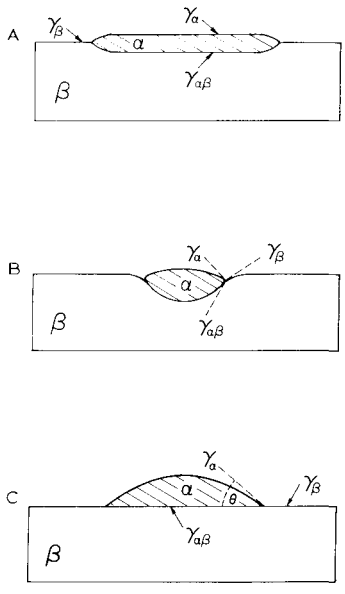

Fig. 2. Spreading or retraction of liquids is determined by the relative values of the interfacial energy terms (γ_α, γ_β, $\gamma_{\alpha\beta}$). A. Non-equilibrium: will a smear of liquid α spread or retract on liquid β? B. Equilibrium of a non-spreading drop on a liquid. C. Equilibrium of a non-spreading drop on a planar solid.

foams and frother–collector interaction.

A floating drop of oil which has come to equilibrium illustrates classical capillarity theory; at its periphery the three surface tensions balance in a triangle of forces (Figure 2B). The angles between the phases adopt unique values that give this balance (otherwise, of course, the contact line would move). Meanwhile, the orientation of the contact region to the vertical must also satisfy hydrostatics and balance the weight of the drop; and if the drop is large its bounding surfaces will depart from spherical form. It is a nice calculational problem! But note that the balance of the tensions is not itself directly affected by gravity.

This independent working of surface forces and gravitational forces, as Gibbs proved more than a century ago, is a direct consequence of the basic assumption that interfaces are of negligible thickness — negligible, that is, compared with the size of the bodies being studied.

Incidentally, Gibbs did also envisage the possibility that a correction might be needed for "line tension", as around the periphery of a floating drop. Many experimenters have tried to detect and measure line tension. Not surprisingly, results have been close to the limits of experimental error and mutually discordant; for if interfaces are exceedingly thin, the amount of matter specially affected at the 3-phase line is, of course, orders of magnitude smaller than that present in the two-

dimensional areas. A line tension will have a significant effect only in systems with a very small radius of curvature; and that probably means particles so small that the classical assumption of constancy of *surface* tension also beings to fail anyway, because of interaction between adjoining interfaces. The problem of thickness of interfaces must be reconsidered later.

The spreading behaviour of liquids is greatly complicated if one or both of them is a *solution*, because there can be simultaneous changes of the three tensions, with partial dissolution of some components until equilibrium is reached. Then the principles outlined above will apply.

Liquid-on-solid

Spreading or retraction of a liquid over a solid depends on the same principles as for liquid-on-liquid, though with certain reservations. Firstly, γ_β and $\gamma_{\alpha\beta}$ cannot be identified with measurable tensions, but must be read as surface free energies. Secondly, the problem is simplified only if the solid surface can be assumed to be ideally smooth and uniform in molecular nature; if it is not, there may be barriers to the movement of a meniscus (see below). Thirdly, the liquid is assumed to be both pure and a non-solvent for the solid.

As with liquid substrates, three types of behaviour may be found with different materials. There may be complete spreading, as with water on perfectly clean glass. Or there may be non-spreading, the liquid shrinking into one drop (e.g. mercury on glass, water on paraffin wax). Or there may be initial spreading, followed by liberation of droplets with an invisible monolayer between them — as happens with certain polar oils on metals or polar solids.

In an ideal system of the kind defined above, a retracting drop shrinks in area until it reaches an equilibrium form. Its perimeter can be seen to meet the solid at a certain angle, the angle of contact, θ, measured in the liquid phase at the 3-phase line (Figure 2C). The equilibrium angle corresponds again to the net minimum of surface free energies, $\Sigma \gamma A$, for which Thomas Young in 1805 gave the equation named after him, namely:

$$\gamma_{SV} = \gamma_{SL} + \gamma_{LV} \cos\theta$$

where the subscripts S, L and V stand for the solid, liquid and vapour phases, respectively. As before, the γ values must be those for mutually equilibrated phases. The form of the *bulk* of the drop is governed by the minimum of surface plus gravitational energy, unaffected by θ.

Regrettably, a great deal of nonsense has been written about Young's equation. Claims that θ is affected by gravity or by drop size are mistaken; in an ideal system, θ is a unique consequence of the materials of the phases. But there are plenty of cases where variation *is* noted for one reason or another. In practice, a meniscus on a solid almost always shows considerable *hysteresis* of contact angle, the angle when the liquid is advancing, θ_A, being larger than when receding, θ_R. Neither of these

angles can be taken to be the equilibrium angle required for Young's equation, nor related to it in any simple way.

Several factors are liable to cause hysteresis of movement of a contact meniscus:

(a) roughness, whether on an obvious or microscopic scale;

(b) penetration of the liquid into the solid (e.g. water into nylon);

(c) chemical heterogeneity of the solid (e.g. a calendered plastic sheet, or — for the present context — a fractured mineral crystal);

(d) impurities in the liquid, on its surface, or on the surface of the solid (e.g. a city raindrop on a car's windscreen!); it is surprisingly difficult to effectively exclude impurities in experiments with water and solids of high surface energy, even in a "clean-room" laboratory.

Often, several of the factors listed above operate simultaneously. Indeed, perfect reversibility of movement is very exceptional. Experimenters measuring contact angles should not fool themselves, but should inspect the contact line through a low-power binocular microscope and observe its form and movement. Most commonly the contact line will be found to be irregular and to change shape from place to place as the liquid advances and recedes. Any macroscopic measures of θ_A and θ_R must then be treated with reserve, at least until the reasons for the hysteresis have been identified.

In the famous froth flotation process, use is made of differences between contact angles on different minerals. The property of "flotability" depends on having a substantial contact angle at an air/water/mineral interface. Generally, the larger the contact angle, the more readily is the mineral floated, while no flotation occurs with zero contact angle.

A few minerals possess natural flotability (e.g. sulphur, graphite, talc) whereas the majority have zero contact angle; hence the former can be easily separated from the latter. More often, however, the flotation process depends on applying chemical reagents to differentially change contact angles, either upwards or downwards, with "collectors" or "depressants" respectively. Experiment shows that a coating of the order of thickness of a single monolayer of certain reagents is sometimes sufficient to generate a substantial contact angle. Here is one indication of the shortness of range of the surface forces involved.

Further details of static and dynamic contact angle phenomena can be left to Chapter 5. Our next basic question is how it is possible to modify surfaces by very small amounts of soluble substances. The phenomenon, of course, is *adsorption* and it is so widespread and important that it could well be called the crux of surface chemistry. Here again, there are two approaches — the classical (macroscopic) and the modern (molecular).

Adsorption

The macroscopic view of adsorption is the change of chemical content of phases at an interface — most commonly the accumulation of one component, either from the gas phase or from solution. The effect is detected as a change in concentration of that component in the bulk phase, and is therefore most noticeable with solid adsorbents of high specific surface area (e.g. porous charcoal, or finely particulate clays). If one component of a solution is adsorbed, other components show an apparent increase of concentration and are said to be negatively adsorbed, though only relatively.

Some cases of adsorption are purely physical in nature, and akin to condensation; others involve chemical reaction. It is important, though not always easy, to identify particular cases, because the controlling laws are quite different.

Physisorption

For example, the uptake of non-reactive vapours by charcoal is clearly physical, as indicated by the following criteria. An equilibrium is quickly reached. The vapours can be recovered unchanged by pumping, the process being perfectly reversible and repeatable. The amount of vapour adsorbed increases with its partial pressure, but decreases with rise of temperature. Correspondingly, adsorption is exothermic, with a heat of the same order as the latent heat of condensation.

Another class of physisorption process occurs at the surface of solutions. Dilute aqueous solutions of alcohols have been much studied. Adsorption is indicated by a marked reduction of the surface tension and can be verified by analyzing the foam produced by passing air through the solution. (Such solutions foam copiously, whereas pure liquids do not.) Obviously, accumulation of an alcohol at an air/water interface is purely physical.

As early as 1878 Gibbs deduced the thermodynamic relationship between the amount of adsorption, Γ, per unit area, and the reduction of surface tension, γ_c. In its approximate form, the Gibbs adsorption equation reads:

$$\Gamma = \frac{-c}{RT}\frac{\mathrm{d}\gamma_c}{\mathrm{d}c}$$

Consequently, Γ can be evaluated from measurements of γ_c. The meaning of Γ is excess mass of solute, per unit area of interface; that is, in excess over what would be found there if the two phases were uniform in composition right up to a planar junction. Nothing is said about the thickness of the interface. The theory has been checked in modern times by experiment. However, the rigorous thermodynamic theory for the surfaces of mixtures is fraught with difficulties, especially when electrolytes are involved. Simple inorganic salts (e.g. NaCl) *raise* the surface tension of water; they are therefore negatively adsorbed, the interfacial region having a slight excess of water. In contrast, an important class of organic electrolytes, exemplified

by the soaps, are very strongly positively adsorbed, lowering the surface tension remarkably. These are the so-called surface-active electrolytes. Such striking differences must be considered later from the molecular point of view, while emphasizing here that the thermodynamics applies to all cases.

In broad terms, the adsorption of alcohols, etc., can be thought of as being "driven" by the resulting reduction of surface free energy. The same principle must apply to the physical adsorption of vapours on charcoal, although the surface free energy of the solid, before and after adsorption, cannot be measured. Nevertheless, the reduction can be deduced from measurements of the adsorption, employing the Gibbs adsorption equation in a reversed, integrated form, namely (Bangham, 1937):

$$(\gamma_0 - \gamma_p) = RT \int_0^p \Gamma \, \mathrm{d}(\ln p)$$

By analogy with the solid/gas interface, the l.h.s. is said to be the "surface pressure" of the adsorbed gas, and is often written as π, defined as $(\gamma_0 - \gamma_p)$.

The r.h.s. can be evaluated from measurements of the adsorption, Γ, of vapours from pressure zero up to p. The result is an absolute measure of the intensity of adsorption. Unfortunately, this approach does not provide a rigorous method of evaluating γ_0 itself, without introducing dubious non-thermodynamic assumptions, for example, about the surface energy of the solid at saturation with the vapour.

The chief use of measurements of physical adsorption of gases in mineral processing research is for determining the specific surface area of finely-divided solids, such as ground or porous minerals or clays. The adsorption of nitrogen at the temperature of liquid nitrogen is commonly used; alternatively, the use of krypton gives advantages for low specific surface areas. Interpretation of the data depends on molecular theories of adsorption, such as the famous Brunaer-Emmett-Teller (BET) theory (1938).

Chemisorption

At the other extreme, there are many examples of adsorption where a chemical reaction is obviously involved. In Langmuir's classic researches with metal filaments (1916), he discovered that many metals, if truly "clean", take up various gases so powerfully that the gases cannot be recovered by pumping. For example, oxygen is held so strongly by tungsten that it cannot be removed except at a high temperature, when it comes off as WO_3. Many other gases, including nitrogen, hydrogen and carbon monoxide, are similarly "chemisorbed" by metals. Hydrogenation and other catalytic processes on nickel or platinum, etc., depend on chemisorption. The heat of chemisorption is large and catalytic reactions often require an activation energy. These surface chemical reactions may be quite different from common reactions in bulk.

An example of this last statement in mineral chemistry is provided by the oxides in contact with water vapour. Although a few oxide minerals do undergo slow three-

dimensional reaction with water [e.g. $MgO + H_2O \rightarrow Mg(OH)_2$], others react only on the surface, and, indeed, do not possess thermodynamically stable hydroxides — e.g. SiO_2, Fe_2O_3. The latter slowly chemisorb water only on exposed surface groups. That it is chemically bound is shown by its non-removal by pumping and by the development of characteristic bands in the infra-red spectrum, due to SiOH or FeOH groups.

A very different class of surface reaction was discovered by two agricultural chemists, Spence and Way (1845–1850) and originally called "base exchange". They found that when bases such as ammonium are abstracted from solution by soils or clays an equivalent quantity of calcium is released into solution. If a solution of ammonium sulphate is shaken with a certain quantity of soil, a cation-exchange equilibrium is soon set up, which approximately follows the law of mass action. The anion (sulphate) does not take part.

Analogous surface ion-exchange reactions accompany the adsorption of dyes by salt-type solids such as barium sulphate. Similarly, the adsorption of anions by oxides is generally accompanied by release of hydroxyl ions, and it therefore becomes responsive to their concentration [OH^-], and thus to pH.

A simple test for a possible chemical surface reaction is to see whether the adsorbed substance can be removed by washing with pure solvent; if not, it may be possible to displace it by adding the likely soluble product of the reaction, which, of course, may be detected by analysis.

A peculiar problem arises with minerals which are slightly soluble and capable of reacting to precipitate a less soluble product when in contact with a given reagent. For example, sodium oleate (a common soap, used as a flotation collector) will certainly react, given time, with calcite ($CaCO_3$) to precipitate calcium oleate, which has a low solubility product. The uptake of oleate ions is simply governed by mass action. However, some authors maintain that flotation can be obtained with quantities of oleate barely sufficient to produce a monolayer on the calcite, and this is supposed to be adsorbed before bulk calcium oleate precipitates. If so, here is a surface reaction, not physical adsorption, and no doubt an equivalent quantity of carbonate ion is released into solution.

The adsorption of polymers* and other substances of complex structure and high molecular weight exhibits other peculiarities, notably, slowness of equilibration and reluctance to desorb. The reason for both is the multiplicity of points of attachment of the macromolecules to the surface. It is not uncommon for macromolecules to

---

**Editors' note:* Since 1979 there has been a marked surge of interest in polymer adsorption and its effect on colloid stability, a little of which is described in Chapter 3. The interested reader is referred to the literature for a detailed treatment, particularly the following papers:

a J.M.H.M. Scheutjens and G.J. Fleer, J. Phys. Chem., 83 (1979): 1619.

b M.A. Cohen Stuart, T. Cosgrove and B. Vincent, Adv. Coll. Int. Sci., 24 (1986): 143.

c G.J. Fleer and J.M.H.M. Scheutjens, Croatica Chem. Acta, 60 (1987): 477.

be attached by different groupings to different molecular "sites", some perhaps by physical and others by chemical interaction.

Surfaces as molecular assemblages

It is remarkable how far classical physics was able to treat surfaces without any knowledge of the size and shape of molecules and the nature of their interactions; but when this information did become available, little by little, it vastly enlarged understanding of surface phenomena.

Historical

The early founders of capillarity theory — including Newton, Hawksbee, Segner, Young, Poisson, Laplace — were aware that surface tension, wetting, capillary rise, and contact angles are a consequence of the cohesive forces which hold together the "ultimate particles of matter" on the liquid or solid state. Indeed, it is evident from a simple inspection of physical constants that surface tension values of liquids correlate rather well with the "cohesive energy density", irrespective of the nature of the substances. For example, to take four very dissimilar liquids — ethyl ether, ethanol, water, mercury — the latent heats of vaporization per unit volume are respectively 0.31, 0.67, 2.42 and 4.09 (kJ cm^3), while the surface tensions run roughly parallel, namely, 17, 22, 72 and 434 (mN m^{-1}). The intermolecular forces must be of very short range. Attraction energy must predominate (to account for the latent heat of vaporisation), but there must be a "steep" repulsion at short distances, to account for the resistance to compression. If molecules can be treated as mutually attracted hard spheres, their interaction energy, Φ, might be supposed to follow a 2-term power law of the kind used by Mie (1903) and others, namely:

$$\Phi = A\,a^{-n} - B\,a^{-m}$$

where a is the intermolecular distance, n and m are more or less universal constant [12 and 6, respectively, according to Lennard-Jones (1930)] and A and B are specific coefficients for particular substances. Such a formula should be able to account for a range of bulk properties such as compressibility, non-ideality of compressed gases, etc. It should also account for the cohesive energy of liquids (and hence their surface tension) and the work of adhesion of liquid to solid and hence contact phenomena. (This last requires a theory to calculate interactions of unlike molecules from the constants of the individual substances.)

Theoretical attempts along the above lines have been made since about 1900, with fair success, and they are still proceeding. An interesting resume of this approach was given by Padday [2] in 1969. A major development, since that article was written, has been the use of increasingly powerful computer methods to evaluate multi-molecular interactions, using either the "molecular dynamics" or the "Monte Carlo" techniques to arrive at equilibrium structures and energies. Current theory

gives a good account of the surface energy of simple liquids such as argon, deriving interaction energy constants from bulk properties. Calculations of the adsorption energy of an atom adsorbed on a given site of a crystal face are also feasible, provided interactions of the atom with the unlike atoms in the substrate can be correctly summed.

As soon as molecules of more complicated form than quasi-spherical are considered, the problem of *orientation*, as well as packing, of surface molecules becomes important. This leads to the question of interactions which are neither central (e.g. dipoles) nor non-specific (e.g. hydrogen bonding). Clearly, the general problem (for substances more interesting than liquid argon!) is excessively complicated for *ab initio* calculations. Nevertheless, chemists have long used descriptive models which help to explain many important surface phenomena in a qualitative way. They use two powerful guiding principles:

(1) Firstly, the great range of cohesive energy densities of various liquids and solids can be ascribed to the well-known spectrum of intermolecular forces. Although this is a continuous series, the broad classes, in order of increasing strength, are (in the simplest terms): (a) non-polar, (b) dipolar, (c) hydrogen bonding, (d) ionic, and (e) metallic.

(2) Secondly, the key to solubility is "like-dissolves-like", in terms of these classes; there is only limited acceptance of neighbouring classes.

The solubility principle is, of course, familiar from the behaviour of common liquids (e.g. hydrocarbons are mutually miscible, slightly soluble in ethanol, practically insoluble in water, and absolutely insoluble in mercury). The basis for the rule of thumb is the intensity of the intermolecular forces (*A–A*, *A–B*). In group (a) only the weak Van der Waals (or dispersion) forces operate. These forces are also present in the other groups but are there overshadowed by the stronger forces between dipoles, ions or metallic bonding. Consequently, a non-polar molecule is literally "squeezed out" of a polar medium. ("Salting out" of slightly soluble organic substances from water works on this principle.) Conversely, a dipolar substance gets minor benefit from its dipole when in a non-polar medium — hence the low solubility of water in paraffins.*

Now the solubility principle also applies to the surface of solutions, because the force field there is weaker than in the interior. It is one-sided! That is why fluorocarbons tend to adsorb on the air/hydrocarbon surface and — to mention an

---

**Editors' note:* In recent times, colloid chemists and physicists have applied these theories of the liquid state to colloidal dispersions. Various choices of pair (or interaction) potential may be made (e.g. "hard" or "soft"), depending on the system one wishes to describe. Thermodynamic properties and phase transitions can be predicted.

d A. Vrij et al., Faraday Discussions on the Chemical Society Number 65, Colloid Stability, 1978.

e R.J. Hunter (Editor), Foundations of Colloid Science, Volume II, Chapter 14, Clarendon Press, Oxford, 1989.

extreme example — why dissolved carbon and sulphur are adsorbed at the surface of molten steel!

Remarkably, the same solubility principle applies to *different parts* within one molecule, if these component parts separately would fall into different force groups. The consequences are vitally important for surface chemistry. They include: (1) oriented adsorption at interfaces, (2) hydrophobic interactions, (3) micellization, an extreme form of (2), and (4) selective adsorption of groups on heterogeneous sites.

As interfaces are junctions of phases of different molecular type or cohesive energy density, molecules having dual character are likely to be retained at the interface and oriented so that their moieties are in the appropriate phase. For example, at an oil/water interface an alcohol molecule is turned with its $-OH$ group in the aqueous phase and its alkyl group in the oil. At an air/water interface an alcohol is adsorbed with its alkyl group away from the water. These dual-nature molecules are said to be "surface active". Surface activity can be weak (e.g. methanol) or strong (e.g. hexanol) as reflected in the lowering of surface tension per unit of concentration (a linear relationship holds at very low concentrations). If a compound is practically insoluble, it may still be active as a surface-spreading insoluble monolayer (e.g. cetyl alcohol on water).

Surface activity in water

Surface activity can be found with all manner of materials and interfaces; but particular interest attaches to aqueous solutions, both from the scientific and technological points of view. *Water is truly special!* Not only is it the most common liquid and the basis of all life, it is also one of the most peculiar. Early physical chemists recognized its "anomalous" properties which they correctly ascribed to an "associated structure". In solid ice each H_2O molecule participates in four hydrogen bonds in tetrahedral configuration, two as H-donor and two as acceptor. That well known structure, of course, explains its low density and high latent heat of vaporization. The heat of fusion of ice is relatively small because a good deal of structure remains in liquid water near 0°C (as shown by its X-ray diffraction pattern) but diminishes as the temperature is raised. (For a readable account of modern ideas, see "Water" by F. Franks [3].)

Solute molecules perturb the structure of water in various ways, not yet understood in detail. Certainly, ions — and particularly small cations — attract shells of oriented water molecules around them ("hydration"). Non-polar molecules (or non-polar portions of dual-type molecules, such as the CH_3CH_2- group in ethanol) impose structural changes in the water around them, perhaps simply because they are non-participant foreigners in a specially structured medium. Work is required to insert such foreigners. Therefore they appear to be expelled from an aqueous medium and hence are designated "hydrophobic" (water-hating), in contrast to polar groups, which are clearly hydrophilic (water-loving).

Because molecular groups act almost independently on the water close to them, it is possible to draw up lists of groups in the order of hydrophobic-to-hydrophilic character. For example, in the following short list:

$$-CF_3 > -CH_3 > -CH{=}CH- > -C.Cl > -COC- > -NH_2 > -COH > -COOH > -COO^-$$

the fluorocarbon group is the most hydrophobic and the carboxylate ion group the most hydrophilic. Estimates of the free energy of immersion of various groups in water have been made from thermodynamic data.* Qualitatively, the relative solubility of a series of structurally similar compounds, such as Ph–X, indicates the "hydrophilicity" of the radical –X. For example, toluene ($Ph–CH_3$) is soluble in cold water to the extent of about 0.05%; aniline ($Ph–NH_2$) 3.4%; phenol (PhOH) 6.7%, while above 60°C it is completely miscible, because the water structure is loosened as temperature rises. Thus, the hydrophilic –OH group can be said to solubilize the hydrophobic phenyl group.

Because phenol has this dual character ("amphipathic" or "amphiphilic") it is also surface active at an air/water interface. The surface tension is lowered from 72 to 42 ($mN\ m^{-1}$) by addition of 5.6% of phenol to the aqueous phase. This suggests that the surface of the solution is composed largely of phenol molecules — a fact which can be deduced quantitatively by application of the Gibbs adsorption equation.

Soluble compounds that are *highly* surface active are known as *surfactants*. To qualify as a surfactant, a substance must, firstly, contain substantial hydrophilic and hydrophobic moieties, spacially separated for orientation at an interface. Secondly, there must be a suitable balance between these dissimilar groups to provide adequate solubility in the given medium. Hence, there are water-soluble and oil-soluble surfactants.

The oldest commercial surfactants were, of course, the fatty-acid soaps such as sodium stearate, $(CH_3)(CH_2)_{16}COO^-Na^+$, whereas the commonest modern surfactant is an alkyl benzene sulphonate, $R.C_6H_4.SO_3^-Na^+$. These are both anionic surfactants. The simplest cationic surfactants encountered in mineral processing are alkylamine salts, such as dodecylamine hydrochloride, $C_{12}H_{25}NH_3^+Cl^-$. In order to obtain a powerful surfactant with *non-ionic* character, it is necessary to have several polar groups to balance one substantial hydrophobic unit — e.g.

---

* One well-known classification system is the HLB (hydrophilic-lipophilic-balance) scale devised for emulsifying agents by Griffin (1949). However, this is empirical, not fundamental.**

** *Editors' note:* It has subsequently been demonstrated that the HLB is directly linked to the packing ratio proposed by Ninham and co-workers [f, g] so that there is now a firmer theoretical foundation for this most used scale.

f P.J. Becher, Disp. Sci. Tech. 5 (1984): 81.

g J.N. Israelachvili, D.J. Mitchell and B.W. Ninham, J. Chem. Soc. Faraday Trans. 2, 72 (1976): 1525.

$R(CH_2OCH_2)_nCH_2OH$, a derivative of polyethylene oxide. If R is a long alkyl chain and n a rather small number, the compound will be oil-soluble, though still surface active. For reasons of cost, only a few of the hundreds of synthetic surfactants that have been described are in commercial use, but the quantities consumed world-wide for innumerable applications are enormous. Surfactants have a key role in flotation, firstly to establish suitable contact angles and secondly to provide a foam.

The property of foaming is common to all surfactant solutions, though the persistence of their foams varies greatly. (Of course, pure liquids do not foam at all.) Liquid films formed from surfactant solutions possess true elasticity — that is, their tension increases with extension, at least transiently. The reason is the time required for adsorption to restore surface layer when it is depleted by stretching. Lagging adsorption means a temporary local rise of surface tension (the so-called dynamic surface tension) which automatically opposes thinning of the lamella at that place because the temporary gradient of surface tension causes flow of liquid towards the thinning place ("surface transport"). Clearly, very dilute solutions of highly surface-active solutes are good candidates for this transient type of foaming. (Long-lived foams have another mechanism.) In the froth flotation process a short-lived foam is required simply to carry off the floated particles. For many years natural pine oil was used, containing a mixture of terpene alcohols. Synthetic non-ionic surfactants tend to be preferred nowadays (e.g. methyl iso-butyl carbinol).

It should not be forgotten that many macro-molecular substances, natural and synthetic, are markedly surface active. Proteins are a prime example. They are amphoteric and their polypeptide backbone carries a variety of amino-acid units, some of which carry polar and other non-polar groups. Consequently, proteins are adsorbed at air/water or oil/water interfaces. They are also adsorbed by most solids. This versatility is due to two factors — firstly, the variety of functional groups (which can "seek" appropriate sites for adsorption), and secondly, the very multiplicity of attachment points that any long, flexible, macromolecule can provide. It is particularly remarkable that water-soluble proteins such as gelatin form monomolecular coatings on solids as different as calcium carbonate, asbestos, (both polar), graphite, and pure paraffin oil. Physical adsorption on to inert, non-polar substrates is ascribed to a special effect known as "hydrophobic association", which has many facets.

Hydrophobic association

Besides proteins, surfactants of all types — anionic, cationic, amphoteric or non-ionic — are found to adsorb on to inert, non-polar substrates. Of course, this is physical and easily reversible adsorption; the surfactant can be readily washed off. The "driving force" is evidently the tendency of hydrophobic units to "escape" from water by mutual association. A more rational-sounding explanation is that by association of two hydrophobic bodies some of the water which was originally

disturbed in structure by proximity with the hydrophobic materials is released to join the normally-structured medium. (Correspondingly, there exists an attractive force between two hydrophobic bodies in close proximity.)

Self-association also causes long hydrocarbon chains to coil up when in water, and the same effect is reflected in the association of surfactant molecules in solution — the well known phenomenon of *micellization*. Many physico-chemical properties of dilute solutions of soaps, etc. show remarkably sharp alterations at a certain concentration, known as the critical micelle concentration (c.m.c.). There is a break point in the curves for osmotic coefficient, surface tension, electrical conductivity, light-scattering, etc., indicating the presence of aggregates of around 100 surfactant molecules. Increasing the concentration above the c.m.c. increases the number of micelles, with very little increase in the numbers of single molecules in equilibrium.

Micellization is analogous to the coalescence of small drops of oil into larger drops, being attended by a decrease of oil/water interfacial area. But, unlike coalescence, micellization stops at a certain aggregate size because the hydrophobic sections (known as "tails" by surface chemists) in surfactants carry polar groups ("heads") at their ends. The simplest micelle is therefore a cluster of tails surrounded by a shell of heads.*

Because the interior of a micelle is like a micro-droplet of oil, solutions of surfactants above their c.m.c. have the property of solubilizing non-polar substances. Mixed micelles can be formed. There is some evidence, also, that mixed species may be adsorbed together on to solid substrates — for example, soaps + fatty acids. In biological systems hydrophobic association is an important factor in the behaviour of proteins and lipids and in their response to other "amphipathic" molecules such as hormones, anaesthetics, surfactants and drugs. Cell membranes, consisting structurally of back-to-back lipid bilayers, are the site, par excellence, of hydrophobic interactions, accompanied, of course by powerful polar interactions. (For deeper study, read Tanford's monograph [4].)

The above principles apply also to the simpler interaction of surfactants with minerals. Hydrophobic interactions are generally secondary to ionic or dipolar forces; but if an ionic surfactant is attracted to a mineral by its head group the lateral hydrophobic interactions between the chains enhance the adsorption. The longer the chains, the stronger the adsorption. This process, sometimes called hemi-micellization, occurs more easily — that is, at a lower concentration of the surfactant — than does ordinary micellization in solution. The hemi-micelle structure

---

* *Editors' note:* Ninham and co-workers [h] have revived and refined an idea first proposed by Hartley in 1941, based on the idea of an orientated wedge. The packing ratio V/la_0 compares the volume, v, of the hydrocarbon chain of a surfactant to the chain length, l, and the head group area, a_0. The value of V/la_0 dictates whether one obtains spherical micelles, cylindrical micelles, vesicles, etc., and has now led to the development of molecularly tailored membranes.

h D.J. Mitchell and B.W. Ninham, J. Chem. Soc. Faraday Trans. 2, 77 (1981): 601.

forms a monolayer with tails presented to the aqueous solution. This is the mechanism by which hydrophilic solids can be converted into hydrophobic, as required in the flotation process (e.g. the use of alkylamines as "collectors" for silicates). If the surfactant concentration is raised above that needed to complete the hemi-micelle, a second layer begins to deposit by hydrophobic association, and this layer has heads outside. Thus, the contact angle passes through a maximum and eventually falls to zero near the c.m.c.

Adsorption of water-soluble polymers, etc.

To be soluble in water, macro-molecular substances must carry a sufficient proportion of polar groups. For example, natural gums are carbohydrates, with plenty of hydroxyl and carboxyl groups. Their dissolution is improved by rise of pH which converts $-COOH$ groups into the ionic $-COO^{-}Na^{+}$ form. Similarly, synthetic polyacrylic acid is caused to expand and dissolve by conversion into sodium polyacrylate, and the specific viscosity of the solution increases dramatically because of the dilation of the chains. It is a typical "polyelectrolyte".

The adsorption of such compounds by surfaces is determined primarily by electrostatics. Polyacrylate, for example, would be attracted strongly to cationic sites and repelled from anionic sites. Less powerful interactions can occur through hydrogen bonding. The adsorption of polyethylene oxide on to silica and of polyvinyl alcohol on to clays has been studied. As mentioned earlier, adsorption of macromolecular substances can be very strong, despite weak monomer attachment, because of multiple point bonding. Quite often polymer adsorption appears irreversible, in that the substance is difficult to wash off; but a change of conditions, such as pH, may displace the substance quite readily by a process of "unzipping". Generally a linear polymer will be attached by only a proportion of its functional groups; short sections of the chain may be attached ("trains") while other sections loop out into the solution ("loops"). There is a dynamic equilibrium between attached and free sections. The relevance of this molecular picture to the process of flocculation by "bridging" adsorption will be considered more fully elsewhere in this book (Chapter 3), as will the theory of adsorption of polymers (Chapter 2). Finally, it should be mentioned that the coating of solids with adsorbed hydrophilic macromolecular substances (such as gelatin or dextrin) guarantees overall hydrophilic character. This is important in flotation control and in the stabilization of various colloids.

Electrical effects at interfaces

Several different electrical effects turn up at the contact of two phases; amongst them, static electric charges, Galvani cell potentials, and Fermi potentials of metals and semi-conductors are well-known. Nevertheless, it is curious that there are conceptual difficulties in defining, and consequently in measuring, meaningful dif-

ferences of potential across an interface composed of different substances. (The literature is a nightmare, best ignored!)

As *water* is a moderate conductor of electricity, no differences of potential can persist on a macroscopic scale in the absence of applied current. There is a great deal of evidence, however, for the existence of gradients of electrical potential near interfaces, *on a molecular scale*, and the phenomena have an important bearing on mineral processing science.

The clearest indications are provided by the electrokinetic effects. There are four of them — electrophoresis, streaming potential, electro-osmosis and sedimentation potential. They are physically equivalent manifestations of slight charge separations between the two sides of an interface. Electro-osmosis was the first one discovered. Reuss (1808) observed that when an electric current was passed through a U-tube packed with quartz sand in water the water rose on the cathode side (and fell on the other). It seemed as though the quartz were negatively charged with respect to the water. An alternative experiment, leading to the same conclusion, is to force the water through the packed bed and measure the (small) potential difference thus generated between the two ends of the bed. This is the streaming potential effect.

In electrophoresis microscopic particles suspended in an aqueous medium are found to migrate if an electric field is applied. The electrophoretic velocity is directly proportional to the applied field strength. (The converse of electrophoresis is the Dorn (1880) effect; sedimenting particles generate a vertical potential gradient.) It seems that the particles carry an electric charge. It may be positive or negative, depending on the surface chemistry of the materials. Obviously, the particles cannot be carrying a net electrostatic charge in the macroscopic sense; if they are filtered off, there is no detectable charge on the filter-paper! Neither is any potential difference measurable with a probe micro-electrode moved towards an interface. The charge separation is confined to sub-microscopic distances (at least, it is in water).

The concept of the *electrical double layer* is ascribed to Helmholtz (1879). Without specifying the chemistry (which depends on the materials), it is postulated that the solid acquires a certain surface charge density (σ) of one sign while the adjoining liquid gains an equal charge of opposite sign. The former is fixed to the solid whereas the charged liquid is mobile under the influence of applied potential gradient or hydrodynamic shearing — hence the electro-kinetic effects. Helmholtz assumed that the two sheets of charge were like the plates of a planar condenser, but very close. The spacing, δ, might be one molecular diameter. However, later calculations, independently by Gouy and Chapman (1910), recognized that the charges are ions; and free ions tend to diffuse through thermal agitation and form a cloud rather than a planar sheet. They cannot escape entirely because their displacement away from the fixed charges generates a restoring potential. The Gouy-Chapman theory describes the distribution of ions in a diffuse layer, on the basis of various simplifying assumptions. A later refinement of the theory (by Stern, 1924) allowed for the possibility that some of the "free" ions ("counterions") might be held to the

surface by specific adsorption forces. That would reduce the surface charge in both layers.

Incidently, the theory of diffuse double layers shows that the fixed charge density, σ, is mainly balanced by counterions of opposite sign, but partly by repulsion of "co-ions" in the electrolyte — that is, a deficit of ions of the same sign as the fixed charge. Experimentally this appears as negative adsorption of external electrolyte.

There is an impressive and quite fascinating body of theory about how to get at the parameters of real double layers by experimental measurements on one or other of the electrokinetic effects. The parameters envisaged by Helmholtz are σ, δ and the potential difference between the two lots of charge, denoted ζ, the zeta potential. Actually, only zeta comes into the equations of the electro-kinetic effects. As the counterions are in a diffuse cloud, the position of the nominal charge is assumed to be around the centre of charge of the mobile layer. There is no means of getting at σ and δ independently, except by assuming the Gouy-Chapman theory and conceding some other assumptions.

In colloid chemistry it has become traditional to gloss over the complications and use approximate formulae to arrive at a nominal zeta potential. This is near enough for chemical considerations. For example, from a measured electrophoretic velocity, U, expressed in μm s^{-1} per V cm^{-1}, zeta in mV is given by $\zeta \approx 12,8U$ (at 25°C). (This formula comes from the theory of Smoluchowski (1914), with the assumptions that the dielectric constant and viscosity of the water in the diffuse double layer have the values for normal water.)

Experimental results usually fall in the range 0 to $\pm$100 mV. The value depends on the chemistry and on the composition of the aqueous solution. The zeta potential is interpreted as the p.d. between the fixed sheet of charge and the "centre" of the counterion cloud. Calculation of the surface charge density shows that it is "low" — meaning the fixed ions are a long way apart, far from close-packed. The calculated "thickness" of the diffuse layer is greatest in pure water — about 0.1 μm — and is inversely proportional to the ionic strength; in 0.1 N solution of 1 : 1 electrolyte it is only 1 nm, i.e. a few molecular diameters.

Despite the reservations attached to the interpretation of zeta potentials, their experimental values do provide valuable information about the surface chemistry of solids and liquids in contact with water. (A full account can be found in Hunter's monograph [5].) Even "inert" solids such as diamond exhibit significant zeta potentials which vary with the composition of the aqueous phase. In mineral processing research, zeta potentials give a clue to the chemistry and the effect of added reagents. For example, a sample of graphite shows a small negative potential; it carries a few acidic groups. On addition of low concentrations of a cationic surfactant the potential falls to zero (because the groups are neutralized) and then at slightly higher concentrations the potential goes positive ("reversal of charge"). The first step involves electrostatic attraction of the surfactant, while the second indicates hydrophobic adsorption. Similarly, non-ionic polymers such as polyvinyl

alcohol always *reduce* the zeta potential towards zero when they are adsorbed; this is a hydrodynamic effect, the polymer chains obstructing flow of the diffuse double layer.

The chemistry of the charging process can generally be identified by precise chemical (or radiochemical) analysis. There are two principal mechanisms for charging of non-conductors — release of ions from the substrate, or adsorption of ions from the solution side. An important case is charging by dissociation of surface groups as acids or bases. For example, alumina, Al_2O_3. is known to react with water to form surface –AlOH groups; and, being amphoteric, these can ionize either as $-AlO^- + H^+$ (nominal) or as $-Al^+ + OH^-$, according to the pH. Careful microtitration gives the amount of acid or base bound by the solid. (This is not necessarily equal to δ.) Another type of ionizing solid is the sparingly soluble salt. The classic example is silver iodide, AgI. Its solubility product is about 10^{-16} (mol $l^{-1})^2$. One might suppose that in pure water it would release equal concentrations of Ag^+ and I^- ions ($= 10^{-8}$) and so be uncharged; but experiment shows it to be negatively charged. Evidently, iodide is more strongly held *on the surface* than Ag^+. The "point of zero charge" is around 10^{-6} of Ag^+ (10^{-10} of I^-). (Foreign ions can also influence the zeta potential, but more feebly.)

The counterions in an electrical double layer are kinetically "free" and so can exchange with ions of the same sign from the solution, on an equivalent basis. Thus every double layer has a certain ion-exchange capacity. Similarly, the counterions can migrate (parallel with the surface) when an electric field is applied. This is the phenomenon of surface conductivity. (The migration through a porous bed also drags water with it — i.e. electro-osmosis.) Finally, although the thickness of double layers is sub-microscopic (so there is no possibility of measuring the potential gradient with a micro-electrode), in a concentrated suspension of particles there *is* a perceptible effect on electrode potentials — the so-called suspension effect. A glass electrode, for example, registers an erroneous pH.

Interaction of double layers

As already mentioned, colloid chemists long ago suspected that particles in stable hydrophobic colloids (e.g. AgI sols) depend on electrical repulsion between their surface "charges". The Gouy-Chapman theory showed that the charges are actually electrical double layers and the diffuse parts extend for considerable distances (on a molecular scale) in to the solution. Repulsion between particles therefore comes about by interaction of diffuse double layers. If the double layers are destroyed by counteracting the charging mechanism, or the diffuse layers are collapsed by raising the ionic strength, the colloid is coagulated. The model seems reasonable; but what is the evidence?

The repulsion effect can be convincingly demonstrated by a simple experiment due to von Buzagh (1929). If a dilute suspension of finely ground quartz in pure

water is examined on a quartz slide under a microscope (say × 300), the particles which have settled on to the slide are seen to be in perpetual Brownian motion, both translational and rotational, despite gravity; if, now, the pH is lowered to 2 (or if any "indifferent" electrolyte is added in sufficient concentration) the motion ceases and the particles adhere to the slide. The dancing particles were obviously kept away from the slide by repulsion between their negative double layers. The attraction between *oppositely* charged double layers can be demonstrated by mixing suspensions of finely-ground ion-exchange resins of strong-acid (−ve) and strong-base (+ve) type in water; they immediately coagulate into voluminous flocs which can be seen under a microscope to consist of alternate cation and anion exchangers. (Identification is facilitated by dyeing one of the resins.)

Another line of evidence is provided by the stability (strictly metastability) of soap films at equilibrium. Dynamic surface tension accounts only for transient film elasticity; but horizontal soap films can be preserved for days and soon adopt an equilibrium thickness at which the Laplace suction is counterbalanced by double-layer repulsion between the two opposing adsorbed layers of soap. The thickness ranges from about 150 nm in 10^{-4} N down to about 10 nm in 10^{-1} N KCl.

An analogous system for study is the equilibrium "wetting films" formed by a dilute aqueous solution on a smooth, hydrophilic, solid such as polished quartz. Such films were first investigated by Derjaguin and Kusakov (1936). Here again capillary suction is balanced by double-layer repulsion.

Attempts to *calculate* the forces of repulsion between over-lapping double layers began around 1938. Langmuir obtained an approximate formula, valid, for example, for thick wetting films. A more general solution to the problem was arrived at during World War 2 — independently, and unknown to each other — by Derjaguin and Landau in Moscow and by Verwey and Overbeek in The Netherlands. Their calculations confirmed that the interaction forces can be substantial and also showed how they depend quantitatively on surface potential, ionic strength and distance between the surfaces. When combined with forces of other origin (see below), the theory of double-layer interaction accounted very satisfactorily for the phenomenon of stability and coagulation of hydrophobic colloids in water. This is the famous DLVO theory of colloid stability.

The precise *measurement* of forces of repulsion between like surfaces in water and as a function of the separation between them has been one of the outstanding achievements of modern experimental colloid science. The first successful solution to this difficult problem was reported by Israelachvili and Adams (1977) working in Canberra and using smooth mica plates as the experimental bodies. This research was a natural sequel to several previous studies of the more general forces that exist between bodies *in vacuo* — namely, the macroscopic dispersion forces (see below).

Other surface forces

Double-layer interaction is but one example of what Russian surface scientists have called "surface forces of the second kind", to distinguish them from ordinary capillary forces. Interactions can arise because interfaces often have appreciable thickness and two such interfaces cannot get too close without disturbing one another. If the force is a mutual repulsion, as with similar double layers, it is referred to as a "disjoining pressure" (cf. von Buzagh's experiment, above). Attraction between interfaces is also common (e.g. in a temporary film over a hydrophobic solid) — a "negative disjoining pressure". These forces are sometimes called "long range", in contrast to simple intermolecular forces, though there is no sharp distinction in range.

Two important sources of long-range forces are well substantiated. Firstly, as was realised in the 1930's, the attractive force between atoms and molecules due to electromagnetic fluctuations [the "dispersion force" of F. London (1930)] is approximately additive for multi-atomic bodies. Hence, a single molecule can be adsorbed on to a smooth solid by multiple attraction to all the relatively near atoms in the surface of the solid. The attraction is not only magnified, it falls off less sharply with distance. This is even more so with two macroscopic bodies. Hamaker (1937) obtained formulae for the attraction between parallel plates or spheres, in vacuum or in a liquid medium. These long range dispersion forces are the reason why colloids coagulate and dust particles stick to one another or to clean smooth solids. They are the universal attractions incorporated in the complete DLVO theory. Nowadays the dispersion force between multimolecular bodies (e.g. plates, particles, droplets) is calculated by a sophisticated theory developed by Lifshitz (1967, 1970), which employs spectroscopic and dielectric properties of the macroscopic bodies, rather than atomic or molecular properties. The theory of these universal forces has been impressively verified by direct measurements.

The other type of long-range force arises from the altered structure of the liquid medium in the vicinity of an interface. The effect is particularly significant with polar liquids. Their natural "structure" may be influenced to a considerable depth. When two such regions approach one another and begin to overlap a disjoining pressure develops. With hydrophilic solids it is a repulsion. For example, silica sols are still rather stable at pH 2, although this is the point of zero charge. Perhaps the surface –SiOH groups can be regarded as hydrated, influencing water structure for several molecular diameters. A different type of structural alteration occurs near hydrophobic surfaces, for these apparently attract one another. These structural components of disjoining pressures are superimposed on the dispersion and double-layer components. The latter has the longest range, as Blake (1972) proved; he found that the thickness of equilibrium wetting films on quartz agrees with double-layer theory and is independent of whether the quartz is clean (and thus hydrophilic) or surface-methylated (and so hydrophobic). If the double layer is eliminated, the

wetting film ruptures on the hydrophobic surface.

At present there is no theory for calculating the structural component of disjoining pressure in water. But the various long-range surface forces are clearly relevant to processing of finely-divided minerals, for they enter into flocculation, flotation, slime coating, dispersion, filtration, sediment packing and flow properties of slurries (which may switch from Newtonian to thixotropic or dilatant according to the character of the surface forces). The theory of these forces is considered in more detail elsewhere in this book and there are two recent monographs on the subject [6, 7].

Mineral surfaces

Particulate minerals

The term "mineral processing" is mainly associated with techniques for extracting valuable minor components from mined rocks — for example, a few percent of galena, PbS, from an ore containing also small amounts of sphalerite, ZnS, pyrite, FeS_2, etc., embedded in a major proportion of a silicate "gangue". Nowadays processing of one kind or another is also applied to a variety of "industrial minerals", even such bulk materials as coal and clays. The present book does not deal with mechanical or physical methods of separation (e.g. jigging, heavy media, magnetic, electrostatic or optical sorting). It is concerned primarily with what has been aptly named "fine particle technology".

There are three areas where colloid-chemical effects come into play:

(1) The separation of very small grains of mixed minerals which have resulted from fine grinding of an ore (generally by crushing and ball-milling) in order to "liberate" the individual mineral species.

(2) The "beneficiation" of minerals which occur naturally in micro-particle form, notably the more valuable clays.

(3) The control of waste slurries, muds, etc., which must not be allowed to pollute the environment.

All three depend on surface properties. As a general principle, surface effects become increasingly prominent, in comparison with body forces such as weight and inertia, as particle size decreases. Of course there is no sharp switch-over from body to surface control. Coal grains as large as 1 mm can be floated by surface tension. The sediment volume of quartz silts up to 10 μm size is influenced by electrical double layer forces; the rheological properties of even coarser sediments are affected by surfactants, and the pumping of slurries can be facilitated by control reagents.

Because very small particles stick to one another through dispersion forces and electrostatic charging, little processing can be done with *dry* powders; water is the only economic dispersion medium. Consequently, the basic question is the nature

of the water/mineral interface. This is a rather imperfectly explored area of surface-physical-chemistry.

The major point to be emphasized is that *no minerals*, however inert they may seem, *are totally without chemical interaction with water.* It may be confined to the outermost atomic layer, it may involve considerable dissolution, or it may transform the whole particle. (For example, there are some obviously reactive mineral species in certain igneous rocks, e.g. periclase, MgO, which slowly converts to brucite [$Mg(OH)_2$].)

Classification of minerals by crystal-chemical type

The bulk of the earth's crust consists of small, poorly-developed, intermingled crystals, quite unlike the beautiful specimens seen in museums — those are the rarities. Nevertheless, X-ray diffraction shows recognizable crystalline species, not only in obviously crystalline rocks like granite, but even in amorphous-looking solids such as flint, china-clay and fuller's earth. (A few are only proto-crystalline e.g. coal.) From X-ray analysis of well-formed specimens, crystallographers have determined the precise lattice structure of all the important minerals. This structure refers to the *ideal* crystal.

Mineralogists have identified thousands of distinct minerals. Fortunately, the task of elucidating their inactions with water does not require completely new researches for every species, as broad principles can be applied to related groups of minerals. For a simplified introduction, six *chemical* classes can be distinguished (see Table 2).

Minerals in water

Although the research literature of mineral processing contains many papers touching on the aqueous surface chemistry of industrially important minerals, few (if any) of them can be said to be thoroughly investigated. There are several obstacles. Firstly, approach to equilibrium is often very slow — not that full equilibrium

TABLE 2

Classification of minerals by chemical type

Class	Examples of minerals (idealized formulae)
A. Elements	gold (Au); sulphur (S); diamond (C); graphite (C)
B. Sulphides	galena (PbS); sphalerite (ZnS); pyrite (FeS_2); chalcopyrite ($CuFeS_2$)
C. Oxides, simple	quartz (SiO_2); corundum (Al_2O_3); hematite (Fe_2O_3)
D. Oxides, mixed	ilmenite ($FeTiO_3$); spinel ($MgAl_2O_4$)
E. Silicates and alumino-silicates	zircon ($ZrSiO_4$); orthoclase ($KAlSi_3O_8$); talc [$Mg_3Si_4O_{10}(OH)_2$]; kaolinite [$Al_2Si_2O_5(OH)_4$]
F. Salts, sparingly soluble	apatite [$Ca_5(PO_4)_3(OH,F,Cl)$];scheelite ($CaWO_4$)

is achieved in plant practice. Secondly, there are often impurities which complicate the chemistry. Thirdly, low specific surface area of samples and, often, low concentrations of some of the dissolved species make analysis difficult. Yet it is clear that some understanding of the basic water/mineral interactions is an essential preliminary to any rational control process. It should be acknowledged that in the past a good deal of reasonably successful processing has been achieved on the basis of only a crude model of the chemistry, supported by a great deal of *ad hoc*, trial-and-error, test-work. That approach is now failing with the more difficult tasks being posed.

The rationale for fundamental study of a particular mineral in water runs as follows.

(1) Examine the crystallographers' lattice structure for the ideal mineral and assume exposed faces of the real mineral have the same structures as in the model.

(2) If thermodynamic data are available for all the relevant water-soluble species, compute the "speciation diagram", showing their theoretical concentrations in equilibrium with the crystalline mineral (taking account, of course, of ambient pH, temperature, etc.).

(3) Consider how appropriate chemical reagents might interact with the various substances.

(4) Now perform chemical analyses, zeta-potential and contact angle measurements (remembering kinetic factors) and try to reconcile the experimental results with the foregoing considerations. Small-scale flotation tests on "value" and gangue minerals should now follow.

To illustrate the chief principles, some of the factors that govern the surface chemistry of the mineral classes (A) to (F) can be briefly summarized.

(A) Elements. Here the atoms are bound together by powerful covalent or metallic bonds; consequently, the elementary solids are virtually insoluble as such and theoretically unreactive with water. Yet all show zeta-potentials that change with pH. At one time, it was thought that OH^- ions are adsorbed by inert surfaces. A more likely explanation is the presence of oxidized sites on the edges of crystals; some of them act as acids or bases. Even gold is known to chemisorb oxygen. Broken carbon–carbon bonds on faces of diamond or edges of graphite sheets are presumably reactive. Certainly coal, which is quasi-graphitic, is subject to progressive oxidation in air, with formation of –COOH and other groups. Impurity species could also play a part. Spectroscopic methods have revealed various groups even on the surface of diamond. However, no elementary mineral has had its surface chemistry exhaustively examined.

(B) Sulphides show certain similarities to the elements. Their solubility is so low (e.g. PbS) that the minerals might be assumed inert; but they are not. All the sulphides are reactive with oxygen — some slowly (e.g. sphalerite), some faster (e.g. pyrite). The oxidation products are appreciably soluble, so that a ground sulphide

mineral in aerated water soon yields, for example, metal ions (e.g. Pb^{2+}_{aq}) or their hydrated oxides (e.g. Fe_2O_3 from pyrite) and anions such as thiosulphate and sulphate. As many sulphides are electronic semi-conductors, their oxidation processes take on the character of electrolytic corrosion reactions; certain areas oxidize preferentially while others are cathodic, as in the rusting of iron. Several research schools have placed great emphasis on the *n*– and *p*– semi-conductor character of various samples of sulphide mineral and its relation to surface reactions with flotation reagents such as xanthate.

Oxidation processes of sulphide minerals can be manipulated by controlling the redox potential (Eh) of the pulp during processing.

(C) Oxides, simple. Quartz is probably the most researched mineral, and one of the least impure. Its hardness (No. 7) relates to its three-dimensional network of alternating Si^{4+} and O^{2-} ions in 2,4 coordination. The Si–O bond is said to have about 50% covalent character and is certainly strong. Neither of the nominal ions can exist as such in water, yet quartz has an appreciable solubility amounting to about 10 mg l^{-1} at 25°C, resulting from the reversible reaction $SiO_2 + 2H_2O = Si(OH)_4$ aq. As the orthosilicic acid is a weak acid, rise of pH displaces the reaction to the right as silicate ions are formed and so increases the solubility. Equilibrium can be reached only at temperatures above about 90°C.

The *surface* of quartz also combines with water, which can be removed by heating above about 400°. Infra-red spectroscopy shows that siloxane groups, –SiOSi–, are converted by water into silanol groups, –SiOH, which are weakly acidic. This is why quartz in water shows a negative zeta potential, reaching about -120 mV in very dilute alkali and falling to nearly zero at about pH 2. The hydroxylated quartz is strongly hydrophilic, showing zero contact angle and a thick equilibrium wetting film due to the electrical double layer; but when the surface is dehydroxylated by strong heating it becomes definitely hydrophobic, probably because the siloxane groups have ether-like properties and are weak acceptors of protons, whereas silanols participate in hydrogen-bonding.

The most remarkable feature of the reversible silica–water reaction is its extreme slowness; apparently a large activation energy is required unless hydrogen or hydroxyl ions are provided to act as catalysts. At ambient temperatures, neither the dissolution nor the recrystallization proceed at a convenient rate. Rock crystal has been formed under hydrothermal conditions (and synthetic quartz crystals are grown in autoclaves). Conversely, if silica is precipitated by neutralizing dilute sodium silicate solution it forms a colloidal sol whose particles are so small that the equilibrium concentration of dissolved silicic acid is 100 mg l^{-1} — i.e. ten times that of quartz — but no quartz forms. In fact, hydrated polysilicic acid in the form of opal or diatomaceous earth has survived without crystallizing for geological ages!

The oxides of most divalent and trivalent metals are amphoteric and their surfaces after hydroxylation show a positive charge at low pH and a negative at high

pH, with a point-of-zero-charge (pzc or zpc) somewhere between — for example at pH 9 for Al_2O_3. Any dissolution is in the form of the hydroxide, dissociated into its constituent ions (e.g. $Mg^{2+} + 2OH^-$). Apparently corundum (Al_2O_3) hydroxylates only on its exposed atoms, despite the thermodynamic preference in this case (the opposite to quartz) for the formation of gibbsite, $Al(OH)_3$. Surface hydroxylation may be slow to reach equilibrium on cassiterite, SnO_2, while redox reactions — especially Fe^{2+}/Fe^{3+} — depend on the Eh of the medium.

It is obvious that more thorough studies are still needed for the majority of oxide materials.

(D) Oxides, double. The principle here is the same as in *(C)*, but now there are two cations with different characteristics. Dissolution ("leaching") is likely to change the properties of the remaining surface, so the zeta potential probably drifts with repeated washing of the sample.

(E) Silicates and alumino-silicates are by far the most abundant minerals. They are also the joy of mineralogists and crystallographers on account of their wonderful variety and complexity! Furthermore, the variety is multiplied enormously by isomorphous substitution with varying proportions of minor elements. In fact, few silicate minerals conform to their idealized textbook formulae. Perhaps this is one reason why few silicates have been studied by surface chemists. However, the basic principles are clear and can be summarized briefly.

The *orthosilicates*, such as forsterite, Mg_2SiO_4, are structurally like simple salt-type crystals, with an ionic lattice; but the SiO_4^{4-} ion cannot dissolve as such, only by hydrolysis. The ultimate products of leaching of forsterite would be dissolved magnesium hydroxide and silicic acid. (On the way, they might form the hydrous "clay" sepiolite, which forms long flat needles only 0.1 μm thick.) Other orthosilicates, however, are highly resistant to leaching and provide semi-precious gems (e.g. zircon). Presumably surface layers are hydroxylated.

All other silicates contain linked structures forming rings, chains, sheets or three-dimensional networks in which O-atoms join Si- or Al-atoms or both. The diversity of the crystal chemistry gives rise to the well known diversity of morphology — for example, the needles of chrysotile asbestos (which are actually bundles of submicroscopic hollow rolled sheets); the large sheets of muscovite mica, the microplatelets of kaolinite (china clay) or the swelling clay montmorillonite; the submicroscopic needles of palygorskite clay; the large, strong, crystals of felspars and the molecularly porous and cation-exchangeable hydrated alumino-silicates of the zeolites.

Two properties they all have in common; firstly, they cannot dissolve "congruently", only by hydrolytic decomposition (there is no true reversible solubility at room temperature), and secondly, almost invariably certain cations will be leached out of the surface layers before others — often alkali metal ions, then alkaline

earths. As hydrolytic reactions are responsible for any dissolution, the kinetics and the products are likely to be dependent on pH. For example, in dilute acids Mg can be leached out of the needles of chrysotile asbestos [idealized formula $Mg_3(Si_2O_5)(OH)_4$], leaving a "pseudomorph" of hydrated silica. This is an extreme example where the process can go all the way through the needles within a reasonable time. But the principle is the same for hard silicates that seem to be resistant; the difference is only kinetic. For example, the felspar crystals [idealized formula (K, Na)$(AlSi_3O_8)$], in granite are well known to be unstable to weathering. They lose their alkalis and leave various products such as the clay kaolinite, $A1_4Si_4O_{10})(OH)_8$. But kaolinite itself is never in reversible equilibrium with water at ordinary temperatures. Probably the paired alumina-silica sheets are resistant to attack on the basal planes (kinetics!) and only exposed edges are nibbled away. In acids alumina is preferentially leached out; in concentrated alkali soluble aluminate and silicate are formed.

The zeta-potential of alumino-silicate particles, such as kaolinite, is a weighted mean of the various exposed faces and it obviously depends on the pre-treatment of the sample. There is a long-standing theory (now almost a dogma!) that, in pure water, the edges of kaolinite are positively charged and the faces negatively. This derives from two observations. Firstly, Thiessen (1942) published electron micrographs showing particles of colloidal gold deposited preferentially on the *edges* of kaolinite plates. Gold sols are negatively charged, while kaolin in water is also negative on average. So the edges *may* be positive, accounting for +− coagulation. However, gold sols are stabilized by traces of aurichloride ions and are exceedingly sensitive to coagulation by low concentrations of aluminium salts. Secondly, Schofield and Samson (1954) found that the sodium form of kaolinite is coagulated in pure water (though dispersed by a small rise of pH). This was explained as face(−)-to-edge(+) attraction. The supporting evidence for positive sites is that these clays have a large cation- and a small *anion*-exchange capacity (e.g. adsorbing sulphate or phosphate) and this latter capacity increases with fall of pH — just like alumina. What is not made clear in the literature is that all these effects depend on having the clay "cleaned up" before use, to remove the coagulating effect of Ca, etc., on the outer surface. Generally prolonged dialysis, electrodialysis or ion-exchange resin treatment is used, and it commonly involves exposure to acid conditions. There is evidence that Al is leached out. On washing to pH 7 dilute Al-salts begin to hydrolyse and deposit polymeric hydroxy-ions — perhaps most thickly around the leached edges, for colloidal alumina is known to deposit on to hydrated silica. The "alumina" sites may be artefacts rather than intrinsic to the crystal.

This brief case study indicates that there is no procedure for cleaning the surface of kaolinite (or any other alumino-silicate) to obtain a perfect, pristine, surface for study. The surface depends on its pre-history. Even with this simple mineral our present knowledge is inadequate.

(F) Sparingly-soluble salts. Minerals with ionic lattices, such as barite, $Ba^{2+}SO_4^{2-}$, have an intrinsic solubility product (e.g. $[Ba^{2+}][SO_4^{2-}] \approx 10^{-10}$) and their lattice ions will generally be "potential-determining" for zeta potential. Anion and cation are unlikely to be equally strongly absorbed (cf. the example of AgI mentioned earlier) and either or both may be subject to hydrolysis (e.g. $CO_3^{2-} \rightarrow HCO_3$) depending on the pH. Hydrolysis thus shifts the *ratio* of the potential-determining ions and hence shifts the zeta potential indirectly. Whether pH also affects the surface charge directly by hydrolysis of surface groups (e.g. replacement of some surface CO_3^{2-} groups on calcite by HCO_3^-) is problematical.

The first step in investigating one of these minerals is to establish the equilibrium concentration diagram of all relevant species in solution — as has been done in detail for calcite, fluorite, apatite, etc. Then it is possible to consider what reactions are to be expected with simple reagents that may be present or added. For example, it is readily shown from the thermodynamic data that small concentrations of sodium carbonate should convert fluorite to calcite or barite to witherite ($BaCO_3$). (This is simple classical physical chemistry.) Zeta-potential measurements do indeed show the expected changes in surface properties. Of course the form that the product takes is not revealed.

Caution is needed in using thermodynamic data in this way. The literature data may not be reliable and constants that apply to well-crystallized solids may be inappropriate for colloidal or ill-formed substances or surface compounds. Furthermore, full equilibrium between sparingly soluble salts and aqueous solutions may need long times — typically hours or days. Therefore, kinetic studies of surface properties are needed. Practical processing of minerals generally provides "conditioning time" of only seconds or minutes; the direction and the rate of reactions needs to be established.

... but REAL minerals are non-ideal, imperfect

In order to elucidate the principles governing the surface chemistry of particular minerals, researchers choose to work with pure, synthetic, crystals or, failing that, with selected pieces of the best obtainable mineral specimens — often misleadingly described by the suppliers as "pure". It needs to be emphasized that few natural minerals have their textbook composition and that most are significantly non-ideal in one or more of the following ways.

Elemental analysis

Perusal of any modern textbook of mineralogy which includes analytical data (for example, that of Deer, Howie and Zussman [8]) reveals considerable departures from the ideal formula for many minerals; and often there are wide divergencies of analysis for specimens from different places. There are two reasons for such

divergencies — (a) isomorphous substitution in the lattice, or (b) the presence of small inclusions of a foreign mineral within the specimens analyzed.

(a) Isomorphous replacement is limited by elemental abundance and by atomic (ionic) radius. A pair which have similar charge, radius and abundance are Fe^{2+} and Mg^{2+}; they commonly substitute for one another (and there even appears to be a continuous series of solid solutions from magnesite, $MgCO_3$, to siderite, $FeCO_3$). Other pairs are OH^-/F^-, K^+/Rb^+, Sr^{2+}/Ca^{2+} and Cr^{3+}/Fe^{3+}. For charge balance, $Mg^{2+} + Si^{4+}$ can replace $2Al^{3+}$; similarly, $Na^+ + Si^{4+}$ for $Ca^{2+} + Al^{3+}$. The modern technique of electron probe micro-analysis can show up analytical differences not only between different grains in a nominally homogeneous sample but also across a single grain.

(b) Inclusions are also common and difficult to avoid unless the ore happens to be coarsely crystalline and amenable to clean "liberation" by crushing and physical separation. Intergrowths and microscopic "ex-solution" specks (formed from the solid during cooling) are common, for example in sulphide minerals. On a coarser scale, the composite particles knows as "middlings" are common in practical mineral processing, because liberation by comminution is often imperfect. That may not matter on the plant (where a second stage of grinding on the first concentrate may be economic); but for surface-chemical studies such a concentrate is likely to be unsuitable.

A few percent of an impurity mineral may not seem important. Research reports sometimes lightly pass it off "... the mineral analyzed 98.2% pure ...", even failing to identify the impurities. But impurities often concentrate on the surfaces of grains. The following examples show how disastrous this pitfall can be. Both are taken from research students' studies of asbestos minerals. Student A made painstaking analyses, using sensitive methods, of the slow leaching of crushed chrysotile and then proposed an elaborate theory about incongruent dissolution of this magnesium silicate. What was overlooked was that the chrysotile had a small excess of magnesium, probably present as needles of brucite, $Mg(OH)_2$, which releases Mg^{2+} and OH^- faster than does chrysotile. Repeated leaching of the specimen might have exposed this error. Similarly, Student B studied the release of Fe^{2+} in acid leaching of amosite, an iron-magnesium silicate, but overlooked the presence of a small amount of ankerite, a ferruginous kind of dolomite (Ca, Mg, Fe carbonate). Of course he ought to have detected sites of effervescence, but didn't think to make close visual examination! Needless to say, either of these researches would have been seriously misleading if published, because the vital impurity would not have been even mentioned.

Non-uniform surface properties

The surface chemistry of minerals is generally investigated with material of small particle size, for convenience of sampling and analysis as well as availability. Perhaps this is the reason why researchers often fail to take account of the well-known fact

that crystals do not have absolutely uniform surface properties. This applies particularly to the *chemical reactivity* of mineral grains, though it is true to some extent for other properties and virtually all crystals. Quite apart from differences of crystal faces (obvious for needles and platy crystals), even well-formed crystals possess dislocations, steps, re-entrant corners, etc: and crystal growth and dissolution centre around such features, not on perfect planes. Features of the surface topography are revealed by electron microscopy, especially with the techniques of shadowing and "decoration" with very small colloidal particles of high electron density, such as gold sols (which tend to collect along steps). Modern surface analysis techniques often reveal unexpected coatings — e.g. graphite material on certain sulphide mineral grains.

In minerals there are additional reasons for heterogeneity — notably, strains of geological origin; foreign or ex-solution substances concentrated at grain boundaries (and thus likely to be prominent when the ore is crushed); "active" ("disturbed") solid produced by grinding. There is a great deal of evidence for the view that fine grinding produces unstable fragments having more rapid dissolution or reaction and higher thermodynamic activity (thus solubility) than stable crystals. Even coarse ground grains may contain incipient fracture lines.

In short, there are sound reasons for *expecting* mineral particles to show differences of reactivity from grain to grain and from place to place on single grains. But it is difficult to test the hypothesis. The eminent Russian expert, I.N. Plaksin, published autoradiographs of mineral grains treated with various reagents labelled with radio-isotopes; the results always showed "patchy" deposition of the reagent. The present writer obtained similar results with S^{2-} on anglesite ($PbSO_4$), Pb^{2+} exchange on anglesite, and CO_3^{2-} exchange on Iceland spar (calcite). These examples all refer to multi-molecular deposits over small areas. There appears to be no precise autoradiographic work on surfaces where only a monolayer or bilayer is expected (e.g. dodecylamine on quartz?).

Possible evidence for non-uniformity of sorption of flotation collectors might come from a study of the kinetic flotability of nominally pure and uniform size mineral fractions. It is known that first-order kinetics do not fit perfectly, some of the sample floating more easily than other parts. But this difference might be due to differences of shape. It would be interesting to collect the fast, medium, and slow floating fractions and analyze them for amount of sorbed collector. I am not aware of any such experiments.

In the absence of topochemical information, researchers divide the amount of reagent adsorbed by the mineral by its BET surface area and report the uptake as "statistical monolayers"; but of course the actual deposit could equally well consist of multimolecular patches separated by bare areas. Similarly, the observation that quartz will float with less than one statistical monolayer could mean that some areas take up more than average and the particles float on these areas. The question might be settled by skilful measurements of contact angles on coarse quartz grains

under a binocular microscope, with a capillary air supply moved around the particle on a micro-manipulator. (The quartz would have to be well cleaned with alkali beforehand, super-pure conditions would be essential, and the reagent would have to be a strongly-bonded one; not an easy experiment, but it could be conclusive.)*

Problems with mineral mixtures

As the objective of most mineral processing schemes is to separate mineral species from particulate mixtures, the logical strategy is to study the surface chemistry of the various minerals separately and then devise conditions and reagents to get a differential response. The plan is next tried out on synthetic mixtures and finally on the actual ore. Complications often occur through interference between the different minerals present.

It might be supposed that the minerals *in an ore* would be mutually in equilibrium, having remained in close proximity for millions of years. But fine-grinding of an ore in water may set off new processes through dissolution, hydrolysis, adsorption, oxidation or colloidal interaction. The active surfaces of freshly crushed crystals may adsorb ions from slightly soluble constituents; for example, a trace of Pb^{2+} coming from oxidizing galena may be sufficient to "activate" silicate towards flotation reagents. A trace of hydrolyzing Fe^{3+} ions, coming from steel grinding balls, has been known to depress the zeta potential of quartz and colloidal ferric oxide readily deposits onto sulphide mineral grains. Or suppose there are two calcium minerals in the ore, say calcite and fluorite, what will determine the level of dissolved Ca^{2+}? In addition, the plant water is likely to contain solutes, especially as it is generally recycled.

Colloidal interactions involving the "slimes" fraction of ground minerals (i.e. <10 μm) are well known. To get the slimes (including natural clays) colloidally dispersed requires careful attention to the pH and ionic content of the suspension ("pulp"). The aim is to get a high zeta potential (usually negative) and a low content of divalent and trivalent cations. For clay dispersal sodium silicate or tripolyphosphate may be added. If the conditions are not favourable for dispersion of the slimes, not only will they coagulate but they will also deposit on to larger grains by a process known in the industry as "slime coating". (Derjaguin has proposed the term "adagulation" for deposition of colloidal particles on to larger solid substrates.)

**Editors' note:* Optical grade, carefully sized angular quartz particles whose surfaces were methylated to various known surface coverages have been studied by Ralston and co-workers. The particles showed the same maximum adsorption density independent of particle size. Similarly, at a specific adsorption density, contact angles measured on an assembly of such particles were the same as on flat plates. When a tightly sized particle size fraction was floated, the largest particles floated most quickly, as is described in detail in the literature.

i R. Crawford, L.K. Koopal and J. Ralston, Colloids and Surfaces, 27 (1987): 57.
j R. Crawford and J. Ralston, Int. J. Min. Proc., 23 (1988): 1.

Adagulation is not specific for particular pairs of materials, though it is particularly marked when the pair carry opposite sign of zeta potential — for example, calcite and quartz in a narrow range of conditions of pH and calcium ion concentration. It can occur wherever double-layer repulsion is too low to maintain a force barrier against Brownian motion. For example, galena slimes can deposit on galena crystals. Of course slime coating is detrimental to good separation in flotation because the differences between the surface properties are screened by foreign particles on the surfaces.

In conventional flotation processes the slimes are treated as a nuisance to be removed (for example, in a hydrocyclone) before the coarser grains are separated by flotation. For economic reasons in future it may become necessary to work out separation processes that will operate in the slimes range — such as selective flocculation — and then the chemical conditions required to disperse the slimes just sufficiently will become critical. Here again experiment shows that procedures which look promising with synthetic mixtures are liable to fail on actual plant slimes, possibly because of "smearing" during comminution or possibly mutual interference of the chemically active material produced during grinding, or soluble or colloidal material in the plant water. A particularly difficult problem for the researcher arises if samples taken at the plant undergo changes on storage before laboratory research can be done on them!

It is clear that no general guidelines can be laid down in this area of colloid-chemistry-applied-to-mineral processing beyond remarking that every case has to be investigated *ab initio*. Clearly, there is still a large area of technology awaiting development.

References

1 D.H. Everett, Basic Principles of Colloid Science, Royal Soc. Chem., London, 1988.
2 J.F. Padday, Surface Tension, in: E. Matijevic (Editor), Surface and Colloid Science, Vol. 1., Wiley-Interscience, New York, N.Y., 1969.
3 F. Franks, Water, Royal Soc. Chem., London, 1983.
4 C. Tanford, The Hydrophobic Effect, J. Wiley, New York, N.Y., 2nd edition, 1980.
5 R.J. Hunter, The Zeta-Potential in Colloid Chemistry, Academic Press, London, 1981.
6 J.N. Israelachvili, Intermolecular and Surface Forces, Academic Press, London, 1985.
7 B.V. Derjaguin, N.V. Churaev and V.M. Muller, Surface Forces, Consultants Bureau, New York, N.Y., 1987 (English translation).
8 W.A. Deer, R.A. Howie and J. Zussman, An Introduction to the Rock-Forming Minerals, Longmans, London, 1966.

Chapter 2

Adsorption

LUUK K. KOOPAL

Introduction

Adsorption at the mineral solution interface is of major importance for the behaviour of mineral particles in solution. Adsorption of simple ions will determine the charge of the particles and therefore affect the colloid stability and the adsorption of other charged components at the particles. Adsorption of surfactants is used in mineral technology to control the dispersion stability and/or the wetting behaviour of the particles. Polymer adsorption may cause destabilisation of a mineral dispersion at low concentrations or enhance stabilisation at high concentrations.

It is the purpose of this chapter to discuss the principles of adsorption with emphasis on modelling aspects. In the available space it is impossible to give a complete review on the adsorption of ions, surfactants and polymers. We start with a summary of the most important thermodynamic relations and a brief description of perfect and regular behavior. In the second part some headlines of the adsorption of inorganic ions, organic molecules, surfactants and polymers will be presented. With the organic molecules a distinction will be made between rigid and flexible molecules. A series of reviews considering the adsorption of various components at the solid/liquid interface can be found in "Adsorption from solution at the solid/liquid interface" [1]. "Surfactant Science Series" volume 27 is devoted to "Reagents in mineral technology" [2]. The solid/gas interface will not be considered. A treatment of the use of gas adsorption for the characterization of solids has been given by e.g. Gregg and Sing [3].

Thermodynamics of adsorption from solution

In this section a brief account of the equilibrium thermodynamics is presented in the form of a summary of the more important thermodynamic relations for the bulk phases and the interfacial region. Equilibrium thermodynamics is a helpful tool in

stating the restrictions imposed on any model of a system or an interface and can help to derive relations between variables which otherwise are difficult to formulate [4]. A textbook, covering the thermodynamics of interphases, is that of Defay et al. [5].

Characteristic functions for a bulk phase

We start with the assumption that any bulk phase will have a well defined value for the internal energy U, the entropy S, the volume V, the number of moles n_i of component i, the temperature T, the pressure p and the chemical potential μ_i of component i. According to the first and second law of thermodynamics [4] a variation of U, the internal energy of a bulk phase, α, is given by:

$$dU = TdS - pdV + \sum_i \mu_i dn_i \tag{1}$$

The condition for equilibrium in an isolated system is that the internal energy has its minimum value for a given value of the entropy. This may be expressed as:

$$(dU)_S = 0 \tag{2}$$

Equilibrium within an isolated phase α is established by allowing the interchange of entropy, volume and matter between different regions in α to satisfy equation (2). At equilibrium the intensive variables T, p and μ_i are uniform throughout the entire phase.

By integration of equation (1) at constant intensive variables we obtain the characteristic energy function U:

$$U = TS - pV + \sum_i \mu_i n_i \tag{3}$$

As equation (3) is an equation of state, it is possible to define other energy functions for a bulk phase by combining the state variable U with other state variables. Usually these functions include the enthalpy H:

$$H = U + pV = TS + \sum_i \mu_i n_i \tag{4}$$

$$dH = TdS + Vdp + \sum_i \mu_i dn_i \tag{5}$$

the Helmholtz energy F:

$$F = U - TS = -pV + \sum_i \mu_i n_i \tag{6}$$

$$dF = -SdT - pdV + \sum_i \mu_i dn_i \tag{7}$$

and the Gibbs energy G:

$$G = U - TS + pV = H - TS = \sum_i \mu_i n_i \tag{8}$$

$$\mathrm{d}G = -S\mathrm{d}T + V\mathrm{d}p = \sum_i \mu_i \mathrm{d}n_i \tag{9}$$

From any of these functions so called Maxwell relations can be obtained by noting that the order of obtaining second derivatives of U, H, F and G is arbitrary. Important examples are:

$$\frac{\partial}{\partial p}\left(\frac{\partial G}{\partial n_i}\right) = \left(\frac{\partial \mu_i}{\partial p}\right)_{T,n_i} = \frac{\partial}{\partial n_i}\left(\frac{\partial G}{\partial p}\right) = \left(\frac{\partial V}{\partial n_i}\right)_{T,p,n_j} = V_i \tag{10}$$

$$\frac{\partial}{\partial T}\left(\frac{\partial G}{\partial n_i}\right) = \left(\frac{\partial \mu_i}{\partial T}\right)_{p,n_i} = \frac{\partial}{\partial n_i}\left(\frac{\partial G}{\partial T}\right) = -\left(\frac{\partial S}{\partial n_i}\right)_{T,p,n_j} = -S_i \tag{11}$$

where n_j indicates $n_j \neq n_i$. Derivatives of the form:

$$Y_i = \left(\frac{\partial Y}{\partial n_i}\right)_{T,p,n_j} \tag{12}$$

where Y is any extensive quantity, are known as partial molar quantities. According to equation (12) at constant temperature and pressure, Y follows from:

$$Y = \sum_i n_i Y_i \tag{13}$$

The Gibbs-Duhem equation and the chemical potential in a bulk phase

An important thermodynamic relation for an open system is the Gibbs-Duhem equation. This equation can be obtained by differentiation of equation (3) and combination of the result with (1):

$$S\mathrm{d}T - V\mathrm{d}p + \sum_i n_i \mathrm{d}\mu_i = 0 \tag{14}$$

According to equation (14) at given temperature and pressure the chemical potential of each component is a function only of the phase composition. This can be expressed as:

$$\mu_i = \mu_i^\circ + RT \ln f_i x_i \tag{15}$$

where μ_i° is the chemical potential of the pure component at the same temperature and pressure, R the gas constant, and x_i and f_i are the mole fraction and activity coefficient of i, respectively. The separation between x_i and f_i as made in equation (15) is arbitrary but very common in the discussion of thermodynamics of solutions

and mixtures [4, 5]. In literature deviations from ideality are often expressed as excess molar quantities taking the so called perfect behavior at the same conditions of temperature, pressure and composition as reference state. For a discussion of the calculation of f_i from experimental results the reader is referred to [6], where also various expressions for $\ln f_i$ can be found.

Perfect solutions

As reference system for ideal behaviour we will use the concept of the perfect (p) solution, defined as one in which all components satisfy [4, 5]:

$$\mu_i^{\mathrm{p}} = \mu_i^{\circ} + RT \ln x_i \tag{16}$$

As standard state the pure component is chosen. The concept of perfect behavior is based on a lattice model for the solution. The partial molar volumes, the partial molar energies (or enthalpies) and the thermal part of the partial molar entropies in a perfect solution are assumed to be independent of the composition and equal to their molar equivalents. Comparison of equations (15) and (16) shows that $\ln f_i$, can be obtained as:

$$\ln f_i = \frac{(\mu_i - \mu_i^{\mathrm{p}})}{RT} \tag{17}$$

Pure components show perfect behavior, hence for $x_i = 1$ also $f_i = 1$.

For any extensive quantity Y the change $\Delta_{\mathrm{m}}Y$ on mixing the pure components to form n moles of mixture is given by:

$$\Delta_{\mathrm{m}}Y = \sum_i n_i Y_i - \sum_i n_i Y_i^{\circ} \tag{18}$$

where Y_i° is the molar quantity of the pure component. The change in Gibbs energy on mixing $\Delta_{\mathrm{m}}G$ is given by equations (18), (15) and (8) as:

$$\Delta_{\mathrm{m}}G = \sum_i n_i RT \ln f_i x_i \tag{19}$$

In the case of a perfect solution by definition $\Delta_{\mathrm{m}}V = 0$, $\Delta_{\mathrm{m}}H = 0$ and $f_i = 1$, hence:

$$\Delta_{\mathrm{m}}G^{\mathrm{p}} = \sum_i n_i RT \ln x_i \tag{20}$$

In general, at constant temperature $\Delta_{\mathrm{m}}G = \Delta_{\mathrm{m}}H - T_{\mathrm{m}}S$ so that according to equation (20) we obtain for the entropy of mixing of a perfect mixture:

$$\Delta_{\mathrm{m}}S^{\mathrm{p}} = -\sum_i n_i R \ln x_i \tag{21}$$

Equations (19)–(21) play a central role in the thermodynamics of solutions and mixtures.

Open system with an interface

So far we have only considered a bulk phase. In treating a system consisting of two phases α and β meeting at a planar interface of area A, it should be realized that to bring molecules from the interior of the phase into the surface, work must be done against the cohesive forces in the liquid. The internal energy change dU in extending the surface area by an amount dA is defined as the surface tension, γ, provided S, V and n of the system are kept constant:

$$\gamma = \left(\frac{\partial U}{\partial A}\right)_{S,V,n_i} \tag{22}$$

For a system containing two phases meeting at a plane interface, equation (1) therefore has to be extended to include the work term for the interface:

$$dU = TdS - pdV + \gamma dA + \sum_i \mu_i dn_i \tag{23}$$

Combination of equation (23) with the energy functions defined in equations (4), (6) and (8) allows us to redefine γ as:

$$\gamma = \left(\frac{\partial U}{\partial A}\right)_{S,V,n_i} = \left(\frac{\partial H}{\partial A}\right)_{S,p,n_i} = \left(\frac{\partial F}{\partial A}\right)_{T,V,n_i} = \left(\frac{\partial G}{\partial A}\right)_{T,p,n_i} \tag{24}$$

The last expression provides the most convenient definition of γ for pure systems.

Because of the finite range of action of the intermolecular forces an interphase should in general be regarded as a region of finite thickness across which the energy, density and other thermodynamic properties change gradually, see Figure 1. Nevertheless a generally adopted approach [5, 7] is to introduce an imaginary dividing surface (plane) between the two bulk phases and to acknowledge the presence of

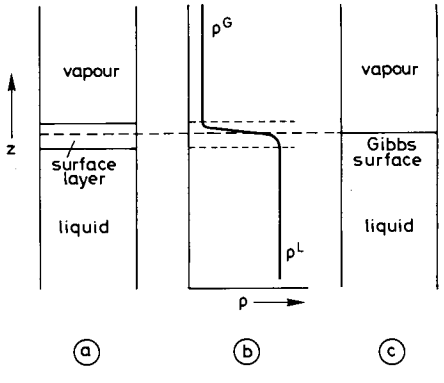

Fig. 1. Schematic representation of a surface of a pure liquid. a. Surface layer; b. variation of the density through the surface region; c. the Gibbs model of the interphase.

the interfacial region by defining surface excess quantities. At the dividing surface, also called the Gibbs plane, it is assumed that there is a discontinuity in density, mass, energy, entropy, force and molecular composition. This approach is called the Gibbs convention.

Any choice of the Gibbs plane defines two volumes, V^α of phase α and V^β of phase β, such that:

$$V = V^\alpha + V^\beta \tag{25}$$

V^α and V^β extend up to the dividing plane, making the volume of the interfacial region $V^s = 0$. Any other extensive property, Y, of the system is supposed to have a certain value in each of the bulk phases up to the dividing plane, plus a surface excess amount defined as:

$$Y^s = Y - Y^\alpha - Y^\beta \tag{26}$$

or more explicitly:

$$Y^s = Y - V^\alpha y^\alpha - V^\beta y^\beta \tag{27}$$

where y^α and y^β are the densities Y^α/V^α and Y^β/V^β in the homogeneous phases α and β, respectively. Using these concepts any variation in internal energy for the whole system can now be subdivided in a variation in internal energy of phase α:

$$\mathrm{d}U^\alpha = T\mathrm{d}S^\alpha - p\mathrm{d}V^\alpha + \sum_i \mu_i \mathrm{d}n_i^\alpha \tag{28}$$

of phase β:

$$\mathrm{d}U^\beta = T\mathrm{d}S^\beta - p\mathrm{d}V^\beta + \sum_i \mu_i \mathrm{d}n_i^\beta \tag{29}$$

and the surface excess energy:

$$\mathrm{d}U^s = T\mathrm{d}S^s + \gamma\mathrm{d}A + \sum_i \mu_i \mathrm{d}n_i^s \tag{30}$$

Equation (30) is obtained by subtracting equations (28) and (29) from equation (23) for the system as a whole. The condition for internal equilibrium [equation (2)] ensures that $T^\alpha = T^\beta = T^s = T$, $\mu_i^\alpha = \mu_i^\beta = \mu_i$ and $p^\alpha = p^\beta = p$. The latter relation implies a planar interface. For curved interfaces p^α and p^β differ by an amount equal to the Laplace pressure [5].

Integration of equation (30) at constant intensive variables leads to the characteristic function:

$$U^s = TS^s + \gamma A + \sum_i \mu_i n_i^s \tag{31}$$

Similarly as for the bulk phase other surface excess functions can also be defined [8]. The surface excess enthalpy is obtained by realizing that with the Gibbs convention for an interface the pV term should be replaced by a γA term:

$$H^s = U^s - \gamma A = TS^s + \sum_i \mu_i n_i^s \tag{32}$$

$$\mathrm{d}H^s = T\mathrm{d}S^s - A\mathrm{d}\gamma + \sum_i \mu_i \mathrm{d}n_i^s \tag{33}$$

The surface excess Helmholtz energy is defined in the conventional way:

$$F^s = U^s - TS^s = \gamma A + \sum_i \mu_i n_i^s \tag{34}$$

$$\mathrm{d}F^s = -S^s\mathrm{d}T + \gamma\mathrm{d}A + \sum_i \mu_i \mathrm{d}n_i^s \tag{35}$$

The latter relation is especially useful for processes at constant A. The surface excess Gibbs energy can be defined as:

$$G^s = U^s - TS^s - \gamma A = F^s - \gamma A = \sum_i \mu_i n_i^s \tag{36}$$

$$\mathrm{d}G^s = -S^s\mathrm{d}T - A\mathrm{d}\gamma + \sum_i \mu_i \mathrm{d}n_i^s \tag{37}$$

Equation (37) is well suited to describe processes at constant γ. The above set of definitions has the advantage that the expression for the surface excess Gibbs energy is analogous to the corresponding expression for the bulk phases, equation (8). From equation (34) it can be deduced that the surface tension can be identified with:

$$\gamma = \frac{F^s - \sum_i \mu_i n_i^s}{A} = f^s - \sum_i \mu_i \Gamma_i \tag{38}$$

This equation shows that γ is not simply an excess energy per unit area. Only for pure liquids for which $\Gamma_i = 0$, γ equals the surface excess Helmholtz energy per unit area.

The Gibbs equation

Differentiation of equation (31) yields in combination with (30):

$$S^s\mathrm{d}T + A\mathrm{d}\gamma + \sum_i n_i^s \mathrm{d}\mu_i = 0 \tag{39}$$

Equation (39) is the surface analogue of the Gibbs-Duhem relation (14). Defining

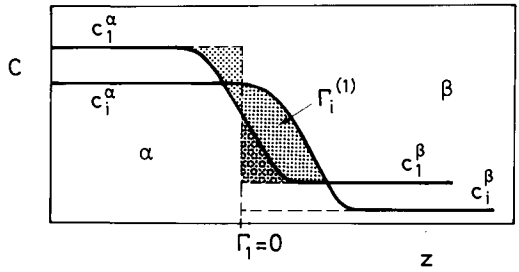

Fig. 2. Gibbs dividing plane and surface excess amounts of solvent (1) and solute (i). The position of the Gibbs plane is chosen such that the surface excess of solvent is zero ($\Gamma_1 = 0$). The surface excess of solute with the dividing surface defined by $\Gamma_1 = 0$ is indicated by the lightly shaded area.

surface excess quantities per unit area, i.e.:

$$y^s = \frac{Y^s}{A} \tag{40}$$

we may write equation (39) as:

$$\mathrm{d}\gamma = -s^s \mathrm{d}T - \sum_i \Gamma_i \mathrm{d}\mu_i \tag{41}$$

where $\Gamma_i = n_i^s/A$ is the "adsorption" of i. Equation (41) is known as the Gibbs equation, it plays a central role in the description of surface phenomena. At constant temperature and pressure equation (41) relates the change in surface tension as a consequence of a variation in μ_i to the adsorption of i.

Above it has been assumed that the Gibbs plane was fixed in order to define V^α and V^β and the excess quantities. However its location, which determines the magnitude of the excess quantities such as s^s and Γ_i, was not discussed. The situation is illustrated in Figure 2, where the concentration profile in the interfacial region is shown for two components, 1 and 2. The Gibbs plane is fixed by assuming that $\Gamma_1 = 0$, this leads to a large positive value for Γ_2 (the lightly shaded area). Clearly the surface excess of component 2 depends on the choice we made for Γ_1.

In order to omit this problem it should be realized that the chemical potentials in equation (41) are not independent of one another. One variable, say μ_1, can be eliminated with the aid of the Gibbs-Duhem equations for the bulk phases. In doing this, one obtains:

$$\mathrm{d}\mu_1 = \left[\frac{(S^\alpha/V^\alpha) - (S^\beta/V^\beta)}{c_1^\alpha - c_1^\beta}\right] \mathrm{d}T - \sum_{i=2} \left(\frac{c_i^\alpha - c_i^\beta}{c_1^\alpha - c_1^\beta}\right) \mathrm{d}\mu_i \tag{42}$$

where c_i denotes the concentration. Substitution of this expression in the Gibbs equation gives:

$$\mathrm{d}\gamma = -s^{(1)} \mathrm{d}T - \sum_{i=2} \Gamma_i^{(1)} \mathrm{d}\mu_i \tag{43}$$

where $s^{(1)}$ is the relative surface excess entropy per unit area and $\Gamma_i^{(1)}$ the relative adsorption of component i, respectively defined as:

$$s^{(1)} = s^s - \Gamma_1 \left\{ \frac{(S^\alpha/V^\alpha) - (S^\beta/V^\beta)}{c_1^\alpha - c_1^\beta} \right\} \tag{44}$$

$$\Gamma_i^{(1)} = \Gamma_i - \Gamma_1 \left(\frac{c_i^\alpha - c_i^\beta}{c_1^\alpha - c_1^\beta} \right) \tag{45}$$

The relative surface excess quantities are independent of the choice of the Gibbs plane. This can be shown by writing equation (43) for constant T and μ_j, leading to:

$$\left(\frac{\partial \gamma}{\partial \mu_i} \right)_{T,\mu_j} = -\Gamma_i^{(1)} \tag{46}$$

Since the quantity $(\partial\gamma/\partial\mu_i)_{T,\mu_j}$ is independent of the choice of the dividing plane, it follows that also $\Gamma_i^{(1)}$ must be independent. It is common practice to fix the position of the Gibbs plane by taking $\Gamma_1 = 0$. However, when another choice of the location of the dividing plane is more convenient this may also be done.

The Gibbs adsorption equation can be applied to all types of interfaces. It provides a relation between γ, $\Gamma_i^{(1)}$ and μ_i or x_i. If we know the relation between two of these variables, the third variable can be calculated. Schematically this is shown in Figure 3. The relation between γ and $\Gamma_i^{(1)}$ is called the two dimensional or 2D equation of state. Such a 2D equation of state contains only surface excess properties. The relation between $\Gamma_i^{(1)}$ and x_i is the adsorption isotherm.

For fluid interfaces γ can be measured as a function of the composition of a solution in which the mole fraction or concentration of i is varied, whereafter $\Gamma_i^{(1)}$ can be calculated. Experimental measurement of Γ_i (exp) is often difficult because of the rather small interfacial area. For solid interfaces in contact with a gas phase or a solution phase γ is not directly measurable, but in this case the adsorption of component i can often be obtained. In most cases $\Gamma_i^{(1)}$ can be identified with

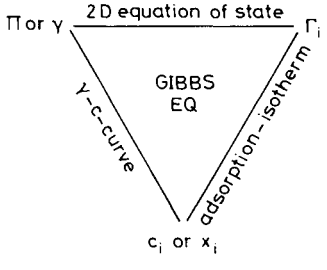

Fig. 3. Central role of the Gibbs equation (43).

Γ_i (exp), and from the adsorption isotherm the change in γ due to adsorption can be calculated according to:

$$\Pi = \gamma^{\circ} - \gamma = -(\gamma - \gamma_{\circ}) = \sum_{i=2} \int_{\Gamma_i^{(1)}=0}^{\Gamma_i^{(1)}} \Gamma_i^{(1)} \, \mathrm{d}\mu_i \tag{47}$$

where Π is called the surface pressure or spreading pressure. For the simple case of adsorption of one component from the gas phase the summation contains only one term and $\Gamma_i^{(1)}$ should be replaced by $\Gamma_1^{(S)}$ with $\Gamma_S = 0$, where S denotes the solid. For fluid interfaces the relation between γ or Π and $\Gamma_i^{(1)}$ is directly measurable with a so called Langmuir trough [9, 10], provided that the surface active material spread in the interface is insoluble in the fluid phase(s). References and reviews of the classical work on insoluble monolayers on fluid interfaces can be found in the book of Davies and Rideal [9] and the monograph of Gaines Jr. [10].

Adsorption from solution in a monolayer

Chemical potential in a perfect monolayer

For the description of physico-chemical equilibrium between a bulk phase and an adjacent interphase it is convenient to have an expression available relating the surface excess quantities of i to the chemical potential of i in the interphase. In order to obtain such an expression the easiest case to consider is that of a perfect monolayer in contact with a perfect solution [5, 11, 12]. Treating the interfacial layer as a monolayer is a common practice to simplify the situation. The monolayer is located in between the two bulk phases. The Gibbs dividing plane is placed between the surface layer and one of the bulk phases. In the monolayer a partial molar area a_i of species i can be defined as:

$$a_i = \left(\frac{\partial A}{\partial n_i^{\mathrm{s}}} \right)_{T, n_j, \gamma} \tag{48}$$

For a perfect monolayer a_i is equal to the area occupied by one mole of i, a_i°, which is independent of the surface composition. It then follows that:

$$\sum_i n_i^{\mathrm{s}} a_i^{\circ} = A \tag{49}$$

$$\sum_i \Gamma_i a_i^{\circ} = 1 \tag{50}$$

Using these definitions the surface mole fraction x_i^{s} of component i can be defined by:

$$x_i^s = \frac{\Gamma_i}{\sum_i \Gamma_i} \tag{51}$$

For a perfect monolayer all molecules are of the same size and equation (51) can be simplified to:

$$x_i^s = \frac{\Gamma_i}{\Gamma_m} \tag{52}$$

where Γ_m is the total number of moles per unit area.

The chemical potential in the monolayer can be obtained by considering the G^s function. According to equation (37) we may write:

$$\left(\frac{\partial G^s}{\partial n_i^s}\right)_{T,\gamma,n_j} = \mu_i^s \tag{53}$$

Differentiation of G^s as defined in (36) leads to:

$$\left(\frac{\partial G^s}{\partial n_i^s}\right)_{T,\gamma,n_j} = \left(\frac{\partial U^s}{\partial n_i^s}\right)_{T,\gamma,n_j} - T\left(\frac{\partial S^s}{\partial n_i^s}\right)_{T,\gamma,n_j} - \gamma\left(\frac{\partial A}{\partial n_i^s}\right)_{T,\gamma,n_j} \tag{54}$$

For a perfect monolayer $(\partial U^s/\partial n_i^s)_{T,\gamma,n_j} = U_i^{os}$ and $(\partial S^s/\partial n_i^s)_{T,\gamma,n_j} = S_i^{os} - R\ln x_i^s$, where U_i^{os} and S_i^{os} are molar quantities of pure i. Substitution of these relations in equation (54) and taking into account (53) and (48) we find:

$$\mu_i^{s,p} = U_i^{os} - TS_i^{os} + RT\ln x_i^s - \gamma^p a_i^o \tag{55}$$

where the superscript (p) indicates perfect behavior. For a monolayer of pure i, $x_i = 1$ and:

$$\mu_i^{s,p} = U_i^{os} - TS_i^{os} - \gamma_i^o a_i^o \tag{56}$$

At equilibrium this expression for μ_i^s can be equated to that for the pure bulk phase, μ_i^o, so that we have:

$$U_i^{os} - TS_i^{os} = \mu_i^o + \gamma_i^o a_i^o \tag{57}$$

Substitution of this relation in equation (55) leads to the sought expression:

$$\mu_i^{s,p} = \mu_i^o + RT\ln x_i^s - (\gamma^p - \gamma_i^o)a_i^o \tag{58}$$

Note that (58) is the surface analogue of the relation:

$$\mu_i = \mu_i^o(p_i^o) + RT\ln x_i + (p - p_i^o)V_i \tag{59}$$

for a bulk solution whose pressure p differs from that of the vapour pressure of pure i.

Chemical potential in a real monolayer

With the model of a perfect monolayer as the standard of reference for the adsorbed phase, and that of a perfect solution for the liquid phase we can now turn to real systems. For a real monolayer, at the same value of x_i^s, component i has a chemical potential μ_i^s and an interfacial tension γ. Analogous to the situation in bulk solution [see equation (15)] we define the chemical potential of i in the real monolayer as [12, 13]:

$$\mu_i^s = \mu_i^o + RT \ln f_i^s x_i^s - (\gamma - \gamma_i^o) a_i \tag{60}$$

This implies that the activity coefficient f_i^s is defined as [13]:

$$\ln f_i^s = \frac{(\mu_i^s - \mu_i^{s,p}) + a_i(\gamma - \gamma^p)}{RT} \tag{61}$$

Again a monolayer of pure i is used as standard state, so that for $x_i^s = 1$ also $f_i^s = 1$. For a discussion of the definition of f_i^s and ways to calculate f_i^s from experimental results we refer to the work of Everett et al. [12, 13]. It is also possible to derive expressions for f_i^s by assuming a model for the non-ideal monolayer. Lattice models are most popular for this purpose [4, 13–15]. We return to this in a later section.

Monolayer adsorption from a mixture

For the adsorption from a multicomponent mixture of molecules of the same size the following exchange reaction can be considered:

$$(1)^s + i \rightleftharpoons 1 + (i)^s \tag{62}$$

where 1 is the solvent and i the component we study. The superscript s denotes the surface layer. The condition for equilibrium is that $\mu_i^s = \mu_i$ or:

$$\mu_1^s + \mu_i = \mu_1 + \mu_i^s \tag{63}$$

Insertion of the expressions for the chemical potentials leads to:

$$K_{i1}^p = \left(\frac{f_1 f_i^s}{f_i f_1^s}\right)\left(\frac{x_1 x_i^s}{x_i x_1^s}\right) \tag{64}$$

where:

$$K_{i1}^p = \exp\left\{\frac{a_i^o(\gamma_1^o - \gamma_i^o)}{RT}\right\} \tag{65}$$

K_{i1}^p is the thermodynamic equilibrium constant of equation (62), it is a measure of the preference of i for the adsorbed layer with respect to component 1. As indicated, K_{i1}^p is related to the surface tensions γ_1^o and γ_i^o. For adsorption from a mixture at a

L/L or a L/G interface γ_1° and γ_i° are directly measurable. For S/L interfaces γ_i° is related to the heat of immersion of the solid in pure i [16, 17]. In principle $(\gamma_1^\circ - \gamma_i^\circ)$ can also be obtained from wetting studies [16]. In practice K_{i1}^p can simply be used as the adsorption or affinity constant.

Equation (64) can be used to define the selectivity coefficient K_{i1}^*:

$$K_{i1}^* = \frac{x_1 x_i^s}{x_i x_1^s} = K_{i1}^p \left(\frac{f_i f_1^s}{f_1 f_i^s} \right) \tag{66}$$

The selectivity coefficient is experimentally accessible. A plot of K_{i1}^* versus x_i shows the deviations from perfect behaviour.

It should be noted that for adsorption from non-dilute solutions the individual adsorption x_i^s should not be confused with the experimentally obtained adsorption, $n^\circ \Delta x_i / A$, where n° is the total number of moles of solution, and Δx_i is the change in mole fraction of i upon adsorption. The relation between $n^\circ \Delta x_i / A$ and x_i^s is:

$$\frac{n^\circ \Delta x_i}{A} = \Gamma_m (x_i^s - x_i) \tag{67}$$

For adsorption from dilute solutions, i.e. $K_{i1}^p \gg 1$ and $x_i \ll x_i^s$ the individual adsorption $\Gamma_m x_i^s$ corresponds with $n^\circ \Delta x_i / A$.

Perfect behaviour

In the case of perfect behaviour and a strong preference of component i for the adsorbed layer as compared to the other components equation (64) becomes the well known Langmuir [18] equation:

$$\Gamma_i^{(1)} = \frac{\Gamma_m x_i K_{i1}^p}{(1 + x_i K_{i1}^p)} \tag{68}$$

The corresponding equation for the surface pressure can be obtained by combining the Gibbs equation (43) with (68). The result is:

$$\Pi = RT\Gamma_m \ln(1 + x_i K_{i1}^p) \tag{69}$$

This relation is known as the Von Szyszkowski [19] equation. It relates the surface pressure to the affinity constant and the mole fraction of i in solution. An alternative formulation of equation (69) is found by realizing that, according to equation (68) $\ln(1 + x_i K_{i1}^p) = -ln(1 - x_i^s)$. Substitution in (69) gives:

$$\Pi = -RT\Gamma_m \ln(1 - x_i^s) \tag{70}$$

This is a 2D equation of state which can be used to describe the behaviour of (insoluble) perfect monolayers [9, 10]. Both the Langmuir and the Von Szyszkowski equation represent highly idealized situations, nevertheless they are often used in practice.

Regular behaviour

In the preceding sections either non-ideality in general or perfect behaviour has been assumed. In order to describe the properties of a non-ideal liquid mixture quantitatively Hildebrand [20] introduced the regular solution as one in which: (1) the components mix without volume change, and (2) the entropy of mixing is given by that corresponding to an ideal solution. The implication of these conditions are: (a) the forces of interaction between the various pairs of molecules are not too different, (b) the different molecules are about the same size, and (c) the arrangement of the molecules is completely random. Based on these assumptions several models have been developed for liquid mixtures or solutions [6]. As non-ideality often plays a crucial role in adsorption phenomena, we will apply a simple lattice model to derive expressions for the activity coefficients in the case of regular behaviour.

In a lattice theory all the molecules are situated on lattice points which are equidistant from one another. Molecular vibrations and rotations about the equilibrium position of a molecule are not affected by the mixing process. For a given temperature the lattice spacings for the pure components and for the mixture are the same, independent of composition. The potential energy of the mixture is obtained by assuming that only nearest neighbour interactions need to be considered and that the pairwise interactions are simply additive. As a consequence of the random mixing assumption the number of nearest neighbour contacts i–j between a molecule i and a molecule j is simply proportional to the product of their mole fractions $x_i x_j$

On the basis of these assumptions the change in Gibbs (or Helmholtz) energy $\Delta_m G$ on mixing a set of pure components to form n moles of mixture can be found as [4, 6]:

$$\frac{\Delta_m G}{RT} = \sum_i \left(n_i \ln x_i + 0.5 \sum_j \chi_{ij} n_i x_j \right) \tag{71}$$

where $\Delta_m G$ is defined in equation (18) and χ_{ij} is the so-called Flory-Huggins interaction parameter:

$$\chi_{ij} = \left(\frac{N_A Z}{RT} \right) \{ \varepsilon_{ij} - 0.5(\varepsilon_{ii} + \varepsilon_{jj}) \} \tag{72}$$

with Z the number of nearest neighbours to a given lattice site, N_A Avogadro's number, and ε_{ii}, ε_{jj} and ε_{ij} the pair-wise interaction potentials. The summations over i and j in equation (71) both include all components and the factor 0.5 corrects for counting the interactions double. Note that according to its definition $\chi_{ii} = \chi_{jj} = 0$. When $\chi_{ij} = 0$ for all i and j the mixture is perfect and equation (71) reduces to equation (20). Since ε_{ij}, ε_{ii} and ε_{jj} are in general of negative sign, positive values of χ_{ij} result if like contacts are preferred over unlike contacts.

Differentiation of $\Delta_m G$ with respect to dn_i at constant T, p and n_j gives $\mu_i - \mu_i^\circ$. For a two component mixture we find:

$$\mu_i = \mu_i^\circ + RT \ln x_i + RT\chi_{ij}(1 - x_i)^2 \tag{73}$$

The corresponding expression for the activity coefficient equals according to equation (17):

$$\ln f_i = \chi_{ij}(1 - x_i)^2 \tag{74}$$

The latter result is equivalent to what is known in the chemical engineering literature as the two-suffix Margules equation [6]. It can be shown [6] that, according to equation (74), in a mixture an incipient instability occurs for $\chi_{ij} = 2$ at $x_i = 0.5$. For $\chi_{ij} > 2$ mixtures are unstable, at sufficiently high mole fractions a phase separation in two stable phases occurs.

To discuss adsorption in a monolayer we also need an expression for f_i^s. To find this expression it is necessary to subdivide the phases on each side of the surface plane in parallel layers one molecular diameter thick. Usually the monolayer with the adsorbed molecules is noted as layer 1, and layer 2 is the first layer in the bulk solution. On the other side of the surface plane we find the solid phase (layer 0). In general the mole fractions for any component i in the layers adjacent to the monolayer differ from that of the monolayer itself. Hence for an appropriate calculation of the potential interactions "site fractions" should be used. The site fraction of i in a lattice layer z can be defined as a weighted average of x_i over the layers $z - 1, z$ and $z + 1$:

$$\langle x_i(z)\rangle = \lambda_1 x_i(z - 1) + \lambda_0 x_i(z) + \lambda_1 x_i(z + 1) \tag{75}$$

where λ_0 is the fraction of nearest neighbours in layer z and λ_1 that in each of the two neighbouring layers. Obviously, $\lambda_0 + 2\lambda_1 = 1$. For a monolayer adjacent to a solid we have for component i ($i \neq s$), $x_i(0) = 0$, $x_i(1) = x_i^s$ and $x_i(2) = x_i$. So that $\langle x_i(1)\rangle = \langle x_i^s\rangle = \lambda_0 x_i^s + \lambda_1 x_i$. The derivation of the activity coefficient f_i^s of component i in the monolayer is analogous to that for the bulk solution provided that the interactions are counted on the basis of site fractions. For a two component mixture the resulting expression for f_i^s is:

$$\ln f_i^s = \chi_{ij}(1 - \langle x_i^s\rangle)^2 \tag{76}$$

For the chemical potential of component i we find:

$$\mu_i^s = \mu_i^\circ + RT \ln x_i^s + RT\chi_{ij}(1 - \langle x_i^s\rangle)^2 - (\gamma - \gamma_i^\circ)a_i^\circ \tag{77}$$

For a binary system the adsorption isotherm for component 2 is obtained by combining equations (64), (74) and (76). The result is:

$$\frac{x_2^s}{1 - x_2^s} = \frac{x_2}{1 - x_2} K_{21}^p \exp\{2\chi_{21}(\langle x_2^s\rangle - x_2)\} \tag{78}$$

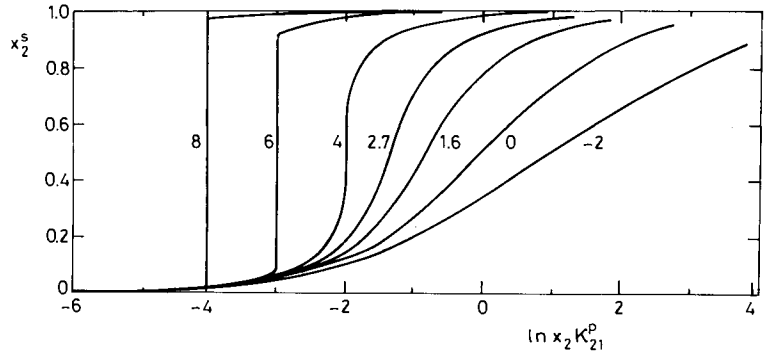

Fig. 4. Theoretical adsorption isotherms according to the FFG equation (80) or (114) for a series of χ_{21} (or $\tilde{\chi}$) values as indicated with the curves. For $\chi_{21} = 0$ the Langmuir isotherm results. In practice values of $\chi_{21} > 2$ will only occur for solute molecules larger than the solvent molecules. In that case equation (114) applies.

Some illustrations of equation (78) can be found in [13].

The expression for the selectivity coefficient K_{21}^* in the case of regular behaviour is obtained through equations (66) and (78):

$$\ln K_{21}^* = \ln K_{21}^p + 2\chi_{12}(\langle x_2^s \rangle - x_2) \tag{79}$$

For adsorption from dilute solutions (i.e. $K_{21}^p \gg 1$ and $x_2 \ll x_2^s$) and a hexagonal lattice ($\lambda_0 = 0.5$), equation (78) reduces to the Frumkin-Fowler-Guggenheim (FFG) [21, 22] equation:

$$\frac{x_2^s}{1 - x_2^s} = x_2 K_{21}^p \exp(\chi_{21} x_2^s) \tag{80}$$

For positive values of χ_{21} like contacts are preferred over unlike contacts and the adsorption will be cooperative. In Figure 4 the adsorption according to the FFG equation is shown for a series of χ_{21} values. Remember that in solution incipient instability occurs for $\chi_{21} = 2$ and two stable liquid phases are formed for $\chi_{21} > 2$. Evidently equation (80) can only be used up to the mole fraction for which the phase separation occurs. In the monolayer incipient instability occurs for $\chi_{21} = 4$ and a phase separation or "2D condensation" for $\chi_{21} > 4$ [23, 24]. Figure 4 illustrates this. The association of the molecules in the monolayer increases with increasing χ_{21} and the condensation step becomes larger. It should be noted that values of χ_{21} considerably higher than about 2 will only occur for solute molecules much larger than the solvent molecules.

Equation (80) applies for solutions so dilute that $d\mu_i = RT d \ln x_i$. Combination of the Gibbs equation (43) with (80) and subsequent integration leads to:

$$\Pi = -RT\Gamma_m \left\{ \ln(1 - x_2^s) - 0.5\chi_{21}(x_2^s)^2 \right\} \tag{81}$$

This is the 2D equation of state corresponding with the FFG equation. It can be used to describe (insoluble) non-ideal monolayers. Equations (80) and (81) are considerably more realistic than respectively the Langmuir (69) and the Von Szyszkowski equation (70).

For a discussion of the regular behaviour theory, its application to experimental results and possible improvements we refer to Prausnitz et al. [6]. For ternary or higher order component systems expressions for the isotherm or the selectivity coefficient can be obtained in a similar way [25].

Ion adsorption

The electrical double layer

In aqueous solutions adsorbents are often charged because there are almost always ionic species present with a strong preference for the surface. Alternatively, adsorbents may become charged by dissociation of surface groups, i.e. by preferential desorption of an ionic species. We will call these ions "surface charge determining". The adsorption of surface charge determining ions is followed by a positive adsorption of counter-ions and negative adsorption or exclusion of co-ions in the immediate vicinity of the surface in order to satisfy the requirements of electroneutrality. The charged interface plus the solution region in which the surface charge is counterbalanced is called "the electric double layer". The charges in solution are mobile, contrary to those on the surface which are generally assumed to be localized. Due to the opposing actions of energy (Coulombic) and entropy the counter-ions and co-ions are distributed in a "diffuse layer". The situation is very similar to that in electrolyte solutions as described in the Debye-Hückel theory [26]. The main difference is that near a surface the potentials can be much higher than around simple ions. Some double layer models to describe the situation are treated below.

Diffuse double layer

The distributions of ions of type i in the field of the surface can be described by a Boltzmann distribution for all ion types. If it is assumed that the ions are point charges which only interact through Coulombic forces this distribution can be expressed as:

$$n_i(z) = n_i(\infty) \exp\left\{\frac{-\tau_i F \psi(z)}{RT}\right\} \tag{82}$$

where $n_i(z)$ is the number of ions i per unit volume at distance z from the surface, τ_i the charge number of the ions, including their sign, F Faraday's constant, and $\psi(z)$ the potential in the double layer. The reference point for the potentials is the

bulk solution where $\psi(\infty) = 0$ and the concentration of each type of ion is its bulk concentration. For the subtleties of potentials we refer to [27]. Equation (82) is in agreement with the statement that counter-ions are attracted and co-ions are repelled.

The space charge density $\rho(z)$ is obtained by:

$$\rho(z) = \sum_i n_i(z)\tau_i e \tag{83}$$

where e is the elementary charge. The additional relation between $\psi(z)$ and $\rho(z)$ is given by the Poisson equation:

$$\nabla^2\psi(z) = \frac{-\rho(z)}{\varepsilon_o\varepsilon_r(z)} \tag{84}$$

where ε_o is the permittivity of vacuum and $\varepsilon_r(z)$ the relative dielectric constant at distance z from the surface. The classical solution of these equations has been given by Gouy [28] and Chapman [29] and can be found in many textbooks, see e.g. [30, 31]. Starting points of the theory are that the surface charge density σ_s, and the surface potential $\psi_s = \psi(z = 0)$ are average, smeared out, quantities, that the surface is planar and that ε_r is independent of the field strength. According to the Gouy-Chapman (GC) theory for a symmetrical indifferent electrolyte, the charge density of the diffuse layer, σ_d, is:

$$-\sigma_d = (8RT\varepsilon_o\varepsilon_r n_s)^{0.5} \sinh\left(\frac{\tau F\psi_s}{2RT}\right) \tag{85}$$

where $\tau = \tau_+ = -\tau_-$ and $n_s = n_+(\infty) = n_-(\infty)$. It should be realized that because of electroneutrality of the double layer as a whole $\sigma_d = -\sigma_s$.

The GC theory also allows us to calculate the ionic components of charge of a diffuse layer, i.e. the surface excess amounts of the cations and anions to compensate the surface charge [32, 33]:

$$\Gamma_{+,d} = \left(\frac{2RT\varepsilon_o\varepsilon_r n_s}{\tau^2F^2}\right)^{0.5}\left[\exp\left(\frac{-\tau F\psi_s}{2RT}\right) - 1\right] \tag{86}$$

and:

$$\Gamma_{-,d} = -\left(\frac{2RT\varepsilon_o\varepsilon_r n_s}{\tau^2F^2}\right)^{0.5}\left[\exp\left(\frac{\tau F\psi_s}{2RT}\right) - 1\right] \tag{87}$$

Differentiation of σ_s with respect to ψ_s provides the relation for the differential capacitance of the diffuse layer:

$$C_d = \varepsilon_o\varepsilon_r\kappa \cosh\left(\frac{\tau F\psi_s}{2RT}\right) \tag{88}$$

where κ is defined by:

$$\kappa^2 = \left(\frac{F^2}{\varepsilon_o \varepsilon_r RT}\right) \sum_i n_i \tau_i^2 \tag{89}$$

κ has the dimension of a reciprocal length and κ^{-1} is called the "Debye length" or the "double layer thickness". For aqueous solutions of symmetrical electrolytes at room temperature equation (89) gives:

$$\kappa = (10c\tau^2)^{0.5} \qquad (\mathrm{nm}^{-1};\ c \text{ in mole } \mathrm{dm}^{-3}) \tag{90}$$

For the potential–distance relation the GC theory results in:

$$\tanh\left(\frac{\tau F \psi(z)}{4RT}\right) = \tanh\left(\frac{\tau F \psi_s}{4RT}\right) \exp(-\kappa z) \tag{91}$$

For small potentials (Debye-Hückel or DH model), that is for $(\tau F \psi_s / 4RT) \ll 1$, the approximation $\tanh x = x$ can be used and (91) reduces to:

$$\psi(z) = \psi_s \exp(-\kappa z) \tag{92}$$

This equation shows that at $z = \kappa^{-1}$, $\psi(z) = \psi_s / e$, illustrating why κ^{-1} is called the double layer thickness. Note that for small ψ_s equation (85) reduces to:

$$\sigma_s = \varepsilon_o \varepsilon_r \kappa \psi_s \tag{93}$$

This again shows the physical meaning of κ^{-1}, i.e. as the plate distance of a condenser. An interesting implication of equation (85) or (93) is that, if we assume ψ_s to be constant, then σ_s becomes a function of the ionic strength. Conversely, if σ_s is assumed to be constant, ψ_s is a function of κ. For a constant surface charge the effect of the electrolyte concentration on $\psi(z)$ is shown in Figure 5a. Figure 5b shows the constant surface potential case (realize that $\sigma_s = \varepsilon_o \varepsilon_r (\mathrm{d}\psi/\mathrm{d}z)_{z=0}$).

Stern-Gouy-Chapman double layer

The limitations of the GC theory are primarily due to the inexactness of the initial assumptions [31, 33]. The point charge assumption for the ions in solution is most likely to be unsatisfactory for the ions in the first molecular layer near the surface, where the distance of closest approach is limited by the size of the ions. Taking into account a charge free layer between the surface and the diffuse layer with a thickness of the order of an ion radius largely eliminates this problem. This improvement was first introduced by Stern [34]. The concept of this charge free layer is frequently used and the layer is generally called the Stern layer. The boundary of the Stern layer and the diffuse layer is called the Stern plane.

Stern also pointed out that counter-ions may not only interact with the surface by electrical forces, but also by "chemical" or "specific" (i.e. non Coulombic forces). "Specific" adsorption will lead to a better screening of the surface charge than

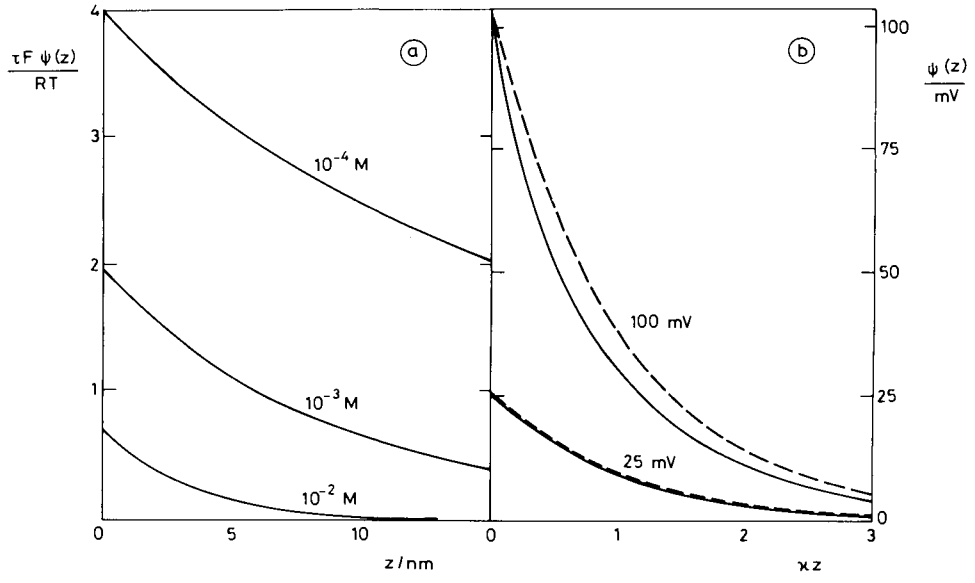

Fig. 5. Potential decay in the diffuse layer as a function of the distance from the surface, see equation (91). a. At constant surface charge (σ_s = 4.3 mC m^{-2}), for three values of the salt concentration (1–1 electrolyte). The value of the surface potential at each salt concentration is calculated with equation (85). b. At constant surface potential, for two values of ψ_s. The dashed curves represent equation (92). For ψ_s = 25 mV the results obtained with both equations cannot be discriminated. Note that κx depends on the ionic strength.

through diffuse ions only and hence to higher surface charges. In the most simple model the Stern plane is also the adsorption plane for the specifically adsorbing ions.

In the case of specific adsorption of counter-ions the surface charge is compensated by the sum of charges at the Stern plane, σ_1, and in the diffuse layer, σ_d,:

$$\sigma_s = -(\sigma_1 + \sigma_d) \tag{94}$$

The presence of the Stern layer has considerable consequences for the potential distribution. Across the Stern layer the potential drops linearly from ψ_s to ψ_d, the potential of the Stern plane. Often ψ_d is considerably lower then ψ_s, especially in the case of specific adsorption. Away from the Stern plane the diffuse layer extends, this implies that in the Stern-Gouy-Chapman (SGC) model ψ_s has to be replaced by ψ_d and σ_s by $-\sigma_d$ in equations (85)–(93). A sketch of the potential distribution according to the SGC model is shown in Figure 6.

With the SGC model we may write for the surface potential:

$$\psi_s = (\psi_s - \psi_d) + \psi_d \tag{95}$$

Dividing by σ_s at constant κ gives:

$$\frac{\psi_s}{\sigma_s} = \frac{\psi_s - \psi_d}{\sigma_s} + \left(\frac{\psi_d}{-\sigma_d}\right)\left(\frac{-\sigma_d}{\sigma_s}\right) \tag{96}$$

or:

$$\frac{1}{K_t} = \frac{1}{C_1} + \frac{1}{K_d}(1 - R) \tag{97}$$

where $K_t = \sigma_s/\psi_s$ and $K_d = -\sigma_d/\psi_d$ are the integral capacitances of the total double layer and the diffuse layer, respectively, C_1 is the Stern layer capacitance, and $R = \sigma_1/\sigma_s$ is a measure of the specific adsorption. For non-metallic surfaces it is mostly assumed that C_1 is a constant independent of σ_s and κ. In that case we may write:

$$C_1 = \frac{\varepsilon_o \varepsilon_1}{d_1} \tag{98}$$

where ε_1 is the relative dielectric constant of the Stern layer and d_1 its thickness. The value of ε_1 is affected by the nature of the surface. As a rule of the thumb we may say that for hydrophilic surfaces ε_1 is of the same order of magnitude as ε_r, whereas for hydrophobic surfaces ε_1 is considerably smaller than ε_r in the solution [35]. K_d follows from the GC theory. From equation (97) it can be inferred that K_t is dominated by the smallest of the two capacitances. At low electrolyte concentrations, where both K_d and R are small, K_t is dominated by the last contribution. For high electrolyte concentration C_1 is likely to dominate K_t.

Stern's approach has been refined by locating the specifically adsorbed ions in a plane inside the Stern layer. This extension is known as the "Helmholtz-Grahame" or "triple layer" (TL) model [32, 36]. In the TL model the so called inner Helmholtz plane is the location for (dehydrated) specifically adsorbed ions,

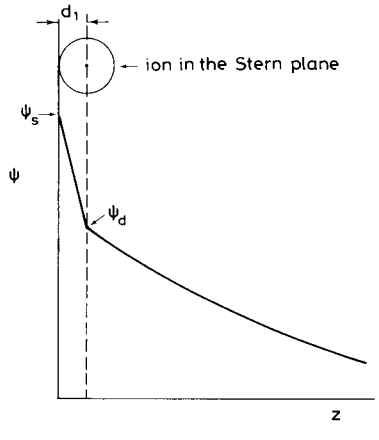

Fig. 6. Schematic representation of the potential distribution according to the Stern-Gouy-Chapman model.

the outer Helmholtz plane coincides with the Stern plane. For perfectly flat interfaces, such as the mercury/solution interface this detailed treatment has been quite successful [33, 37, 38]. For ordinary solid surfaces with a certain surface roughness or with surface groups protruding in the solution, such a refinement can hardly be justified and the SGC model in its simple form is recommended.

Adsorption of surface charge determining ions

Modelling the charging of solid surfaces has received much attention in literature. An integrated approach based on earlier work has been reviewed and reformulated by Healy and White [39] and by James and Parks [40]. In these models, generally known as site binding models, the surface charge is attributed to the ionization of discrete surface groups or conversely to desorption of charge determining ions from discrete surface sites. In addition to the charging of the surface specific adsorption may occur. This specific adsorption is also called surface complexation: complexes are formed between the charged surface sites and the major electrolyte ions.

For the description of the adsorption of the charge determining ions the monolayer model as derived above can be used. The activity coefficient, $\gamma_{\pm}$, for the ions in the bulk solution can be found from the Debye-Hückel theory or one of its extensions such as the Davies equation [41]. At constant background electrolyte concentration these activity coefficients can be taken as constants.

Furthermore it should be realized that the probability of finding an ion in the vicinity of the surface is affected by the electrical field of the particles. This effect can be accounted for by a Boltzmann factor, $\exp\{-\tau_i F\psi(z)/RT\}$:

$$x_i(z) = x_i(\infty)\exp\left\{\frac{-\tau_i F\psi(z)}{RT}\right\} \tag{99}$$

where $x_i(z)$ is the mole fraction of i at a distance z from the surface. Equation (99) implies that interactions other than Coulombic are neglected and that the potential is equipotential in planes parallel to the surface, i.e. $\psi(z)$ is a "smeared out" potential. For $z = 0$ the potential is equal to ψ_s. Substitution of $x_i(0)$ for x_i in equation (68) leads to a simple expression for the isotherm of the charge determining ions.

The description of specific adsorption of the background electrolyte ions is in principle similar to that of the protons. For specific adsorption at the Stern plane ψ_d is the leading potential instead of ψ_s.

Monofunctional surface groups

For non-amphoteric surfaces containing groups which can associate with a proton according to:

$$S^- + H^+ \rightleftharpoons SH \tag{100}$$

the proton adsorption isotherm equation based on equations (100), (68) and (99) reads:

$$\frac{\theta_H}{1-\theta_H} = K_H a_H \exp\left(\frac{-F\psi_s}{RT}\right) \tag{101}$$

where θ_H is the fraction of SH groups, K_H the equilibrium constant, $a_H = x_H\gamma_\pm$ is the proton activity, and ψ_s is the potential at the surface plane. Equation (101) can also be obtained by application of the mass action law to equation (100) and using $x_H(0)$ as the relevant mole fraction of protons. The surface charge density equals:

$$\sigma_s = -F[S^-] = -FN_s(1-\theta_H) \tag{102}$$

where N_s is the total site density (=$[S^-]$ + [SH]) and $(1-\theta_H)$ the degree of dissociation. Note that also the surface charge is considered as smeared out, discrete charge effects are neglected. Equation (101) describes in principle the proton adsorption, however, ψ_s is in general not known and difficult to obtain experimentally. Sometimes the electrokinetic or ζ-potential [42] is substituted for ψ_s but this is a rather poor approximation. Alternatively a double layer model, such as the SGC model, can be used to provide a relation between σ_s and ψ_s. In general we may write:

$$\psi_s = \frac{\sigma_s}{K_t} = \frac{-FN_s(1-\theta_H)}{K_t} \tag{103}$$

where K_t is the (integral) electrostatic capacitance of the double layer given by the double layer model. In general K_t will be a function of σ_s or θ_H. Substitution of the expression for ψ_s in equation (101) provides an alternative form of the isotherm equation:

$$\frac{\theta_H}{1-\theta_H} = K_H a_H \exp\left\{\frac{F^2 N_s(1-\theta_H)}{K_t RT}\right\} \tag{104}$$

From equation (104) it follows that both N_s and K_t are important variables for the description of the adsorption. Some examples of the dissociation behavior of a surface group according to equation (104) in combination with the SGC model, for which K_t is given by equation (97), are shown in Figure 7. Figure 7a shows the effect of N_s, Figure 7b that of the salt concentration c_s and Figure 7c that of the Stern layer capacitance C_1, on the dissociation behaviour.

Equation (104) can be used to describe the behaviour of charged latex particles. James et al. [43] have used equation (104) in combination with the TL model for the description of conductometric and potentiometric titrations of carboxylate latices.

Amphoteric surfaces

For the adsorption of surface charge determining ions on the much more important amphoteric surfaces a similar reasoning can be used. However, in this case

normally at least two types of surface groups should be considered, namely positive and negative groups. Healy and White [39] have discussed several possibilities. In order to find an expression for ψ_s an extra assumption with respect to the topology of the surface groups is required. For a regular mixture or a random arrangement of the different groups the surface potential can be interpreted as the smeared-out

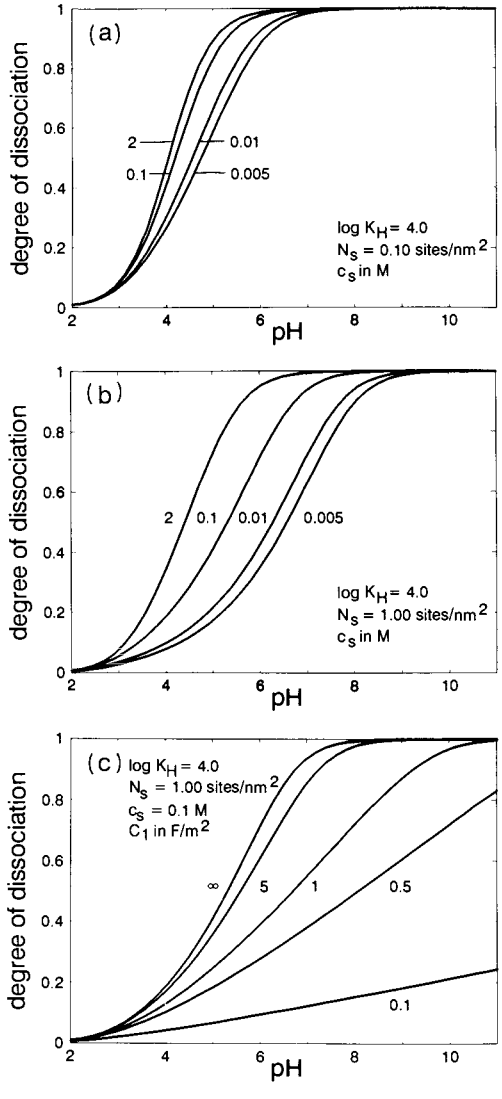

Fig. 7. Surface charge density as a function of pH for a surface with one type of acid surface groups and a SGC double layer. The effect of the site density N_s and the saltconcentration c_s (a and b) and the effect of the Sternlayer capacitance C_1 (c) on the dissociation behaviour.

potential of the entire surface, whereas for a patchwise arrangement of the surface groups ψ_s is the local or patch potential [35]. In most papers ψ_s is taken as a potential for the entire surface.

When the two groups are chemically independent, for each of the two groups an equation similar to (104) can be derived. Harding and Healy [44, 45] have used this type of modelling to analyse the double layer properties of amphoteric latex colloids.

Oxide surfaces

Another type of amphoteric surface is encountered with the mineral oxides. The oxide surfaces have been studied extensively. In most models for oxides the proton association is described by two interdependent reactions:

$$SO^- + H^+ \rightleftharpoons SOH \tag{105}$$

$$SOH + H^+ \rightleftharpoons SOH_2^+ \tag{106}$$

each characterized by its own pK_H value and equilibrium relation. The thus obtained "two-pK" model is a simplification of reality (see Figure 9), but combination of the equilibrium relations based on equations (105) and (106) with double layer models have led to successful descriptions of the proton adsorption/desorption isotherm for many oxides. A review of these models has been presented by Westall and Hohl [46].

Schindler and Stumm and coworkers [47–52] prefer a constant capacitance (CC) model to describe the double layer properties. In this model the double layer is treated as a plate condensor with a constant capacitance. This is a reasonable approximation at high ionic strength and strong specific adsorption of the background electrolyte. Under these conditions K_d is large and R is large so that the Stern layer capacitance dominates the total capacitance [see equation (97)]. At low ionic strength and absence of specific adsorption a constant capacitance is however a rather poor approximation.

Huang et al. [52, 53] and Dzombak et al. [54, 55] have made tabulations of results obtained with the GC model. The different oxides are characterized via N_s and ΔpK, where ΔpK is the difference between the pK_H values corresponding with equations (105) and (106). A disadvantage of this type of modelling is that the solution side of the double layer is fully independent of the type of oxide.

Schindler, Stumm and Huang apply mostly a graphical method to determine the intrinsic affinity constants. It should be noted that in this case the implicit assumption is made that the ΔpK value is large [56]. This is by no means evident [56–58].

Combination of the two-pK model with the TL model is also popular [40, 56, 59–64]. In Figure 8 comparison is made between experimental and calculated results

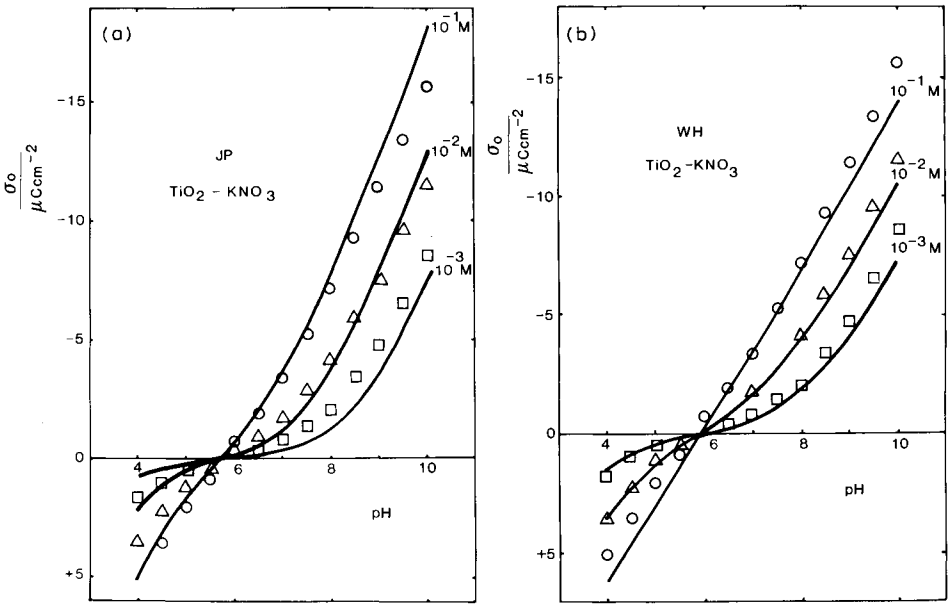

Fig. 8. Surface charge of TiO_2 as a function of pH and KNO_3 concentration. Comparison between experimental results [61] and predictions made with the two-pK TL model and allowing for specific adsorption of electrolyte ions. (From [56].) a. Results obtained by James and Parks [40]. Parameter values: pK = −2.7; pK(SO^-) = 9.1; pK(KOH) = −7.2; pK(HNO_3) = 4.2; C_1 = 1.10 F m^{-2}; N_s = 12.2 sites nm^{-2}; outer Helmholtz layer capacitance, C_2 = 0.20 F m^{-2}. b. Results obtained by Westall and Hohl [46]. Parameter values: pK = −5.15; pK(SO^-) = 6.61; pK(KOH) = −5.15; pK(HNO_3) = 6.61; C_1 = 0.70 F m^{-2}; N_s = 12.2 sites nm^{-2}; C_2 = 0.20 F m^{-2}.

as obtained for rutile. The experimental data are obtained by Yates [60, 61]. The theoretical descriptions as shown have been given by James and Parks [40] and by Westall and Hohl [46]. Unfortunately the parameters used for the calculations are rather different (see Figure 8), but in both cases the fit is reasonably good.

It is impossible to obtain a unique set of parameter values for the rather complex "two-pK TL model", also when information is available on the ζ–(pH) relation [56]. This obscures the physical interpretation of the parameters. Consequently, the TL model should be used with hesitation, unless most of the parameters have been obtained in an independent way.

It should be remarked that in many studies with the TL model an a priori value of 200 mF m^{-2} is assumed for the outer Helmholtz capacity. This value is derived from studies of the hydrophobic Hg- and AgI-solution interfaces [61, 63, 65]. Using the same value for hydrophilic surfaces, such as oxides, is by no means evident. The nature of the surface affects the water structure adjacent to the surface and thereby the electrostatic capacitance(s) of the Stern layer. In modelling the AgI–electrolyte interface a low Stern layer capacitance is required in order to predict the

relatively low values of the surface charge [66]. Oxides however build up a much higher surface charge and a high Stern layer capacitance is required [67]. A low value of the outer Helmholtz layer capacitance prevents effective screening of the charge. In order to overcome this problem and to predict the experimental results with a thus used TL model, a strong specific adsorption at the inner Helmholtz plane and a high inner Helmholtz layer capacitance are required. The latter is in contradiction with the low outer Helmholtz capacity, and the specific adsorption is easily overestimated.

In view of the difficulties encountered with the TL model, Van Riemsdijk et al. [67, 68] prefer to use the SGC model for the calculation of K_1. Neglecting specific adsorption, the two-pK SGC model can describe the σ_s(pH) curves for oxides with three adjustable parameters (N_s, ΔpK, C_1). For the total site density, N_s, a reasonable estimate can be found from crystallographic data [61, 69]. For rutile and hematite an equally good fit between experimental and predicted results is obtained as with the considerably more complicated two-pK TL model.

An alternative and more simple description of the oxide surfaces has been suggested by Van Riemsdijk et al. [67, 68, 70–72]. In this model the charging of the amphoteric surface is described as (see Figure 9):

$$SOH^{1/2-} + H^+ \rightleftharpoons SOH_2^{1/2+} \tag{107}$$

i.e. only one adsorption step is considered. The model is therefore called a "one-pK" model.

The adsorption isotherm equation corresponding to equation (107) is:

$$\frac{\theta_H}{1-\theta_H} = K_H a_H \exp\left\{\frac{-0.5F^2 N_s(1-\theta_H)}{K_1 RT}\right\} \tag{108}$$

where θ_H is the fraction of $SOH_2^{1/2+}$ groups, K_H the equilibrium constant, and use is made of the fact that:

$$\sigma_s = N_s F(\theta_H - 0.5) \tag{109}$$

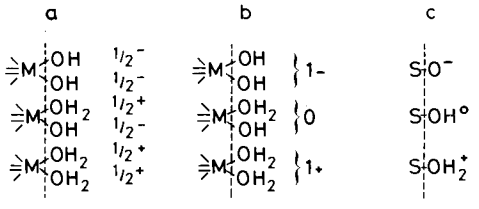

Fig. 9. Schematic representation of the surface configuration at the pristine point of zero charge for the one-pK model (a) showing only two kinds of surface groups, and an analogous picture for the two-pK model (b and c) showing three different kinds of surface groups (from [68]).

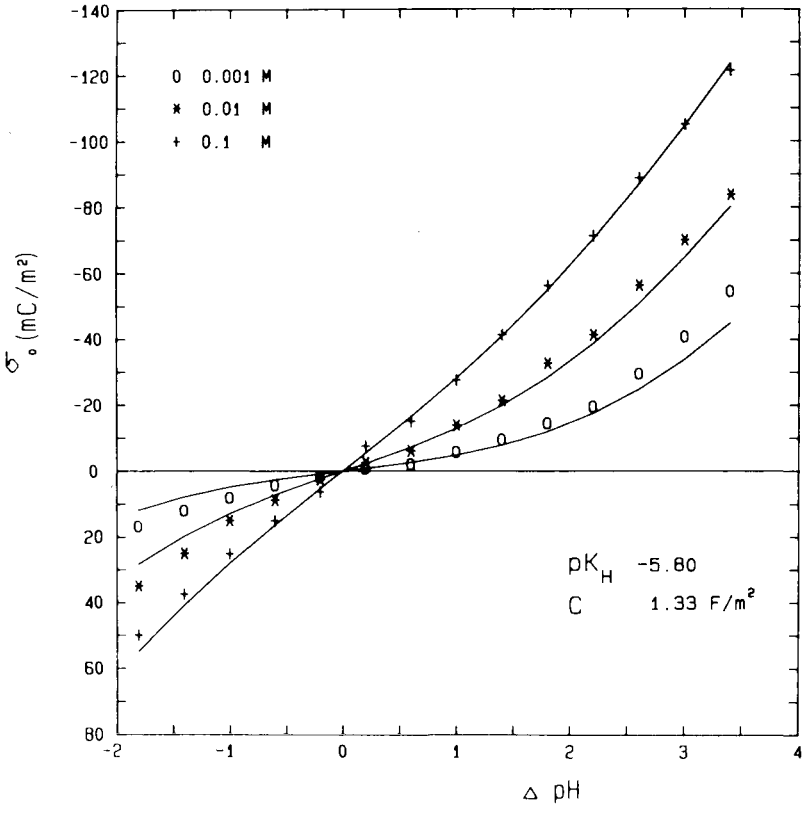

Fig. 10. Surface charge of TiO_2 as a function of ΔpH [=pH − pH(pzc)] and KNO_3 concentration. Comparison between experimental results [61] and predictions made with the one-pK SGC model in the absence of specific adsorption. (From [67].)

Note that N_s is different by a factor 2 from N_s used in the two-pK models (see Figure 9). In order to obtain K_t the same double layer models can be used as before [67, 68]. In most studies the SGC model has been used. Figure 10 shows a comparison of the results obtained for rutile. The curves are the predictions by the one-pK SGC model, the points show the experimental results. Figure 10 can be compared with Figure 8. When the total site density is known, only one adjustable parameter (C_1) is required to obtain this result. Nevertheless the fit is as good as that obtained with the two-pK TL model. A slightly better fit can be obtained by incorporating specific adsorption [67].

Gibb and Koopal [73] have used the one-pK SGC model for the description of rutile, hematite and mixtures of these two oxides. For a precise fit of the results specific adsorption of the background electrolyte ions is required. The mixtures could be described by weighted summation of the σ_s (pH) curves of the individual

oxides. Hiemstra et al. [72] have applied the one-pK SGC model to aluminium oxides.

In general the description of the charging behaviour of oxides with either a two- or a one-pK model is a simplification. Recently, Hiemstra et al. [57, 58] have presented a fundamentally better description of the charging by considering the fact that ordinary oxide surfaces contain various types of surface groups. Based on the behaviour of the metal hydroxides in solution a method is proposed to estimate the intrinsic affinity constants for the various hydroxy and oxy groups on oxide surfaces. The reaction of a proton with a particular surface group and the effective charge of the group depend on the number, n, of metal cations coordinated with the surface oxygen and on the "formal bond valence" [74] of the Me_n–O(H) bond. According to this treatment the simple one-pK model as given by equation (107) provides an accurate approximation for the proton adsorption on gibbsite. For the adsorption on rutile, goethite, hematite and amorphous iron oxide the simple one-pK model is a reasonable approximation and considerably more satisfactory than the two-pK model. For silica the two-pK model is appropriate although the reaction leading to a positive surface hardly occurs in practice. A difficulty with regard to practical application of the treatment by Hiemstra is that the fractions of each type of surface group present should be known, but this does not invalidate the insight gained in the principles of the charging mechanism of oxides.

Finally it should be remarked that the site binding models predict that the surface potentials of oxides behave in general non-Nernstian [59, 56, 73]. Pseudo Nernstian behaviour has been observed for hematite [75] and ruthenium oxide [76], whereas for γ-Al_2O_3 non-Nernstian behaviour has been reported [77]. Fokkink et al. [78, 79] argue that the similarity of the surface charge–pH curves for a series of crystalline oxides (TiO_2, RuO_2, α-Fe_2O_3 and Al_2O_3) strongly suggests (pseudo) Nernstian behaviour for these oxides. Pseudo Nernstian behaviour of $\psi_{s(pH)}$ is in agreement with predictions of the one-pK SGC model for high values N_s and pH values around the point of zero charge (pzc) [73]. The two-pK TL model with large ΔpK values, as worked out by Davis et al. [63] and James and Parks [40] for various oxides, predicts non-Nernstian behaviour. This is an extra argument in favor of the one-pK SGC models.

Specific adsorption of (polyvalent) ions

In many systems related to mineral flotation polyvalent ions such as phosphate, sulfate and metal ions adsorb specifically. The description of the adsorption of polyvalent ions on a charged surface is considerably more complex than that of protons or simple monovalent ions.

The first complication rises because of the speciation in bulk solution. Some polyvalent ions react with a proton, others hydrolyse at high pH values. Secondly, when the polyvalent ions react with the same surface sites as the charge determining

ions, competition occurs and the stoichiometry of the binding reaction is important. A divalent ion may react with one or two monovalent surface groups. Alternatively, it can be assumed that the surface sites for the polyvalent ions are completely independent of the sites for the charge determining ions. In that case there is no competition, but the electrostatic interactions are still present. Finally, surface heterogeneity may complicate the situation [35, 68]. All these aspects make a unique description of polyvalent ion adsorption difficult if not impossible.

Independent of competition or stoichiometry of the reaction, adsorption of polyvalent ions will affect the electric field around a particle. This in turn affects the adsorption of the primary charge determining ions. For instance, metal ion adsorption will in general enhance the desorption of protons (or uptake of hydroxyl ions). Consequently a proton/metal ion "exchange ratio" will result which is only partly due to the stoichiometry of the reaction.

Most studies of metal ion adsorption rely on a specific stoichiometric reaction or combinations of stoichiometric reactions with surface hydroxyls (surface complexation). Schindler [48, 80, 81] and Stumm et al. [49–51] treat the electric double layer as a plate condensor with a constant capacitance. For this type of modelling a capacitance value and a metal ion affinity constant are required at each value of the ionic strength. Huang et al. [82] and Dzombak [54, 55] tabulate ion affinity constants on the basis of the two-pK GC model. Leckie and coworkers [83–87] model cation and anion adsorption with the two-pK TL model. They make a distinction between strongly and weakly adsorbing ions.

Van Riemsdijk et al. [68] were the first to show that electrostatic effects could explain non-stoichiometric exchange ratios. In their treatment of metal ion adsorption on oxides a one-to-one reaction of the metal ion species with the proton sites was assumed. Predictions with the one-pK SCG model and the two-pK SGC model were both in a good agreement with experimentally observed proton/metal ratio's (1.6 to 1.9) and metal ion adsorption isotherms at a series of pH values for rutile, hematite and amorphous iron oxide. With this type of modelling metal ion binding at various pH values and electrolyte levels can be described by using only one additional constant representing the (intrinsic) metal-surface interaction. In contrast with Benjamin and Leckie [88], Van Riemsdijk et al. [68] conclude that incorporation of surface heterogeneity is not required for a description of the cadmium adsorption on amorphous iron oxide.

Bowden et al. [89] and Fokkink et al. [79, 90] in their treatment of metal ion adsorption on oxides use a set of metal ion adsorption sites which is completely independent of the adsorption sites for the protons. In these treatments the precise nature of the metal-surface complex does not have to be specified. Fokkink et al. [79] show that the SGC model in combination with the Nernst equation, relating ψ_s to the pH (approximately correct around the pzc), can describe the proton/metal ion exchange ratios for a whole series of oxides on a purely electrostatic basis. Nevertheless, the use of an independent set of metal adsorption sites seems not

entirely realistic as inorganic species will most probably form some sort of complex with the underlying surface groups [91, 92].

A relatively simple way to obtain information on a system, omitting the use of double layer models, is the combination of electrokinetic measurements with adsorption isotherms and complexation or solubility diagrams. The electrokinetic measurements can provide an impression of the electrostatic potential of the particles in the presence of the polyvalent ions at various pH values, or of the ζ-potential as a function of the concentration of polyvalent ions at constant pH, see for instance [93–95]. For the interpretation of the results still an assumption has to be made about the stoichiometry of the adsorption reaction(s). An extra problem might be the conversion of mobilities into ζ-potentials [42].

In general the adsorption of polyvalent ions is found to be strongly pH dependent. A rapid increase in uptake of the polyvalent ions usually occurs over a narrow pH range [51, 93, 96, 97]. The affinity of a surface for different metal ions is often studied by comparing the metal ion uptake as a function of pH at a given initial metal ion concentration.

A series of reviews on ion adsorption can be found in "Adsorption of inorganics at solid/liquid interfaces". Schindler [79], James [64] and Morel et al. [98] consider general aspects of surface complexation. Hingston [99] reviews anion adsorption, Kinniburgh and Jackson [100] cation adsorption. Huang [53] concentrates on experimental aspects and the two-pK GC model. Adsorption versus precipitation is described by Corey [101]. The latter subject has been worked out in more detail by Farley et al. [102]. Some aspects of metal ion complexation in relation to metal ion solubility have been discussed by McBride [92]. The emphasis in the latter review is on spectroscopic evidence for metal ion complexation. A general review of the adsorption of ions in soil systems can be found in Sposito's book [97].

Adsorption of organic molecules

The description of the adsorption of small inorganic ions as given in the previous section is based on an extension of the Langmuir equation with electrostatic interactions. For organic molecules, with (strong) non Coulombic interactions and often a size difference with the solvent molecules, a simple Langmuir type isotherm is no longer appropriate. Specific lateral interactions and size differences should be considered explicitly. A distinction has to be made between small, fairly rigid molecules and flexible chains. The difference between the two groups lies in the fact that adsorbed rigid organic molecules are only restricted in their orientation, whereas flexible molecules adapt their entire conformation upon adsorption. Consequently, the expression for the standard Gibbs energy of adsorption of the flexible molecules is much more complicated than that of rigid molecules. We will therefore treat the adsorption of these two types of molecules separately.

Rigid organic molecules

The regular behaviour model for adsorption of equal sized molecules can easily be extended to organic molecules adsorbing in a given orientation. The size of the organic molecules is measured relative to that of the solvent molecules by a parameter r. In the ideal situation r is the ratio of molar volumes of solute and solvent. The "monolayer" assumption now applies to the organic molecules. In the monolayer a uniform density of the components is assumed. Based on such assumptions several authors have extended the regular behaviour model (see e.g. [6]). The main modification is related to the entropy of mixing. The change in entropy on mixing the pure components to form n moles of mixture is no longer given by equation (21), but as [103, 104]:

$$\Delta_m S = -R \sum_i n_i \ln \phi_i^b \tag{111}$$

where ϕ_i^b is the volume fraction of i in bulk solution:

$$\phi_i^b = \frac{n_i r_i}{\sum_i n_i r_i} \tag{112}$$

Equation (111) is derived for chain molecules where r_i is the number of segments in the chain. On the basis of equation (111) the change in Gibbs energy $\Delta_m G$ on mixing can be approximated by equation (71), after substitution of ϕ_i^b for x_i and ϕ_j^b for x_j. Starting from Δ_mG expressions for the chemical potentials can be derived and from these and the adsorption equilibrium equation, the isotherm can be obtained. The general result for adsorption of a solute from a dilute solution ($\phi_2^b \ll \phi_1^b$) is:

$$\frac{\phi_2^s}{(1-\phi_2^s)^r} = \phi_2^b K_m \exp(r\overline{\chi}_{21}\phi_2^s) \tag{113}$$

where ϕ_2^s is the volume fraction of the organic component in the adsorbed layer, ϕ_2^b that in bulk solution, K_m the effective affinity constant, $\overline{\chi}_{21}$ the effective Flory-Huggins parameter, and $r_2 = r$. The magnitude of K_m depends on the orientation of the adsorbed molecules and the number of solvent molecules, m, replaced from the surface upon adsorption. The entropy loss due to the restricted orientation of the molecules in the adsorbed layer is small and also included in K_m. Equation (113) is very similar to equation (80) for regular behaviour, apart from the volume fractions; the main difference is the exponent r on the LHS of (113) and the fact that $\overline{\chi}_{21}$ (RHS of 113) is multiplied by r. For $\phi_2^s \ll 1$ the factor $(1-\phi_2^s)^{r-1}$ can be expanded in an exponential series; retaining the first term only, equation (113) becomes:

$$\frac{\phi_2^s}{1-\phi_2^s} = \phi_2^b K_m \exp(\bar{\chi}\phi_2^s) \tag{114}$$

where $\tilde{\chi} = r(\overline{\chi}_{21} - 1) + 1$. Equation (114) is equivalent to the FFG equation (80). However, the interaction parameter $\tilde{\chi}$ in (114) is a function of the chemical interactions and the size of the molecules. The correspondence of equations (114) and (80) illustrates that neglecting the size of the molecules often does not lead to serious errors, if both the affinity and the lateral interaction parameter are seen as adjustable parameters. By considering K_m and $\tilde{\chi}$ as adjustable parameters the formal expression for the selectivity coefficient, which follows from equation (114), is also equivalent to that for regular behaviour, equation (79). By using equation (114) it should be realized the lateral interaction parameter in the adsorbed layer is different from that in the bulk solution. This difference is in the first place due to the simplified treatment. Pseudo-perfect behaviour will occur if $\tilde{\chi} = 0$. A discussion of equations (113) and (114) in relation to the rule of Traube has been given in [105]. Figure 4 presents an illustration of equation (114). In the case of strong lateral attraction $\tilde{\chi}$ may become considerably larger than χ_{21}.

Kronberg et al. [106–108] and Koopal et al. [105, 109] have presented adsorption models for small (flexible) chain molecules which adsorb with a given number of segments in direct contact with the surface and form a (nearly) homogeneous surface layer. The derived isotherm equations are equivalent to equation (113) if the conformational entropy loss is incorporated in K_m [109].

For molecules of arbitrary size and shape, $\Delta_m S$ is somewhere in between equation (21) and equation (111) [110]. Prausnitz et al. [6, 111, 112] have shown that equation (111) can be used for arbitrary shaped molecules too, if r is seen as a parameter depending on both the size and the shape of the molecules. For long chains r equals the number of segments and for large bulky (spherical, cubic) molecules r tends to unity.

Rigid organic ions

To describe the adsorption of rigid charged organic molecules, equation (113) can easily be adapted by adding a Boltzmann factor, $\exp(-\tau_i F\psi_a/RT)$, expressing the Coulombic interactions:

$$\frac{\phi_2^s}{(1-\phi_2^s)^r} = \phi_2^b K_m \exp\left\{r\overline{\chi}_{21}\phi_2^s - \left(\frac{\tau_2 F\psi_a}{RT}\right)\right\} \tag{115}$$

where ψ_a is the potential at the location of the charge centre of the organic ion. The magnitude of ψ_a is determined by the surface charge and the charge due to the adsorbed organic ions.

In general the charge centre of the organic ion is a small distance away from the surface. For compact molecules ψ_a can therefore be approximated reasonably well by the ζ-potential. The use of ζ-potential measurements as a function of the concentration of organic component in combination with adsorption measurements has often led to considerable insight in the adsorption behaviour [42, 113–116].

An alternative way is to use a double layer model to obtain further insight. Some general solutions for the situation that ψ_a is relatively low ($< |50|$ mV; DH model) have been worked out by Koopal and Keltjens [117]. Extension of equation (114) with a Boltzmann factor expressing the Coulombic interactions leads, in the limit of low potentials, again to equations of the FFG type if pH and ionic strength are kept constant [117]. The advantage of such a simplified treatment is that the essential factors which govern the adsorption are clearly illustrated. For instance, for an organic electrolyte adsorbing on an oppositely charged surface an increase in electrolyte strength decreases the affinity with the surface and the lateral repulsion between the adsorbed ions. As a consequence the initial slope of the isotherm will become weaker, but the pseudo saturation value will increase upon salt addition.

Flexible chain molecules

The main class of truly flexible organic chain molecules are the polymers. The specific effects due to the chain nature of polymer molecules have been emphasized already long ago, both for their behaviour in solution [103] and near an interface [118–121]. For an extensive review of the polymer adsorption theories we refer to the literature [122, 123]. In the present text the polymer adsorption theory developed by Scheutjens and Fleer [120] will be explained briefly. This theory is very "flexible" and can easily be extended to copolymer [124–127], polyelectrolyte [128–131] and surfactant [124, 132, 133] adsorption.

The self consistent field lattice theory for adsorption

In the self consistent field lattice theory for adsorption (SCFA) of chain molecules developed by Scheutjens and Fleer [120], each molecule is seen as a sequence of segments equal in size to a solvent molecule. The molecules are placed in a lattice to

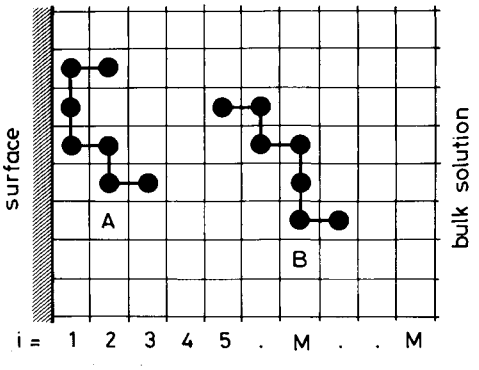

Fig. 11. Schematic illustration of the lattice model. Indicated are two possible conformations for a heptamer, one in the adsorbed state (*A*), one in solution (*B*). The solvent molecules, filling all other sites, are not indicated.

facilitate the counting of the conformations, see Figure 11. The lattice is divided in layers (z) parallel to the surface which are numbered $z = 1,\ldots,M$, where $z = 1$ corresponds to the layer adjacent to the surface and $z = M$ is a layer in the bulk solution.

The various segmental interactions (i.e. with other segments or with solvent molecules) are accounted for on the basis of the regular behaviour model, they result for each layer in a set of Boltzmann factors, one for each segment type. The chain conformations in the adsorbed layer can be described as step-weighted walks in the lattice. All possible conformations in equilibrium with the bulk solution are evaluated using a self consistent field method, viz. by minimizing the Gibbs energy of the system. This results for each type of segment in its equilibrium segment density profile near the surface. Based on these segment density profiles other adsorbed layer properties can be calculated. Below the basic principles of the SCFA theory will be illustrated for the simple case of a binary mixture of solvent molecules (monomers) and polymers.

Segmental weighting factors

The SCFA treatment starts with the derivation of an expression for the segmental weighting factor $G_i(z)$, or the probability of finding a free segment i in layer z with respect to finding a segment i in bulk solution. $G_i(z)$ is related to the selectivity constant expressed in equation (79). In the present situation a selectivity coefficient for each layer z is required. The selectivity coefficient $K^*_{i1}(z)$ of the exchange of a solvent molecule 1 for a free segment i in layer z is defined as:

$$K^*_{i1}(z) = \frac{\phi_i(z)\phi^b_1}{\phi_1(z)\phi^b_i} \tag{116}$$

As we work with chain molecules volume fractions are used instead of site fractions, ϕ^b_i denotes a fraction in bulk solution, $\phi_i(z)$ the fraction of i in layer z. The weighting factor for segment i can now be expressed as:

$$G_i(z) = \frac{\phi_i(z)}{\phi^b_i} = \frac{\phi_1(z)}{\phi^b_1} K^*_{i1}(z) \tag{117}$$

Substitution of the expression for K^*_{i1} [see equation (79)] gives $G_i(1)$. For an arbitrary chosen layer z we find:

$$G_i(z) = \frac{\phi_1(z)}{\phi^b_1} K^p_{i1}(z) \exp\left\{2\chi_{i1}\left(\langle\phi_i(z)\rangle - \phi^b_i\right)\right\} \tag{118}$$

The quotient $\phi_1(z)/\phi^b_1$ is related to the entropy of mixing; it expresses the fact that all lattice sites, have to be filled. If it is assumed that the interactions with the surface extend to the first layer only $K^p_{i1}(z) = K^p_{i1}(1)$ for the first layer, and $K^p_{i1}(z) = 1$ for $z \neq 1$.

Conformation probability and amount adsorbed

Based on the expression for the segmental weighting factor $G_i(z)$, the probability P_c of finding a chain in a certain conformation c can be described as a step-weighted walk in the lattice. A conformation is defined as the sequence of lattice layers that are visited during the walk. Each step in the walk is weighted by a segmental weighting factor $G_i(z)$ and a "bond" weighting factor λ_{z-z} expressing whether the next segment is in the same layer (λ_0) or crosses to one of the neighbouring layers ($\lambda_{-1} = \lambda_{+1} = \lambda_1$). Under these conditions P_c can be written for a two component system as:

$$P_c = \omega_c \prod_z G_i(z)^{r_{i,c}(z)} \tag{119}$$

where $G_i(z)$ is given by equation (118), $r_{i,c}(z)$ is the number of segments i that conformation c has in layer z, and ω_c expresses the multiple product of bond weighting factors of conformation c:

$$\omega_c = \lambda_0^q \lambda_1^{r-1-q} \tag{120}$$

In equation (120) q is the number of bonds parallel to the surface, and $(r-1-q)$ the number of bonds perpendicular to the surface.

The relative weight of all possible conformations c can now be evaluated provided $\phi_i(z)$ is known for all z. In turn the volume fraction profile is the result of all possible chain conformations. The volume fractions $\phi_i(z)$ of which the concentration profile is made up are therefore implicit functions, which have to be determined self consistently by minimizing the Gibbs energy. In general $\phi_i(z)$ is the result of all conformations c which have at least one segment in z:

$$\phi_i(z) = \phi_i^b \sum_c \frac{r_{i,c}(z)}{r} P_c \tag{121}$$

where $r_{i,c}(z)/r$ is the fraction of segments i that a chain in conformation c has in z, ϕ_i^b enters because P_c is expressed relative to the bulk solution behaviour. The amount adsorbed, expressed as excess surface coverage, θ^{ex}, simply follows from $\phi_i(z)$:

$$\theta^{ex} = \sum_z \{\phi_i(z) - \phi_i^b\} \tag{122}$$

Defined in this way, θ^{ex} is expressed in equivalent monolayers.

Equations (118)–(121) form a set of implicit functions which can be solved to find $\phi_i(z)$ for each layer, using the matrix method given in [120, 134, 135]. Once the segment densities are known, other properties, such as the equilibrium probability of each conformation and the amount adsorbed can be calculated. The adsorption isotherm is obtained by doing these calculations for a series of values of ϕ_i^b.

The present treatment can easily be extended to adsorption from multi component solutions [124–127, 132, 133]. The SCFA theory is not restricted to the rigid surfaces, also fluid interfaces [136] and solid surfaces with grafted chains [137] can be considered. Recently it has been shown how the theory can be modified to describe the behaviour of amphiphilic molecules in association colloids such as membranes [138, 139] or micelles [124, 140].

For polyelectrolytes or charged surfactants the Coulombic interactions have to be taken into account. This presents a special problem because these interactions extend over relatively long distances. Solutions for this problem have been presented by Van de Schee et al. [128, 129] and Evers et al. [130] by considering the indifferent electrolyte as point charges and by Böhmer et al. [131] using a full lattice treatment. In the next sections some examples of results obtained with the SCFA theory will be given for the various types of molecules and a brief comparison will be made with experimental results.

Polymers

Polymer adsorption is used extensively to modify properties of interphases. Such modifications may lead to stabilization or destabilization of colloidal dispersions. The SCFA theory has given a clear insight in both the adsorption [120] and the stability [141] aspects. For an extensive treatment of the theory and its results we refer to the original literature and to three review articles which also cover experimental results [122, 123, 142]. A brief selection of the results, chosen to illustrate some prominent features, will be given here.

A series of adsorption isotherms of homopolymers as a function of the chain length are given in Figure 12 for a theta or pseudo-ideal solvent ($\chi_{21} = 0.5$) and for a perfect or athermal ($\chi_{21} = 0$) solvent, considering a dilute concentration

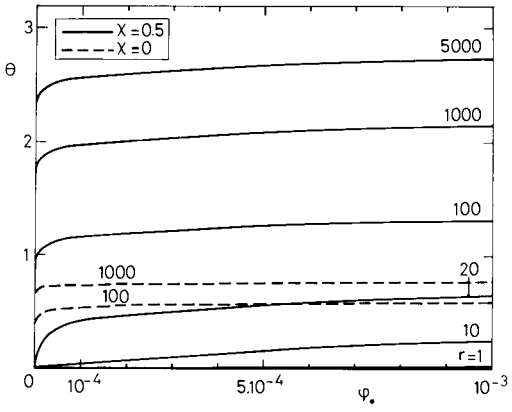

Fig. 12. Polymer adsorption isotherms in a dilute concentration region according to the SCFA theory. Full curves: $\chi_{21} = 0.5$; dashed curves: $\chi_{21} = 0$; $\ln K_{21}^{p}(1) = \chi_s = 1$. (From [120].)

region ($0 < \phi_2^b < 10^{-3}$) The adsorbed amount is expressed as number of segments adsorbed per surface site. Figure 12 shows that for the selected value of K_{21}^p (corresponding to an exchange Gibbs energy of one RT) monomers hardly adsorb, oligomers have Langmuir type isotherms and polymers show a very high affinity for the surface. In poor solvents ($\chi_{21} = 0.5$) the pseudo saturation value increases strongly with molecular weight, whereas in a perfect solvent ($\chi_{21} = 0$) the molecular weight dependence is relatively small. All these trends are in good agreement with experimental findings on well defined monodisperse polymer systems.

In relation to colloidal stability the segment density distribution in the adsorbed layer is important. Figure 13 shows a segment density profile for very long chains adsorbed from a dilute solution. The contribution of the loops and tails to the total segment density are indicated. The segment density of the loops decays exponentially with the distance to the surface. Close to the surface the segment density is dominated by the loop segments, but at large distances tail segments dominate. The volume fraction of segments in the tail region is small, but of the same order of magnitude as that within a free coil in solution.

The theoretical predictions on the segment concentration profile are difficult to check experimentally. Recently, small-angle neutron scattering studies [143, 144] have been applied to particles with an adsorbed polymer layer. A reasonable agreement is found, but the segment density in the outer region is too small to be seen. An indirect way to obtain information about the tail region are hydrodynamic measurements [145, 146]. Computations based on the SCFA theory in combination with the Navier-Stokes equation have demonstrated that the hydrodynamic layer thickness is determined by the tails [146–148]. Layer thicknesses measured by hydrodynamic techniques turn out to be much greater than the thickness calculated on the basis of the small-angle neutron scattering results [145].

The contribution of tails to the adsorbed layer profiles is smaller for shorter

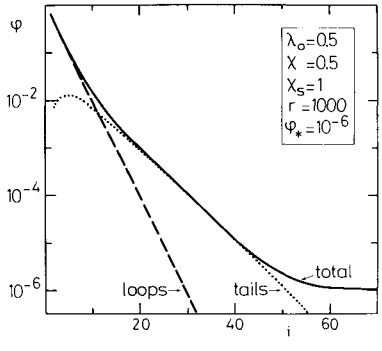

Fig. 13. The volume fraction $\phi(z)$ (full line) and its contributions due to loops (broken line) and tails (dotted line) on a logarithmic scale as a function of the distance z from the surface (SCFA theory). The loop contribution decreases exponentially with z ($\chi_{21} = \chi$; $\phi_2^b = \phi^*$ and $\ln K_{21}^p(1) = \chi_s$. (From [120].)

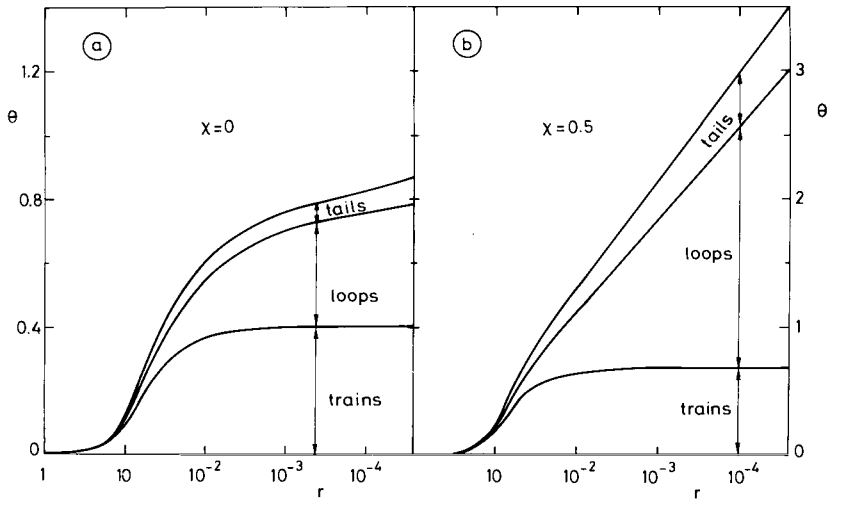

Fig. 14. Predicted chain length dependence of the adsorbed amount (upper curve) and its contributions due to trains, loops and tails; a. for a good ($\chi_{21} = \chi = 0$) solvent; b. for a θ-solvent ($\chi_{21} = \chi = 0.5$); $\ln K_{21}^{p}(1) = \chi_s = 1$; $\phi_2^b = 10^{-3}$ (from [142]).

chains and for perfect ($\chi_{21} = 0$) solvents. Figure 14 shows the chain length dependence of the adsorbed amount separated in the contributions of trains, loops and tails for two solvent qualities. For not too short chains the number of train segments is independent of the chain length. The contribution of the loops is rather different for the two solvents. In a poor solvent the loop contribution is much larger than in a good solvent and it steadily increases with increasing chain length. In both solvents the number of tail segments gradually increases with r. Realizing that each adsorbed molecule has only two tails, this result is equivalent to a considerable increase in tail length with increasing molecular weight. As mentioned before, these long tails largely determine the hydrodynamic layer thickness. Secondly, the long tails are of importance with respect to colloidal stability. For not fully covered particles the tails may form bridges between particles and induce flocculation (bridging attraction or flocculation), whereas for highly covered particles the tails cause a steric stabilization.

In general it is believed that upon interaction between particles covered with a polymer layer a restricted or local equilibrium situation applies [141, 142]. The time scale of a collision between two particles covered with polymer is too small to allow the polymer to desorb. The polymer is trapped in the gap between the particles and only the solvent can leave the gap. If, for instance, complete equilibrium is maintained during the collision, the polymer will leave the gap between the two approaching particles. Under these conditions the theory predicts only attraction, see Figure 15, and a homopolymer cannot stabilize the colloidal system [141]. This is in marked contrast with experimental observations.

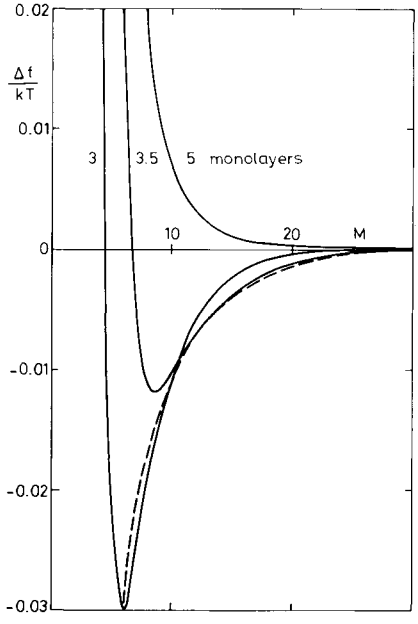

Fig. 15. Interaction free energy per surface site between two plates with adsorbing polymer as predicted with the SCFA theory. The dashed curve is for complete equilibrium and $\phi_2^b = 10^{-6}$. The solid curves apply to restricted equilibrium where the amounts of polymer is fixed at its value and plate separation of 80 lattice layers. The amounts are 3, 3.5 and 5 monolayers, corresponding to equilibrium (at M > 80) with a solution of $\phi_2^b = 10^{-12}$, 10^{-6} and 10^{-2}, respectively. $r = 1000$, $\chi_{21} = 0.5$, $\ln K_{21}^p(1) = \chi_s = 1$. (From [142].)

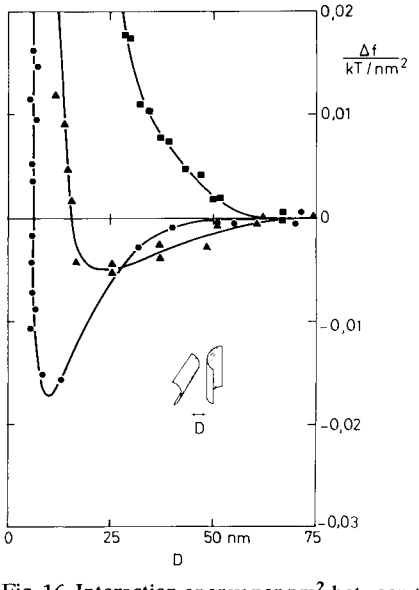

Fig. 16. Interaction energy per nm^2 between two mica surfaces covered with polystyrene in cyclopentane at different amounts adsorbed, compare Figure 15 (data from [156], fig. 5).

Under conditions of a restricted equilibrium, with a constant amount of polymer in local equilibrium between the two phases, the free energy of interaction can also be calculated [141, 149]. In very dilute solutions an attractive potential is predicted, which is deep enough to cause flocculation, see Figure 15. The long dangling tails are adsorbing on the opposing surface to form bridges. For high adsorption values a strong repulsive interaction is dominant, especially in good solvents. This is due to entropic restrictions of the dense polymer layers on both particles (steric stabilization). These trends in stability are confirmed by experimental results [150–152]. Experimental results which can be compared directly with the theoretical interaction curves have been provided mainly by Klein et al. [153–156] and Marra et al. [see 157] for mica surfaces and by Sonntag et al. [158] for quartz surfaces covered with various polymers. In general a good agreement is found. In Figure 16 some of the results as obtained by Klein [156] are replotted.

It should be realized that in a flocculation process kinetic effects may play an important role and such effects are of course not included in the SCFA treatment. As kinetic effects are strongly dependent on the concentration and the size of the particles these factors will be important together with the hydrodynamic situation. Recently, Pelssers et al. [159, 160] have treated the kinetics of polymer induced flocculation in more detail.

Many colloidal systems are stabilized by chemically attached chains. In this case the SCFA theory predicts that the structure of the adsorbed layer depends on the solvent quality and whether or not the segments adsorb. Especially a non-adsorbing grafted polymer in a good solvent extends far in the solution [137] and is an effective stabilizer [161].

Recently, also theoretical work has been done on the adsorption random [125] and of block copolymers [124, 126, 127]. Through their chemical structure, AB block copolymers offer the possibility to adhere strongly with their solvophobic block to the surface, whereas the solvophilic block protrudes far in the solution, resembling grafted chains. For high adsorbed amounts the segment density profile of the less-adsorbing or non-adsorbing block is highly dependent on the solvent quality. ABA triblock copolymers with adsorbing A segments form, at high adsorbed amounts, dangling tails with "sticky" ends. Experimental results on the interaction between mica surfaces covered with di- and triblock copolymers are given by Patel et al. [162] and Marra and Hair [163].

Polydisperse polymers

Most polymers used in practical systems are polydisperse with a wide molecular weight distribution. This polydispersity has considerable consequences for the adsorption behaviour [164–166]. The reason is that polydisperse polymer solutions are essentially a multi component mixture from which preferential adsorption of certain species may occur. As shown in Figure 12, the affinity for the surface and the

adsorbed amount increase with increasing chain length, especially in poor solvents. Consequently, from a polydisperse polymer sample preferential adsorption of the high molecular weight species over the lower molecular weight species occurs. Further theoretical and experimental evidence for preferential adsorption can be found elsewhere [122, 123, 167]. Preferential adsorption has important consequences for the shape of the isotherm [165–168]. If an adsorption isotherm is measured by increasing the polymer concentration at a fixed area-to-volume ratio, A/V, the total amount of high molecular weight polymer in the system becomes larger if the concentration increases. The highest molecular weight species prefer to be adsorbed and the larger the polymer concentration is, "the more selective the surface can be". As a result the adsorbed amount increases with increasing concentration and, unlike monodisperse polymers, polydisperse polymers show a rounded isotherm which gradually increases with polymer concentration. Rounded isotherms are commonly found in practice.

An other consequence of preferential adsorption is that a measured isotherm will depend on the A/V ratio [166]. This effect is shown in Figure 17. The smaller the A/V ratio, "the more selective the surface can be" and the higher is the amount adsorbed. The various isotherms coincide in a master isotherm if the amount adsorbed is plotted as a function of $c_p V/A$. Other examples of this behaviour have been reported by Cohen Stuart et al. [165] and by Hlady et al. [168].

A third rather important implication of preferential adsorption from a polydisperse mixture is that adsorption isotherms are more rounded than "desorption" isotherms obtained by dilution with solvent. This is due to the fact that the solution composition is different for the adsorption and desorption experiment. In the desorption experiment the short chains in solution are diluted and the long chains on the surface only desorb to a very small extent following the isotherm of a monodisperse polymer with essentially a horizontal plateau. Appreciable desorption only occurs if the solution becomes extremely dilute, ie. in the order of one molecule per dm^3 [122, 123]. In practice, it is therefore impossible to desorb polymers fully by simple dilution. Dilution experiments and the hysteresis loop in the adsorption "desorption" isotherm can therefore not be used to conclude that polymer adsorption is irreversible.

Removal of polymers from a surface by displacement is quite well possible. Preferential adsorption of high molecular weight species is essentially achieved by the displacement of the more rapidly adsorbing smaller polymer chains. Low molecular weight species which strongly adsorb can be used as effective "displacers" of adsorbed polymers [169]. Displacement experiments provide an elegant way to measure the segmental adsorption energy of polymers [169, 170].

Finally it should be realized that preferential adsorption of high molecular weight species from a polydisperse sample may strongly affect the hydrodynamic thickness of the adsorbed layer and thus the colloidal stability. By selection of the A/V ratio it is possible to "adjust" the layer thickness of the adsorbed polymer layer [145].

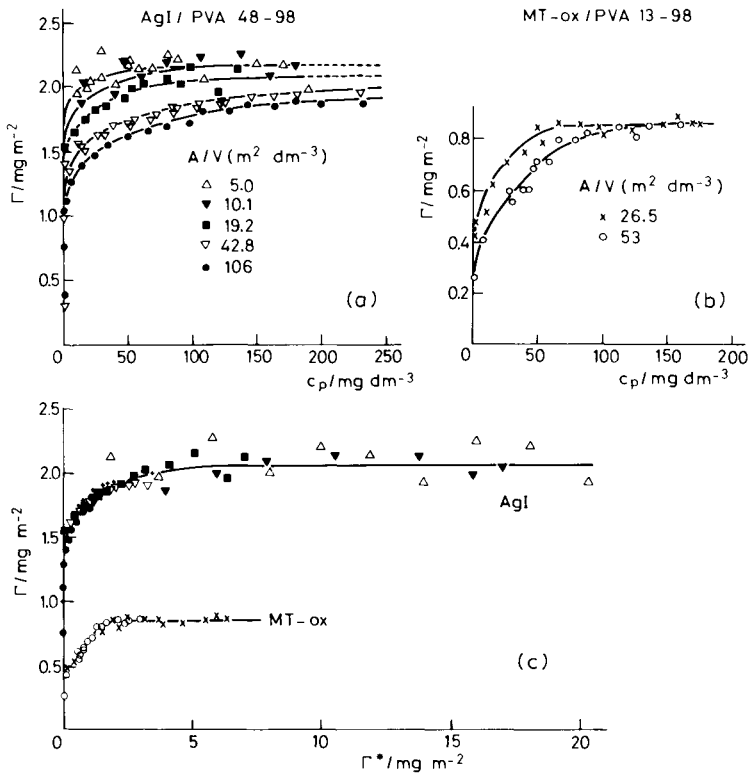

Fig. 17. Effect of the area to volume ratio on the shape of the adsorption isotherm as measured for the AgI–PVA (a) and Sterling MT-ox carbon–PVA systems (b). The A/V ratio is indicated. In (c) the data are replotted as a function of $\Gamma^* = c_p A/V$. This leads to a mastercurve for each system and indicates that the differences in (a) and in (b) are due to polydispersity effects. (From [166].)

In relation to polymer adsorption and colloidal stability electrophoresis can provide good insights in both the electrostatic potential of the particles and the adsorbed layer thickness [145].

Polyelectrolytes

The adsorption of polyelectrolytes is of considerable practical and theoretical interest similar to that of uncharged polymers. Polyelectrolytes are used both as flocculants and stabilizers. The adsorption of flexible polyelectrolytes has much in common with adsorption of uncharged polymers, but also distinct differences exist, which result from the occurrence of the long range electrostatic interactions.

Theoretical work on polyelectrolyte adsorption has started from any of the models for adsorption of uncharged polymer by incorporating the electrostatic free energy in the partition function [171, 128–131]. Essential in such a type of extension

is to allow the segment density profile to adjust itself to all the interactions. This has been achieved by extending the polymer adsorption theory of Roe [128, 129] and the SCFA theory [128, 130, 131]. In the SCFA theory the electrostatic interactions, which a segment experiences due to the presence of the other (charged) segments and the (charged) surface, have to be incorporated in the segmental weighting factor. This is done by multiplying the appropriate segmental weighting factor for the uncharged molecule with the Boltzmann factor expressing the Coulombic interactions:

$$G_i^{\text{Coul}}(z) = \exp\left\{\frac{-\tau_i \alpha_i(z) F \psi(z)}{RT}\right\} \tag{123}$$

where $\alpha_i(z)$ is the degree of dissociation in layer z, and $\psi(z)$ is the electrostatic potential in layer z relative to the potential in bulk solution. The long range effect of the electrostatic interactions is included through the fact that $\psi(z)$ is determined by the charge density in each layer. Both Van der Schee and Evers have evaluated $\psi(z)$ by assuming that the salt ions are point charges, whereas the polyelectrolyte segments and the solvent molecules are assigned the size of a lattice site. The charge of the polyelectrolyte segments is located on planes through the centers of the lattice layers. Van der Schee only considers strong polyelectrolytes, Evers has extended the treatment to weak polyelectrolytes. Very recently, Böhmer et al. [131] have extended the SCFA theory in such a way that not only the segments and the solvent molecules occupy lattice sites, but also the salt ions. The results of this treatment are similar to the results obtained by Evers et al. [130]. Böhmer has also considered the interaction between two plates covered with polyelectrolyte.

A selection of the theoretical results is presented below. For a more complete description the reader should consult the cited literature. A brief review on polyelectrolyte adsorption discussing both theory and experimental results has been given by Cohen Stuart [172].

An important feature of polyelectrolyte adsorption, as compared to homopolymer adsorption, is the much smaller adsorption. Figure 18 summarizes some results of Van der Schee et al. [128, 129]. Adsorption isotherms are shown for strong acid polyelectrolytes ($\alpha_2 = 1$) and neutral polymers ($\alpha_2 = 0$). The "chemical" interaction parameters (χ_{21} and K_{21}^{p}) are assumed to be the same for both polymers. The polyelectrolyte isotherms apply to adsorption on an uncharged surface ($\sigma_s = 0$) at high ionic strength and to adsorption on a surface with a high positive charge ($\sigma_s = 40$ mC m^{-2}) at an intermediate value of the ionic strength. In both cases the polyelectrolyte adsorption is much smaller than that of the uncharged polymer. The charges on the polyelectrolyte groups let water behave as a very good solvent. Even at 1 M salt, where the screening of the charges is considerably, the residual repulsion between the polyelectrolyte groups is large enough to let water penetrate between the groups.

The difference in behaviour of a polyelectrolyte and a neutral polymer is illus-

trated in more detail in Figure 19, where the segment density profiles in the plateau of the adsorption isotherms are shown. Note that the volume fraction is given on a logarithmic scale. At low ionic strength (0.01 M) a clear minimum occurs in the segment profile, caused by the repulsion of the free polyelectrolyte chains by the adsorbed molecules. The surface charge is overcompensated by the adsorbed segments. The minimum is very pronounced on the logarithmic scale, but would be hardly noticeable on a linear $\psi_2(z)$ scale. It is obvious from Figure 19 that at low ionic strength adsorbed segments are only present in the first layers near the surface, i.e. a rather flat adsorption. This flat conformation also leads to a very weak molecular weight dependence of the adsorption. For entirely flat adsorption, the amount adsorbed is independent of the chain length. The adsorption is promoted by either strong electrostatic or chemical attraction between the polymer and the surface. At high ionic strength values the minimum in the segment density profile diminishes or disappears. The decay is smooth and similar to that of the neutral polymer, pointing to the occurrence of loops and tails. In this case the molecular weight dependence of the adsorption is more pronounced than at low ionic strength.

The adsorption of weak polyelectrolytes strongly depends on the degree of dissociation and hence on the pH value [130]. The change from high adsorption values

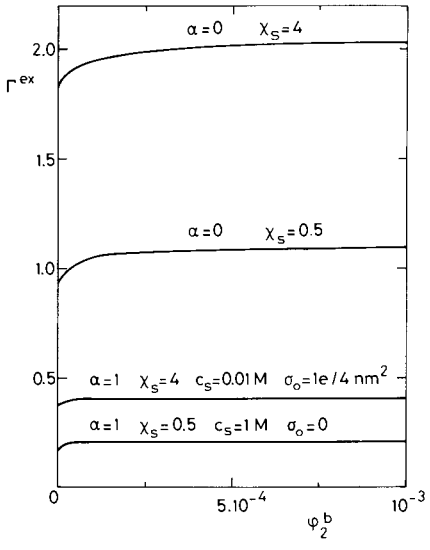

Fig. 18. Comparison of adsorption isotherms of strong polyelectrolytes ($\alpha_i = \alpha = 1$) and neutral polymers ($\alpha_i = \alpha = 0$) on a surface of low ($\ln K_{21}^{p}(1) = \chi_s = 0.5$) and high ($\ln K_{21}^{p}(1) = \chi_s = 4$) affinity. The adsorption is expressed as θ^{ex} ($=\Gamma^{ex}$, number of equivalent monolayers). The polyelectrolyte isotherms apply to an uncharged surface ($\sigma_s = \sigma_o = 0$) at high saltconcentrations ($c_s = 1$ M), and to a highly charged surface of opposite charged sign ($\sigma_s = \sigma_o = 0.25$ electron charges per nm^2 or 40 mC m^{-2}) at low salt concentration ($c_s = 0.01$ M). Hexagonal lattice, lattice step length 1 nm, $r = 500$ and $\chi_{21} = 0.5$. (Data from [120, 129].)

for $\alpha_2(z) = 0$ to low adsorption values for $\alpha_2(z) = 1$ occurs around pH = pK_d, where K_d is the dissociation constant of the charged groups. The situation is complicated by the fact that the dissociation is influenced by the local environment. An interesting observation is that, for an oppositely charged surface, the adsorbed amount passes through a maximum at about pH = pK_d − 1 [130, 131]. At this point the degree of dissociation of the segments in the first layer adapts itself to neutralize the surface charge, leading to a maximum electrostatic attraction. For higher pH values the repulsion between the segments increases, for lower pH values the electrostatic attraction decreases. The effect is enhanced by taking into account competition between negative salt ions and polyelectrolyte segments [131].

Experimentally the adsorption behaviour of polystyrene sulphonate and polylysine (see [172]) on various surfaces is well studied. The trends obtained are in good agreement with the predictions. An unexplained feature is the gradual increase in adsorption with polyelectrolyte concentration as found for polystyrene sulphonate adsorbed on silica and polyoxymethylene. In a recent study by Blaakmeer et al. [173] on the adsorption of weak polyelectrolytes a comparison is made between experimental results and predictions obtained with the SCFA theory as extended by Böhmer [131]. Apart from his own results Blaakmeer also discusses recent work of other authors with respect to the theoretical predictions.

Colloid stability in relation to polyelectrolyte adsorption has been studied by Böhmer et al. [131]. Böhmer predicts that the interaction between two charged surfaces in the presence of adsorbing polyelectrolyte resembles that of two neutral surfaces in the presence of neutral polymer, see Figure 20, provided the affinity

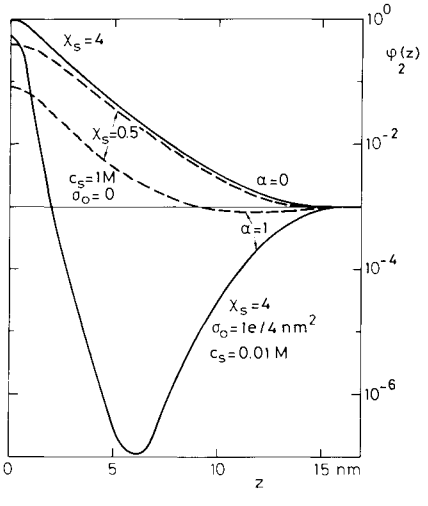

Fig. 19. Logarithm of the segment density $\phi_2(z)$ as a function of the distance to the surface in the plateau region ($\phi_2^b = 10^{-3}$) for the four isotherms shown in Figure 18 (data from [129]).

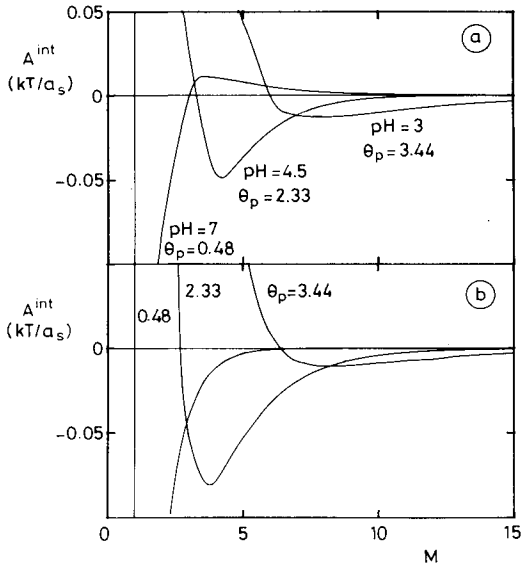

Fig. 20. The interaction free energy per surface site between two plates covered with polyelectrolyte (a) or an equal amount of neutral polymer (b). The amounts adsorbed are indicated. The curves apply to restricted equilibrium, where the amount of polyelectrolyte or polymer is fixed at its value of large plate separation (60 lattice layers). For Figure 20a the surface charge is 50 mC m^{-2}, z_o = 0.6 nm, pK_d of the polyelectrolyte equals 5, and the saltconcentration is 0.1 M 1–1 electrolyte. For both polymers r = 500, $\phi_2^b = 10^{-4}$, $\ln K_{21}^p(1) = 1$ and the electrolyte solution is a theta solvent. (From [131].)

of the segments for the surface is not too high. For the calculations it has been assumed that the amount of polymer is independent of the surface separation (local equilibrium). In Figure 20a the interaction curves are given for two charged surfaces (σ_s = 50 mC m^{-2}) in the presence of an adsorbing weak polyacid at three pH values and a ionic strength of 0.1 M. The amount of polyacid between the plates is indicated in the figure. The pK_d of the polyacid is 5. At pH = 7 the polyelectrolyte is almost fully dissociated. At pH = 3 the adsorbed polyacid is weakly negative due to the enhanced dissociation in the first layer (induced by the electrostatic field of the surface). In all cases the positive surface charge is effectively neutralized by the polyelectrolyte and the electrostatic potential in layer 1 is negative. For not too high surface charges this is generally the case.

Figure 20b shows the interaction curves for two uncharged surfaces (σ_s = 0 mC m^{-2}) covered with a neutral polymer ($\alpha_2(z)$ = 0). The differences between Figure 20a and b are relatively small. For the lowest amount of polymer between the plates a repulsion is observed at large plate separations. Comparison of Figure 20a and b shows that this repulsion is due to electrostatic interactions between the charged polyelectrolyte segments on each of the particles. At small separation distances bridging attraction occurs for both the neutral polymer and the polyelec-

trolyte. For the uncharged polymer this bridging attraction sets in at a larger plate separation. Very close to the surface ($z \approx 1$) a strong steric repulsion appears. For $\theta_p = 2.33$ and 3.44 the behaviour is very similar in both cases: bridging attraction starting at relatively large plate distances and steric repulsion at short distances. For the polyacid and not too low amounts adsorbed the bridging attraction is slightly stronger than the electrostatic repulsion, whereas for the very small amount adsorbed the electrostatic repulsion dominates. For other values of the ionic strength the picture remains about the same. For a strongly adhering highly dissociated polyelectrolyte the effect of the electrostatic repulsion becomes more pronounced at low salt levels.

Interaction curves obtained by direct force measurements for the mica–polylysine system [174] and the mica–poly(2-vinylpyridine) system [175] resemble the trends shown above.

Surfactants

Surfactants are frequently used to control the colloid stability and/or the wetting behaviour of solid dispersions. Applications are in detergency, pigment, pesticide and pharmaceutical formulations, mineral separation processes, printing, enhanced oil recovery, etc. As a consequence of such ubiquitous use there is a vast amount of literature on surfactants and surfactant adsorption. General reviews on surfactants, including surfactant adsorption, can be found in the Surfactant Science Series [176]. A recent textbook on surfactants, with contributions of various authors, has been edited by Tadros [177]. Surfactant adsorption has recently been reviewed by Clunie and Ingram (non-ionics) [178] and by Hough and Rendall (ionics) [115]. Surfactant adsorption in relation to flotation has been treated by Dobias [179], Moudgil et al. [116] and Clark and Wilson [180]. Some aspects of modelling of surfactant adsorption including the SCFA treatment of surfactants will be given below.

The adsorption of surfactants is mostly treated by neglecting the conformational changes which the molecules undergo upon adsorption. Popular descriptions of the adsorption of ionic surfactants often rely on FFG type equations extended with Coulombic interactions or on the even more simple Stern-Langmuir equation [116]. An overview of these models can be found in [105]. In the FFG type equations the "chemical" lateral interactions are accounted for on the basis of a "Bragg-Williams" or mean field approximation. Wilson et al. [180] have considered surfactant adsorption on the basis of the "quasi-chemical" approach, but these authors neglect size effects. Cases et al. [181, 182] introduce surface heterogeneity in their adsorption models. For the "local" isotherm equation, that is to say the isotherm equation for a group of "equal-energy" sites, Cases assumes a step function corresponding with 2D condensation. Such a step function is a reasonable approximation for the local isotherm in the case of very strong lateral attraction. Scamehorn et al. [183] and Harwell et al. [184] have extended the approach of Cases by considering the forma-

tion of "ad-micelles" on the surface. Fuerstenau [185] and Gu et al. [186, 187] have developed models based on "hemi-micelle" formation. Hemi-micelles [185, 188] are 2D surfactant aggregates, whereas ad-micelles [184] are aggregated bilayer structures. A three-stage adsorption model for non-ionic surfactants has been developed by Klimenko [189, 190] and is reviewed in [178]. In all these models the flexibility of the molecules is not treated (explicitly). Kronberg [106–108] has derived a relatively simple equation for the adsorption of non-ionic surfactants by treating the surfactant as a simple polymer and the adsorbed layer as a homogeneous mixture of surfactant and solvent. The loss of conformational entropy is however not included in this treatment.

Koopal et al. [109] have made a naive attempt to account for the conformational changes upon adsorption by using a simplification of the SCFA theory. Both ionic and non-ionic surfactants have been considered. For the adsorption from dilute solutions (i.e. strong adsorption below the CMC), the general equation for the surfactant isotherm can be written as:

$$\theta_2 = \phi_2^b W (1 - \phi_2^s)^r (\overline{K}_{21})^m \exp\left[2r\overline{\chi}_{21}\phi_2^s - \left\{\frac{\tau_2 F\psi(t)}{RT}\right\}\right] \tag{124}$$

In the derivation of equation (124) it is assumed that each surfactant molecule consists of r segments (about equal in size to a water molecule) of which m ($1 \leq m \leq r$) are adsorbed in direct contact with the surface. In equation (124) θ_2 is the adsorbed amount, which is equal to $r\phi_2^s/m$, ϕ_2^b is the bulk volume fraction of surfactant, W a factor related to the conformational entropy loss upon adsorption, ϕ_2^s the volume fraction surfactant in the nearly homogeneous adsorbed layer, $\overline{K}_{21}$ the effective affinity constant for a segment in direct contact with the surface, $\overline{\chi}_{21}$ the average Flory-Huggins interaction parameter, and $\psi(t)$ the electrostatic potential at the location (t) of the charged headgroups. The parameters, $\overline{K}_{21}$, $\overline{\chi}_{21}$ and $\psi(t)$, depend on the orientation of the surfactant molecules in the adsorbed layer, but not on the chain conformation as long as m is a constant. The conformational entropy loss, $-k \ln W$, can be approximated by assuming that only the m segments in direct contact with the surface contribute to W. In that case the expression for W reads [109]:

$$W = \lambda_0^{m-1}\lambda_1 \tag{125}$$

indicating that W is also constant for a fixed value of m. An analytical expression for the electrostatic potential can only be given for low potentials, i.e. in the Debye-Hückel limit ($\psi(t) < |50|$ mV). For dilute solutions and the headgroup located in lattice layer t the general expression for $\psi(t)$ equals [105]:

$$\psi(t) = \frac{\sigma_s}{\varepsilon_o\varepsilon_r\kappa}\left[\exp\{-\kappa z_o(t-1)\}\right] + \frac{\sigma_2(t)}{2\varepsilon_o\varepsilon_r\kappa}\left[1 + \exp\{-2\kappa z_o(t-1)\}\right] \tag{126}$$

where σ_s is the surface charge density, $\sigma_2(t)$ is the charge density due to surfactant in layer t, and z_o is the lattice layer distance. For adsorption of the headgroups in layer 1, equation (126) reduces to:

$$\psi(1) = \frac{\sigma_s + \sigma_2(1)}{\varepsilon_o \varepsilon_r \kappa} \tag{127}$$

The charge density $\sigma_2(1)$ can be replaced by $\tau_2 F \phi_2^s / ma$. Equations (124–127) are well suited to give a semi-quantitative insight in factors which determine the adsorption behaviour.

In the case of non-ionic surfactants, equation (124) can be used with $\tau = 0$. Koopal et al. [109] have shown that (for dilute solutions) the thus obtained equation is very similar to the adsorption isotherm equation for non-ionics as formulated by Kronberg [106].

Equation (124) does not apply to "bilayer" adsorption. However, with some further approximation (124) can be used for the description of the adsorption of a ionic surfactant in a "bilayer", once the "monolayer" is formed. Roughly speaking this point is reached when the surface charge is just compensated by the adsorbed surfactant charge. This isoelectric point corresponds with the intersection point of surfactant isotherms measured at different salt concentrations [191]. With "bilayer" formation the affinity of the surfactant for the surface with the adsorbed "monolayer" is merely due to lateral interactions, so that $\overline{K}_{21} = 1$. Moreover, the conformational entropy loss of surfactants adsorbed in the bilayer mode is small so that $W = 1$ is a reasonable approximation. The expression for $\psi(t)$ is very similar to that of equation (126) if it is assumed that the headgroup is adsorbing in layer t at some distance of the surface. The only difference is that σ_s has to be replaced by $\sigma_s + \sigma_2(1)$, where $\sigma_2(1)$ represents the charge present in the first layer due to "monolayer" adsorption. The total surfactant adsorption is found by adding the "monolayer" and the "bilayer" adsorption together. This two-step treatment should be seen as a first order approximation. The model of Harwell et al. [184] for admicelle adsorption is rather more complicated but not necessarily better, because it treats the electrostatic interactions with an unrealistic amount of detail and neglects the specific chain nature of the molecules.

The disadvantage of all treatments mentioned so far is that many simplifying assumptions have to be made with respect to the segment density distributions in the adsorbed layer. In order to overcome these simplifications, the SCFA theory offers, at the moment, the most promising alternative. In order to be able to use the SCFA theory for the description of surfactant adsorption an extension of the theory is required which describes micellization. Such an extension has been derived by Leermakers et al. [124, 140]. The description of micellization is important because above the CMC (critical micelle concentration) the volume fraction of free surfactant hardly increases upon an increase of the total volume fraction of surfactant in the solution. Consequently, the chemical potential of the free surfactant will hardly

increase above the CMC and this in turn will lead to a (pseudo) saturation value of the adsorption. Theoretical models which do not include micellization are necessarily restricted to very dilute solutions, i.e. surfactant concentrations below the CMC.

Results for surfactants as obtained with the extended SCFA theory are limited to block-type non-ionic surfactants [132, 133] and simple ionic surfactants [197, 198]. Some results about micellization and adsorption of a series of alkyl-polyoxyethylenes are reproduced in Figures (21–24). The alkyl-polyoxyethylenes are noted as an A_nB_x, where A represents an aliphatic segment and B an ethyleneoxide segment. The Flory-Huggings interaction parameter χ_{AW} between A and solvent (water) is set equal to 2, reflecting the poor solubility of A in W. For χ_{BW} a value of 0.4 is assumed in accordance with measurements of Van den Boomgaard [192] and Amu [193]. For χ_{AB} a value of 2 is chosen; this high value promotes the separation between segments A and B.

Predictions with respect to the CMC for spherical micelles $A_{10}B_x$ as a function of the B (= EO) block length are shown in Figure 21 [133]. Also indicated are the critical concentration for the formation of flat membranes and the concentration where (bulk) phase separation occurs. According to Figure 21 the CMC increases linearly with the number of B segments. This agrees with experimental results [192, 193] and supports the chosen values for the χ_{ij} parameters. It is predicted that spherical micelles are formed at lower concentrations (and hence at lower chemical potentials) than flat membranes. For the given type of surfactant also this is in agreement with practice.

Figure 22 shows the calculated density profiles of segments A and B in micelles of $A_{10}B_6$ and $A_{10}B_{40}$. The hydrophobic core of the $A_{10}B_6$ micelles is much bigger than that of the $A_{10}B_{40}$ micelles. Steric hindrance between the B blocks prevents the formation of large micelles of $A_{10}B_{40}$.

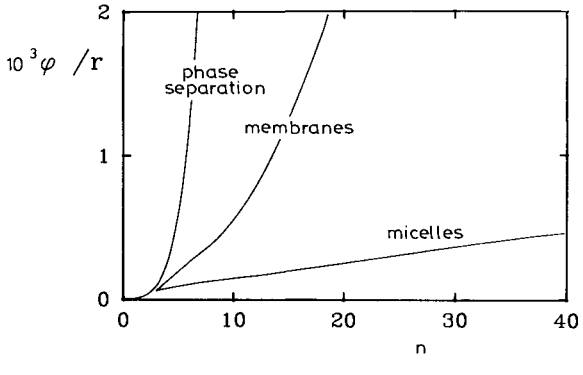

Fig. 21. Theoretical predictions of the equilibrium volume fractions of $A_{10}B_n$ molecules for phase separation, membrane (flat) formation and micelle (spherical) formation as a function of the B block length. Interaction parameters $\chi_{AW} = 2$, $\chi_{AB} = 2$, $\chi_{BW} = 0.4$. (From [133].)

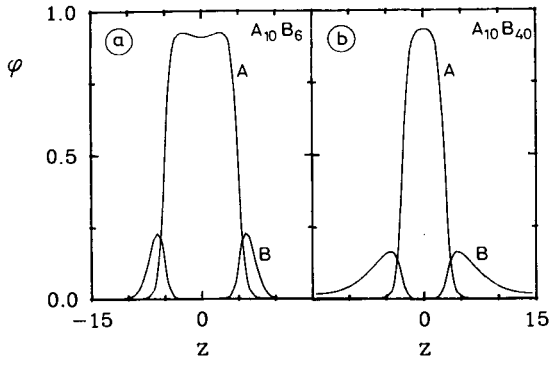

Fig. 22. Predicted volume fraction profiles for $A_{10}B_6$ (a) and $A_{10}B_{40}$ (b) micelles. The volume fractions for segments of type A and B are indicated. The overall concentration φ/r of surfactant is 5×10^{-4}. Interaction parameters: see Figure 21. (From [133].)

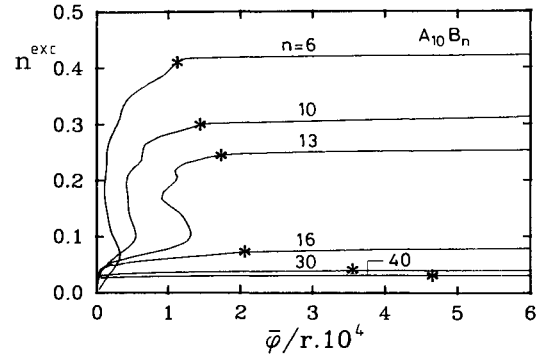

Fig. 23. Calculated adsorption isotherms for a homologous series of amphiphilic chain molecules $A_{10}B_n$ on a hydrophilic surface. The CMC values are indicated with an asterisk. Interaction parameters: $\chi_{AW} = 2$, $\chi_{AB} = 2$, $\chi_{BW} = 0.4$, $\ln K^{p}_{AW}(1) = 0$, $\ln K^{p}_{BW}(1) = 1.6$. (From [133].)

Predicted adsorption isotherms of a homologous series $A_{10}B_x$ on a hydrophilic surface are shown in Figure 23 [132, 133]. The asterisk marks the CMC. The interaction parameters are the same as above, for the affinity constant per B segment a value of 5 is used, corresponding with a standard Gibbs energy of adsorption (an exchange quantity) of $1.6RT$. For the A segments the standard Gibbs energy of adsorption is assumed to be zero. For short B blocks the isotherms reach high adsorption values, long B blocks lead to a low adsorption. Conversely, the initial slope of the isotherm is the steeper the larger the B block, indicating a relatively flat adsorption. Chains with many B segments have a high adsorption energy in the limit of isolated adsorbed chains.

The cooperativity in adsorption already begins at extremely low concentrations. The A segments associate to reduce the number of AW contacts. The association

is more pronounced if the A/B ratio increases. Steric hindrance between the B blocks prevents association similarly as in the micelles. For A/B ratios of about one the isotherm shows a phase transition region or "2D" condensation step. (The small irregularities in the adsorption isotherms are caused by lattice artifacts.) At the condensation step a "bilayer" is formed. Steric hindrance between the B blocks prevents "bilayer" formation for A/B ratio's much smaller than one. The general trends observed in Figure 23 correspond well with experimental results [194–195]. In practice, bilayer formation may occur in local aggregates if the A/B ratio is much smaller than one. A problem with a comparison with experimental results is that most non-ionic surfactants are polydisperse, so that no sharp CMC and/or 2D phase transitions are observed.

Segment density distributions in the adsorbed layer just before the CMC is reached are shown in Figure 24 for $A_{10}B_6$ and $A_{10}B_{40}$. The density distribution of the B segments of $A_{10}B_6$ clearly shows the "bilayer" formation. For $A_{10}B_{40}$ no maximum in the volume fraction of B segments is found at the solution side of the interfacial region. Note that the adsorbed layer thickness is considerably smaller than twice ($A_{10}B_6$) or once ($A_{10}B_{40}$) the extended chain length.

For a hydrophobic surface, for which it is assumed that only the aliphatic segments adsorb, a comparable set of predictions has been made [133]. Also in this case a good agreement with experimental results is observed [108, 196]. Again association of the hydrophobic segments determines the shape of the isotherm. In this case no bilayer formation occurs.

Predictions for the adsorption of ionic surfactants on charged interfaces, using the SCFA theory, are in progress [197]. The first results on micellization are promising [198]. Preliminary results on adsorption show that the ionic strength and the surface charge are important parameters (as predicted by the simple theories). Cal-

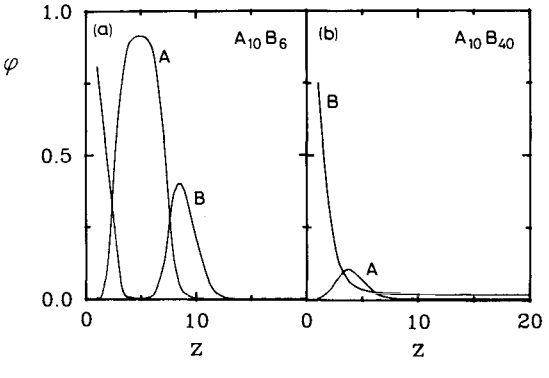

Fig. 24. Volume fraction profiles of $A_{10}B_6$ (a) and $A_{10}B_{40}$ (b) in the adsorbed layer at the plateau of the isotherm on a hydrophilic surface. The volume fractions of the segments A and B are indicated. See Figure 23 for the interaction parameters. (From ref. [133].)

culations show that at coverages of a few percent strong association of the molecules starts, whereas "bilayer" formation will occur at about 0.1 of the CMC, when the headgroups and the surface are oppositely charged. The headgroups at the solution side of the "bilayer" are not located in one plane but distributed over a number of lattice layers (compare also Figure 24) to minimize the electrostatic repulsion. Interesting aspects which have to be studied are the differences between adsorption on fixed and variably charged surfaces.

So far no predictions have been made using the SCFA theory with respect to surfactant induced colloidal stability. However, it will be clear that further progress can be made. Necessarily, results obtained with lattice theories, such as the SCFA, have the drawback that lattice artifacts may obscure some results. Other high level theoretical developments are therefore most welcome. The present advantage of the SCFA theory over, for instance, molecular dynamics or Monte Carlo studies is that complicated systems can be considered at the expense of relatively little computer time.

References

1 G.D. Parfitt and C.H. Rochester (Editors), Adsorption from solution at the solid/liquid interface, Academic Press, London, 1983.

2 P. Somasundaran and B.M. Moudgil (Editors), Reagents in mineral technology, Surfactant Science Series, Vol. 27, Marcel Dekker, New York, N.Y., 1988.

3 S.J. Gregg and K.S.W. Sing, Adsorption surface area and porosity, 2nd edition, Academic Press, London, 1982.

4 E.A. Guggenheim, Thermodynamics, 5th edition, North Holland Publishers, Amsterdam, 1967.

5 R. Defay, I. Prigogine, A. Bellemans and D.H. Everett, Surface tension and adsorption, Longmans, London, 1966.

6 J.M. Prausnitz, R.N. Lichtenthaler and E. De Azevedo, Molecular thermodynamics of fluid-phase equilibria, 2nd edition, Prentice-Hall, Englewood Cliffs, N.J., 1986.

7 J.W. Gibbs, The scientific papers of J. Willard Gibbs, Vol. 1, pp. 55–371, Dover, New York, N.Y., 1961.

8 D.H. Everett, Pure Appl. Chem., 31 (1972): 579.

9 J.T. Davies and E.K. Rideal, Interfacial phenomena, 2nd edition, Academic Press, New York, N.Y., 1963.

10 G.L. Gaines jr., Insoluble monolayers at liquid–gas–interfaces, Interscience, New York, N.Y., 1966.

11 D.H. Everett, Trans. Faraday Soc., 60 (1964): 1803.

12 D.H. Everett, in: D.H. Everett (Editor), Colloid Science, Specialist Periodical Reports, Vol. 1, The Chemical Society, London, 1973, Chapter 2.

13 D.H. Everett, Trans. Faraday Soc., 61 (1965): 2478.

14 J.E. Lane, in: G.D. Parfitt and C.H. Rochester (Editors), Adsorption from solution at the solid/liquid interface, Academic Press, London, 1983, Chapter 2.

15 S.G. Ash, D.H. Everett and G.H. Findenegg, Trans Faraday Soc., 66, (1970): 708.

16 D.H. Everett and R.T. Podoll, in: D.H. Everett (Editor),, Colloid Science, Specialist Periodical Reports, The Chemical Society, London, Vol. 3, 1979, Chapter 2.

17 S. Sircar, J. Novosad and A.L. Myers, Ind. Eng. Chem. Fundam., 11 (1972): 249.
18 I. Langmuir, Am. Chem. Soc., 39 (1917): 1848.
19 B. Von Szyszkowski, Z. Phys. Chem., 64 (1908): 385.
20 J.H. Hildebrand, J.M. Prausnitz and R.L. Scott, Regular and related solutions, Van Nostrand Reinhold, New York, N.Y., 1970.
21 A.N. Frumkin, Z. Phys. Chem., 116 (1925): 466.
22 R.H. Fowler and E.A. Guggenheim, Statistical thermodynamics, Cambridge University Press, Cambridge, 1956, p. 426.
23 B.B. Damaskin, O.A. Petrii and V.V. Batrakof, Adsorption of organic compounds on electrodes (translated from Russian by E.B. Uvarov; R. Parsons, Editor), Plenum Press, New York, N.Y., 1971.
24 W.A. Steele, The interactions of gases with solid surfaces, Pergamon Press, Oxford (1974).
25 C. Minka and A.L. Myers, AIChE J., 19 (1973): 453.
26 P. Debye and E. Hückel, Physik Z., 24 (1923): 305.
27 S. Trasatti, in: J.O'M. Bockris, B.E. Conway and E. Yeager, (Editors), Comprehensive treatise of electrochemistry, Vol. 1: The double layer, Plenum Press, New York, N.Y., 1980, Chapter 2.
28 G. Gouy, J. Phys., 9 (1910): 457.
29 D.L. Chapman, Phil. Mag., 25 (1913): 475.
30 P.C. Hiemenz, Principles of colloid and surface chemistry, 2nd edition, Marcel Dekker, New York, N.Y., 1986.
31 R.J. Hunter, Foundations of colloid science, Clarendon Press, Oxford, 1987.
32 D.C. Grahame, Chem. Rev., 44 (1947): 441.
33 R. Reeves, in: J.O'M. Bockris, B.E. Conway, E. Yeager (Editors), Comprehensive treatise of electrochemistry, Vol. 1: The double layer, Plenum Press, New York, N.Y., 1980, Chapter 3.
34 O. Stern, Z. Elektrochem., 30 (1924): 508.
35 L.K. Koopal and W.H. Van Riemsdijk, J. Colloid Interface Sci., 128 (1989): 188.
36 J.O'M. Bockris, M.A. Devanathan and K. Muller, Proc. R. Soc. London, Ser. A., 274 (1963): 55.
37 M.A. Habib and J. O'M Bockris, in: J.O'M. Bockris, B.E. Conway and E. Yeager (Editors), Comprehensive treatise of electrochemistry, Vol. 1: The double layer, Plenum Press, New York, N.Y., 1980, Chapter 4.
38 M.J. Sparnaay, The electrical double layer, Pergamon Press, Oxford, 1972.
39 T.W. Healy and L.R. White, Adv. Colloid Interface Sci., 9 (1978): 303.
40 R.O. James and G.A. Parks, in: E. Matijevic (Editor), Surface and Colloid Science, Vol. 12, Plenum Press, New York, N.Y., 1982, Chapter 2.
41 C.W. Davies, Ion association, Butterworths, London, 1962.
42 R.J. Hunter, Zeta potential in colloid science, principles and applications, Academic Press, London, 1981.
43 R.O. James, J.A. Davis and J.O.Leckie, J. Colloid Interface Sci., 65 (1978): 331.
44 I.H. Harding and T.W. Healy, J. Colloid Interface Sci., 89 (1982): 185.
45 I.H. Harding and T.W. Healy, J. Colloid Interface Sci., 107 (1985): 382.
46 J. Westall and H. Hohl, Adv. Colloid Interface Sci., 12 (1980): 265.
47 P.W. Schindler and H. Gamsjäger, Kolloid Z. Z. Polym., 250 (1972): 759.
48 P.W. Schindler, in: H. Sigel (Editor), Metal ions in biological systems, Vol. 18: Circulation of metal ions in the environment, Marcel Dekker, New York, N.Y., 1984, Chapter 7.
49 H. Hohl and W. Stumm, J. Colloid Interface Sci., 55 (1976): 281.
50 W. Stumm, H. Hohl and F. Dalang, Croat. Chem. Acta, 48 (1976): 491.
51 P.W. Schindler and W. Stumm, in: W. Stumm (Editor), Aquatic surface chemistry, J. Wiley, New York, N.Y., 1987, Chapter 4.
52 C.P. Huang and W. Stumm, J. Colloid Interface Sci., 43 (1973): 409.

53 C.P. Huang, in: M.A. Anderson and A.J. Rubin (Editors), Adsorption of inorganics at solid/liquid interfaces, Ann Arbor Science, Ann Arbor, Mich., 1981, Chapter 5.
54 D.A. Dzombak, Towards a uniform model for the sorption of inorganic ions on hydrous oxides, Ph.D. Thesis, Massachusetts Institute of Technology, Cambridge, 1986.
55 D.A. Dzombak and F.M.M. Morel, Surface complexation modeling hydrous ferric oxide, Wiley, New York, N.Y., 1990.
56 L.K. Koopal, W.H Van Riemsdijk. and M.G. Roffey, J. Colloid Interface Sci., 118 (1987): 117.
57 T. Hiemstra, W.H. Van Riemsdijk and G.H. Bolt, J. Colloid Interface Sci., 133 (1989): 91.
58 T. Hiemstra, J.C.M. De Wit and W.H. Van Riemsdijk, J. Colloid Interface Sci., 133 (1989): 105.
59 S. Levine and A.L. Smith, Disc. Faraday Soc., 52 (1971): 290.
60 D.E. Yates, S. Levine and T.W. Healy, Trans. Faraday Soc., 70 (1974): 1807.
61 D.E. Yates, The structure of the oxide/aqueous electrolyte Interface, Ph.D. Thesis, University of Melbourne, Melbourne, 1975.
62 D. Chan, J.W. Perram, L.R. White and T.W. Healy, J. Chem. Soc. Faraday Trans., 1, 71, (1975): 1046.
63 J.A. Davis, R.O. James and J.O. Leckie, J. Colloid Interface Sci., 63 (1978): 480.
64 R.O. James, in: M.A. Anderson and A.J. Rubin (Editors), Adsorption of inorganics at solid/liquid interfaces, Ann Arbor Science, Ann Arbor, Mich., 1981, Chapter 6.
65 J. Lyklema, Kolloid Z. Z. Polym., 175 (1961): 129.
66 B.H. Bijsterbosch and J. Lyklema, Adv. Colloid Interface Sci., 9 (1978): 147.
67 W.H. Van Riemsdijk, G.H. Bolt, L.K. Koopal and J. Blaakmeer, J. Colloid Interface Sci., 109 (1986): 219.
68 W.H. Van Riemsdijk, J.C.M. De Wit, L.K. Koopal and G.H. Bolt, J. Colloid Interface Sci., 116 (1987): 511.
69 P. Jones and J.A. Hockey, Trans Faraday Soc., 67 (1971): 2679.
70 G.H. Bolt and W.H. Van Riemsdijk, in: G.H. Bolt (Editor), Soil chemistry, B: Physico-chemical models, 2nd edition, p. 459. Elsevier, Amsterdam, 1982.
71 W.H. Van Riemsdijk, L.K. Koopal and J.C.M. De Wit, Neth. J. Agric. Sci., 35 (1987): 241.
72 T. Hiemstra, W.H. Van Riemsdijk and M.G.M.Bruggenwert, Neth. J. Agric. Sci., 35 (1987): 281.
73 A.W.M. Gibb and L.K. Koopal, J. Colloid Interface Sci., 134 (1990): 122.
74 L. Pauling, J. Am. Chem. Soc., 51 (1929): 1010.
75 N.H.G. Penners, L.K. Koopal and J. Lyklema, Colloids Surf., 21 (1986): 457.
76 S. Ardizonne, P. Siviglia and Trasatti, S., J. Electroanal. Chem., 122 (1981): 395; P. Siviglia, A. Daghetti and S. Trasatti, Colloids Surf., 7 (1983): 15.
77 L. Bousse, N.F. De Rooij and P. Bergveld, Surf. Sci., 135 (1983): 479.
78 L.G.J. Fokkink, A. De Keizer, J.M. Kleijn and J. Lyklema, J. Electroanal. Chem., 208 (1986): 401.
79 L.G.J. Fokkink, A. De Keizer and J. Lyklema, J. Colloid Interface Sci., 118 (1987): 454.
80 P.W. Schindler, in: M.A. Anderson and A.J. Rubin (Editors), Adsorption of inorganics at solid/liquid interfaces, Ann Arbor Science, Ann Arbor, Mich., 1981, Chapter 1.
81 P.W. Schindler, B. Fürst, R. Dick and P.U. Wolf, J. Colloid Interface Sci., 55 (1976): 469.
82 C.P. Huang, Y.S. Hsieh, S.W. Park, M. Ozden, A.R. Bowers and H.A. Elliot, in: J.W. Patterson and R. Passino (Editors), Metals speciation, separation and recovery, Lewis Publishers, Michigan, 1987, p. 437.
83 J.A. Davis and J.O. Leckie, J. Colloid Interface Sci., 67 (1978): 90.
84 J.A. Davis and J.O. Leckie, J. Colloid Interface Sci., 74 (1980): 32.
85 K.F. Hayes and J.O. Leckie, in: J.A. Davis and K.F. Hayes (Editors), Geochemical processes at mineral surfaces, Am. Chem. Soc., Washington, D.C., 1986, p. 114.
86 K.F. Hayes and J.O. Leckie, J. Colloid Interface Sci., 115 (1987): 564.
87 K.F. Hayes, C. Papelis and J.O. Leckie, J. Colloid Interface Sci., 125 (1988): 717.

88 M.M. Benjamin, J.O. Leckie, J. Colloid Interface Sci., 79 (1981): 209.
89 J.W. Bowden, A.H. Posner and J.P. Quirk, Austr. J. Soil Res., 15 (1977): 121.
90 L.G.J. Fokkink, A. De Keizer and J. Lyklema, J. Colloid Interface, Sci., 135 (1990): 118.
91 H. Motschi, Colloids Surf., 9 (1984): 333; H. Motschi, in: W. Stumm (Editor), Aquatic surface chemistry, J. Wiley, New York, N.Y., 1987, Chapter 5.
92 M.B. McBride, Advances in Soil Science, Vol. 10, Springer Verlag, New York, N.Y., 1989, p. 1.
93 R.O. James and T.W. Healy, J. Colloid Interface Sci., 40 (1972): 53.
94 M.C. Fuerstenau and K.E. Han, in: P. Somasundaran and B.M. Moudgil (Editors), Reagents in mineral technology, Surfactant Science Series, Vol. 27, Marcel Dekker, New York, N.Y., 1988, Chapter 13.
95 D.D. Hansmann and M.A. Anderson, Environ. Sci. Technol., 19 (1985): 544.
96 R.O. James and T.W. Healy, J. Colloid Interface Sci., 40 (1972): 42, 65.
97 G. Sposito, The surface chemistry of soils, Oxford University Press, New York, N.Y., 1984.
98 F.M.M. Morel, J.C. Westall and J.G. Yeasted, in: M.A. Anderson and A.J. Rubin (Editors), Adsorption of inorganics at solid/liquid Interfaces, Ann Arbor Science, Ann Arbor, Mich., 1981, Chapter 7.
99 F.J. Hingston, in: M.A. Anderson and A.J. Rubin (Editors), Adsorption of inorganics at solid/liquid Interfaces, Ann Arbor Science, Ann Arbor, Mich., 1981, Chapter 2.
100 D.G. Kinniburgh and M.L. Jackson, in: M.A. Anderson and A.J. Rubin (Editors), Adsorption of inorganics at solid/liquid Interfaces, Ann Arbor Science, Ann Arbor, Mich., 1981, Chapter 3.
101 R.B. Corey in M.A. Anderson and A.J. Rubin (Editors), Adsorption of inorganics at solid/liquid Interfaces, Ann Arbor Science, Ann Arbor, Mich., 1981, Chapter 4.
102 K.J. Farley, D.A. Dzombak and F.M.M. J. Morel, Colloid Interface Sci., 106 (1985): 226.
103 P.J. Flory, Principles of polymer chemistry, Cornell University Press, Ithaca, N.Y., London, 1953.
104 M.L. Huggins, Ann. N.Y. Acad. Sci., 43 (1942): 1.
105 L.K. Koopal and J. Ralston, J. Colloid Interface Sci., 112 (1986): 362.
106 B. Kronberg, J. Colloid Interface Sci., 96 (1983): 55.
107 B. Kronberg and P. Stenius, J. Colloid Interface Sci., 102 (1984): 410.
108 B. Kronberg, P. Stenius and Y. Thorssell, Colloids Surf., 12 (1984): 113.
109 L.K. Koopal, G.T. Wilkinson and J. Ralston, J. Colloid Interface Sci., 126 (1988): 493.
110 J.H. Hildebrand, J. Chem. Phys., 15 (1947): 225.
111 R.N. Lichtenthaler, D.S. Abrams and J. Prausnitz, Can. J. Chem., 51 (1973): 3071.
112 M.D. Donohue and J. Prausnitz, Can. J. Chem., 53 (1975): 1586.
113 P. Somasundaran, T.W. Healy and D.W. Fuerstenau, J. Phys. Chem., 68 (1964): 3562.
114 K. Osseo-Asare and D.W. Fuerstenau, Croat. Chem. Acta, 45 (1973): 149.
115 D.B. Hough and H.M. Rendall, in: G.D. Parfitt and C.H. Rochester (Editors), Adsorption from solution at the solid/liquid interface, Academic Press, London, 1983, Chapter 6.
116 B.M. Moudgil, H. Soto and P. SomasundaraN, in: P. Somasundaran and B.M. Moudgil (Editors), Reagents in mineral technology, Surfactant Science Series, Vol. 27, Marcel Dekker, New York, N.Y., 1988, Chapter 3.
117 L.K. Koopal and L. Keltjens, Colloids Surf., 17 (1986): 371.
118 A. Silberberg, J. Colloid Interface Sci., 38, (1972): 217; J. Chem. Phys., 48 (1968): 2835; J. Chem. Phys., 46 (1967): 1105.
119 C.A.J. Hoeve, J. Polym. Sci., Polym. Symp., 61 (1977): 389; J. Polym. Sci. (C), 34 (1971): 1; J. Polym. Sci. (C), 30 (1970): 361; J. Chem. Phys., 44 (1966): 1505.
120 J.M.H.M. Scheutjens and G.J. Fleer, J. Phys. Chem., 83 (1979): 1619; J. Phys. Chem., 84 (1980): 178; Adv. Colloid Interface Sci., 16 (1982): 341.
121 R.J. Roe, J. Chem. Phys., 60 (1974): 4192.
122 G.J. Fleer and J. Lyklema, in: G.D. Parfitt and C.H. Rochester (Editors), Adsorption from solution

at the solid/liquid interface, Academic Press, London, 1983, Chapter 4.
123 G.J. Fleer, in: P. Somasundaran and B.M. Moudgil (Editors), Reagents in mineral technology, Surfactant Science Series, Vol. 27, Marcel Dekker, New York, N.Y., 1988, Chapter 4.
124 B. Van Lent and J.M.H.M. Scheutjens, Macromolecules, 22 (1989): 1931.
125 B. Van Lent and J.M.H.M. Scheutjens, J. Phys. Chem., 94 (1990): 5033.
126 O.A. Evers, J.M.H.M. Scheutjens and G.J. Fleer, Macromolecules, (1991), in press.
127 O.A. Evers, J.M.H.M. Scheutjens and G.J. Fleer, J. Chem. Soc. Faraday Trans. 1, 86 (1990): 1355..
128 H.A. Van der Schee and J. Lyklema, J. Phys. Chem., 88 (1984): 6661.
129 J. Papenhuijzen, H.A. Van der Schee and G.J. Fleer, J. Colloid Interface Sci., 104 (1985): 540.
130 O.A. Evers, G.J. Fleer, J.M.H.M. Scheutjens and J. Lyklema, J. Colloid Interface Sci., 111 (1986): 446.
131 M.R. Böhmer, O.A. Evers and J.M.H.M. Scheutjens, Macromolecules, 23 (1990): 2288..
132 L.K. Koopal and M.R. Böhmer, in: A. Mersmann and S.E. Scholl (Editors), Fundamentals of Adsorption, Vol. III, Engineering Foundation, Am. Inst. Chem. Eng., New York, N.Y., 1991, p. 435.
133 M.R. Böhmer and L.K. Koopal, Langmuir, 6 (1990): 1478.
134 E.A. DiMarzio, J. Chem. Phys., 42 (1965): 2101.
135 R.J. Rubin, J. Chem. Phys., 43 (1965): 2392.
136 J.M.H.M. Scheutjens, F.A.M. Leermakers, N.A.M. Besseling and J. Lyklema, in: K.L. Mittal (Editor), Surfactants in solution, Modern applications, Plenum Press, New York, N.Y., Vol. 7, 1990, p. 25.
137 T. Cosgrove, T. Heath, B. Van Lent, F. Leermakers and J. Scheutjens, Macromolecules, 20 (1987): 1692.
138 F.A.M. Leermakers, J.M.H.M. Scheutjens and J. Lyklema, Biophys. Chem., 19 (1983): 352.
139 F.A.M. Leermakers and J.M.H.M. Scheutjens, J. Chem. Phys., 88 (1988): 3264; J. Chem. Phys., 89 (1988): 6912.
140 F.A.M. Leermakers, P.P.A.M. Van der Schoot, J.M.H.M. Scheutjens and J. Lyklema, in: K.L. Mittal (Editor), Surfactants in solution, Modern applications, Plenum Press, New York, N.Y., Vol. 7, 1990, p. 43.
141 J.M.H.M. Scheutjens and G.J. Fleer, Macromolecules, 18 (1985): 1882.
142 G.J. Fleer, J.M.H.M. Scheutjens and M.A. Cohen Stuart, Colloids Surf., 31 (1988): 1.
143 K.G. Barnet, T. Cosgrove, T.L. Crowley, Th.F. Tadros and B. Vincent, in: Th.F. Tadros (Editor), The effect of polymers on dispersion properties, Academic Press, London, 1982, p. 183.
144 T. Cosgrove, T.G. Heath, K. Ryan and B. Van Lent, Polym. Comm., 28 (1987): 64.
145 L.K. Koopal, V. Hlady and J. Lyklema, J. Colloid Interface Sci., 121 (1988): 49.
146 T. Cosgrove, B. Vincent, T.L. Crowley and Cohen M.A. Stuart, in: Polymer adsorption and dispersion stability, ACS Symp., Ser. 240 (1983): 147.
147 M.A. Cohen Stuart, F.H.W.H. Waajen, T. Cosgrove, B. Vincent and T.L. Crowley, Macromolecules, 17 (1984): 1825.
148 J.L. Anderson and J.O. Kim, J. Chem. Phys., 86 (1987): 5163.
149 G.J. Fleer and J.M.H.M. Scheutjens, Croat. Chem. Acta, 60 (1987): 477.
150 J.A. Kitchener, Brit. Polym. J., 4 (1972): 217.
151 B. Vincent, Adv. Colloid Interface Sci., 4 (1974): 193.
152 D.H. Napper, in: Colloidal dispersions, Spec. Publ. R. Chem. Soc., Vol. 43, 1982, p. 99.
153 J. Klein, Adv. Colloid Interface Sci., 16 (1982): 101.
154 J. Israelachvili, M. Tirrell, J. Klein and Y. Almog, Macromolecules, 17 (1984): 204.
155 J. Klein and P.F. Luckham, Nature (London), 308 (1984): 836.
156 Y. Almog and J. Klein, J. Colloid Interface Sci., 106 (1985): 33.
157 J. Marra and H. Christenson, J. Phys. Chem., 93 (1989): 7180.

158 Th. Götze and H. Sonntag, Colloids Surf., 31 (1988): 181.
159 E.G.M. Pelssers, M.A. Cohen Stuart and G.J. Fleer, Colloids Surf., 38 (1989): 15.
160 E.G.M. Pelssers, M.A. Cohen Stuart and G.J. Fleer, J. Chem. Soc. Faraday Trans. 1, 86 (1990): 1355.
161 B. Van Lent, R. Israels, J.M.H.M. Scheutjens and G.F. Fleer, J. Colloid Interface Sci., 137 (1990): 380.
162 S. Patel, M. Tirrell and G. Hadziioannou, Colloids Surf., 31 (1988): 157.
163 Marra, J. and M.L. Hair, Colloids Surf., 34 (1989): 215.
164 R.E. Felter and L.N. Ray, J. Colloid Interface Sci., 32 (1970): 349.
165 M.A. Cohen Stuart, J.M.H.M. Scheutjens and G.J. Fleer, J. Polym. Sci., Polym. Phys. Ed., 12 (1980): 559.
166 L.K. Koopal, J. Colloid Interface Sci., 83 (1981): 116.
167 J.M.H.M. Scheutjens and G.J. Fleer, in: Th.F. Tadros (Editor), The effect of polymers on the dispersion properties, Academic Press, London, 1982, p. 145.
168 V. Hlady, J. Lyklema and G.J. Fleer, J. Colloid Interface Sci., 87 (1982): 395.
169 M.A. Cohen Stuart, G.J. Fleer and J.M.H.M. Scheutjens, J. Colloid Interface Sci., 97 (1984): 515; idem, 97 (1984): 526.
170 G.P. Van der Beek, M.A. Cohen Stuart, G.J. Fleer and J.E. Hofman, Langmuir, 5 (1989)1180.
171 F.Th. Hesselink, J. Electroanal. Chem., 37 (1977): 317; J. Colloid Interface Sci., 60 (1977): 448.
172 M.A. Cohen Stuart, J. Phys. France, 49 (1988): 1001.
173 J. Blaakmeer, M.R. Böhmer, M.A. Cohen Stuart and G.J. Fleer, Macromolecules, 23 (1990): 2301.
174 T. Afshar-Rad, A.I. Bailey, P.F. Luckham, W. MacNaughtan, and D. Chapman, Colloids Surf., 31 (1988): 125.
175 J. Marra and M.L. Hair, J. Phys. Chem., 92 (1988): 6044.
176 M.J. Schick and F.M. Fowkes (Consulting Editors), Surfactant Science Series, Marcel Dekker, New York and Basel.
177 Th.F. Tadros (Editor), Surfactants, Academic Press, London, 1984.
178 J.S. Clunie and B.T. Ingram, in: G.D. Parfitt and C.H. Rochester (Editors), Adsorption from solution at the solid/liquid interface, Academic Press, London, 1983, Chapter 3.
179 B. Dobias, in: C.K. Jørgensen (Editor), Structure and bonding, Springer, Berlin-Heidelberg, 1984, p. 92.
180 A.N. Clarke and D.J. Wilson, Foam flotation: theory and applications, Marcel Dekker, New York, N.Y., 1983, Chapter 4.
181 J.M. Cases, Bull. Minéral., 102 (1979): 684.
182 J.M. Cases, G. Goujon and S. Smani, AIChE. Symp. Ser., 71 (1975): 100.
183 J.F. Scamehorn, R.S. Schechter and W.H. Wade, J. Colloid Interface Sci., 85 (1982): 463.
184 J.H. Harwell, J.C. Hoskins, R.S. Schechter and W.H. Wade, Langmuir, 1 (1985): 251.
185 S. Chander, D.W. Fuerstenau and D. Stigter, in: R.H. Ottewill, C.H. Rochester and A.L. Smith (Editors), Adsorption from solution, Academic Press, London, 1983, p. 197.
186 T. Gu, Y. Gao and L. He, J. Chem. Soc. Faraday Trans. 1, 84 (1988): 4471.
187 B-Y. Zhu and T. Gu, J. Chem. Soc. Faraday Trans. 1, 85 (1989): 3813; B-Y. Zhu, T.Gu. and X. Zhao, J. Chem. Soc. Faraday Trans. 1, 85 (1989): 3819.
188 A.M. Gaudin and D.W. Fuerstenau, Trans. AIME, 202 (1955): 958.
189 N.A. Klimenko, Kolloidn. Zh., 40 (1978): 1105.
190 N.A. Klimenko, Kolloidn. Zh., 41 (1979): 781.
191 A. de Keizer, M.R. Böhmer, T. Mehrian and L.K. Koopal, Colloids Surf., 51 (1990): 339.
192 A. Van den Boomgaard, The effect of electrolytes on emulsions stabilized by nonionic surfactants, Ph.D. Thesis, Wageningen Agricultural University, Wageningen, The Netherlands, 1985.
193 T.C. Amu, Polymer, 23 (1982): 1775.

194 P. Levitz, H. Van Damme and D. Keravis, J. Phys. Chem., 88 (1984): 2228.
195 P. Levitz and H. Van Damme, J. Phys. Chem., 90 (1986): 1302.
196 B. Kronberg, P. Stenius and G. Ingeborn, J. Colloid Interface Sci., 102 (1984): 418.
197 M.R. Böhmer and L.K. Koopal, Langmuir (to be published).
198 M.R. Böhmer, L.K. Koopal and J. Lyklema, J. Phys. Chem., accepted (1991).

Chapter 3

Interparticulate forces

R.M. PASHLEY

Introduction

Once it was recognised (by Graham in the mid 19th century) that a non-molecular (crystalloid), colloidal solution could be formed by dispersion of one phase in another, it was also immediately obvious that the solution could be destroyed by altering conditions so as to cause coagulation. This phase-change can, in general, be easily described in terms of attractive and repulsive contributions to the interaction between particles of the dispersed phase. The same description also, of course, applies to intermolecular forces, where attractive forces cause condensation to more condensed states of matter.

The most important property, then, of the colloidal state must be this interaction potential and over the last 100 years the search for a detailed understanding of this interaction has been vigorously sought.

In 1892 Linder and Picton [1] demonstrated that in aqueous solutions, colloidal particles of one type move to one electrode under the influence of an applied electric field. The charged nature of the particles thus gave the first explanation of how the colloidal solution could be stabilised against the effect of the ubiquitous, attractive Van der Waals forces. The 1882 observations by Schulze [2] on the enhanced coagulating powers of multivalent electrolytes also supported the concept that it is the electrical nature of these colloids that determines their stability. These ideas led Hardy [3] and Freundlich [4] to postulate that colloids are coagulated at their iso-electric point. This was later (1912–1915) refined by Ellis [5] and Powis [6] who introduced the concept of a critical zeta (ζ) potential, which is the magnitude of the electrostatic potential at the colloid surface (measured by an electrophoretic process) below which the colloid is precipitated. The value ζ critical was found to be typically about 30 mV for a "lyophobic" colloid. As early as 1932 Kallmann and Willstätter [7] suggested that the total interaction between colloid particles could be obtained on the basis of electrostatic double-layer and dispersion (VDW) forces.

Earlier, Gouy [8] and Chapman [9] had developed a theory of the ion distribution in solution next to a charged surface.

At this point it is perhaps worth digressing to look at a problem in terminology for the two main categories of colloids: lyophobic and lyophilic. As will become clear later in this chapter the differences between these two types of colloids have now become less obvious but for the moment we will stick to the original definitions which are based on experimental observations. Thus, a lyophobic colloidal system refers to one in which work has to be done to produce the dispersion (e.g. an aqueous silica sol), whereas a lyophilic colloid forms a solution spontaneously (e.g. surfactants and some proteins). The problem with this nomenclature arises when we examine the nature of the colloid surface in each case, as we will see later.

In 1938 Irving Langmuir [10] made a major step forward in the understanding of colloidal stability by deriving an approximate analytic equation for the repulsive pressure developed in the diffuse electrical double-layer between two charged, flat surfaces. Schofield [11] then used this result to explain the water wetting films on mica and glass measured earlier by Derjaguin and Kussakov [12]. These forces, which were clearly responsible for determining the thickness of wetting films, must also give rise to a repulsive force between identical colloid particles preventing coagulation.

DLVO theory

A comprehensive theory of the interaction potential between colloidal particles was put together by Derjaguin and Landau [13] and Verwey and Overbeek [14] during the second world war. This 'DLVO theory' combined the electrostatic repulsive forces with the attractive Van der Waals forces between spherical particles, which had been developed in the 1930's by London [15], Bradley [16], de Boer [17] and Hamaker [18]. In 1937 Hamaker had also analysed colloidal interactions using these forces [19].

Let us now look at this theory in more detail. It turns out that although calculation of the Van der Waals force between spherical particles is mathematically complex the resulting equation (accurate for most purposes) is simple and has the form:

$$V_A = -A_{121}\frac{r}{12d} \qquad (r \gg d) \tag{1}$$

where V_A is the interaction energy between spheres, r is the radius of either of two equal spheres and d is the distance of closest approach between the spheres (see Figure 1). The complex part of the calculation is involved in determining the Hamaker constant A_{121} from the dielectric properties of the media 1 and 2 [20]. However, tables of these values for most systems of interest are available [20] and for most purposes in colloid science it is reasonable to make the assumption that

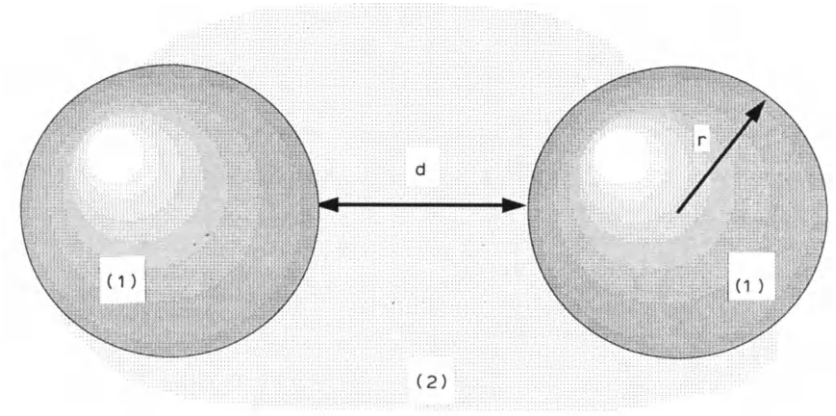

Fig. 1. Interaction between two identical colloid spheres.

the Hamaker constant is not a function of distance. Thus, for example, the Hamaker constant for the common quartz/water/quartz system is 1.0×10^{-20} J, which allows a fairly accurate calculation of the Van der Waals attraction between two colloidal size quartz particles in water.

For any given colloidal system, the Van der Waals force is essentially independent of almost any changes we may wish to make to the solution (e.g. by addition of electrolyte). Even the adsorption of a surfactant monolayer onto the particle surface will have only a slight effect on the Van der Waals attraction [21]. This suggests that in order to change the stability of a colloidal solution we will have most effect by altering the electrostatic double-layer forces in the system, which is indeed the case. Once again, the mathematical problems involved in calculating the double-layer force between colloidal particles are rather serious and numerical approximation methods have usually been applied. It is possible to obtain an approximate, analytic equation which shows all the main features of the exact solution and so we will derive this result here.

The basic equations for the electrostatics next to a surface are derived from Maxwell's equations, which can be simplified for the case of a potential decay away from a flat, charged wall (see Figure 2). The decay in electrostatic potential away from a surface is contained in the fundamental equation (S.I. units):

$$\frac{d^2\psi(x)}{dx^2} = -\frac{\rho(x)}{\varepsilon_o \varepsilon_r} \tag{2}$$

where $\psi(x)$ and $\rho(x)$ are the electrostatic potential and charge density at distance x away from the charged surface, ε_o is the permittivity of free space and ε_r the dielectric constant of the medium. In order to determine $\rho(x)$ we can apply the Boltzmann distribution equation to any ion contributing to the total charge density at x. Thus, for an ion i of charge $Z_i|q_e|$ (where $|q_e|$ is the positive value of the

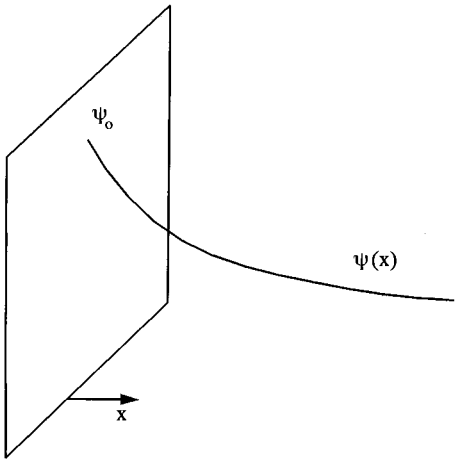

Fig. 2. Electrostatic potential decay away from a flat surface immersed in electrolyte solution..

electronic charge) and bulk concentration $\rho_i(B)$ the concentration at a distance x from the surface must be given by:

$$\rho_i(x) = \rho_i(B) \exp\left\{-\frac{Z_i|q_e|\psi(x)}{kT}\right\} \tag{3}$$

It therefore follows that the total charge density at x:

$$\rho(x) = \Sigma_i Z_i|q_e|\rho_i(x)$$

$$= \Sigma_i Z_i|q_e|\rho_i(B) \exp\left\{-\frac{Z_i|q_e|\psi(x)}{kT}\right\} \tag{4}$$

hence, substitution in equation (2) gives the important Poisson-Boltzmann (P-B) equation used in the Gouy-Chapman theory of the diffuse electrical double layer:

$$\frac{d^2\psi(x)}{dx^2} = -\left[\frac{|q_e|}{\varepsilon_o\varepsilon_r}\right] \Sigma_i Z_i \rho_i(B) \exp\left\{-\frac{Z_i|q_e|\psi(x)}{kT}\right\} \tag{5}$$

This equation can be substantially simplified by placing the restriction of only using symmetrical electrolytes (e.g. 1:1, 2:2) and introducing the Debye length:

$$\kappa^{-1} = \left[\frac{\varepsilon_o\varepsilon_r kT}{2|q_e|^2 Z^2 \rho(B)}\right]^{1/2} \tag{6}$$

where Z is the valency of the symmetrical electrolyte and ρ(B) the bulk concentration of the electrolyte. Thus, equation (5) becomes:

$$\frac{d^2y}{dX^2} = \sinh y \tag{7}$$

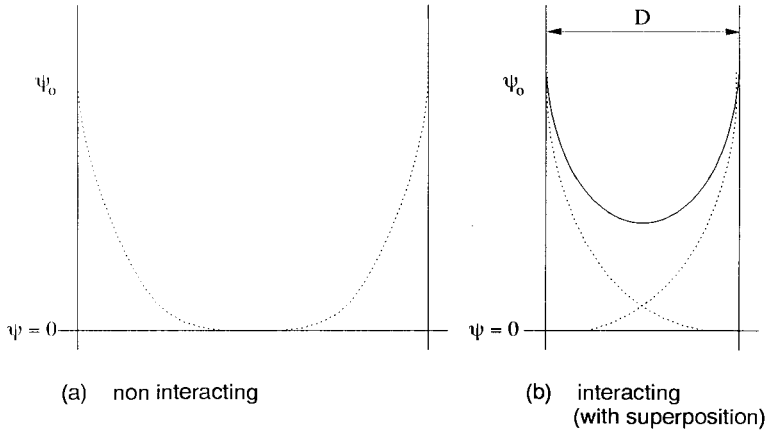

Fig. 3. Electrostatic potential profiles for two interacting flat surfaces.

where the scaled distance $X = \kappa x$, and y is the dimensionless potential given by $Z|q_e|\psi(x)/kT$.

Double integration of equation (7) with the boundary conditions $x \rightarrow \infty$, $dy/dX \rightarrow 0$, $y \rightarrow 0$ and $y = y_o$ at $X = 0$ gives the exact, analytic result:

$$y = 2 \ln_e \left[\frac{1 + \gamma \exp(-X)}{1 - \gamma \exp(-X)}\right] \tag{8}$$

where:

$$\gamma = \frac{[\exp(y_o/2) - 1]}{[\exp(y_o/2) + 1]}$$

This equation allows us to calculate exactly the decay in electrostatic potential away from a flat, charged surface of potential ψ_o. This decay in potential is shown schematically in Figure 3 for two facing, charged surfaces. In case 3a, the surfaces do not "see" each other and are not interacting, whereas in case 3b the diffuse layers overlap and an interaction occurs.

If we now make the superposition approximation, that the resulting potential (in case b) is simply the sum of the potentials due to each surface when the other is not present we can easily calculate the potential at the mid-plane between the surfaces (ψ_m or y_m). It turns out that this assumption is reasonable for low potentials (<25 mV) and hence this procedure produces an equation known as the "weak overlap approximation". Since we are only using equation (8) at large separations (i.e. where the potentials are low) we can expand and simplify the equation (for $X \gg 1$) to obtain:

$$y \sim 4\gamma \exp(-X) \tag{9}$$

and hence:

$$y_m \sim 8\gamma \exp\left(-\frac{D\kappa}{2}\right) \tag{10}$$

where D is the separation distance between the surfaces. Having obtained $y_m = f(D)$ it is a relatively simple problem to relate y_m to the repulsive pressure between the surfaces. This is because at the mid-point between the surface there is no electric field and so we only need consider the osmotic pressure at this plane. The osmotic pressure is given simply by:

$$P_{os} = nkT \tag{11}$$

where n is the solute concentration. Since we know ψ_m (through y_m) we can easily calculate the total solute (counterions and co-ions) concentration at the mid-plane and hence the osmotic pressure relative to the bulk concentration. The osmotic pressure difference between the mid-plane and the bulk solution is equal to the repulsive pressure (P) between the surfaces and is given (for symmetrical electrolytes) by:

$$P = 2\rho(B)kT\{\cosh(y_m) - 1\} \tag{12}$$

Now, this result can also be simplified since $y_m \ll 1$ and the cosh function can then be approximated to give:

$$P = \rho(B)kTy_m^2 \tag{13}$$

Then, substitution of y_m gives:

$$P = 64\rho(B)kT\gamma^2 \exp(-\kappa D) \tag{14}$$

which shows that the repulsive pressure decays exponentially with distance with a decay length equal to the Debye length. We can now integrate the pressure to obtain the corresponding interaction energy V_R between the surfaces:

$$V_R = -\int_{\infty}^{D} P \, dD$$

$$\therefore \quad V_R = \left[\frac{64\rho(B)kT}{\kappa}\right]\gamma^2 \exp(-\kappa D) \tag{15}$$

Equation (15) is known as the weak-overlap approximation and is accurate for any surface potential but only at large separations where the interaction is weak.

For the common case of colloidal particles of radius (r) much larger than the range of the double layer force (i.e. $\kappa r \gg 1$) we can use the Derjaguin approximation [22] to obtain the equivalent interaction energy between two spheres:

$$V_S = \left[\frac{64\pi r\rho(B)kT\gamma^2}{\kappa^2}\right]\exp(-\kappa H) \tag{16}$$

where H is the distance of closest approach between the spheres.

The repulsive and attractive terms in equations (1) and (16) can now be combined to give the total interaction potential between two colloidal particles. Several typical cases are shown in Figure 4. The solution is (meta-) stable if the repulsive barrier is above about 10 kT. In all cases at short-range, the Van der Waals attractive force will dominate and pull the particles (if smooth) into an almost infinitely deep primary minimum. However, it is also possible to obtain a secondary minimum (see Figure 4b) from which re-dispersal should be possible (e.g. by diluting the electrolyte solution).

The unique case in Figure 4c was used by Verwey and Overbeek [14] to theoretically derive the experimental Schulze-Hardy rule, where the critical coagulation concentration (c.c.c.) was found to be inversely proportional to the sixth power of the valency of the counterion. The combination of equations (1) and (16) with the additional conditions that $\gamma = 1$ and $dV/dH = 0$ at $H = 0$ at the critical coagulation condition does indeed give a value of the c.c.c. proportional to $1/Z^6$. However, to obtain this result the surfaces were assumed to have a very high potential (i.e.

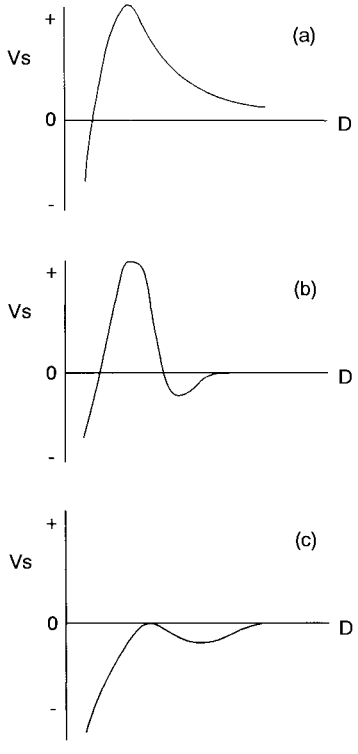

Fig. 4. Interaction energy (V_S) curves for two spherical colloids separated by distance D. The strength of the electrostatic repulsion decreases from (a) to (c).

$\gamma = 1$) which is quite contrary to widespread observation that coagulation occurs under low potential conditions. If a similar procedure is followed for the more realistic low potential (i.e. linear approximation) case it is found that the predicted c.c.c. $\alpha(1/Z^2)$.

The problems with this type of approach to coagulation arise mainly because it is implicitly assumed that coagulation is caused by a decrease in Debye length or range of the double-layer force by adding electrolyte. The fact is that for most colloids the surface potential ψ_o is substantially altered by the electrolyte both by specific ion adsorption and by screening effects. Indeed, the low potential approximation leads to an equation of the form: c.c.c. $\alpha(\psi_o^4/Z^2)$, which has a strong surface potential dependence, as expected. Closer examination of a wide range of colloidal systems also shows up many exceptions to the Schulze-Hardy rule. In addition, coagulation data obtained in trivalent ion electrolytes must be treated with caution because of the extensive hydrolysis which occurs and which can give rise to significant adsorption. As we shall see later, a complete double-layer model including ion-adsorption/regulation and screening effects must be used to accurately describe electrostatic interactions.

Structural forces

Although, many colloidal systems are clearly stabilised by electrostatic forces (and have therefore been labelled "electrocratic" by Freundlich [4]), there is a large body of observations which do not fit into the DLVO scheme of colloid stability. One common example is the repeptization process, which should not occur, according to theory, after coagulation into a primary minimum, although secondary minimum repeptization is possible. Dried clay minerals [23] and multibilayer phospholipids [24] often spontaneously swell in water, which also should not be possible according to this theory. The common silica sol does not coagulate at the isoelectric point or under conditions of high salt [25]. In addition, the coagulation behaviour of highly charged amphoteric latex particles (which are well-defined in terms of monodispersity and sphericity) in various electrolyte solutions cannot be explained by DLVO theory alone [26].

The dramatic prevention of bubble coalescence by the addition of electrolytes [27] is another good example of a simple observation in complete contradiction of DLVO theory. This process is important in froth flotation but is not at all understood.

One of the most elegant demonstrations of the inadequacy of this theory was presented by Laskowski and Kitchener [28]. They demonstrated that the conversion of water-wetting, clean hydrophilic silica to non-wetting, methylated silica could not be explained by DLVO forces because both double-layer and Van der Waals forces remained unaltered after the methylation process. That is, in both cases the theory predicts that a stable wetting film should be formed, which is not observed.

Observations of this nature have been made over at least the last fifty years and there have been two main explanations proposed. One of these is derived from the universal problem in surface chemistry of contamination. In many systems the surface area is low and the adsorption of some other unknown material may completely alter the surface interaction forces. However, this is not likely in very high surface area systems such as in swelling clays. A related problem is that of the colloid surface reacting with the dispersion fluid, as in the case of the proposed gel-layer formation on silica [29]. Of course, the polywater episode itself was caused by dissolution of silica and other materials from the surface of the capillaries in which this so-called new state of water was formed [30].

The other explanation is based on the reasonable supposition that the presence of a surface may alter the nature of the fluid in the regions close to the surface. Such an effect will give rise to solvation forces between colloids which are not described in the DLVO model. This idea goes back to at least 1876, when Clerk-Maxwell suggested [31] that the ordering of water molecules in thin films might extend several molecular diameters. This idea was also taken up by Hardy [32], but he anticipated that such effects might extend hundreds of microns, which is much further than work in recent years has indicated. Kruyt and Bungenberg de Jong [33] used the idea of solvation forces directly in a colloidal system to explain the stability of biocolloids.

Although indirect experimental evidence for these types of interparticle forces has been amassed over at least the last eighty years, it is only in the last ten years that theories of liquid structure have been developed and direct surface force measurements made of sufficient accuracy to test these theories. The author of this article has been involved in some of the experimental developments in this area, especially with the Surface Forces Apparatus (SFA) developed by Israelachvili and colleagues at the Australian National University in Canberra. The wide-ranging results on surface forces in aqueous solutions obtained in recent years using this technique are of direct, fundamental relevance to interparticulate forces and colloid stability and some of these results are presented here.

A diagram of the SFA is shown in Figure 5. In this technique multiple-beam interferometry is used to measure the distance between two, curved, macroscopic crystals of muscovite mica [34] down to an accuracy of about ± 0.02 nm (for very thin films).

The total interaction force between these molecularly smooth crystals is measured using a spring device, where the deformation of the spring gives the force down to a sensitivity of about 1 μN. Using this instrument it is possible to measure surface forces between molecularly smooth mica surfaces in a wide range of electrolyte, surfactant and polymer solutions as well as in non-aqueous liquids. In addition, the mica crystals can be coated to give hydrophobic [35] and lipid [36] bilayer surfaces and, more recently, metallic surfaces [37]. The technique has also been successfully used with thin sapphire crystals [38]. The surface forces measured

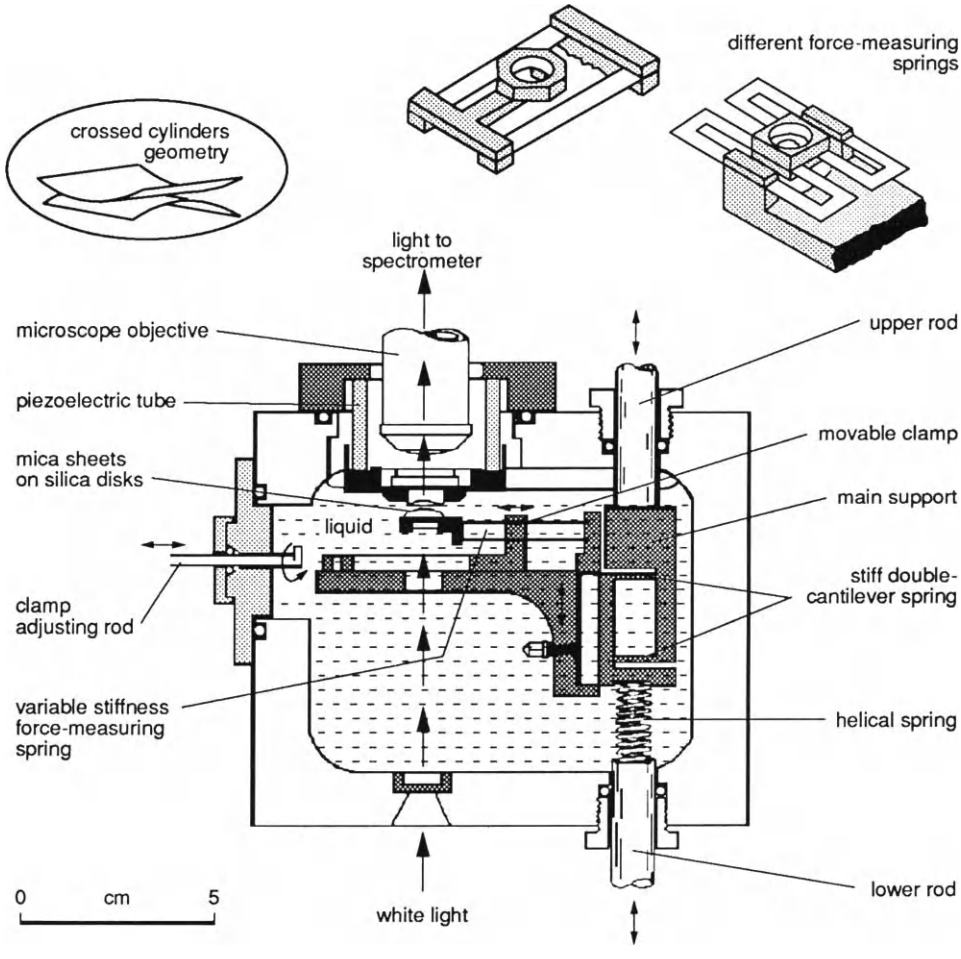

Fig. 5. Surface force apparatus (SFA) for directly measuring the total interaction forces between curved sheets of molecularly smooth muscovite mica.

in these various systems can be directly related to particle–particle interactions under similar surface and solution conditions.

Early work using the SFA technique was aimed at testing the validity of the DLVO theory. One of the most remarkable results was obtained for mica crystals interacting in pure water [39] which is shown in Figure 6. Because of the accuracy of the results it was necessary to use an exact numerical solution [40] to the Poisson-Boltzmann equation and the theoretical curves are shown as solid lines. The limiting boundary condition of constant surface charge [41] was used in this case. The long Debye length was as expected for pure water equilibrated with atmospheric carbon dioxide and, in addition, the force maxima at about 2.4 nm due to the short-range Van der Waals attraction was also observed. The agreement with DLVO theory

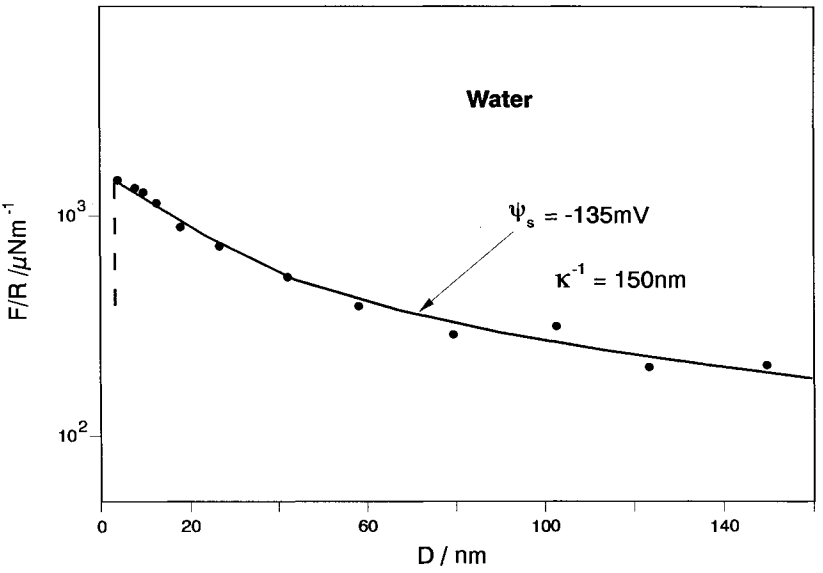

Fig. 6. Total force F between mica surfaces of mean radius R separated by distance D in distilled water. The parameter F/R is equal to $2\pi E$, where E is the corresponding interaction energy per unit area between flat surfaces. The solid line is calculated from an exact numerical solution to the Poisson-Boltzmann equation (see text). The long Debye length is consistent with the low electrolyte concentration in distilled water. The surfaces jump into contact from a separation of about 3.4 nm because of Van der Waals attractive forces which, as predicted by DLVO theory, dominate at short-range. The surfaces are seen to jump because of the spring device used to measure forces (see Figure 5). At $D = 0$ the mica crystals are held in an adhesive primary minimum. These results are in excellant agreement with both electrostatic double-layer and Van der Waals forces.

under these conditions is very close. It should be pointed out here that because of the spring device, used to measure forces, no measurements can be made beyond the force maximum from which the surfaces jump together into an adhesive primary minimum.

The separations from which the mica surfaces jump into contact and the forces measured around a secondary minimum can be used to obtain the attractive Van der Waals force law. Results from a series of these experiments [42] are shown in Figure 7 for mica surfaces in aqueous electrolyte solutions. At separations below about 7 nm the force-law follows the non-retarded Hamaker equation $F/R = A/6D^2$, with a Hamaker constant $A = 2.2 \times 10^{-20}$ J. The more complicated Liftshitz theoretical calculation using spectral data for mica and water [20] is also shown for comparison. At separations greater than about 7 nm the force decays more rapidly, as expected from the onset of retardation effects.

These results clearly demonstrate that the DLVO model represents an accurate picture of surface interactions. However, it turns out that this *complete* agreement is more the exception than the rule! This is well illustrated by Figure 8, which

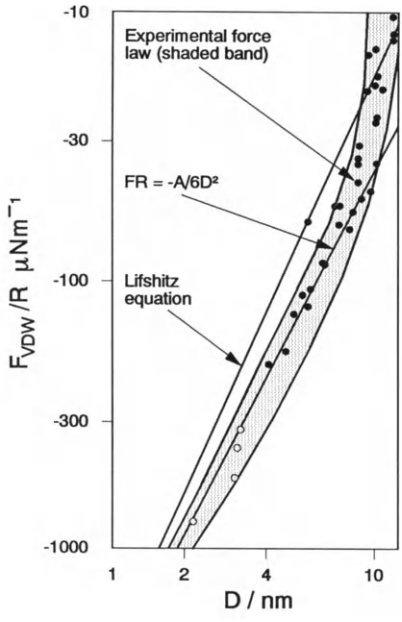

Fig. 7. Measured attractive forces between mica surfaces immersed in a range of aqueous electrolyte solutions. The open circles were obtained using a DLVO fit to the observed forces near the force maximum, whereas the filled circles were from systems with a secondary minimum.

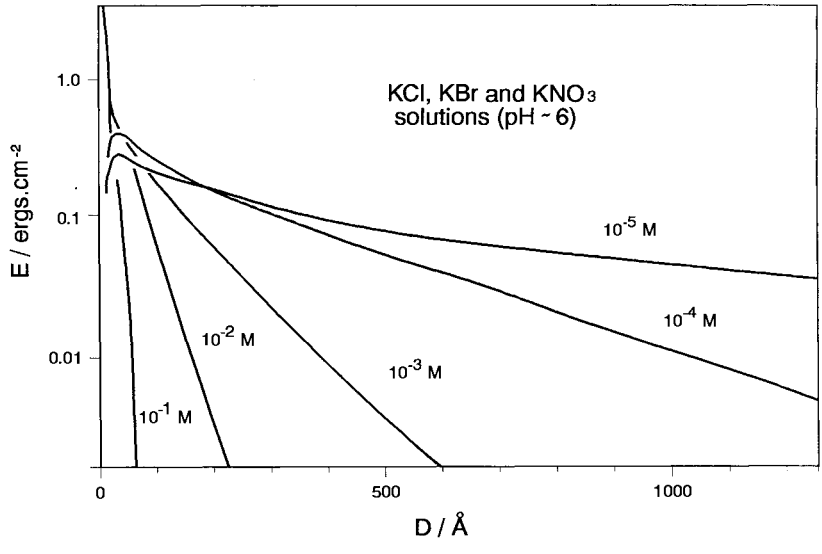

Fig. 8. The interaction energy E per unit area between flat mica surfaces (calculated from the measured F/R values) is shown as a function of separation distance D for a range of K^+ salts in aqueous solution. As the concentration increases the observed Debye length decreases in accordance with Gouy-Chapman theory. However, above a certain concentration the short-range jump into a primary minimum is replaced by a strong repulsive force, identified as a solvation or hydration force.

shows the effect on the interaction of adding KCl/KNO_3 electrolyte at increasing concentrations. Although the decay length of the forces is precisely given by the calculated Debye length, the short-range forces at the higher concentrations are quite unlike those expected from DLVO theory. Instead of a jump to primary minimum no such minimum was observed and an additional short-range repulsion arises. In order to understand these results it is important to realise that the surface of the mica crystals is an almost ideal ion-exchange surface and on immersion in water almost all of the original K^+ ions present on the cleaved surface are replaced by hydronium ions. On increasing the K^+ ion concentration this exchange is reversed and the mica re-adsorbs these ions. The short-range repulsive force is clearly related to the adsorption of these ions. Further study of a wide range of other cations [43] confirms this and, in addition, strongly supports the idea that the short-range repulsion was due to the work required to de-hydrate these adsorbed ions on forcing the mica surfaces together. The strength and range of the additional force was found to follow the trend:

$$La^{3+} \gg Mg^{2+} > Ca^{2+} > Li^+ \sim Na^+ > K^+ > Cs^+ \gg H_3O^+$$

which is generally consistent with that expected for the degree of hydration of these ions. The one exception to this hydration by adsorption process (sometimes referred to as secondary hydration) is the H_3O^+ ion, which is the reason why DLVO forces were observed in pure water and no short-range repulsive forces are observed for mica in acid solutions [39]. The explanation for this exception must be related to some kind of specific bonding of the H^+ ion to the negatively charged oxygen ring on the surface of mica. This binding must be of sufficient strength to remove the hydration properties of the ion. It is possible that the proton may actually penetrate the mica lattice and hence not be present on the surface at all. Further support for this comes from the observation that the proton has a significantly stronger binding energy to mica than any of the other cations studied [43].

Closer examination of the short-range forces in this system have led to the discovery of some remarkable solvent structural effects. Figure 9 shows the measured forces in KCl solution just at the point where significant hydration forces arise [44]. From this data it is clear that the short-range hydration repulsion is actually oscillatory with a periodicity close to the size of a water molecule. That such oscillations in the force should exist for interactions in very thin films was predicted theoretically from Monte Carlo and molecular dynamics simulations [45]. Stable states exist only at integral numbers of solvent molecules where the packing is the most favourable. This oscillatory force has been identified as the same as that observed in the so-called crystalline swelling of clays [46]. The fact that a common clay mineral Na-montmorillonite can be prevented from swelling by the addition of calcium salts is used in many industrial processes such as in agriculture and oil recovery. The swelling of these parallel aluminosilicate layers is prevented beyond about 0.9 nm [47] on addition of Ca^{2+}. The most likely cause of these specific distances, also

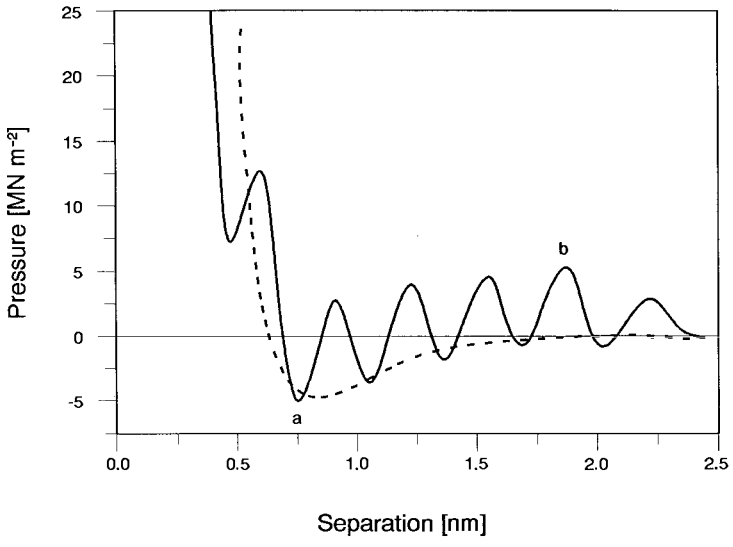

Fig. 9. Semi-schematic representation of the interaction law between mica surfaces in 0.15 M $CaCl_2$ solution. This figure was constructed from a combination of experimental and theoretical (dotted line) results on this system. The overall minimum at a separation of about 0.75 nm is apparently caused by an ion-ion correlation effect. The oscillatory structure is produced by molecular layering of water. This minimum is closely related to the well known effect of Ca^{2+} ions on swelling clays.

observed in other clay systems [47], is the packing of the water layers. However, the remaining question as to why a particular oscillation should be strongly adhesive has only been addressed very recently [48].

In summary, it has been established that these forces decay with separation and oscillate about whatever background force is present — e.g. hydration force, double-layer or Van der Waals force. Under certain conditions, however, it is possible to obtain a double-layer force which is strongly attractive only over a fairly narrow distance region. Such a situation has been shown to arise for divalent counterions, such as Ca^{2+}, in highly charged clay swelling systems [48]. This attraction arises because of ion–ion correlation effects which are not included in the Poisson-Boltzmann equation. A schematic diagram of the resultant total force is shown in Figure 8. In this case the clay mineral would swell only to a water separation of about 0.75 nm. Direct experimental support for this model has recently been obtained using the SFA technique [47].

Although these oscillations or structural solvation forces are of fundamental importance to the understanding of clay swelling in aqueous and organic solvents, most other colloidal solutions do not contain molecularly smooth particles and it has been shown that under these conditions the oscillatory structure is smoothed out. Thus, for a rough hydrated surface such as polished silica [49] and lipid bilayers [24], only the background monotonic hydration force has been observed.

Combination of a short-range repulsive hydration force with a Van der Waals attraction can produce an adhesive minimum (called a hydration minimum) which is much weaker than a primary minimum. Alteration of solution conditions can then cause repeptization (as is often observed) of the colloid coagulated into this minimum, which would be impossible from a primary minimum.

Since a hydrated surface gives rise to short-range repulsive forces it is perhaps not surprising that a hydrophobic surface gives an additional attractive force and this has indeed been observed [35, 50]. The forces measured between mica surfaces coated with a hydrophobic monolayer are shown in Figure 10. These forces are much stronger than those expected for Van der Waals forces and at separations less than about 10 nm, decay exponentially with distance. The strength of the attraction appears to be related to the degree of hydrophobicity of the surfaces and there is evidence that the attraction has a weak tail extending out to more than 50 nm for the most hydrophobic surfaces. However, it is possible that this longer range force may originate in some residual mosaic of charge imbalance on each surface.

Once these surfaces have been pulled into adhesive contact by this force it is interesting to note that on forcing them apart again in water a cavitation process occurs, producing a bridging vapour meniscus between the surfaces. This phenomena

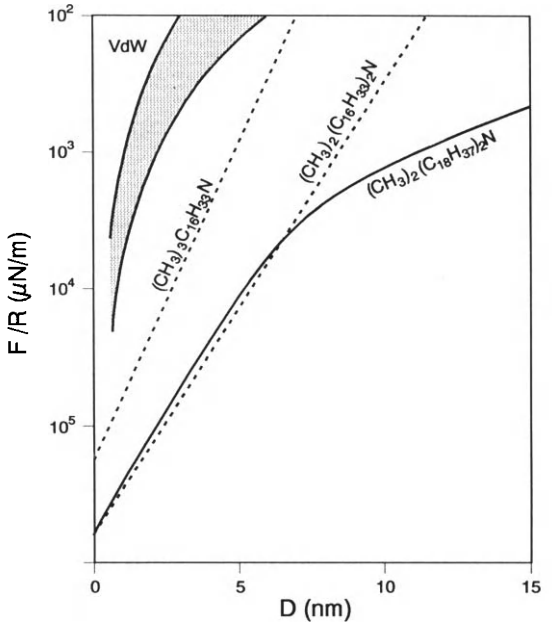

Fig. 10. A comparison of the magnitude of the hydrophobic interaction measured in three different systems and the non-retarded Van der Waals (VDW) force. The shaded limits of the VDW force were calculated using Hamaker constants of 2.2×10^{-20} J (as for mica|water|mica) and 5×10^{-21} J (as for hydrocarbon|water|hydrocarbon). The lines are for three cationic surfactants adsorbed as monolayers on mica.

has been predicted [51] for surfaces with a water contact angle greater than 90°. It is worth pointing out here that even though this attractive force is much stronger than the Van der Waals force for these systems a "hydrophobic colloid" solution would still be stable for any significant surface potential (e.g. >50 mV) in dilute electrolyte. However, as the Debye length of the solution approaches the decay length of the hydrophobic attraction, coagulation would be expected.

The precise cause and mechanism for the interaction between hydrophobic surfaces is clearly complex and has not been fully elucidated. This phenomenon is of central importance in biological systems as well as industrial surface chemistry processes, such as froth flotation. In the latter case, the attachment of a hydrophobic particle to an air bubble must involve electrostatic, Van der Waals, hydrophobic and hydrodynamic forces. Both the air bubble and particle surfaces are usually charged and may be considered to be hydrophobic. The air bubble apparently has a natural negative charge [52] in pure water but will take up a charge determined by adsorption of surfactants present in the flotation cell. The extent of this adsorption will also determine the hydration status of the bubble surface. Optimum bubble capture would be expected for a lowly charged or oppositely charged system, with both particle and bubble hydrophobic. A strong enhancement for capture would only be expected for particles with a water contact angle greater than 90°, where spontaneous cavitation has been observed. Such a high angle is both unusual and unnecessary for efficient flotation.

Hydrodynamic forces involved in particle capture depend largely on the size, shape and density of the particle and the viscosity of the solution. Recent SFA studies have convincingly laid to rest the suggestion that the viscosity of water may be higher than bulk near to the particle surface. Viscosity measurements [53] down to water films as thin as 5 nm or less have produced bulk values even in the presence of solvation effects.

As a final example, the SFA technique has also been used to investigate "steric" forces between surfaces in polymer solutions. Long and short-chain polymers are often used to stabilize colloids (e.g. in paints and inks) by adsorption of a relatively thick layer which has the effect of preventing close approach and hence adhesion of the particles. Klein and Luckham [54] measured forces between mica surfaces in a range of aqueous polyethylene oxide solutions. The repulsive forces they observed extended to about 80 nm, way beyond the effective range of Van der Waals forces. The solvation of the polymer chains and their attachment to the particle surface give rise to the repulsive forces and hence stability. These forces could therefore be classed as solvation forces.

The effect the adsorbing polymer has on colloid stability depends also on surface coverage [55]. Thus, at intermediate to low coverage significant bridging can occur between particles which produces polymer flocculation. At high coverage this is not possible and if the chains are solvated the polymer-coated particle will be stable even in concentrated electrolyte solution.

Addition of non-adsorbing polymer to the colloidal solution can give rise to attractive forces due to depletion layer effects [56]. These forces arise once the gap between the interacting surfaces becomes depleted of polymer compared with the bulk density, that is when the separation distance approaches the radius of gyration of the polymer.

Conclusions

The results of surface force measurements over the last ten years indicate that the interaction between most colloidal particles is well described by the classical theory of Poisson-Boltzmann electrostatics and non-retarded Hamaker forces at separations greater than about 5-10 nm. Interactions at shorter distances will often be dominated by the solvation properties of the colloid surface. In some cases (e.g. for highly charged surfaces with divalent counterions) it has also become clear that a more sophisticated electrostatic theory including ion size and ion correlation effects is necessary to adequately describe short-range electrostatic forces.

Finally, it is interesting to note that the classic definitions of lyophobic and lyophilic colloids are not based on the nature of their surfaces, once formed. However, it is quite clear from this recent experimental work that it is the nature of this surface which is of the utmost importance with regard to colloid stability.

References

1 H.T. Pledge, Science Since 1500, Science Museum, London, 1966.
2 H. Schulze, Z. Prakt. Chem., 25 (1982): 431.
3 W.B. Hardy, Proc. R. Soc., 66 (1900): 110.
4 H. Freundlich, Colloid and Capillary Chemistry, 3rd edition, Methuen, London, 1926.
5 R. Ellis, Z. Phys. Chem., 89 (1914): 145.
6 F. Powis, Z. Phys. Chem., 89 (1914): 186.
7 H. Kallmann and M. Willstatter, Naturwissenschaften, 20 (1932): 952.
8 M. Gouy, J. Phys., 9 (1910): 347.
9 D.L. Chapman, Phil. Mag., 25 (1913): 475.
10 I. Langmuir, Science, 88 (1938): 430; J. Chem. Phys., 6 (1938): 873.
11 R.K. Schofield, Trans. Faraday Soc., XL11B (1946): 219.
12 B.V. Derjaguin and M. Kussakov, Acta Physicochim., 10 (1939): 25; 10 (1939): 153.
13 B.V. Derjaguin and L. Landau, Acta Phys. Chim. U.R.S.S., 14 (1941): 633; JETP (USSR), 15 (1945): 633.
14 E.J.W. Verwey and J.Th.G. Overbeek, Theory of the Stability of Lyophobic Colloids, Elsevier, Amsterdam, 1948.
15 F. London, Z. Phys., 63 (1930): 245; Z. Phys. Chem., B11 (1930): 222.
16 R.S. Bradley, Phil. Mag., 13 (1932): 853.
17 J.H. de Boer, Trans. Faraday Soc., 32 (1936): 10.
18 H.C. Hamaker, Physica, 4 (1937): 1058.

19 H.C. Hamaker, Recueil des Travaux Chimiques des Pay-Bas, 56 (1937): 727; 56 (1937): 1.
20 D.B. Hough, and L.R. White, Adv. Colloid Int. Sci., 14 (1980): 3.
21 J. Mahanty and B.W. Ninham, Dispersion Forces, Academic Press, London, 1976.
22 B.V. Derjaguin, Kolloid Z., 69 (1934): 155: and: R.J. Hunter, Foundations of Colloid Science, Vol. 1, Clarendon Press, Oxford, 1987.
23 H. Van Olphen, Clay Colloid Chemistry, 2nd edition, Wiley, New York, N.Y., 1977, p. 107.
24 D.M. LeNeveu, R.P. Rand, V.A. Parsegian and D. Gingell, Biophys. J., 18 (1977): 209.
25 L.H. Allen and E. Matijevic, J. Colloid Interface Sci., 31 (1969): 287.
26 T.W. Healy, A. Homola and R.O. James, Faraday Soc. Disc., 65 (1978): 156.
27 J.B. Melville and E. Matijevic, in: R.J. Akers (Editor), Foams, Academic Press, 1976; and: A. Detwiler and D.C. Blanchard, Chem. Eng. Sci., 33 (1978): 9.
28 J. Laskowski and J.A. Kitchener, J. Colloid Interface Sci., 29 (1969): 670.
29 J.A. Kitchener, Disc. Faraday Soc., 52 (1971): 379.
30 B.V. Derjaguin, and N.V. Churaev, Nature, 244 (1973): 430.
31 J.C. Maxwell, Capillary Action (1875), in: Encyclopaedia Britannica, 9th edition, updated by Lord Rayleigh in 11th edition, 1911.
32 W.B. Hardy, Kolloid Z., 46 (1928): 268.
33 H.R. Kruyt and H.G. Bungenberg de Jong, Z. Physik. Chem., 100 (1922): 250; Kolloidchem. Beihefte, 28 (1928): 1.
34 J.N. Israelachvili and G.E. Adams, Faraday Trans. I, 74 (1978): 975.
35 J.N. Israelachvili and R.M. Pashley, Nature, 300 (1982): 341.
36 R.M. Pashley and J.N. Israelachvili, Colloids Surf., 2 (1981): 169.
37 J.L. Parker and H.K. Christenson (to be published).
38 R.G. Horn, D.R. Clarke and M.T. Clarkson (to be published).
39 R.M. Pashley, J. Colloid Interface Sci., 80 (1981): 153.
40 D.Y.C. Chan, R.M. Pashley and L.R. White, J. Colloid Int. Sci., 77 (1980): 283.
41 D.Y.C. Chan and D.J. Mitchell, J. Colloid Interface Sci., 95 (1983): 193.
42 J.N. Israelachvili and R.M. Pashley, J. Colloid Interface Sci., 98 (1984): 500.
43 R.M. Pashley, J. Colloid Interface Sci., 83 (1981): 531.
44 J.N. Israelachvili and R.M. Pashley, Nature, 306 (1983): 249.
45 B. Jonsson, Chem. Phys. Lett., 82 (1981): 520; and: N.I. Christou, J.S. Whitehouse, D. Nicholson and N.G. Parsonage, Faraday Symp. Chem. Soc., 16 (1981): 139.
46 R.M. Pashley and J.N. Israelachvili, J. Colloid Interface Sci., 101 (1984): 511.
47 J.P. Quirk, Israel J. Chem., 6 (1968): 213.
48 R. Kjellander, S. Marcelja, R.M. Pashley and J.P. Quirk, J. Phys. Chem., 92 (1988): 6489.
49 G. Peschel, P. Belouschek, M.M. Muller, M.R. Muller and R. Konig, Colloid Polym. Sci., 260 (1982): 444.
50 H.K. Christenson, P.M. Claesson and R.M. Pashley, Proc. Indian Acad. Sci., 98 (1987): 379.
51 Y.I. Rabinovich, B.V. Derjaguin and N.V. Churaev, Adv. Colloid Interface Sci., 16 (1982): 63.
52 G.L. Collins, M. Motarjemi and G.J. Jameson, J. Colloid Interface Sci., 63 (1978): 69.
53 J.N. Israelachvili, J. Colloid Interface Sci., 110 (1986): 263.
54 J. Klein and P.F. Luckham, Macromolecules, 17 (1984): 1041.
55 J. Rubio and J.A. Kitchener, J. Colloid Interface Sci., 57 (1976): 132.
56 B. Vincent, J.M.H. Scheutjens and G.J. Fleer, ACS Symp. Ser., 240 (1984): 245.

Chapter 4

Dispersions stability and dispersing agents

JANUSZ S. LASKOWSKI and ROBERT J. PUGH

Introduction

Flotation process requires the use of various reagents ranging from collectors, through different groups of modifiers to frothers. Perhaps the most important, the collectors, are designed to adsorb selectively onto minerals and render them hydrophobic. Since the treated minerals are quite commonly very similar to each other from the crystallochemical point of view, their separation requires, in addition to collectors, the use of modifiers which enhance the selectivity of the collectors.

The group of flotation modifiers includes a wide variety of both inorganic and organic reagents. They are referred to as activators and depressants, dispersants and aggregating chemicals (coagulants and flocculants), pH regulators, etc.

The dispersants are used in the mineral processing field to prevent fine particle aggregation; in flotation systems, this is quite commonly an aggregation of slimes (very fine particles) onto coarse particles. This so-called slime coating is in many flotation operations responsible for poor floatability of valuable mineral constituents. Removal of slimes from the surfaces of valuable coarser particles requires the use of dispersing agents. Thus, it is obvious that these agents increase flotation recovery, but may also increase separation selectivity. In the systems where selective flocculation is applied, dispersants are used to prevent initial heterocoagulation and by doing this to furnish the conditions for subsequent selective flocculation [1]. Dispersants have also recently found important applications as viscosity reducing agents in wet grinding [2] and in preparation of coal/water fuels [3].

Depressants are also used to increase flotation selectivity by inhibiting flotation of unwanted mineral species. Since dispersion is associated with an increase in hydrophilic character, it is often impossible to distinguish between dispersion and depression, and some chemicals are utilized in flotation processes as both depressants and dispersants. To clarify such terminological ambiguities, it will be necessary to go back to basic principles.

Dispersing/depressing agents in mineral processing

The function of a depressant is the opposite of that of a collector; it inhibits flotation of a given mineral. This can be achieved either by (a) preventing collector from adsorbing onto a given mineral, or by (b) making the mineral surface hydrophilic. There are, therefore, various depressants with quite different modes of action.

Simple inorganic chemicals such as pH regulators, or strongly reducing compounds such as, for example, Na_2S, can be categorized in the former group of flotation depressants. They can prevent the collector from adsorbing. The latter group includes mostly polymeric hydrophilic compounds which form strongly hydrophilic protective layers on mineral surfaces. This usually also leads to a displacement of a collector from mineral surface, but examples of a quite different mechanism are also known. For instance, Somasundaran [4] found that the oleate flotation of calcite was depressed with starch but not by the classical competitive adsorption mechanism. In the presence of starch, oleate adsorption was found to be enhanced, and vice versa starch adsorbed better onto calcite in the presence of oleate. Apparently, what was important here was the formation of a strongly hydrophilic layer on calcite, which made flotation impossible.

Analysis of the stabilization process, which will be discussed in detail in the next section, reveals that there are basically two possibilities to prevent fine solid particles suspended in a liquid from aggregating. This can be accomplished either by (a) increasing coulumbic repulsive forces (electrostatic stabilization), or by (b) constructing a physical barrier around interacting particles which will prevent them from approaching one another to a distance where there is a significant attractive force (steric stabilization) [5]. According to some researchers [6], the real resistance to squeezing out the intervening layer is the difficulty of removing solvent from the adsorbed lyophilic stabilizer. Simple monomeric compounds, mostly inorganic, are used to increase electrostatic repulsive forces between interacting solid particles, while polymeric compounds (both inorganic and organic) are utilized to impose also steric effect on the system [7]. Thus, the polymeric substances, which adsorb onto mineral particles and form hydrophilic protective layers, used as flotation depressants, are exactly the same as those agents classified into the second group of dispersing agents. The same modifying agents, such as pH regulators for example, can also be used as depressants or as dispersants. This results from the fact that H^+ and OH^- are potential determining ions for many mineral systems, and so they act primarily by controlling the surface charge of mineral particles. In this way they affect both interparticle interactions and collector adsorption. Sodium sulphide, a well known depressing agent in xanthate flotation of sulphides, makes the mineral surface more negatively charged, and so it is also affecting the stability of mineral dispersions.

The classification of both depressing and dispersing agents, and the comparison of various groups, shows that the second group of dispersing agents and the second

group of depressants include similar compounds. The first groups may be different, and we will not discuss the similarities and differences between them any further here.

Classification of dispersing agents

A classification of dispersing agents, which follows, is based on the classification offered earlier [7] and on that by Lovell [8].

Dispersing agents used in the mineral processing field can be broadly classified into inorganic compounds, polymeric dispersants derived from natural sources, and synthetic polymeric dispersants.

Inorganic dispersants

Probably best known are sodium silicate (water glass) and sodium phosphate salts.

The composition of sodium silicate can be expressed by the general formula of $m\mathrm{Na_2O}n\mathrm{SiO_2}$. The ratio n/m, referred to as the modulus of sodium silicate, is quoted by Leja [9] after Vail to vary from 1.6 to 3.75. Klassen and Mokrousov [10] state that sodium silicate whose modulae vary from 2.2 to 3.0 are frequently used in flotation.

Sodium silicate undergoes hydrolysis in aqueous solution which results in the production of hydroxylated species: $\mathrm{Si(OH)_4}$, $[\mathrm{SiO(OH)_3}]$, $[\mathrm{SiO_2(OH)_4}]^{4-}$, but also dimeric $[\mathrm{Si_2O_3(OH)_4}]^{2-}$, trimeric $[\mathrm{Si_4O_8(OH)_4}]$ and probably other polymeric species. Peskov, as quoted by Klassen and Mokrousov [10], postulated that aqueous solutions of sodium silicate may also contain highly charged colloidal species.

Polymerization of sodium silicate solutions with polyvalent cations improves the dispersing ability of the product. Yang [11] described the preparation of a very stable dispersing agent in which $\mathrm{Na_2SiO_3}$, $\mathrm{Fe(NO_3)_3.9H_2O}$ and $\mathrm{H_2SO_4}$ are reacted at the ratio of 5 : 1 : 1.

Sodium polyphosphates are another important group of inorganic dispersants. Both linear polyphosphates and cyclic metaphosphates are used.

Linear polyphosphates form anions of the general formula $[\mathrm{P}_n\mathrm{O}_{3n+1}]^{(n+2)-}$. An orthophosphate ion, a dipolyphosphate ion $\mathrm{P_2O_7^{4-}}$ (pyrophosphate) and tripolyphosphate ion, $\mathrm{P_3O_{10}^{5-}}$, shown below, belong to this group.

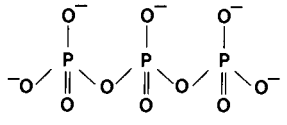

The cyclic compounds include tetrametaphosphate, $Na_4P_4O_{12}$, and hexametaphosphate, $Na_6P_6O_{18}$. The hexametaphosphate formula is shown below:

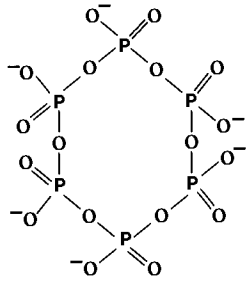

$+ 6Na^+$

Polymeric dispersants

Polymeric dispersants derived from natural sources

(a) Polysaccharides. Starch and starch derivatives. Starch contains a water-soluble straight chain fraction, amylose, and a water-insoluble branched fraction, amylopectin. The basic structural unit for polysaccharides is D-glucose, whose chemical structure is shown schematically in Figure 1a. As indicated in Figure 1b, these basic units can be connected through α-1.6 linkages, or α-1.4 linkages. While α-1.6 linkages are present in the linear amylose, both α-1.4 and α-1.6 linkages appear in amylopectin with branching occurring approximately every 25 glucose units [13–15]. The average number of glucose units per polysaccharide molecule is called the degree of polymerization, DP.

In an aqueous solution, amylose behaves as a random coil or helix with six glucose residues per turn. The helix is hydrophobic in the interior, and hydrophilic on the exterior. Branched polymers, such as amylopectin, do not seem to have such a structure.

Unmodified corn starch is negatively charged [16]. Electrophoretic studies with potato starch in basic solutions have shown migration of starch towards cathode, indicating negative charge [17]. This can be due to the ionization of starch hydroxyls (pK about 12) as well as to some impurities [18]. Modification, which can take place at the hydroxyl groups through oxidation, esterification, or ether formation can significantly change the properties of the original material. Hydroxyl groups on C-6 are the most reactive [19].

Dextrin is derived from starch by thermal degradation under acidic conditions. Depending on the degree of conversion, dextrin may exhibit varying solubility in water. White dextrins, which are only slightly converted and have limited solubility in water, are produced at low temperature (80–120°C). The yellow or canary dextrins are the products of longer conversion times (6–18 h) at higher temperatures (150–180°C and with lower concentrations of acid). Canary dextrins have a higher degree of conversion and are 90–100% soluble in cold water [20]. Both starch and dextrin

form colloidal systems in water. The main difference between them is that dextrin is a highly branched smaller molecule, with its molecular weight ranging from 800 to 79,000 [21, 22], whereas starch is made up of much larger molecules of both linear and branched components. Dextrins can also be produced from starch by the action of enzymes (amylases, and cyclic Schardinger dextrins).

Heating starch to the range of 170–195°C without addition of acids leads to British gums. Both dextrins and British gums have highly branched structures and low molecular weights [15].

Also *galactomannans* belong to the groups of branched polysaccharides. The most important species containing galactomannans is *guar gum* [23]. Different steric configuration of neighbouring OH groups in guar and starch, as depicted below, was claimed to have a pronounced effect on much higher reactivity of guar [24].

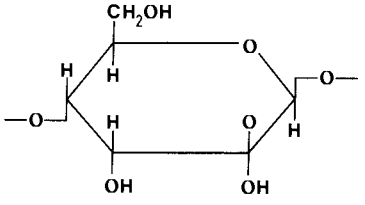

Galactomannan

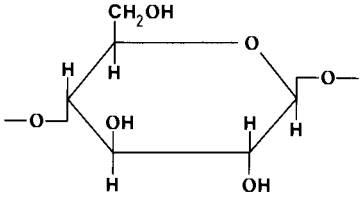

Starch

Acidic polysaccharides, such as gum tragacanth (GT), which is based on polygalacturonic acid (PGUA), have also been described as efficient stabilizers [25, 26]. The chemical structures of PGUA and GT are shown in Figure 2a and b.

Cellulose constitutes the fibrous tissue of all plants, its long chain polymer is built from glucose units bonded by β-1.4 link. Of cellulose derivatives the most widely used is *carboxymethyl cellulose.* Its glucose unit is shown below. The presence of a carboxylic group makes it an anionic polymer, which is fully ionized in alkaline solutions.

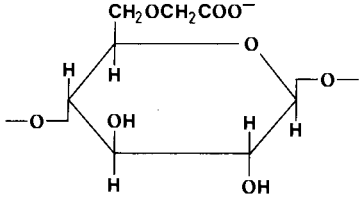

(b) Polyphenols. Tannin extracts, quebracho and *wattle bark*, as well as *lignin*, are classified in this group. An excellent review of the methods of their production, and their properties can be found in Leja's classic [9].

Wood consists of about 50% cellulose fibers, about 30% lignin and 20% carbohydrates. Tannin extracts obtained from two types of trees are well-known modifying

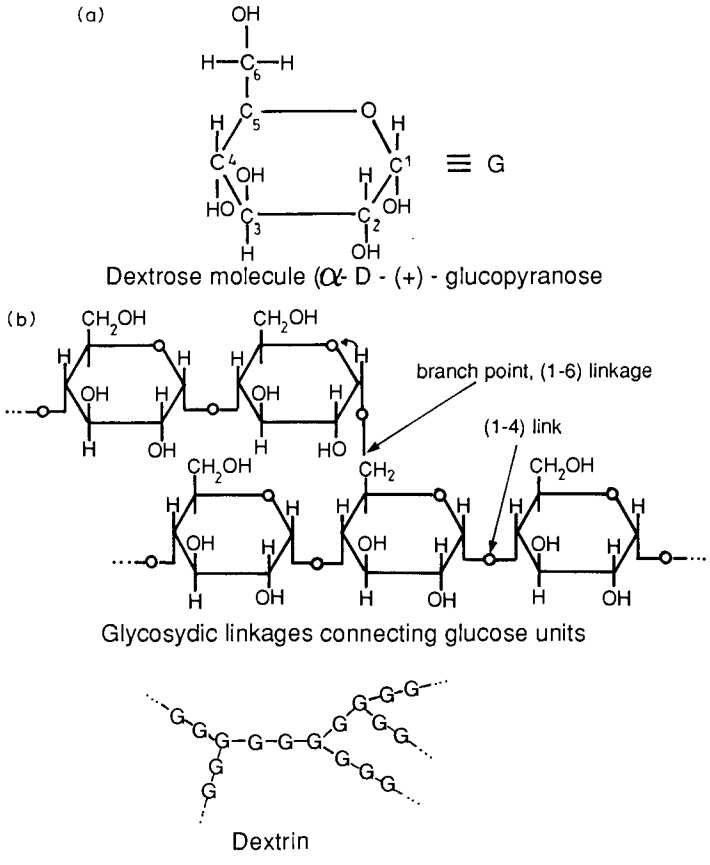

Fig. 1. Starches and dextrins are polymers of dextrose monomeric units linked through 1–4 glycosidic joints in straight chain polymolecules, and 1–6 joints in branch chain polymolecules.

agents: quebracho and wattle bark. The chemical composition of *quebracho* is shown below:

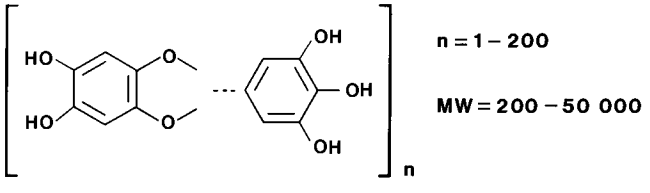

Lignin, which binds together the cellulose fibers of wood, represents an extremely complex mixture of monomeric cyclic species with polymers which are both two- and three-dimensional. A dioxyphenyl propyl unit, which Leja quotes as an important

repeating unit of most lignin components, is depicted below:

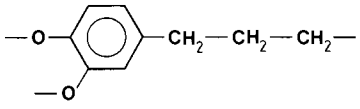

Lignin sulphonates have found broad applications as dispersing agents.

Humic acids and their sodium salts will also be classified in this group (humic acids are now commercially available [27]). These are highly reactive, amorphous, predominantly aromatic complex anionic polyelectrolytes with carboxylic and phenolic groups [28]. According to Jensen et al. [29], coal oxidation involves two simultaneous but unrelated reactions which result in the development of acidity and skeletal breakdown (degradation). The latter leads to the alkali solubility of coal with the dissolved product being humic acids. By the way, one of the methods used

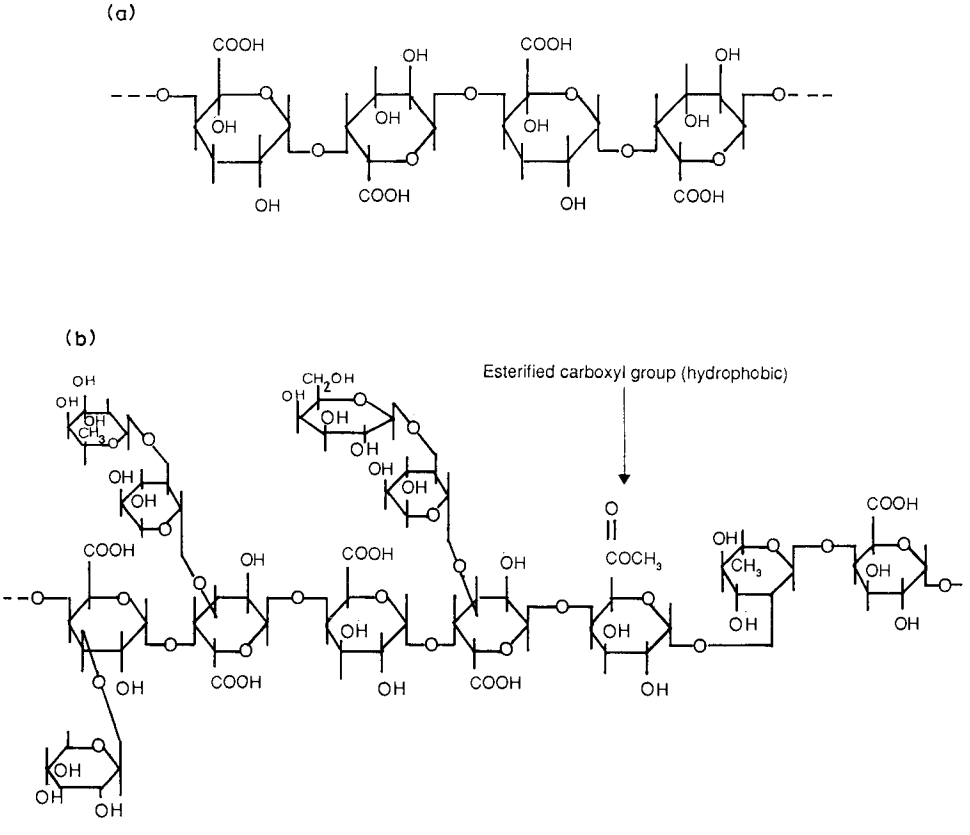

Fig. 2. Chemical structure of polygalacturonic acid (a) and gum tragacanth (from Yokohama et al. [25] with permission).

to determine coal oxidation consists in the boiling of a coal sample in NaOH solution, followed by the colorimetric determination of the humic acids in the pregnant solution [30]. Humic acids, also referred to as humic substances, appear widely in all natural waters [31] and impart brown or yellow coloration to them. Depending on the source, humic acids may widely differ. They form complexes with metallic ions, clays and other aluminosilicate minerals [32, 33].

Synthetic polymeric dispersants

Polygycol ethers. Any organic compound containing reactive hydrogen, as in alcohols (ROH), carboxylic acids (RCOOH), alkyl phenols (RC_6H_4OH), etc., can react with alkyl oxides ($C_nH_{2n}O$) giving polyoxy derivatives as in the following example:

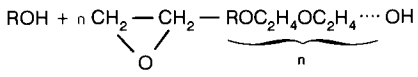

Since the water molecules are affixed to the ether oxygen by hydrogen bonding, the oxyethylene chain imparts hydrophilic properties to the molecule and thus the surface activity and solubility depend finally on the number of ethoxy units in the molecule and the number of carbon atoms in R. In other words, the hydrophile–lipophile balance (HLB) of the molecule can then be controlled by a number of ethoxy-units and by a number of carbon atoms in the side chain R.

Condensation products of propylene and ethylene oxides with methyl alcohol (or other alcohols) form an important group of the flotation frothers (for example, Dowfrothers). Polyoxyethylene nonylphenols, shown schematically below, have emulsifying and dispersing abilities.

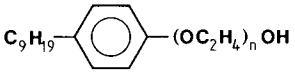

The group of synthetic polymeric dispersants also includes various *polyelectrolytes*, such as low molecular weight polyacrylates (e.g. Cataflot manufactured by Pierrefitte-Auby Co) [34], low molecular weight copolymers of the polyacrylate type (e.g. *Dispex* manufactured by Allied Colloids Ltd.) [35], etc. Many reagents of this and the similar type have recently been offered under various trade names [2]; their chemical compositions were not, however, disclosed.

It is worthy of mention that all water soluble polymers can either be used as flocculants or dispersants. While the former are linear and are characterized by high molecular weight (around and above 10^6), the latter are of low molecular weight (in the range of 10^4) and may be of branched structure. One must, however, bear in mind that all polymers under certain conditions, irrespective of their molecular weight, and especially at high concentrations may cause dispersion [36, 37].

Particle interactions in dispersed systems

In most mineral processing operations such as flotation, wet grinding, dewatering, and pumping in general, the slurry contains a mixture of different particles and is subject to turbulence and shear forces. The degree of turbulence can vary according to the type of operation and often depends on the design of the equipment. For example, in a flotation cell the flow conditions depend on the type of impeller, the geometry of the inserts and the volume of the vessel. Typical impeller rotation speeds are in the order of 3 s^{-1} and although the primary function of the stirring is to generate air bubbles and produce bubble–particles collisions, it also serves to whirl up and re-disperse the larger particles and flocs from the base of the tank. In addition, it helps to redistribute the reagent throughout the pulp.

Another important aspect to consider is the wide particle size range involved. Generally, in the Mineral Processing Industry, particles are classified into coarse, and fine fractions. The so-called 1–10 μm slime fraction, however, is not truly colloidal. Under these circumstances it is important to consider the influence of particle size on the interparticle interactions particularly with respect to Brownian, hydrodynamic, gravitational or inertial effects resulting from fluid shear.

Warren [38] emphasized the fact that surface forces such as Van der Waals, electrostatic and Brownian motion can only dominate over gravitational and inertial forces for particles in the 0.1 μm size range. For larger particles in the 1–10 μm size range, the inertial and gravitational forces are more dominant under non-quiescent flow conditions and the fluid can confer enormous energies to the particles. Under

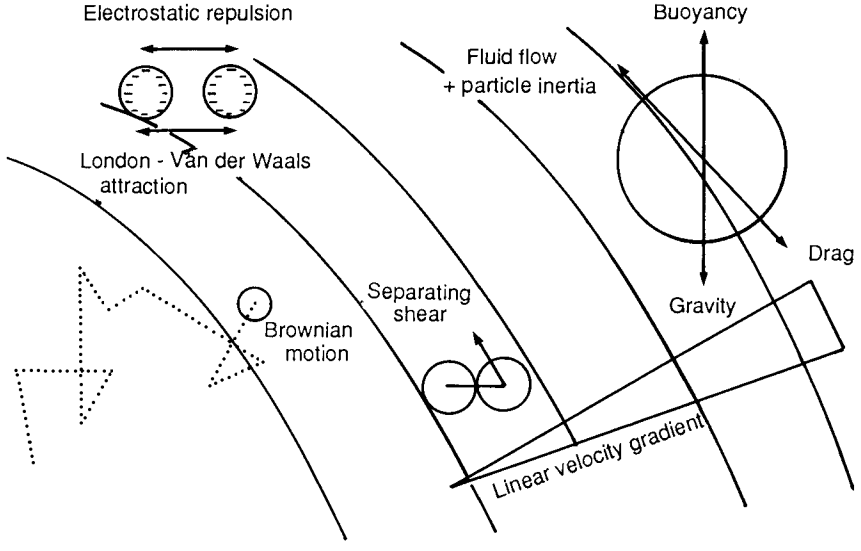

Fig. 3. Forces acting on and between the particles in a suspension in laminar flow (from Warren [38] with permission).

these latter conditions, the mechanical forces can cause coagulation by overcoming the repulsive energy barriers between particles, or they may aid dispersion by forcing particles apart. In Figure 3, the forces acting on particles under laminar flow conditions are illustrated.

Since it is often necessary to have precise control of the state of the dispersions for the whole range of particle sizes to prevent loss in recovery or reduction in grade, all these forces must be taken into consideration. Generally, the suspension contains dissimilar particles and the overall behaviour can successfully be controlled by addition of a dispersing agent. Simple chemical dispersants produce a strong electrostatic repulsive force between interacting particles. In addition, particles may also be stabilized by the adsorption of a hydrophilic polymer (steric stabilization). Finally, in many cases stabilization can be achieved by a combination of both steric and electrostatic stabilization. These three cases are considered in Figure 4.

To begin with, we will discuss the principles governing electrostatic stabilization but it is also important to consider the effect of hydrodynamic conditions (interactions under conditions of Brownian diffusion and fluid shear).

Particle interactions under perikinetic conditions (DLVO theory)

Over the past sixty years or so most colloidal stability theory has been based on perikinetic phenomenon, where the liquid is assumed to be stationary and collisions occur from Brownian translational motion. Essentially Brownian motion is thermal in origin and follows random statistics. Also, for particles in the 0.1 μm size range, inertial and gravitational effects can be neglected. DLVO theory [39], which serves as the main framework for electrostatic stability studies, deals with the pairwise interaction of particles by the summation of the potential energy of electrostatic repulsion (V_E) and the Van der Waals attraction (V_A):

$$V_T = V_E + V_A \tag{1}$$

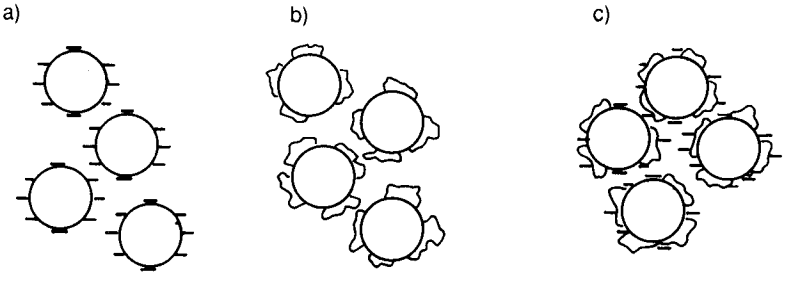

Fig. 4. The stabilization of mineral particles by: (a) electrostatic charge achieved by change in pH or the adsorption of charged ions from solution; (b) steric stabilization achieved by adsorption of an uncharged polymer; (c) a combination of steric and electrostatic stabilization achieved by adsorption of a charged polymer.

A useful practical form of expressing V_A and V_E to allow for dissimilar particles (with surface potentials ψ_1 and ψ_2) with unequal sizes (radii a_1 and a_2) has been formulated by Hogg, Healy and Fuerstenau [40] and takes the form:

$$V_E = F \times \frac{\varepsilon}{4} \left\{ 2\psi_1\psi_2 \ln \left[\frac{1 + \exp(-\kappa H_o)}{1 - \exp(-\kappa H_o)} \right] + (\psi_1^2 + \psi_2^2) \ln[1 - \exp(-2\kappa H_o)] \right\} \quad (2)$$

and:

$$V_A = -F \frac{A}{6H_o} \quad (3)$$

where A is the net Hamaker-London constant for material 1 and 2 in medium 3 and is given by $A = A_{12} + A_{33} - A_{13} - A_{23}$, F is the form factor, $a_1a_2/(a_1 + a_2)$, κ is the Debye-Hückel reciprocal length parameter which is related to the ionic strength of the medium, ε is the di-electric constant of the liquid, and H_o is the interparticle separation distance. In the case of monodispersed particles, $a_1 = a_2$ and for a system with only one type of particle, $\psi_1 = \psi_2$.

In using equations (2) and (3), it is usually assumed that the surface potentials ψ_1 and ψ_2 are relatively low and can be replaced by the zeta potential of the mineral particles. Also, two limiting cases are implied: (a) completely relaxed double layers, and (b) total unrelaxed double layers as the particles approach. The first corresponds to constant potential of the interacting surfaces and the second to constant charge density. Recent experiments suggest that for many cases the real situation is somewhere intermediate in between these two extremes.

From equation (1), the total potential energy of interaction (V_T) gives a potential energy against interparticle separation, and the curve when plotted against distance exhibits several characteristic features which can be used to describe the stability of the system. Essentially, a "primary minimum" exists at close distances of separation and a "primary maximum" height (V_{MAX}) which acts as a barrier. This maximum must be surmounted before the particles fall into the "primary minimum" and make contact (coagulate). If we consider two particles colliding, then the amount of energy involved will be about 10^{-20} J ($\approx k_B T$) where k_B is the Boltzmann's constant and T the temperature. In principle, when V_{MAX} is sufficiently high in terms of $k_B T$ (i.e. at least $5k_B T$), the particles will not be able to surmount the barrier and the dispersion will be stable.

At larger interparticle separation distances, a secondary net attraction or "secondary minimum" (V_{MIN}) may also be predicted from the potential interparticle distance plot, which becomes deep enough with particles larger than a few microns to cause interparticle association. In Figure 5, the total potential energy of interaction versus interparticle distance curves show four classes of shapes with large variations in stability. In the first case (curve A), the particles experience no repulsive forces and fall directly into the deep "primary minimum". Under these circumstances "fast coagulation" occurs and the system is completely unstable. In

case *B*, coagulation in the primary minimum may be prevented by a fairly high V_{MAX} energy barrier, but "weak coagulation" may occur in the secondary minimum. This "secondary minimum" effect is more pronounced with particles of large radii and for flat particles than with spherical ones. It is interesting to note that while the potential energy against coagulation (V_{MAX}) rises approximately proportionate to the increase of particle radius, the depth of V_{MIN} is also increasing with the radius. This fact suggests that larger sized particles, which are prevented from reaching the primary minimum, are likely to deposit in the "secondary minimum". Particles held in the secondary minimum (which is not deep) are separated by a thin disjoining film and may diffuse out again producing a dispersed system, whereas the primary minimum is too deep to allow the trapped particles to escape. An interesting feature of the secondary minimum instability, which has been reported to have been identified in several experimental systems, is that the particles may undergo rotational and Brownian motion. In Figure 5, curve *C*, the V_{MAX} value is sufficiently high

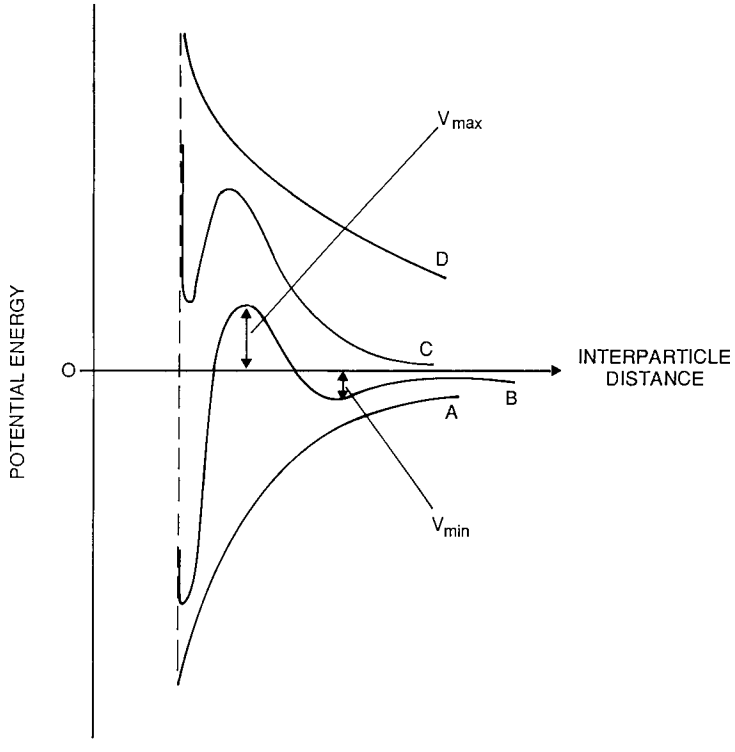

Fig. 5. Total potential energy versus interparticle distance curves between two particles showing four different types of interactions. *A* = fast coagulation into primary minimum; *B* = weak secondary minimum coagulation; *C* = no primary coagulation due to high V_{MAX} energy barrier; *D* = spontaneous dispersion of particles (---- indicates particle contact). From Tabor [41] with permission.

to prevent coagulation, and finally curve D represents only strong repulsive forces producing a dispersed system.

Generally, the primary minimum stability will be reduced by lowering V_{MAX} (by reducing the electrostatic repulsion term). In practice, this may be achieved either by increasing the ionic strength of the solution which decreases κ^{-1} (the double layer thickness) and "screens" out the surface charge, or by decreasing the surface potential, ψ of the particles.

The rate of coagulation (Smoluchowski/Müller theory)

Smoluchowski originally formulated the theory of fast coagulation (assuming no V_T, V_A or V_R) for monodispersed spherical particles forming doublets and the equations were later elaborated by Müller [43]. Smoluchowski [42] showed that the rapid rate of disappearance of primary particles $-(dN/dt)_p^f$ in the initial stage of the fast perikinetic coagulation process could be expressed similar to that of a bimolecular reaction by:

$$-\left(\frac{dN}{dt}\right)_p^f = k_p^f N_o^2 \tag{4}$$

where N_o is the number of primary single particles per unit volume initially present, and k_p^f is the fast perikinetic rate constant. For rapid coagulation (in the absence of an energy barrier) then:

$$k_p^f = 8\pi DR \tag{5}$$

where R is the collision diameter or distance between the centres of the two particles at which a lasting contact is formed. In the case of particles of radii a, $R = 2a$. The diffusion coefficient for single particles, $D = k_B T/6\pi\eta a$. Hence, the rate of fast perikinetic coagulation of the monodispersed particles may be expressed by:

$$-\left(\frac{dN}{dt}\right)_p^f = \frac{8k_B T N_o^2}{3\eta} \tag{6}$$

However, in the early derivation of these equations no account was taken of the effects of hydrodynamic interactions, V_R or V_A between particles. Subsequent analysis of the problem showed that if diffusion in the presence of a potential energy barrier is considered (slow coagulation) then DLVO theory must be taken into consideration and a perikinetic collision factor (α_p), which quantifies the fraction of collisions leading to agglomeration, and a perikinetic slow rate constant, k_p^s, may be introduced, where $k_p^s = \alpha_p \times k_p^f$. Under these conditions the rate of slow perikinetic coagulation, $-(dN/dt)_p^s$ can be expressed by:

$$-\left(\frac{dN}{dt}\right)_p^s = \alpha_p k_p^f N_o^2 \tag{7}$$

and the α_p value can be related to a perikinetic stability factor (W_p) by:

$$\alpha_p \approx \frac{1}{W_p} \tag{8}$$

In addition, from DLVO theory it was shown that $W_{p(1,2)}$ the perikinetic stability factor between particles 1 and 2, could be related to the interparticle potential, V_{12} by the equation:

$$W_{p(1,2)} = 2\bar{a} \int_{2\bar{a}}^{\infty} \exp \frac{V_{12}}{k_B T} \frac{dr}{r^2} \tag{9}$$

where r is the distance between the centres of the two particles, i.e. $r = a_1 + a_2 + H_o$ and $\bar{a} = (a_1 + a_2)/2$.

Equation (9) can be presented in an approximate form by:

$$W_{p(1,2)} \sim \frac{1}{2\kappa\bar{a}} \exp\left(\frac{V_{MAX}}{k_B T}\right) \tag{10}$$

where V_{MAX} (see page ?? and Figure 5) is defined as the maximum height of the potential energy barrier.

These equations have been used by Pugh and Kitchener [45] to compute a series of stability curves relating $W_{p(1,2)}$ to the radii a_1 and a_2, and the surface potentials ψ_1, ψ_2 of two species for various values of the Hamaker constant A and the Debye-Hückel reciprocal length parameter, κ. Plots were computed for both constant charge and constant potential conditions. In addition, a rough guide to secondary minimum could be evaluated from the curves. These plots give a useful general guide to the stability of electrostatically charged colloidal dispersions.

Over the past 35 years the DLVO theory has been generally successful in describing stability of colloidal particles under perikinetic conditions. However, it is important to note the following restrictions.

(1) The theory only applies to monodispersed electrostatically charged sols which collide to form doublets, a quantitative theory of polydispersed slurries is far too complex to be derived at present. Even with model colloids, the Smoluchowski approach applies only to the early stages, i.e. the interaction between two particles, but in high solid pulps several interactions may occur simultaneously. Also according to Verwey and Overbeek [46] orthokinetic collisions with particles becomes more important as the early aggregates grow over 1 μm in size. The perikinetic stage is hence only a minor process in the coagulation of moderately concentrated slurries; the major process is the orthokinetic stage where sweeping up of the small particles by hydrodynamic collisions with smaller ones occurs.

(2) Van der Waals and double layer interactions are only considered. "Structural" hydration and hydrophobic interactions are not included. There is no general theory to deal with these additional forces, because such forces often depend on specific features of the surface.

(3) The theory only applies to colloids with smooth, well characterized surfaces. It is sometimes difficult to apply this knowledge to minerals with rough and dirty surfaces.

Although DLVO theory can often be used to predict primary minimum coagulation for model colloidal systems, the theory has been found to be less successful in explaining secondary minimum effects. For example, in DLVO theory a decrease in electrolyte concentration increases κ^{-1} and decreases the depth of the secondary minimum or removes it altogether. Also, in many concentrated colloidal model systems containing monodispersed spherical particles, a decrease in electrolyte concentration has been shown to produce a stabilized ordered phase. This can be explained by an increase in the range of the electrostatic repulsive forces and as the concentration of the particles is increased, a situation is reached when the particles maintain repulsive contacts over a long period of time. Such colloidal order-disordered transitions cannot be explained by DLVO theory. In concentrated suspensions all particles interact simultaneously with several neighbouring particles and to some extent the simpler types of model systems can be treated successfully by statistical thermodynamics.

The essential structural features of an electrostatically stabilized aqueous dispersion of charged monodispersed, spherical colloidal particles are shown schematically in Figure 6. This shows that at intermediate electrolyte concentrations (10^{-3} M) and low volume fraction, the sol undergoes random Brownian motion with constant repulsion as the particles collide. If the electrolyte concentration is reduced (10^{-5} M), the range of the electrostatic repulsion (as indicated by the circular dashed line) becomes extended producing a larger effective "charged particle diameter" beyond the true diameter. This can restrict the movement of particles so they form an ordered structure. The degree of order depends on particle size, polydispersity and can lead to a liquid type state or crystallization. Most of these studies have been made with model polymer colloids. From structure analysis by small angle neutron scattering it has been shown that the dispersions of spherical particles can exist in states which are analogous in structure to the molecular states of vapours, liquids, crystals and gases [47]. Although such structures cannot occur in concentrated mineral suspensions since the particles are nonspherical with a wide distribution in size, the electrical double layer will still play an important role in defining the stability and rheology.

Particle interactions under orthokinetic conditions

Gentle stirring causes coagulation due to the liquid velocity gradient which induces different interparticle velocities leading to collisions. Early theoretical studies dealt with unidirectional flow at a constant velocity gradient. This is difficult to achieve in practice but the annular gap between coaxial rotating cylinders (couvette) are usually taken as the nearest conditions. In recent years many attempts have been

made to extend the simplified theories dealing with uniform shear fields to velocity gradients under turbulent flow conditions which are more realistic in practice.

Smoluchowski [42] studied simple orthokinetic coagulation (in a laminar flow) for monodispersed particles and formulated the fast coagulation rate as:

$$-\left(\frac{dN}{dt}\right)_o^f = \left(\frac{32}{3}\right) D_v a^3 N_o^2 \tag{11}$$

where D_v is the mean velocity gradient, and in the case of a slow orthokinetic coagulation:

$$-\left(\frac{dN}{dt}\right)_o^s = \left(\frac{32}{3}\right) \alpha_o D_v a^3 N_o^2 \tag{12}$$

where α_o is the collision factor under orthokinetic conditions.

From equations (6) and (12), and assuming the collision factors are equal, $\alpha_o = \alpha_p$, i.e., the ratio of the collision rates by orthokinetic agglomeration and

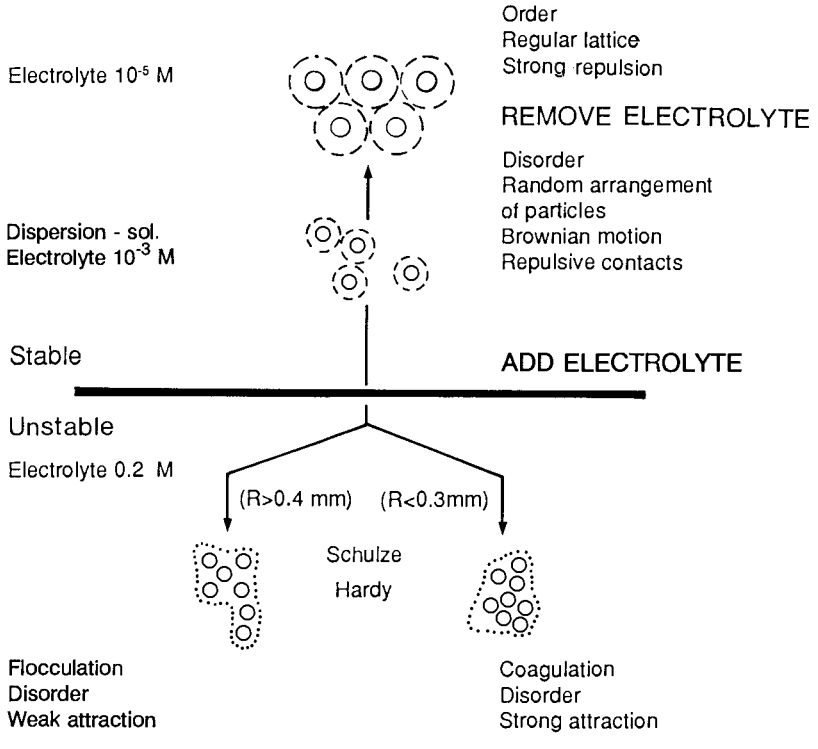

Fig. 6. Concentrated monodispersed suspensions showing the effect of electrolyte on the stability and states of the suspension (from Ottewill [46] with permission).

the collision rates of perikinetic coagulation are about the same then:

$$\frac{(dN/dt)_o}{(dN/dt)_p} = \frac{4D_v a^3}{k_B T}\eta \tag{13}$$

Also providing that the volume of solid remains constant during the coagulation process, and that it can be defined by $\phi = (4\pi/3)a^3 N_o$, then equation (12) can be re-expressed as:

$$-\left(\frac{dN}{dt}\right)_o^s = \frac{8}{\pi}\phi D_v N_o \alpha_o \tag{14}$$

If we assume additivity of the separate mechanisms, the total rate of coagulation of particles of any size may be expressed by:

$$-\left(\frac{dN}{dt}\right)_{o+p}^s = \alpha_p \frac{8k_B T}{3\eta} N_o^2 + \alpha_o \frac{8\phi D_v N_o}{\pi} \tag{15}$$

Usually at low mean velocity gradients for particles with $d > 1$ μm, the first term becomes negligible. For particles with $d < 1$ μm, the second term becomes less important than the first term.

These fairly simplified models essentially apply to monodispersed particles. For polydispersed systems, the particle size and distribution of particle sizes can have a complex influence on the kinetics. The rates at which heterodispersed systems coagulate has been summarized by Stumm and Morgan [47] for the various transport mechanisms (i.e. Brownian diffusion, fluid shear and differential settling).

Further theoretical developments to orthokinetic coagulation theory have been made by Curtis and Hocking [48] who improved on the Smoluchowski contribution to shear induced coagulation of interacting uncharged spherical particles by introducing the Van der Waals attraction term. Later Batcheler and Green [49] improved the hydrodynamic solutions for binary interactions. More recent advances were made by Van de Ven and Mason [50–52] in which DLVO theory was included, however, these calculations are restricted to laminar shear flow. Zeichner and Schowalter [53] present a more general approach and consider non-equational trajectories with uniaxial extensional as well as laminar shear flow.

Under laminar shear flow conditions several researchers found that a suspension containing large particles ($\approx$1 μm) could become unstable at very low shear rate due to agglomeration in the DLVO secondary energy minimum, and, yet, stable at intermediate shear rates due to the large hydrodynamic forces which are sufficient to push the particles out of the shallow secondary minimum. At high shear rates, the system becomes again unstable because the hydrodynamic forces are then large enough to overcome V_{MAX}, the primary energy barrier, and to allow the particles to coagulate into the primary minimum. Stability shear domains plots relating stability to surface potential and ionic strength for monodispersed particles are shown in Figures 7 and 8, respectively. Essentially the stability diagrams define the state of

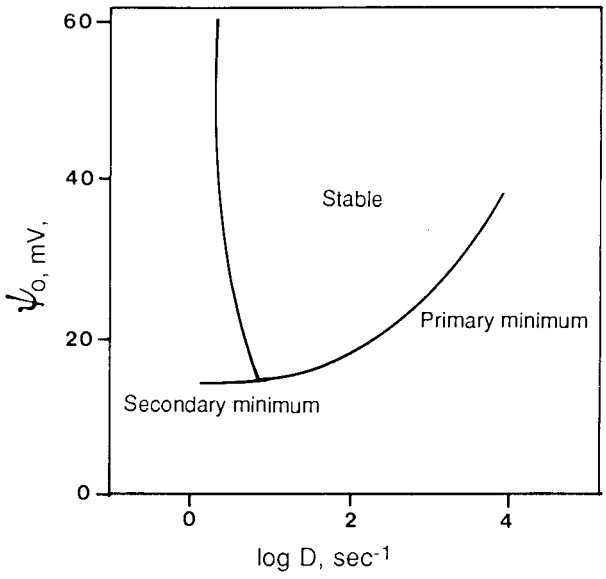

Fig. 7. The effect of surface potential and shear rate on stability. The system is unstable at low and high shear rates but remains stable at intermediate values [from Van de Ven and Mason [51] with permission).

the dispersion as a function of dimensionless groups characterizing the relative strength of the interparticle and viscous forces.

Turbulent flow conditions

For turbulent conditions the situation becomes extremely complex. Theories of coagulation have been derived by Camp and Stein [54], Saffman and Turner [55] and Levich and Probstein [56]. Generally, assuming homogeneous isotropic turbulence, two different mechanisms have been considered which depend on the particle size, relative to the microscale length of turbulence (λ_o) where:

$$\lambda_o = \left(\frac{\nu^3}{\bar{\varepsilon}}\right)^{1/4} \tag{16}$$

where $\nu = \eta/p$ is the kinematic viscosity, and $\bar{\varepsilon}$ is the average rate of energy dissipation per unit mass of suspension. Typically λ_o has a magnitude of 25 μm in stirred tanks.

For small particles (relative to λ_o), assuming that there is no energy barrier to prevent coagulation, then from a simplified interpretation of the Smoluchowski orthokinetic kinetics, the rate of coagulation under turbulent flow conditions can be

given by:

$$-\left(\frac{dN}{dt}\right)_{o/t} \propto \left(\frac{\bar{\varepsilon}}{\nu}\right)^{1/2} (a_1 + a_2)^3 N_1 N_2 \tag{17}$$

where N_1 and N_2 are the concentrations of particles of radii a_1 and a_2, respectively, and assuming no break up of the flocs occurs.

For larger particles ($a > \lambda_o$):

$$-\left(\frac{dN}{dt}\right)_{o/t} \propto (\bar{\varepsilon})^{1/3} (a_1 + a_2)^{7/3} N_1 N_2 \tag{18}$$

Chia and Somasundaran [57] have studied the coagulation of fine anatase and coarse oleate coated calcite mineral particles under intense agitation using these equations. Unfortunately, the theories were difficult to verify, since in many systems the larger aggregates break up above a critical size and it is necessary to introduce so-called break-up models. In laboratory experiments, this effect can be seen from particle size measurements where a maximum size coagula is produced.

The influence of intense agitation on the state of a dispersion has also been studied in theory and practice by Tomi and Bagster [58, 59]. Some qualitative predictions were made of the size of the aggregates produced under hydrodynamic forces in industrial equipment and these predictions were tested with a flocculated

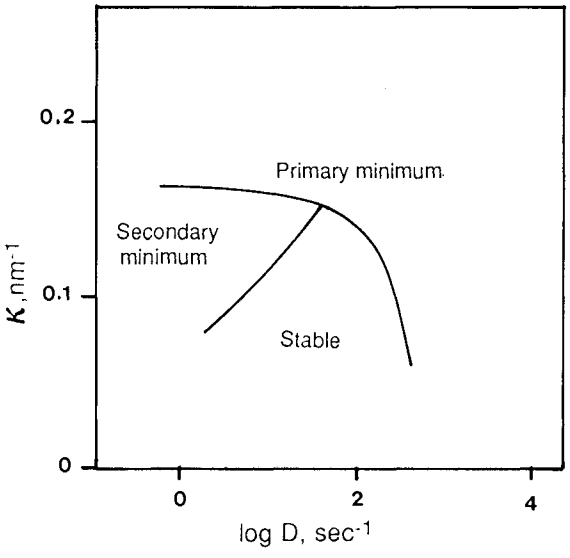

Fig. 8. The effect of ionic strength and shear rate on stability. The system is unstable at low and high shear rates but remains stable at intermediate values (from Van de Ven and Mason [51] with permission).

galena suspension. It was shown that the aggregates build up to a maximum size and thereafter a slow process of irreversible degradation occurs.

Steric stabilization

In addition to low molecular weight inorganic dispersing agents which operate by stabilizing electrostatically the particles, polymers are often used to stabilize sterically the mineral particles. In fact, high molecular weight polymers such as proteins and gums have a long history as stabilizing agents. Steric stabilization between adsorbed polymer layers was first discussed by Heller and Pugh [60], although steric hindrance was also considered by Koelman and Overbeek [61] in 1954. The presence of an excess of non-adsorbed polymer can cause depletion stabilization but this is not considered in the present text.

Although the theoretical aspects of the mechanism of steric stabilization by adsorbing polymer is still not well understood today, it is clear that an additional repulsive term, V_S, must be introduced into equation (1) to account for the repulsive component caused by the overlap of the adsorbed polymer outer segments as they begin to overlap. Hence, the total interaction equation (1) must be modified to:

$$V_T = V_E + V_A + V_S \tag{19}$$

where V_S is a short range structural term and rises rapidly at short interparticle distances. Several theoretical approaches have been made to describe steric stabilization. These have been reviewed by Sato and Ruch [62] and generally fall into two main groups: (a) entropic stabilization theories, and (b) osmotic stabilization theories. In the entropic theories, the layers of adsorbed polymers do not penetrate when the particles collide but the compression effects cause a decrease in entropy. This results in an increase in Gibbs free energy causing interparticle repulsion.

According to the osmotic theories, the polymer chains can penetrate on collision causing an increase in Gibbs free energy due to the reduction of polymer chains in contact with the dispersion medium which increases the enthalpy. Also the configurational entropy of the adsorbed polymer is reduced.

Both types of approaches are complex and controversial and verification of these theories is extremely sparse. Experimental studies of steric interactions have so far been restricted to homopolymers adsorbed on mica. A number of surface force measurements have been reported but these experiments only give data which represent the very slow approach of the two mica sheets. Most of the theories of steric interactions are equilibrium theories but in practice it appears unlikely that two rapidly approaching mineral particles under thermal motion or shear will not respond to the equilibrium conditions. Steric forces are time-dependent and rate-dependent due to the rheological behaviour of adsorbed polymers. Also, in the case of ionic polymers the adsorbed layers can also effect V_E and V_A in addition to V_S.

For a highly solvated macromolecular film, the refractive index and hence the effective London-Hamaker constant will be close to the value of water. Under these circumstances the layer will contribute only weak interparticle attractive forces (V_A) when the layers touch and we can assume that the layers are not easily compressed. For extended hydrated polymer chains which may be compressed it is necessary to predict the configuration changes to calculate the elastic force (or osmotic pressure to remove solvent from the coating) and this is extremely difficult.

Unfortunately, many of these models for the treatment of steric repulsion are rather too sophisticated and uncertain to apply to dispersed mineral systems. However, for practical purposes an estimate can be made of the thickness of the adsorbed layer required for steric stabilization of a spherical particle providing no compression occurs and if we select a model where there is only Van der Waals attraction, and the repulsion becomes infinite as soon as the adsorbed layers come into contact ("non-penetration" of adsorbed polymer layers). Under these circumstances the approaching particles will be held in an energy minimum, the depth of which, V_M, depends on the thickness of the adsorbed layer.

If we take V_A^{121} to represent the total energy of attraction between two equal-sized spherical particles of the same mineral (1) in water (2) (when the polymer layers coating the two approaching particles touch), then this value should be greater than k_BT, the average kinetic energy per particle in order that sticking will occur on

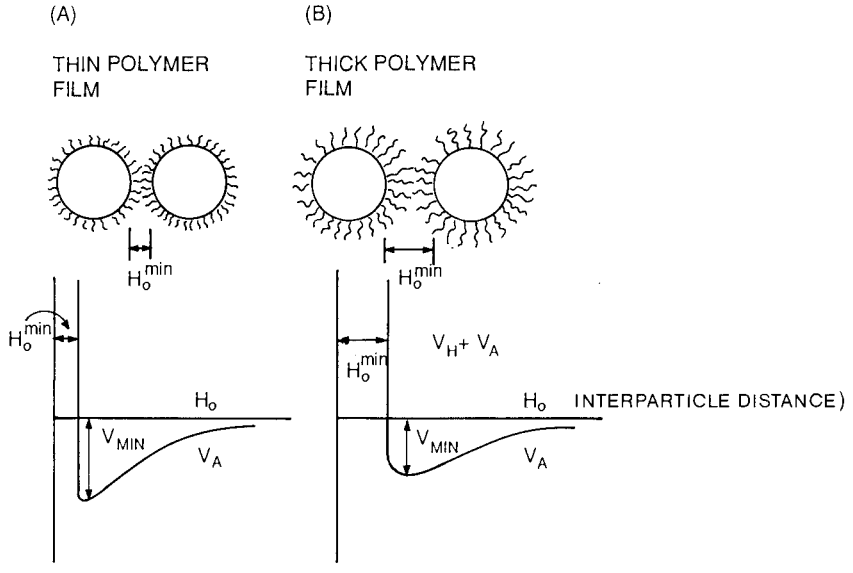

Fig. 9. Systematic representation of the potential energy of interaction versus interparticle distance curves for two approaching mineral particles with a film thickness of adsorbed dispersant of $H_o^{min}/2$. In order for sticking to occur $V_{MIN} > k_BT$. Two situations are considered with a thin and a thick adsorbed film.

contact (Figure 9). If the value is less than k_BT the particles will not stick but will redisperse.

The energy of attraction at short interparticle distances may be represented by:

$$V_A^{121} = -\frac{aA_{121}}{12H_o} \times f \tag{20}$$

where a is the particle radius, f is the retardation factor, and H_o is the interparticle distance.

The shortest interparticle distance of separation, H_o^{min}, for the particles to remain stable when the particles are touching (assuming $V_A^{121} \approx -k_BT$ at this point) can be given by:

$$H_o^{min} = \frac{aA_{121}}{12k_BT} \times f \tag{21}$$

The requirement for stability is that a particle must have a minimum film thickness of adsorbed dispersant of $H_o^{min}/2$. The retardation effects on the London forces (f) may be calculated from the equations derived by Schenkel and Kitchener [63] so that equation (21) may be re-expressed as:

$$H_o^{min} = \frac{aA_{121}}{12k_BT}\left(\frac{1}{1 + 1.77p_o}\right) \qquad \text{for} \quad 0 < p_o < 2 \tag{22}$$

and:

$$H_o^{min} = \frac{aA_{121}}{12k_BT}\left(\frac{+2.45}{5p_o} - \frac{2.17}{15p_o^2} + \frac{0.59}{35p_o^3}\right) \qquad \text{for} \quad 0.5 < p_o < \infty \tag{23}$$

where A_{121} is the Hamaker constant of the mineral (2) in water (1), $p_o = 2\pi H_o/\lambda_a$, and λ_a is the wavelength corresponding to the intrinsic electronic oscillation of atoms ($\approx$1000 Å for the minerals in water). Using these equations the minimum film thickness of the dispersant (to establish stability) can be related to the particle radius for mineral particles dispersed in water (see Figure 10).

Hydration forces

The DLVO theory was developed from two types of interactions — electrical double layer repulsion and Van der Waals attraction. More recently, discrepancies in DLVO theory have been explained by additional forces which are thought to be of a "structural" nature and arise from the re-arrangement of water molecules near the interface. The structural forces are known to be important at close distances and produce either repulsion in the liquids that are able to wet the substrate, or attraction when the solid is poorly wetted by the liquid [64]. The hydrophobic structure forces can cause a very strong attraction [65]. The development of a theory for structural forces is today only in the initial stages [66, 67].

Estimates of the range of these forces have varied from a few molecular diameters to much larger distances. With high molecular weight hydrated dispersants such as starch and tannins the hydration force appears to be combined with the steric repulsion force. This may be explained by the simple fact that a steric stabiliser requires the polymer to have some degree of hydration. At first sight, this suggests that steric stabilization by polymeric surfactants automatically involves hydration forces. However, recent studies have shown that a low molecular weight polyethylene oxide can stabilize and act as depressant and dispersant for colloidal talc particles [68]. With such a short-chain nonionic surfactant, steric stabilization appears unlikely. Since the efficiency of steric stabilizers generally decreases with decrease in chain length and increase in flexibility, it seems likely that many low molecular weight nonionic hydrophilic polymers stabilize colloidal systems by hydration forces to some extent. With high molecular weight polyethylene oxide (PEO) polymers probably a combination of steric and hydration forces arise. Particles stabilized by PEO type molecules can be destabilized if the solvency of water for the PEO chain is reduced, for example by adding large amounts of electrolyte, or by increasing the temperature.

Generally, repulsive hydration forces occur whenever molecules are strongly hydrated or water is strongly bound to hydrophilic groups such as –OH, $-PO_4^{3-}$,

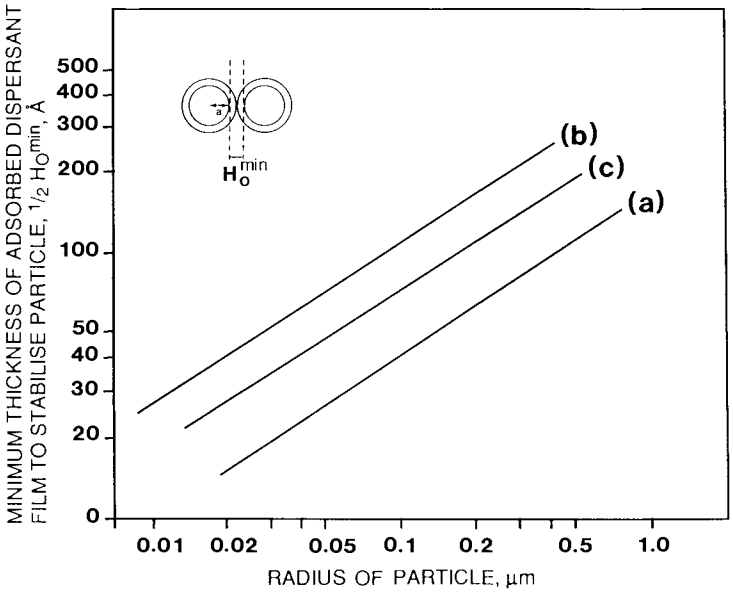

Fig. 10. Steric stabilization of mineral particles with adsorbed dispersant film. The minimum thickness of the film ($H_o^{min}/2$) to achieve stability versus the radius of the particle. *a*: Fused quartz particles in water with $A_{121} = 0.8 \times 10^{-20}$ J; *b*: Al_2O_3 in water with $A_{121} = 4 \times 10^{-20}$ J; *c*: clay particles in water with $A_{121} = 2 \times 10^{-20}$ J.

$-N(CH_3)_3^+$, etc., and their strength depends on the energy needed to disrupt the ordered water structure and ultimately dehydrate the end groups of the adsorbed molecules. The effectiveness to induce hydration effects depends on such factors as the size of the head group, the number of head groups and their mobility. In the case of macromolecular depressant films such as starches, tannins, polyphenols, dyes, etc., where the molecules are associated with multitudes of hydrophilic groups, it may be suggested that the strong ion-dipole effects may impose a structure on the neighbouring water. The extent that these forces propagate into solution would depend upon the conformation and type of adsorbed polymer.

Another example where hydration force arises is where high concentrations (>1 mM) of hydrated cationic counterions are adsorbed on minerals (i.e. clay surfaces). This has been demonstrated by the surface force apparatus [69]. Two mica surfaces in concentrated electrolyte solution are gradually pushed together. At close distances dehydration of the cations must occur, leading to an increase in free energy and repulsion. The value of the repulsive force increases with the hydration of the adsorbed cation following the lyotropic series $Li^+ \approx Na^+ > K^+ > Cs^+$ and have been shown to be exponential with a decay length of about 1 nm. At low ionic strength no hydration force was found and the repulsion followed DLVO theory.

Dispersing agents at solid/liquid interfaces

Inorganic dispersants

According to Leja [9], water glass (sodium silicate) and polyphosphates are used primarily to control the charge density at the solid/liquid interface. This makes them typical dispersing agents; at higher concentrations, they are also used as flotation depressants.

Many authors believe that polysilicic acid belongs to the most active species in sodium silicate aqueous solutions. Since the polymerization involves both H_3SiO_4 ion and $Si(OH)_4$ molecule it depends on pH, but it is also accelerated by polyvalent cations, and an increased temperature speeds up the polymerization process [70].

Synergistic effects of polyvalent cations and sodium silicate were extensively investigated by Russian authors. Fatty acid adsorption on such minerals as fluorite, barite, calcite, etc., was found to decrease in the presence of sodium silicate. Sodium silicate activity was found to be extremely sensitive to the presence of polyvalent cations. Klassen and Mokrousov [10] reviewed these works and concluded that the formation of polysilicic acid seemed to be responsible for increased activity of sodium silicate.

Polysilicic acid (a weak acid) is partly ionized in aqueous solutions. Its adsorption must lead to an increased negative charge of the solid and, consequently, must stabilize mineral systems against aggregation. The results of direct sedimentation

experiments which support such a conclusion can be found in technical literature [10]. Parsonage et al. [71] are of the opinion that polymeric sodium silicate adsorbs by multiple weak bonds to form hydrated layers at the mineral surface. In consequence, dispersion is due to both an increased negative zeta potential values and hydrated layers.

Generally, it may be expected that good complexing agents will exhibit high adsorption. Since polyphosphates have strong affinity for the surface and can adsorb either electrostatically or by hydrogen bonding, or by forming strong covalent bonds with a number of metallic cations, these are very powerful dispersing agents [72].

In a very extensive comparative study of various dispersing agents for cassiterite suspensions, aminopolyphosphates and polyphosphates were found to the most effective [73].

Changgen and Yongxin [74] concluded that while the zeta potential of the studied minerals (scheelite, calcite, fluorite) was becoming much more negative in the presence of polyphosphates, they were not able to detect any adsorption of polyphosphate anions on the mineral surfaces. The adsorption of sodium oleate, which was used as a collector in the flotation of the minerals they studied, was much lower when these minerals had been first contacted with polyphosphates. Based on these observation, the quoted authors [74] postulated that phosphates form complexes with calcium and selectively dissolve calcium ions from the mineral surface. Thus, this mechanism imparts a negative charge to the particles via decreasing the number of positively charged active centers on the mineral surface.

A mixture of sodium salts of cyclic hexametaphosphoric acid and linear dimeric pyrophosphoric acid ($H_4P_2O_7$) is a commercially produced dispersant under the trade name Calgon.

Organic polymeric dispersants

Where a small but finite adsorption affinity exists for a monomeric substance, adsorption is greatly enhanced on going to an analogous polymeric compound. The reason is simply that the mean translational energy of all molecules, large or small, remains at $3/2(k_BT)$, whereas the adsorption energy increases proportionally to the number of links, thus the probability of adsorption rises steeply with molecular weight. To illustrate this point, Kitchener uses, as an example, polyphosphate effectiveness in imparting a strong negative charge to oxides [75].

Since in this chapter we are dealing with dispersants, one has to bear in mind that a too long hydrocarbon chain of an organic polymer may eventually lead to flocculation [34, 76]. In accordance with this principle, polysaccharides of lower molecular weight, such as dextrins, are commonly used as dispersants, whereas starches are also used as flocculants.

The mechanism of interaction of polysaccharides with mineral surfaces was studied extensively by Iwasaki and his co-workers [17, 77–80). Since electrophoretic

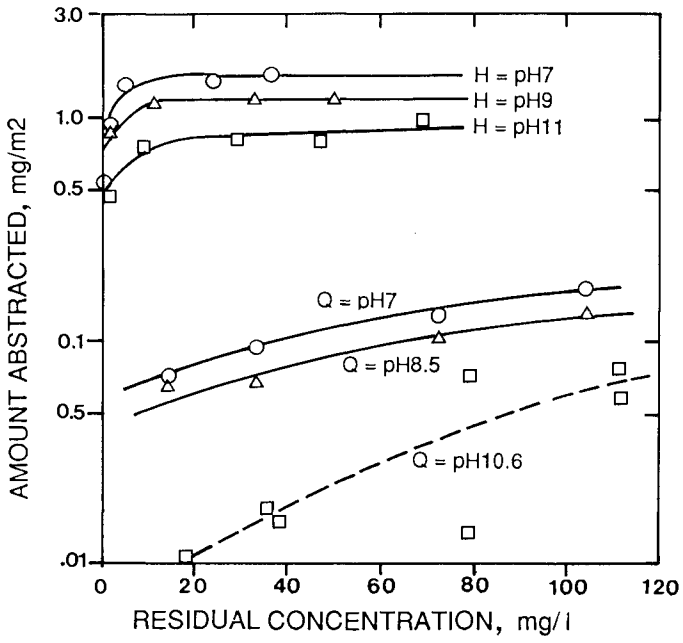

Fig. 11. Adsorption of corn starch on hematite (H) and quartz (Q) (from Balajee and Iwasaki [17] with permission).

tests revealed that in alkaline solutions potato starch migrated towards the cathode, indicating its negative charge, Balajee and Iwasaki [17] postulated that starch is more strongly adsorbed on less electronegative hematite than on quartz. Their experimental adsorption results are shown in Figure 11.

It is obvious that coulombic repulsive forces acting between the mineral surface and starch molecules hinder adsorption, but the adsorption is obviously caused by nonionic interactions. In this and other cases of starch adsorption, hydrogen bonding is silently believed to be primarily responsible for adsorption.

Klassen in his monograph on coal flotation [81], reviewed various experimental data on the adsorption of dextrin and of starches on coal and concluded that both make the coal surface very hydrophilic. Flotation of coal was shown to be depressed in the presence of dextrin and starch. Klassen pointed out that branched polysaccharides were superior depressants. In line with these findings, Wie and Fuerstenau [82] showed that dextrin depresses the floatability of molybdenite. J. Miller and his co-workers [22, 83] obtained similar results for other hydrophobic minerals. All these data led to the hydrophobic bonding theory.

Our tests with carboxymethyl cellulose [84] clearly indicated, however, that while carboxymethyl cellulose adsorbed strongly onto high quality Ceylon graphite, it did not adsorb on the same graphite which was further purified by leaching with acids.

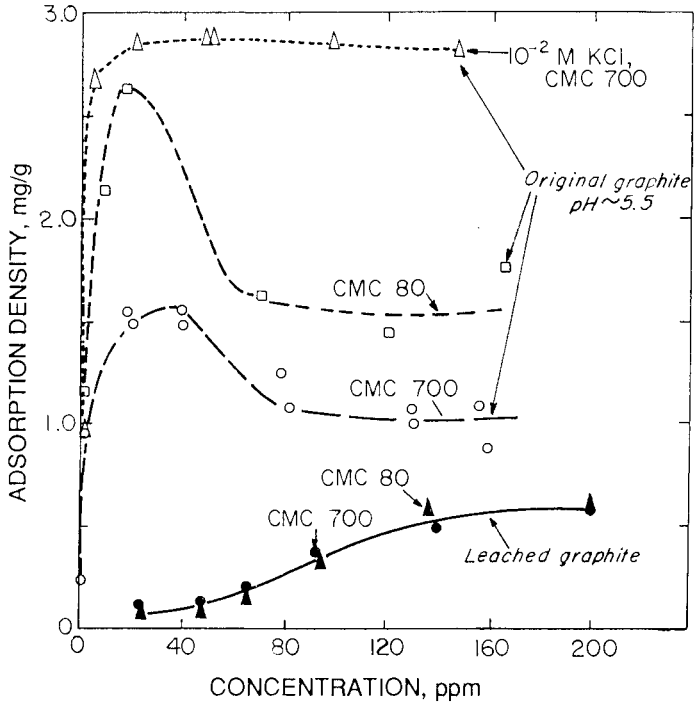

Fig. 12. Adsorption isotherm of carboxymethyl cellulose on original high quality graphite and graphite purified further by leaching, pH 5.5, 25°C; 800 and 700 stand for molecular weight of carboxymethyl cellulose of 80,000 and 700,000, respectively (from Solari et al. [84]).

Obviously this treatment removed adsorption centers such as Fe, Ca and Mg from the graphite surface, and this completely altered the adsorption isotherm from a high affinity type to a low affinity type (Figure 12).

Following these results, Liu and Laskowski [85–87] reinvestigated the mode of adsorption of dextrin onto mineral surfaces. In these tests, pure quartz was used as a model of a hydrophilic solid, methylated quartz [88] was used as a model hydrophobic surface; in some tests both were also activated by treatment with lead. Dextrin of low molecular weight, the same that was used by Wie and Fuerstenau [82], did not adsorb onto either hydrophilic quartz or methylated hydrophobic quartz. Dextrin, however, did adsorb quite strongly onto both hydrophilic and methylated hydrophobic quartz activated with lead (Figure 13) [86].

The results of Figure 14 [85] reveal the effect of pH on the interaction between dextrin and $Pb(NO_3)_2$ in aqueous solution. As seen, in the pH range from 10 to 11 both dextrin and lead interact, co-precipitate, and disappear from the solution. As shown in Figure 13, dextrin is strongly adsorbed onto lead-coated quartz exactly over the same pH range.

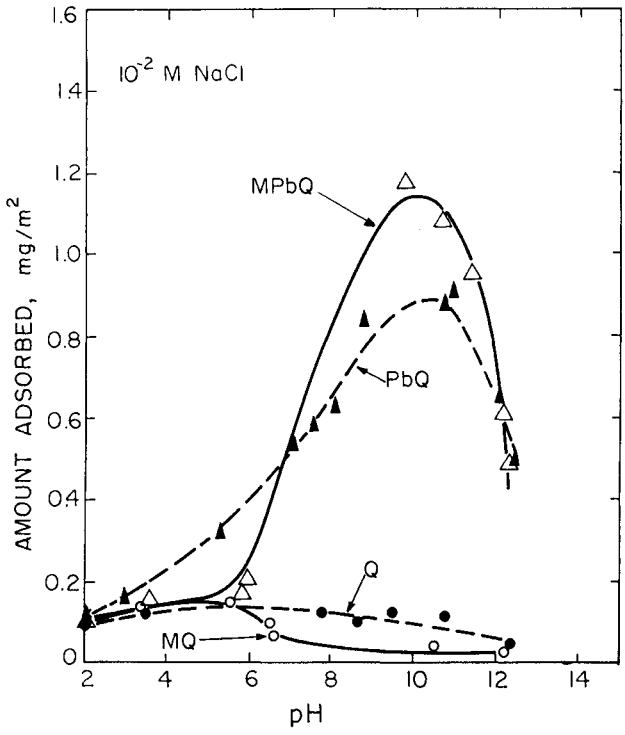

Fig. 13. Effect of pH on adsorption of dextrin on pure hydrophilic quartz (Q), quartz made hydrophobic by methylation (MQ), lead-coated hydrophilic quartz (PbQ) and hydrophobic methylated lead-coated quartz (MPbQ), initial concentration of dextrin was 50 ppm (from Liu and Laskowski [86].

These results are further corroborated by adsorption isotherms shown in Figure 15 [86]. As it is seen, low affinity type isotherms were obtained for hydrophilic and hydrophobic quartz samples which did not contain any metallic adsorption centers. High affinity type adsorption isotherms obtained for the samples containing lead indicate strong chemical in nature interaction between the lead coated surface and dextrin in the pH range from 9 to 11. Based on the infrared spectra, it was postulated that the interaction between $Pb(OH)_2$ and dextrin takes place according to the reaction [85, 86]:

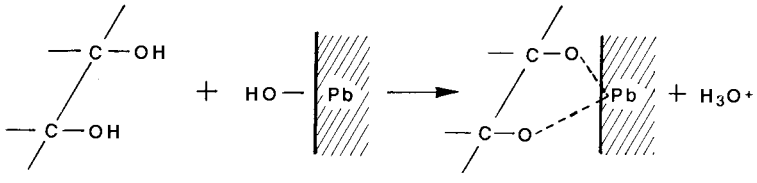

(24)

In line with this model it was shown that it was possible to separate galena from

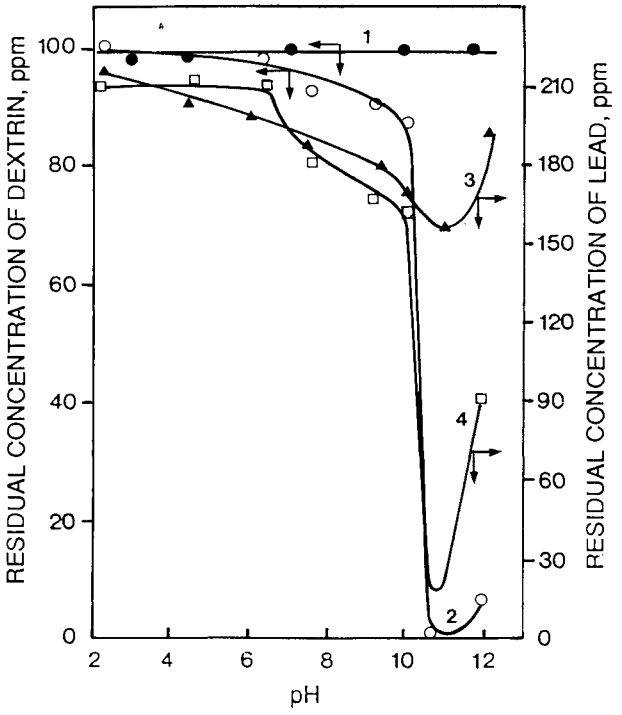

Fig. 14. Effect of pH on the residual concentration of dextrin and lead, after centrifuging at 8000 rpm for 3 min. Residual concentration of dextrin: *1* = dextrin solution; *2* = dextrin-$Pb(NO_3)_2$ solution. Residual concentration of lead: *3* = $Pb(NO_3)_2$ solution; *4* = $PB(NO_3)_2$-dextrin solution (from Liu and Laskowski [85]).

chalcopyrite in the flotation with xanthate and dextrin when the pH was accordingly adjusted [87].

These findings will require a lot of additional work to clarify all the interrelated questions before a comprehensive adsorption model, which will take into account all experimental facts, is put forward. It is to be pointed out, however, that there is no doubt that the primary reason for dextrin adsorption onto quartz is the presence of metallic adsorption centers (Figures 13 and 15), but the surface which was hydrophobic and contained lead, adsorbed more dextrin than the hydrophilic lead-coated quartz. This suggests that while the surface hydrophobicity is not the primary factor in dextrin adsorption onto solids, it still contributes to the behaviour of dextrin at such an interface. Hydrophobicity of the matrix on which lead adsorption centers rest seems to enhance further dextrin adsorption by the synergistic effect between the dextrin–mineral surface chemical interaction and some type of hydrophobic bonding.

It is worth pointing out that according to Rubio and Kitchener [89] and Rubio

[90], a combination of hydrogen bonding and hydrophobic interaction are responsible for the adsorption of polyethylene oxide on mineral surfaces. The ether groups which provide aqueous solubility of the PEO and presumably operate as hydrogen-bond acceptors to water molecules are also capable of acting as links to hydrophilic substrates. The CH_2CH_2 groups in PEO are sufficiently hydrophobic to lead to physical adsorption. As a result PEO adsorbs onto those minerals which may be referred to as hydrophobic. In line with this concept PEO was found to adsorb onto anthracite, but not onto strongly oxidized anthracite [91].

Parsonage and Marsden [73] pointed out that alcoholic –OH groups do not confer dispersant properties on a molecule, however, if hydroxybenzene has –OH groups on adjacent carbon atoms (catechol and pyrogallol). These groups dissociate when adsorbing on positive sites increasing the solid net negative charge. The effectiveness of hydroxybenzenes as dispersants for cassiterite was further greatly increased by introducing carboxyl groups into their molecules. A similar mechanism was earlier postulated by Baldauf and Schubert [92].

Lin and Burdick [24] concluded that galactomannan with two neighbouring –OH groups in a dextrose unit in cis-configuration should have better ability to associate with adsorption sites on the mineral surface than starch or dextrin. Their flotation results obtained with potash ore seem to confirm that galactomannan exhibited better dispersing properties than dextrin.

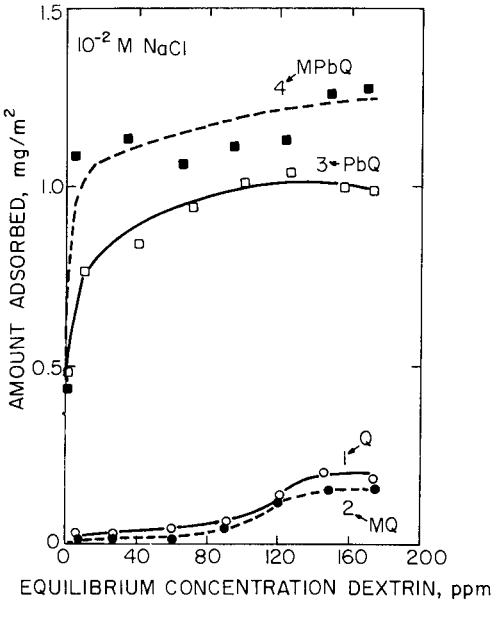

Fig. 15. Adsorption isotherm of dextrin on different quartz samples (symbols as in Figure 13; from Liu and Laskowski [86]).

It is obvious that large polysaccharide molecules with their great number of hydrophilic groups interacting strongly with water will also impose steric effects on the disperse system. Such effects were found when gum arabic was used to stabilize suspensions of calcite, dolomite and apatite [71].

In the study on the effect of gum tragacanth (an acidic polysaccharide based on galacturonic acid) on the stability of the polystyrene latex disperse system, pH was discovered to have little effect on the adsorption isotherm of the gum, but influenced significantly the stability [93]. Gum tragacanth turned out to be an effective stabilizer at low concentrations and at low pH values. As the pH was lowered, the thickness of the adsorbed layer increased significantly due to the change of conformation at the surface resulting from the formation of loops and tails. Such thick adsorbed layers on the latex particles provided strong steric repulsive forces.

Schulze et al. [94] maintain that tannins become chemisorbed on the calcium minerals through Ca^{2+} ions, either in the surface of the mineral lattice or as Ca^{2+} adsorbed on it from the solution. Pure quartz cannot be floated with oleate, but in the presence of Ca^{2+} ions floats very well at pH 12. Addition of quebracho depresses such a flotation very efficiently and confirms that quebracho is mainly adsorbed by "calcium bridging" [95].

Soluble lignin derivatives are commonly used as cheap dispersing agents. In the extensive study on the effect of sodium lignosulphonate on dispersion of TiO_2 suspension it was established that adsorption of the lignin on rutile increased the stability of the suspension [96]. The best lignosulphonate dispersants for TiO_2 were those with molecular weight from 10,000 to 40,000. The results also indicated that the dispersion power correlated approximately with the sulphur content. Strongly anionic lignosulphonates were also shown to adsorb onto negatively charged polystyrene latex particles, but the lignin with the lowest degree of sulphonation gave the highest adsorption [97, 98]. The zeta potential of the latex particles stabilized with lignosulphonate was found to be very sensitive to concentrations of Ca^{2+} ions and this was mirrored by the dependence of the stability of the lignin-stabilized latex on concentration of Ca^{2+} ions. This demonstrates that electrostatic effects play a very important role in the stabilization mechanism with lignosulphonates. Lignosulphonate was also found to be an efficient stabilizer of barite suspensions [99].

O'Melia [100] maintains that the surface properties and stability of colloidal suspensions in natural waters are affected by naturally occurring organic substances (humic acids) dissolved in these waters. His review indicates that several authors noted that all solids become moderately electro-negative in natural seawater and this seems to be due to the adsorbed organic matter. These observations also indicate that colloids in rivers can be stabilized by dissolved organic matter, but are destabilized by magnesium and calcium ions through specific chemical and electrostatic interactions with these ions. While humic substances stabilize hematite suspensions, calcium ions enhance coagulation of such systems [101]. Humic substances adsorb on alumina and kaolinite and impart negative charge to the particles.

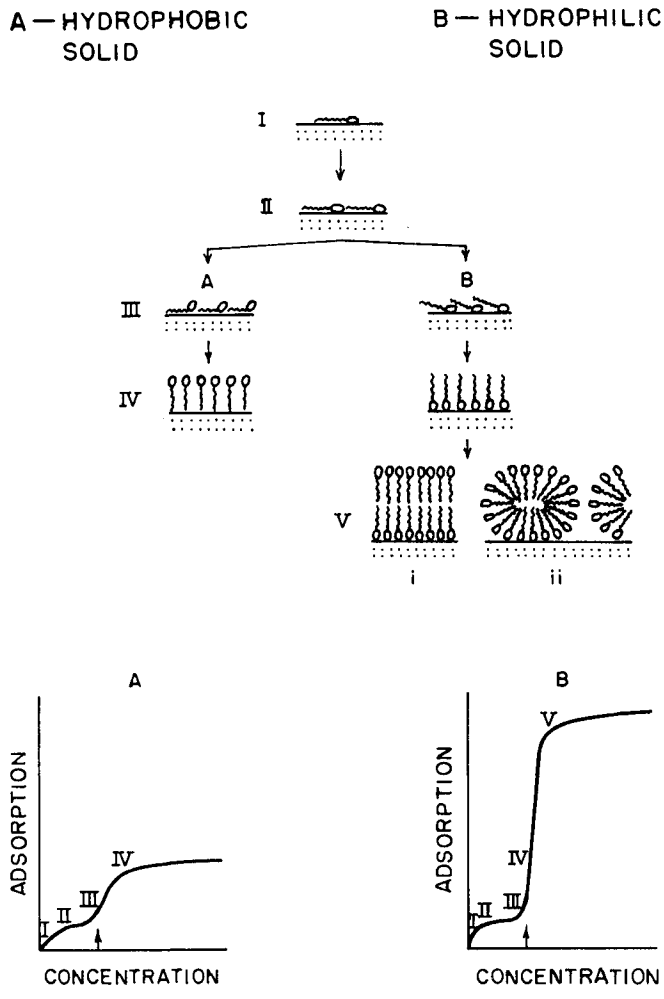

Fig. 16. Model for adsorption of nonionic polyoxy-surfactant onto hydrophobic (A) and hydrophilic (B) surfaces, and corresponding adsorption isotherms (from Clunie and Ingram [107] with permission).

Calcium enhances the adsorption of organic matter onto alumina at high pH, and reduces its adsorption at pH less than 7–8. Humic acids were also shown to adsorb onto hydrophobic solids, such as graphite, and to render them hydrophilic [102]. Measured stability factors indicated variation in particle stability among Swiss lakes. The lakes with dissolved organic content less than 2 mg l^{-1} exhibit substantial coagulation, whereas colloidal systems were found to be quite stable in the lakes with dissolved organic content in the 3–5 mg l^{-1} range [100].

All these results indicate that humic substances are quite efficient stabilizers; they seem to increase stability through both electrostatic and steric effects. The

use of humic substances as stabilizers may, however, be quite complicated for the following reasons. According to Jensen et al. [29], the molecular weight of humic acids obtained by oxidizing coal may range from less than 600 to more than 10,000. Humic matter is also leached and extracted from brown coal, pit [103], soil, natural waters, etc. Many functional groups, such as carboxylic, phenolic and alcoholic –OH as well as amino acids, have been identified in such matter [33, 104]. The number of products identified in humic matter following chemical degradation procedures amounted to 100 or more [105]. It is obvious then that the chemical composition of these substances varies enormously and that the use of such an ill-defined stabilizer can lead to quite unexpected results.

Polyoxy surfactants are another group of common dispersants. Ottewill [106] studied the effect of such components on the stability of silver iodide colloid. He observed that with an increase in concentration of polyoxy surfactant, the part played by steric stabilization increased substantially making the electrostatic stabilizing factor a less important parameter. Figure 16 summarizes after Clunie and Ingram [107] the mode of adsorption of polyoxy nonionic surfactants onto hydrophobic and hydrophilic solids. Due to various orientations and packing at the solid/solution interface, such molecules can adsorb on both hydrophobic and hydrophilic substrates. In both cases the solid surface becomes covered with the oriented layer of molecules with their polar heads facing the aqueous phase. As shown by Scales et al. [108], who measured the wettability of the hydrophobic methylated quartz and hydrophilic quartz surfaces in the solutions of nonyl polyoxy phenols, at the concentration exceeding the critical micelle concentration of the

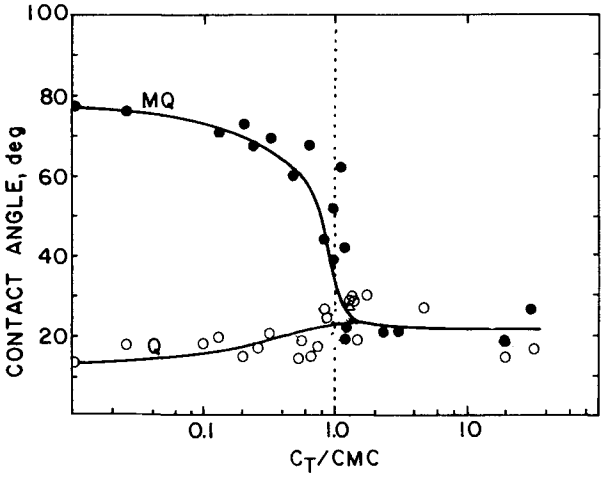

Fig. 17. Calculated equilibrium contact angles on hydrophilic silica and methylated hydrophobic silica versus normalized equilibrium concentration of nonyl polyoxyphenols with 5, 9 and 30 ethoxy units per molecule (from Scales et al. [108] with permission).

surfactant both surfaces become completely hydrophilic (Figure 17). These experimental results agree reasonably well with Ottewill's concept that steric stabilizing effects are predominant in the mechanism by which polyoxy surfactants stabilize disperse systems.

Stability measurements of dispersed systems

The assessment of the dispersibility or stability of a suspension is one of the most difficult experimental aspects of dispersion science. To begin, it is important to distinguish between dispersibility which is the resistance to break apart or separate aggregates (by chemical and mechanical methods) and stability which is a measure of the rate of reaggregation. In the case of dilute suspensions the dispersion and stability behaviour may occur on different time scales so that they can be treated as separate processes. However, in concentrated suspensions assuming there is no stability barrier, the two processes may superimpose since the dispersion step is rapidly reversed by coagulation. This may be illustrated from the Smoluchowski theory which describes the rate of fast coagulation [see equation (6)]. On integration the half life $t_{1/2}$ (the time required to half the number of particles in the system) may be expressed by:

$$t_{1/2} = 3\eta/4k_BTN_o \approx 2 \times 10^{11}/N_o \quad \text{(sec)} \tag{25}$$

For a dilute suspension ($N_o = 10^7$ particles cm^{-3}) in water, at room temperature $t_{1/2}$ would be several hours, whereas for a concentrated suspension $\approx 5\%$, ($N_o = 10^{14}$ particles cm^{-3}) $t_{1/2}$ would be reduced to milliseconds and the process is reversed extremely rapidly. Colloid stability in concentrated dispersions cannot easily be followed by experimentally measuring the change in turbidity in light scattering as in dilute suspensions, and it is necessary to study rheology or neutron scattering, or taking a more simplified approach by measuring the sedimentation volume. Unfortunately, many of the techniques used to measure stability, such as rheology and microscopy, tend to disturb the system. A general guide of the simpler methods of stability measurements will be given below.

Optical microscopy

This usually involves counting the number of particles over a projected area using an eyepiece graticule. The number particle size distribution can be converted into a weight size distribution but a sufficiently large number of particles must be counted to have statistical significance. For many dilute suspensions, one can also study the interparticle collisions as they occur and observe interparticle repulsion or attraction and floc formation or disruption. After certain time intervals the coagulation process can be stopped by adding arabic or gelatin solution. The particles

may then be accurately counted. Several instrumentation techniques have now been developed so the counting method are no longer tedious or time consuming. For very small particles the electron microscope is useful (<1–2 μm) but the sample preparation methods are more specialized.

Scattering methods

Particle-size-distribution analysis by photon-correlation spectroscopy is a useful method for studying the stability but is restricted to dilute solutions of small particles. New laser diffraction instruments such as the Master Sizer (Malvern Instruments) can now deal with much greater size ranges (from 0.1 to 600 μm, covered by two overlapping ranges from 0.1 to 80 μm and 1.2 to 600 μm). The technique is based on laser diffraction where small and large particles diffract light at large and small angles, respectively. Measurement of the scattered light is carried out over a wide range of angles in the near forward direction. The instrument is suitable for on-line use and can be utilized for determining the particle size in aqueous and non-aqueous suspensions.

Electronic counting techniques

Several instruments have been devised to count the change in electrical resistance that occurs when a non-conducting particle dispersed in an electrolyte flows through a small orifice, i.e. Coulter Counter (Coulter Electronics) or Elzone Particle Sizer (Particle Data Inc., U.S.A.). The instruments usually measure only in dilute dispersions. Particle sizes in the 1–400 μm range can be easily measured accurately, however, and the sensitivity of the apparatus can be altered since it depends on the ratio of the particle radius to the orifice radius. The method is useful for counting a large number of particles and can be used for stability measurements by providing counts on singlets, doublets, triplets, etc., related to coagulation kinetics. Unfortunately, the instrument is not accurate for floc sizes or volumes and treats aggregates as solid spheres composed of primary particles with no water included. Also loose flocs may be sheared by the velocity gradients in the flow as they pass through the orifice.

Electrokinetics

The zeta potential (ζ) is the potential drop across the mobile part of the double layer (dl) that surrounds a colloidal particle and is responsible for the electrokinetic behaviour of the particle under an electric field. From double layer theory, the ζ-potential may be equated to the Stern layer potential ψ_δ and enables a basic understanding of types of ions and species which determine the structure of the dou-

ble layer. This type of information is important with regard to suspension stability, rheology and sediment characteristics.

For solids for which H^+ and OH^- ions are potential determining, the pH value at which the charge on the surface is zero is called the zero point of charge (pH_{zpc}). This value is determined by titration with potential-determining ions. Conditions under which the ζ-potential is zero is called the iso-electric point (pH_{iep}). For oxide minerals when the zeta potential measurements are carried out in the presence of non-specific adsorbing ions, $pH_{iep} \approx pH_{zpc}$. However, in the presence of specifically adsorbing species such as polyvalent or surface active dispersant species, the pH_{zpc} may not be identical to the pH_{iep}. Hence, the difference between these two values can sometimes be useful for understanding the adsorption mechanism.

For oxide systems the zeta potential versus pH curves (assuming OH^- and H^+ are potential determining ions) are fairly reproducible with well defined pH_{iep}. These values are characteristic of the oxide type and generally reflect the varying degree of basicity or acidity of the hydrated surface. Differences in pH_{iep} for a certain type of oxide mineral can be explained by difference in degree of purity, hydration, cleavage, crystallinity etc. For other minerals such as sulphides, a wide spectrum of values have been reported which can be explained by considering the complicating effects associated with the oxidation kinetics of the surface [109]. For salt type minerals, the situation is perplexing due to the effect of both the pH and the concentration of all potential determining ions released by dissolution from the lattice and complexed in solution.

Zeta potential measurement can be made using instruments based on the following principles: (a) *electrophoresis* — the movement of the charged particle under an applied field relative to the surrounding liquid; (b) *electro-osmosis* — the movement of the liquid relative to a charged surface (capillary or plug); (c) *streaming potential* — the electric field created when a liquid flows along a stationary charged surface; and (d) *sedimentation potential* — the electric field created when charged particles move relative to a stationary liquid [110, 111]. Several types of commercial instruments are available to determine the zeta potential, i.e. Zeta Sizer, (Malvern Instruments), Zetameters (Zetameter Inc., Penkem, Rank Bros.), etc. For larger particles the zeta potential may be determined by streaming potential technique. Most ζ-potential measurements today are carried out on small particles in dilute suspensions using the electrophoresis technique. For concentrated suspensions, instruments have been developed to use electric and ultrasonic impulses to determine zeta potential values [112].

Earlier measurements on concentrated dispersions were made using boundary methods, electrophoresis mass transfer and instruments built to determine the mass of particles deposited on an electrode. However, these types of instruments have begun to be replaced by acoustic techniques. The original principle of the acoustic method, that sound waves passing through a suspension of charged particles could generate a force causing an electric field due to a difference in relative motion of

the two phases, was originally proposed by Debye [113]. The sinusoidal-colloidal-vibration potential is measured between electrodes and the acoustic mobility value can be calculated providing the density and volume fraction are known and from the acoustic mobility data, zeta potential values can be determined. Several new instruments have recently been introduced where it is possible to measure both surface charge (by titration) and the zeta potential by acoustophoretic measurements on concentrated dispersions. This enables both the pH_{iep} and pH_{zpc} to be determined on the same sample. In cases where the two values differ, it becomes possible to understand the role of the potential determining ion, indifferent ion and chemically adsorbed ion on the stability of the system. The principles of the technique have been recently reviewed by Babchin et al. [114] where acoustophoretic mobility results are compared to electrophoretic mobility data for several dispersed systems.

Rheology

Rheological measurements have been widely used to characterize the dispersibility and stability of mineral systems although the exact interpretation of the observed phenomenon for heterodispersed non-spherical particles in concentrated systems is difficult. In fact, most of the fundamental studies have been carried out with large suspensions of spheres at a low solid concentration. These idealistic particulate suspensions usually show Newtonian flow behaviour where the shear (τ) is linearly dependent on the shear rate (D) and their ratio is constant over the whole shear rate range giving a value of the coefficient of viscosity (η):

$$\tau = \eta D \tag{26}$$

Unfortunately, in the mineral processing industry many different types of less expensive viscometers are used, such as the capillary flow type or the coaxial cylindrical type (the Brookfield which consists of a motor-driven bob and a dynamometer to measure the torque). This has led to a tendency to characterize suspensions by determining a simple rate of flow at a given shear rate giving only an apparent viscosity:

$$\eta_a = \frac{\tau}{D} \tag{27}$$

This value implies that the flow curve is linear passing through the origin and that the suspension exhibits Newtonian behaviour. However, many mineral suspensions show non-Newtonian plastic or pseudoplastic rheological behaviour in which the apparent viscosity of the suspension and shear stress are dependent on the shear rate. For such cases Bingham's equation can often be used to describe the flow behaviour:

$$\tau = \tau_B + \eta_{pl} \cdot D \tag{28}$$

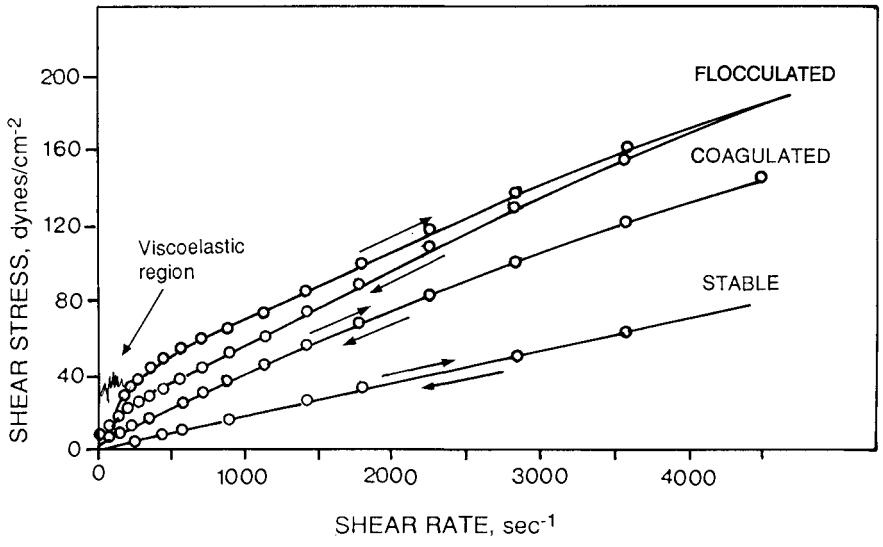

Fig. 18. Rheological properties of calcite suspensions (10% w/w) with different degrees of aggregation (from Friend and Kitchener [115] with permission).

where τ_B is the Bingham yield value and η_{pl} is the plastic viscosity or the Herschel-Bulkley equation:

$$\tau = \tau_o + AD^b \tag{29}$$

where A and b are constants.

Friend and Kitchener [115] carried out rheological measurements using a Weissenberg rheogoniometer with calcite: (a) dispersed to a stable slurry, (b) after ionic coagulation with electrolyte, and (c) after flocculation with a high molecular weight polyelectrolyte. The rheological plots of shear stress as a function of shear demonstrated the widely different rheological behaviour of the three systems and is shown in Figure 18 (for more information see [116]).

By definition, the gradient of this curve at any point is the apparent viscosity of the suspension at the relevant shear rate. It can be seen that the stable suspension exhibits Newtonian behaviour, the coagulated suspension shows reversible plastic behaviour (decreasing viscosity up to a constant value as the shear rate increases) and the flocculated suspension shows irreversible pseudo-plastic behaviour with initial viscoelasticity. The hysteresis in the latter case results from irreversible breakdown of the larger flocs. However, the average floc size remaining after periods of intense shear is still greater than in the case of the coagulated suspensions. This indicates that the flocs are strongly held together and cannot be easily ruptured. Figure 19 illustrates the different degrees of aggregation present in (a) a stable suspension, (b) an ionically coagulated suspension, and (c) a flocculated suspension

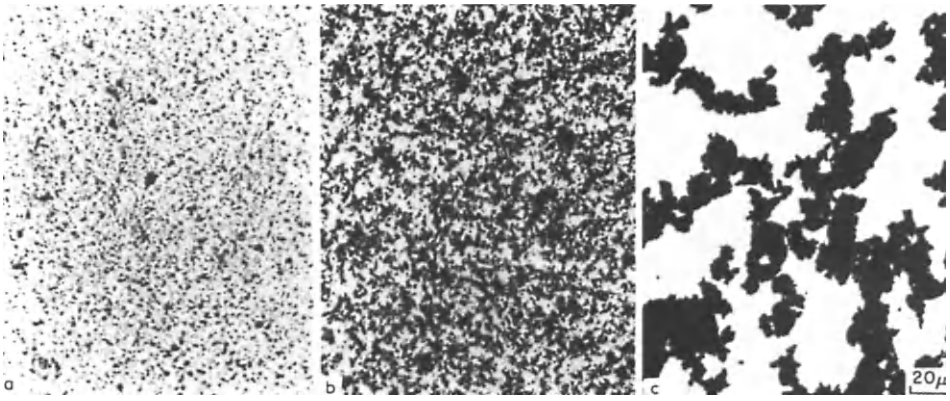

Fig. 19. Finely divided ferric oxide with different degrees of aggregation. (a) Dispersed with non-ionic surfactant (large energy barrier); (b) coagulated by addition of electrolyte (no energy barrier); (c) flocculated with a polymeric flocculant. The flocs are much larger than the coagula (from Friend and Kitchener [115] with permission).

of hematite. These flocs are much larger for the suspension flocculated with polymer (for more information on rheology of sedimenting suspensions see [118]).

Sedimentation rate and sedimentation bed volume

Useful information on dispersion stability can be obtained by simply allowing the suspension to settle and by observing the boundary. As most mineral slurries contain submicron particles as well as large particles, a graded turbidity can be expected as the particles sediment separately at different rates. For a coagulating suspension, a sharp upper boundary with a clear supernatant can often be seen. The measurement of the rate of fall of the boundary can also be informative. From Stokes law the velocity of an isolated spherical sedimenting particle (V_S) can be related to the second power of the diameter by the equation:

$$V_S = \frac{2g}{9\eta}(\rho_s - \rho_l)a^2 \tag{30}$$

where η is the viscosity of the liquid and ρ_s and ρ_l are the densities of the solid and liquid.

Sedimentation balances or Andreasen pipettes can be used to follow the sedimentation process. Photosedimentation measurements are less tedious to carry out (Figure 20). The method is only valid for dilute suspensions $<0.2\%$ volume as for higher solids content $>1\%$ hindered settling occurs and the behaviour of the dispersion will depend on the structure as well as the particle size and density. Modern sedigraphs incorporate a finely collimated beam of low energy X-rays and a detector to determine the distribution of particle sizes in a cell containing a sedimentation

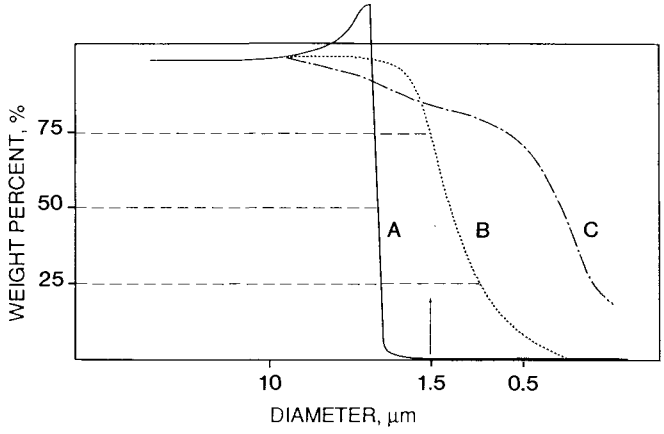

Fig. 20. Particle size distribution on a sedigraph analyzer of a calcite suspension. *A* = after flocculation with polyacrylate; *B* = non-flocculated suspension; *C* = dispersed using ultrasonics (from Foissy et al. [117]).

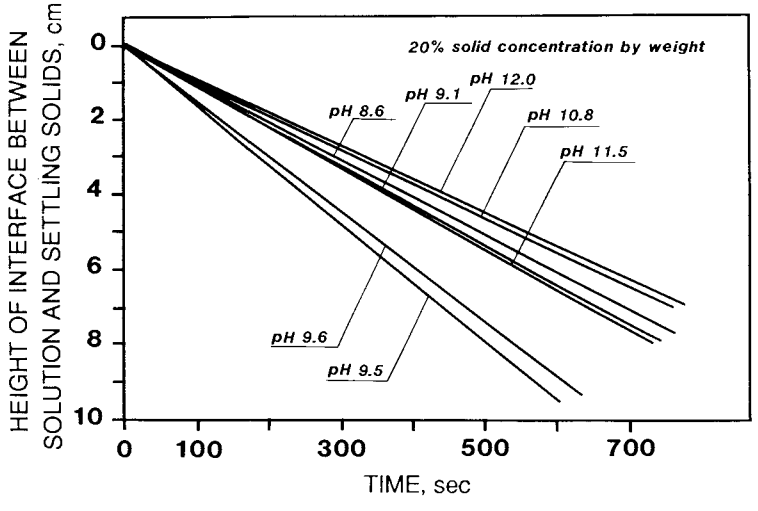

Fig. 21. Hindered settling of dolomite suspensions at 20 wt.% solids. pH values are indicated on the curves (from Sadowski and Laskowski [120]).

liquid (Sedigraph 5100). The X-ray source and detector assembly are stationary, and the cell containing the sample moves vertically between them. The X-ray pulses passes through the cell and determines the distribution of particle mass at various points in the cell from the number of pulses reaching the detector. The instrument covers particle sizes from 0.1 to 300 μm and gives the distribution and the percent mass at given particle diameters.

Laskowski et al. [119, 120], measured hindered settling rates of several mineral slurries and related the results to the stability of the systems. For unstable suspensions, aggregation of the particles is promoted during the sedimentation process due to the weak shear forces. It was found that the mean Stokes diameter, $\bar{d}$, of the slurry particles or aggregates depended on the suspension pH. The value of $\bar{d}$ was designated the apparent mean diameter and could be related directly to the stability of the suspension. The hindered settling technique was therefore found to be an extremely useful method to study aggregate stability of quartz, dolomite, magnesite and calcite suspensions and also for determining the pH_{iep} of the mineral system where the coagulation is maximum (Figures 21 and 22).

In concentrated suspensions hindered settling occurs and several equations have been proposed to describe the process. Usually the hindrance is considered to be dependant on the solids volume fraction. Three different methods were used by Dollimore and Horridge [121] to determine the limiting settling rate at zero solids concentration. The value was obtained by extrapolation of the directly determined settling rate (Q) to zero solids concentration by assuming that the modified rate equals the Stoke's settling rate V_S. From the limiting settling rates the particle radius was calculated from equation (30) which was assumed to correspond to the

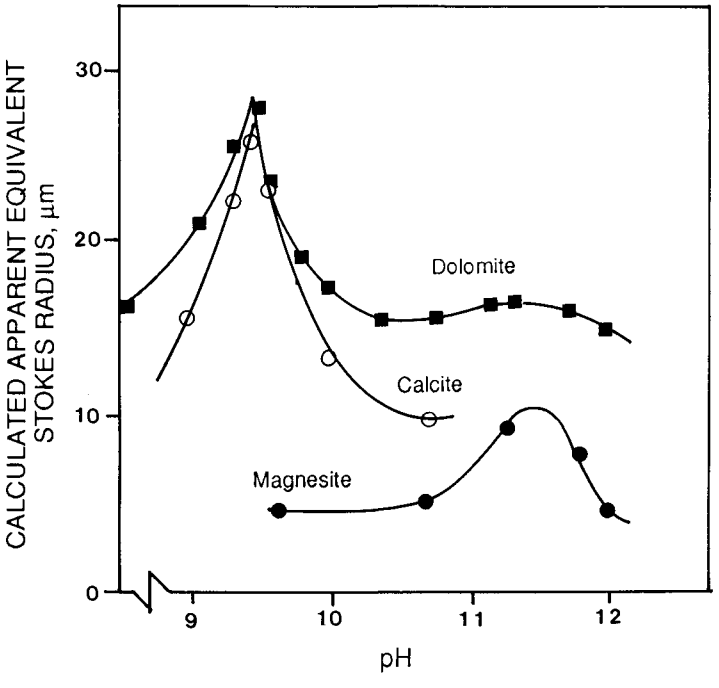

Fig. 22. Mean apparent equivalent Stokes radii calculated from hindered settling experiments performed at various pH values (from Sadowski and Laskowski [120]).

radius of an undisturbed floc consisting of primary particles. In the first method V_S was determined by plotting log Q versus the solid concentration C, where Q is the rate of fall of the interface. In the second method a modification of the Steinour equation was used:

$$Q = V_S \epsilon^2 10^{-B(1-\epsilon)} \tag{31}$$

where ϵ is the liquid volume fraction and B is the slope of the plot of log Q/ϵ^2 versus ϵ. The Stokes' sedimentation rate V_S was obtained by extrapolating to $\epsilon = 1$. Finally the floc size was calculated from the empirical equation of Richardson and Zaki [122]:

$$Q = V_S \epsilon^n \tag{32}$$

where n is the slope of log Q against log ϵ. V_S is obtained at $\epsilon = 1$. Le Bell [123] used these methods to study the hindered settling rates of kaolin in sodium chloride solution with lignosulphonate dispersants. All cases yielded straight line plots and the limiting settling rates V_S were obtained by extrapolating to zero solids concentration. All three methods gave the same V_S value and a typical set of results is shown in Figure 23. From such data the efficiency of the dispersant throughout a range of concentrations can be evaluated.

In addition to the sedimentation rate, the sedimentation volume also gives useful information concerning the degree of aggregation of the system. The arrangements in which the particles pack in concentrated suspensions give an indication of the

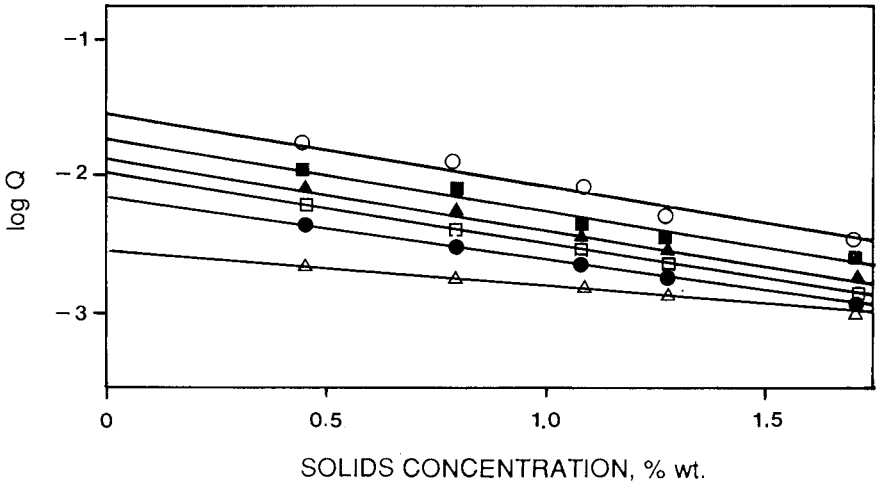

Fig. 23. Plot of log Q (where Q is the hindered settling rate as determined from measurements of the interface) versus the % solids at a range of lignosulphonate dispersant concentrations: ○ = 0, ■ = 1, ▲ = 2, □ = 5, ● =10 and △ = 30 mg l^{-1} (in 0.1 M NaCl at pH 6; from Le Bell [123] with permission).

interparticle binding forces and are a useful criteria to stability. For well dispersed systems the repulsive force dominates and keeps the particles apart by means of a fluid layer such that they can slide under their own weight without adhesion and assemble into a close packed array with low sedimentation volume (SV). Under coagulation conditions the particles adhere on contact and random aggregates form after collision since the interparticle fluid layer is considerably reduced and they cannot slide against each other. This leads to a disordered array with a higher void space.

Two other situations are also feasible: First, in cases where positively charged particles are in the presence of negatively charged particles leading to heterocoagulation, and finally in cases where polymeric solution species (organic or inorganic) are present at low concentration leading to flocculation. The latter situation can lead to fluffy flocs giving high SV values. In addition, it is possible for the superimposition of the various states to occur. In Figure 24 the various states of the colloidal dispersions are related to the sedimentation volumes.

Pugh and Bergström [124] studied the sedimentation behaviour of α-Al_2O_3 and SiC dispersions coagulated by hydrolyzing Mg(II) ions and many of the above features were observed. Similar sedimentation behaviour has also been observed from concentrated silica suspensions coagulated by Ca(II) electrolyte solution [125]. To interpret the electrokinetic and stability data in some detail it was necessary to review the solution equilibria of the cation and the current models dealing with specific adsorption and precipitation.

An estimate of the floc sizes from sedimentation volumes requires knowledge of the effective density of the floc. The density can be calculated providing the ratio of water to solids in the floc is known. Michaels and Bolger [126] related the sediment volume to the initial volume of the suspension, the ratio of floc to solid volume ratio, the solid volume concentration and a volume of a so-called zone of non-uniform lower density.

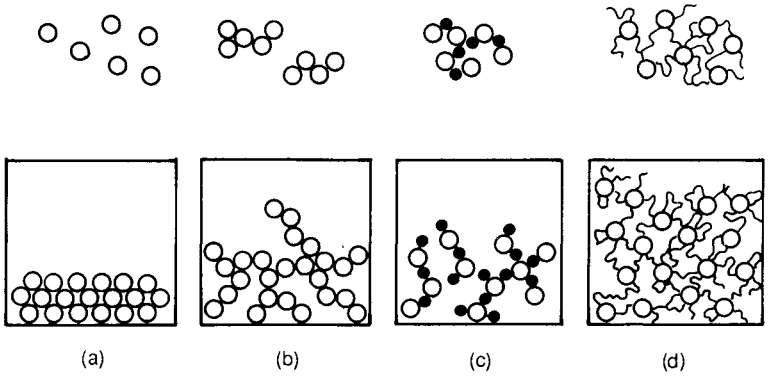

Fig. 24. States of colloidal dispersions (upper sketch) and settled volumes (lower sketch). (a) Stable dispersion, (b) coagulation, (c) heterocoagulation, (d) flocculation (from Ottewill [125] with permission).

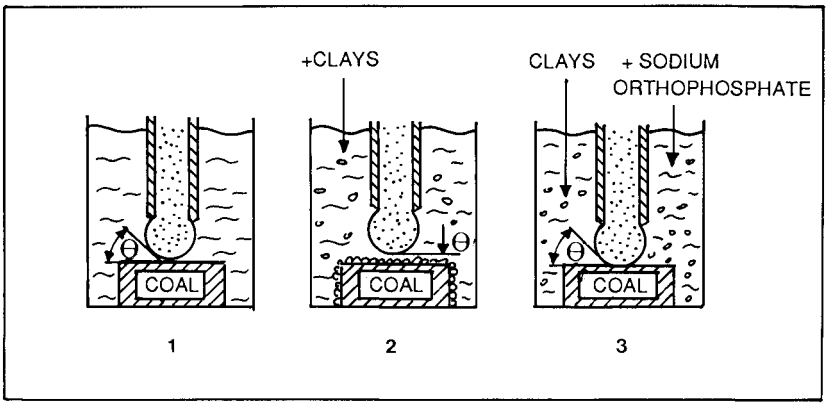

Fig. 25. Effect of clays and dispersant (phosphates) on wettability of coal surface in aqueous solution (from Jowett et al. [128] with permission).

Also, the rheological properties of the sediments formed from coagulated suspensions differ from those formed from stabilized suspensions and this gives some measure of the dispersibility. For example, sediments formed from well dispersed and stable quartz particles, are dense, well packed and dilatant (capable of flow under weak field). Sediments formed from rapidly coagulated slurries show plastic flow-initial shearing stress with a yield point (showing characteristics of a floc structure). It is important, however, that the measurements are made after a critical settling time to ensure that the equilibrium sediment structure has been reached.

Recent studies based on fractal geometry have been used to describe the concentration of the sediment formed by the settling of colloidal aggregates [127]. It was predicted from this study that the sediment concentration depended on the size of the settling particles in addition to the interparticle adhesive forces.

Industrial applications

The most instructive example which illustrates industrial applications of dispersants in flotation processes was provided by Jowett and his co-workers [128]. These researchers showed that hydrophobic coal particles become completely hydrophilic in the presence of clays which form a "slime coating" on coal surfaces (Figure 25). Coal hydrophobicity could, however, be restored by simply adding a dispersant, sodium hydrogen phosphate. Both the coal and clay particles were found to acquire more negative zeta potential values in 50–100 mg l^{-1} sodium hydrogen phosphate solutions (Figure 26). This is then a clear example of electrostatic stabilization; the specific adsorption of phosphate anions increases the negative charge of the coal

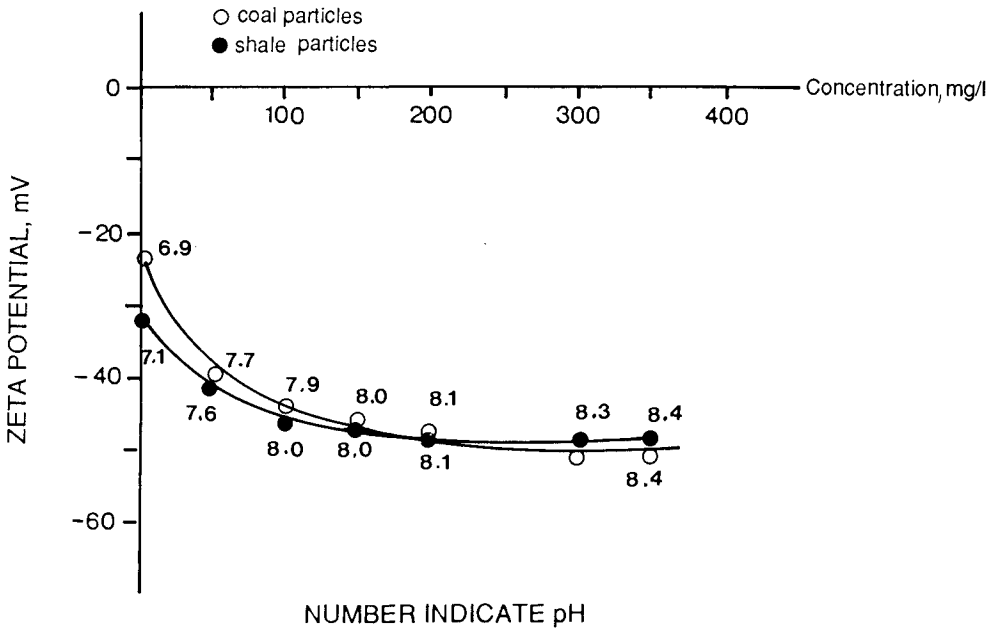

Fig. 26. Effect of sodium hydrogen phosphate on the zeta potential of coal and clay particles (from Jowett et al. [128] with permission).

and clay particles, bringing about strong coulombic repulsion which keeps clay particles apart from the coal surface thereby restoring the natural floatability of coal.

This example illustrates very well the slime coating phenomenon which is usually observed in the presence of colloidal minerals, that is the minerals which occur either naturally as sub-micron particles (clays) or as artificial mineral slimes resulting from fine grinding [129]. Since de-sliming before separation can only very rarely be applied, the use of dispersing agents to prevent slime coating is quite common.

Useful information on the role of an optimum dispersion in flotation can be found in Yang's publications [11]. His paper also brings interesting information on how the sodium silicate dispersing capability can be enhanced by the incorporation of polyvalent metallic cations.

As specified by Yarar and Kitchener [1], one of the conditions necessary to achieve selective flocculation is initial complete dispersion of all suspended mineral constituents. Adjustment of the pH and the use of dispersants serves this purpose. This is clearly seen in the Tilden Mine selective flocculation/flotation flowsheet [130]. Hematite and silica particles are separated in this plant following very fine grinding of the ore. The pulp is dispersed by adjusting pH to about 11 and by using dispersants, either sodium silicate or sodium polyphosphates. Introduction of starch under such conditions leads to its selective adsorption onto hematite (Figure 11),

resulting in hematite flocculation. The fine quartz particles are left suspended and are removed in the thickener overflow.

As it is seen from Figure 18, particle aggregation alters the rheological properties of a disperse system. While a stable, well dispersed system may display Newtonian behaviour, aggregated suspensions exhibit pseudo-plastic behaviour. Since in a wet grinding in tumbling mills, the basic mechanism involves an impact breakage of particles by falling balls (or rods), the process should be affected by pulp viscosity. As Klimpel [2, 131–133] maintains, from a maximum throughput basis, tumbling media mills need to operate on a slurry basis that is as thick as possible, yet still offers a low enough viscosity to keep grinding in a first-order manner. The use of dispersing agents, referred to as grinding aids, improves mill throughput and the yield of fines in the grinding product. The dispersing aids which reduce the yield stress of a slurry, or maintain pseudo-plastic behaviour without a yield stress, were found to be the best [2]. Low molecular-weight water-soluble polymers, sodium silicate, sodium tripolyphosphate and hydroxides to maintain high pH, were all listed among those which provide encouraging results.

The coal–water fuel technology is another area in which dispersing agents find broad applications. Coal–water slurries (CWS), also referred to as coal–water fuels (CWF), are concentrated suspensions of finely ground coal in water [3]. CWS typically contains 60 to 75% coal by weight (usually 80–90% below 100 μm), 0.5 to 1.5% chemical additives and water. The additives include: a viscosity reducing dispersant, a defoamer and a stabilizer.

Coal–water fuels have the advantage over pulverized coal in that they can be handled in an environmentally acceptable manner similar to heavy fuel oils. Because water — which must be evaporated during combustion — lowers the calorific value of CWS, coal–water fuels are required to contain at least 70% coal, to not exceed viscosity in the range of 1 Pa.s and be stable towards sedimentation.

Since these are highly concentrated disperse systems, it would, perhaps, be advisable to look at the effect of aggregation in such system on the system's properties (Figure 27).

Aggregation increases the size of the sedimenting unit but decreases the effective particle density due to the immobilization of the liquid within aggregate. For small aggregates in a dilute system the first effect is dominant, increasing both the sedimentation rate and the volume of the settled bed. For more extensive aggregation in a concentrated system, the lower density and decreased effective void volume become dominant, thus increasing stability towards sedimentation. On the other hand, when interparticle repulsion is high, stability of a relatively coarse system toward sedimentation will be poor with no mass subsidence, but with individual particles sedimenting at rates depending upon their size thus resulting in a compacted bed. The viscosity will be low, but the settled bed will be hard packed and difficult to resuspend. Because of this, water was found to be the preferred additive for coal–oil mixtures because it produces weakly aggregated soft sediments [134].

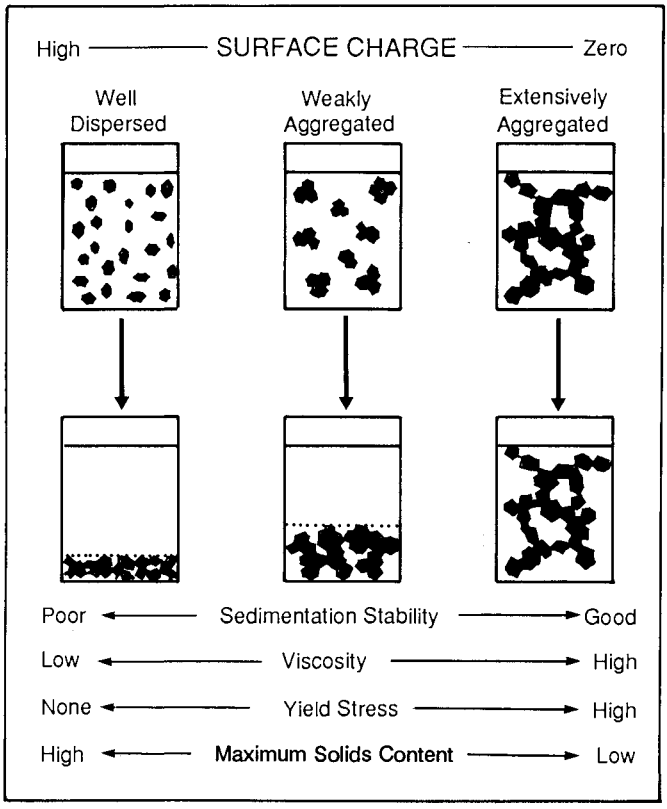

Fig. 27. Relationship between surface charge and the properties of concentrated suspensions (from Atlas et al. [150] with permission).

Coal surface wettability was shown to have a profound influence on coal–water slurry properties. Major factors affecting coal surface wettability were identified as follows [135, 136]:

(a) the hydrocarbon skeleton (related to the rank of coal);

(b) the number and type of polar groups (mostly oxygen functional groups: phenolic and carboxylic);

(c) the content of inorganic impurities.

While the hydrocarbon matrix imparts hydrophobicity to coal particles, the polar groups and inorganic impurities make the coal surface hydrophilic. This situation is further complicated by the heterogeneity of coal organic matter which is composed of macerals of quite different chemical composition and properties [137]. The macerals may exhibit distinct surface properties [138].

It has been well established that coal wettability depends on coal rank. Figure 28 shows contact angle plotted versus coal volatile matter content which is used as a main coal classification parameter in all classification systems. As indicated by

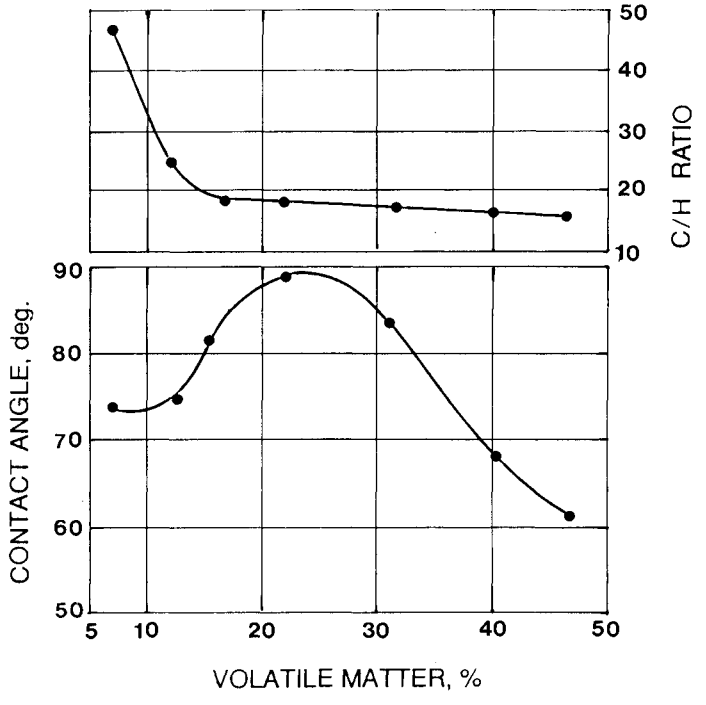

Fig. 28. Effect of coal rank on coal surface wettability (from Klassen [81]).

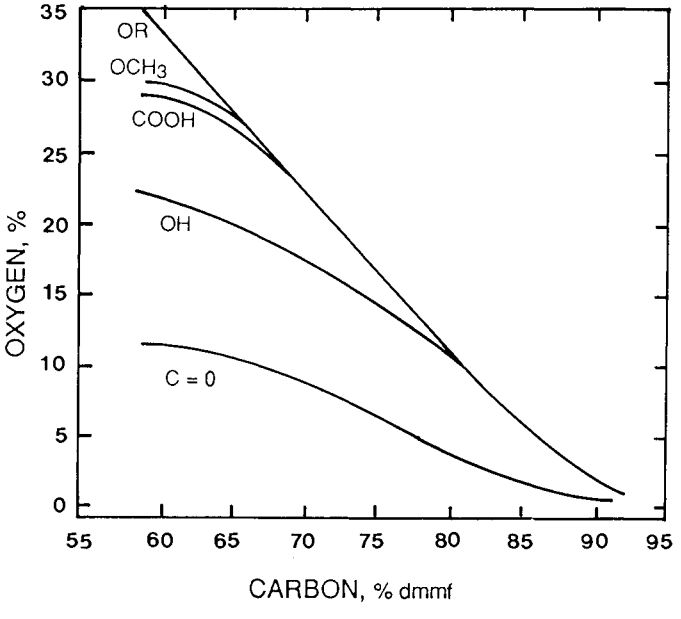

Fig. 29. Oxygen functional groups in coal of different rank (from Ihnatowicz [139] with permission).

Klassen [81], coal wettability reflects varying coal chemical composition, for example its varying C/H ratio. Coal wettability is better understood if the relationship $\theta = f$ (coal rank) is compared with the relationship oxygen content $= f$ (coal rank) (Figure 29) [139]. As it is seen, low rank coals contain a lot of oxygen, also in the form of phenolic and carboxylic groups, and these coals are not hydrophobic. Hydrophobicity increases for bituminous coals in which oxygen content is much lower; very hydrophobic metallurgical coals do not contain practically any phenolic and carboxylic oxygen. This correlates very well with the results published by Rosenbaum et al. [136], who found that not total oxygen content, but rather phenolic and carboxylic oxygen content is interrelated with coal wettability. Additional evidence for this type of conclusion provides the electrokinetic measurements which for various coals were summarized as shown in Figure 30 [140]. As seen, deviation from linearity of the zeta potential-pH curves for lower rank coals can be attributed to acidic oxygen functional groups.

Kaji et al. [141] confirmed the relationship between coal wettability and coal oxygen content. Further tests [142] corroborated that the main factor in determining coal surface wettability is the content of coal phenolic and carboxylic groups.

As seen from Figure 28, low volatile bituminous coals are the most hydrophobic. If it is further assumed that the surface of coal is built up with micro-bricks, being either paraffinic or aromatic hydrocarbons, polar groups and inorganic impurities, then it is also necessary to take into account the increasing ratio of C to H with rank, that is increasing coal aromaticity [81]. The sharp increase of this ratio is especially

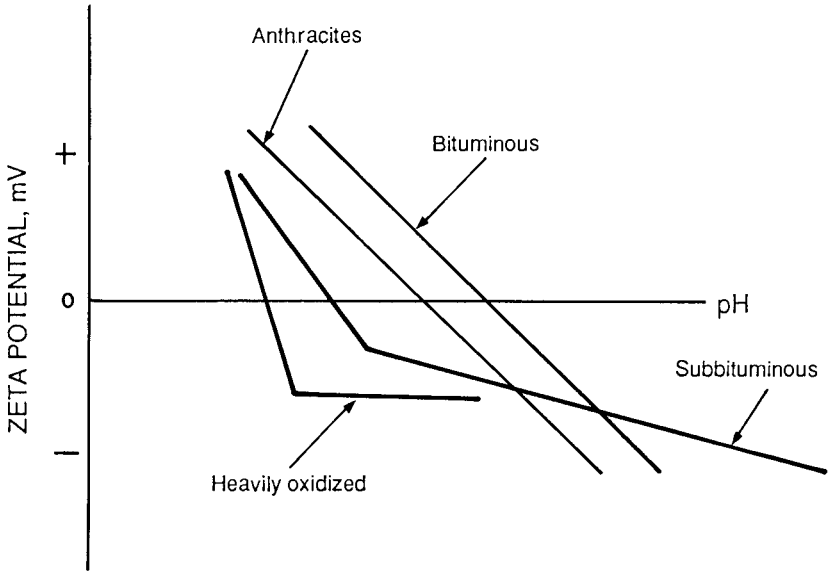

Fig. 30. Generalized zeta-potential versus pH diagram for coals of various rank (from Laskowski and Parfitt [140]).

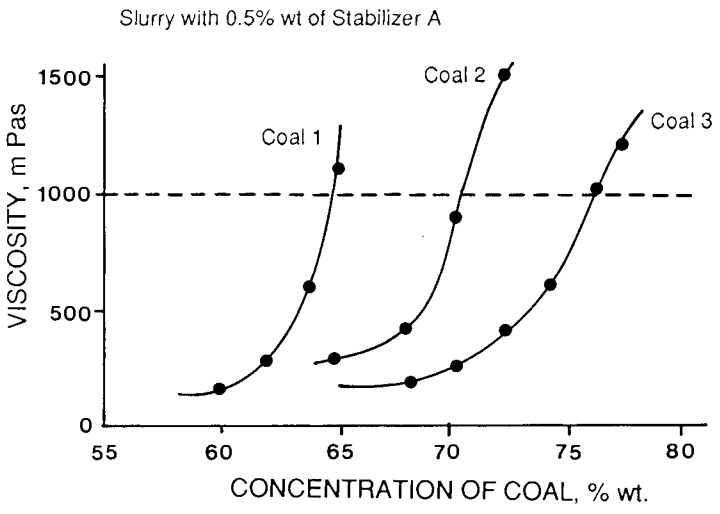

Fig. 31. Apparent viscosity of coal-water slurries prepared with the use of the same stabilizer (0.5%) and three different coal samples: Coal 1, Coal 2 and Coal 3 (from Schwartz [145] with permission).

significant for very high rank coals. Numerical evaluations confirm such assumptions [143, 144].

Coal surface wettability affects the "slurryability" which is characterized by the coal concentration at which the CWS viscosity increases sharply. Figure 31 shows the slurryability of the three coal samples tested by Schwartz [145]. The C/O and C/H ratios in the three samples are given in the table below:

Ratio of elements	Coal 1	Coal 2	Coal 3
C/O	4.6	12.7	20.8
C/H	13.6	15.8	18.5

Coal 1 was wetted completely by water and by the aqueous solution of stabilizer, while the contact angle measured for water sessile droplets on Coal 2 and Coal 3 was about 90 degrees; these angles decreased to about 40 degrees for Coal 2 and almost to 20 degrees for Coal 3 in the aqueous solution of stabilizer, a nonionic ethylene oxide/propylene oxide block copolymer. As seen from Figure 31, for Coal 1 the limit (coal percent content in CWS giving a slurry viscosity of 1000 mPA.s) is reached at 64% solids, whereas for Coal 2 and Coal 3 solid concentrations for the same viscosity is much higher (70 to 74%). These results agree very well with the findings by Japanese researchers [142] who showed a very good correlation between the CWS viscosity and coal oxidation. It is evident from these results that coal surface properties affect CWS rheology and stability. Water wets hydrophilic coals and will penetrate the capillaries in coal; this will reduce free water and will result in increased slurry viscosity. On the other hand, the formation of hydration

layers around coal particles stabilizes the suspension against aggregation, reduces the degree of aggregation and thus viscosity. However, the hydration layers will also increase the effective particle volume and thus, in concentrated suspensions (coal–water slurry), will give higher viscosity. These various trends, depending on the coal, may lead to quite a different rheology and stability [146]. As reported by Taweel et al. [147] the oxidation of coal initially provided lower apparent viscosity, probably due to an increased hydration of coal particles, but this was followed by an increase in apparent viscosity for longer oxidation times which is likely to result from the increased effective volume of the coal particles.

The use of higher rank coals and appropriate stabilizers seems to lead to better rheological characteristics of CWS. Since coal has to be cleaned prior to the preparation of CWS, the effect of the inorganic impurity reduction has also been studied [148]. In agreement with what has already been concluded on the effect or rank, coal cleaning permits higher solid loading.

Some authors claim [149] that coal cleaning may have both beneficial and adverse effects on the performance of coal water slurries. While removal of inorganic impurities and sulphur from finely ground coal prior to the CWS production has a positive effect on the performance, the final effect also depends on coal cleaning technique. Use of oil agglomeration or flotation to clean fine coal results in a more hydrophobic final product which will require more expensive nonionic dispersants (over less costly anionic dispersants, such as, for example, ammonium ligno-sulphonate, which can be used to prepare CWS from unbeneficiated coal).

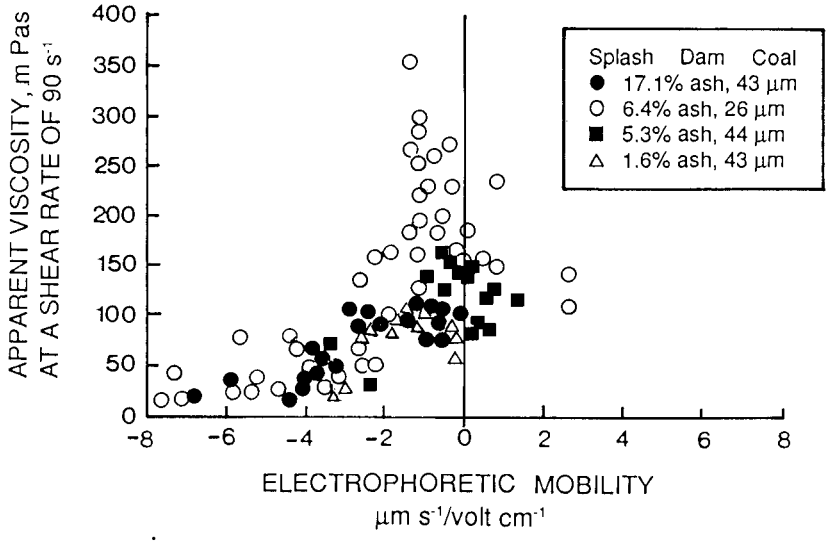

Fig. 32. Relationship between viscosity and electrophoretic mobility in 50 wt% coal-water slurries (from Atlas et al. [150] with permission).

An interesting observation was made by Atlas et al. [150], who found a clear correlation between apparent viscosity of CWS and electrophoretic mobilities of coals stabilized with different additives if the electrophoretic mobility was measured at 50% coal content (Figure 32). Apparently, the zeta potential of coal particles in coal water slurries is affected by a high solid concentration, and possibly also by the double layer overlap.

Because of the high solid content, coal particle size distribution plays a primary role and bi-modal particle size distributions are known to be essential to achieve high loading [151]. The use of stabilizers and viscosity reducers is absolutely necessary. However, since coal — as discussed above — is extremely heterogenous, it is very unlikely that a universal chemical additive will be found which is able to disperse coal from various sources and produce a suspension with the desirable properties [152].

Many authors find that poly-oxy type non-ionic surfactants are more promising than ionic surfactants. The adsorption of a non-ionic poly-oxy surfactant on coal particles is complex and is determined by the interaction of alkyl groups with coal hydrophobic spots, and also by hydrogen bonding of ethoxy (or propoxy) groups with coal polar sites. In the quoted paper, Tadros [152] compared two non-ionic agents with 54 and 88 EO units and showed that for a particular coal much higher loading could be achieved with the use of the agent containing 88 EO units.

Another group frequently tested are non-ionic polymers which are used both to stabilize the suspension and also to provide some degree of structuring to prevent the formation of hard sediments. The use of non-ionic surfactants and non-ionic polymers together may also lead to good results. Polysaccharides (xantham gum), cellulose esters, ligno-sulphonates (ammonium lignosulphonates), polycarboxylates and polyethoxysulphonates are commonly tested.

CWS stabilized by non-ionic additives are not sensitive to the concentration of the electrolyte, in contrast to those stabilized by ionic surfactants. However, since the solvency of non-ionic surfactants depends on temperature, the coal–water slurries obtained with the use of non-ionic additives may exhibit properties very much dependent on temperature.

Botsaris and Glazman [146] quote after other authors that promising results have also been reported with additives consisting of alkali or ammonium salt of naphthalene sulfonic acid formaldehyde condensate and a water-soluble polymer selected from group gum karaya, mixtures of gum karaya and polyacrylamide, sodium alginate, guar gum, locust bean gum and carboxymethylhydroxypropyl guar gum.

References

1 B. Yarar and J.A. Kitchener, Trans. IMM., Sec. C., 79 (1970): C23.
2 R.R. Klimpel, in: P. Somasundaran and B.M. Moudgil (Editors), Reagents in Mineral Technology, Marcel Dekker, New York, N.Y., 1988, Chapter 6.

3 G. Papachristodoulo, G. and O. Trass, Can. J. Chem. Eng., 65 (1987): 186.
4 P. Somasundaran, J. Colloid Interface Sci., 31 (1969): 557.
5 D.H. Napper, Polymeric Stabilization of Colloidal Dispersions, Academic Press, London, 1983.
6 A. Silberberg, Progr. Colloid Polym. Sci., 59 (1976): 33.
7 J.S. Laskowski, in: S.H. Castro and J.A. Alvarez (Editors), Froth Flotation, Elsevier, 1988, pp. 1–16.
8 V.M. Lovell, in: R.P. King (Editor), Principles of Flotation, S. Afr. Inst. Min. Metall., Johannesburg, 1982, pp. 73–89.
9 J. Leja, Surface Chemistry of Froth Flotation, Plenum Press, 1982.
10 V.I. Klassen and V.A. Mokrousov, An Introduction to the Theory of Flotation, Butterworths, 1963, p. 322.
11 D.C. Yang, in: P. Somasundaran and N. Arbiter (Editors), Beneficiation of Mineral Fines, AIME, 1979, pp. 295–308.
12 L.H. Lange, US Patent 1,914,695, 1931.
13 G.O. Aspinal, Polysaccharides, Pergamon Press, New York, N.Y., 1970.
14 M.L. Wolfram and H.E. Khadem, in: E.L. Whistler and E.F. Paschall (Editors), Starch: Chemistry and Technology, Academic Press, New York, N.Y., 1965, pp. 251–278.
15 R.H. Whistler and J.R. Daniel, in: M. Grayson (Editor), Kirk-Othmer Encyclopedia of Chemical Technolgy, 3rd edition, Wiley, New York, N.Y., Vol. 21 (1983): 492–507.
16 J.R. Radley, Starch and Its Derivatives, Chapman and Hall, London, 1968, p. 20.
17 S.R. Balajee and I. Iwasaki, Trans. AIME, 244 (1969): 401.
18 V.K. La Mer and R.H. Smellie, J. Colloid Sci., 11 (1956): 704.
19 E.A. Davidson, Carbohydrate Chemistry, Holt, Rinhart and Winston, 1967.
20 D. Horton, in: R.L. Whistler and E.F. Paschall (Editors), Starch: Chemistry and Technology, Vol. 1, Academic Press, New York, N.Y., 1965, pp. 421–438.
21 G.V. Caesar, in: J.A. Radley (Editor), Starch and Its Derivatives, Chapman and Hall, London, 1969, p. 282.
22 H.H. Haung, J.V. Calara, D.L. Bauer and J.D. Miller, in: Recent Developments in Separation Science, Vol. 4, CRC Press, Chicago, 1978, p. 115.
23 S.F. Krishnan, and Y.A. Attia, in: P. Somasundaran and B.M. Moudgil (Editors), Reagents in Mineral Technology, Marcel Dekker, 1988, pp. 485–518.
24 K.F. Lin, and C.L. Burdick, Polymeric Depressants, in: P. Somasundaran and B.M. Moudgil (Editors), Reagents in Mineral Technology, Marcel Dekker, New York, N.Y., 1988, Chapter 15.
25 A. Yokoyama, K.R. Srinivasan and H.S. Foglier, J. Colloid Interface Sci., 126 (1982): 141.
26 A. Yokoyama, K.R. Srinivasan and H.S. Fogler, Langmuir, 5 (1989): 534.
27 P. MacCarthy and R.L. Malcolm, The Nature of Commercial Humic Acids, in: I.H. Sufflet and P. MacCarthy (Editors), Aquatic Humic Substances, Am. Chem. Soc., Adv. Chem. Ser., Washington, D.C., 219 (1989): 55–64.
28 R.L. Wershaw, D.C. Pinkney and S.E. Brooker, U.S. Geol. Surv. J. Res., 5 (1977): 49, 571
29 E.J. Jensen, N. Melnyk, J.B. Wood and N. Berkowitz, Adv. Chem. Ser., 55 (1966): 621.
30 D.E. Lowenhaupt and R.J. Gray, Int. J. Coal. Geol., 1 (1980): 63.
31 D.E. Thurman, Organic Chemistry of Natural Waters, Martinus Nijhoff, Dordrecht, 1986.
32 J.A. Marinsky, S. Gupta and P. Schindler, J. Colloid Interface Sci., 89 (1982): 401.
33 S.E. Manahan, R.E. Poulson, J.B. Green and D.S. Farrier, Coal Humic Substances and Their Application to Pollution Control in the Synthetic Fuels Industry, US Dept. of Energy, LETC/RI-78/5, Sept. 1978.
34 A. van Lierde, Int. J. Miner. Process. 1 (1974): 81.
35 Z. Sadowski and J.S. Laskowski, in: P. Somasundaran (Editor), Fines Particles Processing, Vol 2, Soc. Min. Eng., AIME, New York, N.Y., 1980, pp. 1083–1103.

36 K. Furusawa, Y. Tezuka and N. Watanabe, J. Colloid Interface Sci., 73 (1988): 21.
37 J. Lyklema and G.J. Fleer, Colloids Surf., 25 (1987): 357.
38 L. Warren, in: Principles of Mineral Flotation (Editor), M.H. Jones and J.T. Woodcock, Australasian Inst. Min. Metall. 1984, p. 185.
39 J.Th.G. Overbeek, in: H.R. Kruyt (Editor), Colloid Science, Vol. 1, Amsterdam, 1960.
40 R. Hogg, T.W. Healy and D.W. Fuerstenau, Trans. Faraday Soc. 62 (1966): 1638.
41 D. Tabor, Gases, Liquids and Solids, 2nd edition, Cambridge University Press, 1979.
42 M. von Smoluchowski, Phys. Z., 27 (1916): 585; Z. Phys. Chem. 92 (1917): 129.
43 H. Müller, Kolloid Z., 38 (1926): 1; 26 (1928): 25.
44 E.J.W. Verwey and J.Th.G. Overbeek, Theory of the Stability of Lyophobic Colloids, Elsevier, Amsterdam, 1948.
45 R.J. Pugh and J.A. Kitchener, J. Colloid Interface Sci., 35 (1971): 656.
46 R. Ottewill, Chem. Ind., May 1980, p. 377.
47 W. Stumm and J.J. Morgan, Aquatic Chemistry, Wiley Interscience, New York, N.Y., 1970.
48 A.S.G. Curtis and L.M. Hockings, Trans. Farady Soc., 66 (1970): 1381.
49 G.K. Batchelor and J.T. Green, J. Fluid Mech., 56 (1972): 375.
50 T.G.M. van de Ven and S.G. Mason, J. Colloid Sci., 57 (1976): 517
51 T.G.M. van de Ven and S.G. Mason, J. Colloid Sci., 57 (1976): 505
52 T.G.M. van de Ven and S.G. Mason, Colloid Polym. Sci., 255 (1977): 794.
53 G.R. Zeichner and W.R. Schowalter, J. Colloid Interface Sci., 71 (1979): 237.
54 T.R. Camp and P.G. Stein, J. Boston Soc. Civil. Eng., 30 (1943): 219.
55 P.G. Saffman and J.S. Turner, J. Fluid Mech., 1 (1956): 16.
56 V.G. Levich, Physiochemical Hydrodynamics, 2nd edition, Prentice-Hall, New Jersey, 1962.
57 Y.H. Chia and P. Somasundaran, Colloids Surf., 8 (1983): 187.
58 D.T. Tomi, and D.F. Bagster, Trans. I. Chem. E., 56 (1978): 1
59 D.T. Tomi and D.F. Bagster, Trans. I. Chem. E., 56. (1978): 9
60 W. Heller and T.L. Pugh, J. Chem. Phys., 22 (1954): 1774.
61 H. Koelmann and J.Th.G. Overbeek, Disc. Faraday Soc., 18 (1954): 52.
62 R. Sato and R. Ruch, in: Stabilization of Colloidal Dispersions by Polymer Adsorption, Marcel Dekker, New York, N.Y., 1980.
63 J.H. Schenkel and J.A. Kitchener, Trans. Faraday Soc. 62 (1966): 1638.
64 N.V. Churaev and B.V. Derjaguin, J. Colloid Interface Sci., 103 (1985): 542.
65 J. Israelachvili and R. Pashley, Nature, 300 (1982): 341.
66 B.V. Derjaguin and N.V. Churaev, Colloids Surf., 41 (1989): 223.
67 B.V. Derjaguin, Theory of Stability of Colloids and Thin Films, Consultants Bureau, New York, N.Y., 1989.
68 K. Tjus and R.J. Pugh, in: G.S. Dobby and S.R. Rao (Editors), Proc. of Int. Symp. of Processing Complex Ores, Can. Inst. Min. Metall., Pergamon Press, 1989, pp. 121–130.
69 R.M. Pashley, J. Colloid Int. Sci., 83 (1981): 531.
70 F.G.R. Gimblett, Inorganic Polymer Chemistry, Butterworths, London, 1963, p. 170.
71 P. Parsonage, D. Melven, A.F. Healey and D. Watson, in: M.J. Jones and R. Oblatts (Editors), Reagents in the Minerals Industry, Inst. Min. Metall., London. 1984, pp. 33–40.
72 R.F. Conley, J. Paint Technol., 46 (July 1974): 51.
73 P. Parsonage and A. Marsden, Int. J. Miner. Process., 20 (1987): 161.
74 Changgen, Li and Yongxin, Lu, Int. J. Miner. Process., 10 (1988): 219.
75 J.A. Kitchener, in: K.J. Ives (Editor), The Scientific Basis of Flocculation, Sijthoff and Noordhoff, 1988, pp. 283–328.
76 K. Furusawa, Y. Tezuka and N. Watanabe, J. Colloid Interface Sci., 73 (1980): 21.
77 I. Iwasaki and R.W. Lai, Trans. AIME, 232 (1965): 364.

78 I. Iwasaki, Trans. AIME, 232 (1965): 383.
79 I. Iwasaki, W.J. Carlson and S.M. Paramerter, Trans. AIME, 244 (1969): 88.
80 I. Iwasaki, in: P. Somasundaran and N. Arbiter (Editors), Beneficiation of Mineral Fines, AIME, 1979, pp. 257–262.
81 V.I. Klassen, Coal Flotation, Gosgortiekhizdat, Moscow, 1963.
82 J.M. Wie and D.W. Fuerstenau, Int. J. Miner. Process., 1 (1974): 17.
83 J.D. Miller, C.L. Lind and S.S. Chang, Coal Preparation, 1 (1984): 21.
84 J.A. Solari, A.C. de Araujo and J.S. Laskowski, Coal Preparation, 3 (1986): 15.
85 Qi Liu and J.S. Laskowski, J. Colloid Interface Sci., 130 (1989): 101.
86 Qi Liu and J.S. Laskowski. Int. J. Miner. Process., 26 (1989): 297.
87 Qi Liu and J.S. Laskowski, Int. J. Miner. Process., 27 (1989): 147.
88 J.S. Laskowski and J.A. Kitchener, J. Colloid Interface Sci., 29 (1969): 670.
89 J. Rubio and J.A. Kitchener, J. Colloid Interface Sci., 57 (1976): 132.
90 J. Rubio, Colloids Surf., 3 (1981): 79.
91 R.J. Gochin, M. Lekili and H.L. Shergold, Coal Prep., 2 (1985): 19.
92 H. Baldauf and H. Schubert, in: P. Somasundaran and B.M. Moudgil (Editors), Reagents in Mineral Technology, Marcel Dekker, 1988, pp. 471–484.
93 A. Yokoyama, K.R. Srimikvasan and H.S. Fogler, J. Colloid Interface Sci., 126 (1988): 141.
94 J.H. Schulze, H.S. Hanna and U. Bilsing, Freiberg. Forschungsh., A476 (1970): 33.
95 J. Iskra, C. Gutierrez and J.A. Kitchener, Trans. IMM, Sec. C, 82 (1973): C73.
96 A. Rezanowich, J.F. Jaworzyn and D.A.I. Goring, Pulp Paper Mag. Canada, 62 (January 1961): T-172.
97 Th.F. Tadros, Colloid Polym. Sci., 258 (1980): 439.
98 Th.F. Tadros, Colloid Polym. Sci., 261 (1983): 49.
99 Z. Sadowski and R.W. Smith, Miner. Metall. Process., (1985): 217.
10 C.R. O'Melia, in: W. Stumm (Editor), Aquatic Surface Chemistry, John Wiley, New York, N.Y., 1987, pp. 385–404.
101 E. Tipping and D.C. Higgins, Colloids Surf., 5 (1982): 85.
102 K. Wong and J.S. Laskowski, Colloids Surf., 12 (1984): 319.
103 A. Andreasson, B. Jönsson and B. Lindman, Colloid Polym. Sci., 266 (1988): 164.
104 B. Leuenberger and P.W. Schindler, Anal. Chem., 58 (1986): 1471.
105 M.H.B. Hayes and R.S. Swift, in: Greenland and M.H.B. Hayes (Editors), The Chemistry of Soil Organic Colloids, 1978, pp. 179–320.
106 R.H. Ottewill, in: M. Schick (Editor), Surfactant Science Series, Marcel Dekker, 1967, pp. 627–682.
107 J.S. Clunie and B.Y. Ingram, in: G.D. Parfitt and C.H. Rochester (Editors), Adsorption from Solution at the Solid/Liquid Interface, Academic Press, 1983, pp. 105–152.
108 P.J. Scales, F. Grieser, D.N. Furlong and T.W. Healy, Colloids Surf., 21 (1986): 55.
109 R.J. Pugh, in: E. Forssberg (Editor), Proc. XVI Int. Miner. Process. Congr., Elsevier, 1988, pp. 751–62.
110 R.J. Hunter, Zeta Potential in Colloid Science, Principles and Applications, Academic Press, London, 1981.
111 D.J. Smith, Electrophoresis, Academic Press, 1969.
112 B.J. Marlow, D. Fairhurst and H.P. Pendse, Langmuir, 4 (1988): 611.
113 P. Deby, J. Chem. Phys., 1 (1933): 13.
114 A.J. Babchin, R.S. Chow and R.P. Sawatzky, Adv. Colloid Surf. Sci., 30 (1989): 111.
115 J.P. Friend and J.A. Kitchener, Chem. Eng. Sci., 28 (1973): 107.1
116 Th.F. Tadros, in: B.M. Moudgil and B.J. Scheiner (Editors), Flocculation and Dewatering, Engineering Foundation, New York, N.Y., 1988.

117 A. Foissy, J. Persello, J.M. Lamarche and G. Robert, J. Dispersion Sci. Tech., 3(2) (1982): 105.
118 B. Klein, S.J. Partridge and J.S. Laskowski, Coal Prep., 8 (1990) 123.
119 J. Mager and J. Laskowski, Colloid Polym. Sci., 257 (1979): 328.
120 Z. Sadowski and J. Laskowski, Colloids Surf., 1 (1980): 151.
121 O. Dollimore and T.A. Horridge, Trans. Br. Ceram. Soc., 70 (1971): 191.
122 J.F. Richardson and N.N. Zaki, Trans. Inst. Chem. Eng., 32 (1954): 35.
123 J.C. Le Bell, Colloids Surf., 5 (1982): 285.
124 R.J. Pugh and L. Bergström, J. Colloid Interface Sci., 124 (1988): 570.
125 R. Ottewill, Phil. Trans. R. Soc. Lond., A310 (1983): 67.
126 A.S. Michaels and J.C. Bolger, Eng. Chem. Fundam., 1 (1962): 153.
127 M. Zrinyi, M. Kabai-Faix and F. Horkay, Progr. Colloid Polym Sci., 77 (1988): 165.
128 A. Jowett, H. El-Sinbawy and H.G. Smith, Fuel, 35 (1956): 303.
129 J.A. Kitchener, Filtr. Sep., 6 (1969): 553.
130 A,.F. Colombo, in: P. Somasundaran and N. Arbiter (Editors), Beneficiation of Mineral Fines, 34 (1982): 1665.
131 R.R. Klimpel. Min. Eng., 45 (1982): 1665.
132 R.R. Klimpel, Min. Eng., 35 (1983): 21.
133 H.E. El-Shall, in: P. Somasundaran and B.M. Moudgil (Editors), Reagents in Mineral Technology, Marcel Dekker, New York, N.Y., 1988, pp. 159–178.
134 V.P. Singh, Coal-#2 Oil Mixtures — Effect of Additives on Stability and Theological Properties, Proc. 4th Int. Symp. Coal Slurry Combustion, U.S. Dept. of Energy, Pittsburgh, Pa., 1982.
135 J.S. Laskowski, Surface Chemistry Aspects of Fine Coal Beneficiation, Proc. 1st Meeting of the Southern Hemisphere on Mineral Technology, Rio de Janeiro, December, 1982, Vol. 1, pp. 59–69.
136 J.M. Rosenbaum, D.W. Fuerstenau and J.S. Laskowski, Colloids Surf., 8 (1983): 153.
137 D.W. van Krevelen, Coal, Elsevier, Amsterdam, 1961.
138 B.J. Arnold and F.F. Aplan, Fuel, 68 (1989): 651.
139 A. Ihnatowicz, Bull. Centr. Res. Min. Inst., No. 125, Katowice, 1952 (in Polish).
140 J.S. Laskowski and G.D. Parfitt, in: G.D. Botsaris and Y.M. Glazman (Editors), Interfacial Phenomena in Coal Technology, Marcel Dekker, New York, N.Y., 1989, pp. 279–327.
141 R. Kaji et al., Effects of Coal Type, Surfactant, and Coal Cleaning on the Rheological Properties of Coal Water Mixture. In: Proc. 5th Int. Symp. Coal Slurry Combustion and Technology, Tampa, 1983, U.S. Dep. of Energy, Pittsburgh, Pa., 1983, Vol. 1, pp. 151–175.
142 T. Igarashi et al., Effects of Weathering of Coals on Slurriabilities. In: 6th Int. Symp. Coal Slurry Combustion and Technology, Orlando, 1984, U.S. Dep. of Energy, Pittsburgh, Pa., 1984, pp. 283–303.
143 J.M. Rosenbaum and D.W. Fuerstenau, Int. J. Miner. Process., 12 (1984): 313.
144 B.V. Keller, Colloids Surf., 22 (1987): 21.
145 E. Schwartz, Physical Properties of Coal Surfaces and Their Interrelation with Stabilizers. In: Proc. 7th Int. Symp. Coal Slurry Fuels Preparation and Utilization, New Orleans, 1985, U.S. Dept. of Energy, New Orleans, La., 1985, pp. 41–49.
146 G.D. Botsaris and Y.M. Glazman, in: G.D. Botsaris and Y.M. Glazman (Editors), Interfacial Phenomena in Coal Technology, Marcel Dekker, New York, N.Y., 1989, pp. 199–277.
147 A.M. Taweel, O. Fadalay and J.C.T. Kwak, Effect of Coal Properties on the Rheology and Stability of CWS Fuels, in: Proc. 7th Int. Symp. Coal Slurry Fuels Preparation and Utilization, New Orleans, 1985, U.S. Dept of Energy, New Orleans, La., 1985, p. 15.
148 J.M. Ekmann and D.J. Wildman, The Influence of Additives on Coal–Water Mixtures Prepared with Beneficiated Coal. A.I.Ch.E. Spring National Meeting, New Orleans, La., 1985, p. 15.
149 A.B. Walters, Chemical Effects of Beneficiation on Coal–Water Fuel Properties, in: Proc. 8th Int. Symp. Coal Slurry Fuels Preparation and Utilization, Orlando, 1986, U.S. Department of Energy,

Pittsburgh, Pa., 1986, pp. 222–225.

150 H. Atlas, E.Z. Casassa, G.D. Parfitt, A.S. Rao and E.W. Toor, in: Proc. 10th Annual Powder and Bulk Solids Conf., Chicago, Ill., May 1985.

151 F. Ferrini, V. Battara, E. Donati and C. Piccinini, Optimization of Particles Grading for High Concentration Coal Slurry, 9th Int. Conf. Hydraulic Transport of Solids in Pipes, Roma, October 1984.

152 Th.F. Tadros, in: Second European Conference on Coal Liquid Mixtures, Inst. Chem. Eng. Symp. Ser., No. 95, London, 1985, pp. 1–12.

Chapter 5

Static and dynamic contact angles

J. RALSTON and G. NEWCOMBE

Introduction

The contact angle has been extensively used and misused in mineral processing theory and practice. The thermodynamic origin of contact angle and its link to surface energetics first appeared in the work by Thomas Young in 1805 [1]. The subject was extended in the lucid treatment of the thermodynamics of wetting by Gibbs in 1878 [2]. Where necessary, reference will be made to the work of Gibbs without rederiving all of his essential equations. Numerous reviews of both static and dynamic contact angles have appeared over the past two decades or so [3, 4] and modern theories of interfacial forces have provided revealing insights into wettability [5]. Furthermore recent advances have been made in the measurement of contact angles on particles [6, 7], so that our knowledge base both in theory and experiment is expanding rapidly.

For a bubble or an oil droplet to actually adhere to a mineral particle so that the latter can be recovered, a finite contact angle must exist at the three-phase line of contact. Contact angle is not the sole criterion responsible for mineral recovery, but is rather one of *the* important contributing factors. The purpose of this chapter is to examine the fundamental features of both static and dynamic contact angles which are of central importance to mineral processing. The relationship between particle size and contact angle is dealt with in Chapter 6, whereas the principles of surfactant adsorption are described in Chapter 2 with applications appearing in the second half of this volume (e.g. Chapters 7 and 11).

Static contact angles

Ideal surfaces

A bubble or droplet minimizes its free energy by adopting a spherical shape in the absence of gravity. When the bubble or droplet contacts either a solid or a liquid substrate, it will still minimize its free energy, as originally noted by Gibbs [2].

Essentially the sum:

$$\gamma_{LV}A_{LV} + \gamma_{SV}A_{SV} + \gamma_{SL}A_{SL}$$

must be minimized where γ is a surface or interfacial tension, A is an area and LV, SV and SL denote the respective interfaces between the liquid, vapour and solid phases.

If, say, a drop is placed on a solid surface it may spread to form a thin liquid film or it may remain as a discrete droplet. In the first instance the behaviour may be described as complete wetting whilst the latter corresponds to partial wetting. Similar behaviour is exhibited by a bubble contacting a substrate.

There will certainly be some interaction between the fluid and the solid substrate upon which it rests, even if this is due only to Van der Waals forces [5]. Some type of surface interaction, such as adsorption or ionization of surface groups is likely in many cases.

As shown in Figure 1, the contact angle is the angle contained between planes tangent to the surfaces of the solid and the liquid at the wetting perimeter. In the example shown, θ is measured through the vapour phase. This is of primary importance in mineral flotation, for we are concerned as to whether or not a bubble will cling to a solid surface. The wetting perimeter is frequently referred to as the three-phase line of contact (tplc) but really is a small zone where the three phases merge [8]. One needs to distinguish, in practice, between situations where the fluid is tending to advance over or retreat from the surface in question. The limiting static angles determined for these two cases correspond to the advancing (θ_A) and receding (θ_R) contact angles. As noted by Huh and Scriven [9] and by Blake [10], it would be more logical to use the terms "advanced" and "recessed" to describe the static case, however common practice dictates otherwise.

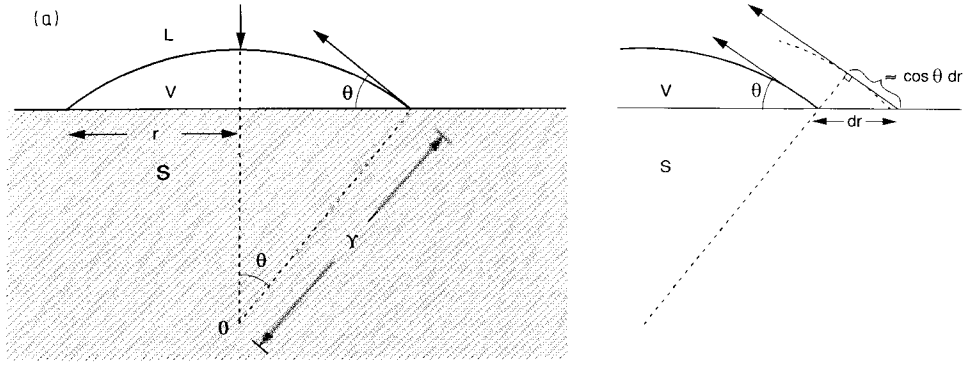

Fig. 1. (a) Sessile bubble with axial symmetry on a solid surface immersed in a liquid in a constant temperature chamber. S = solid, L = liquid, V = vapour. (b) Changes at the three-phase contact line for slight changes in the solid (S)–vapour (V) area of contact for the sessile bubble in (a).

In general, $\theta_A \geq \theta_R$, any difference normally being ascribed to hysteresis, a topic which is dealt with in the section on "Non-ideal surfaces", below.

Young's equation

Consider an axially symmetric bubble (Figure 1) resting on a planar solid substrate, in an aqueous environment at constant temperature and bubble volume. We can readily calculate the change in Helmholtz free energy, F, for the situation where the bubble increases its area infinitesimally at constant volume. The argument follows that of Gibbs [2]. Changes in the respective interfacial areas occur ("dA"), as the radius of the bubble perimeter at the SL interface increases from r to $r + dr$:

$$\text{SL interface:} \quad dA_{SL} = 2\pi r dr \tag{1}$$

$$\text{LV interface:} \quad dA_{LV} = \left(\frac{1}{R_1} + \frac{1}{R_2}\right) dV + 2\pi r dr \cos\theta \tag{2}$$

where R_1 and R_2 are the principal radii of curvature of the bubble. The first term is derived from the Young-Laplace equation whilst the second term is the outer surface area of the wedge shown in Figure 1. Since the volume of the bubble is constant, dV is constant (d$V = 0$) and:

$$dA_{LV} = 2\pi r dr \cos\theta = dA_{SL} \cos\theta \tag{3}$$

Therefore:

$$dF = \gamma_{SV}(-dA_{SV}) + \gamma_{SL}(dA_{SL}) + \gamma_{LV} dA_{LV}$$

and, since:

$$-dA_{SV} = dA_{SL}$$

$$dF = (\gamma_{LV} \cos\theta + \gamma_{SL} - \gamma_{SV}) dA_{SL}$$

Under conditions of mechanical equilibrium, $dF/dA_{SL} = 0$, hence:

$$\cos\theta = \frac{\gamma_{SL} - \gamma_{SV}}{\gamma_{LV}} \tag{4}$$

This is an energy-balance statement of Young's equation, commonly derived through force-balance arguments.

If the SL and SV interfaces meet at a sharp edge and there is no common tangent at the wetting line, the three-phase equilibrium condition is given by:

$$\gamma_{LV} \cos\alpha \leq \gamma_{SL} - \gamma_{SV} \tag{5}$$

$$\gamma_{LV} \cos\beta \leq \gamma_{SV} - \gamma_{SL} \tag{6}$$

reducing to equation (4) when $\alpha + \beta = 180°$, where α and β are the angles occupied by the liquid and vapour phases.

Equation (4) supposes that γ_{SV} represents the surface tension of a solid in equilibrium with adsorbed vapour, i.e. the surface tension of the pure, dry solid, γ_{S^o}, has been reduced by adsorption. The reduction of surface tension by the adsorbate molecules is given by:

$$\pi_e = \gamma_{S^o} - \gamma_{SV} \tag{7}$$

where π_e is commonly referred to as the equilibrium spreading pressure. One might therefore expect bubble (or drop) shape to be sensitive to the magnitude of π_e.

Several further conditions apply to Young's equation. The solid should not be deformable, for there must be a steady state of strain at the surface of the solid and within its bulk [11]. Recent work, however, has been directed at the wetting of deformable solids [12]. Secondly, considerable care needs to be exercised in dealing with γ. The latter is defined as:

$$\gamma = \left(\frac{\partial F}{\partial A}\right)_{T,V,N_i} = \left(\frac{\partial G}{\partial A}\right)_{T,P,N_i} \tag{8}$$

where F is the Helmholtz and G the Gibbs free energy. N_i refers to the number of mole of species i. In our example, V is constant so that γ is defined in terms of the Helmholtz free energy.

Suppose we consider the work done in extending the surface of a one component isotropic solid by an amount A [13]. Then:

$$dw = \gamma_{S^o} dA \tag{9}$$

and:

$$dw = d(AF_G) \tag{10}$$

where F_G is the specific excess Helmholtz free energy (the subscript G is consistent with the notion of a Gibbs excess quantity).
Hence:

$$\gamma_{S^o} dA = d(AF_G)$$

and:

$$\gamma_{S^o} = F_G + A\left(\frac{dF_G}{dA}\right) \tag{11}$$

Clearly $\gamma_{S^o} = F_G$ only when $dF_G/dA = 0$. This is true for a one component liquid but is not generally true for a freshly formed pure solid surface, since the atoms are not in their equilibrium positions.

γ_{S° and F_G may be equal for an equilibrium solid surface, a situation unlikely to be ever encountered in mineral processing. γ_{S° is referred to as the surface tension or, *rather loosely*, as a "surface energy". For a solid surface, Gibbs [2] did not even give a name to γ_{S°!

Furthermore, for any interface, γ and F^* are certainly not equal when adsorption occurs. Here F^* may be the specific excess Helmholtz surface free energy, F_G (Gibbs model) or the specific total surface free energy, F_S (surface phase model). In either case [13]:

$$F^* = \gamma + \Sigma_i \mu_i \Gamma_i \tag{12}$$

and $F^* \neq \gamma$ since Γ_i is never zero. Γ_i is of course the adsorption density in mol m^{-2} of species i.

From Figure 1 and equation (4) if the magnitude of the contact angle is decreased, better flotation might be anticipated as stronger bubble–solid adhesion is expected. The Young equation does not provide direct information as to what surface tension changes might be expected for the interfaces. The latter information can only be obtained through the Gibbs adsorption equation.

Recall Figure 1 and let us suppose that a non-volatile flotation collector C is present and that the vapour phase is nitrogen saturated with water vapour. Assume that the nitrogen is insoluble in the water. The Gibbs adsorption equation (14) links changes in interfacial tension to adsorption density. At constant temperature and pressure:

$$-d\gamma = \Sigma_i \mu_i \Gamma_i \tag{13}$$

For the solid–liquid interface:

$$d\gamma_{SL} = -\Gamma_C^{(1)SL} d\mu_C \tag{14}$$

where $\Gamma_{H_2O}^{SL} = 0$ and $\Gamma_C^{(1)SL}$ denotes the surface excess concentration of C.
At the solid–vapour interface

$$-d\gamma_{SV} = \Gamma_C^{SV} d\mu_C + \Gamma_{H_2O}^{SV} d\mu_{H_2O} + \Gamma_{N_2}^{SV} d\mu_{N_2} \tag{15}$$

At equilibrium, the chemical potential of collector and water must be the same throughout the system. Recalling the Gibbs-Duhem equation for the bulk aqueous and vapour phases at constant temperature and pressure:

$$\text{aqueous phase:} \quad x_C d\mu_C + x_{H_2O} d\mu_{H_2O} = 0 \tag{16}$$

$$\text{vapour phase:} \quad P_{H_2O} d\mu_{H_2O} + P_{N_2} d\mu_{N_2} = 0 \tag{17}$$

where x_i and P_i represent the mole fraction and partial pressure of species i, respectively.

Substitution of equations (16) and (17) into (15) yields:

$$-d\gamma_{SV} = \left[\Gamma_C^{SV} - \frac{x_C}{x_{H_2O}}\Gamma_{H_2O}^{SV} - \frac{x_C P_{H_2O}}{x_{H_2O} P_{N_2}}\Gamma_{N_2}^{SV}\right] d\mu_C \tag{18}$$

Since the concentration of collector is rather low and $P_{H_2O} \ll P_{N_2}$, then $x_C P_{H_2O}/x_{H_2O} P_N$ 1, and choosing $\Gamma_{H_2O}^{SV} = 0$, then:

$$d\gamma_{SV} = -\Gamma_C^{(1)SV} d\mu_C \tag{19}$$

Subtracting equation (19) from (14) yields:

$$d(\gamma_{SL} - \gamma_{SV}) = \left(\Gamma_C^{(1)SV} - \Gamma_C^{(1)SL}\right) d\mu_C \tag{20}$$

Comparison with equation (4) shows:

$$\frac{d\gamma_{LV} \cos\theta}{d\mu_C} = \Gamma_C^{(1)SV} - \Gamma_C^{(1)SL} \tag{21}$$

Thus for the contact angle to decrease with increasing collector concentration (i.e. for the bubble to spread and displace the aqueous phase) and $d\cos\theta/d\mu_C$ to be positive:

$$\Gamma_C^{(1)SV} > \Gamma_C^{(1)SL}$$

i.e. the adsorption density at the solid–vapour interface must exceed that at the solid–liquid interface. This finding was first noted by de Bruyn et al. [15] and confirmed experimentally by Smolders [16], but has essentially laid dormant as far as flotation research and practice are concerned.

From time to time the validity of Young's equation has been questioned, prompted by the difficulty in providing experimental justification. The arguments have principally centred on the distinction between microscopic and macroscopic contact angles [17]. White [6] has shown, however, that there is a clear differentiation between these two angles and that it is the macroscopic contact angle which obeys Young's equation. It is pertinent to invoke a physical description of the contact zone. Recall Figure 1 for the moment and imagine that the contact angle θ is obtuse. At the SV interface a nominal monolayer coverage of water molecules will be present on the solid surface (together with collector molecules if the latter has been added), establishing a π_e. The gradient of the LV interface will gradually increase from zero as we move towards the bulk liquid phase, until a liquid thickness is reached where any solid–liquid–vapour interaction energy is negligible compared with γ_{LV}. The contact angle at this thickness equals that expected from Young's equation if the interaction energy is only due to dispersion forces, which will occur when the liquid film has exceeded about 1 nm in thickness.

In mineral flotation we are intensely interested in the manner in which a particle is attached to a bubble. This topic is addressed in some detail in Chapter 6. For

the present, we can consider a rather simplified case because it demonstrates how Young's equation is a natural outcome of particle bubble adhesion.

The situation is depicted in Figure 2. A spherical, solid particle is located at the interface between two fluid phases. All phases are assumed to have the same density. For the particle to have achieved a stable equilibrium position, the total surface free energy must be minimized. Let h be the distance of penetration of the particle in phase α. The system is considered to be at constant volume.

The area of the solid–fluid α interface is $2\pi r^2$ whilst the solid–fluid β interface is $4\pi r^2 - 2\pi rh$. The area of the $\alpha\beta$ interface occupied by the solid is $\pi(2rh - h^2)$.

For equilibrium:

$$dF = \gamma_{S_\alpha}(2\pi r\, dh) + \gamma_{S_\beta}(-2\pi r\, dh) - \gamma_{\alpha\beta}\pi(2r - 2h)\, dh = 0 \tag{22}$$

or:

$$\gamma_{S_\alpha} - \gamma_{S_\beta} = \left(1 - \frac{h}{r}\right)\gamma_{\alpha\beta} = \gamma_{\alpha\beta}\cos\theta \tag{23}$$

i.e. Young's equation (4) is recovered. Thus a particle will be stable at the $\alpha\beta$ interface if θ is finite and will occupy a position which satisfies Young's equation and where θ is the equilibrium contact angle.

Some further insight into Young's equation may be gleaned from calorimetry. If a dry, powdered solid is immersed in a liquid, heat will be evolved during the wetting process, i.e. an exothermic process takes place where the heat of immersion, ΔH_{imm} is given by:

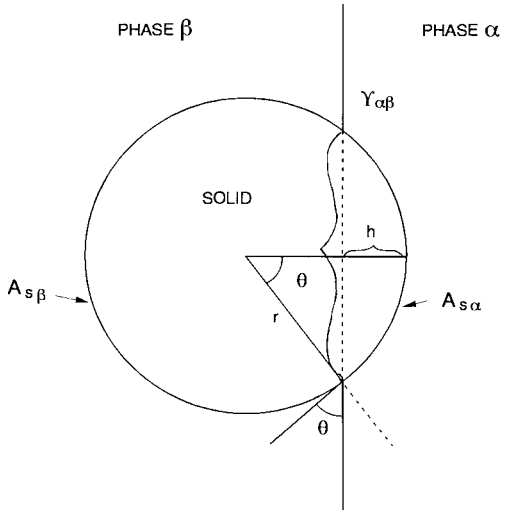

Fig. 2. Location of a solid, spherical particle at an interface between two fluid phases α and β. The system is gravity free. All phases are assumed to have the same density.

$$\Delta H_{imm} = H^S_{SL} - H^S_{S^o} \tag{24}$$

Here H^S_{SL} is the enthalpy of the solid in contact with the liquid (the "wet" solid) and $H^S_{S^o}$ is the enthalpy of the dry solid [refer equation (7)]. From basic thermodynamics [13]:

$$H^S = \gamma - T\left(\frac{d\gamma}{dT}\right) \tag{25}$$

and thus:

$$\Delta H_{imm} = \left[\gamma_{SL} - T\left(\frac{d_{SV}}{dT}\right)\right] - \left[\gamma^o_S - T\left(\frac{d\gamma^o_S}{dt}\right)\right] \tag{26}$$

From equation (4), for a dry solid:

$$\gamma_{LV}\cos\theta = \gamma_{S^o} - \gamma_{SL}$$

thus:

$$-\Delta H_{imm} = \gamma_{LV}\cos\theta - T\frac{d}{dT}(\gamma_{LV}\cos\theta)$$

and:

$$-\Delta H_{imm} = \gamma_{LV}\cos\theta - T\cos\theta\frac{d\gamma_{LV}}{dT} - T\gamma_{LV}\frac{d\cos\theta}{dT} \tag{27}$$

Equation (27) shows directly the thermodynamic significance of contact angle. Provided that ΔH_{imm}, $d\gamma_{LV}/dT$ and $d\cos\theta/dT$ can be determined with sufficient precision and accuracy, it is possible to obtain $\cos\theta$ and θ [18]. Although this thermodynamic technique is little used in mineral processing research it is of considerable importance to selective oil agglomeration techniques.

Wetting

From equation (4) and Figure 1, when the air bubble completely spreads over, or totally wets, the solid surface, θ is zero and equation (4) becomes:

$$\gamma_{LV} = \gamma_{SV} - \gamma_{SL} \tag{28}$$

which immediately begs a question concerning the absence of the three-phase wetting line. The validity of this equation has been demonstrated experimentally by Johnson and Dettre [3] and given a firm thermodynamic basis by Melrose [11] and Rowlinson and Widom [19]. The argument and physical picture is very similar to that advanced by White [8] in distinguishing between microscopic and macroscopic contact angles, as discussed in the section on "Non-ideal surfaces", below.

Recalling equation (7), equation (28) may be expressed as:

$$\gamma_{LV} = \gamma^o_S - \pi_e - \gamma_{SL} \tag{29}$$

Where a liquid (or indeed any fluid) spreads over a solid surface, π_e will increase, reducing γ_{SV} until it equals $\gamma_{LV} + \gamma_{SL}$. This will occur when the thickness of the adsorbed film reaches the point where it exhibits the properties of a bulk liquid with separate and distinct γ_{LV} and γ_{SL} values, i.e. it is a duplex film. Only when equation (28) is applicable will the adsorbed film adopt the properties of the bulk liquid. A disjoining pressure (Chapters 3 and 6) will exist within the thin aqueous film between an air bubble and a solid particle as the two approach in water. This disjoining pressure acts normal to the plane of the film, varies with film thickness and can prevent thinning. If θ is finite, the disjoining pressure will, at some point, become negative and thus a draining film, upon reaching a certain thickness will spontaneously rupture. A stable contact angle will be formed, with a freshly exposed SV interface formed under the "spread" air bubble. This situation (θ finite) constitutes a case of partial wetting of the solid by the air (or liquid, depending on how one defines θ).

A probe, inserted through the LV interface, would not see a "dry" solid surface, but rather one containing microdroplets of aqueous phase in equilibrium with multilayers of water molecules. If collector molecules are present they will also be distributed at the SV interface and at a greater density than for the SL interface [recall equation (21)]. The adsorption and orientation of collector molecules at the SV and SL interfaces, their influence on the contact angle during movement etc. are subjects of intense research interest (e.g. [4, 20]) and it is not possible to give an accurate global description. Orientation changes at the SV and SL interfaces are certainly expected on theoretical and experimental grounds [20, 21]. Patchwise collector adsorption is anticipated from the early autoradiographic work of Plaksin [22]. As the techniques of scanning tunnelling microscopy, atomic force microscopy, in-situ Fourier Transform Infrared Spectroscopy, neutron scattering and the like become more widely applied in mineral flotation research, considerable advances in our understanding of collector adsorption will take place.

For rather small systems, an additional problem may exist, i.e. the three-phase wetting line may be in a state of tension, as first proposed by Gibbs [2]. Under such circumstances, for the air bubble depicted in Figure 1, equation (4) should be expressed as:

$$\gamma_{LV} \cos\theta = \gamma_{SL} - \gamma_{SV} - \frac{\kappa}{r} \tag{30}$$

where κ is the line tension and r is the radius of curvature of the wetting line in the plane of the solid. κ may be positive or negative and is apparently of order 10^{-10}–10^{-11} N or so (e.g. [23]). Thus corrections to Young's equation are only likely to be significant where r is less than 100 nm, with $\kappa/r \leq 1$ mN m^{-1}. Thus line tension is likely to be significant when phenomena such as droplet coalescence, heterogeneous nucleation, the stability of free liquid films and condensation in porous solids are

involved [10, 23]. It *may* be important in bubble–particle adhesion in flotation, however evidence to date suggests that this is unlikely (Chapter 6).

For the majority of cases in mineral processing, Young's equation is perfectly acceptable for describing wetting equilibria. However other terms are frequently invoked in the colloid and surface chemistry literature, e.g. spreading coefficient, work of adhesion. It is not the purpose of the present chapter to define these terms in detail, rather the interested reader should consult the extensive literature on the subject [13, 14, 24].

The influence of surface charge on contact angle

Electrical double layer effects have a significant influence on wetting behaviour, a contribution which is frequently overlooked, despite the pioneering efforts of Frumkin and others [25]. For silver iodide and surface modified silicas, the influence of surface charge on the solid–liquid–vapour contact angle, θ, measured through the aqueous phase, has been determined by Billett et al. [26] and Laskowski and Kitchener [28], respectively. These studies indicate that θ is a maximum at the point of zero charge (p.z.c.) of the solid and is strongly dependent on pX (i.e. pAg or pI for AgI, pH for quartz). Apart from these studies, the bulk of reported θ values do not specify the exact experimental conditions (i.e. pX, concentration of supporting electrolyte) under which they were obtained [24].

In the case of the mercury-aqueous electrolyte system, the influence of electrostatic effects has been examined. Here the dependence of θ on electrical parameters is obvious, for the specific interfacial energy of the mercury–solution interface, γ_{Hg-sol}, is itself a function of charge and potential, as shown through the Lippmann equation:

$$-\left(\frac{\delta\gamma_{Hg-sol}}{\delta E}\right)_{\mu_s,T} = \sigma_o \tag{31}$$

where E is the applied potential, σ_o is the charge per unit area at the mercury–solution interface and μ_s is the chemical potential of the supporting electrolyte.

From equations (4) and (31), the dependence of $\cos\theta$ (θ measured through vapour phase) on σ_o is given as:

$$\cos\theta = \frac{\int_o^E \sigma_o \, dE - \gamma_{Hg-V}}{\gamma_{sol-V}} \tag{32}$$

a relationship which has been validated experimentally by Nakamura et al. [28].

In the case of a solid substrate, charged through adsorption of potential determining ions (i.e. a reversible electrode interface), the dependence of the interfacial energy, γ_{SL} on the electrical parameters is less obvious.

Application of equation (31) to this group of systems is of little help, because γ_{SL} cannot be measured in practice and one must consequently seek an alternative

route. As a first approximation, the presence of a double layer may be considered to only affect γ_{SL}. It should be recognized that charge present at the solid–solution interface may have some influence on the equilibrium spreading pressure, π_e, and thus on γ_{SV}. However, there is no hard evidence available for the influence of electrical double layers on π_e for these ionizable solids. Indeed, the definition of pX, say, in such ultra-thin films of liquid adsorbed at the SV interface is troublesome. In this respect it is noteworthy that Gee [29] has shown that the adsorption of water molecules at the modified silica–water vapour interface, as a function of the relative vapour pressure of water, may be adequately described by Van der Waals contributions alone. Our arguments here are developed for the solid-vapour-aqueous solution system, however a parallel analysis may equally well be developed for the solid-oil-aqueous solution case.

The change in γ_{SL} is caused by adsorption of potential determining ions and diffuse adsorption of counterions in the simplest case (we can neglect any specific adsorption for the present). In principle, the change in γ_{SL} can be determined from the Gibbs equation (14).

However, closer consideration of the formation of electrical double layers in contact angle systems leads to a more informative approach to θ (pX) relationships at reversible solid–electrolyte interfaces [30]. Electrical double layers are formed spontaneously in these systems and the free energy of their formation is therefore always negative [31]. At reversible interfaces, double layers are formed by the adsorption of potential determining ions from the bulk solution, accompanied by a rearrangement of compensating charge in the diffuse layer. If, in a three-phase contact angle system, the composition of the liquid phase is such that a soluble layer is present at the SL phase boundary, i.e. if pX $\neq$ p.z.c., the system is able to minimize its free energy by increasing the area of the SL interface. At a fixed bubble volume where θ is measured through the vapour phase, this must automatically cause an increase in θ. This leads to the phenomenological conclusion that for reversibly charged solids θ is a *minimum* at the p.z.c. (i.e. the air bubble clings most tightly to the surface). Or, in other words, the presence of surface charge renders a solid more hydrophilic. θ measured through the solution phase will of course be a *maximum* at the p.z.c. This conclusion is of significance for mineral flotation practice. In collectorless flotation, the separation efficiency could be improved in some cases by pX control. This has not always been realized, but might well explain some pH trends observed in flotation studies (e.g. [32, 33]).

In the presence of surface charge, the free energy of the SL interface can be formally written as:

$$\gamma_{SL} = \gamma_{SL}^{\circ} + \Delta F_{d.l.} \tag{33}$$

where γ_{SL} is the total free energy per m^2 of SL interface, γ_{SL}° is the "chemical" contribution to that energy (and equals γ_{SL} at the p.z.c.), and $\Delta F_{d.l.}$ is the free energy of double layer formation. This dissection of γ_{SL} into chemical and electrical con-

tributions is formally equivalent to that performed for the electrochemical potential of a charged species. Substituting equation (33) in Young's equation yields, for the case where θ is measured through the vapour phase, θ_V:

$$\cos\theta_V(pX) = \frac{[\gamma^\circ_{SL} + \Delta F_{d.l.}(pX)] - \gamma_{SV}}{\gamma_{LV}} = \frac{\Delta F_{d.l.}(pX)}{\gamma_{LV}} - \cos\theta_V(\text{p.z.c.}) \quad (34a)$$

Since $\Delta F_{d.l.} < 0$, therefore $\theta_V(\text{pX}) > \theta_V(\text{p.z.c.})$ in all cases. Where θ is measured through the solution phase, θ_{sol}:

$$\cos\theta_{sol}(pX) = \cos\theta_{sol}(\text{p.z.c.}) - \frac{\Delta F_{d.l.}(\text{pX})}{\gamma_{LV}} \quad (34b)$$

According to Verwey and Overbeek [31], the free energy of single double layer formation is given by:

$$\Delta F_{d.l.} = -\int_o^{\psi_o} \sigma_o \, d\psi \quad (35)$$

where ψ_o is the electrical potential of the SL interface. Equation (35) is valid for Nernstian surfaces, i.e. surfaces for which $\psi_o(\text{pX})$ follows the Nernst equation (31). For non-Nernstian surfaces, configurational contributions can be included in equation (35):

$$\Delta F_{d.l.} = -\int_o^{\psi_o} \sigma_o \, d\psi + \Delta F_{conf}(\text{pX}) \quad (36)$$

where ΔF_{conf} is the pX dependent configurational entropy contribution to the double layer free energy, but are not considered further here [34].

The $\Delta F_{d.l.}$ contribution in equation (34) can be calculated from double layer theory. For Nernstian surfaces this can be achieved by computing $\sigma_o(\psi_o)$ from the Poisson-Boltzmann (P-B) equation and carrying out the integration in equation (35).

For a flat diffuse double layer present at a Nernstian solid–solution interface the free energy of double layer formation is given by (14):

$$\Delta F_{d.l.} = -\frac{8n^\circ kT}{\kappa}\left(\cosh\frac{ze\psi_o}{2kT} - 1\right) \quad (37)$$

where n_o is the concentration of the symmetric $z:z$ electrolyte, k the Boltzmann constant, κ the reciprocal double layer thickness, and e the elementary charge.

Theoretical $\theta_{sol}(\text{p,X})$ relations for solids with different intrinsic hydrophobicities [i.e. $\theta_{sol}(\text{p.z.c.})$ values] calculated from equations (34b) and (37) are given in Figure 3. It follows that for rather hydrophobic solids, θ_{sol} essentially decreases to zero over a narrow pX range of one to two units, a prediction which is supported by measurements on the trimethylchlorosilane (TMS) modified silica system by Laskowski and Kitchener [27]. A decrease in θ_{sol} with increasing indifferent electrolyte concentration under otherwise identical conditions is theoretically expected (Figure

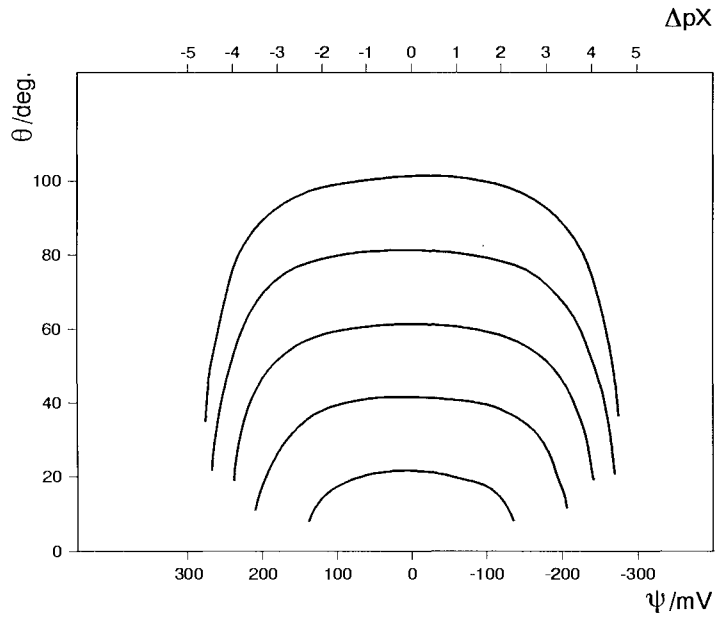

Fig. 3. Macroscopic water contact angle θ_{sol} as a function of surface potential in the presence of a diffuse double layer for different intrinsic hydrophobicities. Electrolyte: 10^{-2} M (1–1), temperature: 298 K. (From Fokkink and Ralston [30], with permission.)

4) and is indeed observed for the wetting of TMS treated quartz as indicated in the figure.

For a quantitative treatment of θ(pX), a more realistic description of the double layer is required. If, for a practical system, $\sigma_o(\psi_o)$ can be described by an appropriate model, the double layer contribution in equation (34) follows from theory. In most practical systems, however, a suitable model is not readily available. In these cases $\Delta F_{d.l.}$ can be obtained by numerical integration of experimental σ_o(pX) data. The vexing problem of pX to ψ_o conversion (i.e. the "Nernst" analogue) remains in most instances. For silver iodide–solution interfaces it is fundamentally sound to apply the Nernst equation (14) and thus one has a very suitable system with which to test this simple approach.

Billett et al. [26] measured θ_{sol}(pAg) on smooth, well-characterized AgI films. These data are reproduced in Figure 5. For this system, the electrostatic contributions to θ can be accounted for through equations (34b) and (35). $\Delta F_{d.l.}$ may be obtained by numerical integration of σ_o(pAg) in 10^{-4} M indifferent electrolyte (35). γ_{LV} and pAg° were taken as 73 mN m^{-1} and 5.6, respectively. The calculated dependence of θ on pAg is also given in Figure 3. Although Billett et al. [26] did not maintain a constant indifferent electrolyte level in their experiments, the agreement between experiment and theory is quite satisfactory.

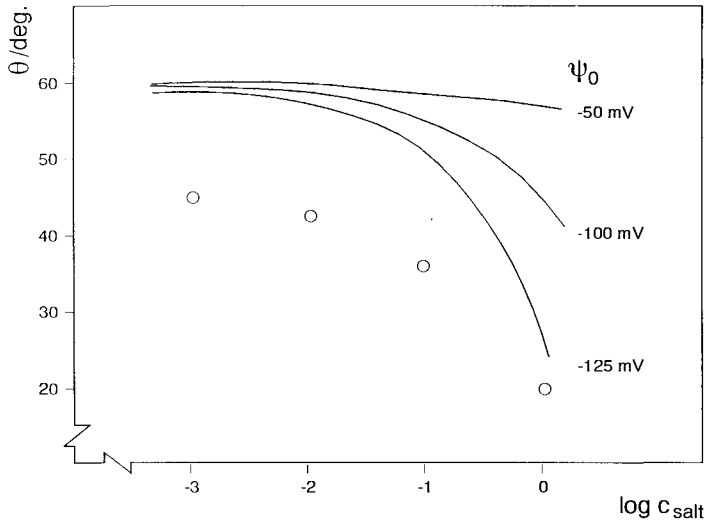

Fig. 4. Influence of indifferent (1–1) electrolyte concentration on θ at different surface potentials (ΔpX) in the presence of a diffuse double layer. Experimental points refer to advancing water contact angles measured on TMS-quartz in KNO_3 at pH 11. Temperature: 298 K. (From Fokkink and Ralston [30], with permission.)

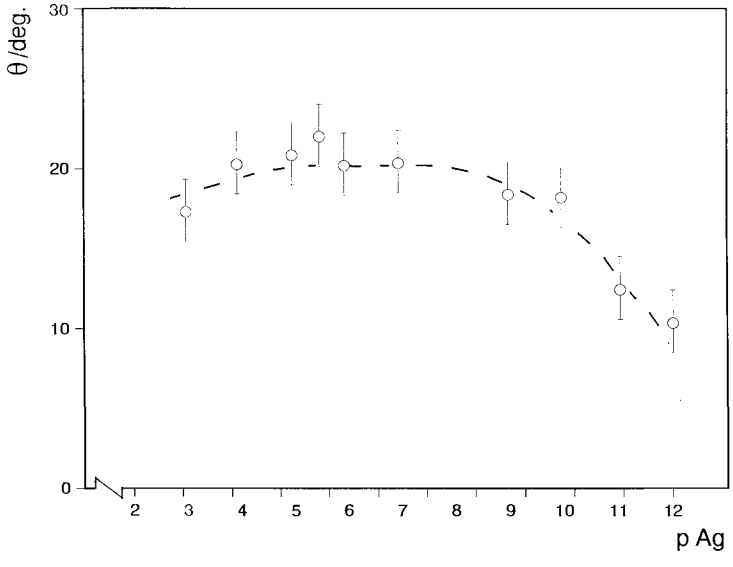

Fig. 5. pAg dependence of the contact angle θ_{sol} on smooth AgI film. Experimental points taken from [26], broken line calculated from double layer data, equation (34b). (From Fokkink and Ralston [30], with permission.)

Thus in any consideration of contact angle in mineral processing one should recognize that:

(a) electrostatic contributions in wetting phenomena are significant and may be accounted for by double layer thermodynamics; and

(b) contact angle measurements should be reported under well-defined conditions, i.e. θ_V or θ_{sol}, pX, electrolyte concentration.

Theoretical approaches to interfacial tension and contact angle

Virtually since Rayleigh's time [36] there has been a strong interest in calculating the specific interfacial energies γ_{SL}, γ_{SV} and γ_{LV} since a knowledge of these will enable the contact angle θ to be calculated, through equation (4), as well as other wetting parameters such as work of adhesion.

The most comprehensive pioneering work in this field was performed by Fowkes [37], catalyzed by the prior efforts of Girifalco and Good [38]. Fowkes maintains that when two immiscible liquids are in contact, the dominant interaction is due to the Van der Waals dispersion interaction. In the specific case of a hydrocarbon in contact with a liquid, Fowkes regards this dispersion contribution as the only important interaction. γ_{HV}, the surface tension of the pure hydrocarbon is reduced by the interaction that the surface hydrocarbon molecules have with the adjacent liquid atoms and, similarly, this second liquid will have its surface tension reduced. According to the Berthelot principle, the interaction constant for two different phases is given by the geometric mean of the interaction constant for the individual phases. By analogy, then, the interfacial tension, γ_{HgH}, between a simple hydrocarbon and mercury is given by:

$$\gamma_{HgH} = \gamma_M + \gamma_H - 2\left(\gamma_H^d \gamma_M^d\right)^{1/2} \tag{38}$$

where γ_M is the surface tension of mercury, γ_H the surface tension of the hydrocarbon and γ_M^d, γ_H^d are the respective dispersion only contributions to the surface tensions. Fowkes assumes that for the hydrocarbon–vapour interface:

$$\gamma_H = \gamma_H^d \tag{39}$$

i.e. the dispersion contribution is completely dominant. In this instance, equation (38) contains only one unknown quantity and by comparing the measured interfacial tensions of a series of hydrocarbons against mercury, it is possible to estimate the dispersion component, γ_M^d, of mercury. Fowkes determines this to be 200 ± 7 mJ m^{-2} at 293 K against an experimental value of 484 mJ m^{-2} for γ_M. The difference was ascribed to metallic bonding in liquid mercury. If this same argument is applied to the water–hydrocarbon interface, a value for $\gamma_{H_2O}^d$ of 21.8 mJ m^{-2} is obtained at 293 K. Turning to the mercury–water interface and assuming that only the dispersion contribution is significant, equation (38) becomes, at 293 K:

$$\gamma_{HgH_2O} = \gamma_{Hg} + \gamma_{H_2O} - 2\left(\gamma^d_{Hg})\gamma^d_{H_2O}\right)^{1/2}$$

$$= 484 + 72.8 - 2(200 \times 21.8)^{1/2} = 424.8 \text{ mJ m}^{-2}$$

which compares favourably with the experimental value of 426 mJ m^{-2}, indicating that there is a negligible contribution from the water molecule's permanent dipole moment. Whilst this is an important finding, only in selected circumstances is it valid to consider only the dispersion contribution from water. The surface tension of water is 72.8 mJ m^{-2} at 273 K, some 50 mJ m^{-2} of which cannot be accounted for by dispersion theory and which is attributed to hydrogen bonding. The formation of a hydrogen bond is a short range, coulombic interaction caused by the asymmetrical distribution of electron density around the water molecule. In such cases, this interaction determines the structure of the fluid. When a free air–water interface is formed and the hydrogen bonding structure readjusts to the change, one should not expect simple alkane molecules to markedly influence this structure. Thus simple alkanes (e.g. pentane, heptane, etc.) spread happily on water [39].

For a liquid droplet resting on a solid surface in air and where θ is measured through the liquid phase, from equation (4):

$$\cos\theta = \frac{\gamma_{SV} - \gamma_{SL}}{\gamma_{LV}} \tag{40}$$

and, introducing π_e from equation (7):

$$\cos\theta = \left(\frac{\gamma^o_S - \pi_e - \gamma_{SL}}{\gamma_{LV}}\right) \tag{41}$$

The presence of the π_e term in equation (41) normally makes the theoretical calculation of θ intractable. For low surface energies π_e is zero, i.e. the vapour of a high surface energy liquid will not adsorb on to a low energy solid because this will not lower the surface energy of the system. Examples of such solids include paraffin, polythene and poly(tetrafluoroethylene); the latter is commonly known as "Teflon".

Assuming that only the dispersion force contribution is important, combining equation (41) and an analogue of equation (38) for low energy surfaces yields:

$$\cos\theta = \frac{\gamma^o_S - \left[\gamma^o_S + \gamma_{LV} - 2\left(\gamma^d_S\gamma^d_{LV}\right)^{1/2}\right]}{\gamma_{LV}} \tag{42}$$

$$= -1 + 2\left(\gamma^d_s\right)^{1/2}\left[\frac{\left(\gamma^d_{LV}\right)^{1/2}}{\gamma_{LV}}\right] \tag{43}$$

This approach was initially used by Fowkes [37], who demonstrated that a plot of the measured contact angle versus $(\gamma^d_{LV})^{1/2}/\gamma_{LV}$ for a range of liquids on low energy surfaces did obey equation (43), allowing γ^d_S for the solid to be estimated. Zisman

and co-workers [40] found that for a given substance and a series of related liquids (e.g. *n*-alkanes, siloxanes or dialkyl ethers), $\cos\theta$ shows a reasonably linear dependence on γ_{LV}. The point where $\cos\theta = 1$ corresponds to the critical surface tension of wetting, γ_C. In practice, the measurement of γ_C requires that one uses a range of liquids of varying surface tension and with $\gamma_{LV} > \gamma_C$. This has tempted investigators to use a series of aqueous surfactant solutions of varying concentrations or mixtures of, say, alcohol in water. The latter approach has been used to achieve selectivity in flotation separations [41]. Preferential adsorption of one or other component can lead to quite spurious γ_C data.

The macroscopic approach may also be focussed on wetting behaviour [5]. Let us consider that we have a solid–vapour–liquid system at constant volume and denote the total free energy per unit area of the planar, parallel interfaces as $F_{SVL}(d)$, where d is the thickness of the vapour film. When the solid–vapour and liquid–vapour interfaces are separated by an infinite thickness of vapour, then:

$$F_{SVL}(\infty) = \gamma_{SV} + \gamma_{LV} \tag{44}$$

where γ_{SV} and γ_{LV} are the solid–vapour and liquid–vapour interfacial tensions, respectively. The interaction free energy per unit area is given by:

$$E_{SVL}(d) = F_{SVL}(d) - F_{SVL}(\infty) = F_{SVL}(d) - \gamma_{SV} - \gamma_{LV} \tag{45}$$

If d is reduced to zero, the total free energy must be that of the solid–liquid interface, i.e.:

$$F_{SVL}(0) = \gamma_{SL} \tag{46}$$

Combination of equations (45) and (46) yields:

$$\gamma_{SL} = \gamma_{SV} + \gamma_{LV} + E_{SVL}(0) \tag{47}$$

Here $E_{SVL}(0)$ represents the work of adhesion between the solid and the liquid. $E_{SVL}(0)$ is of course opposite in sign to the conventionally defined reversible work of adhesion [42].

If $E_{SVL}(0) < 0$, $\gamma_{SL} < \gamma_{SV} + \gamma_{LV}$ and the liquid will form a finite contact angle given by Young's equation, viz:

$$\cos\theta = \frac{\gamma_{SV} - \gamma_{SL}}{\gamma_{LV}} \tag{40}$$

and hence:

$$\cos\theta = -1 - \frac{E_{SVL}(0)}{\gamma_{LV}} \tag{48}$$

When two semi-infinite blocks of solid and liquid, both of unit area, are brought from infinity until they are almost touching at some critical separation d_C, Lifshitz theory [5] shows that the interaction energy per unit area is given by:

$$E_{SVL}(0) = \frac{-A_{SVL}}{12\pi d_C^2} \tag{49}$$

where A_{SVL} is the Hamaker constant for the system solid–vapour–liquid (recall Chapter 3). d_C is typically 0.15 to 0.2 nm and is invoked since the two blocks cannot approach to $d = 0$ due to the finite size of their constituent atoms.

For two identical liquid interfaces separated by vapour, by a similar argument leading to equation (47) where E_{LVL} is now equal in magnitude, but opposite in sign, to the work of cohesion [42]:

$$\gamma_{LV} = -\frac{1}{2}E_{LVL}(0) \tag{50}$$

Introducing a new cut-off distance d_C^i we obtain:

$$\gamma_{LV} = \frac{A_{LVL}}{24\pi d_C^{i2}} \tag{51}$$

so that the contact angle, θ, from equations (48), (49) and (51) is:

$$\cos\theta = \frac{2A_{SVL}}{A_{LVL}}\left(\frac{d_C^i}{d_C}\right)^2 - 1 \approx \frac{2A_{SVL}}{A_{LVL}} - 1 \tag{52}$$

if $d_C^i = d_C$ to a good approximation. Of course one may determine the value of d_C^i from equation (51) and experimental values of γ_{LV}. The reader should note the similarities between equation (43) and (52). This macroscopic approach has been found to yield good agreement between theory and experiment for contact angles of alkanes on poly(tetrafluoroethylene), but has certainly not been universally adopted at this stage. The use of d_C as an adjustable "cut off" does not always work and alternative approaches are often very difficult to apply or the necessary experimental spectral data are unavailable.

The somewhat empirical but nevertheless useful approach of Fowkes and the fundamental, macroscopic approach of Lifshitz can both be brought to bear on contact angles and wettability in mineral processing. Numerous problems and an absence of data will ensure an active research field for many years.

Non-ideal surfaces

To this point only ideal, smooth surfaces have been considered. In practice, solid surfaces are almost always rough and heterogeneous so that it is necessary to consider how these impact on the approach taken to date. In brief, roughness can either enhance or decrease wettability whilst chemical surface heterogeneity produces a composite contact angle which reflects the contribution from the various chemical "patches". Hysteresis, the discrepancy between advancing and receding contact angles (recall previous section) is a reflection of both roughness and heterogeneity.

Note that hysteresis is used to describe differences in static states and *not* kinetic effects. The latter are described in the next section on "Dynamic contact angles", below. Let us see if these effects can be quantified, noting only the major points, for excellent reviews are available in the literature [3, 4].

For a droplet of liquid, resting on a solid in contact with a vapour and forming a finite contact angle θ, equation (40) applies:

$$\cos\theta = \frac{\gamma_{SV} - \gamma_{SL}}{\gamma_{LV}} \tag{40}$$

Wenzel [43] argued that the validity of this expression depends upon the surface being smooth. If this is not the case, the surface area of the solid is $r(\gamma_{SV} - \gamma_{SL})$ and the apparent contact angle is given by the Wenzel equation:

$$\cos\theta_r = \frac{r(\gamma_{SV} - \gamma_{SL})}{\gamma_{LV}} \tag{52}$$

where:

$$r = \frac{\text{actual surface area}}{\text{geometric surface area}} \tag{53}$$

and θ_r is the contact angle observed on a surface of roughness r. Shuttleworth and Bailey (1948) among others also derived equation (52).

Cassie and Baxter [45], using similar reasoning to Wenzel, derived an expression to describe the behaviour of contact angles on *chemically heterogeneous* and *porous* surfaces. They considered that a heterogeneous surface of unit area consisted of two domains, the first having an area fraction f_1 with a contact angle of θ_1 and the second having an area fraction f_2 with a contact angle of θ_2, where:

$$f_1 + f_2 = 1 \tag{54}$$

The Gibbs free energy gained per unit area when a liquid droplet spreads across the surface is thus:

$$\Delta G = f_1 (\gamma_{S_1V} - \gamma_{S_1L}) + f_2 (\gamma_{S_2V} - \gamma_{S_2L})$$

where γ_{S_1V} and γ_{S_1L} refer to the first domain and γ_{S_2V} and γ_{S_2L} refer to the second. In combination with equation (40) and following similar reasoning to that leading to equation (4), the Cassie equation is derived:

$$\cos\theta_C = f_1 \cos\theta_1 + f_2 \cos\theta_2 \tag{55}$$

where θ_C represents the composite (advancing *or* receding) contact angle. In cases where the second region is air, for example where a porous medium is involved, γ_{S_2V} is zero and γ_{S_2L} becomes γ_{LV}, therefore equation (55) reduces to:

$$\cos\theta_C = f_1 \cos\theta_1 - f_2 \tag{56}$$

Israelachvili and Gee [46] have recently investigated the validity of the Cassie equation on a chemically heterogeneous surface. If a surface contains a mixture of hydrophobic and hydrophilic groups the application of the Cassie equation on a molecular level may not be valid in the light of current theories dealing with intermolecular and surface forces. The Cassie equation can easily be derived by averaging energies of cohesion. However, in considering the theories of Van der Waals and electrostatic forces, it is not cohesive energy that should be averaged but rather the polarizability, dipole moments or surface charges of the surface. Using this approach, Israelachvili and Gee derived a new relationship between θ_C and the contact angles of atomic or molecularly sized patches on the surface. For a two component surface:

$$(1 + \cos\theta_C)^2 = f_1(1 + \cos\theta_1)^2 + f_2(1 + \cos\theta_2)^2 \tag{57}$$

Crawford, Koopal and Ralston [47] have recently measured advancing and receding contact angles on smooth quartz surfaces of known area fractions of trimethylsilyl and silanol groups. Their results for advancing contact angles measured on

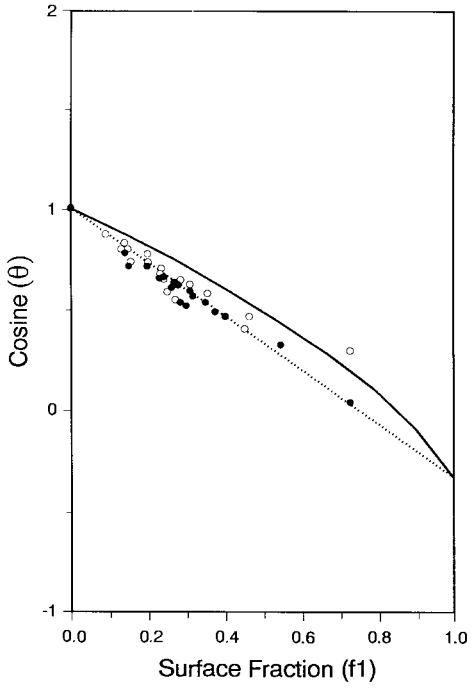

Fig. 6. Theoretical advancing water contact angle as a function of surface coverage of trimethylsilyl groups on quartz surfaces. Dotted line corresponds to the Cassie equation (55), solid line to Israelachvili and Gee, equation (57). (Experimental advancing water contact angle data are taken from Crawford et al. [47], with permission: • refer to smooth quartz plates; o to packed beds using the dynamic Washburn technique.)

smooth plates and packed powder beds are shown in Figure 6 and are compared with Cassie equation predictions [equation (55)] and those of equation (57). The data of Crawford et al. adhere more closely to equation (55) than to (57). The Cassie equation always predicts larger values than that of equation (57), however it is impossible at this point to say with any certainty which approach is more correct, particularly since the disposition of surface groups is presently undefined, i.e. are they in macroscopic or molecular patches? New surface analytical techniques can be focussed on this problem.

Johnson and Dettre [48] examined the problem of surface roughness by considering an idealised *rough* surface, symmetrical about the z-axis with a cross-sectional shape and a corresponding sinusoidal wave form which could therefore be mathematically described. The radius of the drop was larger than the distance between successive peaks and gravity was neglected. Their analysis, based upon Wenzel's approach and using an overall free energy minimisation approach, revealed the existence of a large number of metastable states. These metastable states display a range of apparent contact angles, thus providing a theoretical basis for contact angle hysteresis, i.e. as a liquid advances or retreats over a solid surface, various apparent (measured against some defined reference line) angles are seen. The microscopic contact angle is still the same as that obtained for a molecularly smooth surface, however the apparent angle depends on the angle of the true surface to the reference line at the three-phase line of contact. The equivalence of this microscopic angle on a rough surface with that determined on a smooth surface was confirmed by Oliver et al. [49] from a scanning electron microscope study of mercury droplets clinging to a finely grooved nitrocellulose surface. Importantly, Oliver et al. also showed that the three-phase line of contact could "stick" at edges, an effect predicted theoretically by Huh and Mason [50].

For the case of porous, composite surfaces, Oliver et al. [49] derived, for the case of a spherical drop resting on a series of concentric grooves:

$$\cos\theta_r = \frac{L_1}{2r}\cos\theta - \frac{L_2}{2r} \tag{58}$$

where L_1 and L_2 are the arc lengths of the solid–liquid and liquid–vapour interfaces and $2r$ is the diameter of contact of the droplet on the solid. For drops much larger than the wavelength of the roughness, equation (58) reduces to equation (56), i.e. Oliver et al. argue that the Cassie equation is a special case of equation (58). The problems alluded to in connection with equation (57) still remain, however.

Why are these effects important to mineral processing? In the act of attachment of an air bubble or an oil droplet to a mineral particle immersed in water, the water must retreat over the previously wetted mineral surface. This could lead to hysteresis in a manner already described above. Rough surfaces may result in sluggish liquid retreat over the surface, inhibiting movement at edges and thus limiting the time available, under flotation conditions, for the formation of a wetting

perimeter and a stable bubble or droplet–particle union. However the three-phase line of contact may be stabilized at edges, resisting the advancement of the liquid front and thus stabilizing bubble–particle contact. Finally, on the composite surfaces invariably encountered in mineral processing, patches of isolated water may be left in the wake of the retreating water, indicating a reduction in hydrophobicity. This latter effect is certainly observed in wettability investigations of packed beds of particles [51].

Certainly non-ideal surfaces complicate our interpretation of contact angles but do not diminish their importance to mineral processing. We must next decide how best to measure them.

Measurement of contact angles

A succinct review of the major techniques used for measuring contact angles on flat plates and powders is now given. The reader is referred to an extensive literature on the subject for specific details (e.g. [14, 24]).

Flat plates

(a) Drop profile. The measurement of contact angles is dependent upon the nature of the substrate under consideration. If the solid surface is a flat plate then the most widely used and most contemporary technique is a direct measurement of the angle by viewing the drop profile. The angle formed by a sessile drop or, alternatively, an adhering gas bubble can be determined to an accuracy of $\pm 2°$ for contact angles greater than about 20° [14]. Zisman and co-workers [40] were mainly responsible for popularising the method through the use of a goniometer eyepiece. Leja and Poling [52] photographed sessile (hanging) bubbles at slight angles so that a reflection occurs with the surface of the solid, thus the contact angle is half the angle subtended by the direct and reflected images. A bubble may be brought into contact with a plate with the use of a micrometer syringe and then either a goniometer eyepiece may be used to measure the contact angle directly or the bubble may be photographed and the angle measured with a protractor. This technique readily lends itself to the measurement of advancing or receding angles — the bubble size can be increased or reduced accordingly.

In cases where droplets are used and the equilibrium spreading pressure, π_e is appreciable, the observed contact angle may depend upon whether or not equilibrium with respect to adsorption has been reached.

(b) Drop dimensions. Contact angle may be obtained through the measurement of the drop dimensions when a sessile drop rests on a surface. Bashforth and Adams [53] used the Laplace equation to describe the droplet shape from a theoretical perspective. Smolders and Duyvis [54] selected a number of coordinate points and

applied a curve fitting technique, enabling the simultaneous determination of γ_{LV} and θ.

Fisher [55] developed a relationship between contact angle, radius and volume in order to measure small contact angles for sessile drops. An analytical balance was used to determine mass and, with a known ρ, volume, whilst the radius was determined from a photograph of the drop.

(c) Wilhelmy plate. Macroscopic contact angles do not necessarily have to be measured from angles formed with bubbles or droplets. When a smooth, vertical plate is brought in contact with a liquid, if the contact angle is less than 90° a downward force, W_F, is exerted on the plate, viz (e.g. [56]):

$$W_F = p\gamma_{LV} \cos\theta \tag{59}$$

where p is the perimeter of the line of contact. If the depth of immersion is not equal to zero then a volume V of liquid will be displaced. Consequently, the effect of buoyancy must be taken into account when considering the force exerted:

$$W_F = p\gamma_{LV} \cos\theta - V\Delta\rho g \tag{60}$$

Thus, if the surface tension is known, the contact angle can readily be calculated.

The plate should be smooth, otherwise a contact angle less than the true contact angle will be obtained. Indeed, if the plate is sufficiently roughened a contact angle of zero will be obtained which, in turn, provides a useful method for determining surface tension.

This technique, used in conjunction with an electronic balance, lends itself to the measurement of contact angles with time [57]. Processes such as adsorption and temperature effects can be observed.

Furthermore, both advancing and receding contact angles can be measured. Advancing angles are obtained by slowly bringing the plate and liquid surface together, whereas the receding angles are obtained by immersing the plate in the liquid and then withdrawing it a little.

(d) Capillary rise. The Wilhelmy plate technique may be modified so as to measure the capillary rise at a vertical plate. This method has been reported to be capable of increasing precision to 0.1°. When a liquid comes in contact with a vertical plate it will rise up and the height which it attains can readily be determined by the application of the Laplace equation, yielding:

$$\sin\theta = 1 - \frac{\Delta\rho g h^2}{2\gamma_{LV}} \tag{61}$$

The edge of the meniscus under appropriate illumination is usually quite sharp, hence, with the use of a travelling microscope, the height can be determined to a high degree of accuracy and precision.

Powders

The measurement of contact angles on powders is difficult and frequently highly unreliable. Numerous qualitative techniques are used with the majority of the quantitative methods dealing with compressed powders or the dynamic techniques popularised by Washburn [58], developed theoretically by Levine et al. [59] and Good and Lin [60] and carefully validated for narrow capillaries by Fisher and Lark [61]. These dynamic techniques are always plagued by problems such as depletion of surfactant molecules at a moving wetting front, lack of knowledge of the powder bed geometry, possible lack of attainment of thin film equilibria if "wetting" liquids are used to calibrate a particular powder bed, etc.

Non-equilibrium effects, which seriously complicate the analysis of dynamic wetting measurements, are overcome in static measurements such as the method originally proposed by Bartell and co-workers [62]. The theory underlying this method has been revived and elegantly extended by White [63]. The pressure required to prevent movement of liquid through a packed bed of particles, opposes the sum of the Laplace pressure, ΔP, and the hydrostatic head. The Laplace pressure is defined by:

$$\Delta P = \frac{2\gamma_{LV} \cos\theta}{r_{eff}} \tag{62}$$

where γ_{LV} is the liquid–vapour surface tension, θ is the contact angle of the liquid against the solid, measured through the liquid phase, and r_{eff} is the effective capillary radius.

The White derivation is a macroscopic thermodynamic argument where γ_{LV} and $\cos\theta$ enter equation (1) only after the Young-Dupre equation has been invoked. Most importantly, r_{eff}, inadequately described in the Bartell approach, is cogently defined by White as:

$$r_{eff} = \frac{2(1-\phi)}{\phi\rho A} \tag{63}$$

where ϕ is the volume fraction of solid in the packed bed, ρ is the density of the solid material, and A is the specific surface area per gram of solid. Combining equations (62) and (63) yields the Laplace-White equation, which is a strict expression for ΔP in porous media, viz:

$$\Delta P = \frac{\gamma_{LV} \cos\theta \phi A \rho}{(1-\phi)} \tag{64}$$

A capillary method for testing the White approach has been reported by Dunstan and White [64]. Broad agreement between theory and experiment was obtained for cleaned and chemically treated smooth glass Ballotini.

The method has been extensively developed by Diggins et al. [65] and has been shown to give reliable contact angle determinations on angular, chemically treated

quartz particles such as those encountered in mineral processing. Moreover the Cassie equation [equation (55)] was, for the first time, validated for packed beds of mixtures of hydrophobic and hydrophilic particles.

Dynamic contact angles

When the thin liquid film between, say, an air bubble and solid surface has drained and ruptured, a three-phase contact line (tpcl) is formed. A similar event occurs if an oil droplet is involved. If flotation is to occur, a particle/air bubble contact area sufficiently large to ensure aggregate stability must form in the contact time available. The kinetics of movement of the tpcl over the solid may therefore determine whether or not the particle will adhere to the bubble after film rupture. The kinetics of movement of the tpcl, what influences the movement and the contact angles formed as a result of this movement are of central importance to mineral processing.

The contact angles formed during the movement of the tpcl, i.e. the dynamic contact angles, are strongly dependent on both the velocity and direction of the contact line. In the case where a liquid displaces air, as the velocity of the tpcl increases, the dynamic contact angle increases. If the velocity is high enough a dynamic contact angle of 180° leads to the entrainment of a film of air at the solid surface, as shown in Figure 7. The recovery of crude oil from capillaries in oil bearing rock often involves flooding the capillaries with gas. If the oil is displaced by air the dynamic contact angle at the air/oil/solid contact line will decrease with increasing velocity. At a critical velocity the dynamic contact angle will be zero and a layer of oil will be entrained at the solid surface, decreasing the recovery.

The tpcl movement illustrated is an example of forced movement. An external force is required to move the liquid/gas interface over the solid surface. Spontaneous movement of the tpcl occurs when the system is relaxing from a non-equilibrium to an equilibrium state. An air bubble expanding over a hydrophobic surface is an example (see Figure 8), as is the spreading of a drop of liquid on a solid. Consider that, as before, the processes occur at constant volume.

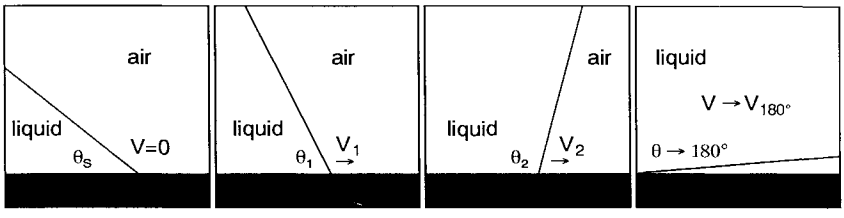

Fig. 7. Variation of contact angle with increasing tplc velocity (left to right) for liquid displacing air on a solid surface. Eventually, entrainment occurs in this case of forced spreading.

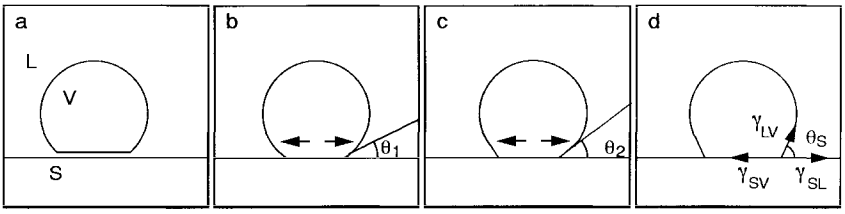

Fig. 8. Spontaneous expansion of a bubble, immersed in a liquid, on a solid surface. (a) shows film thinning prior to rupture, (b) and (c) correspond to dynamic spreading, (d) to the final static state.

Spontaneous spreading occurs when the Helmholtz free energy change, ΔF, given by:

$$\Delta F = \gamma_{LV}\Delta A_{LV} + \gamma_{SV}\Delta A_{SV} + \gamma_{SL}\Delta A_{SL} \tag{65}$$

is negative; γ_{LV}, γ_{SV} and γ_{SL} are of course the interfacial tensions for the liquid–vapour, solid–vapour and solid–liquid interfaces, respectively, and ΔA_{LV}, ΔA_{SV} and ΔA_{SL} are the changes in area of those interfaces caused by the spontaneous spreading. In the case of an air bubble spreading on a solid surface, illustrated in Figure 8, ΔA_{SV} is positive and equal to the decrease in A_{SL} and ΔA_{LV} is determined by the geometry of the bubble and the equilibrium contact angle. Clearly, for spontaneous spreading to occur, F (spread state) $<$F (unspread state).

The hydrodynamics of tpcl motion are obviously very important but difficulties arise when flow at the solid surface is considered. According to the classical "no slip" boundary condition of fluid mechanics there is no relative motion between the liquid and the solid at the solid surface. Application of this condition leads to the unlikely result that shear stress and pressure fields increase without bound as the contact line is approached, in other words the contact line should not move at all [66]. By assuming the surface is pre-wetted by a thin film of the liquid, or allowing for slip in the immediate vicinity of the contact line, this problem can be overcome but an assumption must be made about the correct form of the slip condition [4, 67].

The role of surface forces in controlling motion of the tpcl is of particular significance. Recalling equation (40), for a liquid droplet resting on a solid surface in air:

$$\cos\theta_S = \frac{\gamma_{SV} - \gamma_{SL}}{\gamma_{LV}} \tag{40}$$

and:

$$\gamma_{SV} = \gamma_{SL} + \gamma_{LV}\cos\theta_S \tag{66}$$

where θ_S is the static contact angle (Figure 8d).

Consider the case where the thin film between an air bubble and a solid surface has ruptured and the tpcl has just begun to move (Figures 8b and c).

θ_1, the initial dynamic contact angle, generally specified as θ_d, is much smaller than θ_s. If we assume that the interfacial tensions remain constant, which would be expected in the absence of soluble surfactants, immediately after rupture $\gamma_{SV} < \gamma_{SL} + \gamma_{LV} \cos\theta_d$ and there is an imbalance of forces acting on the tpcl. The movement of the three-phase boundary is considered to be caused by this imbalance and the driving force of the motion, D_F, is given as:

$$D_F = (\gamma_L + \gamma_{LV} \cos\theta_d) - (\gamma_{SL} + \gamma_{LV} \cos\theta_s) = \gamma_{LV}(\cos\theta_d - \cos\theta_s) \quad (67)$$

The driving force is therefore dependent on the difference between the *cosines* of the dynamic and equilibrium contact angles and is often written as $\theta_{LV}\Delta\cos$. The force decreases as θ_d increases and approaches zero as $\theta_d \rightarrow \theta_s$. Inertial and frictional forces oppose the motion of the tpcl but terms describing these factors contain unknowns such as the surface viscosity and the velocity of the fluid normal to the solid surface [4].

In the analysis of the kinetics of movement of the tpcl there are two strong schools of thought:

(a) The dynamic contact angles formed at the tpcl during displacement are an indication of the work needed to overcome an energy barrier to the movement at a molecular level. This is the "surface chemical" school where all observations are attributed to the influence of interfacial forces. Hydrodynamic contributions are generally ignored. The relationship between θ_d and V is due to the interaction between molecules of the liquid and adsorption sites on the solid surface [10, 68, 69].

(b) The apparent dynamic contact angles observed at the tpcl are determined by the hydrodynamics of the system only, and surface forces are disregarded [10, 70].

(a) and (b) have been combined by a number of authors who propose that the surface chemical approach holds in certain circumstances but the hydrodynamics of the system dominates at other times [71, 72].

Overall, there is a plethora of theories in this field, mirrored in the vast number of published papers. Experimental data generally agrees well with theory for a particular set of experimental conditions, but agreement is rarely seen between different systems. Part of the problem at least is due to the fact that poorly characterized experimental systems have been used, e.g. time dependent adsorption processes occur in the presence of soluble surfactants. The subject warrants intense study on well characterized systems [73].

Summary

In this chapter we have explored the thermodynamic origins of the contact angle and linked them to collector adsorption and electrical double layer effects. We have demonstrated that contact angle has a rigorous theoretical basis. Rough and

composite surfaces, typical of those encountered in mineral processing, force us to modify our "ideal surface" approach to contact angle, but do not diminish its importance. Static and dynamic contact angles can both be measured. Our understanding of contact angle is extensive, but far from complete, and as new approaches and techniques focus on collector adsorption mechanisms, surfactant reorientation effects, improved models of dynamic contact angles and the like, extensive benefits to mineral processing are anticipated.

References

1 T. Young, Phil. Trans. R. Soc. (London), 95 (1805): 65.
2 J.W. Gibbs, The Collected Works of J. Willard Gibbs, Volume 1, Longmans-Green, New York, N.Y., 1928.
3 R.E. Johnson and R.H. Dettre, in: E. Matijevic (Editor), Surface and Colloid Science, Vol. 2, Wiley-Interscience, New York, N.Y., 1969.
4 P.G. de Gennes, Rev. Mod. Phys., 57 (1985): 827.
5 J.N. Israelachvili, Intermolecular and Surface Forces, Academic Press, London, 1985.
6 L.R. White, J. Colloid Interface Sci., 90 (1982): 536.
7 D. Diggins, L.G.J. Fokkink and J. Ralston, Colloids Surf., 44 (1990): 299.
8 L.R. White, J. Chem. Soc. Faraday Trans. I, 73 (1977): 390.
9 C. Huh and L.E. Scriven, J. Colloid Interface Sci., 35 (1971): 85.
10 T.D. Blake, in: T. Tadros (Editor), Surfactants, Academic Press, London, 1984.
11 J.C. Melrose, in: Society for Chemical Industry (London), Monograph, No 25 (1967): 123.
12 A.I. Rusanov, J. Colloid Interface Sci., 63 (1978): 330.
13 R. Aveyard and D.A. Haydon, Introduction to the Principles of Surface Chemistry, Cambridge University Press, Cambridge, 1973.
14 R.J. Hunter (Editor), Foundations of Colloid Science, Vol. 1, Clarendon Press, Oxford, 1987.
15 P.L. de Bruyn, J.Th.G. Overbeek and R. Schulman, Trans. Am. Inst. Min. Eng., 199 (1954): 519.
16 C.A. Smolders, Rec. Trav. Chim., 80 (1961): 699.
17 G.J. Jameson and M.C.G. del Cerro, J. Chem. Soc. Faraday Trans. I, 72 (1976): 883.
18 A. Neumann, Adv. Colloid Interface Sci., 4 (1974): 105.
19 J.S. Rowlinson and B. Widom, Molecular Theory of Capillarity, Clarendon Press, Oxford, 1982.
20 P.M. McGuiggan and R.M. Pashley, Colloids Surf., 27 (1987): 277.
21 M.A. Cohen Stuart, T. Cosgrove and B. Vincent, Adv. Colloid Interface Sci., 24 (1986): 143.
22 I.N. Plaksin, Proc. 5th Int. Miner. Process. Congr., IMM, London, 1960, p. 253.
23 I.B. Ivanov, B.V. Toshev and B.P. Radoev, in: J.F. Padday (Editor), Wetting, Spreading and Adhesion, Academic Press, London, 1978.
24 A.W. Adamson, Physical Chemistry of Surfaces, 3rd edition, John Wiley, New York, N.Y., 1976.
25 V.I. Klassen and V.A. Mokrousov, An Introduction to the Theory of Flotation (translated by J. Leja and G.W. Poling), Butterworths, London, 1963.
26 D.F. Billett, D.B. Hough and R.H. Ottewill, J. Electroanal. Chem., 74 (1976): 107.
27 J. Laskowski and J.A. Kitchener, J. Colloid Interface Sci., 29 (1969): 1970.
28 Y. Nakamura, K. Kamada, K. Katoh and A. Watanabe, J. Colloid Interface Sci., 44 (1973): 517.
29 M. Gee, Ph.D. Thesis, University of Melbourne, Australia, 1987.
30 L.G.J. Fokkink and J. Ralston, Colloids Surf., 36 (1989): 69.
31 E.J.W. Verwey and T.Th.G. Overbeek, Theory of the Stability of Lyophobic Colloids, Elsevier, Amsterdam, 1948.

32 B.V. Derjaguin and N.D. Shukakidse, Int. Min. Metall. Trans., 70 (1960–61): 569.
33 R.A. Hayes, D.M. Price, J. Ralston and R.W. Smith, Min. Proc. Extr. Metall. Rev., 2 (1987): 203.
34 D.Y.C. Chan and D.J. Mitchell, J. Colloid Interface Sci., 95 (1983): 193.
35 J.A.W. van Laar, Ph.D. Thesis, University of Utrecht, Utrecht, The Netherlands, 1952.
36 Lord Rayleigh, Phil. Mag., 30 (1890): 285.
37 F.M. Fowkes, J. Phys. Chem., 66 (1962): 382.
38 L.A. Girifalco and R.J. Good, J. Phys. Chem., 64 (1960): 561.
39 D.B. Hough and L.R. White, Adv. Colloid Interface Sci., 14 (1980): 3.
40 W.A. Zisman, Adv. Chem. Ser., 43 (1964): 1.
41 B. Yarar and J. Kaoma, Colloids Surf., 11 (1984): 429.
42 R. Defay, I. Prigogine, A. Bellemans and D.H. Everett, Surface Tension and Adsorption, Longmans, Green, London, 1966.
43 R.N. Wenzel, Ind. Eng. Chem., 28 (1936): 988.
44 R. Shuttleworth and G.L.J. Bailey, Disc. Faraday Soc., 3 (1948): 16.
45 A.B.D. Cassie and S. Baxter, Trans. Faraday Soc., 40 (1944): 456.
46 J.N. Israelachvili and M.L. Gee, Langmuir, 5 (1989): 288.
47 R. Crawford, L.K. Koopal and J. Ralston, Colloids Surf., 27 (1987): 57.
48 R.E. Johnson and R.H. Dettre, Adv. Chem. Ser., 43 (1964): 112.
49 J.F. Oliver, C. Huh and S.G. Mason, J. Adhesion, 8 (1977): 223.
50 C. Huh and S. Mason, J. Colloid Interface Sci., 60 (1977): 11.
51 D. Diggins, M.App.Sc. Thesis, South Australian Institute of Technology, 1990.
52 J. Leja and G.W. Poling, Proc. 5th Int. Miner. Process. Congr., IMM, London, 1960, p. 325.
53 F. Bashforth and J.C. Adams, An Attempt to Test the Theory of Capillary Action, CUP, Cambridge, U.K., 1892.
54 C.A. Smolders and E.M. Duyvis, Rec. Trav. Chim. Pays-Bas, 80 (1961): 635.
55 L.R. Fisher, J. Colloid Interface Sci., 72 (1979): 200.
56 G.L. Gaines, Insoluble Monolayers at Liquid–Gas Interfaces, Interscience, New York, N.Y., 1965.
57 J.D. Andrade, L.M. Smith and D.E. Gregonis, in: Surface and Interfacial Aspects of Biomedical Polymers, Vol. 1, Plenum Press, New York, N.Y., 1985.
58 E.W. Washburn, Phys. Rev., 17 (1921): 273, 374.
59 S. Levine, J. Lowndes, E.J. Watson and G.J. Neale, J. Colloid Interface Sci., 73 (1980): 136.
60 R.J. Good and N.J. Lin, J. Colloid Interface Sci., 54 (1976): 52.
61 L.R. Fisher and P.D. Lark, J. Colloid Interface Sci., 69 (1979): 486.
62 F.E. Bartell and C.W. Walton, J. Phys. Chem., 38 (1934): 503.
63 L.R. White, J. Colloid Interface Sci., 90 (1982), 536.
64 D. Dunstan and L.R. White, J. Colloid Interface Sci., 111 (1986): 60.
65 D. Diggins, L.G.J. Fokkink and J. Ralston, Colloids Surf., 44 (1990): 299.
66 C. Huh and L.E. Scriven, J. Colloid Interface Sci., 35 (1971): 85.
67 E.B. Dussan V and S.H. Davis, J. Fluid Mech., 65 (1974): 75.
68 T.D. Blake and J.M. Haynes, J. Colloid Interface Sci., 30 (1969): 421.
69 M.C. Wilkinson, R. Ellis, M.P. Aronson, J.W. Vanderhoff and A.C. Zettlemoyer, J. Colloid Interface Sci., 68 (1979): 543.
70 E. Rillearts and P. Joos, Chem. Eng. Sci., 35 (1980): 883.
71 G.F. Teletzke, H.T. Davis and L.E. Scriven, Chem. Eng. Commun., 55 (1987): 41.
72 A.M. Schwartz and S.B. Tejada, J. Colloid Interface Sci., 38 (1972): 359.
73 G. Newcombe, M.App.Sc. Thesis, South Australian Institute of Technology, 1989.

Chapter 6

The influence of particle size and contact angle in flotation

J. RALSTON

Introduction

When an ore is ground so as to liberate, either fully or partially, desired mineral particles from the surrounding matrix or gangue, a distribution of particle sizes inevitably results. Nowadays, particle size is often measured and controlled in flotation concentrators. For example, hydrocyclones may be used to remove fine particles or to send coarse particles back to the grinding circuit and on-stream particle size analysis is common. The finest particles possess the largest *specific* surface area (m^2 kg^{-1}). The term "fine particle", expressed as a particle diameter, describes a particle which is a lot larger for coal flotation (e.g. 100 to 200 μm) than for sulphide or oxide flotation (circa 5 μm or less). Fines are often a metallurgist's curse, being difficult to float, showing a tendency to "slime" or coat coarse material and consuming, per unit mass, much larger quantities of collector compared with intermediate and coarse particles. The former are generally the most readily floatable, although middlings (composites of two or more minerals) can still respond poorly to flotation, whilst coarse particles are often lost due to turbulent forces breaking bubble–particle contact in the flotation cell. Thus a flotation concentrator will typically exhibit an "elephant" shaped flotation curve, with a marked decrease in recovery for both fine and coarse particles. Part of our task in this present chapter is to try and understand why particles of different sizes respond poorly or well in flotation.

We should note that the influence of particle size on flotation was recognised in the landmark paper by Gaudin et al. [1]. Similarly the principles of selective adsorption and their link to contact angle have been developed over many years and are discussed in chapters 2 and 5.

The diagnostic value of size by size recovery curves has now permeated flotation research and practice to some degree [2], demonstrably leading to improved metallurgical performance [3, 4]. In contrast, questions dealing with the degree of hydrophobicity required to float a particle of a given size under specific conditions have generally remained unanswered, despite their immense importance. Only

rarely has there been any real attempt to marry contact angle to particle size and then use this liaison to investigate flotation performance [2, 5, 6].

The origins of this difficulty lie in elucidating the underlying colloid science, a task which is the subject of this present chapter.

It is instructive to recall that flotation is essentially a dynamic process where kinetics and energetics are inextricably mixed. Focussing on the kinetic aspects of flotation for a moment allows us to obtain a perspective view of the link between particle size and contact angle before teasing out the threads of the relationship further.

Kinetic considerations in bubble–particle interaction

For batchwise flotation processes, such as those which take place in the Hallimond Tube, Fuerstenau cell, Denver and Agitair cells etc., the rate of removal of particles may be described by a first order rate equation, viz.:

$$\frac{dC}{dt} = -kC \tag{1}$$

where C is the particle concentration in mass per unit volume and k is a "rate constant". The reference volume (V_r) requires some consideration — it may be taken as the total pulp volume, the volume of water alone, the volume of water plus air, etc. This reference volume needs to be kept constant for a particular investigation.

From equation (1):

$$\int_{C=C_0}^{C=Ct} \frac{1}{C}\,dC = \int_{t=0}^{t=t} -k\,dt$$

and:

$$C = C_0 e^{-kt} \tag{2}$$

The recovery, R may be conveniently defined in a number of ways, noting the number, mass and concentration of particles at various times in the reference volume V_r:

Time	Number of particles, N	Mass, M	Concentration, C
0	N_0	M_0	C_0
t	N	M	C
∞	N_∞	M_∞	C_∞

Thus:

$$R = \frac{M_0 - M}{M_0} = \frac{N_0 - N}{N_0} = \frac{C_0 - C}{C_0}$$

$$\frac{dR}{dt} = k(1 - R) \tag{3}$$

and:

$$R = 1 - e^{-kt} \tag{4}$$

After prolonged flotation, some material may remain in the pulp, i.e. is unfloatable and may be represented by C_∞. Thus C is replaced by $C - C_\infty$, and C_0 is replaced by $C_0 - C_\infty$, hence:

$$R = R_\infty(1 - e^{-kt}). \tag{5}$$

As the bubble rises in the cell it collects particles with a collection efficiency E and carries them out of the cell.

The concentration of particles at any time t is N/V_r where N is the total number of particles in the cell whose reference volume is V_r.

For large bubbles, of 1 mm diameter or so, as are often found in flotation, and not overly large particles, in an agitated pulp the total number of particles removed by a bubble as air rises through the liquid in the cell, of depth h is:

$$E\left(\frac{\pi d_b^2 h}{4}\right)C$$

where d_b is the bubble diameter.

E, the flotation probability or collection efficiency is given by $E = E_c E_a E_s$ where E_c is the collision efficiency, E_a is the attachment efficiency and E_s is the stability efficiency of the bubble/particle aggregate. This dissection of collection efficiency is both instructive and common, serving to focus the reader's attention on the three zones of bubble–particle interaction originally proposed by Derjaguin and Dukhin [6].

If the gas volumetric flow rate is G_{fr}, the number of bubbles formed per unit time is $G_{fr}/(\pi d_b^3/6)$.

The rate of removal of particles from the cell is:

$$\frac{dN}{dt} = \frac{-6G_{fr}}{\pi d_b^3} \times E\frac{\pi d_b^2 h}{4} \times C = -\frac{3}{2}\frac{G_{fr}Eh}{d_b}C$$

Since $C = N/V_r$, then:

$$\frac{dC}{dt} = -\frac{3}{2}\frac{G_{fr}Eh}{d_b V_r}C \tag{6}$$

or, expressing C in terms of recovery, R:

$$\frac{dR}{dt} = +\frac{3G_{fr}Eh}{2d_b V_r}(1 - R) \tag{7}$$

Comparing equation (7) with (3) and (4):

$$R = 1 - \exp\left(-t\frac{3G_{fr}E_cE_aE_sh}{2d_bV_r}\right) \tag{8}$$

$$k = \frac{3G_{fr}E_cE_aE_sh}{2d_bV_r} \tag{9}$$

The rate constant k is directly analogous to that obtained in chemical reaction kinetics. Its value will be partly determined by the slow step(s) in bubble–particle collision, attachment and detachment processes, as well as by physical variables such as G_{fr}.*

Equation (4) has been shown to apply to a system of monodisperse polystyrene latex particles, for example, floating under batchwise conditions (e.g. [7, 67]). A plot of $\ln(1 - R)$ versus t yields the rate constant k. For systems which are polydisperse in particle size and/or in which particles of different hydrophobicities are present, the recovery then becomes the sum of a series of exponential terms and the plot of $\ln(1 - R)$ versus t will show curvature, reflecting the different contributions from the various particles in the pulp to the recovery.

In the metallurgical literature R versus t data are analysed by assuming that the pulp consists of "fast" and "slow" floating components, allowing the respective rate constants (k_f and k_s) and fractions (f_f and f_s) to be determined (e.g. [2, 8]). Although this is a gross simplification of the real multi-component situation, much valuable information may be gleaned from such a simplified analysis. In fact the latter is frequently used to examine the flotation behaviour of particles of a specific size range in flotation circuits, where the behaviour of an individual flotation cell or bank of cells may be approximated to a batchwise process [8].

Derjaguin and Dukhin were the first to distinguish three zones of approach of a bubble and a particle on the basis of the different kinds of force occurring in them (Figure 1). This model is a very useful one and serves to stress the significant contributions to collection efficiency. It should not be taken to mean, however, that there are well defined boundaries between each zone; rather they grade into one another, the importance of the various contributing effects in each zone being more accurately identified as further experimental results become available in the literature.

Zone 1 is a region far from the bubble surface where hydrodynamic forces are dominant, controlling E_c in equation (9). Hydrodynamic drag forces act to sweep the particle around the bubble, viscous forces tend to retard this relative motion between the two whilst particle inertial and gravity forces force the particle towards the bubble. It is not our present purpose to focus on collision theory, however some passing comment at least must be made on a topic which is adequately dealt with

* For a constant G_{fr} and constant bubble size distribution, d_b will be an appropriate average.

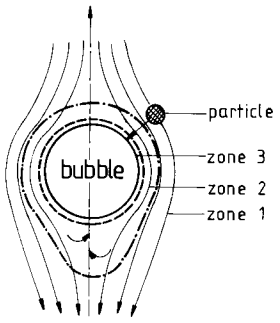

Fig. 1. Hydrodynamic (*1*), diffusiophoretic (*2*) and interparticle (*3*) force zones of interaction between a bubble and a particle (from Derjaguin and Dukhin [6], with permission).

elsewhere (e.g. [9]). It should be noted that as the particular model of collision efficiency varies, the dependence of dR/dt on bubble diameter changes [67].

Broadly speaking, all models of collision efficiency predict that E_c decreases with particle size at constant bubble size down to a diameter of circa 0.5 μm. At this value, Brownian diffusion takes over as the predominant capture mechanism, the collision efficiency increasing with decreasing size as the tiny particles (virtually "solute molecules") move towards the surface of a spherical bubble. Sutherland [10] made the first significant contribution to the treatment of collision efficiency. His hydrodynamic treatment of the process of particle and bubble approach in zone 1 was carried out without any consideration of particle inertia, bubble deformation or film thinning, deficiencies which were in part recognised by Sutherland and Wark [11].

The Sutherland theory, based on potential theory or streamline flow and corrected by Dobby and Finch [12] shows that the concentration, C, of mineral floated at a time t is related to its initial concentration, C_0, by the recovery, R as:

$$R = \frac{C}{C_0} = \left\{1 - \exp -t \left[\frac{3\pi\phi R_B R_p V_t N_B}{\cosh^2 3V_t\lambda/2R_B}\right]\right\} \tag{10}$$

where R_B and R_p are the bubble and particle radii, V_t is the bubble–particle relative velocity, λ is the induction time, N_B is the number of bubbles per unit volume, and ϕ is the fraction of particles retained in the froth following bubble–particle attachment. The reader should note the relationship between equations (4), (8) and (10). Despite the deficiencies of the Sutherland model, addressed in detail in the literature (e.g. [13–16]), his "first approximation theory" yields results which are in fair agreement with experimental determinations of particle trajectories, touching angles and collision efficiencies, obtained from model experiments performed in a vertical flow tube with individual particles and a single bubble, as noted by Schulze [9]. For more detailed treatments of the hydrodynamic aspects of bubble–particle

collision the reader is referred elsewhere, particularly to the overview of Schulze [9, 68], the excellent blend of theory and experiment by Anfruns and Kitchener [15] and the combination collision and attachment model of Dobby and Finch [13]. The inability of collision theory to adequately describe the collection process between bubbles and smooth and angular particles is vividly demonstrated by Anfruns and Kitchener [15]. Their experiments — *still the only measurements of absolute rate of capture* — gave results in good agreement with collision theory, assuming every collision resulted in capture of their very hydrophobic particles.

Derjaguin and Dukhin [6] identified zone 2 as that region where diffusion effects are important. A strong electric field exists in this zone, for the liquid flow around the moving bubble gives rise to a tangential stream at its surface which destroys the equilibrium distribution of adsorbed ions there. Surfactant is continually swept from the upper to the lower surface of the bubble. Transport of ionic surfactant to the moving bubble surface therefore takes place, leading to the establishment of a concentration gradient. A strong electric field of order 3000 V cm^{-1} is established when the cation and anion diffusion coefficients differ, as they generally do. Hence charged particles entering zone 2 will experience an electrophoretic force in precisely the same way as in an electrophoresis cell [17] and would be either attracted towards, or repelled from the bubble surface. Derjaguin and Dukhin coined the term "diffusiophoresis" for this phenomenon i.e. the "diffusiophoretic force" therefore acts on the particle as an additional force.

To date however, there is absolutely no unequivocal experimental evidence confirming the presence or absence of diffusiophoresis in flotation aside from some very preliminary work [18]. Apart from noting its possible contribution to *collision* efficiency it is not pursued further here.

In zone 3, interparticle forces of the type described in Chapter 3 predominate once the thin film between the bubble and the particle is reduced much below a few hundred nanometer. These interparticle forces can *accelerate*, *retard* or even *prevent* the thinning of the liquid film between the particle and the bubble. From a thermodynamic point of view, the free energy of a liquid film differs from the bulk phase from which it is formed. This excess free energy was originally called the "wedging apart" or "disjoining" pressure by Derjaguin [19] and represents the difference between the pressure within the film, p^f and that in the bulk liquid adjacent to the solid surface, p^l. Note that for a bubble pushed against a flat solid surface, immersed in water, p^b, the pressure within the bubble, is equal to p^f. Derjaguin and Titievskaya [20] and Scheludko and Exerowa [21] performed experimental measurements of disjoining pressures, providing both the first real verification of the DLVO theory as well as the first accurate experimental estimates of the Hamaker constant, respectively. The disjoining pressure (π) depends on the film thickness, h, and:

$$\pi(h) = p^f - p^l \tag{11}$$

For mechanical equilibrium in a stable film $\pi(h) > 0$ and $d\pi/dh < 0$.

If the liquid film is stable at all thicknesses the liquid is said to completely wet the solid. This occurs, for example, when an air bubble approaches a clean silica surface immersed in water — in this instance the Hamaker constant is negative and the corresponding Van der Waals force is repulsive for the silica/water/air triple layer [22]. For an unstable film the thin film must drain then rupture and the resulting three phase line of contact (tplc, vapour–water–solid) must expand to form a wetting perimeter before the particle can adhere to the bubble. Each of these events will have a characteristic time associated with them, the sum of which must be less than the contact time between the bubble and the particle if flotation is to occur. The contact time is generally of the order of 10^{-2} seconds or less. The induction time, λ [see equation (10)] is normally [9] taken as the time required for bubble–particle adhesion to occur, once the two are brought into contact. i.e. it is the sum of the thin film drainage/rupture and tplc spreading times ($t_{\text{film}} + t_{\text{tplc}}$) and is synonymous with the attachment time. Occasionally λ is restricted to encompass only the first of these processes.

The thermodynamic and kinetic properties of thin liquid films are described in reviews by Buscall and Ottewill [23], Aveyard and Vincent [24] and Ralston [25] as well as in the books by Sonntag and Strenge [16], Hunter [27] and Ivanov [69]. Several of the salient findings with respect to mineral processing are summarised here. The reader should refer to Chapter 3 and references therein for a description of the role of interparticulate forces.

The mechanism(s) of thin film drainage have received a great deal of attention, with particular emphasis being placed on symmetric films [26]. At large distances, film drainage between surfaces obeys the Reynold's equation. Reynolds [28] used the basic hydrodynamic equations of Navier and Stokes to analyse the flow between two parallel flat plates. For the case of a circular disc of radius r approaching a stationary, flat surface, where radial flow from the centre is assumed and the velocity at each interface is taken to be zero, the force F pressing on the disc is given by:

$$F = \frac{3\eta\pi r^4}{2h^3}\left(\frac{\mathrm{d}h}{\mathrm{d}t}\right) \tag{12}$$

where η is the liquid viscosity. Further:

$$\frac{\mathrm{d}\{1/h^2\}}{\mathrm{d}t} = \frac{4P}{3\eta r^2} \tag{13}$$

where $P = F/A$ and A is the disc area (i.e. πr^2). As an integrated form:

$$\frac{4P}{3\eta r^2}(t_{\mathrm{t}} - t_0) = \frac{1}{h^2} - \frac{1}{h_0^2} \tag{14}$$

This treatment of Reynolds for zero velocity at each interface was extended by Scheludko and Platikanov [29] to the case of one surface being a free liquid. With

these new boundary conditions, equation (13) becomes:

$$\frac{d\{1/h^2\}}{dt} = \frac{16P}{3\eta r^2} \tag{15}$$

For a bubble being pushed against a flat plate in a liquid, an experimental system frequently used in flotation related studies, from equations (11) and (15):

$$\frac{d\{1/h^2\}}{dt} = \text{constant } \left[p^1 - \pi(h)\right] \tag{16}$$

and the integrated form becomes:

$$\left(\frac{1}{h^2} - \frac{1}{h_0^2}\right) = \text{constant } \left[p^1 - \pi(h)\right](t - t_0) \tag{17}$$

Thus, from a plot of $(1/h^2) - (1/h_0^2)$ against time, whether or not the disjoining pressure is attractive or repulsive may be readily detected. Under conditions where true Reynolds flow occurs $[\pi(h) = 0]$ the plot will be linear, as expected for thick films where $h \rightarrow \infty$ and $\pi(h) \rightarrow 0$. Various optical methods (e.g. interferometry) may be used for following film drainage [26].

Chan and Horn [30] measured the drainage rates for non polar liquid films constrained between two molecularly smooth mica surfaces. The liquids studied were octamethylcyclotetrasiloxane, *n*-tetradecane and *n*-hexadecane, all three of which exhibit Newtonian behaviour. For film thicknesses down to 50 nm the drainage rates adhered to Reynolds' equation. Below 50 nm the drainage rate was retarded, an observation which Chan and Horn accounted for by assuming that the liquid within several molecular layers of each mica surface does not undergo shear. In such ultra thin films, the continuum theory advanced by Reynolds disintegrates and drainage takes place in a stepwise fashion, the step size mirroring the molecular layer thickness in the liquid. This behaviour is reminiscent of the oscillatory short-range forces due to solvent structural effects which have been detected in accurate force-distance measurements, as discussed in Chapter 3.

When a bubble is pressed against a solid surface, through water, the intervening film is generally not plane parallel. Rather the edge of the film thins quickly and a small, thicker dimple is trapped in the centre. This is essentially a kinetic phenomenon, caused by the flow being greatest at the very edge of the film in the initial stages of drainage. The existence of this dimple has been detected by Scheludko [31], Prokhorov [32] and others. Hydrodynamic theories attempting to describe the profile and evolution of the dimple have been proposed by Frankel and Mysels [33] and Hartland and Robinson [34], with rather limited success in describing experimental data [35].

Experimental evidence relating to film drainage in systems where soluble surfactants are present is rather equivocal. Adsorption and desorption processes coupled with possible molecular reorientation make any theoretical interpretation difficult.

Unfortunately these are the very systems which are of primary interest to mineral processing. Furthermore additional complications ensue when one considers a particle approaching a bubble in flotation. The nature of the bubble surface (i.e. the boundary condition) will influence the evolution of the thin film between bubble and particle. If the bubble surface is mobile, as will be the case in the absence of surfactant, the particle should *slide* over the bubble. If surfactant is present, as commonly occurs in practice, and the bubble surface is immobilized, the particle should *roll* over the bubble [36]. This makes any solution of the Navier Stokes equation for film drainage extraordinarily difficult, if not intractable, particularly in the case of the angular particles that are normally present in flotation. It is worth recalling at this point the observations that smooth spheres float more slowly than angular particles under otherwise identical conditions [15, 37] presumably because the asperities on the angular particles lead to increased film drainage rates and/or rupture.

The kinetics of movement of the three phase line of contact (tplc) are of central importance in many processes, apart from flotation. During the movement of the tplc a dynamic contact angle is established, as discussed in Chapter 5. Irrespective of whether the "surface chemical", "hydrodynamic" or mixed "surface chemical/hydrodynamic" approaches are used, there is as yet no general theory which adequately describes tplc kinetics. One cannot generally calculate ab initio what the spreading velocity of the tplc will be when an air bubble spreads over a mineral surface immersed in water in the presence of a surfactant. Part of the problem at least is due to the fact that poorly characterized experimental systems have been used where any generalization has been obscured by the same time dependent adsorption/desorption/molecular reorientation processes which plague thin film drainage rate studies.

It should be noted that at present only the crudest estimates of t_{film} and t_{tplc} can be made [68]. Hence various experimental methods for determining λ are frequently resorted to. Ye and Miller [38] have recently developed a potentially valuable approach to the calculation of induction times, based essentially on bubble deformation and restoration.

These experimental methods for determining induction times are generally based on either pressing a bubble against a smooth mineral surface or against a bed of particles. The disadvantages of all current methods for determining λ include: (1) insufficient understanding of the process of bubble deformation and energy dissipation during bubble/particle collision; (2) insufficient information concerning the behaviour of the attractive hydrophobic forces during the bubble/particle interaction (e.g. how the thin film of liquid evolves with time, during the time a particle slides or rolls around a bubble; it may well be incorrect to assume that bubble–particle interaction ceases when the particle passes the bubble equator [9, 13]); (3) data on t_{film}, e.g. influence of surfactant type and concentration on thin-film drainage mechanisms and rate; and (4) data on t_{tplc} as a function of hydrophobicity, surface roughness and surfactant type.

The most appropriate method for determining induction times is probably through direct observation of bubble/particle interactions in a flotation cell under well-defined conditions. The necessary theory can then be developed. For the present the Sutherland approach [equation (10)] serves as a useful approximation in determining λ from experimental flotation data of the type normally generated. Such λ values probably contain the information described in (1) to (4) above at least and can be considered as a reflection of attachment efficiency, E_a, for the present.

Kinetic effects certainly have a strong influence on bubble–particle collision and attachment efficiencies. *Once attachment has occurred*, the interplay between particle size and contact angle and the consequent stability of the bubble–particle aggregate in the environment of the flotation cell becomes of paramount importance and is the next subject of this chapter.

Bubble–particle aggregate stability

Flotation limits for coarse particles

The essential problem in understanding bubble–particle aggregate stability is to determine whether or not the adhesive force, acting on the three phase contact line, is large enough to prevent the destruction of the aggregate under the *dynamic* conditions which exist in flotation.

It is important that the reader understands the physics of the problem before moving on to a mathematical description. Let us consider a smooth spherical particle located at a fluid interface. Once the equilibrium wetting perimeter has been established following spreading of the three phase contact line, the static buoyancy of this volume of the particle will act against the gravitational force (Figure 2). The hydrostatic pressure of the liquid column of height Z_0 acts against the capillary pressure. The "other detaching forces" require further discussion — since they

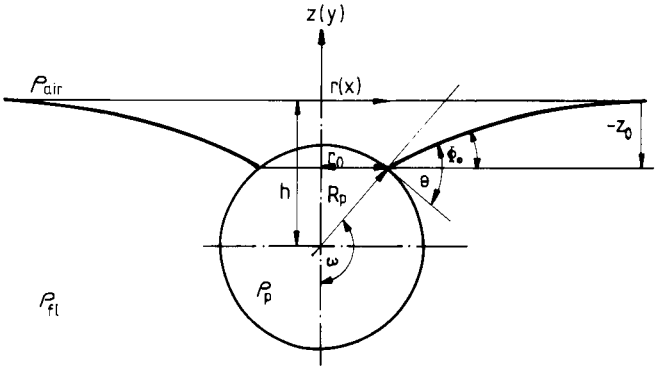

Fig. 2. Location of a smooth spherical particle at a fluid interface (from Schulze [9], with permission).

arise from the particle motion relative to the bubble, velocity dependent drag forces will oppose the detachment of the particle from the bubble. An analysis of these forces is extremely complex and has not been reported to date. Therefore any force balance will necessarily be quasistatic.

The net adhesive force, F_{ad}, is therefore equal to the sum of the attachment forces, F_a, minus the detachment forces, F_d, i.e.:

$$F_{ad} = F_a - F_d$$

An equilibrium position is achieved if F_{ad} is zero. The particle will not remain attached to the bubble if F_{ad} is negative but will report to the liquid phase.

The mathematical description of the various forces which dictate the equilibrium position of particles at liquid–vapour or liquid–liquid interfaces has followed an evolutionary trail. Analogous processes of interest, for example, include pigment "flushing", where a solid particle is induced to transfer from one liquid phase to another by appropriate surface modification with surfactants [39] and the stabilization of emulsion droplets by solid particles [40]. A very simple thermodynamic description of the equilibrium position of a particle at a liquid–liquid interface is given in Chapter 5.

The actual problem of the balance of forces operating on a particle at a liquid–air interface has its historical origins in the work of Wark [41] and Kabanov and Frumkin [42], who considered the case of a gas bubble attached to a plane solid surface of infinite extent and used this as a model for bubble–particle adhesion in flotation. Since this early work there have been notable contributions from Morris [43], Nutt [44], Scheludko [45] and others. It was Princen [46] who proposed the first extensive and generalized treatment of the forces acting on a particle at fluid interfaces. This theory was developed further by Schulze in 1977 [47] and expanded in 1984 [9].

It is now pertinent to consider the case of a spherical particle at liquid–air interface, following the work of Princen [46] and Schulze [9, 47]. The force balance will be used and then linked to the energy balance. We assume that the system is in a quasistatic state and that the contact angle corresponds to that obtained for a static system. In Chapter 5 it was pointed out that the dynamic contact angle can depart significantly from the static value, depending in part on the velocity of the three phase line of contact. If the particle oscillates around its equilibrium position, the tplc would be expected to move to some extent. Hence a full analysis would need to account for the velocity dependent drag forces mentioned above and link these to contact angle dynamics. This is not a tractable problem at present so that a simpler approach is necessary.

Let us suppose that a spherical particle of radius R_p is attached to a bubble of radius R_b where R_b is much greater than R_p, as shown in Figure 2. The forces acting upon the particle are the:

(1) Capillary force, F_c, acting in the vertical direction along the three phase line of contact:

$$F_c = 2\pi r_0 \gamma \sin \Phi_0 = -2\pi R_p \gamma \sin\omega[\sin(\omega + \theta)] \tag{18}$$

where γ is the liquid–vapour surface tension.

(2) Static buoyancy of the fractional volume of the immersed particle, F_b:

$$F_b = \pi R_p^3 \rho_l g[(1 - \cos\omega)^2(2 + \cos\omega)] \tag{19}$$

(3) Hydrostatic pressure, F_h, of the liquid column of height Z_0 on the contact area:

$$F_h = -\pi r_0^2 \rho_l g Z_0 = -\pi R_p^2 (\sin^2\omega)\rho_l g Z_0 \tag{20}$$

(4) Capillary pressure, F_p, in the gas bubble which acts on the contact area πr_0^2:

$$F_p = P_\gamma \pi r_0^2$$

which is given approximately as:

$$F_p \approx \pi R_p^2 \sin^2\omega \left(\frac{2\gamma}{R_b} - 2R_b\rho_l g\right) \tag{21}$$

for a spherical bubble.

(5) Gravitational force, F_g:

$$F_g = \frac{4}{3}\pi R^3 \rho_p g \tag{22}$$

where ρ_p is the particle density.

(6) Extra detaching forces, F_d, which are denoted approximately and generally as the particle mass multiplied by a generalized acceleration b_m in the flotation cell:

$$F_d \approx \frac{4}{3}\pi R^3 \rho_p b_m \tag{23}$$

It is worth remarking that it is bubble–particle aggregates which are actually accelerated in the flotation device, thus ρ_p is in fact an approximation ($\Delta\rho = \rho_p - \rho_{fl}$).

At equilibrium, the sum of these forces, $\sum F$, must equal zero.

Following Schulze [9, 47] it is possible to make these equations dimensionless by noting that $Z_0 = -h - R\cos\omega$ and dividing by $2/3\pi R_p^3 g \rho_{fl} = f$.

The dimensionless force sum $\sum F^*$ is:

$$\sum F^* = 1 + \frac{3h}{2R_p}\sin^2\omega - \cos^3\omega - \frac{3}{a^2 R_p^2}\sin\omega\sin(\omega + \theta)$$

$$- \frac{2\rho_p}{\rho_l} - \frac{2\rho_p b_m}{\rho_l g} - \frac{3b\sin^2\omega}{R_p \rho_l} \tag{24}$$

with the capillary constant $a = \rho_l g/\gamma$ and the bubble-capillary pressure constant $b = \gamma/(R_b g) - R_b \rho_l$.

The Laplace equation describes the shape of the meniscus profile and enables h to be determined by numerical integration. This can be performed with little error for the case where $R_b \gg R_p$ and the numerical solution for unbounded menisci is used. i.e. where the menisci are not bounded by a solid wall or otherwise affected [48, 49].

The energy of detachment, E_{det}, corresponds to the work done in forcing a particle to move from its equilibrium position, $h_{eq}(\omega)$ at the liquid–vapour interface to some critical point, $h_{crit}(\omega)$, where detachment occurs and the particle moves into the liquid phase. The sum of the various forces, $\sum F$, is related to E_{det} by:

$$E_{det} = \int_{h_{eq}(\omega)}^{h_{crit}(\omega)} \sum F \, dh(\omega) \tag{25}$$

Equation (25) may be solved by substituting (24) and carrying out a numerical integration. The procedure is lengthy, and suitable data are tabulated by Schulze [9]. The detachment process takes place when the kinetic energy of the particle equals E_{det}. The kinetic energy of the particle is given by $2/3\pi R_p^3 \rho_p V_t^2$, where V_t is the relative (turbulent) velocity of the particle, acquired due to stresses on the bubble–particle aggregate in the turbulent field of the flotation cell, as the aggregate collides with other bubbles or aggregates or due to other modes of excitation. V_t corresponds to the velocity of gas bubbles in the flotation cell [9, 45].

The maximum floatable particle diameter based on the kinetic theory, $D_{max,K}$, is therefore given as:

$$D_{max,K} = 2\left[\frac{3}{2\pi\rho_p V_t^2}\int_{h_{eq}(\omega)}^{h_{crit}(\omega)}\left\{\frac{2}{3}\pi_p^3\rho_{fl}g \times\left(1 - \frac{2\rho_p}{\rho_{fl}} - \cos^3\omega + \frac{3h}{2R_p}\sin^2\omega - \frac{3}{a^2R_p^2}\sin\omega\sin(\omega+\theta)\right)\right.\right.$$
$$\left.\left. -\pi(R_p\sin\omega)^2\left(\frac{2\gamma}{R_b} - 2R_B\rho_{fl}g\right)\right\}dh\right]^{1/3} \tag{26}$$

Equation (26) may also be solved by numerical integration or by plotting each of the kinetic and detachment energies as a function of R_p at constant γ and ρ_p and specified V_t. In the absence of kinetic effects which exist under normal turbulent flotation conditions, the maximum particle size which can be floated is essentially due to a balance of capillary and gravitational forces. For spherical particles between approximately 300 to 500 μm and bubbles of about 1×10^{-3} m in diameter hydrostatic and capillary pressure terms may be neglected [9] and the maximum size of particles which can be floated is given by:

$$D_{\max,G} = 2 - \frac{3}{2}\left[\frac{\gamma \sin\omega^* \sin\{\omega^* + \theta\}}{\Delta\rho g}\right] \tag{27}$$

where the subscript G signifies gravitational limit, $\omega^* = 180° - 1/2\theta$ for $\theta < 90°$ and refers to the location of the particle at the water–vapour interface, $\Delta\rho$ is the density difference between the particle and fluid, and g is the gravitational constant.

Scheludko et al. [45] derived an equivalent expression for spheres located at a water–vapour interface, assuming the volume of contact above the wetting perimeter was small in comparison with the total volume of the sphere (for $\theta \leq 40°$):

$$D_{\max,G} = 2\left(\frac{3\gamma}{2\Delta\rho g}\right)^{1/2} \sin\frac{\theta}{2} \tag{28}$$

Huh and Mason [50] have presented a more general analysis of the Scheludko result. Whilst these equations are instructive, they cannot reasonably be expected to describe the dependence of particle size on contact angle which occurs under the turbulent conditions in a flotation cell. Rather they correspond to the conditions experienced when a captive bubble, constrained at the end of a capillary, is gently brought to bear against a given particle. Under such quiescent conditions, the bubble may or may not lift the particle, depending on whether or not the conditions in equations (27) and (28) are satisfied.

Flotation limits for fine particles

The only theoretical study to date dealing with the limit of floatability of fine particles was proposed by Scheludko et al. [45]. The limit is the critical work of expansion required to initiate a primary hole or three phase contact line, a requirement which is met by the kinetic energy of the particles. The matching of these two quantities enables a minimum particle diameter, $D_{\min,K}$ for flotation to be obtained:

$$D_{\min,K} = 2\left[\frac{3\kappa^2}{V_t^2 \Delta\rho\gamma\{1 - \cos\theta\}}\right]^{1/3} \tag{29}$$

where κ is the line tension, opposing expansion of the three phase contact. It was Gibbs [51] who first identified the importance of line tension, using as example the line of intersection of the three surfaces of discontinuity which exist when two gas bubbles adhere together. Molecules which are present in a line have a free energy which is different from those at a surface — in fact there is an excess linear free energy and a linear tension in an analogous fashion to that of excess surface free energy and surface tension.

In fact, as shown by Pethica [52]:

$$\kappa = \left(\frac{\partial F}{\partial L}\right)_{T,V,W} \tag{30}$$

where F is the Helmholtz free energy, L is the contact line, and W is the thermodynamic work. The Young-Dupre equation becomes:

$$\gamma_{S/V} - \gamma_{S/L} = \gamma_{L/V} \cos\theta \pm \frac{\kappa}{r} \tag{31}$$

The line tension is important only for small contact radii [52, 53] and can oppose or reinforce $\gamma_{L/V} \cos\theta$. It counteracts the formation of the three phase contact line in Scheludko's theory, the latter neglecting thin film drainage and other hydrodynamic effects.

Experimental verification of flotation limits

The forces which operate on a sphere as it is pulled out of a liquid have been determined by Schulze [47] and are in good agreement with theoretical predictions.

Attempts to relate theoretical and practical flotation limits have by and large led to only broad qualitative agreement [54]. Certainly no successful studies have been reported where particle size and contact angle have been systematically varied until the recent work of Crawford and Ralston [5]. Previous attempts to link particle size and contact angle have been unsuccessful because where water soluble collectors are present, bubble size, electrical double layer properties, surface tension, the kinetic aspects of collector adsorption and other variables may vary which has made it a very difficult task to develop firm experimental data with which to compare theoretical predictions.

In order to circumvent these difficulties, a model system of angular quartz particles was therefore developed whose surfaces were tailored to varying, but *known* surface coverages by a methylation reaction using trimethylchlorosilane [55], following earlier work by Laskowski and Kitchener [70]. Trimethylsilyl groups are firmly attached to the quartz surface and do not desorb, neither are the electrical double layer or Van der Waals forces detectably influenced by the ultra-thin trimethylsilyl adsorption layer. Advancing water contact angles measured on these particles by both dynamic and equilibrium techniques are in good agreement with angles measured on similarly treated quartz plates as well as with Cassie equation predictions [56, 57].

The results of batchwise flotation experiments conducted with these particles in a Hallimond tube, in the absence of frother, under conditions of known bubble size, bubble density, pulp density, pH and ionic strength are shown in Figures 3 and 4.

The major features are:

(a) There is a critical advancing water contact for each particle below which flotation does not occur under the prevailing experimental conditions (Figure 3).

(b) For the fine (e.g. 15 μm) particles, flotation recovery increases only weakly at contact angles above the threshold value and does not plateau, in marked contrast to the intermediate and coarse particles (Figure 3c).

(c) A flotation domain is clearly evident, within which flotation occurs, outside of which there is no flotation. Both coarse and fine particles require a larger advancing water contact angle to float than do the intermediate particles (Figure 4a).

(d) There is a particular particle size (circa 38 μm) at which a minimum advancing water contact angle is required to initiate flotation under the experimental conditions examined (Figure 4a).

The experimental results obtained from the study by Crawford and Ralston [5] are shown in Figure 4 and are plotted on two scales for comparison purposes. The dependence of $D_{max,G}$ on θ obtained from equation (27) predicts the flotation of much larger particles, for a given θ, than is observed experimentally.

The dependence of $D_{max,K}$ on θ from equation (26) is shown for $V_t = 20 \times 10^{-2}$ ms^{-1} and 30×10^{-2} ms^{-1}, corresponding to the predominant range of bubble sizes and velocities observed. ρ_p was taken as 2,600 kgm m^{-3} and γ was measured as 72.0×10^{-3} N m^{-1}. For the experimental system, the measured advancing water

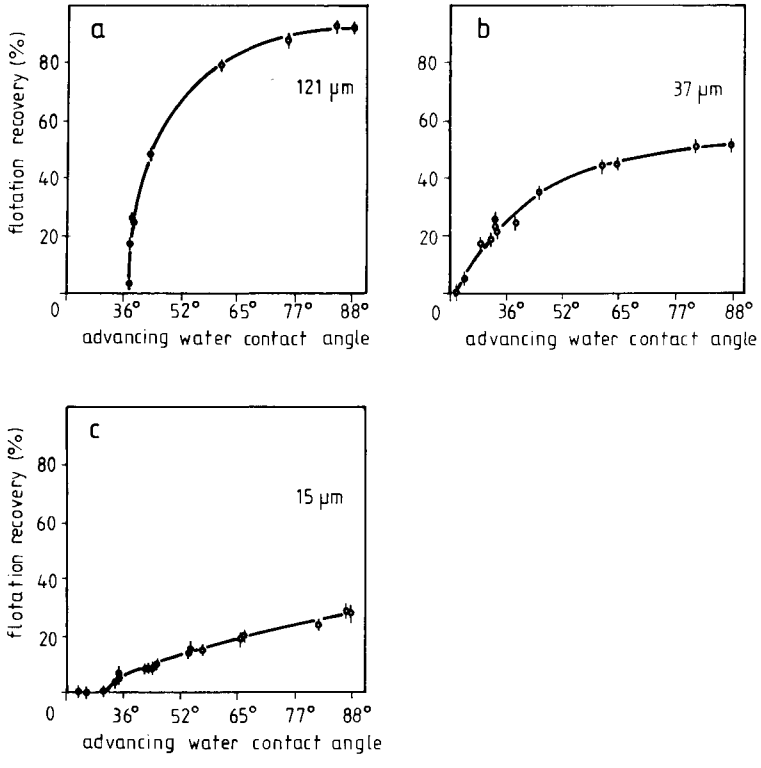

Fig. 3. Flotation recovery as a function of advancing water-contact angle for 121 μm, 37 μm and 15 μm methylated quartz particles; pH = 5.6, $I = 10^{-3}$ M KNO_3. These three curves show critical contact angles below which flotation does *not* occur under the particular experimental conditions (from Crawford and Ralston [5], with permission).

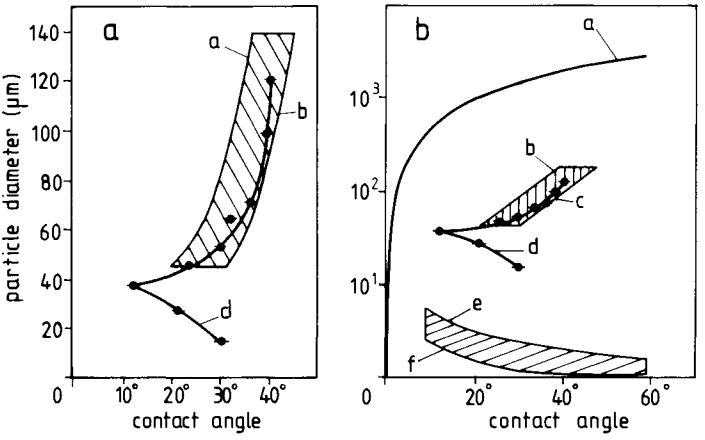

Fig. 4. Experimental threshold values (mean particle size and advancing water contact angle) showing flotation domain compared with theoretical predictions. Vertical scale is altered in (a) and (b) for comparison purposes; pH = 5.6, $I = 10^{-3}$ M KNO_3. (a) Line *a* corresponds to equation (26) with $V_t = 20 \times 10^{-2}$ m s^{-1}; line *b* to $V_t = 30 \times 10^{-2}$ m s^{-1}. (b) Line *a* corresponds to static conditions [$D_{max,G}$, equation (27)]; lines *b*, *c* to equation (26) with $V_t = 20$, respectively 30×10^{-2} m s^{-1}; line *d*, with symbols, refers to experimental data; line *e* to equation (29) with $\kappa = 5.6 \times 10^{-10}$ N, $V_t = 20 \times 10^{-2}$ m s^{-1}; line *f* to equation (29) with $\kappa = 2.8 \times 10^{-10}$ N, $V_t = 30 \times 10^{-2}$ m s^{-1}. V_t is bubble velocity, κ is line tension (see text). From Crawford and Ralston [5], with permission.

contact angle has been used; clearly the liquid advances as the particle is ejected from the water/air interface. For particles between 45 and 125 μm in diameter there is reasonably good agreement between the experimental results and those predicted from equation (26). Within the accuracy of the experiment, the flotation response of methylated, angular quartz particles, whose advancing water contact angles have been measured independently, agrees with that predicted by Schulze for smooth spheres. Microscopic events associated with surface roughness and particle shape (e.g. [50, 58]) are evidently of insufficient magnitude to detectably influence the $D_{max,K}$- versus $-\theta$ threshold behaviour under turbulent flotation conditions.

These results indicate that the flotation behaviour of coarse, angular quartz particles, typical of those encountered in flotation pulps, can be predicted reasonably well by equation (26), despite its inherent approximations.

The variation of $D_{min,K}$ as a function of θ is given through equation (29). The value and importance of the line tension κ is very uncertain. Experimental data are both scarce and of doubtful reliability, so that calculations involving line tension are hazardous. Using the extreme κ values of 2.8 and 5.6×10^{-10} N determined by Scheludko et al. [45], values of $D_{min,K}$ were computed with V_T at 20 and 30×10^{-2} m s^{-1}. The density difference $\Delta\rho$ was taken as 1600 kg m^{-3} and γ was measured as 72.0×10^{-3} N m^{-1}. Receding water contact angles (the liquid front recedes as the three-phase contact expands) determined from the Cassie equation were

used in this calculation, because receding angles could not be measured on the methylated particles using the dynamic contact angle technique [56]. Nevertheless the good agreement between measured advancing angles on similarly treated plates and particles and those predicted by the Cassie equation suggests that this is a reasonable approximation. The results of these calculations are shown in Figure 4.

There is a qualitative agreement between the predictions of equation (29) and the experimental data, i.e. for a smaller particle with less kinetic energy, a larger contact angle is required for it to float. For the experimental data and theory to be reconciled, however, the value of κ would need to be at least an order of magnitude larger than those determined to date. κ should also depend on contact angle as well as on the geometry of the three-phase contact line [9, 60]. A much clearer interpretation of κ is required before it can be used in calculations with any confidence. The evidence to date indicates that the concept of line tension, in its present form, is inapplicable to flotation studies.

It is significant to note that the kinetic theories of flotation limits for coarse and fine particles together predict both the existence of a flotation domain and a minimum contact angle, optimum particle size for flotation under specified conditions, i.e. the interaction of the $D_{\max,K}$ and $D_{\min,K}$ curves. It is clearly evident in figure 6 of the paper by Scheludko et al. [45] as well as in figures 5–12 of the monograph by Schulze [9]. Both features have been observed in the study by Crawford and Ralston [5], as is clearly evident in Figure 4. The precise reasons for the changeover in mechanism from coarse- to fine-particle behaviour remain obscure. It is probable that for the finer particles the hydrodynamic resistance of the thin liquid film between the particle and bubble and/or some sluggishness in the rate of formation of the wetting perimeter may well contribute to the divergence between theoretical predictions and the results of the experimental investigation.

In this chapter we have thus far identified the importance of the collision, attachment and stability efficiencies. Particular attention has been paid to the stability of the bubble–coarse particle aggregate, *once formed*, as well as to the flotation limits of fine particles. It is now pertinent to recall our earlier kinetic analysis in order to see how rate constant depends on particle size and contact angle.

Kinetics revisited

Theoretical studies of rate constant and its dependence on particle size [14, 16] often suggest that:

$$k \propto d_p^n$$

where d_p is the particle diameter and $1.5 < n < 2$, whereas the earlier work of Sutherland [10] predicts $n = 1$ as is recalled in equation (10). Some flotation experiments performed with spherical particles [61] support a value for n falling between 1.5 and 2, whereas for oil droplets values are reported as unity [62], 1.2

and 1.8 [64]. On the other hand, the data from a large number of batch flotation tests indicates that n is unity [2]. It is well known that the mechanism of bubble/particle attachment differs markedly for angular particles compared with smooth spheres [15, 37], as does the coalescence of oil droplets dispersed in water in the presence and absence of solid crystals at the oil/water interface [65]. These different attachment mechanisms may well account for the various sets of n values.

In the study by Crawford and Ralston [5], the dependence of $\log k_f$ versus $\log d_p$ for three different particle sizes at advancing water contact angles from 50° to 88° is shown in Figure 5. This type of plot is commonly used in the literature in order to extract a value of n. There are deficiencies apparent in this method however. Within experimental error, $n = 1.0 \pm 0.1$ over the range of θ, and particle sizes examined in Figure 5. Although smaller particle sizes were not dealt with, evidence to date suggests that this trend will persist down to particles smaller than one micron in diameter [62, 64]. At some point of course (<1 μm or so), a diffusion rather than a collision mechanism might be anticipated to control bubble/"particle" collection. The behaviour of the angular, hydrophobized quartz particles used is in agreement with the results of batch flotation studies performed with particles produced by crushing and grinding rather than with smooth spheres. A value of unity for n is consistent with Sutherland's model [10]; however, the Crawford and Ralston data [5]

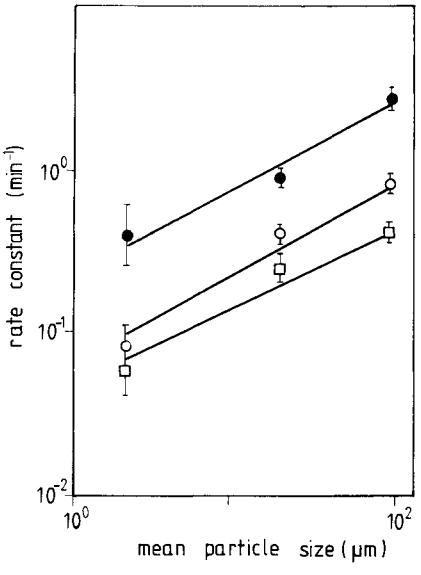

Fig. 5. Log_{10} (fast rate constant) as a function of $\log_{10}$ (particle diameter) at various advancing water contact angles; pH = 5.6, $I = 10^{-3}$ M KNO_3. ● = 88°, $n = 1.0 \pm 0.2$; ○ = 60°, $n = 1.1 \pm 0.1$; □ = 50°, $n = 1.0 \pm 0.1$. (N.B.: 88° predicted from Cassie equation; see Crawford et al. [56].) From Crawford and Ralston [5], with permission.

are not sufficiently accurate to reveal the possible influence of λ on the rate constant in the exponential term in equation (10). Assuming for the present argument that this equation is valid, with all variables such as R_b, V_t, etc. constant, the first order rate constant k = constant $R_p f(\lambda)$; thus $\log k = \log k' + \log[R_p f(\lambda)]$, where k' is a constant. For the dependence of k on R_p to be strictly linear in Figure 5, $f(\lambda)$ would need to be constant at a given contact angle. λ mirrors attachment efficiency, and since it is well known that the attachment efficiency of spheres and angular particles is different, the reported variations in "n" values probably reflect differences in the dependence of λ with particle size for spheres and angular particles. Thus, when experimental k values are plotted against R_p it is really $R_p f(\lambda)$ in equation (10) which should be the variable, not R_p alone.

Applications and summary

The existence of a flotation domain is of practical significance (Figure 4). Assume that value particles of, say, about 1 to 100 μm diameter produced from the milling circuit are presented to the flotation cells. At the "starvation" collector additions which are typical of operating conditions in many flotation concentrators, the value particles should all adsorb the same collector concentrations *per unit area* and possess the same contact angle (disproportionate collector consumption per unit area with varying particle size is not considered here and is *not* observed in gas adsorption studies). This could correspond to a contact angle of 25° in Figure 4. At constant collector addition, with all other variables constant, particles within the flotation domain possessing contact angles equal to or less than 25° will float, whilst coarser and finer particles will consume collector and will not float. Split conditioning and the separate treatment of fine, medium, and coarse particles are therefore desirable practices. A cautionary note at this juncture is necessary. The flotation domain in Figure 4 is not a universal one. It will alter as the turbulent conditions change [equation (26), V_t] and as the particle density alters [equation (26), ρ_p] as well as with d_p and θ. Each system will possess its own unique domain. Importantly, if the turbulence in the flotation cells is increased, the recovery of coarser particles may decrease sharply. Curve *b* or *c* in Figure 4b will shift to the right.

Fine particles will probably be recovered more efficiently under conditions where contact time is maximized and relatively low V_t is encountered, as occurs in column flotation. Coarse particle recovery is also favoured by a low V_t. It remains to be proven whether or not high degrees of turbulence actually enhance the attachment efficiency of fine particles (e.g. by reducing t_{film} or t_{tplc}) or if the observed increased recoveries are due to particle/particle coagulation and a consequent increased collision efficiency of the coarser aggregates.

The overall collection process in mineral flotation can only be properly described when the collision, attachment and stability efficiencies are understood. It is a futile exercise to assume that one or other efficiency is important to the exclusion of the

others, a mistake all too commonly made in the literature.

In this chapter the important relationship between particle size and contact angle in mineral flotation has been developed through a study of the underlying colloid science. The picture is far from complete and we are still a long way from the *ab initio* calculation (or estimation) of rate constants for either laboratory or plant studies. Perhaps the reader will be stimulated to probe further.

References

1 A.M. Gaudin, J.O. Groh and H.B. Henderson, Am. Inst. Min. Metall. Eng., Tech. Publ. No. 414, 1931.
2 W.J. Trahar, Int. J. Miner. Process., 8 (1981): 289.
3 D.F. Kelsall, P.S.B. Stewart and W.J. Trahar, Symp. Opt. Control Miner. Process. Plants, Brisbane, Australia, 53, July 1974.
4 S.R. Grano, J. Ralston and N.W. Johnson, Miner. Eng., 1 (1988): 137.
5 R. Crawford and J. Ralston, Int. J. Miner. Process., 23 (1988): 1.
6 B.V. Derjaguin and S.S. Dukhin, Bull. Inst. Min. Metall., 70 (1961): 221.
7 G.L. Collins and G.J. Jameson, Chem. Eng. Sci., 31 (1976): 985.
8 A.J. Lynch, N.W. Johnson, E.V. Manlapig and C.G. Thorne, Mineral and Coal Flotation Circuits, Their Simulation and Control, Elsevier, Amsterdam, 1982.
9 H.J. Schulze, Physicochemical Elementary Processes in Flotation, Elsevier, Amsterdam, 1984.
10 K.L. Sutherland, J. Phys. Chem., 52 (1948): 394.
11 K.L. Sutherland and I.W. Wark, Principles of Flotation, Aus. IMM, Melbourne, 1955.
12 G.S. Dobby and J.A. Finch, J. Colloid Interface Sci., 109 (1986): 493.
13 G.S. Dobby and J.A. Finch, Int. J. Miner. Process., 21 (1986): 241.
14 D. Reay and G.A. Ratcliff, Can. J. Chem. Eng., 51 (1973): 178.
15 J.F. Anfruns and J.A. Kitchener, Trans IMM Sect. C, 86 (1977): C9.
16 L.R. Flint and W.J. Howarth, Chem. Eng. Sci., 26 (1971): 1155.
17 R.J. Hunter, Zeta Potential in Colloid Science, Academic Press, London, 1981.
18 G.J. Lyman, M.E. Thesis, McGill University, Montreal, 1974.
19 B.V. Derjaguin and M. Kussakov, Acta Physicochim., 10 (1939): 25.
20 B.V. Derjaguin and A.S. Titievskaya, Proc. 2nd Int. Congr. on Surface Activity, 1 (1957): 536.
21 A. Scheludko and D. Exerowa, Kolloid Z., 168 (1960): 24.
22. D.B. Hough and L.R. White, Adv. Colloid Interface Sci., 14 (1980): 3.
23 R. Buscall and R.H. Ottewill, Colloid Science, Vol. 2, A Specialist Periodical Report, The Chemical Society, London, 1975, Chapter 6.
24 R. Aveyard and B. Vincent, Progress in Surface Science, 8 (1977): 59.
25 J. Ralston, Adv. Colloid Interface Sci., 19 (1983): 1.
26 H. Sonntag and K. Strenge, Coagulation and Stability of Disperse Systems, Halsted Press, New York, N.Y., 1972.
27 R.J. Hunter, Foundations of Colloid Science, Volume 2, Oxford University Press, Oxford, U.K., 1989.
28 O. Reynolds, Phil. Trans. R. Soc., 177 (1886): 157.
29 A. Scheludko and D. Platikanov, Kolloid Z., 175 (1961): 150.
30 D.Y.C. Chan and R.G. Horn, J. Chem. Phys., 83 (1985): 5311.
31 A. Scheludko, Kolloid Z., 155 (1957): 39.
32 P.S. Prokorov, Disc. Faraday Soc., 18 (1957): 41.

33 S. Frankel and K. Mysels, J. Phys. Chem., 66 (1962): 190.
34 S.D. Hartland and J.D. Robinson, J. Colloid Interface Sci., 60 (1977): 72.
35 D. Platikanov., J. Phys. Chem., 68 (1964): 3619.
36 R. O'Brien, pers. commun., University of New South Wales, 1988.
37 P. Blake and J. Ralston, Colloid. Surf., 16 (1985): 41.
38 Y. Ye and J.D. Miller, Coal Prep., 5 (1987): 1.
39 G.D. Parfitt, Dispersions of Powders in Liquids, 3rd edition, Applied Science, Essex, U.K., 1981.
40 P. Becher (Editor), Encyclopedia of Emulsion Technology, Vol. 1, Basic Theory, Marcel Dekker, New York, N.Y.., 1983.
41 I.W. Wark, J. Phys. Chem., 37 (1933): 623.
42 B. Kabanov and A. Frumkin, Z. Phys. Chim., A165 (1933): 433.
43 T.M. Morris, Am. Inst. Metallurg. Eng. Trans., 187 (1950): 91.
44 C.W. Nutt, Chem. Eng. Sci., 12 (1960): 133.
45 A. Scheludko, B. Tosev and B. Bogadiev, J. Chem. Soc. Trans. Faraday 1, 72 (1976): 2815.
46 A. Princen, in: E. Matijevic (Editor), Surface and Colloid Science, Volume 2, John Wiley, New York, N.Y., 1969, Chapter 2.
47 H. J. Schulze, Int. J. Miner. Process., 4 (1977): 241.
48 C. Huh and L. E. Scriven, J. Colloid Interface Sci., 30 (1969): 323.
49 J.F. Padday, Phil. Trans. R. Soc., London, 275 (1973): 489.
50 C. Huh and S. G. Mason, J. Colloid Interface Sci., 47 (1974): 271.
51 J.W. Gibbs, The Collected Works, Longmans, Green, New York, N.Y., 1928.
52 B.A. Pethica, J. Colloid Interface Sci., 62 (1977): 567.
53 J.E. Lane, J. Colloid Interface Sci., 52 (1975): 155.
54 J.A. Finch and C.W. Smith, Miner. Sci. Eng., II (1979): 36.
55 P. Blake and J. Ralston, Colloid. Surf., 15 (1985): 101.
56 R. Crawford, L. Koopal and J. Ralston, Colloid. Surf., 27 (1987): 57.
57 D. Diggins, L.G.J. Fokkink and J. Ralston, Colloid. Surf., 44 (1990): 299.
58 J.F. Oliver, C. Huh and S.G. Mason, J. Adhes., 8 (1977): 223.
59 J.A. Mingins and A. Scheludko, J. Chem. Soc. Faraday Trans. 1, 75 (1979): 1.
60 L.R. White, pers. commun., University of Melbourne, 1986.
61 D. Reay and G.A. Ratcliff, Can. J. Chem. Eng., 53 (1975): 479.
62 A. Larson, P. Stenius and L. Odberg, Sven. Papperstid., 18 (1984): R165.
63 N.D. Sylvester and J.J. Byeseda, Soc. Pet. Eng. J., 20 (1980): 579.
64 A. Larsson, P. Stenius and L. Odberg, Sven. Papperstid., 18 (1984): R158.
65 P. Walstra, in: P. Becher (Editor), Encyclopedia of Emulsion Technology, Volume 1, Basic Theory, Marcel Dekker, New York, N.Y., 1983, Chapter 2.
66 S.J. Gregg and K.S.W. Sing, Adsorption, Surface Area and Porosity, 2nd edition, Academic Press, London, 1982.
67 N. Ahmed and G.J. Jameson, in: J.S. Laskowski (Editor), Frothing in Flotation, Gordon and Breach, Glasgow, 1989, Chapter 4.
68 H.J. Schulze, in: J.S. Laskowski (Editor), Frothing in Flotation, Gordon and Breach, Glasgow, 1989, Chapter 3.
69 I.B. Ivanov (Editor), Thin Liquid Films: Fundamentals and Applications, Marcel Dekker, New York, N.Y., 1988.
70 J.S. Laskowski and J.A. Kitchener, J. Colloid Interface Sci., 29 (1969): 670.

Chapter 7

An introduction: physicochemical methods of separation

JANUSZ S. LASKOWSKI

Introduction

Mineral processing has traditionally been defined as the art of extracting the useful mineral constituents from ores, in the form of concentrates, without changing the identity of the minerals. Today, however, this traditional definition must be treated with some flexibility as decreasing particle sizes and consequently increasing difficulties with selective separation call for a kind of "activation" which in some cases may quite profoundly change the treated mineral. In such cases the activation is only a pretreatment stage which is always followed by physical separation.

Ore deposits are heterogeneous mixtures of solidified phases with some disseminated valuable minerals. Since *mineral processing separation methods* are based on differences in physical properties of mineral grains, such as density, magnetic susceptibility, electrical conductivity, etc., sufficient *liberation* is the prerequisite to selective separation. Fine dissemination of valuable constituents in the ores of progressively lower content of "valuables" requires very fine grinding. This leads to very fine sizes of the mineral particles in the feeds to the mineral processing plants. Both, the fine size of the valuable mineral constituents which are to be separated, as well as the high content of gangue slimes that interfere with the separation processes, present difficult problems in the mineral processing circuits.

Three classes of mineral fines can be distinguished in mineral processing operations [1]:

(A) Naturally-occurring clay minerals, such as kaolinite, illite, montmorillonite, which are intrinsically composed of very small particles (mainly below 2 μm).

(B) The fines produced during the crushing and grinding of ores in mineral beneficiation operations.

(C) The residues of the leaching of crushed ores in hydrometallurgical processes. Such slimes consist partly of insoluble mineral particles and partly of precipitates (products of chemical reactions).

In the past, the mineral industry has not been too seriously hindered by the awkward colloidal minerals. Where water and space were readily available, slimes were

simply dumped in settling lagoons and lower recoveries could still be profitable. Falling grades of ore bodies bring, however, new technological problems and make the wastage of values in slimes less justifiable. New more stringent environmental regulations make easy-going solutions, which do not protect streams, land nor air from pollution, less acceptable throughout the world.

The history of development in the area of mineral processing is the history of dealing with decreasing sizes of mineral particles. All important breakthroughs involved decreasing the size limits of the handled particles.

Since the size of particles currently processed is rapidly approaching colloidal range, mineral processing is becoming more and more an *applied colloid chemistry*. The simple examples below illustrate this point.

Since the bulk properties such as density (or magnetic susceptibility) are proportional to volume, and the surface effects are proportional to surface area, the ratio of the surface forces to the bulk forces for spheres can be said to be proportional to $6d^{-1}$, where d is the diameter of the sphere. As d decreases, this ratio increases, and at a given size, the surface effects predominate over bulk effects. For such fine particle systems (suspension), the characteristics of the suspension, such as aggregation stability and the resulting settling rate, rheology, etc., depend no longer on the particle bulk properties, but on the particle surface properties.

A decrease in size sharply increases the number of particles per volume. For example, in the case of 1 cm cubes, there will be one particle per cubic centimeter. If the size of cube is made finer under the assumption that the distance between the cubes in the suspension is equal to their size, there will be 25^2 cubes in cubic centimeter of the suspension if their size is 1 mm. For the cubes 1 μm in size, their number in the unit volume of the suspension will increase to 25^5. Such an increasing number of particles accompanied by a sudden decrease in gravity and other bulk forces that act on particles, make all the separation processes radically different.

It is, therefore, obvious that the effectiveness of conventional mineral beneficiation techniques becomes unacceptably low for the separation of values from the fines obtained by excessive comminution of ores. Hence, if the increasing mineral demand is to be met, techniques that enable the recovery of valuable minerals from finely comminuted ores are urgently needed. This can be achieved either by modifying the established processes, so that they can cope with wider size distribution in the feed, or by developing new processes. To place these new emerging processes in their proper perspective, it seems important to classify them according to the principles common to the methods.

General classification of separation methods

The grounds for the separation of particles are differences in the properties of various minerals such as density, magnetic susceptibility, electrical conductivity, dif-

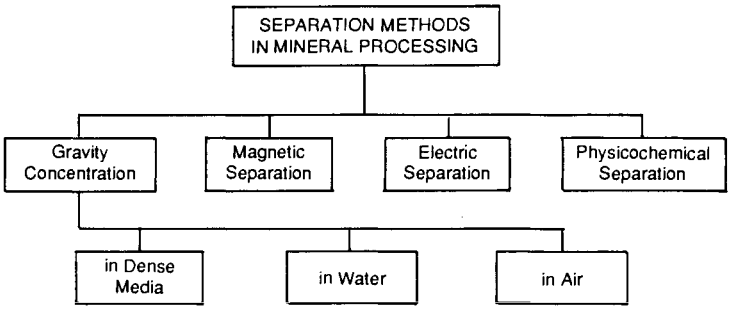

Fig. 1. Classification of mineral processing separation methods.

ferences in friction, radioactivity or colour, and surface properties. Generalization of the basic phenomena involved in mineral separation techniques leads to classification as shown in Figure 1.

Most numerous are the *gravity concentration methods*. These are very effective in dealing with coarse particles (with sizes that fall in the range 10^3–10^5 μm). The size of particles that can be separated with magnetic and electric methods fall in the range of 10^2–10^3 μm. With *flotation methods* (which are classified here as a part of physicochemical methods), the size of mineral grains separated are usually in the range of 10^1–10^2 μm. Another group of physicochemical separation methods, the *colloidal methods*, can practically deal with all very fine particles even as fine as much below 1 μm.

Physicochemical separation methods

Figure 2 shows the classification of the physicochemical separation methods [2]. The classification has been adapted to mineral systems and ignores entirely such processes as ion and precipitate flotation [3, 4], which are of much more interest for chemical and hydrometallurgical rather than mineral processing purposes.

The main subdivision categorizes the physicochemical methods of separation into *flotation* and *colloidal methods*. Both are based on differences in the surface properties of the minerals separated, but, in the case of flotation, the dispersed air is blown in the form of fine bubbles which "pick up" the hydrophobic mineral particles and carry them up to the froth layer with the hydrophilic particles left behind in the pulp. In the colloidal methods, separation can be achieved by *selective aggregation* (coagulation, flocculation, agglomeration) of one of the mineral species into aggregates while leaving the other minerals in a dispersed state. The aggregates can then be separated from the dispersed material by sedimentation, sieving, or other suitable techniques.

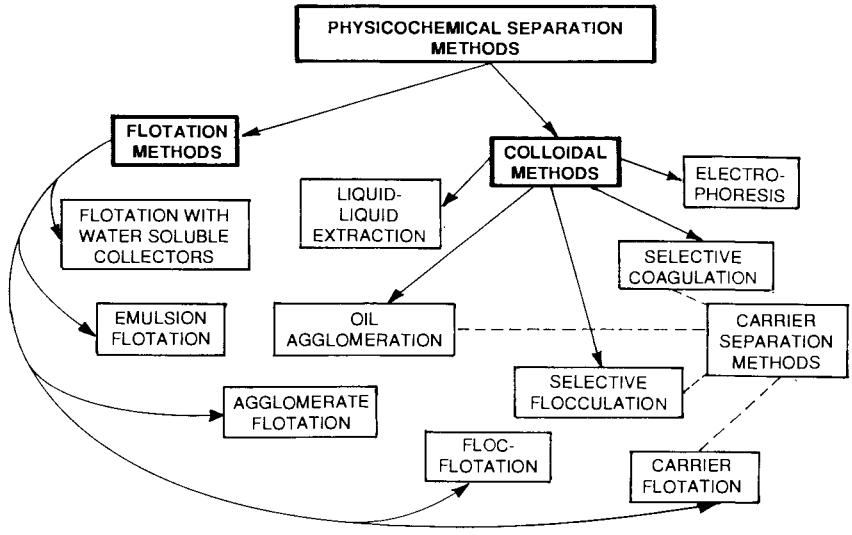

Fig. 2. Physicochemical separation methods.

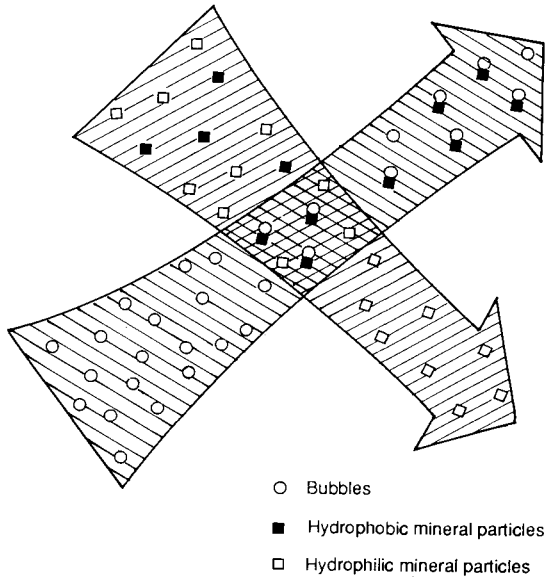

Fig. 3. Separation of hydrophobic from hydrophilic particles in flotation.

Flotation

Froth flotation, as the process is referred to, is a kind of a carrier process in which air bubbles function as the carrier (Figure 3). Since the bubbles can only differentiate between hydrophobic and hydrophilic particles, the selectivity of separation

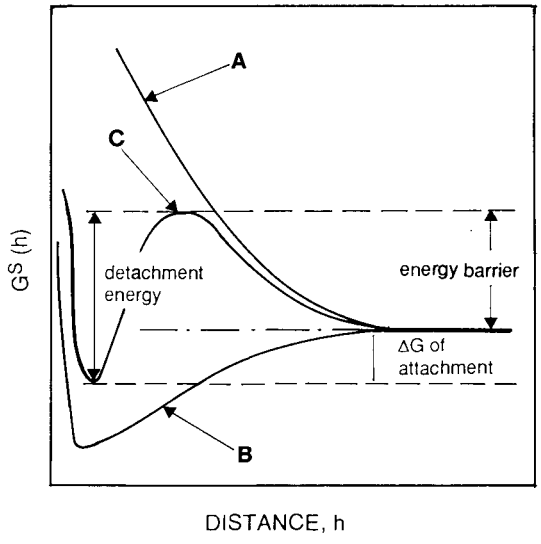

Fig. 4. Schematic energy versus distance profiles for wetting films on solids.

critically depends on differences in the *wettability* between the separated mineral particles.

In a flotation process, mineral particles collide with bubbles. The particles are classified as *floatable* if they attach to air bubbles and are lifted by them to a froth layer.

Figure 4 shows the solid particle and bubble before and after attachment. A classical condition for particle/bubble contact to be possible (on a unit-area basis; temperature, pressure and chemical composition all constant) is that the free energy change (ΔG) during the attachment process (as shown in Figure 4) is negative.

$$\Delta G = G_2 - G_1 = G_2^s - G_1^s = \gamma_{SV} - \gamma_{SL} - \gamma_{LV} < 0 \tag{1}$$

where G_1 and G_2 are Gibbs free energies of the system before the attachment (state 1) and after the attachment (state 2), respectively. G_1^s and G_2^s are corresponding surface free energies which may be equated to G_1 and G_2, respectively, as only the surface portion of the free energy of the system changes during this process; γ_{SV}, γ_{SL} and γ_{LV} are the solid/vapour, solid/liquid and liquid/vapour interfacial tensions, respectively.

By introducing Young's equation, equation (1) can be converted to a more useful form:

$$\Delta G = \gamma_{LV}(\cos\theta - 1) \tag{2}$$

where θ denotes contact angle. Obviously $\Delta G = 0$ for $\theta = 0°$ and $\Delta G < 0$ for $\theta > 0°$.

This well known equation (2) has been called the *thermodynamic criterion of flotation*. Its only strict interpretation is as follows: the more negative the value of ΔG, the greater is the probability of particle dewetting [5, 6].

The attachment process depicted in Figure 4 entirely neglects collision probability and the intermediate attachment stages which involve thinning and rupture of the disjoining film separating a particle and a bubble; this film must rupture during a short time of contact if the collision is to lead to the particle-to-bubble attachment. Since this process does not directly depend on particle wettability, equation (2) is not related to the rate of the process (as, by the way, all thermodynamic formulae). For the flotation to be possible, the contact angle θ must be larger than zero; for the high rate of flotation favourable hydrodynamic and kinetic conditions must exist as well [5–7].

As shown in equation (2), wettability expressed by the value of the contact angle is an important mineral surface property for flotation. Some minerals exhibit high *native floatability*, which simply means that they are floatable even without flotation reagents. Other minerals, which by nature are *hydrophilic*, can be rendered *hydrophobic* with the use of *flotation reagents*, namely flotation collectors.

The fundamental for flotation terms "*hydrophobicity*" and "*hydrophilicity*" will be discussed in the section below following Laskowski and Kitchener's [8] line of reasoning. The classical boundary condition for the hydrophilic–hydrophobic transition is equality of W_A, the work of adhesion of liquid to solid, and W_C, the work of cohesion of the liquid:

$$W_A = \gamma_{SV} + \gamma_{LV} - \gamma_{SL} \tag{3}$$

$$W_C = 2\gamma_{LV} \tag{4}$$

By introducing Young's equation, equation (3) can be converted to:

$$W_A = \gamma_{LV}(1 + \cos\theta) \tag{5}$$

Then:

$$\frac{W_A}{W_C} = \frac{\gamma_{LV}(1 + \cos\theta)}{2\gamma_{LV}} \tag{6}$$

which gives:

$$\cos\theta = 2\frac{W_A}{W_C} - 1 \tag{7}$$

The condition of hydrophobicity follows from equation (7): only for $W_A < W_C$, $\theta \neq 0$.

Figure 5 depicts a sessile liquid droplet resting on a flat solid surface; the values of the work of cohesion of the liquid, and the work of adhesion of the liquid to the solid determine the contact angle at the solid/liqiud/gas interface.

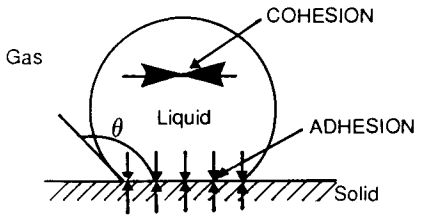

Fig. 5. Illustration of the effect of the work of cohesion of liquid and the work of adhension of liquid to solid on the solid wettability.

According to Fowkes [9] there are three main contributions to the work of adhesion of water to solid:

$$W_A = W_A^d + W_A^h + W_A^e \tag{8}$$

where W_A^d is the contribution from dispersion forces, W_A^h is the contribution from the hydrogen bonding of water to solid surface groups (hydroxyl and similar), and W_A^e is the contribution from the electrical charge at the interface.

According to Fowkes [10] W_A^d can be calculated from:

$$W_A^d = 2\left(\gamma_{H_2O}^d \cdot \gamma_s^d\right)^{1/2} \tag{9}$$

where $\gamma_{H^2O}^d \approx 22$ erg cm^{-2}.

Laskowski and Kitchener [8] indicated that for no substance (except fluorocarbons) is W_A^d as large as the exceptionally high work of cohesion of water ($W_C = 145$ erg cm^{-2}). Therefore because:

$$\cos\theta = 2\left\{\frac{(W_A^d + W_A^h + W_A^{e)}}{W_C}\right\} - 1 \tag{10}$$

for $W_A^h \approx 0$ and $W_A^e \approx 0$,

$$\cos\theta = 2\frac{W_A^d}{W_C} - 1 \tag{11}$$

It follows from equation (11) that the solid is always hydrophobic, $\theta > 0°$, whenever $W_A \approx W_A^d$.

The main conclusion is obvious, *all solids would be hydrophilic if they did not carry polar or ionic groups* [8]. This is perfectly in line with Gaudin [11] who pointed out that all hydrophobic solids present non-polar molecular groups whereas hydrophilic solids have ionic or dipolar groups capable of undergoing hydration.

Equation (10) also explains the effect of the electrical charge of the solid on its wettability. According to this equation, contact angle should reach maximum values, $\theta \to \theta_{max}$ when $W_A^e \to 0$.

Frumkin and co-workers [12] and Smolders [13] confirmed experimentally that the contact angle at the mercury/solution interface reaches maximum values at the electrode potential at which the electrode surface charge is zero.

Elegant confirmation of this relationship for a reversible system (AgI/aqueous solution interface) was offered by Ottewill et al. [14].

The surface charge for AgI/H_2O is given by:

$$\sigma = (\Gamma_{Ag^+} - \Gamma_{I^-})F \tag{12}$$

where Γ stands for adsorption of Ag^+ and I^- ions, respectively, and F is Faraday's constant.

Since for such system the surface potential, ψ_o, is given by the equation:

$$\psi_o = \frac{RT}{F} \ln \frac{a_{M^+}}{a^0_{M^+}} \tag{13}$$

where a_{M^+} and $a^0_{M^+}$ are the activities of Ag^+ ions in solution, and in solution at the point of zero charge, respectively.

From this equation:

$$d\psi_o = 2.3\frac{RT}{F} d\,pAg^+ \tag{14}$$

and from Lippmann's equation:

$$d\gamma = -\sigma d\psi_o \tag{15}$$

The substitution of equations (12) and (14) into (15) gives:

$$d\gamma = -2.3RT(\Gamma_{Ag^+} - \Gamma_{I^-})d\,pAg^+ \tag{16}$$

Thus, the curve $\gamma = f(\psi_o) = f(pAg_{+})$ indicates capillary maximum at:

$$\frac{d\gamma}{d\,pAg^+} = -2.3RT(\Gamma_{Ag^+} - \Gamma_{I^-}) = 0 \tag{17}$$

that is at $\Gamma_{Ag^+} = \Gamma_{I^-}$ which is the p.z.c.

Ottewill et al's experimental results [14], which illustrate the effect of electrical charge on the wettability of the AgI surface in aqueous solution, are shown in Figure 6. Since the p.z.c. for this system is around $pAg^+ \approx 5.5$, the agreement with experiment is very good.

A slightly different approach was offered by Fokkink and Ralston [15] who put that in the presence of surface charge, the free energy of solid/liquid interface can formally be written as:

$$\gamma_{SL} = \gamma^o_{SL} + \Delta G_{d.l.} \tag{18}$$

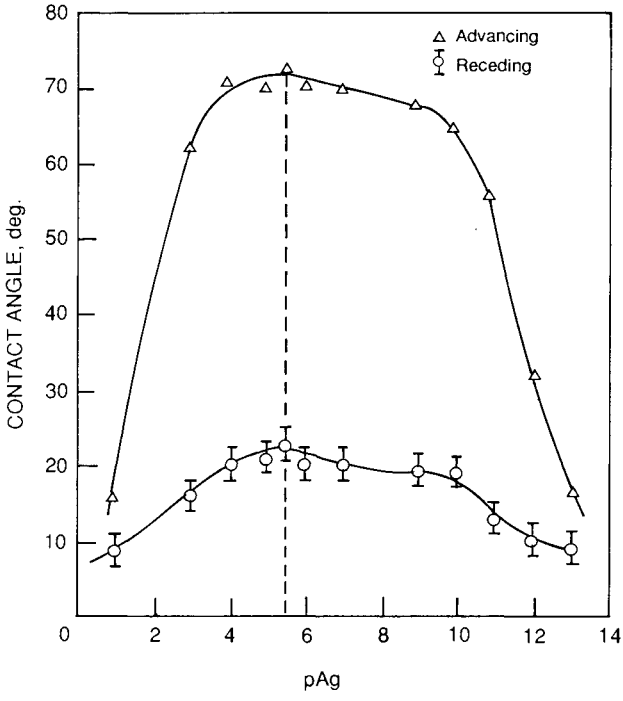

Fig. 6. Contact angle against pAg for measurements on silver iodide thin films: △ = advancing liquid meniscus, o = receding liquid meniscus; broken line indicates position of maximum θ (from Ottewill et al. [14] with permission). y6pt

where γ_{SL} is the total free energy per unit area, γ°_{SL} is the "chemical" contribution to the total energy (and equals γ_{SL} at p.z.c.) and $\Delta G_{d.l.}$ is the free energy of double layer formation. Since:

$$\Delta G_{d.l.} = -\int_0^{\psi_0} \sigma_o \, d\psi \tag{19}$$

where ψ_o is the surface potential at the solid/liquid interface, for the surface for which $\psi_o = f(\text{PDI})$ the use of equations 14–16 leads to the same conclusions, namely that the contact angle vary with ψ_o (that is with the potential determining ions concentration).

Direct contact angle measurements showing the relationship between ionization of the solid ionic groups and the surface wettability can be found in the recent paper by Holmes-Farley et al. [16].

Only one part of the theory interrelating wettability and floatability is clear: the contact angle must be larger than zero for the particle to be able to attach to a bubble [equation (2)].

As seen from Figure 4, the disjoining film between particle and bubble is completely stable when $\theta = 0$ (curve A). Since work is required to reduce the thickness of a stable film, the system reacts as if an additional force was keeping the interfaces apart; this additional force was termed by Derjaguin the *disjoining pressure*:

$$\pi_{(d)} = -\left(\frac{dG^s}{dh}\right)_{T,P,\mu} \tag{20}$$

The disjoining pressure is then positive for curve A (repulsion between interfaces); a negative disjoining pressure corresponds to attraction. Curve B shows the case of a completely unstable film which, when formed, will spontaneously rupture. A negative disjoining pressure must then exist in film C at a critical range of thicknesses. B and C curves are both characterized by contact angles $\theta > 0$. However, while each particle–bubble collision will lead to attachment in case B, this may not be so in case C. *Flotation rates for these two cases will then be quite different.*

Laskowski and Iskra [17] used quartz particles and fused silica plates, both rendered hydrophobic by methylation, to study the relationship between flotation, contact angle and induction time (defined as the time of particle–bubble contact required for successful attachment). Experiments carried out at a constant pH, but varying ionic strength of the solution, revealed only a good correlation between flotation and induction time, no correlation with contact angle was observed under such circumstances. These findings have recently been fully corroborated [18]. The same model system with varying degree of hydrophobicity, fused silica rods and plates, and quartz particles, all rendered hydrophobic by methylation under the same carefully controlled conditions, was utilized in the measurements of contact angle, energy barrier, induction time and flotation rate. The results fully confirmed that the energy barrier is a primary obstacle for particle-to-bubble attachment. For hydrophobic particles ($\theta > 0$), there exists a well pronounced correlation between the energy barrier, induction time and flotation rate constant.

It is noteworthy that Blake and Kitchener [19] observed that thick equilibrium films were formed not only on clean, hydrophilic silica, but also on methylated, hydrophobic silica, when electrical double layers developed at both interfaces [8]. The film stability over the measured range of thicknesses (60–200 nm) was in both cases due to electrical double layers repulsion. However, while the film on the hydrophilic surface was permanently stable, the film on the hydrophobic surface was clearly metastable at smaller thicknesses. Instability of water films of a certain thickness on hydrophobic solids is fundamentally due to a deficiency of hydrogen bonding in these films as compared with bulk water [8].

It is to be pointed out that in flotation processes the natural differences in wettability between *valuable* and *gangue* minerals are generally not sufficient for their selective separation; to aid separation selectivity, various *flotation reagents* are utilized. These include collectors, modifiers (activators, depressants, dispersants, pH

regulators, etc.) and frothers. *Adsorption* of a collector, amphipatic compound (the compound of dual character usually with a long non-polar hydrocarbon chain and a polar group) onto a hydrophilic solid surface, takes place through interactions of the polar groups with the solid surface. This leaves the hydrophobic radicals directed towards the aqueous phase. Such an oriented adsorption layer replaces the hydrophilic solid surface (which interacted actively with adjacent water molecules through electrical forces and hydrogen bonding), with the surface which can interact with water through dispersion forces only. As a result, the surface becomes hydrophobic. All other reagents used along with a collector modify the system so that the differences in the flotation rates become large enough for the selective separation of the valuable from gangue minerals.

Flotation methods

Flotation collectors are usually classified as anionic, cationic and non-ionic. The first two groups are more or less soluble in water and act through selective adsorption onto minerals from the pulp. The selectivity of collector adsorption, which in practice is further enhanced by modifying agents, is a critical factor which determines to a large extent the overall selectivity of the process.

Ionic surfactants, anionic and cationic, can either be weak or strong electrolytes. It is important to bear in mind, therefore, that — as it has recently been pointed out [20–22] — the solution chemistry and properties of the weak and strong electrolyte type collectors can be quite different.

Insoluble in water, nonpolar hydrocarbon "oils" are also used in flotation as collectors [23–25]. Since upon conditioning with the pulp they are emulsified, the process is termed emulsion flotation. Emulsification of such nonpolar reagents prior to flotation aids the process significantly [26]. Since hydrocarbon droplets are hydrophobic, they can attach, in the same way as bubbles, only onto particles with some degree of hydrophobicity. In this case, the selectivity of the process depends on the selectivity of oil droplets' attachment. Since the droplets can only differentiate between hydrophobic and hydrophilic particles [27], the process depends critically on differences in the initial wettability of the separated minerals.

Emulsion flotation is usually applied in the processing of minerals that exhibit native floatability, such as coals, sulphur, molybdenite, talc and graphite [23, 28] (these aspects are further discussed in Chapter 12).

As a result of unfavourable *hydrodynamic conditions*, the efficiency of capturing fine particles by bubbles is very low. Froth flotation is therefore not very efficient in treating very fine particles; particles below let's say, 10 micrometers. Better understanding of particle-to-bubble hydrodynamics [29], resulting in the use of finer bubbles, can further decrease the size limits (see Chapter 13). Nevertheless, the best means of extending froth flotation to lower size ranges is by the use of techniques that permit selective aggregation of fines.

As shown by Gaudin and Malozemoff [30], near-colloidal mineral particles are

best floated if they are first *selectively aggregated* leaving the gangue particles in a dispersed state. It has been known since Rehbinder's early work [31] that fine mineral particles rendered hydrophobic by collectors tend to form larger aggregates. Hydrophobic but electrically charged fine particles can also form stable suspensions. Laskowski and Kitchener [8] observed that silica made hydrophobic by methylation retains its high negative zeta potential and may form quite a stable suspension. According to Warren [32, 33], charged but hydrophobic fine particles, stable on standing, can be aggregated by high intensity shearing. The process is referred to as *shear flocculation* (for further details see Chapter 10). This process requires mechanical energy to overcome energy barriers, arising from the high electrical charge.

Aggregation of fine hydrophobic particles by an emulsified hydrocarbon is much more efficient and is utilized in *agglomerate flotation*. In the *carrier flotation*, fine valuable particles are aggregated onto the larger hydrophobic particles which are then floated up (Figure 7). The rate of attachment of fine particles to larger ones is hydrodynamically much more favourable; it was experimentally observed that the rate of aggregation of small onto large particles was much higher as compared to the rate of aggregation of fine particles among themselves [34, 35].

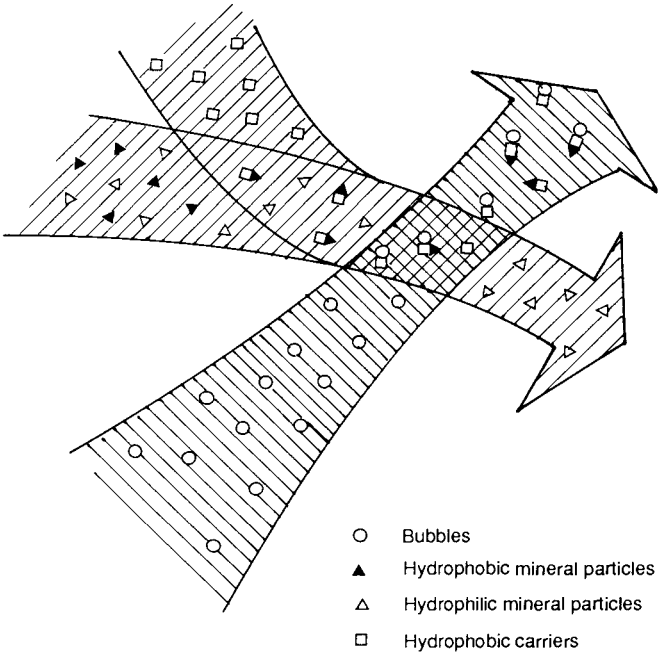

Fig. 7. Separation of hydrophobic from hydrophilic particles in carrier flotation.

From the physicochemical point of view, *agglomerate flotation* is a kind of emulsion flotation. In this process, the flotation stage is preceded by agglomeration of fine particles made hydrophobic with use of an ionic collector. The conditioning of pulp at high solid content (50–70%) with an ionic collector–fuel oil combination prior to flotation [36–39] is a critical step that determines recovery and grade. As proved by Karjalahti [39], the emulsification of non-polar oil prior to the conditioning with pulp improves significantly the process and substantially reduces energy requirements in the conditioning stage.

In the *carrier flotation*, which was used industrially for some years to remove fine iron and titanium oxide mineral impurities (a few microns in size) from kaolin clays, coarse calcite particles were used [40]. Since fatty acids employed as a collector renders hydrophobic both calcite, and iron and titanium oxides, and since calcite particles were about 50 μm in size, the conditioning of kaolin with the carrier led to the aggregation of fine hydrophobic impurities on a large hydrophobic carrier. The basis of the process is not completely clear and is still a subject of research projects [41]. The possible "autogenous" carrier flotation, in which coarse valuable particles are used as a carrier for fine particles of the same mineral [42] is an interesting modification; by the way, this is probably quite an important mechanism by which fine particles report to the concentrate in any froth flotation process.

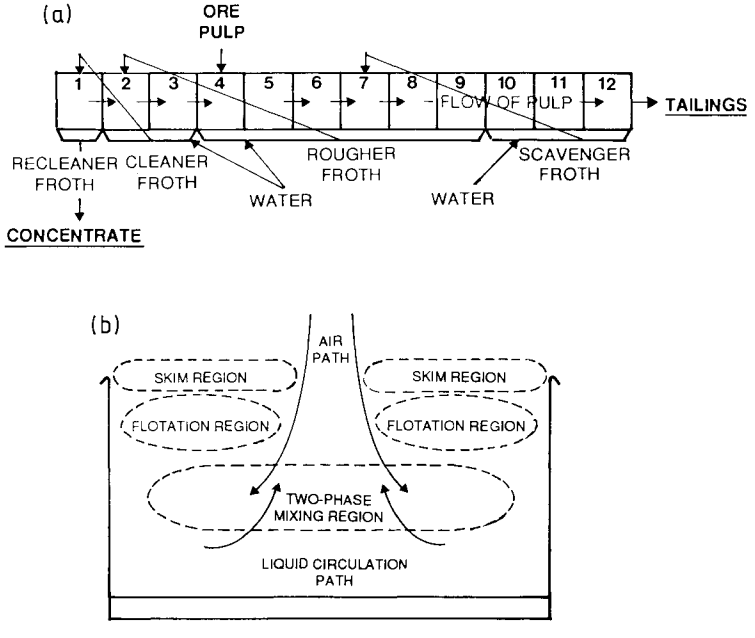

Fig. 8. (a) Schematic representation of a rougher–scavenger–cleaner counter-current flotation circuit. (b) Zones inside flotation mechanical cell.

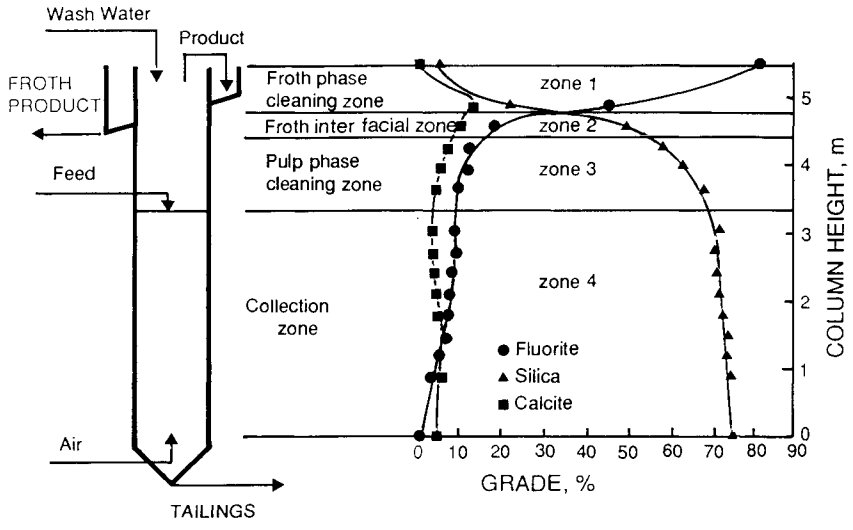

Fig. 9. Delineation of flotation column zones and mineral upgrading profiles (from McKay et al. [45] with permission).

In principle, an industrial flotation machine acts as a continuous *counter-current upgrading device*. The *cleaner cells* have the greatest concentration of valuable minerals, the *rougher cells* the next, and the *scavengers* the least. The flow of concentrates and tailings are in opposite directions as shown in Figure 8a. As seen from Figure 8b, however, the counter-current principle, clearly seen in the bank of cells, may deviate quite far from this principle in each of the *mechanical cells*. High intensity shearing forces in such cells do not promote flotation of aggregates and larger particles. Therefore, the theoretical possibility of using flocculants in flotation, described many years ago by Usoni et al. [43], has not yet found industrial applications. This was however, found by Osborne [44] to be quite possible in *flotation columns*. In this type of strictly counter-current upgrading device (Figure 9) [45], in which a very gentle mixing is provided by a stream of rising bubbles, conditions are very favourable for the flotation of flocs. The only condition which must, however, be satisfied (as in all flotation processes) is that the flocs must be hydrophobic. Combination of polyethylene oxide flocculant, which according to Rubio and Kitchener [46–48] can be used in selective hydrophobic flocculation, is an obvious solution.

The first promising results of *floc-flotation* have already been published [49].

Colloid methods

It is accepted that at a given concentration of potential-determining ions, a positive or negative charge is created at a solid/solution interface. Whereas for many

minerals it is difficult to indicate unequivocally the potential determining ions (e.g. sulphides), H^+ and OH^- ions have been identified to be potential determining for oxides. Different electrical charges that are created on the surface of these minerals at a given pH can then be exploited in the electrophoresis, or selective coagulation, to separate the mixtures of various oxides.

The possibility of *selective coagulation* in colloidal mineral suspensions was investigated by Pugh and Kitchener [50–52]. The process is based on the Derjaguin-Landau-Verwey-Overbeek (DLVO) theory of colloid stability [53–56], which takes electrical and van der Waals forces into account to explain the coagulation process. Recent work by Yoon et al. [57] sheds new light on the question of the effect of surface wettability of solid particles on their coagulation. These researchers have shown that while the weakly hydrophobic fine particles coagulate in accordance with the DLVO theory, the hydrophobic fine particles coagulate even at relatively high value of zeta potential (this subject is further discussed in Chapter 8).

Aggregation of fine particles can be achieved not only by neutralizing the electrical charge of the interacting particles (*coagulation*), but also by bridging the particles with polymolecules (*flocculation*) [58]. The latter process may lead to a selective flocculation of fine particles if the bridging polymer and the physicochemical conditions are properly selected (*selective flocculation*). The first original studies on selective flocculation have come mostly from Kitchener's laboratory [56–61]; in this respect the contribution by Usoni et al. [43] is also noteworthy. The essentials of the process were graphically visualized by Collins and Read [62] (see Chapter 9).

Perhaps the most colloidal among the colloidal separation methods are *carrier separation methods*. In the carrier flotation, hydrophobic flocculation of fine hydrophobic particles onto much larger carrier particles, which are also hydrophobic, is followed by the flotation removal of the aggregates. It is easy to visualize that other carrier properties can also be utilized in the carrier separation techniques. The most obvious is the use of ferromagnetic carrier, such as magnetite, followed by the magnetic separation of the loaded carrier particles [2]. A large number of various phenomena can be exploited to aggregate selectively the particles which are to be removed from the system with magnetite. Perhaps the most interesting in this area is the selective coating of the mineral with colloidal, chemically precipitated magnetite, followed by magnetic separation. Dramatic increase in magnetic response was revealed even for less than 1% amounts of magnetite [63, 64] (These techniques are discussed in Chapter 11).

Finally, it should be emphasized that the practical exploitation of the separation methods mentioned above generally requires an extensive program of chemical research and testing to arrive at suitable surface conditions for the separation stage. Every mineral system demands its own, thoroughgoing, investigation.

References

1 J.A. Kitchener, in: K.J. Ives (Editor), The Scientific Basis of Flocculation, Sijthoff and Noordhoff, Alphen aan den Rijn, 1978, pp. 283-328.
2 J.S. Laskowski, in: E. Matijevic (Editor), Surface and Colloid Science, Vol. 12, Plenum Press, 1982, pp. 315-357.
3 B.L. Karger, R.B. Grieves, R.B. Lemlich, R. Rubin and F. Sebba, Sep. Sci., 2 (1967): 401.
4 R. Lemlich, in: R. Lemlich (Editor,), Adsorptive Bubble Separation Techniques, Academic Press, New York, N.Y., 1972, pp. 1-5.
5 J.S. Laskowski, in: P. Somasundaran (Editor), Advances in Mineral Processing, Soc. Min. Eng., Littleton, 1986, pp. 189-208.
6 J.S. Laskowski, in: J.S. Laskowski (Editor,), Frothing in Flotation, Gordon and Breach, New York, N.Y., 1989, pp. 25-42.
7 J.S. Laskowski, Miner. Sci. Eng., 6 (1974): 223.
8 J.S. Laskowski and J.A. Kitchener, J. Colloid Interface Sci., 29 (1969): 670.
9 F.M. Fowkes, in: Wetting, Society of Chemical Industry Monograph No. 25, London, 1967, pp. 3-30.
10 F.M. Fowkes, Ind. Eng. Chem., 56, No. 12 (1964): 40.
11. A.M. Gaudin, Flotation, 2nd edition, McGraw-Hill, New York, N.Y., 1957.
12 A.N. Frumkin, V.S. Bagotsky, Z.A. Iofa and B.N. Kabanov, Kinetics of Electrode Processes, University of Moscow, Moscow, 1952.
13 C.A. Smolders, Rec. Trav. Chim. Pays-Bas., IA (1961): 650.
14 R.H. Ottewill, D.F. Billett, G., Gonzalez, D.B. Hough and V.M. Lovel, in: J.F. Padday (Editor), Wetting, Spreading and Adhesion, Academic Press, New York, N.Y., 1978, pp. 183-199.
15 L.G.J. Fokkink and J. Ralston, Colloids Surf., 36 (1989): 69.
16 S.R. Holmes-Farley, R.H. Reamey, T.J. McCarthy, J. Deutch and G.M. Whitesides, Langmuir, 1 (1985): 725.
17 J.S. Laskowski and J. Iskra, Trans. IMM, Sec. C, 79 (1970): 6.
18 J.S. Laskowski, Z. Xu and R.H. Yoon, Energy Barrier in Particle-to-Bubble Attachment and Its Effect on Flotation Kinetics. 17th Int. Miner. Process. Congr., Dresden, September 1991.
19 T.D. Blake and J.A. Kitchener, J. Chem. Soc. Faraday Soc. I, 7 (1972): 1435.
20 S.H. Castro, R.M. Vurdela and J.S. Laskowski, Colloids Surf., 21 (1986): 87.
21 J. Laskowski, R.M. Vurdela and Q. Liu, in: K.S. Eric Forssberg (Editor), Proc. 16th Int. Miner. Process. Congr., Stockholm, 1988, Elsevier, Development in Mineral Processing, 1988, Vol 10A, pp. 703-715.
22 J.S. Laskowski, in: K.V.S. Sastry and M.C. Fuerstenau (Editors), Challenges in Mineral Processing, Soc. Min. Eng., Littleton, 1989, pp. 15-34.
23 V.I. Klassen, Coal Flotation, Slask, Katowice, 1966 (Polish edition translated from Russian by J.S. Laskowski).
24 L.Y. Shubov, A.S. Kuzkin and A.K. Lifshitz, Theoretical Bases and Practice of the Application of Nonpolar Collectors in Flotation, Izdat. Nedra, Moscow, 1969 (in Russian).
25 V.I. Klassen, in: I.N. Plaksin (Editor), Physicochemical Bases of the Action of Nonpolar Collectors in Flotation of Ores and Coal, Izdat Nauka, Moscow, 1969 (in Russian).
26 S.C. Sun, L.Y. Tu and E. Ackerman, Min. Eng., 7 (1955): 656.
27. A.R. Burkin and S.C. Soane, in: Proc. 3rd Congr. of Surface Activity, Cologne, Vol. 4 (1960): 430.
28 V.I. Klassen and V.A. Mokrousov, An Introduction to the Theory of Flotation, Butterworths, London, 1963 (English edition translated from Russian by J. Leja and G.W. Poling).
29 R.H. Yoon and G.H. Luttrell, in: J.S. Laskowski (Editor), Frothing in Flotation, Gordon and Breach, New York, N.Y., 1989, pp. 101-122.
30 A.M. Gaudin and P. Malozemoff, J. Phys. Chem., 37 (1933): 597.

31 P.A. Rehbinder, in: I.N. Plaksin (Editor), Role of Gases and Reagents in the Flotation Processes, Izdat. Akad. Nauk. Moscow 1950 (in Russian).
32 L.J. Warren, J. Colloid Interface Sci., 50 (1975): 307.
33 L.J. Warren, Trans. IMM, Sec. C., 84 (1975): C99.
34 B.V. Derjaguin, V.D. Samygin and A.K. Livshitz, Kolloidn. Zh., 26 (1964): 179.
35 V.D. Samygin, L.A. Barsky and S.M. Angelova, Kolloidn. Zh., 30 (1968): 581.
36 E.H. Gates, Trans. AIME, 208 (1957): 1368.
37 U. Runolinna, R. Rinne and S. Kurronen, in: Proc. 5th Int. Miner. Process. Congr., IMM, London, 1960, pp. 447-475.
38 M. Lapidot and O. Mellgren, Trans. IMM, Sec. C., 77 (1968): C149.
39 K. Karjalahti, Trans. IMM, Sec. C., 81 (1972): C219.
40 R.N. Maynard, N. Millan and J. Iannicelli, Clays, Clay Miner., 1 (1969): 59.
41 Y.H. Chia and P. Somasundaran, Colloids Surf., 8 (1983): 187.
42 Wang Dianzuo, Qu Guanzhou and Hu Weibai, in: A.J. Plumpton (Editor), Production and Processing of Fine Particles, Pergamon Press, New York, N.Y., 1988, pp. 309-316.
43 L. Usoni, G. Rinelli and A.M. Marabini, in: Proc. 8th Int. Miner. Process. Congr., Mekhanobr Institute, Leningrad, 1969, Vol. 1, pp. 514-533.
44 D.G. Osborne, Trans. IMM, Sec. C., 87 (1978): C189.
45 J.D. McKay, D.G. Foot and M.B. Shirts, in: K.V.S. Sastry (Editor), Column Flotation '88, Soc. Min. Eng., Littleton 1988, pp. 173-186.
46. J. Rubio and J.A. Kitchener, J. Colloid Interface Sci., 57 (1976): 132.
47 J. Rubio and J.A. Kitchener, Trans. IMM, Sec. C., 86 (1977): C97.
48 J. Rubio, Colloids Surf., 3 (1981): 79.
49 H. Soto and G. Barbery, in: A.J. Plumpton (Editor), Production and Processing of Fine Particles, Pergamon Press, New York, N.Y., 1988, pp. 297-308.
50 R.J. Pugh and J.A. Kitchener, J. Colloid Interface Sci., 35 (1971): 656.
51 R.J. Pugh and J.A. Kitchener, J. Colloid Interface Sci., 38 (1972): 656.
52 R.J. Pugh, Colloid Polym. Sci., 252 (1974): 400.
53 B.V. Derjaguin and L. Landau, Acta Physicochimica URSS, 14 (1941): 633.
54 E.J.W. Verwey and J.Th. G. Overbeek, Theory of the Stability of Lyophobic Colloids, Elsevier, Amsterdam, 1948.
55 B.V. Derjaguin, Disc. Faraday Soc., 18 (1954): 85.
56 B.V. Derjaguin, Theory of Stability of Colloids and Thin Films, Consultants Bureau, New York, N.Y., 1989.
57 Zhenghe Xu and R.H. Yoon, J. Colloid Interface Sci., 132 (1989): 15.
58 R.W. Slater and J.A. Kitchener, Disc. Faraday Society, 42 (1966): 26D.
59 B. Yarar and J.A. Kitchener, Trans. IMM, Sec. C., 79 (1970): C23.
60 J.P. Friend and J.A. Kitchener, Chem. Eng. Sci., 28 (1972): 1071.
61 Y.A. Attia and J.A. Kitchener, in: Proc. 11th Int. Miner. Process. Congr., University of Cagliari, Cagliari, 1975, pp. 1233-1248.
62 D.N. Collins and A.D. Read, Miner. Sci. Eng., 3, No. 2 (1971): 19.
63 P. Parsonage, Trans. IMM, Sec. C., 93 (1984): C37.
64 P. Parsonage, Int. J. Miner. Process., 24 (1988): 269.

Chapter 8

Selective coagulation of colloidal mineral particles

R.J. PUGH

Introduction

Selective coagulation usually occurs in an initially dispersed mixed colloidal system, where differences in the slow rates of coagulation of the various species are of a sufficient magnitude that one species may separate out, leaving the other species in suspension after a certain time period. To avoid rapid mutual coagulation of the components, it is essential that all species carry the same sign of charge. The separation process can be controlled by careful adjustment of the surface potential, so that one of the components is reduced to the point where slow coagulation begins, yet heterocoagulation or mutual coagulation is avoided.

In a binary colloidal system consisting of components 1 and 2, then there exist three distinct interaction rates, namely 1–1, 1–2 and 2–2, to be considered. Separations may be achieved if the rate of coagulation of 1–1 is greater from that of 1–2 and 2–2 by a factor of 100 though possibly not if they differ by only 10. It is therefore not a necessary requirement that one species remains indefinitely stable.

From DLVO theory, the collision frequency of a *fast* coagulation process resulting from such interactions, will be dependent on the different initial particle concentrations and sizes. In the *slow* coagulation process, however, the potential energy barrier makes a major contribution to the stability of the system. The magnitude of this barrier depends on the size of the particles and the surface potentials. The resistance of a sol to coagulation has been defined in terms of the stability factor W, which is the ratio of the initial rate of coagulation to that which would occur if the process was only diffusion controlled (in the absence of an energy barrier).

Since the first parts of the present paper are concerned with the selective coagulation of different types of colloidal particles according to the broad predictions of DLVO theory, it is important to mention certain restrictions to the theory when applied to colloidal mineral mixtures. It must first be noted, that the original DLVO theory is limited to the coagulation and dispersion of particles of identical size and nature and for symmetrical double layer interactions in the electrolyte solution. It

has subsequently been shown that the principles of "heterocoagulation", which describes the coagulation of particles of dissimilar nature, may be developed on the basis of the DLVO theory but there are several difficulties to be considered, before such a theory can be applied to a practical system. For example, the theory applies to spherical colloidal particles of uniform size, whereas most practical dispersions consist of non-spherical particles having a wide size distribution. However, many particles are approximately isometric and the effect of flattening of the sides will be analogous to that of heterodispersity which can be dealt with, schematically at least, in the theory.

Also, it must be realized that DLVO theory has never been precisely confirmed by experiment for any colloidal model; nevertheless, attempts to check it have been met with partial success, and there has been no good reason to doubt its validity. The theory and experiments must also be limited to particles of the order of 1 μm or less, because with larger particles, sedimentation would have to be counteracted by an upflow and inertia factors then become important. It is known that orthokinetic coagulation dominates over perikinetic coagulation with particles above 1 μm. Finally, it must be recognized that so-called hydrophobic and hydration interactions cannot yet be included in DLVO theory. These additional interactions are referred to as "structural forces" and may explain many discrepancies in the theory. It is now known that hydration forces can have an important contribution at close distances, giving rise to a strong repulsion. An additional hydrophobic term can also explain a strong attraction.

DLVO theory applied to selective coagulation

According to classical DLVO theory, the total potential energy of the interaction (V_T) between two particles is defined by:

$$V_T = V_E + V_A \tag{1}$$

where V_E is the electrostatic double layer repulsive potential and V_A the Van der Waals attraction. Hogg et al. [4] have considered the case for spherical particles radius a_1 and a_2 with low surface potentials ψ_1 and ψ_2, ($e\psi/kT \ll 1$) and thin double layers ($a\kappa \gg 1$). In such cases the relation between V_E and V_A and the distance H_o between the surfaces can be described by the following equations:

$$V_E = +\frac{F\varepsilon}{4} \times f(\psi_1, \psi_2, \kappa, H_o) \tag{2}$$

$$V_A = -F \times \frac{A}{6H_o} \tag{3}$$

where F is the form or size factor $a_1a_2/(a_1 + a_2)$. The net Hamaker-London constant, A, for materials 1 and 2 in medium 3, is given by $A = A_{12} + A_{33} - A_{13} - A_{23}$;

ε is the dielectric constant of the medium and κ is the Debye-Hückel reciprocal length parameter.

The repulsion function for the case of constant potentials may be expressed as:

$$f(\psi_1, \psi_2, \kappa, H_o) = 2\psi_1\psi_2 \ln\left[\frac{1 + \exp(-\kappa H_o)}{1 - \exp(-\kappa H_o)}\right] + (\psi_1^2 + \psi_2^2)\ln[1 - \exp(-2\kappa H_o)] \quad (4)$$

It has been shown by Wiese and Healy [5] that the comparable formula for the case of constant surface charge is identical except for a negative sign between the two terms on the right-hand side and ψ_1 and ψ_2 must be taken as the potentials on particles at infinite separation. These workers also took account of the retardation effect on the London forces; as is necessary when considering the possibility of coagulation into the secondary minimum. From Schenkel and Kitchener [6], $-A/6H_o$ in equation (3) may be modified to:

$$\frac{-A}{6H_o}\left[\frac{1}{1 + 1.77p_o}\right] \text{ for } 0 < p_o < 2 \quad (5)$$

where $p_o = 2\pi H_o/\lambda$ (λ being the wavelength corresponding to the intrinsic electronic oscillations of the atoms), and for larger H_o values then:

$$\frac{-2A}{H_o}\left[+\frac{2.45}{60p_o} - \frac{2.17}{180p_o^2} + \frac{0.59}{420p_o^3}\right] \text{ for } 0.5 < p_o < \infty \quad (6)$$

Finally, Wiese and Healy [5] found it was possible to express the stability or coagulation into the primary minimum or secondary minimum for a monodispersed, single component sol by graphs showing a series of zones. These theoretical plots were compared with experimental data. As criteria of stability, they selected an energy barrier of 5 or 10 $\times$ k_BT and a secondary minimum trough of 1.5 or 5 $\times$ k_BT where k_B is the Boltzman constant and T is the temperature.

In order to extend the theory to the problem of selective coagulation, it is necessary to carry the calculations a stage further. What is required, is data for the *rates of coagulation* of the various combinations of particles present in the mixed suspension. Since the rates are functions of the concentrations of the particles concerned and their size, it is not sufficient to adopt simple energy criteria to distinguish rates in a mixture.

From DLVO theory, the coagulation time, $t_{1/2}$, is related to the stability coefficient (W) which provide a quantitative measure of the stability of the dispersions and the initial concentration (N_o) of particles by the equation:

$$t_{1/2} = \frac{3\eta W}{4k_BTN_o} \quad (7)$$

This equation applies for a single type of particle and must be modified to allow for appropriate values of W and $N_{o(1)}$ and $N_{o(2)}$ for collision of unlike particles. If

the colloids are not monodisperse, a range of coagulation times will be obtained for the various possible combinations of sizes. For each combination, W_{12} must be calculated by an extension of the Fuchs theory for spheres of unequal size (cf. Overbeek [7]). Following Hogg et al. [4]:

$$W_{12} = 2\bar{a} \int_{2\bar{a}}^{\infty} \exp\left(\frac{V_{12}}{k_B T}\right) \frac{dR}{R^2} \tag{8}$$

where $R = (a_1 + a_2 + H_o)$. Here V_{12} is the interaction energy between particles 1 and 2 and $\bar{a}$ is the mean of a_1 and a_2. For the purposes of an exploratory survey of the range of W_{12} values likely to be encountered, the crude approximation:

$$W_{12} \approx \frac{1}{2\kappa(\bar{a})} \exp\left(\frac{V_{max}}{k_B T}\right) \tag{9}$$

can be used, where V_{max} is the maximum height of the potential energy barrier (itself proportional to the size factor). This equation describes essentially only the early stages of the process where collisions of single particles are involved and becomes inapplicable once this stage is complete. In fact, no detailed theory is available to describe the kinetics of particles undergoing multiple collisions (even for initially mono-disperse spheres). This definition, however, does give a basis for the prediction of relative coagulation rates in mixed colloidal suspension of different particle size and surface potential.

Using these equations, Pugh and Kitchener [8] computed a series of stability curves relating W_{12} to the radii a_1, a_2 and the surface potentials ψ_1, ψ_2 of two spheres for various values of the Hamaker constant, A, and the Debye-Hückel reciprocal length parameter κ. It was necessary to consider two cases: those of constant surface charge on the particle surface during the interaction and of constant surface potential. In practice the actual interaction must lie somewhere intermediate between the two, depending on the rates of exchange of the potential-determining ions. Generally, the results predict that a wide range of coagulation rates are possible, and by chemical control of the surface potential it should be possible to separate two different colloidal species.

The broad features of these results are shown in Figures 1–4 where $\log W$ is shown plotted against the "size factor" $[a_1 a_2/(a_1 + a_2)]$ for chosen values of ψ_1, ψ_2, κ and A. The spread of values resulting from changes of a, compatible with a given value of the form factor, is small; providing the size ranges are not enormous, they lie within a narrow band. The ordinate in all figures is the logarithm of the size factor, $a_1 a_2/(a_1 + a_2)$, the values of which are marked on the left side. Examples of various size combinations for a_1 and a_2 (expressed in microns) are marked on the r.h.s. It will be seen that the graphs cover all combinations of particle size from 0.01 to 2 μm. The results in Figures 1–4 are based only on the height of the potential energy barrier and are therefore for coagulation into the primary minimum; retardation of the London-Van der Waals forces is then negligible.

Retardation can also be allowed for in Figure 5. This figure shows that coagulation into the secondary minimum becomes significant, i.e., depth $>5k_BT$ (with $A = 3 \times 10^{-20}$ J, a medium value) only at high ionic strengths. It should be noticed that whereas Figures 1–4 show stability increasing to the right (as $\log W$ increases), Figure 5 shows the depth of the secondary minimum (V_{min}) increasing to the right. Thus all systems to the right of, say, $5k_BT$ will be subject to rapid coagulation into the secondary minimum, despite the fact that some of them (e.g., 50, 50 mV) are indicated by Figure 3 to exhibit high stability against coagulation into the primary minimum. This situation becomes more significant as the size factor increases, as an increasing depth of secondary minimum accompanies a rising height of primary maximum. Therefore, the data summarized in Figures 1–4 must be used with the reservation that the secondary minimum must first be proved absent by examination of data such as those in Figure 5 before stability differences of Figures 1–4 are considered.

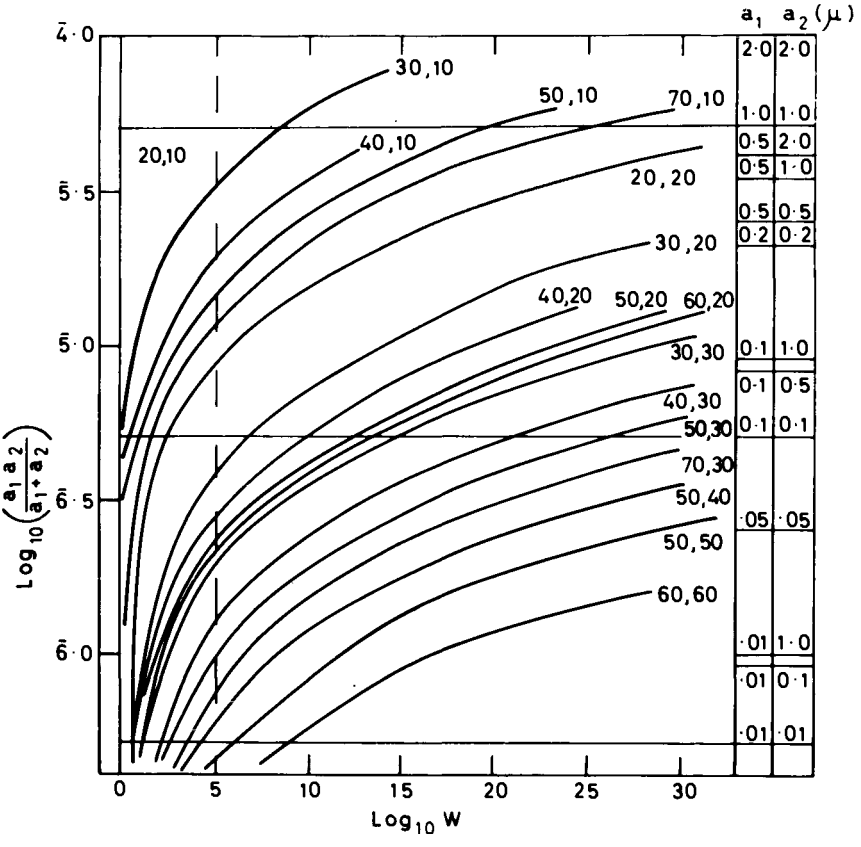

Fig. 1. Stability curves: constant potential; $A = 3 \times 10^{-20}$ J, $\kappa = 10^6$ cm^{-1} (from Pugh and Kitchener [8]).

Comparison of Figure 1 (constant potential) and Figure 2 (constant charge) shows some great differences between the positions of corresponding lines. Constant charge predicts, of course, greater stability. The difference is particularly marked for heterocoagulation of particles of different potential, one high and one low. For large distances of separation, both theories indicate electrical repulsion, but the constant potential theory predicts a transition to attraction at short distances. This is because a reversal of sign of charge is required, in order to maintain constant potential on the lower potential surface as it comes within the influence of the higher potential surface. This switch-over has the effect of considerably reducing the height of the potential barrier (V_{max}), as compared with the case of constant charge.

Implication of theory

Consider a slurry containing about 2×10^{11} particles per cm^3 then the time for half coagulation in the absence of a potential barrier would be of the order of 1 s.

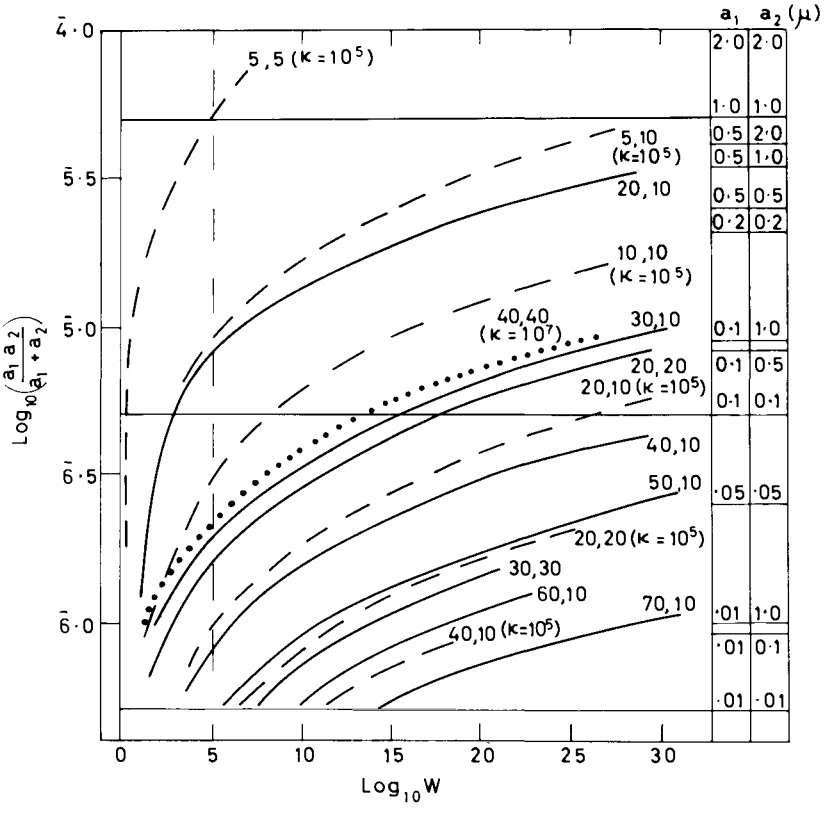

Fig. 2. Stability curves: constant charge; $A = 3 \times 10^{-20}$ J, $\kappa = 10^5$, 10^6, 10^7 cm^{-1} (from Pugh and Kitchener [8]).

At a concentration of 10^{10} particles per cm^3 then the half-life would be about 20 s. However, any practical process would require a longer standing period than this during which the coagulated components could settle out. A suitable period might lie in the range 1–10 hours. Therefore, the stable components would need half-times considerably longer than 1–10 hours — this implies stability factors (W) larger than 4000–40.000; for example, $W = 10^5$ might be taken as typical of a practically stable suspension, which would be readily separable from a rapidly coagulating 1% impurity.

Figures 1–4 show that differences of 10^5 in stability values are well within expectation according to the theory. Indeed, W values up to 10^{30} are predicted for 0.1 μm particles bearing a moderately high potential. It is evident from the curves that separations could be based on any of the following factors (or suitable combinations of them).

(a) Difference of A value, with given size and potential (see Figure 4). For

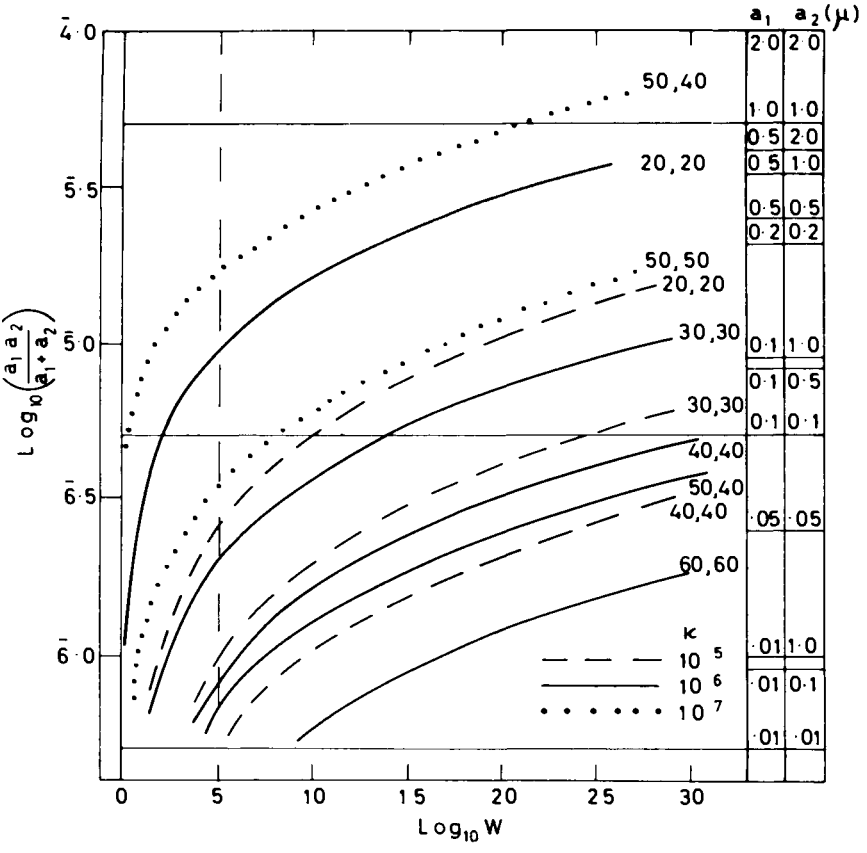

Fig. 3. Stability curves: constant potential; $A = 3 \times 10^{-20}$ J, $\kappa = 10^5, 10^6, 10^7$ cm^{-1} (from Pugh and Kitchener [8]).

example, with $\kappa = 10^6$, $a = 0.1$ μm, a difference of a factor of 3 in net value would be adequate to distinguish two coagulation rates. This type of separation process could be particularly important when dealing with different materials where there is an order of magnitude difference in Hamaker constant. For examples $A \sim 80k_BT$ for gold and $\sim k_BT$ for polystyrene latex.

(b) Differences of potential, or charge, with given A and a. Figure 2 suggests, for example, that very adequate differences of rate would result from having $\psi_1 = 10$ mV, $\psi_2 = 30$ mV ($A = 3 \times 10^{-20}$ J, $\kappa = 10^6$, $a = 0.1$ μm)

(c) Differences of size, with given A and ψ. Consider, for example, the line for 20, 20 mV in Figure 1. The log W values for particle combinations 0.01 + 0.01, 0.01 + 0.1, 0.1 + 0.1, 0.1 + 1.0 and 1.0 + 1.0 (μm) are, respectively, 0.4, 0.5, 3, 5.5 and 35. A check against Figure 5 shows that with $A = 3 \times 10^{-20}$ J and $\kappa = 10^6$ there would be no danger of coagulation of the larger particles into the secondary minimum. Consequently, it should be possible to fractionate heterodisperse lyophobic colloids

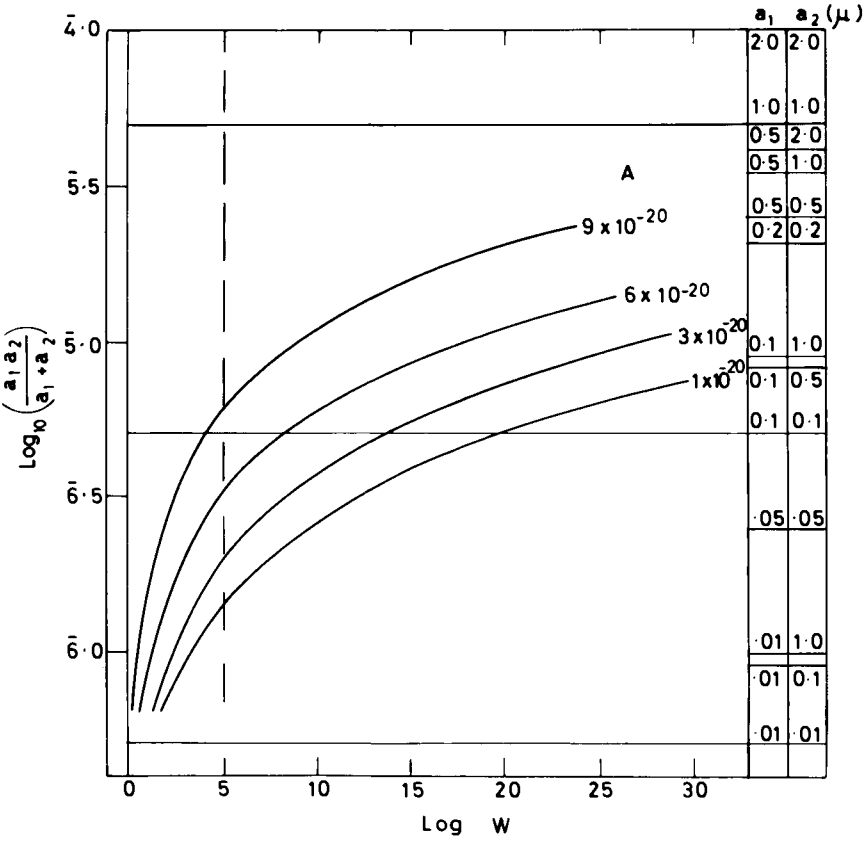

Fig. 4. Stability curves: constant potential (30, 30 mV); $A = 1, 3, 6, 9 \times 10^{-20}$ J, $\kappa = 10^6$ cm^{-1} (from Pugh and Kitchener [8]).

by cautiously lowering the surface potential with potential-determining electrolyte, while keeping the ionic strength below 10^{-3} M of 1 : 1 electrolyte.

To summarize, from numerical calculations carried out with a range of values of a_1, a_2, ψ_1, ψ_2, κ and A, as presented in Figure 1–4, two important points emerge:

(1) W_{12} varies over an enormous range of values.

(2) The changes of W_{12} arising from different size combinations result principally from changes in the exponential term (i.e. the pre-exponential term is relatively insensitive to size combinations).

It would there appear possible to separate a given mixture providing:

(1) The particle size distributions of the main components are known or can be determined.

(2) Approximate values of the Hamaker constants for the various components are known.

(3) The range of zeta potentials obtainable with appropriate potential-determining electrolytes can be determined and explored.

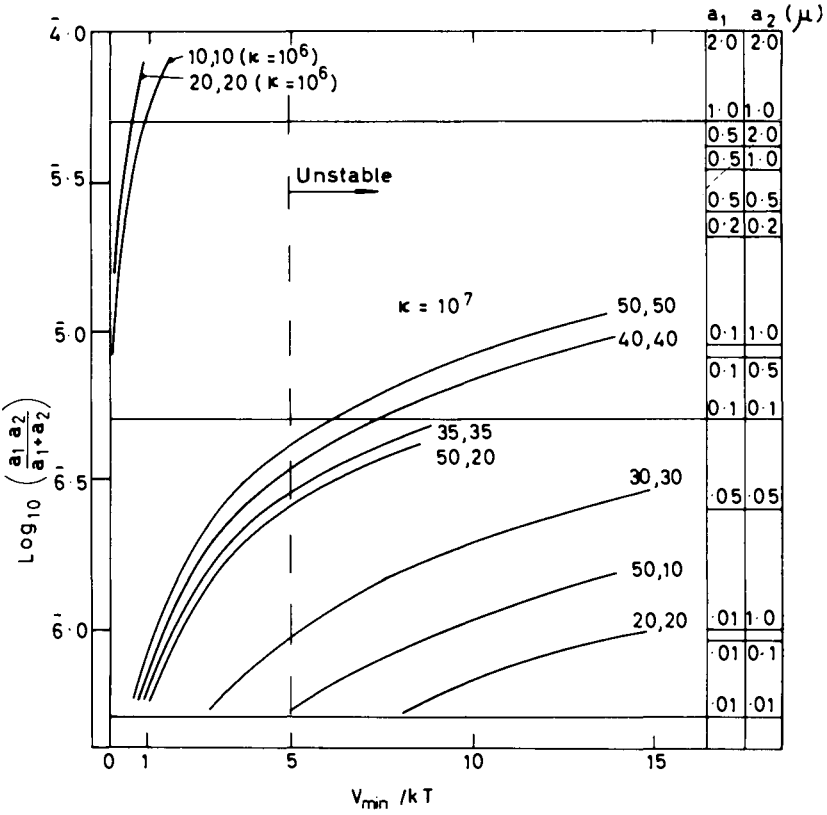

Fig. 5. Depth of the secondary minmum: constant potential; $A = 3 \times 10^{-20}$ J, $\kappa = 10^6$, 10^7 cm^{-1} (from Pugh and Kitchener [8]).

Then, by employing the approximate equations outlined above, the ranges of W values for the various combinations of sizes and types of particles could be determined. From the results, conditions for obtaining large enough differences of rate of coagulation could be predicted.

Selective coagulation in binary mineral mixtures

In order to achieve a clear-cut selective coagulation with an experimental system, it is desirable to choose two components having spherical or, at least spheroidal, particles of narrow size range, which should be below 1 μm in radius to avoid the complications of "secondary minimum instability". Selective coagulation would be operated by exploiting the differences in the coagulation rates of the two components following adjustment of the pH and/or strength medium. Clearly, conditions must be chosen where the two colloids carry the same sign of surface charge and, from the proposed theory of selective coagulation, a large difference in the surface potentials of the two components is required (one component preferably having a low value, while the other component retains a relatively high value).

The procedure was experimentally tested with binary mixtures of colloidal oxides; quartz/rutile [1] and quartz/hematite [2] where H^+ and OH^- are the potential determining ions which control the size and sign of the charge at the mineral/water interface. The quartz and hematite were naturally occurring minerals ground and

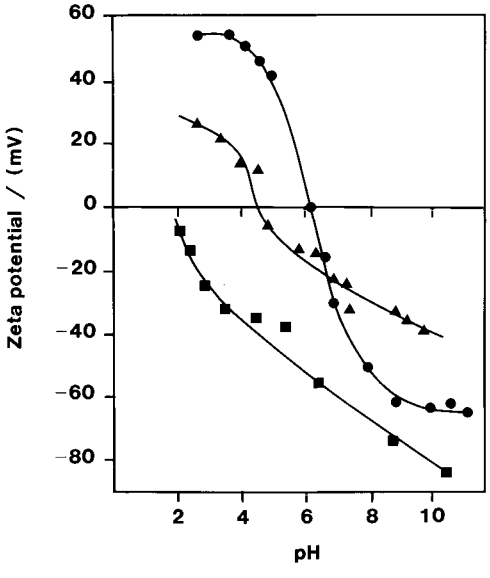

Fig. 6. Zeta potential of the quartz (■), rutile (▲) and hematite (●) versus pH (from Pugh and Kitchener [1, 2]).

fractionated to a size range of between 0.05 and 0.2 μm radius. The rutile used in the experiments was a synthetic sample (supplied by Tioxide Ltd., U.K.) with a diameter of about 0.2 μm. The zeta potential versus pH curves for the three minerals is shown in Figure 6. By careful adjustment of pH and electrolyte concentration it was found that selective coagulation could be achieved in the binary mixtures of minerals.

Quartz/rutile

For the quartz and rutile systems Figure 7A, B show the regions of stability for the two separate components respectively, throughout the pH range and Figure 7C shows those for the mixed suspensions. All the suspensions had 2.2 wt.% solids — in the case of mixtures, 1.1% of each. No addition of electrolyte was made in this

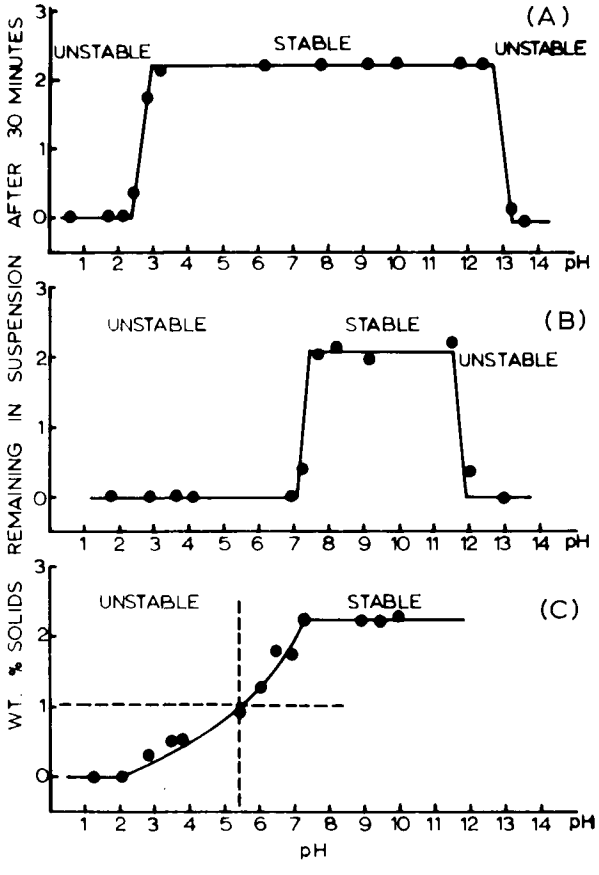

Fig. 7. Stability regions for (A) quartz, (B) rutile and (C) quartz + rutile mixture, without additional electrolyte; stability is measured by wt.% solids remaining in suspension after 30 min. (from Pugh and Kitchener [1]).

TABLE 1

Supernatant and sedimentation analysis in the selective coagulation regions (in Figures 7 and 8) for the SiO_2/TiO_2 system [1]

Fig no.	pH	Electrolyte concentration (NaCl) M	Supernatant liquid analysis (%)		Sediment analysis (%)	
			SiO_2	TiO_2	SiO_2	TiO_2
7C	5.6	–	98	2	7	93
8C	9.5	0.020	95	5	4	96
8C	9.5	0.023	89	11	13	87
8C	9.5	0.0265	87	13	1	90

series of experiments. A region of selective coagulation of the mixtures was anticipated (and found) at about pH 5.6, since at this point the quartz sol remained stable while the rutile was observed to undergo rapid coagulation. From the electrophoresis measurements both components carried a negative surface potential at this pH. Chemical analysis of the supernatant liquid and sediment confirmed selective coagulation occurred (Table 1).

An additional series of investigations in the pH range 7–10 were carried out, in which both quartz and rutile remained stable until electrolyte was added to bring about coagulation. Figure 8A, B show the stability regions of the individual components on addition of increasing amounts of sodium chloride. A study of the coagulation characteristics of the mixture was made by adding electrolyte at pH 9.5 (Figure 8C). The results indicate that selective coagulation should occur between 0.015 and 0.050 M NaCl. In this region the quartz remains stable and the rutile undergoes coagulation, both components again retaining a negative surface potential. Finally, chemical analysis of the supernatant liquid and sediment at three different points confirmed successful separations by coagulation of the rutile, leaving the quartz substantially in suspension (Table 1).

Quartz/hematite

A similar series of experiments with quartz and fractioned finely ground natural hematite were also reported [2]. From Figure 6 it may be observed that hematite has a pH_{iep} of about 6. One would therefore expect from DLVO theory that the requirements for selective coagulation of hematite from quartz to occur in slightly alkaline conditions providing only low concentrations of electrolyte are present in solution. In this region it may be anticipated that quartz will retain a high negative surface potential (and remain stable) while that hematite may be reduced to a low negative value and, therefore, these sols may coagulate. These predictions are confirmed by a detailed investigation of the coagulation behaviour of the mixed suspension.

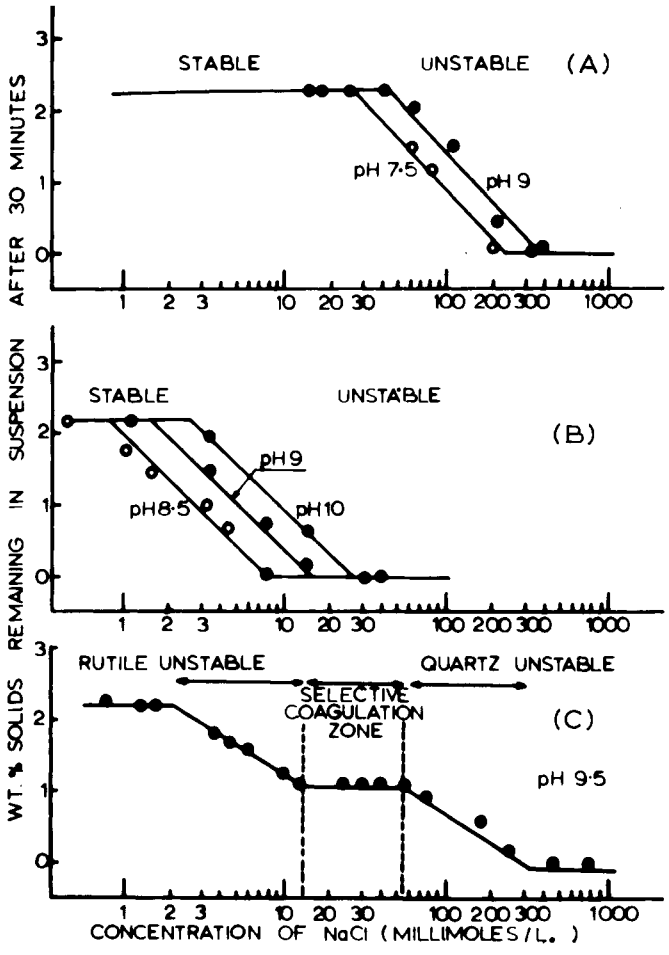

Fig. 8. Stability regions for (A) quartz, (B) rutile and (C) quartz + rutile mixtures in the pH range 7–10; conditions as in Figure 7 (from Pugh and Kitchener [1]).

Figure 9A shows the regions of stability for the two separate components throughout the pH range and Figure 9B shows that for the mixed suspension. Again, all the suspensions had 2.2 wt.% solids — in the case of mixtures, 1.1% of each. No addition of electrolyte was made in this series of experiments. From Figure 9A it can be seen that the quartz suspension became unstable at about the pH_{iep} ($\approx$2). At high pH instability was observed due to the presence of high concentrations of sodium hydroxide having the effect of reducing the double layer thickness. A similar behaviour pattern was observed for hematite instability, about the pH_{iep} ($\approx$6) and also at low and high pH values due to the presence of strong acid and alkali, respectively. A region of selective coagulation of the mixture was predicted (and found) at pH 7–

7.5 (Figure 9B), since in this region the quartz remained relatively stable (having a negative surface potential of about 60 mV) while the hematite was observed to undergo coagulation, having a negative surface potential of about 30–35 mV.

An additional series of investigations were made at pH 9, in which both components remained stable until indifferent electrolyte was added to bring about coagulation. The results are presented in Figure 10. In Figure 10A the stability regions of the individual components are shown on addition of increasing amounts of sodium chloride and Figure 10B the mixture. In the mixture the hematite was observed to start to coagulate in 0.01–0.015 M NaCl. In 0.15 M NaCl at pH 9 the quartz was stable, having a zeta potential of about 70 mV. Coagulation of the quartz suspension began to occur when the electrolyte concentration was increased to about 0.1 M.

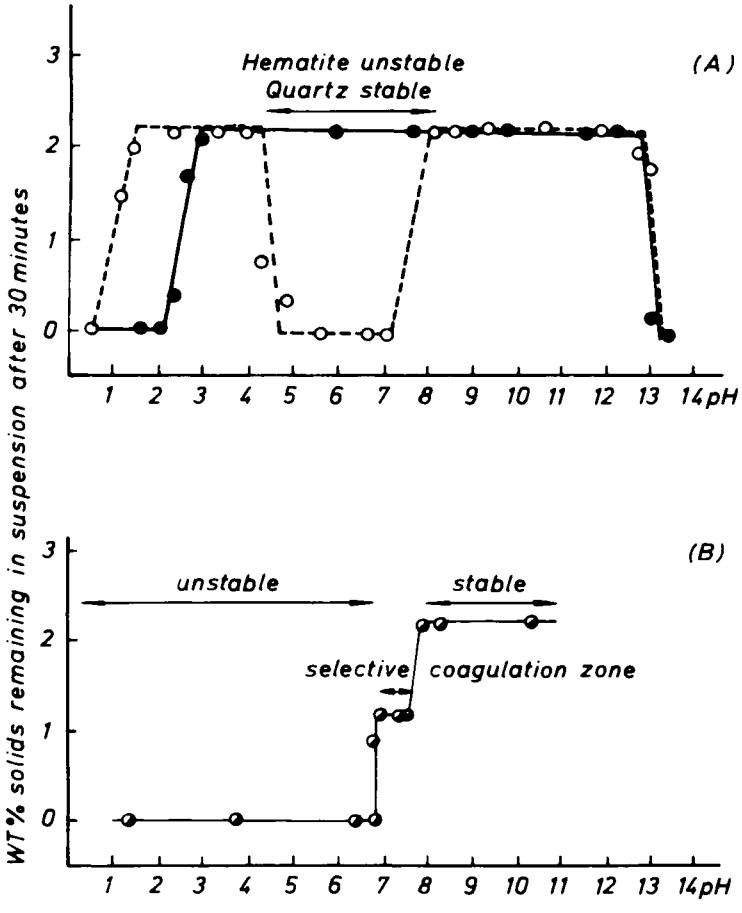

Fig. 9. The stability regions without addition of electrolyte: (A) the hematite suspension (o) and the quartz suspension (●); (B) the hematite/quartz mixed suspension. Conditions as in Figure 7 (from Pugh [2]).

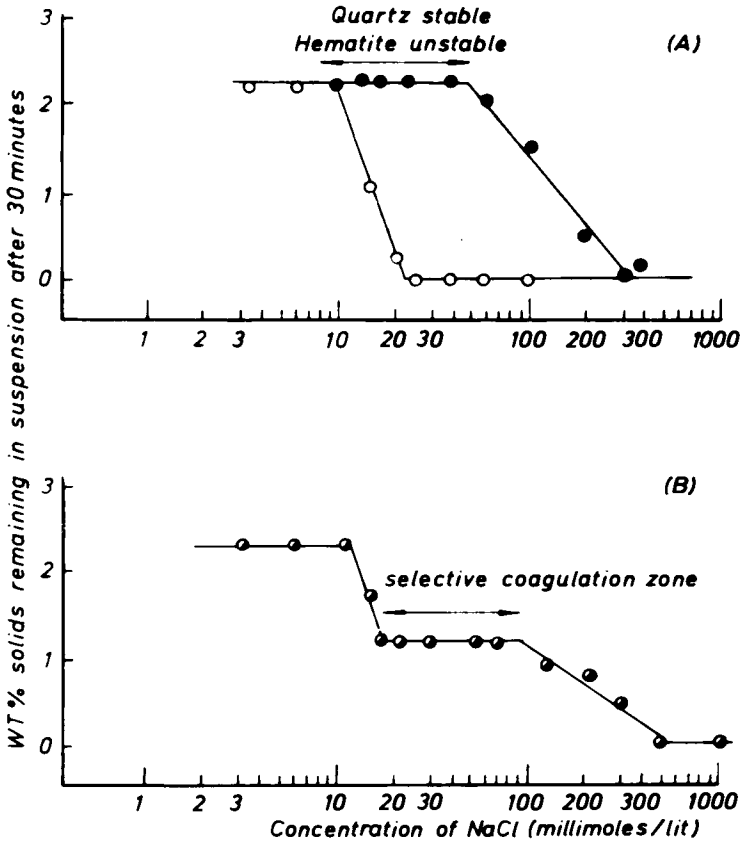

Fig. 10. The stability regions over a range of NaCl concentrations of: (A) the hematite suspension (o) and the quartz suspension (•); (B) the hematite/quartz mixed suspension at pH 9. Conditions as in Figure 7 (from Pugh [2]).

This study of the coagulation characteristics of the system indicated that selective coagulation should occur between 0.015 and about 0.1 M NaCl. In this region the quartz remained stable and the hematite coagulated while both components again retained a negative surface potential. Analysis of sediment and supernatant in the selective coagulation regions are shown in Table 2.

Latex/mineral mixtures

The colloidal stability of different types of mixed colloidal materials such as latex and mineral has become particularly interesting in recent years, since they can be utilized as models to study industrial processes such as the impregnation of fabrics or the preparation of filled and pigmented polymers. Recently, the interaction

TABLE 2

Supernatant and sediment analysis in the selective coagulation regions (in Figures 9 and 10) for the SiO_2/Fe_2O_3 system [2]

Fig no.	pH	Electrolyte concentration (NaCl) M	Supernatant liquid analysis (%)		Sediment analysis (%)	
			SiO_2	Fe_2O_3	SiO_2	Fe_2O_3
9B	7	–	98	2	16	84
10B	9	0.022	99	1	8	92
10B	9	0.033	99	1	8	92
10B	9	0.05	98	2	9	91

between particles of spherical hematite and polymer latex (polytetrafluoroethylene, PTFE) of comparable size have been studied by Visca et al. [3]. The stability of the dispersions was measured as a function of pH and ionic strength, over a wide range of surface potentials, where conditions of selective coagulation and hetero-coagulation could be predicted. The colloidal hematite (narrow size distribution with average diameters about 0.05 μm) were prepared by precipitation from ferric chloride solution as previously described [9]. The particles were carefully washed to remove impurities and the size distribution determined by electron microscope. The PTFE particles were extensively dialyzed and purified with mixed ion-exchange resins to remove surfactant. The electrokinetic properties of the two types of particles (as a function of pH) are shown in Figure 11. The pH_{iep} of the hematite was found to be about pH 6 whereas the PTFE was shown to have a negative charge over the pH range of interest.

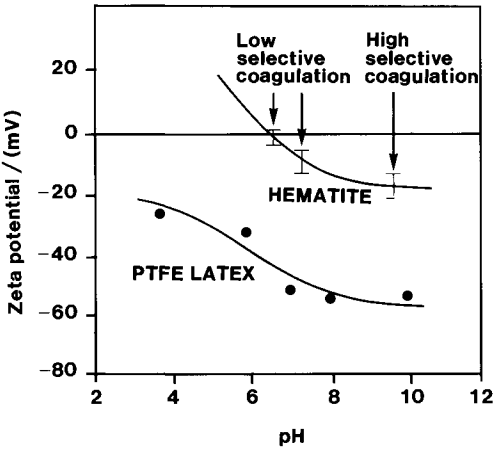

Fig. 11. Zeta potential versus pH for PTFE latex (in 10^{-3} M KNO_3) and hematite (in $\approx 10^{-3}$ M KNO_3) (from Visca et al. [3]).

The relative stability of the α-Fe_2O_3, PTFE latex and mixed dispersions was assessed by determining the concentration of particles remaining in the supernatant solution at different ionic strengths and pH values, after a pre-determined time following the dispersion of the components. The interaction of the mixed systems was studied over the neutral and alkaline pH range where both particles were negatively charged. Simply by minor adjustment of the pH, two different situations were created; in the first case the magnitude of the surface potential on the two different types of particles was comparable whereas in a second case a significant different in potential on the two types of particles was obtained. At pH < 6 the particles had opposite charge and heterocoagulation occurred.

The results of the investigation are presented in Table 3. Table 3A shows the experiments carried out with equal amounts of α-Fe_2O_3 and PTFE latex (total particle concentration 1.2×10^{12} cm^{-3}) at pH 9.4 at a range of electrolyte concentrations. The results confirm that fairly good selective coagulation could be achieved by slow coagulation of the dispersion (about 20 hours) in medium strength electrolyte concentrations (3.6×10^{-2} and 5×10^{-2} M). At higher electrolyte concentrations (7×10^{-2} and 1×10^{-1} M), both components in the dispersion coagulated. The suspensions appear to remain fairly stable at lower electrolyte concentrations for shorter time periods. At pH values within the neutral range (Table 3B, C) with differences in α-Fe_2O_3/PTFE ratio it was also found difficult to selectively coagulate these mixtures.

In an attempt to explain these experimental results, theoretical interaction energy curves for PTFE/PTFE, α-Fe_2O_3/α-Fe_2O_3 and PTFE/α-Fe_2O_3 in water were calculated. Unfortunately, the coagulation kinetics of the systems were not considered by the authors and no attempt was made to calculate *the rates* of coagulation for the various combinations of particles in the mixture. Since the rates are functions of the concentration of particles and size, it is not sufficient to adopt interaction potential criteria to distinguish rate in a mixture. However, the authors showed major differences in the characteristic interaction energy curves for the two types of particles, due to differences in surface potential and values of the Hamaker constant.

Clay mixtures

In mixtures of colloidal clays with different charge or particle size, there exist the possibilities of selective coagulation occurring in dilute electrolyte solution. From the theoretical curves presented in the section on "DVLO theory applied to selective coagulation", it would appear that for clays with the same sign but different magnitude surface charge, selective coagulation would more likely occur in larger particle size systems. However, with hydrophilic colloids such as clays, water "structures" near the surface may reduce the range of the Van der Waals forces and

TABLE 3

Selective coagulation in colloidal latex (PTFE)/mineral (α-Fe_2O_3) mixtures

	pH	Zeta potential		Average particle diameter of hematite (μm)	Original ratio α-Fe_2O_3/latex	Total particle concentration	KNO_3 concentration (mole dm^{-3})	Coagulation time	Particle fractions remaining in suspension		Selectivity
		Latex	α-Fe_2O_3						PTFE	α-Fe_2O_3	
A	9.4	−40	−26	0.045	1	1.2×10^{12}	3.6×10^{-2}	1	1	0.8	Low selectivity
	9.4	−40	−26		1	1.2×10^{12}	3.6×10^{-2}	2	1	0.5	Low selectivity
	9.4	−40	−26		1	1.2×10^{12}	3.6×10^{-2}	20	0.9	0.1	*High selectivity*
	9.4	−34	−22	0.045	1	1.2×10^{12}	5×10^{-2}	1	0.9	0.7	Low selectivity
	9.4	−34	−22		1	1.2×10^{12}	5×10^{-2}	2	0.9	0.5	Low selectivity
	9.4	−34	−22		1	1.2×10^{12}	5×10^{-2}	20	0.7	0.1	*High selectivity*
	9.4			0.045	1	1.2×10^{12}	7×10^{-2}	1	0.3	0.1	Both components
							7×10^{-2}	20	0	0	coagulated
	9.4	−30	−20	0.045	1	1.2×10^{12}	1×10^{-1}	1	0.1	0.1	Both components coagulated
B	7.1	−65	−22	0.057	2	1.5×10^{12}	1×10^{-2}	20	1	1	Individual components remain stable
	7.1	−57	−15	0.057	2	1.5×10^{12}	3.5×10^{-2}	20	0.67	0.47	Poor selectivity
C	6.5	−40	−15	0.045	0.5	1.8×10^{12}	1×10^{-2}	20	0.9	0.7	Poor selective
		−39	−12	0.045	0.5	1.8×10^{12}	2×10^{-2}	20	0.6	0.4	coagulation
					0.5	1.8×10^{12}	4×10^{-2}	20	0	0	Both components
					0.5	1.8×10^{12}	7×10^{-2}	20	0	0	unstable

will additionally produce repulsive hydration forces at close distances. These have not been considered in DLVO theory.

Frey and Lagaly [10] carried out detailed experiments using model clay colloids consisting of sodium smectites which are composed of negatively charged silicate layers about 1 nm thick. Experiments were carried out with high charged and low charged systems and the type of coagulation which occurred (assuming predominant face–face interactions) was determined from crystal analysis of the sediment. For example, for two components consisting of A and B, then in cases of selective coagulation, the coagulate will consists of a *mixture of separate "crystallites"* (i.e. crystallites of layer A and crystallites of layer B). If plates A and B coagulate together (with no selectivity occurring) then they will aggregate in the *same crystal* (producing mixed layer crystals). Hence, the layer sequence of A and B in the crystal can be regular, zonal or random (see Figure 12). A convenient method for analysis of the crystallite structure (to determine the extent of selective coagulation) was carried out by exchanging Na^+ for alkyl ammonium ions and determining the basal spacing of the crystals by X-ray analysis.

In the experimental studies, both low and high charged smectites (montmorillonite and beidellite) were chosen as models. For these systems the interlayer cation density of the colloids was not constant throughout the individual crystals and varies between 16.1 and 24.5 μC cm^{-2} (average 19.2 μC cm^{-2}) for montmorillonite and between 20.1 and 34.7 μC cm^{-2} (average 25.9 μC cm$^{-2)}$ for beidellite (Figure 13A, B). Also two particle fractions <0.1 μm and 0.1–2 μm were chosen.

Critical coagulation concentrations (CCC), corresponding to the lowest electrolyte concentrations to cause face–face coagulation of the separate smectite sys-

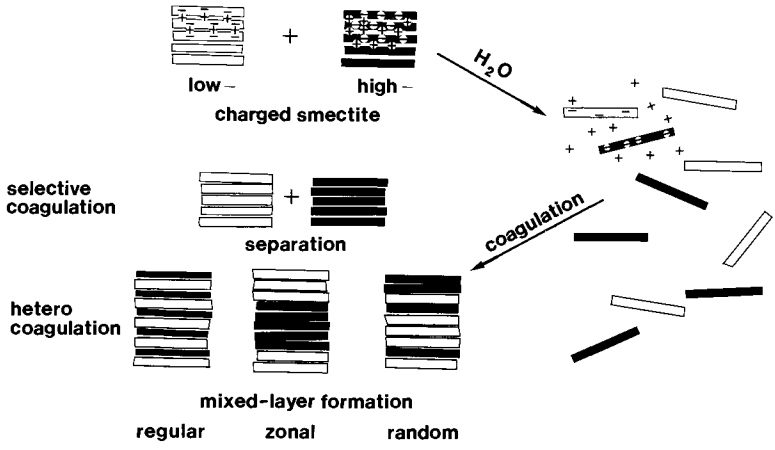

Fig. 12. Disintegration of sodium smectite crystals in water, formation of colloidal suspensions and reaggregation to crystals (surface charges and interlayer cations not entirely shown) (from Frey and Lagaly [10]).

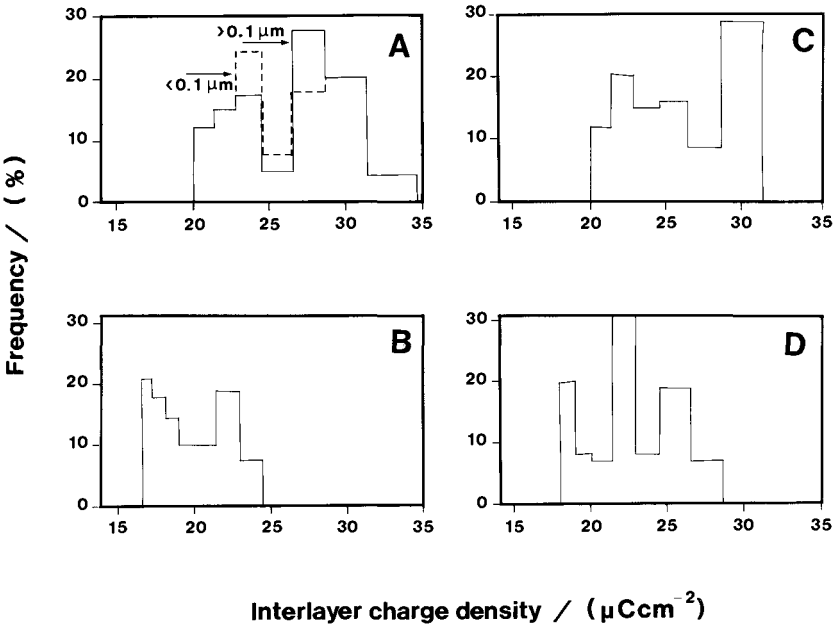

Fig. 13. Interlayer cation densities: A. beidellite; B. montmorrilonite; C. after coagulation of mixed colloidal suspensions, fractions 0.1–2 μm, high-charged component; D. after coagulation of mixed colloidal suspensions, fractions <0.1 μm (from Frey and Lagaly [10]).

tem and for mixtures was determined. To prevent edge–face-coagulation occurring in these systems, it was necessary to add sodium diphosphate (which specifically adsorbs on positively charged edges) and increases the negative charge on the sites. Thus the CCC for edge to face aggregation was increased and became similar or exceeded the concentration required for face-to-face aggregation. The CCC in diphosphate solution was therefore taken as the approximate concentration of face-to-face

TABLE 4

Critical coagulation concentrations (CCC) of sodium chloride in sodium smectite suspensions (0.25 g smectite l^{-1}, pH 6–7) [10]

Smectite	$\bar{\zeta}/2$ [a]	Fraction (μm)	CCC (moles Na^+ l^{-1} in 0.01 M $Na_4P_2O_7$ solutions)
Beidellite	13.0	0.1–2	0.25–0.29
	12.8	<0.1	0.26–0.29
Montmorillonite (Cyprus)	11.3	0.1–2	0.33–0.38
Montmorillonite (Wyoming)	9.6	0.1–2	0.37–0.44
	9.6	<0.1	0.36–0.44

[a] $\bar{\zeta}/2$: average surface charge density (μC cm^{-2})

TABLE 5

Average cation densities $\bar{\zeta}$ of pure and coagulated smectites [10]

Fraction (μm)	Starting materials		After coagulation with NaCl	
	Smectite	$\bar{\zeta}$ (μC cm^{-2})	Coagulum	$\bar{\zeta}$ (μC cm^{-2})
0.1–2	Beidellite	25.9	High-charged crystals	25.5
	Montmorillonite	19.2	Low-charged crystals	≈19
<0.1	Beidellite	25.6		
	Montmorillonite	19.2	Mixed-layer crystals	22.0

coagulation. The results of the coagulation experiments are shown in Table 4.

For the beidellite, both particle size fractions show approximately the same CCC whereas the montmorillonite samples appear to be more stable. Coagulation of beidellite–montmorillonite mixed suspensions were carried out under a range of experimental conditions (smectite concentration, pH, very slow and fast additions of NaCl, etc.) and the following conclusions were drawn:

(1) The particle size of the colloid had the predominant influence on the type of coagulation which occurred.

(2) Larger particles (>0.1 μm) were selectively coagulated. Even rough inspections of the X-ray diagrams reveal that the coagulum consist of crystals of higher-charged layers and crystals of lower-charged layers. The charge distribution histograms (Figure 13C, D) indicate that the high-charged crystals have a similar but by no means identical layer sequence in comparison with pure beidellite (see Table 5). With the appropriate choice of concentrations, beidellite-like plates could be selectively coagulated, while the montmorillonite-like plates remained in colloidal suspension.

(3) Small particles (<0.1 μm) were coagulated to mixed-layer crystals; the charge distribution curve (Figure 13D) clearly showed that high- and low-charged layers are aggregated in the same crystals. However, the mixing of the layers was not completely random.

These experiments show clearly that the low-charged plates segregate predominantly from higher-charged ones, providing the particle size exceeds a critical value. Selective coagulation could not be achieved with small plates.

Natural water systems

The transport of mixtures of colloidal clay particles from freshwater to estuaries (where a salinity transition occurs) may be accompanied by a change in stability. This may be caused by the change in double layer thickness. For fresh water κ^{-1} is typically in the range of 5 to 20 nm. In seawater κ^{-1} is of the order of 0.4 nm which is of a magnitude similar to the radius of the hydrated ion. The double layer

in seawater may therefore be considered to be non-diffused. Clay minerals are the most common colloids in natural water systems and in low salinity water (fresh), a strong negative repulsion usually dominates producing stable suspensions. However, on increasing κ, the double layer is reduced producing flocs whose size and settling rate may be several orders of magnitude higher than the individual particles. In addition, most clay minerals have a relatively high surface area per unit mass so that interparticle forces which control perikinetic coagulation are at least as important as hydrodynamic forces under mild turbulent flow conditions.

In natural water systems containing different types of clay mixtures (all predominantly having the same sign of charge), then it may be anticipated that there would be extensive possibilities of selective coagulation occurring naturally as the clay suspensions are gradually transported to the mouth of the estuary. Evidence for the occurrence of selective coagulation can often be obtained from analysis of the estuary sediment. A detailed investigation dealing with the stability of clay colloids along the 35 mile length of the Pamlico Estuary (flowing from Washington, D.C., USA), was carried out by Edzwald et al. [11]. The salinity of the water was reported to vary

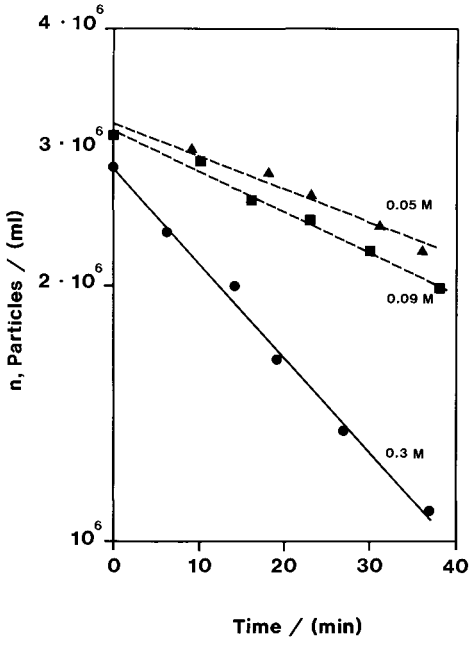

Fig. 14 (left). Coagulation kinetics of kaolinite in buffered NaCl solutions at three ionic strengths. Volume of colloidal particles per volume of suspension 8.81×10^{-5}, root-mean-square velocity gradient 52.4 s^{-1} (from Edzwald et al. [11] with permission).

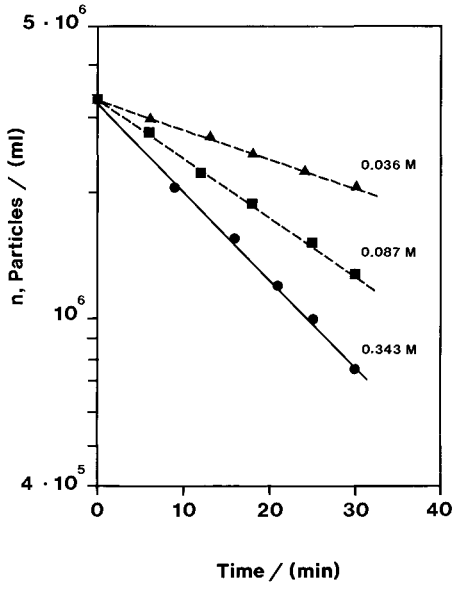

Fig. 15 (right). Coagulation kinetics of kaolinite in synthetic estuarine solutions at three ionic strengths. Volume of colloidal particles per volume of suspension 8.67×10^{-5}, root-mean-square velocity gradient 52.3 s^{-1} (from Edzwald et al. [11] with permission).

TABLE 6

Stability constants for clays in buffered sodium chloride and synthetic estuarine solutions [11]

Ionic strength	Montmorillonite	Kaolinite	Illite
Stability value (buffered NaCl solution)			
0.036 M	0.0075 ± 0.009	0.0245 ± 0.007	0.0128 ± 0.003
0.087 M	0.089 ± 0.006	0.0308 ± 0.004	0.0275 ± 0.005
0.3 M	0.125 ± 0.005	0.0724 ± 0.007	0.0455 ± 0.055
Stability values (synthetic estuarine solution)			
0.036 M	0.0943 ± 0.003	0.0445 ± 0.002	0.0180 ± 0.003
0.087 M	0.113 ± 0.019	0.0915 ± 0.006	0.0701 ± 0.007
0.343 M	0.148 ± 0.006	0.138 ± 0.009	0.0740 ± 0.009

from <0.5 ppt (parts per thousand) to 16 ppt at the mouth. From this study it was generally concluded that kaolinite (a relatively unstable clay) was easily coagulated and deposited in the upstream sediment, whereas illite (a more stable clay) was coagulated and deposited nearer the mouth. There was also a considerable amount of evidence that selective coagulation occurred naturally, along the length of the estuary giving separate fractions.

Initially, detailed experiments were carried out in the laboratory to determine coagulation rates for model clay in sodium chloride solution (pH adjusted to 7.8–8.2) buffered at three ionic strength values and in synthetic estuary electrolyte. Coagulation was carried out under mild shear conditions and typical coagulation plots at the three ionic strengths are shown in Figures 14 and 15. Following Smoluchowski's theory of orthokinetic coagulation, the change in particle number concentration with time could be related to the stability constant for the systems. The change in clay particle numbers over time was observed by using microscopic counting and coulter counter techniques. Values of the stability constant were evaluated from the slopes (Figures 14, 15) and are summarized (Table 6).

From these results, it can be seen that the stability constant increases with increase in ionic strength for both systems (complete destabilization would be characterized by a value of unity). Comparison of sodium chloride solution with the estuary solution indicates higher stability constant values with the estuary water, at about the same ionic strength. This can be expected since the estuary water is known to contain divalent cations. In addition, it was found from the experiments that the clays generally followed the order of stability; (stable) illite > kaolinite > montmorillonite (unstable). To find evidence for selective coagulation in the Palmlico River, sampling of the sediment was carried out and the results compared with the laboratory experiments. Analysis of the sediment composition (<2 μm size fraction) was carried out by X-ray crystallography. Sediment samples were taken at a range of salinity levels from estuary fresh water to points in the upper and lower estuary.

In Figure 16 the change in salinity of the surface water versus distance downstream is shown and in Figure 17, the relationship between the clay sediment composition and the location of the downstream sampling points. These results suggest that the kaolinite selectively coagulates in the upper estuary, where the salinity is lowest and very little was found to be present in the downstream sediments. However, very little illite was found in the upper estuary where it appeared to remain stable but coagulated downstream at higher salinity levels. Montmorillonite was found to be present in minor amounts along the entire length of the estuary indicating an intermediate stability level for this clay. Generally, it was concluded that the results

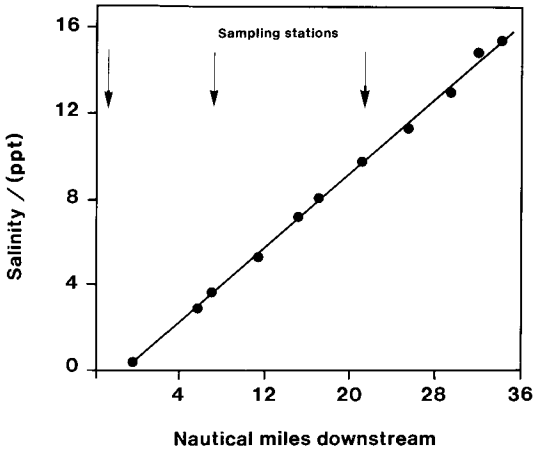

Fig. 16. Salinity of the surface waters of the Pamlico River Estuary (from Edzwald et al. [11] with permission).

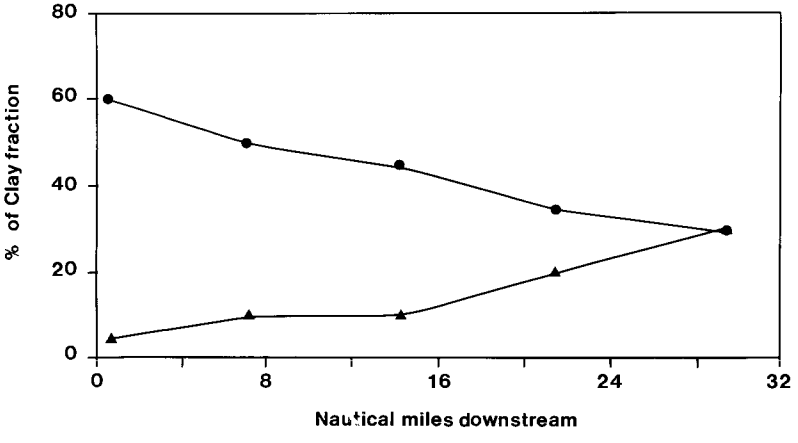

Fig. 17. Clay mineral composition of the Pamlico sediments downstream, kaolinite (●) and illite (▲) (from Edzwald et al. [11] with permission).

of the sampling study were in general agreement with the laboratory experiments in which the individual components were coagulated. This suggested that selective coagulation of the clay colloids was occurring along the length of the estuary, due to the change in ionic strength. Unfortunately no zeta potential measurements or particle size measurements were carried out.

Other examples of selective coagulation in marine environments have also been reported. Parham [12] also found that the landward accumulation of kaolinite relative to illite and smectite occurs during the transport of clays from fresh to saline waters. Thomas and Murray [13] explained the distribution of clay minerals in the Portland Creek area of the Mississippi bay by selective coagulation. The amount of kaolinite found in the area increased west to east and the smectite east to west. Selective coagulation of clays in natural water systems has also been discussed by Gibbs [14].

The coagulation and deposition of suspended solids can have a significant effect on water quality, especially with regard to the biological oxygen demand. Also silting and the formation of deltas and the coagulation of secondary treatment wastes from sewage plants are also important problems to consider. Selective coagulation studies of the colloidal constituents in natural water offers opportunity to control such phenomena. Unfortunately with clay systems, only simplified theories can be used to predict the stability rates which do not incorporate the effects of edge to face coagulation or stabilization by adsorption of trace amounts of hydrolyzed cations.

Different sized particles

It has been shown that selective coagulation may be achieved in hetero-dispersed colloidal systems based on a difference in particle size. For example, Iler [15] showed that larger particles of colloidal silica could be selectively coagulated from the small fraction by careful control of the coagulation condition using calcium ions. Particles of 4 to 130 nm average diameter were studied at the pH range 8.1 to 9.5. Also Frens [16] reported that smaller particles of gold sols were more stable against coagulation with electrolyte, compared to larger particles. In the latter case, however, differences in Hamaker constant were used to explain the results.

Selective coagulation of mineral slimes in magnetic separation processes

The control of the balance of magnetic forces with electrostatic and Van der Waals interactions can also be applied, as an effective coagulation/separation technique for mineral fines. In a homogeneous magnetic field the total interaction potential between the surfaces of colloidal particles may be modified (to a first approximation) to include the magnetic interaction V_M:

$$V_T = V_E + V_A + V_M \tag{10}$$

In strong magnetic fields the value of V_T (separating the primary minimum and secondary minimum) can be reduced, and coagulation may occur, even in cases where the particles have an electrostatic repulsive potential.

Calculations of V_T and coagulation rates suggest that particles such as hematite can flocculate in magnetic fields of about 0.1 T (background magnetic induction) for 1 μm particles and about 3 T for 10 μm particles of mineral slurry with about 10% v/v [17]. Hence, although the magnetic field can suppress V_T for a broad range of particle sizes, for larger particles ($\geq$50 μm) a field greater than 10 T will be required to induce fairly rapid magnetic coagulation. However, since mineral slimes generally contain particles <40 μm (with an average size of about 10 μm) then high gradient magnetic fields in modern separators may easily render the dispersions unstable. In such cases, the surface forces (including magnetic forces) will have an important influence on the probability of capture of a magnetic particle on a matrix, the stability of the build-up profile on the matrix and also possibly the coagulation of the particles in suspension. In the case of low magnetic fields, then electrostatic repulsion may predominate and prevent capture. However, in the case of high magnetic fields with low electrostatic repulsion, although the total interaction will be positive and coagulation may occur, it is also important to consider the hydrodynamic shear stress near the surface of the matrix which may strip-off the particles under high shear flow.

In theory, if we consider two colloidal minerals with different pH_{iep} values, then it should be possible to increase the efficiency of the metallurgical separation process

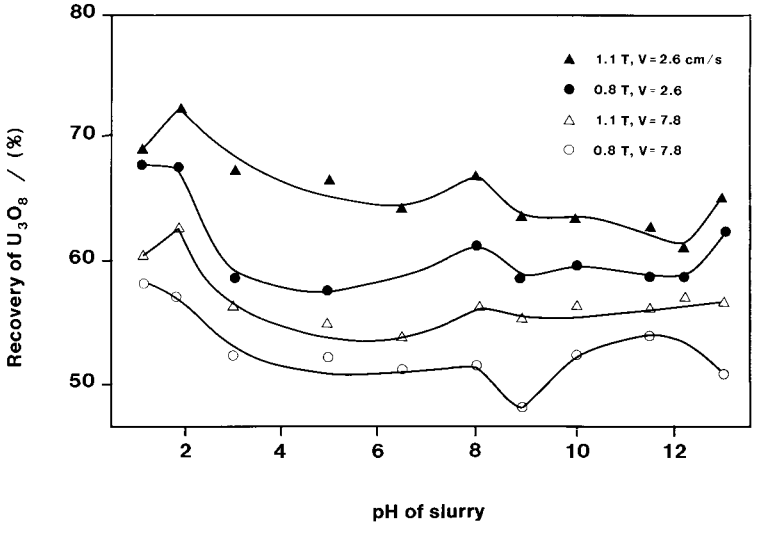

Fig. 18. The dependence of U_3O_8 recovery on the pH of the slurry in magnetic separation on a woven wire-mesh matrix at a range of induction strengths (T) and flow rates (V) (from Svoboda et al. [18] with permission).

by adjustment of the pH (so that both components have significant difference in like charge) before passing through the high grade magnetic separator. An interesting example of what appears to be selective coagulation occurring under a magnetic field, has recently been reported in the separation of uranium/gold tailings from gangue in Witwatersrand, South Africa [18]. In this plant it was found that the highest performance of the separator occurred at a pH value at which the valuable and gangue minerals were the same sign, but not far removed from the pH_{iep} of the valuable mineral.

Trials were carried out with uranium/gold tailing consisting of cyanide leaching residues of complex ores containing quartz, chlorite, mica, pyrophyllite with the valuable minerals present in a variety of forms. The experiments were carried out over a range of pH values (from pH 1.3 to 13) simply by addition of HCl and NaOH. The results shown in Figure 18 relate the dependence of uranium recovery to the pH for a mesh matrix for various values of the magnetic induction and flow rates. The maximum recovery was achieved between pH 1.2 and 1.8 and the recovery decreases with increase in pH. The difference between the maximum recovery and the recovery corresponding to the natural pH of the tailing (pH $\approx$ 9) was about 8% for a mesh matrix and 5% for a ball matrix irrespective of the magnitude of the magnetic field and the flow rate. In Figure 19 the influence of pH on the grade of the magnetic concentrate is shown. The maximum grade was achieved at about pH

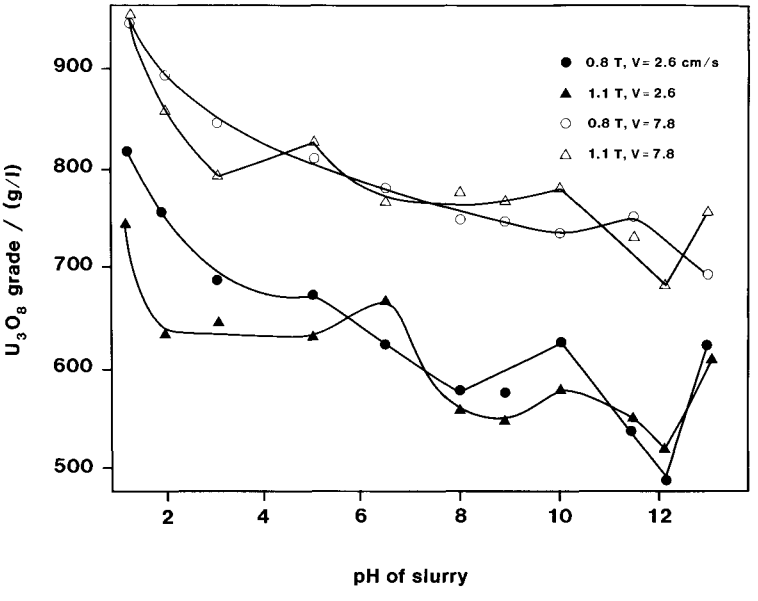

Fig. 19. The depencence of slurry pH on the grade of the U_3O_8 of the magnetic concentrate for a mesh matrix at a range of induction strengths (T) and flow rates (V) (from Svoboda et al. [18] with permission).

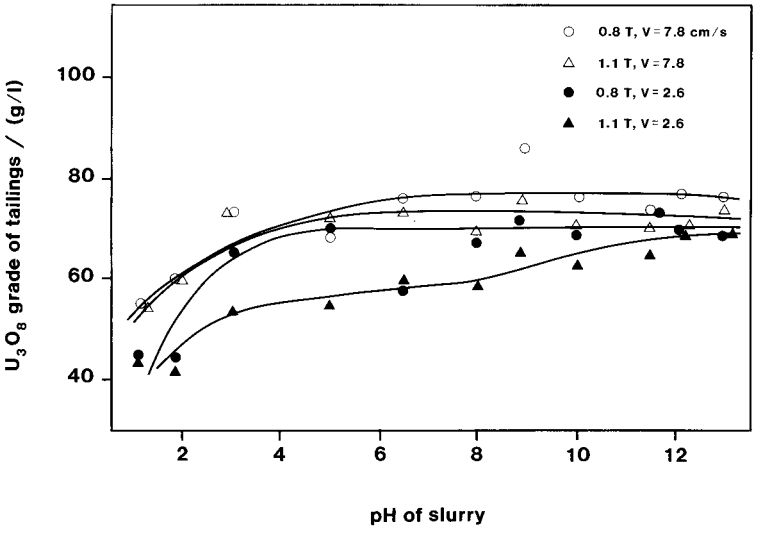

Fig. 20. The dependence on U_3O_8 grade on pH of the slurry of non-magnetic fraction for a mesh matrix at a range of induction strengths (T) and flow rates (V) (from Svoboda et al. [18] with permission).

1.2 and decreased with increase in pH, although a secondary minimum appeared to occur at pH 10. The difference between the maximum grade (pH 1.2) and that at pH 9 is about 20% for both types of matrices at a range of flow rates and magnetic field strengths. As expected, the opposite tend is observed for the non-magnetic fraction (Figure 20); the lowest grade occurring at pH 1.2 and increases by about 20% at the alkaline pH values.

In Figure 21 the zeta potential/pH plots for the mineral particles is shown. The uranium rich ore shows a similar curve to the uraninite ore where the pH_{iep} lies in the pH range 3.0 to 3.2. In the case of the uranium-poor ore, the curve is similar to that of the quartz with the pH_{iep} lying between 2 and 2.3. Generally, the quartz fraction was associated with a low uranium content whereas the iron/quartz fractions (with slightly higher pH_{iep}) were usually enriched with the valuable uranium minerals. In the pH region 1.2 to 1.8 (<1.8) both particle fractions were positively charged but different in stability, especially in the presence of the magnetic field were reported. The gangue fraction did not response to the magnetic field to any great extent. However, on increasing the pH to 2–4, heterocoagulation was thought to occur causing the grade to decrease rapidly. At pH 1.2 both colloidal systems were unstable to some extent but a high grade of concentrate with low entrapment of quartz particles was obtained in this region. Generally, the process appeared most selective in the region of pH 1.2 to 1.8.

For some other types of uranium-rich ores (usually containing iron and aluminium) then the pH_{iep} was shifted to pH 8–9. Under these circumstances then the

pH region 3–9 has to be avoided since the minerals would have opposite charge (assuming quartz gangue has a $pH_{iep} \approx 2$). Under these circumstances high quality concentrates with low quartz entrainment could be obtained at pH 1–2 with the grade rapidly decreasing at pH 2–4 due to coagulation of quartz with uraninite. Also, at pH > 9 good selective separation could also be achieved with increase in grade. From the trials it was concluded that the quality of the magnetic concentrate could be enhanced by about 20% for uranium and about 25% for gold and the recovery of uranium increased by about 6–8% simply by adjustment of pH. (Generally, the gold recover followed the uranium recovery). Also it was reported that no improved recovery of valuable mineral could be achieved by increasing the magnitude of the magnetic field.

Selective coagulation in the presence of magnetic fields would also appear feasible in the areas of water treatment, where finely divided mineral particles with ferromagnetic properties have been successfully used, as a separation technique. When the particles are magnetized they flocculate very strongly giving large flocs with high sedimentation rates comparable to much larger size particles. The feasibility of using similar concepts have been demonstrated for ion exchange reactions utilizing magnetic polymers and for a new water clarification and decolorization process using an alkali treated magnetite. Also magnetic activated carbon particles have been used which selectivity adsorbed small organic molecules. These processes have been reviewed by Bolto [19].

In laboratory experiments, Kallay and Matijevic [20] studied the effects of surface

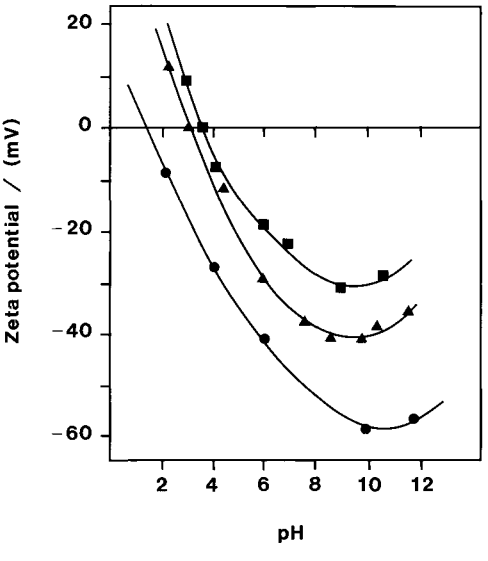

Fig. 21. Zeta potential verus pH plot of an uranium rich ore (▲), uraninite (■) and uranium-poor ore (●) (from Svoboda et al. [18] with permission).

potential, ionic strength and magnetic field on the capture of spherical α-Fe_2O_3 colloidal particles from aqueous solution onto stainless steel balls ($\approx$30 μm). The steel balls were packed in a column and the hematite sol (in neutral electrolyte) fed through the chamber containing the beads. Under these conditions the deposition rate depends on both influence of the magnetic interaction on the α-Fe_2O_3 particles (ordered aggregates can be formed in suspension) as well as between the α-Fe_2O_3 particles and the steel balls. As the surface of the steel collector bed gradually became coated with patches of adhered particles, a reduction of the attachment rate was also reported. This was particularly pronounced at high coverages. This effect occurred in systems where the substrate and particle were opposite in charge due to the repulsion between deposited and incoming colloidal particles.

Selective coagulation by hydrophobic forces

In addition to the control of the magnetic and electrostatic surface potentials, colloidal particles may also be separated using "non-DLVO" forces such as the hydrophobic/hydrophilic interaction.

For example, in Figure 22 the stability to coagulation and zeta potential data is shown (as a function of pH) for both fresh and low temperature oxidized coal [21].

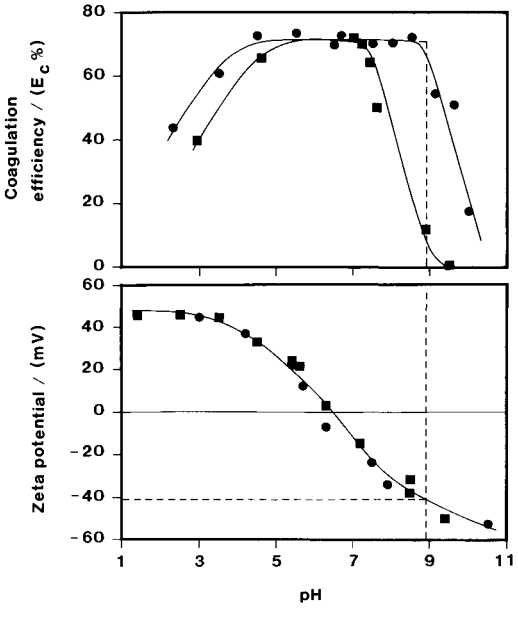

Fig. 22. Coagulation and zeta potential measurements on fresh (●) and oxidized (■, 140°C) coal samples as a function of pH. The coagulation efficiency refers to the amount of coal remaining in suspension after a predetermined coagulation time (from Xu and Yoon [21]).

Although the zeta potential results would suggest identical electrostatic colloidal stability, the fresh coal is shown to be unstable under a much wider range of pH values (pH 3.8 to 8.9). In this system it would appear feasible to selectively coagulate the fresh hydrophobic coal from the oxidized hydrophilic coal by carefully adjustment of the pH to between 9 and 11. Quartz would also be an interesting system to study under similar conditions since the hydrophobic/hydrophilic balance of the surface can also be easily controlled by heat treatment [22].

Selective coagulation by magnetic and hydrophobic forces

The separation of titanium-bearing minerals (anatase and rutile) from fine kaolin have been achieved by magnetic seeding a slurry [23]. It was found that both chemically precipitated and ground magnetite could be used in the process. The separation was achieved in a wire wool matrix with the titaniferous impurities attached to the magnetite. It was also shown that the process could be improved with fatty acids as hydrophobizing agents [24]. A proportion of the magnetite was removed in an initial flotation step, reducing the load on the subsequent magnetic separation process. It was proposed that the titanium minerals were selectively hydrophobically coagulated with the magnetite. Magnetite has also been used to selectively coat calcite and dolomite in conjunction with sodium oleate, in the separation of carbonates from phosphate slurries [25].

Suspension filtration processes

Selective coagulation would also appear feasible in combination with filtration, as an effective separation technique for dilute suspensions. Again adjustment of pH can be used to control the extent of charge. No application of the technique is known by the author.

Other examples of selective coagulation of mineral particles reported in the literature

In industry, attempts to plan separations of mineral suspensions by selective coagulation by theoretical calculation have not been attempted to date. However, there appears to have been several other examples reported in the literature indicating that slow selective coagulation can occur under favourable conditions.

Schwerin [26], as early as 1912, patented a method for partially separating finely divided particles, i.e. sand and iron ore, from a natural aggregated clay mixture, by dispersing the minerals with what was described as a "non-neutral colloidal body",

such as humic acid, silicic acid or acetic acid, and then finally adding a strong base or acid as a coagulant. Several years later, Feldenheimer [27], using a similar clay mixture succeeded in coagulating the finely divided particles with tannic acid or gum arabic, subsequently adding just sufficient sodium chloride or sulphuric acid to coagulate the remaining hydrated clay suspension. After sedimentation was complete, it was possible to observe two distinct layers at the bottom of the vessel, a layer of clay on top of a layer of impurities. A similar separation achieved by adding a critical amount of electrolyte has been reported by Codding [28].

More recently, a technique has been developed by Maynard et al. [29] for removing coloured titanium dioxide mineral impurities from kaolin. The process, apparently discovered empirically, produces a state of slow coagulation of the coloured impurities of titanium and is achieved by dispersing china clay, at about 30% solids, in a solution of sodium hexametaphosphate containing about twice what would be needed for optimal dispersion (judged by minimal viscosity). The resulting slurry presumably undergoes slow coagulation. After a period of 14 hours or more of standing, it is observed that highly discoloured vertical bands appear which subsequently disappear while a yellow sludge slowly collects at the bottom. These coloured impurities (consisting of the titanium minerals, etc.), are present only to the extent of about 1 to 4 percent in the original clay. After a sufficient time (20 hours in an 11 inch column) the coloured material settles to the bottom and the kaolin slurry is decanted and used, its "brightness" as a pigment having been usefully enhanced. It seems from the observations reported that the particles of titanium minerals must have coagulated selectively with one another but not with kaolin particles, nor have kaolin particles coagulated with kaolin appreciably.

There are, in addition, reported cases of selective coagulation achieved by addition of small amounts of surface active substances, which selectively adsorb on the surface of mineral mixtures and appear to have a considerable influence on the zeta potentials and stability of the individual components. A study has been made of the adsorbability of quaternary ammonium components on colloidal clays by measurement of the zeta potential and the stability of the systems recorded in terms of sedimentation volumes [30]. It was observed that the sedimentation volume of the clay minerals attained a maximum value about the point of pH_{iep} as anticipated. In addition, however, the adsorption of the surface active compounds was found to be selective, depending on the type of clay, and by working at or near the maximum differences in sedimentation volumes or zeta potentials, two-component clay mixtures were separated more or less completely.

A further example of selective coagulation by adsorption of polar additives has been reported [31]. In the conditioning of a mixed mineral suspension, consisting of hematite and quartz or barite and quartz, it was found that the addition of a flotation collector such as tall oil, resulted in a first stage coagulation of the fine particles in the mixture. The flocs so formed appeared to be decidedly selective, containing a high percentage of the valuable minerals but very little fine quartz

or other gangue particles. The influence of electrolyte concentration and pH had also a marked effect on the separation, especially at high collector concentrations. Reduction of the pH from 9.5 to about 6.5 produced stable flocs and a high flotation yield could be achieved; but on re-adjustment of the pH by adding NaOH to a value of 9.5, the flocs became extensively dispersed, with the result that the yield and selectivity was reduced and a prolonged flotation time was necessary. It was suggested that this was due to the conversion of the molecular forms of the tall oil adsorbed on the surface to the soluble form of sodium oleate and linoleate. Also Warren [32, 33] has exploited the separation of fine grade scheelite particles in sodium oleate solution by stirring the suspension at high speed. The so-called shear flocculation was explained by formation of aggregates due to hydrophobic association.

Finally, it is also of interest to note that in the early flotation literature, the assumption was often made that the coagulation process often parallels the flotation process. This effect is particularly marked with the fatty acid and xanthate types of collectors; for example, potassium ethyl xanthate is used to render galena hydrophobic (and therefore floatable) but not only attaching non-polar (ethyl groups) but also bringing the surface potential to a low value, without having any appreciable effect on the negatively charged non-metallic gauge minerals present in the pulp. Thus, there is simultaneously a coagulation of the fine galena particles in the pulp as well as a hydrophobic coating.

Acknowledgement

The author would like to sincerely thank J.A.K. for his help and guidance with parts of this work, taken from the author's Ph.D. Thesis, Imperial College, 1972.

References

1 R.J. Pugh and J.A. Kitchener, J. Colloid Interf. Sci., 38 (1972): 657.
2 R.J. Pugh, Colloid Polym. Sci., 252 (1974): 400.
3 M. Visca, S. Savonelli, E. Barouch and E. Matijevic, J. Colloid Interf. Sci., 122 (1988): 567.
4 R. Hogg, T.W. Healy, T.W. and D.W. Fuerstenau, Trans. Faraday Soc., 62 (1966): 1638.
5 G.R. Wiese and T.W. Healy, Trans. Faraday Soc., 66 (1970): 490.
6 J.H. Schenkel and J.A. Kitchener, Trans. Faraday Soc., 56 (1960): 161.
7 J.Th.G. Overbeek, in: H.R. Kruyt (Editor), Colloid Science, Elsevier, Amsterdam, 1960, Vol. 1.
8 R.J. Pugh and J.A. Kitchener, J. Colloid Interface Sci., 35 (1971): 656.
9 J.H. van den Hull and J.W. Vanderhoff, Electroanal. Chem., 37 (1972): 161.
10 E. Frey and G. Lagaly, J. Colloid Interface Sci., 70 (1979): 46.
11 J.K. Edzwald, J.B. Upchurch and C.R. O'Melia, Environ. Sci. Tech., 8, 1 (1974): 58.
12 W.F. Parnham, in: L. Heller and A. Weiss (Editors), Proc. Int. Clay Conf., Vol. 1, Israel Prog. Sci. Trans., 1966, p. 135.

13 A.R. Thomas and H.H. Murray, Clay and Clay Minerals, 37, 2 (1989): 179.
14 R.J. Gibbs, J. Sed. Pet., 47 (1988): 237.
15 R. Iler, J. Colloid Interface Sci., 53 (1975): 476.
16 G. Frens, Kolloid Z. Z. Polym., 250 (1972): 736.
17 J. Svoboda, IEEE Transactions on Magnetics, Col. 18, No 3, 1982, p. 861.
18 J. Svoboda, I.J. Corrans and M.H.E. Spitze, Int. J. Miner. Process., 17 (1986): 83.
19 B.A. Bolt, Proc. Conf. Adsorption from Aqueous Soln., R. Aust. Chem. Inst., Div. Colloid Surf. Chem., Univ. of Melbourne, March 1978, p. 33.
20 N. Kallay and E. Matijevic, Colloid Surf., 39 (1989): 161.
21 Z. Xu and R-H. Yoon, J. Colloid Interface Sci., 132 (1989): 15.
22 R.N. Lamb and D.N. Furlong, J. Chem. Soc., Faraday Trans. I, 78 (1982): 61.
23 A.J. Nott and W.M. Price, Magnetic Beneficiation of Clays Utilizing Magnetic Particles, U.S. Patent 4,125,460 and 4,087,004, 1978.
24 J.A. Cook, Magnetic Beneficiation of Clays Utilizing Magnetic Seeding and Flotation, Patent 2,092,026A (GB).
25 P. Parsonage, Trans. Inst. Min. Metall., Sect. C, Min. Process. Extr. Metall., 93: C37.
26 B. Schwerin, U.S. Patent 1,029,579, 1912.
27 W. Feldenheimer, U.S. Patent 1,324,958, 1919.
28 M.K. Codding, U.S. Patent 1,402.740, 1922.
29 R.N. Maynard, N. Millman and J. Iannicelli, Clays Clay Miner., 17 (1969): 59.
30 S.K. Mukherjee and S.K. Chakravarti., Indian Chem. Soc., 44, 3 (1967): 167.
31 M. Clements, H. Harms and H.M. Trondle, Proc. 9th Int. Min. Prog. Congr. Chechoslav., 1970, p. 179.
32 L.J. Warren, Trans. Inst. Min. Metall., London, 84 (1975): C99.
33 L.J. Warren, J. Colloid Interface Sci., 50 (1975): 307.

Chapter 9

Flocculation

YOSRY A. ATTIA

General flocculation

Introduction and definitions

Primary particles in a dispersed system can be aggregated into larger structures by various mechanisms. Aggregation processes based on reducing interparticle repulsion (i.e. by compressing the electrical double layer thickness or by charge neutralization) are classified as coagulation and the aggregates are known as coagula. If aggregation is induced by polymer bridging action, the process is known as flocculation and the aggregates are referred to as flocs. When aggregation results from the action of an immiscible bridging liquid, such as oil in an aqueous dispersion, the process is known as agglomeration and the aggregates are referred to as agglomerates. In water treatment, metal salts are commonly used. The mechanisms involved include both those in coagulation (i.e. the action of electrolytes) and bridging flocculation by either inorganic polymeric species [1] or by the precipitating metal hydroxide. The latter is known as "sweep" flocculation [2].

Furthermore, flocculation processes using polymers have been classified according to the type of action of the polymer on the particles. For example, bridging flocculation is the result of adsorption of individual (linear) polymer molecules on several particles simultaneously, thus forming molecular bridges between the adjoining particles in the floc. If the polymer molecules are highly branched, or alternatively if two or more types of interacting (linear) polymer molecules are utilized, so that a three dimensional gel-type network, enmeshing the particles into a floc-gel, the process may be appropriately termed as network flocculation. Even with linear polymers, careful control of the polymer addition and hydrodynamic conditions can produce compact and very strong pellet-like flocs. This process is known as pelleting flocculation [3].

The action of cationic polymers on negatively charged particles can be somewhat similar to the action of coagulation, in that charge neutralization is the predominant

mechanism over polymer bridging. This observation gave rise to the "electrostatic patch" flocculation model [2]. However, this does not necessarily mean that the bridging mechanism is absent, but in fact it is always operative, epecially with high molecular weight polymers.

Flocculation by "non-adsorbing" free polymers is known as depletion flocculation. This phenomenon is observed with high concentrations of polymers in suspension; on the order of 0.1–1%, i.e. 1000–10,000 mg l^{-1}. Depletion flocculation is explained as follows [4]: when the distance between approaching particles is smaller than the size of polymer molecules, none of these molecules can enter the region between these particles, which is then composed of the solvent only. The solution outside the particles retains its bulk polymer concentration and therefore exerts an inward force arising from its osmotic pressure. This inward force causes the particles to flocculate. This theory assumes that polymer molecules have rigid conformation in solution, particles are treated as semi-permeable membranes and does not consider the free energy changes involved in bringing the particles to close approach [5]. Apparently, the free polymer can also generate repulsion between colloidal particles, because the creation of microreservoirs of pure solvent must increase the total free energy of the system. This is the origin of depletion stabilization [5]. Evidently, the basis for depletion flocculation and depletion stabilization is still unclear. All the assumptions used to explain the theory are not valid in most cases encountered in particle flocculation practice. In addition, the polymer concentrations required for this "process" are much higher than those needed for mineral particle flocculation where a fraction of 1 mg l^{-1} or a few mg l^{-1} of polymer will be sufficient. Even though proponents of depletion flocculation [4, 6] argue against bridging flocculation in the systems they studied, common experience in particle flocculation by bridging polymers suggests that polymer bridging is likely the reason for flocculation. Only a very small amount of polymer is needed for this. Such a small concentration could well be beyond the detection limit of analytical procedures used for determination of polymer concentration in those systems.

This chapter will deal mainly with bridging flocculation by linear (or slightly branched) polymer molecules, which is the main flocculation mechanism in mineral processing. For bridging flocculation to happen, the adsorption of polymer on the particles will be required. The various theories on polymer adsorption have been addressed in numerous publications and a recent summary has been given by Lyklema [7]. The forces responsible for general and selective polymer adsorption on mineral surfaces are summarized later in this chapter under "Selective flocculation".

Polymeric flocculants

Typically, polymeric flocculants consist of long-chain molecules with molecular weights of 10^6 or greater. They may be either natural, synthetic, or derivatized hybrid organic products. Due to their great molecular chain lengths, they are capable

of adsorbing on several particles simultaneously. The resulting molecular bridging action is believed to be the chief mechanism for binding the adjoining particles within the floc.

There are many ways to classify polymeric flocculants. These classifications might be based on one or more of the polymer properties, such as molecular weight, functional group, charge, chemical structure, or origin. For example, polymeric flocculants may be natural, synthetic or derivatives of both; high or low molecular weight; cationic, anionic or nonionic; specific, chelating or nonspecific; and of myriad forms of chemical structures.

Kirshnan and Attia [8] have tabulated examples of polymeric flocculants based on their structure, origin, functional group and the likely mechanisms of adsorption. Examples of selective polymeric flocculants and dispersants are given under selective flocculation heading.

Kinetics of flocculation

Polymer adsorption and particle flocculation can be considered as transport processes. Rates of these transport processes depend on diffusion and on induced velocity gradients. Velocity gradient effects on polymer–particle collision leading to adsorption, and particle–particle collision resulting in flocculation are predominant where there is a fluid flow (agitation), particle size greater than 1 μm, and very high molecular weight polymers (greater than 10^6). Under these conditions, adsorption rate can be slower than flocculation rate. In the absence of induced velocity gradients, Brownian motion diffusion is the main mechanism for particle collision and polymer adsorption.

Adsorption rate

Gregory [9] pointed out that kinetics of polymer adsorption can be assumed to be transport-limited, i.e., adsorption depends on the rate of arrival (or collision) of polymer molecules at particle surface. This assumption is valid only at low surface coverage, as adsorption rate decreases when the surface becomes more fully covered by adsorbed polymer. Since flocculation does not require high or complete surface coverage, transport-limited adsorption may be justified. The number of particle–polymer collisions in unit volume per unit time, J_{12}, for a suspension containing n_1 number of particles and n_2 polymer molecules is given by:

$$J_{12} = K_{12} n_1 n_2 \tag{1}$$

where K_{12} is a rate constant. The rate constant K_{12} may be determined from the following equations (2) and (3):

$$K_{12} = \left(2K\frac{T}{3\mu}\right)\frac{(a_1 + a_2)^2}{a_1 a_2} \tag{2}$$

or:

$$K_{12} = (413)D(a_1 + a_2)^2 \tag{3}$$

where K = Boltzmann's constant, T = absolute temperature, μ = viscosity, D = velocity gradient or shear rate (s^{-1}), and a_1 and a_2 = radius of particle and polymer, respectively. Equation (2) is applicable for diffusion-controlled adsorption, i.e., in the absence of induced velocity gradient, while equation (3) applies when agitation is used.

Rate of floc formation

Equation (1) is used also to describe the flocculation rate in terms of collision rate between polymer-loaded particles, but with $n_1 = n_2$; i.e.,

$$J = \frac{dn_F}{dt} = K n_1^2 \tag{4}$$

where n_F = number concentration of flocs. However, since not all of the collisions are effective in producing flocculation, a collision efficiency factor E is introduced into equation (4). E was estimated by LaMer et al. [10]:

$$E = \theta(1 - \theta) \tag{5}$$

Thus, the rate of formation of binary particle flocs in the initial stages of flocculation can be determined by the formula of Smellie and LaMer [10]:

$$\frac{dn_F}{dt} = A n_1^2 \theta(1 - \theta) \tag{6}$$

where n_1 and n_F are the number concentrations of primary and binary particles (flocs), θ is the fraction of surface covered by polymer and A is a flocculation rate constant. The rate of flocculation in equation (6) is equal to the product of particle collision frequency and a collision efficiency factor (E): $dn_F/dt = A n_1^2 E$.

Assumptions inherent in LaMer's estimation of collision efficiency factor are:

(1) polymer adsorption takes place only on single particles;

(2) formation of bridges between particles is only possible when a polymer molecule from one particle adsorbs on a vacant site on the second particle;

(3) interaction between two adsorbed molecules, or two bare surfaces(particles) would not cause flocculation;

(4) $E_{max} = 1/4$ at $\theta = 1/2$.

This equation has been criticized on theoretical and experimental grounds by Hogg [11], who derived a more realistic equation for the collision efficiency between two particles of sizes X_i and X_j as:

$$E_{ij} = 1 - \theta^{n_i + n_j} - (1 - \theta)^{n_i + n_j} \tag{7}$$

where n represents the number of sites where the polymer molecules are adsorbed on each particle. According to Hogg, n can be determined by the ratio of surface

area of the particle to the area occupied by a single adsorbed molecule as shown in equation (8):

$$n_i = \frac{K_s X_i^2}{4\overline{R_g^2}} \tag{8}$$

where K_s = particle shape factor, and $\overline{R_g^2}$ = mean square radius of gyration of polymer molecules in solution.

When $n_i = n_j = 1$, equation (7) becomes:

$$E_{ij} = 2\theta(1 - \theta) \tag{9}$$

Extreme caution should be exercised when using equations (5)–(9) as there are many simplifying assumptions which are not valid for many cases. For example, equation (8) assumes that the polymer configuration in solution will be the same on the particle surface, which of course is not very likely. Also, the rate of polymer adsorption, and effect of molecular weight distribution, on the flocculation process are not accounted for. While LaMer's model tends to underestimate the collision efficiency by not allowing for re-orientation of polymer-laden particles, Hogg's model tends to overestimate the collision efficiency. In either case the effects of the prevailing hydrodynamics on particle–polymer–particle collision and subsequent breakage have not been considered.

Deason [12] proposed a model allowing for a minimum distance of approach between two colliding particles (H_{min}) which is determined by a balance of surface forces acting on these particles. He also attempted to account for the non-adsorbed segments of the polymer molecular bridge in solution (i.e., loops) which extend some distance (h) into the liquid from the particle surface. The "corrected" binary-collision bridging efficiency is then expressed as equation (10):

$$E = 1 - [1 - 2\theta(1 - \theta)]^N \tag{10}$$

where N = number of interacting pairs ($N = n_i n_j$ for Hogg's model). The value of N was calculated from the following equations (11) and (12).

For equal size spheres:

$$N = \frac{r(h - H_{min})}{h^2} \tag{11}$$

For unequal size spheres:

$$N = \frac{2r_j}{h^2} \frac{2r_i(h - H_{min}) - (h - H_{min})^2}{2[r_i + r_j - (h - H_{min})]} \tag{12}$$

where j is the smaller particle and i is the larger one. While Deason's model [equation (10)] is a refinement of the previous two models, it also assumes that polymer adsorption rate is not a limiting factor and that no reorientation or multiple bridges

are allowed between the adjoining particles. Also, determination of N for non-spherical particles, floc–floc or floc–particle, is very difficult. In all these models, simultaneous adsorption of polymer molecules on several particles was ignored. The simultaneous adsorption causes instant flocculation. Thus flocculation and adsorption processes are intertwined.

Rate of floc growth

Floc growth occurs by a random process which involves floc–floc collisions as well as floc–particle collision and produces irregular structures. Hogg et al. [13] developed an approximate expression for floc growth rate in agitated suspensions based on theoretical analysis. The rate of floc growth is defined as follows:

$$\frac{d\overline{X}}{dt} = K \cdot E \cdot D \cdot \phi \cdot \overline{X} \tag{13}$$

where $\overline{X}$ = mean floc size at time t, D = mean shear rate due to agitation, ϕ = volume fraction of solids in suspension, E = collision efficiency factor, and K = a constant ≈ 1.

Since E can be assumed to be constant with time, integration of equation (13) leads to:

$$\ln \frac{\overline{X}}{X_0} = K \cdot E \cdot D \cdot \phi \cdot t \tag{14}$$

where X_0 = initial floc size.

Rate of floc breakage

Unlike floc growth, floc disintegration can not be as yet characterized by breakage mode function, dissipation rate or parent floc size, as multiple-level aggregation structures yield disintegration events of different degrees of severities [14]. However, some insight into floc breakage was put forward by Glasgow [15]. If the eddies responsible for floc disintegration can be characterized by the Kolmogorov scales, a rough equality between floc yield stress T_y and dynamic pressure can be made [15]:

$$T_y \approx \frac{1}{2}\rho v^2 \tag{15}$$

where ρ is the fluid density and v is the fluid velocity. The critical characteristic velocity:

$$v_c \simeq \sqrt{\frac{2T_y}{\rho}} \tag{16}$$

Higher velocity than v_c would result in floc breakage. However, floc yield stress has to be independently determined or known before these equations can be used.

Schubert et al. [16] developed a model to determine the maximum stable floc size, d_{max}, in a flocculation process using agitation:

$$d_{max} = \left(\frac{F_H}{\rho_l}\right)^{1/2} (\nu\varepsilon)^{-1/4} \tag{17}$$

where F_H = average adhesion force between particles, ρ_l = fluid density, ν = kinematic viscosity, and ε = energy dissipation rate.

Hogg et al. [17] used population balance models developed for size reduction by grinding to describe the floc degradation process. In this analysis, re-agglomeration of floc fragments was assumed negligible. A mass balance on flocs in some size interval i can be expressed by the following equation:

$$\frac{dW_i}{dt} = \sum_{j=1}^{i=1} b_{ij} S_j W_j - S_i W_i \tag{18}$$

where W_i = mass fraction of flocs in size interval i at time t, S_i = specific rate of breakage of these flocs, and b_{ij} = mass fraction of fragments produced by breakage of flocs of size j which fall into class i. b_{ij} is known as the primary breakage distribution.

Klimpel and Austin [19] assumed that S_i and b_{ij} can be determined as follows:

$$S_i = A\left(\frac{X_i}{X_j}\right)^{\alpha} \tag{19}$$

$$B_{ij} = \phi\left(\frac{X_i - 1}{X_j}\right)^{\gamma} + (1 - \phi)\left(\frac{X_i - 1}{X_j}\right)^{\beta} \tag{20}$$

where A, α, ϕ, γ and β are constants for any given set of conditions, X is the floc size, and B_{ij} is the cumulative breakage distribution function defined by:

$$B_{ij} = \sum_{k=i}^{n} bk_j \tag{21}$$

Application of back calculation procedure to floc size distributions found in excess mixing period of the flocculation process leads to sets of parameters A, α, ϕ, γ and β, which can be used to simulate the breakage process using equation (18). Using this procedure, Hogg et al. [17] appeared to obtain an excellent description of floc breakage in agitated suspensions.

Hydrodynamic effects in flocculation

Hydrodynamic forces in suspension affect all facets of the flocculation process, from dispersion of polymer molecules, to polymer adsorption, floc formation to floc growth and floc break up. The effect of hydrodynamic forces on the various flocculation functions [e.g. equations (1)–(17)] has been represented by the mean shear rate as expressed by the velocity gradient D (s^{-1}). The usual method for calculating D is through Camp and Stein's equation:

$$D = \left(\frac{P}{\mu V}\right)^{1/2} \tag{22}$$

where P = power transmitted to the fluid, μ = viscosity of fluid (or more accurately suspension), and V = fluid volume.

For in-line (plug-flow) mixing system, the power dissipated is given by the following relation:

$$P = \rho Q F \tag{23}$$

where F = head loss due to friction, Q = volumetric flow rate, and ρ = fluid density.

The head loss due to friction can be calculated from Darcy's equation:

$$F = \frac{4fLU^2}{2dg_c} \tag{24}$$

where f = fanning friction factor, L = length of tube, U = fluid velocity, d = tube diameter, and g_c = dimensional constant.

From equations (22)–(24), the following expression for velocity gradient in an in-line, plug-flow mixing is obtained:

$$D = \left(\frac{2\rho}{g_c \mu}\right)^{1/2} \left(\frac{f}{d}\right)^{1/2} U^{3/2} \tag{25}$$

For stirred tank (back flow) mixer, the power dissipated is given by:

$$P = \frac{N_p \rho d_i^5 N^3}{g_c} \tag{26}$$

where N_p = power number, d_i=impeller diameter, N = revolution per second, g_c = dimensional constant, and ρ = fluid density.

From equations (26) and (22), the following expression results:

$$D = \left(\frac{N_p d_i^5 \rho}{g_c \mu V}\right)^{1/2} N^{3/2} \tag{27}$$

The validity of mean velocity gradient (D) as an expression of shear rate acting on individual particle or floc in a turbulent regime under inhomogeneous and anisotropic conditions usually encountered in flocculation processes is questioned. However, D has been commonly used because of the difficulty in determining the actual shear rate acting on the individual particle or floc. In fact, much of the literature in the field of water treatment industry describes the guideline values for good flocculation such as $D = 50\ s^{-1}$ for $t = 20$ min, so that $Dt = 10^4$ or 10^5 [15].

It is known, however, that the energy dissipation rate per unit mass, ε, is much higher in the vicinity of the impeller than some distance away from it, with $\varepsilon_{local}/\varepsilon_{mean} = 100$ in some cases. Floc breakage is usually a consequence of local

microturbulence, not mean flow conditions. Intensity and structure of the microturbulence depend only on the energy dissipation rate ε and kinematic viscosity ν. The mean energy dissipation rate ε_m in a tank containing m mass of fluid and having a power input P is [16]:

$$\varepsilon_m = \frac{P}{m} \tag{28}$$

The local dissipation rate ε varies with the distance X downstream (as measured from the point of issuance) as follows [14]:

$$\varepsilon \approx 5.0 \times 10^4 \exp(-0.14X) \tag{29}$$

Microturbulences influencing the flocculation process are further defined by the Kolmogorov scales. Kolmogorov [20] developed a theory for breakage in homogenous, isotropic turbulence employing eddy acceleration and work performed against surface tension, while Hinze [21] described the relationship between critical eddy scale and parent drop size. Droplets or flocs can be influenced only by eddies of particular scales. Thus large eddies cannot influence (break) small size flocs or droplets, and conversely, small eddies can not break large flocs or droplets. Thus a practical limit for size reduction is defined by Kolmogorov length microscale, η, and time scale, t:

$$\eta = \left(\frac{\nu 3}{\varepsilon}\right)^{1/4} \tag{30}$$

$$t = \left(\frac{\nu}{\varepsilon}\right)^{1/2} \tag{31}$$

where ν and ε are the kinematic viscosity and dissipation rate per unit mass, respectively.

The greatest shear stress results when the floc size is roughly equal to eddy scale, since this situation produces the largest relative velocities. Cleasby [22] states that use of D to express the shear rate is valid only if the particles being flocculated are smaller than the Kolomogorov microscale. He also advocated the use of the energy dissipated per unit volume raised to the two thirds power — $\varepsilon_\nu^{2/3}$ — for systems in which the particles to be flocculated are greater than the microscale. In the case of back flow mixing, the calculated velocity gradient is based on impeller tip speed, and this shear rate is not necessarily the average shear rate in the mixer [23]. There are two reasons why the velocity gradient is still commonly used in spite of these objections. First, D is a relatively accurate estimation of average shear rate, which is directly related to shear stress. Second, D is an easily obtained parameter and familiar to most engineers. For these reasons, Attia et al. [24] used the mean velocity gradient, D, to compare the effects of in-line (plug-flow) mixing

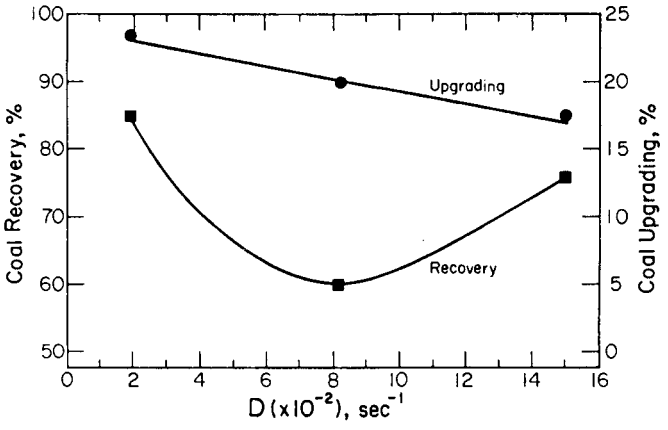

Fig. 1. Upgrading and recovery of coal by selective flocculation as a function of the velocity gradient (D), using a back-flow (stirred) mixer (from [24]).

(Figure 1), with stirred tank (back-flow) mixing (Figure 2) on the performance of selective flocculation process. Figure 1 shows the upgrading and recovery as a function of velocity gradient D in a back flow (stirred baffled tank) mixer. The figure indicates that, at low shear rate, the polymer appeared to have been rapidly and efficiently dispersed which promoted a low rate of floc growth. This resulted in the high recovery and upgrading observed. As the shear rate increased, the recovery and upgrading were seen to decrease. This was probably due to a combination of two factors. At this shear rate (800 s^{-1}) the polymer was not well dispersed as can be observed from the study of kinetics of polymer dispersion (Figure 4). The non-homogeneous polymer dispersion may produce high local concentrations of the polymer yielding small overdosed flocs. The small flocs are formed when the particle surface become saturated with polymer, and form stabilized agglomerates. Since the small flocs have been stabilized by polymer adsorption (steric stablization), there is less tendency for inter-floc growth to occur, and therefore the flocs that have formed remain small. Since the small flocs would take longer to settle, the floc recovery in a given time period will be correspondingly reduced. The other possible factor involved was the breaking of the flocs by the higher shear rate. The floc breakage and reflocculation of the particles also produce small flocs, thus reducing the recovery even further.

When the shear rate was increased beyond 800 s^{-1}, the recovery was seen to increase once again. It is believed that at higher shear rates the polymer dispersion was more homogeneous, thus resulting in an increase in the recovery. However, the recovery was still less than that observed at low shears (i.e. less than 400 s^{-1}), indicating that the redispersion and reflocculation of the flocs was still taking place. It is expected that as the shear rate is increased further (beyond 1500 s^{-1}), the recovery will begin to drop due to the production of more fine flocs.

It appears that the prevailing hydrodynamic conditions affect the efficiency of the polymer mixing process, and the floc formation and growth processes. For example, the gentle, low shear condition (close to the laminar regime) favor good floc formation and result in both high floc recovery and grade. On the other extreme, where turbulent conditions prevail, good performance of the selective flocculation process was also observed. It is in the transition regime between the two conditions where the process performance is somewhat unpredictable. The low shear regime allows for a slow rate of flocculation, and a low rate of floc breakage (i.e. higher floc growth rate). The turbulent conditions provide good polymer dispersion which allows more particles to be flocculated, but higher floc breakage leeds to smaller floc sizes which minimizes entrapment of gangue particles and results in higher floc grades.

Figure 2 shows the effect of velocity gradient in an in-line (plug flow) mixer on the selective flocculation performance. The recovery can be seen to first increase and then begins to decrease at higher shear rates. This trend is the same as the one previously explained from the back flow mixer. The upgrading was somewhat higher in this series of experiments than those using the back flow mixer. This might be the result of continuously adding the flocculant throughout the flocculation period rather than in one dose at the beginning.

The effect of impeller speed in a back flow mixer on the degradation of floc size is shown on Figure 3 [25]. Clearly, the increase in impeller speed, hence the shear rate, has a dramatic impact on reducing the floc size. Even dispersion of polymer molecules in water is affected by the shear rate and time of agitation. Figure 4 [24], demonstrates these effects. From this figure it can be seen that at 600 rpm, a steady-state level for the polymer concentration (±10 percent of the bulk concentration) was achieved in about 15 seconds, whereas at 100 rpm, 32 seconds were required to reach the steady-state value. The reason for this is not clear at the present time.

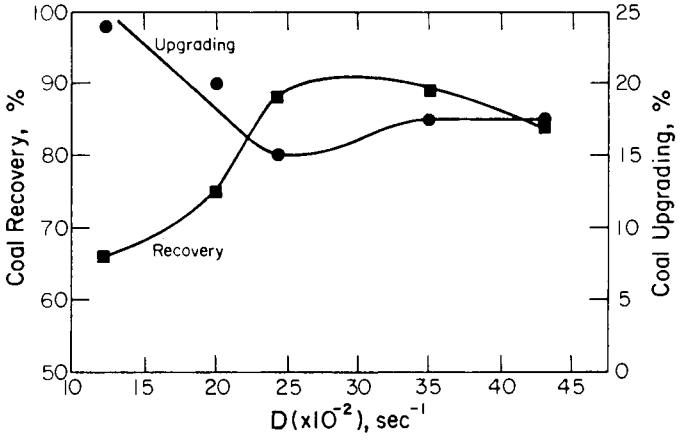

Fig. 2. Upgrading and recovery of coal by selective flocculation as a function of the velocity gradient (D), using an in-line (plug-flow) mixer (from [24]).

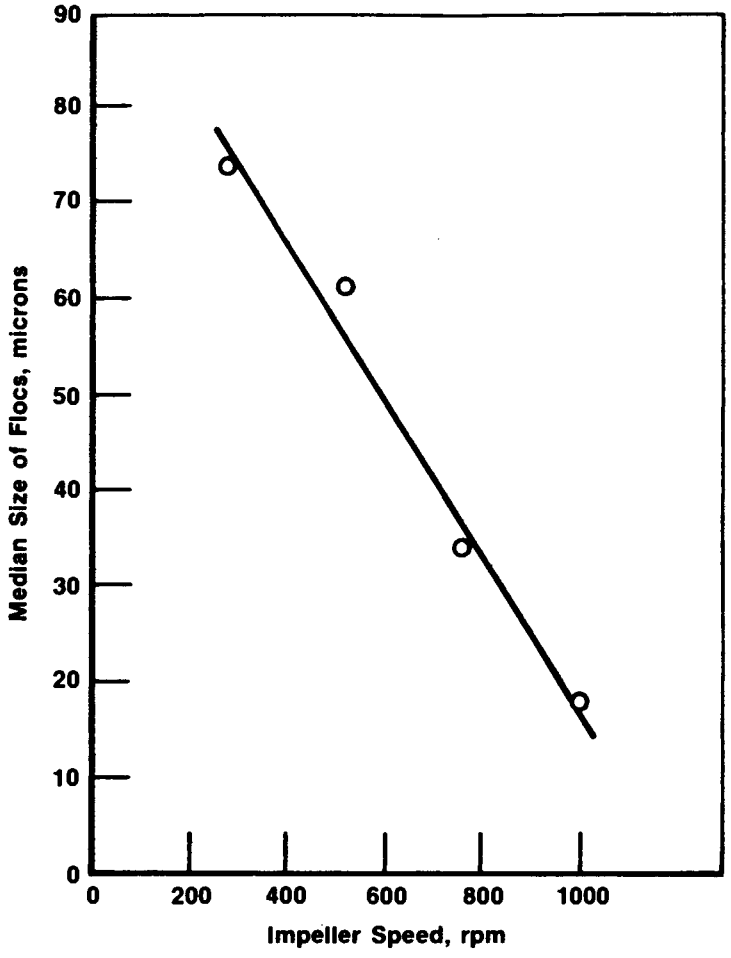

Fig. 3. Effect of impeller speed on size of malachite flocs. Solids 1 g l^{-1}, SHMP 300 mg l^{-1}, PAMG 5 mg l^{-1}, pH 11, conditioning time 5 min (from [25]).

However, the salient conclusion that can be drawn from this observation is that as little as 15 seconds are needed for the adequate mixing of the polymer in solution, and further mixing would be unproductive.

Applications of flocculation in mineral processing

Applications of polymeric flocculation in mineral processing are numerous and varied. Almost every mineral processing plant employs polymeric flocculants in order to aid, enhance, expedite or carry out the overall process or certain aspects of it. Therefore, the applications may be discussed in terms of the relevant unit processes. Unit processes such as flocculation/settling, filtration and centrifugation are essen-

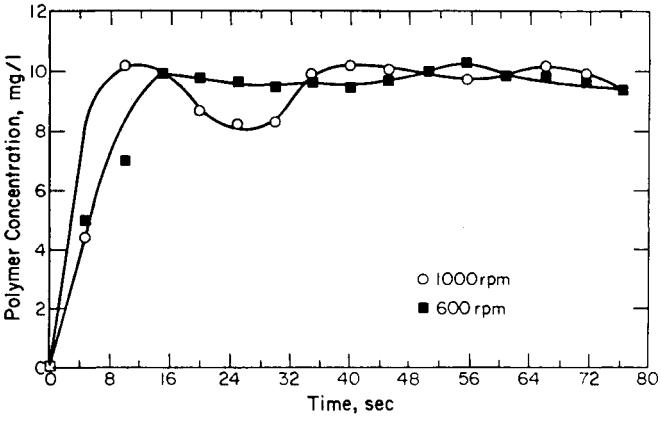

Fig. 4. Kinetics of polymeric flocculant dispersion in water (from [24]).

tial in solid–liquid separation. The objective of the separation may be concentration of the solids, as in tailings disposal, removal of water from concentrate product, or recovery of process water. Processes such as flotation, selective flocculation and selective dispersion may be termed solid–solid separation where recovery of desired particles form finely ground ore particles suspended in water is accomplished. While solid–liquid separation emphasizes the recovery of either the solids or the liquid, in the solid–solid separation, increasing the grade of the solids in the concentrated fraction is the objective. However, it should be noted that though polymeric flocculants are applied in these unit operations, the underlying mechanism of their action is still primarily flocculation of fine particles. Selective flocculation and dispersion are discussed separately later in this chapter.

(a) Flocculation/settling. One of the earliest applications of polymers was in clarification of colliery effluents [26]. The effluents chiefly contain fine shale particles such as kaolinite, illite, vermiculite and quartz. The concentration of these fine particles must be kept to a minimum in the recycled water in order to avoid slime coating of coal, which adversely affects flotation performance. The use of flocculation is, therefore, essential to remove these fine particles. Although earlier, starch was commonly used for this purpose with additions of lime, in current practice synthetic polymers of the polyacrylamide type have largely superseded starch.

(b) Filtration. The chief objective of using polymeric flocculants in filtration processes is to obtain a slurry that forms a filter cake with an open structure of high permeability with no free fines to block the channels or "blind" the filter medium. In settling applications, large, loose flocs are most effective in causing rapid settling. However, they trap water in the floc structure, and are ineffective for filtration

applications because of higher moisture contents of the resulting filter cakes. Generally, flocculants that work best on sedimentation are not the best for filtration. For filtration, flocs that are small, strong and equisized are desirable [27]. Consequently, the kinds of flocculants used in filtration are of importance. With proper choice of flocculants, filtration rates can be improved up to 100 times, especially in the case of difficult-to-filter materials such as fine clays, sludges and tailings [28].

(c) Centrifugation. Another important application of polymeric flocculants is in dewatering of slurries by centrifugation. This technique as commonly carried out in the laboratory, involves the addition of a flocculant prior to centrifugation in order to expedite the dewatering rate. On a larger scale in the minerals industry, this technique appears to be applied primarily in the clay industry. A limitation that was recognized early in the use of flocculants in centrifuges was the lack of adequate resistance of the polymers to very high local shear forces that exist at the point where the suspension enters the bowl via the axial feed and is accelerated to the bowl speed [29]. Many high shear resistant flocculants have been developed to overcome this concern, and also many methods of flocculant addition have been developed.

(d) Flotation. Polymeric flocculants have been used in flotation circuits to improve efficiency of separation and to enhance recovery [8]. Most often the function of the polymeric flocculant is attributed to depression of minerals, while in reality the minerals might be selectively flocculating. The three mechanisms of depression of flotation by polymers are: (a) inhibition of collector adsorption, thus making the solid surface hydrophilic, (b) formation of large aggregates, and (c) complexation of the collector in solution. The distinction between depressing and flocculating action of polymers lies chiefly in the molecular weight of the polymer and its mechanism of action on the mineral surface. In general, polymers having molecular weights of a few hundred thousand or less act as a "depressant"' adsorbing on the mineral surfaces but forming no interparticle bridges, i.e., no flocculation. On the other hand, use of higher-molecular-weight polymer (1 million or more) leads to the formation of flocs. Low-molecular-weight polymers that "depress" flotation act primarily by masking the surface of the minerals from collector adsorption. Use of polymeric flocculants, however, leads to the formation of flocs of one type of mineral, which may be too large for the air bubbles to carry to the top of the flotation cell, hence these minerals are prevented from flotation. On the other hand, if the flocs are not too large, they can be floated, and lead to increased recovery of the minerals. However, it is not possible to distinguish between depression and flocculation in flotation systems from the literatures due to lack of a clear definition of depression and of an understanding of mechanisms involved.

Many examples of application of polymeric flocculants to the various unit processes in solid–liquid separation and in flotation have been reported by Krishnan and Attia [8].

Selective flocculation

Introduction and definitions

Selective flocculation technique is one of the most significant advances in fine particle separation in recent years. This technology aims at recovering valuable minerals from ultrafine ore suspensions [30], and is achieved by selectively aggregating mineral particles in question to such sizes as to enable their effective separation from the suspension. However, selective flocculation is also applied in fine particle/colloid separations in several industries other than minerals. For example, it has been tested for separating low density cholesterol from high density ones [31], and in separation of treated paper from pulp [32].

Selective flocculation utilizes the differences in the physical–chemical properties of the various fine mineral components in the mixed suspension. It is based on the preferential adsorption of an organic flocculant on the particular minerals to be flocculated, leaving the remainder of the particles in suspension.

In some applications, the reverse of selective flocculation, that is selective dispersion of fine mineral particles in mixed suspension, is desirable, as in the purification of kaolin or coal water slurry fuel. Selective dispersion, which also utilizes the differences in the minerals' surface chemical properties, is based on the preferential adsorption of a selective dispersant on the selected particles to be dispersed, leaving the remainder of the suspension particles flocculated by a general-type flocculant.

Elements of selective flocculation

A selective flocculation process, e.g. for cleaning and desulfurization of fine coal slurry, conceptually consists of four major sub-process. As illustrated in Figure 5, these are: (a) general dispersion of mineral particles, in which all the particles are stably and uniformly distributed in the suspension with the individual particles being essentially separate; (b) selective adsorption of flocculant and floc formation; (c) floc conditioning, which aims at obtaining flocs of desired properties for their subsequent separation and with minimum entrapment of dispersed particles; and (d) floc separation from the suspension.

Design of selective flocculation processes

The first and also the most important decision in the design of a selective flocculation process is which type of mineral components of the ore suspension should be selectively flocculated.

In designing a selective flocculation process to separate certain desired particles from mixed suspension with unwanted (gangue) solids, selective flocculation of either the valuable components or the gangue components may be employed depending on which route is more technically and economically feasible. Both of these

routes have been successfully applied on a commercial scale. In one application for processing iron ore [33], the valuable components, i.e. iron minerals, are selectively flocculated, while the associated silicate gangue minerals remain dispersed. The iron mineral flocs are separated from the suspension by gravity settling using a thickener. In the other application processing potash ore [34], the unwanted clay minerals are selectively flocculated, while the halide minerals remain dispersed. The clay flocs are separated from the suspension by flotation of the flocs. Thus, in principle, the separation of certain fine particles from mixed suspensions could be obtained by either route.

In the overall flowsheet design, selective flocculation process can be considered to be either a preparation process for flotation or an independent process. For example, in the Tilden's iron ore plant, selective flocculation process is used prior to flotation for improving flotation efficiency while in another iron ore plant, selective flocculation/settling was demonstrated to achieve high grade iron product.

There are some general guidelines to be followed which are similar to those in the application of froth flotation. More specifically to selective flocculation, the route which results in lower reagent consumption, more efficient separation and lower equipment cost (both capital and operation costs) would obviously be the preferred choice. However, this decision is usually reached after a considerable amount of work on bench and pilot-plant scale. In setting out to design a selective flocculation

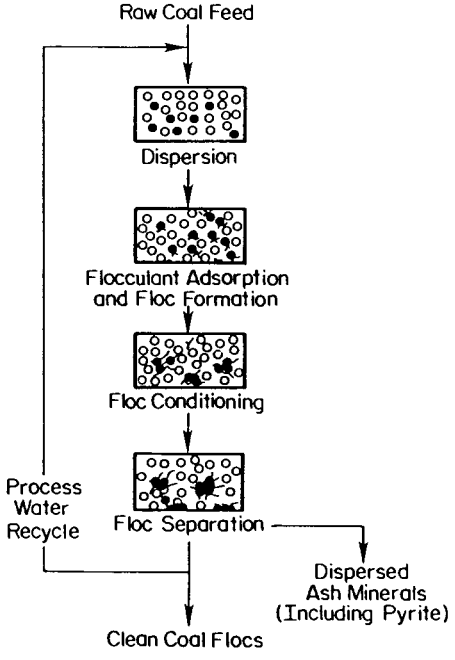

Fig. 5. Conceptual representation of the selective flocculation process for coal cleaning and desulfurization.

process from fundamental or basic levels, knowledge of the various methods of achieving selective flocculation is essential.

Methods of achieving selective flocculation

There are basically three ways to achieve selective flocculation of the mineral of choice (whether it is the valuable or the unwanted one) from a mixed suspension [30]. These are: (1) use of a selective flocculant for the mineral of choice, either alone or in combination with a general, unselective dispersant; (2) use of a selective dispersant in combination with a normally unselective flocculant; and (3) use of a selective activator in combination with a general but non-adsorbing flocculant. Obviously, the use of any combination of these methods would be expected to achieve superior performance to any of the methods alone. However, this might not necessarily be the most cost effective, since the cost of preparing selective reagents might be inherently more expensive, at least at this early stage of development, than the more commercially produced general reagents.

Use of selective flocculants

This route involves employing a selective flocculant either alone or in combination with general dispersants. Selective flocculant adsorption can be achieved by either designing a specific flocculant or enhancing polymer's selectivity by chemical modulation of the interfaces. The specifically designed polymeric flocculants can be classified into three categories:

(a) Chemisorbing or chelating polymers in which the functional groups are strong complex formers with certain ions on the solid surface.

(b) Stereoselective flocculants which rely on the selective effect of the molecular structure such as steric hindrance of adsorption of polymers having bulky constituent groups in their structures.

(c) Hydrophobic or partially hydrophobic flocculants where selective flocculation of hydrophobic colloids from those hydrophilic ones are desired. The details of designing selective flocculants are discussed in next section.

Enhancement of polymer's selectivity by chemical modulation of interfaces could be implemented by regulating the surface electrical potential or by employing competitive dispersion conditions. In the latter, a dispersant (or a depressant) would compete with the flocculant for bonding sites on a certain solid surface, thereby inhibiting its adsorption. This might also be considered as a case of selective dispersion.

Use of selective dispersants

The functions of a dispersant include: (a) reduction of the aggregation and settling rates due to particle–particle attraction (slimes coating, coagulation, and poly-

mer bridging flocculation); and (b) reduction of the gravitational settling rate of the individual particles due to inter-particle repulsion which hinders the settling process. The dispersing agent could either be monomeric or polymeric in nature; the latter could be either linear or branched molecules [30] (see also Chapter 4.) Since more surface coverage is usually required in the case of dispersion compared with the flocculation, branched molecules should be more effective than linear ones. On the contrary, the effective flocculant is normally a linear long-chain, polymeric molecule which is needed for bridging between the adjoining particles in the floc.

In general, dispersants for aqueous solid suspensions may function by one or more of the following mechanisms [39]:

(a) control of surface electrical potential in order to induce repulsion between similarly charged particles;

(b) reduction of interfacial energy of solids by surface-active dispersants;

(c) solvation of particle surface by the adsorption of hydrophilic colloids.

In the last mechanism, the particle–particle interaction would be reduced to liquid–liquid interaction due to the presence of lyophilic layers on the particle surface. It is difficult to single out one mechanism that is the most important for selective dispersion-flocculation, but it is likely that the first mechanism will be the most useful. However, the reader is referred to Chapter 4 for more in depth discussion on this subject.

In addition to the dispersion function, the same reagent must act as a depressant for the flocculant action on the solid particles by competing with it for bonding sites on the surface and thus inhibiting its adsorption. The "dispersant" is also often required to act as a deactivating agent by complexing potential interfering ionic species present in the suspension. Examples of random activation and deactivation in polymer adsorption are well documented in the literature [39, 41].

Use of selective activator

By analogy with the use of selective dispersants and depressants, use of selective activators might also be used to achieve selective flocculation. The use of selective activators for certain components of the mixed suspension which, when used with a general but non-adsorbing flocculant (e.g., a highly anionic flocculant at high pH), may cause the selective flocculation of these components. The choice and design of the selective activating agents are governed by the same principles used for selective flocculants or dispersants.

Design of selective polymers

Selective flocculation of a particular mineral from a mixed suspension cannot be achieved unless the polymeric flocculant is selectively adsorbed on the mineral to be flocculated [35]. Therefore, the ability of the polymer's functional groups to exploit the differences in the surface chemical behaviors of the various mineral particles

to achieve selective adsorption is of basic concern [36, 37]. In order to select a region for selective polymer adsorption, three main interactive factors must be carefully considered. These are: (a) flocculant, (b) mineral surface, and (c) suspending medium.

The effect of the suspending medium, which is aqueous in most applications, can only be considered in conjunction with the behaviors of the flocculant and the mineral surface. It is well known that the aqueous medium affects the electrochemical and physical properties of the polymeric flocculant. Thus, coiling up and uncoiling (or even decomposition) of the polymer are certainly affected by the type and amount of electrolytes in solution, hydrodynamics, pH and the ionic nature of the polymer's functional groups. Similarly, the electrochemical state of the mineral surface is controlled by the aqueous medium. Thus, the adsorption of the polymer on the mineral surface can be strengthened or prevented largely by proper control of the medium. Therefore, although selective polymer adsorption and flocculation depends primarily on the functional groups of the polymer and nature of the surface sites on the mineral, it can be largely influenced by the differential effects of the aqueous medium on the different minerals in the mixed suspension.

Forces in adsorption of polymers

The forces involved in the adsorption of polymeric flocculants on mineral surfaces can either be physical or chemical or both. The forces which are considered to be physical (i.e. do not form chemical bonding and result in physisorption regardless of the chemical nature of interface) include the following:

(a) Electrostatic (Coulombic) forces: these result in the adsorption of polyelectrolyte onto any surface of opposite charge, irrespective of their chemical nature.

(b) Dipole attraction forces: these were suggested [38, 39] to explain the flocculation of ionic-type crystal (e.g. fluorite) by non-ionic polyacrylamide.

(c) London-Van der Waals forces: in these, neutral molecudes or atoms constitute systems of oscillating charges producing synchronized dipoles that attract each other [40].

(d) Hydrophobic association: this is characterized by the tendency of nonpolar molecular groups (or substances) to escape from an aqueous environment.

The important chemical forces resulting in chemisorption, include the following:

(e) Chemical bonding: this is exemplified by reactions of the polymer groups with metallic sites on the solid surface which result in the formation of insoluble compounds by covalent or ionic bonding.

(f) Coordination bonding: this includes chelating or complex formation resulting in polymer attachment to a surface.

(g) Hydrogen bonding: in the organic compounds where the hydrogen atom is combined with a strongly electronegative atom (such as O, S, N), the hydrogen atom is able to accept electrons from atoms on the solid surface, such as from the –OH

groups of the hydrated surface of an oxide mineral, resulting in the formation of a hydrogen bond.

The adsorption of polymers on mineral surfaces by chemical forces against electrostatic repulsion can only happen if the polymer approaches the surface closely by other means or mechanisms. These may be due either to London-Van der Waals forces or to strong collisions between the polymer molecules and the mineral particles.

Design of the polymer's selective functional groups

It is very important to choose a surface property as a basis for selective adsorption of polymer (such as hydrophocity, surface change, or chemical bonding), in which the fine mineral, particles to be separated exhibit a wide difference. The wider the difference in the surface behavior between the fine mineral particles to be separated, the more selective is the adsorption, and thus the easier the separation becomes. However, before the functional group can be selected for incorporation in the polymer's structure, the various mechanisms for polymer adsorption must be recognized.

Possible mechanisms for selective adsorption

Ideally, the design of a specific polymer for particular mineral surface is to achieve a yes or no adsorption. As mentioned earlier, a selective polymeric flocculant or dispersant can be designed based on either: a) chemisorbing or chelating mechanisms, (b) stereoselective effect, or (c) hydrophobic interaction. Similar to flotation, electrostatic attraction can be used as a mechanism for selective adsorption of a polymer on oppositely charged particles and affect their separation from simple mixed suspensions. The design of selective flocculation processes using selective flocculants by one or more of these mechanisms has been the major route followed by researchers thus far.

Selective polymers based on chemisorption

Examples of selective chemisorbing flocculants are found in the literature [42–49]. Notably, the development of polyxanthate flocculants for the selective floccualtion of sulfide minerals and oxidized copper minerals was first reported by Attia and Kitchener [42], and was later confirmed by Sresty et al. [43] and Baudet et al. [44]. A chelating or complexing polymer, polyacrylamide-glyoxal-bis-2-hydroxyanil (PAMG), was designed and used for the selective flocculation of copper minerals from a natural ore [45]. Its possible structure is illustrated in Figure 6. Another example of chemisorbing selective polymers are the polyoximes, which were designed for separation of cassiterite (SnO_2) from quartz (SiO_2) and tourmaline [46, 47]. Figure 7 shows the preparation of polymethylvinyloxime (PMVOX). The use of

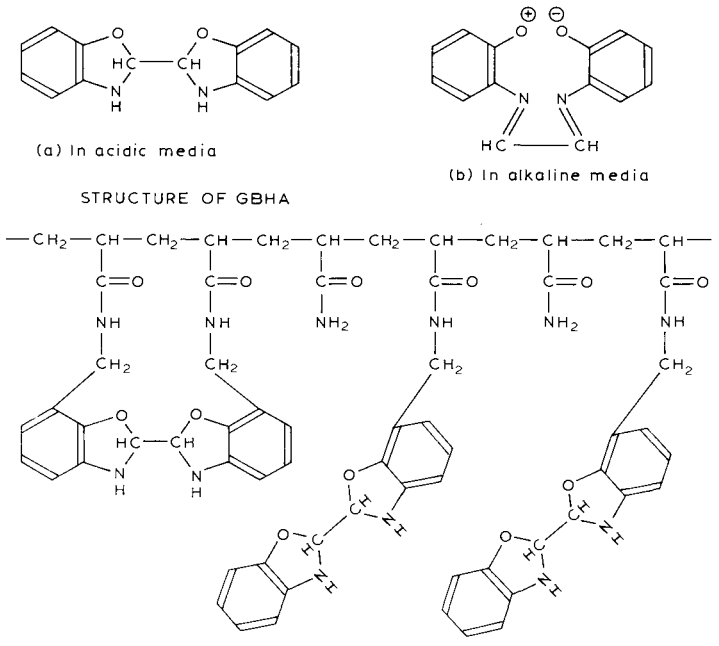

Fig. 6. Possible structure of PAMG chelating flocculant (from [45]).

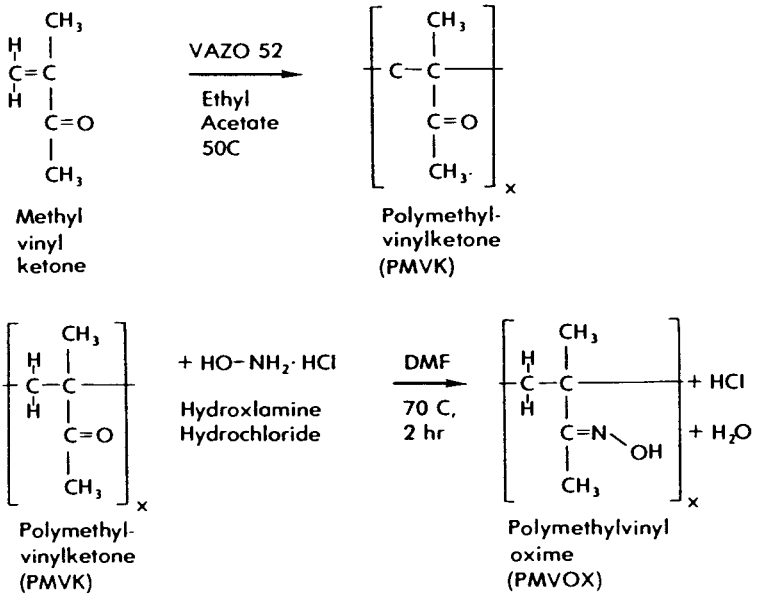

Fig. 7. Preparation of polymethylvinyloxime (PMVOX) (from [46])

chemisorbing or chelating polymers for achieving selective flocculation so far represents the most practical and promising mechanism. These types of flocculants are, therefore, very likely to find wide applications in the mineral processing industry in future.

The possibility of designing selective chemisorbing dispersants was confirmed by Attia [48], who found that by using modified low molecular weight polymers with chemical groups that are selective toward certain solid surfaces in the mixed suspension, selective dispersion and depression could be obtained. Thus the author designed and prepared two novel reagents for magnesium and calcium-bearing minerals, such as calcite and dolomite. The crude solution of one reagent tested exhibited selective dispersant and depressant behavior for calcite and dolomite but to a much lesser degree for feldspar. Lower concentrations of this reagent, compared with the unmodified polymer, enabled more effective selective flocculation of the copper minerals from mixtures with calcite, dolomite, and feldspar. This reagent also proved to be a selective depressant for calcite and fluorite in their separation from barite by flotation. Another example of selective chemisorbing dispersants was that designed by Attia and co-workers [55, 61], which incorporates xanthate groups into a low molecular weight polyacrylic acid. This dispersant, known as PAAX for short, with a possible chemical structure of sodium poly (acrylate-acrylodithiocarbonate), was used for selective dispersion of pyrite from coal.

Selective polymers based on stereoselective effect

Stereoselective flocculants have not yet been designed as such or used in selective flocculation, although their potential has been recognized [49] for some time. The design of this type of flocculants involves the geometrical arrangement of the flocculant's groups, so as to match the geometric structure of the binding ionic (or atomic) sites on certain mineral surfaces, thereby selectively adsorbing and flocculating them. Structural effects, such as steric-hindrance, ring strain, and specific size fit (of a chelating flocculant), could be employed to produce selective flocculation. Y. Attia (unpublished report, 1974), incorporated bulky groups such as Alizarin ($C_{14}H_8O_4$) into long-chain acrylamide polymers to obtain selective flocculants for clay minerals. One such polymer was found to flocculate kaolinite well from suspension, but dispersion of kaolinite was restored on addition of a dispersant (N.O. Clark, English China Clays, 1974). Evidently, the dispersant was able to displace the flocculant, which because of the bulky alizarin groups, was only weakly adsorbed onto the kaolinite particles. This is a case where reversible flocculation can be achieved. Future developments in flocculant design will likely take advantage of this rather sophisticated concept.

Selective polymers based on hydrophobic effect

Hydrophobic or partially hydrophobic polymers appear to have greatest potential for selective flocculation of hydrophobic solids (with natural or induced hydropho-

bicity) in mixed suspensions with hydrophilic solids. The use of this type of flocculants for selectively flocculating naturally hydrophobic solids, such as coal, was suggested by Attia [50]. However, the application of this type of flocculant in selective flocculation of hydrophobized copper minerals was first reported by Rubio and Kitchener [51]. In their application, the initially hydrophilic surfaces of oxidized copper minerals were selectively made hydrophobic by selective adsorption of surfactant or even by sulfidization with sodium sulfide. Then, by introducing a partially hydrophobic flocculant, polyethylene oxide, selective flocculation of oxidized copper minerals from associated hydrophilic silica and silicate minerals was achieved.

Selective polymer adsorption on metallic and industrial minerals

Interaction of a chemical group with a metal ion in solution can be used at least qualitatively as a model for the adsorption of polymers on metallic sites on mineral surfaces. Selective binding of a metal cation in solution by a chemical group (ligand) is basically due to the favorable combination of the ligand's type of donor atom (the central atom in the chemical group which is responsible for binding the metal ion), and ligand structure with the metal cation's type and coordination sphere. The relationships between the selectivity of interactions and each of these factors were defined by Schwarzenbach [52]. The principles of selective interactions were applied for the design of selective polymers [36, 37, 42]. The effects of different types of donor atoms on surface interactions were summarized by Attia [37, 48] and the effects of structural factors on selective interactions were summarized as: (a) formation of closed ring structure — the "chelate" effect, which causes an increase in the system's entropy; (b) formation of rigid structures, where the ligand contains a vacancy which is especially fitting for a particular cation's radius and coordination sphere; and (c) the steric hindrance effect, where the degree of hindrance (and consequently the reduction in complex stability) varies with the cation's radius and coordination sphere as well as the degree of closeness between the ligand donor atom and the metal cation. The steric effect is similar to ring-strain effect, in which normally stable five- and six-membered rings can be made more strained and therefore favor the formation of certain complex structures over others. Only cations with coordination spheres which fit the modified structures are complexed with those ligands.

Selective polymer adsorption on fossil fuel minerals

Fuel minerals such as those in raw coal, tar sands, oil shales and so on, exhibit a wide range of physical and chemical properties. Coal has the greatest near-term potential for application of selective flocculation procedure at present, although selective removal and purification of pigments, graphite and other organics are similarly possible. Raw coal, with a complex and variable organic and inorganic composition, may serve as a general model for fuel minerals systems. An idealized model for the unit structure of coal based on published analytical data summarized

in reference [54], was proposed by Attia [53]. The model shows the coal as having a "sandwich" structure, with bonded layers of condensed aromatic rings on both sides of the sandwich, bridging groups (holding the sandwich together), and interstitial or filler groups. The latter are presumed to constitute the volatile part of coal. The bonded layers of condensed aromatic rings on each side of the sandwich, vary in number with coal rank. Thus, in high rank anthracite and bitumineous coal, as many as 40 layers are bonded together on each side of the sandwich, while in low rank coal, the number might be four or less.

One revealing feature of this model is the sandwich type structure of the coal surface, with aromatic faces and heterogenous edges, in a manner similar to silicate structure. The presence of condensed aromatic groups as well as the methyl, ethyl and other non-polar bridging and filler groups gives rise to the well known hydrophobic characteristics of coal in aqueous suspensions. However, the presence of hydroxyl, phenolic and carboxylic groups gives rise to decreased hydrophobicity of coal surfaces in water as well as to the formation of electrical double layers. The presence of carboxylic and phenolic groups has been shown to increase with the prolonged exposure to oxygen. With severe oxidation, the aromatic rings are broken up to give rise to humic acid type compounds. More discussion on the surface properties of coal is given in Chapter 4.

Since selective flocculation aims at separating the mainly hydrophobic coal particles from the associated hydrophilic shale particles, selective polymer adsorption can be achieved through hydrophobic association of the non-polar groups on the coal surface with the hydrophobic groups in the polymer structure. Figure 8 illustrates the possible structure of hydrophobic polymers [55]. The validity of this approach has been recently verified and the feasibility of selective flocculation-cleaning of raw coals has been confirmed [55]. However, as the surface becomes increasingly oxidized and therefore less hydrophobic, other polymer adsorption mechanisms will have to be utilized. Such mechanisms might include hydrogen bonding and electrostatic attraction (especially when the difference in charge density between the shale and coal surfaces can be exploited), or conceivably through metal-ion bridging.

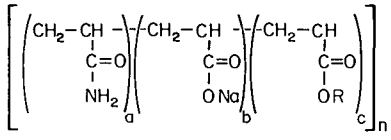

R = Methyl ($-CH_3$);
2-Ethylhexyl ($-CH_2-CH(C_2H_5)-(CH_2)_3-CH_3$)

Fig. 8. Possible structures of hydrophobic polymeric flocculants (from [55]).

TABLE 1

Selective floccuation separation of Upper Freeport coal using sedimentation at pH 7.5, FR-7 dosage = 0.02 mg g^{-1} and SMP = 300 mg l^{-1} [56]

Product	Weight (%)	Ash (%)	Distribution (%)	
			Ash	Coal
Single-step separation				
Flocs	87.0	5.6	32.8	96.4
Dispersed	13.0	76.4	67.2	3.6
Feed	100.0	14.8	100.0	100.0
Flocs	87.7	5.4	33.5	96.7
Dispersed	12.3	77.2	66.5	3.3
Feed	100.0	14.3	100.0	100.0
Flocs	85.4	5.7	32.8	94.6
Dispersed	14.6	68.4	67.2	5.4
Feed	100.0	14.9	100.0	100.0
Two-step separation				
Flocs	80.9	2.7	14.9	92.4
Dispersed 1	11.9	71.8	57.6	3.9
Dispersed 2	7.2	56.5	27.5	3.7
Feed	100.0		100.0	100.0
Flocs	78.9	2.9	15.1	90.0
Dispersed 1	10.5	73.2	51.8	3.3
Dispersed 2	10.6	46.3	33.1	6.7
Feed	100.0		100.0	100.0
Flocs	80.5	2.8	15.4	91.5
Dispersed 1	12.1	72.1	60.4	3.9
Dispersed 2	7.4	47.3	24.2	4.6
Feed	100.0		100.0	100.0

Applications of selective flocculation in mineral processing: case studies

Selective flocculation has been demonstrated to separate various minerals in laboratory and pilot plant testing as well as in several commercial operations in North America. A recent review of the application of selective flocculation in mineral processing was made by Yu and Attia [63]. In this article however, only four case studies on the application of selective flocculation technology in mineral processing are presented.

Separation of coal from mineral matter and pyrite

Various studies on the feasibility of selective flocculation of coal from slurries using hydrophobic flocculants were recently made by the author and his co-workers [55–58]. However, other attempts to utilize this concept have been made [59, 60, 62]. One set of experiments was reported by Attia and Driscoll [52]. In that study, tests were performed under near optimum conditions which were previously de-

termined experimentally. A raw coal sample from the Upper Freeport Seam was crushed and ground to −500 mesh (−25 microns), and a hydrophobic polymer, FR-7 (2,ethylhexylmethacrylate, a latex polymer emulsion provided by Calgon Corp., Pittsburgh, Pa.), was employed as the selective flocculant. Their experimental results are listed in Table 1. In a single step selective flocculation, the ash content was reduced from 14.7% to about 5.5% with 95% of the coal recovered. When a second step of selective flocculation was used, the ash content of the cleaned coal was reduced to 2.7%, with coal recovery over 90%. These results clearly indicated that deep cleaning of coal is technically feasible by selective flocculation. In these experiments, floc separation from suspension was made by preferential gravitational settling (sedimentation).

Since pyrite is also moderately hydrophobic, the hydrophobic polymer used for coal flocculation can also flocculate pyrite and impair its separation from coal. To prevent this, a specially developed hydrophilic anoinic polymeric dispersant, polyacrylic acid-xanthate (PAAX for short), or more accurately, sodium poly(acrylate-acrylodithiocarbonate) [55,61], having a preferential adsorption affinity to pyrite, was employed to depress pyrite flocculation and flotation. The structure of this dispersant/depressant is illustrated in Figure 9. It was also recognized that in the presence of heavy and/or coarse dispersed particles (e.g. pyrite particles, whose specific gravity is about 5.0, in coal slurry), selective flocculation efficiency using differential sedimentation for floc separation will be severly affected. To overcome this problem, Attia and co-workers [61] employed dissolved air flotation technique for separating coal flocs from dispersed particles (particularly pyrite particles). In the separation of the coal flocs from the slurry by disolved air flotation, very fine air bubbles were produced by the dissolved air apparatus. To stabilize the micro air bubble in the flotation system, methyl isobuytl carbinol (MIBC) was used at a dosage of 0.82 g kg^{-1}. The released micro air bubbles attached to the hydrophobic coal flocs, and carried the flocs to the overflow, leaving pyrite and ash mineral particles in the flotation cell. The data listed in Table 2 indicates that this separation was very efficient. In a single step separation, the ash content was reduced from about 7.6% to 3.5%, total sulfur was reduced from 2.76% to 1.64%, and coal recovery was as high as about 95%. In the two step separation, the ash content was reduced to

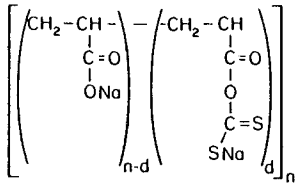

Fig. 9. Postulated structure of PAAX/sodium poly(acrylate-acrylodithiocarbonate) dispersant (from [61])

TABLE 2

Selective flocculation disolved air flotation cleaning of pre-cleaned Pittsburgh No. 8 coal at PAAX concentration = 200 mg l^{-1}, pH 8.0, FR-7 concentration = 5 mg l^{-1}, SMP concentration = 500 mg l^{-1} [61]

Product	Weight (%)	Ash (%)	Total S (%)	Distribution (%)		
				Ash	Total S	Coal
Single-step separation						
Flocs	88.8	3.8	1.72	44.0	52.2	92.5
Dispersed	11.2	38.2	12.25	56.0	47.8	7.5
Feed	100.0	7.6	2.91	100.0	100.0	100.0
Flocs	91.4	3.5	1.64	40.5	54.3	95.7
Dispersed	8.6	54.7	13.81	59.5	45.7	4.3
Feed	100.0	7.6	2.67	100.0	100.0	100.0
Flocs	91.8	4.7	1.67	56.8	57.5	94.7
Dispersed	8.2	40.5	14.65	43.2	42.5	5.3
Feed	100.0	7.7	2.67	100.0	100.0	100.0
Two-step separation						
Flocs	85.5	2.8	0.94	30.5	29.3	90.3
Dispersed 1	6.9	42.5	13.48	36.6	33.9	4.3
Dispersed 2	7.6	34.2	13.27	32.9	36.8	5.4
Feed	100.0	7.9	2.74	100.0	100.0	100.0
Flocs	88.1	2.4	0.97	30.1	30.3	92.4
Dispersed 1	5.8	56.9	14.77	47.2	30.4	2.7
Dispersed 2	6.1	26.0	18.17	22.7	39.3	4.9
Feed	100.0	7.0	2.83	100.0	100.0	100.0
Flocs	86.2	2.3	0.87	25.7	26.6	91.2
Dispersed 1	6.0	45.9	13.30	36.1	28.4	3.5
Dispersed 2	7.8	37.1	16.2	38.2	45.0	5.3
Feed	100.0	7.5	2.81	100.0	100.0	100.0

2.3%, total sulfur was substantially reduced to only 0.9% (i.e. over 90% pyritic sulfur removal), and the coal recovery was still higher than 90%.

Selective flocculation of copper ores

Attia and co-workers [42, 49, 62] studied the mechanisms of selective flocculation of several copper minerals. In their research, a number of water-soluble polymers of high molecular weight, incorporating sulphydryl (–SH) or other groups which selectively complex or chelate heavy metal ions, particularly copper, were tested. Evidence for selectivity of flocculation with synthetc mixtures of finely-divided minerals was obtained. For example, xanthate containing polymers (namely cellulose, cellulose derivatives and PVA xanthates) showed marked selectivity towards minerals like galena, pyrite, chalcopyrite and chrysocolla, while they had little or no flocculating effects on calcite, quartz, feldspar and kaolinite. These polyxanthates almost fulfill the ideal case of yes-or-no adsorption. With these specifically adsorb-

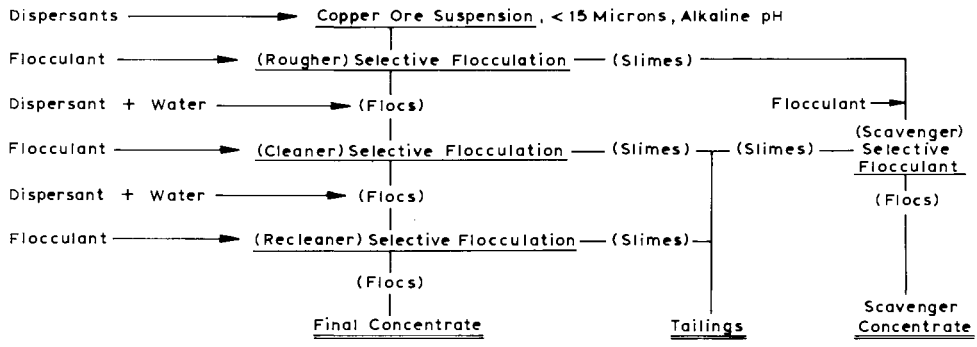

Fig. 10. Flowsheet used for processing a complex copper ore by selective flocculation (from [36])

ing polymers, selective flocculation of chrysocolla from quartz and galena from calcite could be achieved. However, it was found that soluble Cu^{+2} ions can activate mixtures of feldspar and kaolinite, therefore rendering the polyxanthate flocculant unselective. Moreover, by the addition of a masking agent such as Na_2S, this problem could be avoided. The chelating flocculant, polyacrylamide-glyoxal-bis-2-hydroxyanil (PAMG), was found to readily flocculate copper minerals from mixture with calcite, quartz, feldspar, and dolomite in the presence of competitor reagents such as polyphosphates or polyacrylates. Qualitative flocculation tests (color of flocs) at pH 10 showed that chrysocolla was readily separated from calcite; chrysocolla and malachite from mixture with feldspar, calcite and quartz; malachite from dolomite, etc.. Selective flocculation was used to concentrate copper miner-

TABLE 3

Processing complex copper ore by selective flocculation

Products	Cu (%)	Recovery (%)	Conditions
Final concentrate	22.5	69	2.5% solids
Scavenger concentrate	7.3	17	Distilled water
Tailings	1.1	14	
Final concentrate	23.5	64	5.0% solids
Scavenger concentrate	3.8	23	Distilled water
Tailings	1.5	13	
Final concentrate	19.6	62	10% solids
Scavenger concentrate	5.3	12	Tap water
Tailings	2.0	26	
Final concentrate	18.2	62	30.8% solids
Scavenger concentrate	3.0	2	Tap water
Tailings	2.0	36	

Feed: 5.4% Cu; <15 microns; dispersants: Calgon + Dispex N40; flocculant: PAMG

als from a refractory copper ore using the chelating polymer PAMG [48]. In order to obtain a useful enrichment ratio, multiple stages of flocculation and redispersion were found necessary in order to release entrapped, unwanted particles. The typical flowsheet used in separating various copper minerals from natural ore suspensions is outlined in Figure 10 and typical results obtained by this technique are shown in Table 3. General inspection of these results clearly indicates the technical feasibility of processing finely disseminated copper ores by selective flocculation technique.

Selective flocculation of iron ore

Commercial application of selective flocculation for upgrading iron ore is employed by Cleveland Cliffs Company at the Tilden Processing Plant in Michigan [33]. The Tilden operation is based on a selective flocculation-desliming step, where the iron-bearing minerals are selectively flocculated using starch and separated from fine silica particles by settling in a thickener. This step is followed by a cationic flotation step where the entrapped coarse silica particles in the floc are separated from the flocculated iron minerals. The ore feed contains about 36.6% Fe and 46.4% SiO_2, mostly as hematite, magnetite, geothite, chert and quartz (silica). Adequate liberation occurred when approximately 90% of the feed passed through a 400-mesh sieve (37 microns). The plant processes over 40 million tons per year of iron ore to produce about 10 million tons of concentrate containing about 5% SiO_2 and 62–64% Fe, with iron recovery of 75–80%. Another commercial plant operated by the same company, the Empire plant, having the same flowsheet and production capacity as those of Tilden's is in operation also in Michigan.

Selective flocculation of potash (sylvinite) ores

Banks [34] described the development of the commercial application of a selective flocculation-flotation process for upgrading a sylvinite (potash) ore at Cominco Limited's operations in Saskatchewan, Canada. The ore contained sylvinite (KCl + NaCl) as the chief resource for potash, mixed with gangue minerals, such as dolomite, hematite, quartz, kaolinite, illite, chlorite and anhydrite. The gangue minerals amounts to 4.5–8.0% by weight of the total ore. Using the selective flocculation-flotation flowsheet outlined in Figure 11, 86% of commercial grade potash concentrate could be recovered. The reagents used consisted of a non-ionic polyacrylamide flocculant at 13.6 gram per ton of feed, and a cationic collector, Aero 870 (American Cyanamid Company), for selective flocculation-flotation of fine gangue (clay) minerals, and ethoxylated alkylmic alkylguanidine complex, at 18.6 gram per ton of the feed, for flotation of silivinite mineral from coarse gaungue minerals.

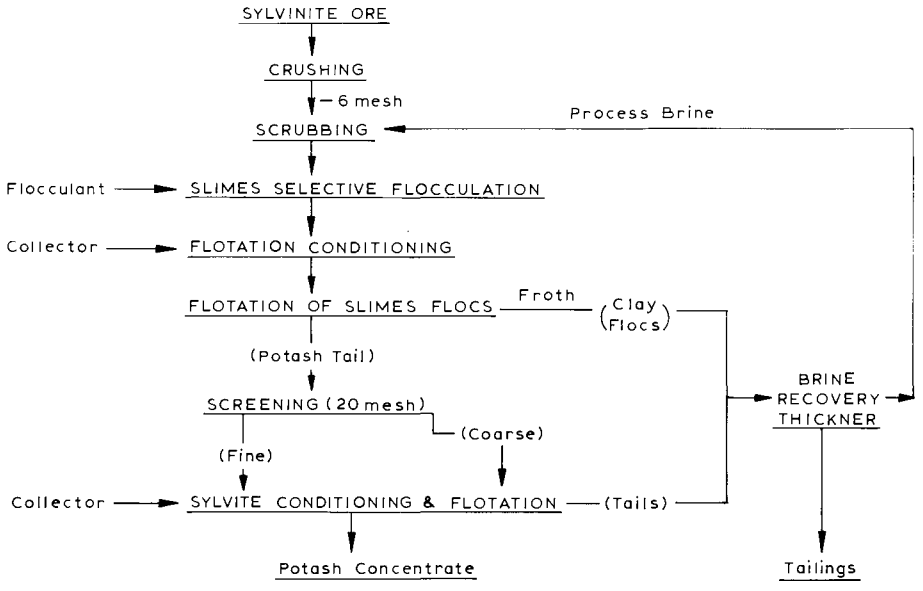

Fig. 11. Selective flocculation–flotation of slimes from Comico's sylvinite ore (from [34]).

Acknowledgements

The author would like to express his gratitude to Mr. S. Yu for his assistance in writing the section on selective flocculation and to Mr. M. Yu for typing and proofing this manuscript.

References

1 C.R. O'Melia, in: B.M. Moudgil and P. Somasundaran (Editors), Flocculation, Sedimentation and Consolidation, Engineering Foundation, New York, N.Y., 1986, pp. 159–169.
2 J. Gregory, in: B.M. Moudgil and P. Somasundaran (Editors), Flocculation, Sedimentation and Consolidation, Engineering Foundation, New York, N.Y., 1986, pp. 125–138.
3 M. Yusa, in: Y.A. Attia (Editor), Flocculation in Biotechnology and Separation Systems, Elsevier, 1987, pp. 755–764.
4 S. Asakura and F. Oosawa, J. Chem. Phys. 22 (1954): 1255.
5 D.A. Napper, Polymeric Stabilization of Colloidal Dispersions, Academic Press, 1983.
6 C. Bondy, Trans. Faraday Soc., 35 (1939): 1093.
7 J. Lyklema, in: B.M. Moudgil and P. Somasundaran (Editors), Flocculation, Sedimentation and Consolidation, Engineering Foundation, New York, N.Y., 1986, pp. 3–21.
8 S.V. Krishnan and Y.A. Attia, in: P. Somasundaran and B.M. Moudgil (Editors), Reagents in Mineral Technology, Marcel Dekker, 1988, p. 485.
9 J. Gregory, in: Y.A. Attia (Editor), Flocculation in Biotechnology and Separation Systems, Elsevier, 1987, pp. 31–44.

10 R.H. Smellie and V.K. La Mer, J. Colloid Sci., 23 (1958): 589.
11 R. Hogg, J. Colloid Sci., 102 (1984): 232.
12 D.M. Deason, in: Y.A. Attia (Editor), Flocculation in Biotechnology and Separation Systems, Elsevier, 1982, pp. 21–30.
13 R. Hogg, in: B.M. Moudgil and B.J. Scheiner (Editors), Flocculation and Dewatering, Engineering Foundation, 1989, pp. 143–152.
14 L.A. Glasgow, Y.H. Kim and J.P. Hsu, in: B.M. Moudgil and P. Somasundaran (Editors), Flocculation, Sedimentation and Consolidation, Engineering Foundation, 1986, pp. 191–204.
15 L.A. Glasgow, Chem. Eng. Progress, August 1989, pp. 51–55.
16 H. Schubert, in: K.V.S. Sastry and M.C. Fuerstenau (Editors), Challenges in Mineral Processing, SME/AIME, 1989, pp. 272–289.
17 R. Hogg, R.C. Klimpel and D.T. Ray, in: B.M. Moudgil and P. Somasundaran (Editors), Flocculation, Sedimentation and Consolidation, Engineering Foundation, 1986, pp. 217–228.
18 L.G. Austin and P.T. Luckie, Powder Technology, 5 (1971): 215.
19 P.R. Klimpel and L.G. Austin, Int. J. Miner. Process., 4 (1977): 7.
20 A.N. Kolmogorov, Doklady Akad. Nauk SSSR, 66 (1949): 825.
21 J.O. Hinze, AICHE, 1 (1955): 289.
22 J.L. Cleasby, J. Environ. Sci., 110 (1984): 875.
23 R.S. Brodkey, personal communication, The Ohio State University, 1986.
24 V. Kogan, K.H. Driscoll and Y.A. Attia, in: Y.A. Attia (Editor), Flocculation in Biotechnology and Separation Systems, Elsevier, 1987, pp. 321–334.
25 S. Krishnan and Y.A. Attia, in: B.M. Moudgil and P. Somasundaran (Editors), Flocculation, Sedimentation and Consolidation, Engineering Foundation, 1986, pp. 229–248.
26 J.A. Kitchener, in: K.J. Ives (Editor), The Scientific Basis of Flocculation, Sijthoff and Noordhoff, 1978.
27 M.J. Pearse, in: Proceedings of Consolidation and Dewatering of Fine Particles Conference, Univ. of Alabama, August 1982.
28 P.J. Lafforgue, N. Peyriere and N.J. Roche, AIME Annual Meeting, Dallas, Feb. 1982, preprint 82-22.
29 R.J. Akers, Flocculation, Institute of Chem. Engineers, London, 1975.
30 Y.A. Attia, Sep. Sci. and Tech., 17 (1982): 485.
31 Malchesky, personal communication, Cleveland Clinic, Cleveland, Ohio, 1988.
32 T. Lindstrom and G. Glad-Nordmark, J. Colloid Interface Sci., 94 (1983): 404.
33 R. Sisselman, Eng. Miner. J., 176 (1975): 52.
34 A.F. Banks, in: P. Somasundaran and N. Arbiter (Editors), Beneficiation of Mineral Fines, NSF Workshop Report, 1979.
35 B. Yarar and J.A. Kitchener, Trans. Inst. Min. Metal., 79 (1970): 23.
36 Y.A. Attia and D.W. Fuerstenau, in: N. Li (Editor), Recent Developments in Separation Science, Vol IV, Ch. 5, CRC Press, Florida, 1978, p. 52.
37 Y.A. Attia, in: Y.A. Attia (Editor), Flocculation in Biotechnology and Separation Systems, Elsevier, 1986, pp. 227–246.
38 J.A. Kitchener, Filtr. Sep., 6 (1969): 553.
39 R.W. Slater, J.P. Clark and J.A. Kitchener, Proc. Brit. Ceram. Soc., 13 (1969): 1.
40 F.M. Fowkes, Chemistry and Physics at Interfaces, Am. Chem. Soc., Washington, D.C., 1965.
41 J. Drzymala and D.W. Fuerstenau, Int. J. Miner. Process., 8 (1981): 265.
42 Y.A. Attia and J.A. Kitchener, Proceedings of 11th Int. Min. Process. Congr., University of Cagliari Press, Calgliari, Italy, 1975.
43 G.C. Sresty, A. Raja and P. Somasundaran, in: N. Li (Editor), Recent Advances in Separation Science, Vol. IV, CRC Press, 1978.

44 G. Baudet, Ind. Miner. Mineralurgie, 1 (1978): 19.
45 Y.A. Attia, Int. J. Miner. Process., 4 (1977): 191.
46 Y.A. Attia, R.G. Sinclair, R.A. Markle, M. Cousin, R.O. Keys and S.V. Krishnan in: Y.A. Attia (Editor), Flocculation in Biotechnology and Separation Systems, Elsevier, 1986, pp. 263–276.
47 C.R.A. Clauss, E.A. Appleton and J. Vink, Int. J. Miner. Process., 3 (1976): 27.
48 Y.A. Attia, Int. J. Miner. Process., 4 (1977): 209.
49 Y.A. Attia, Selective Flocculation of Copper Minerals, Ph.D. Thesis, Imperial College, University of London, 1974.
50 Y.A. Attia, personal communication with J.A. Kitchener and D.W. Fuerstenau, 1975.
51 J. Rubio and J.A. Kitchener, Trans. Inst. Min. Metall., 86 (1978): 97.
52 G. Schwarzenbach, in: H.J. Emeleus and A.G. Sharpe (Editors), Advances in Inorganic Chemistry and Radiochemistry, Vol. 3, Academic Press, 1961, p. 257.
53 Y.A. Attia, 16th Annual Meeting of the Fine Particle Society, April 22–26, 1985, Miami Beach, Fla.
54 C.S. Tsai, Fundamentals of Coal Beneficiation and Utilization, Elsevier, 1982.
55 Y.A. Attia, in: Y.A. Attia (Editor), Processing and Utilization of High Sulfur Coals, Elsevier, 1985, p. 267.
56 Y.A. Attia and K.H. Driscoll, in: Y.A. Attia, B.M. Moudgil and S. Chander (Editors), Interfacial Phenomena in Biotechnology and Materials Processing, Elsevier, Amsterdam, 1988, pp. 317–332.
57 Y.A. Attia, S. Yu and S. Vecci, in: Y.A. Attia (Editor), Flocculation in Biotechnology and Separation Systems, Elsevier, 1987, pp. 547–564.
58 Y.A. Attia and S. Yu, in: Y.P. Chugh and R. Caudle (Editors), Processing and Utilization of High Sulfur Coals — II, Elsevier, 1987.
59 J. Rosenbaum, Y.A. Attia and D.W. Fuerstenau, Unpublished Report, University of California, Berkeley, Calif., 1977.
60 M.J. Littlefair and N.R.S. Lowe, Int. J. Miner. Process., 17 (1986): 187.
61 Y.A. Attia, F. Bavarian and K.H. Driscoll, Coal Prep., 6 (1988): 35.
62 Y.A. Attia, S.V. Krishnan and D.M. Deason, Selective Flocculation Technology, Group Program, Final Report, June 10, 1983, Battelle-Columbus, Ohio.
63 S. Yu. and Y.A. Attia, in: Y.A. Attia (Editor), Flocculation in Biotechnology and Separation Systems, Elsevier, 1987, pp. 601–638.

Chapter 10

Shear-flocculation

L.J. WARREN

The shear-flocculation effect

Shear-flocculation is a method for selectively aggregating very fine particles of one mineral from others in a suspension. Shear flocculation has potential as a means of upgrading deposits of finely-grained minerals, and, more generally, for separating different types of particles suspended in a fluid.

The shear-flocculation effect that is normally observed is one in which ultrafine particles suspended in an aqueous solution of a surfactant are made to aggregate by applying a shear field of sufficient magnitude [1]. The surfactant should be one that renders the particle surfaces hydrophobic and for this purpose reagents often used as flotation collectors are suitable [2]. It is not yet clear what the most appropriate shear field is, but a baffled cylindrical tank is commonly used [3].

In the last ten years there has been an increasing amount of research into shear-flocculation and related aspects, e.g. Xu and Yoon [4], and it is appropriate to review the current state of the art. Warren [1] coined the term "shear-flocculation" to try to distinguish the effect from, for example, coagulation by electrolytes or flocculation by soluble polymers. However, other authors have used different terminology. Wojcik [5] refers to "selective aggregation", Wei Dawei et al. [6] to "hydrophobic agglomeration", Hu Yongping and Yu Mulong [7] to "controlled dispersion–shear flocculation", Lu Shouci et al. [8] to "hydrophobic aggregation" and Li and Fuerstenau [9] to the "influence of surfactant adsorption on stability (of suspensions)".

The key features of shear-flocculation can be made clearer by reference to a typical experiment. Li and Fuerstenau [9] prepared dilute suspensions of fine hematite (Fe_2O_3) particles at pH 3, where the hematite was positively charged and dispersed. There was no change in suspension turbidity after stirring in a baffled vessel at 1600 rpm for 60 min. However, in the presence of 10^{-4} mol l^{-1} sodium dodecyl sulfate (which made the hematite particles hydrophobic and negatively charged) there was extensive aggregation that increased with time of stirring at 1600 rpm. To induce significant aggregation, speeds above 800 rpm were required.

Similar results had been reported by Warren [1] for ultrafine scheelite ($CaWO_4$) suspended in sodium oleate solutions, except that in this case the scheelite particles were highly negatively charged both before and after adsorption of the hydrophobe, sodium oleate.

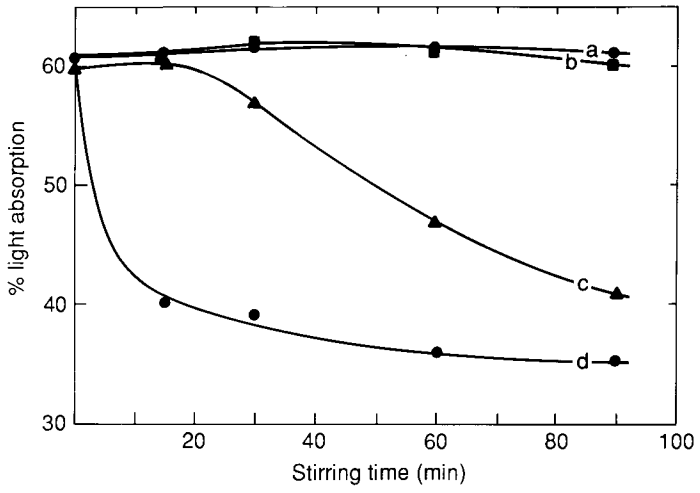

Fig. 1. Change in turbidity of aggregating scheelite suspensions (0.35 g l^{-1}, 0.75-1.4 μm, pH 10, 10^{-4} mol l^{-1} sodium oleate) with time of stirring. Curve *a*: 200 rpm; *b*: 850 rpm; *c*: 1700 rpm; *d*: 1700 rpm; pretreated in 2.5 x 10^{-4} mol l^{-1} $MgCl_2$, pH 9.3. Curve *a* also refers to the suspension stirred in the absence of sodium oleate at 200–1700 rpm. (From Warren [1].)

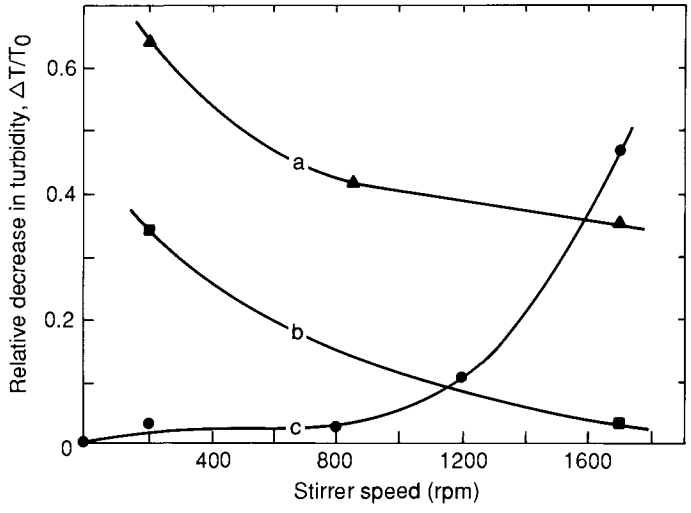

Fig. 2. Relative decrease in turbidity of scheelite suspensions after 90 min stirring as a function of the stirrer speed, for various types of aggregating agents. The greater the relative decrease in turbidity, the greater the degree of aggregation. Curve *a*: coagulation in 0.5 mol l^{-1} NaCl; *b*: flocculation by a nonionic polyacrylamide; *c*: aggregation in 10^{-4} mol l^{-1} sodium oleate. (From Warren [1].)

It was found that:

(a) the particles need to be made hydrophobic before aggregation can occur, given the same speed and time of stirring, and given that the particles are highly charged (Figure 1);

(b) a minimum shear rate is needed to initiate the aggregation process (Figures 1 and 2); and

(c) the flocs formed are stronger than those produced by coagulation or flocculation, since these tend to breakup at higher shear rates (Figure 2).

These characteristics suggest that shear-flocculation may have advantages as a technique for selective aggregation. For example, the flocs produced should be tough enough to withstand the turbulence in mineral processing operations, the flocs will have hydrophobic surfaces and should be able to be separated from remaining hydrophilic dispersed particles by flotation, and, a degree of selectivity in the aggregation should be assured by choosing surfactants already proven as selective collectors in flotation.

Parameters affecting shear-flocculation

Particle hydrophobicity

The observation that particles suspended in aqueous solutions tend to stick together when their surfaces are made hydrophobic pre-dates the present studies of the shear-flocculation effect. Alexander and Iler [10] formed weak, planar aggregates from 50 nm silica particles by mixing with a dilute solution of the quaternary amine, dodecyl trimethyl ammonium bromide. A micelle of amine was thought to adsorb on one silica spheroid and then bridge across to an unoccupied spot on another silica spheroid (Figure 3).

Greene and Duke [11] found that in order to remove small amounts of TiO_2 impurity from clay it was beneficial to add larger calcite ($CaCO_3$) particles and sodium oleate before attempting flotation of the TiO_2. It was proposed that the hydrophobic calcite particles collected the similarly hydrophobic TiO_2 particles in preference to the clay, which was hydrophilic, and that flotation then removed the calcite with its coating of impurity TiO_2. This has been called "carrier flotation" and, although it involves the shear-flocculation effect, will not be considered further in this review. Somasundaran et al. [12] observed that, when colloidal alumina (Al_2O_3) was suspended in dilute solutions of sodium dodecyl sulfonate, increasing the surfactant concentration changed the surface charge of the alumina from positive, through zero to negative, but that the alumina did not redisperse as the alumina became negatively charged; aggregation in fact increased. It was speculated that the adsorbed surfactant might bridge between particles thereby lowering the free energy of the system by removing some of the (hydrophobic) hydrocarbon chains from the aqueous environment.

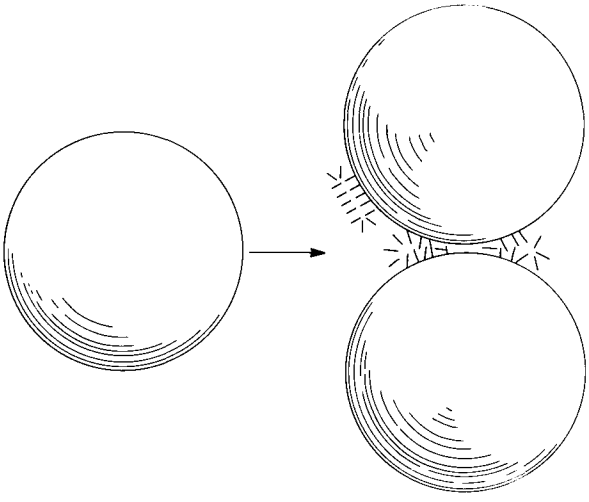

Fig. 3. An early explanation of hydrophobic association between particles involving adsorption of micelles (from Alexander and Iler [10]).

Aggregation between hydrophobic particles is of course a key part of the shear-flocculation of ultrafines and a number of different systems have been discovered that make the surfaces of particular minerals in a mixture hydrophobic. Sodium oleate in alkaline solution and in the presence of sodium silicate selectively adsorbs on scheelite rather than on the silicate mineral, garnet [13]. Alkaline oleate in the presence of sodium silicate and another polymeric dispersant made apatite [Ca_5 (PO_4)$_3$ (OH, F, Cl)] hydrophobic in preference to rhodochrosite ($MnCO_3$) [7]. A 2 : 1 emulsion of kerosene : oleate with sodium hexametaphosphate as dispersant made siderite ($FeCO_3$) hydrophobic in preference to quartz [8]. Particles of coal in a Polish deposit were preferentially aggregated in the presence of siliceous gangue by small additions of diesel oil [5] (see Chapter 12). Acidic solutions of sodium dodecyl sulfate made hematite hydrophobic in preference to quartz [14]. In shear-flocculation of galena (PbS)–quartz and chalcocite (Cu_2S)–quartz mixtures, Dippenaar [15] found that potassium amyl xanthate or potassium hexyl xanthate made the sulfides preferentially hydrophobic.

In some systems the surfactant tends to adsorb on all minerals and to improve selectivity a "modifier" is essential. For example, in shear-flocculation of wolframite [(Fe,Mn) WO_4]–quartz mixtures Wei et al. [16] found that pre-treatment with $CaCl_2$ or $FeCl_3$ was required before sodium oleate would adsorb selectively on the wolframite.

These findings are not surprising to anyone familiar with the technique of froth flotation where the same principles apply.

However, there may be some differences in the degree and type of hydrophobicity required in shear-flocculation and flotation. It seems that for adsorbed surfactants shear-flocculation may require longer chain lengths. Zollars and Ali [17] present evidence suggesting that a chain with 14 carbons is required for good shear-flocculation. Dippenaar [15] found that potassium ethyl xanthate produced very weak flocs with galena whereas the hexyl xanthate gave excellent shear-flocculation. Warren [2] observed that styryl phosphonic acid and benzyl arsonic acid would float cassiterite (SnO_2) but would not induce shear-flocculation. Longer chain surfactants such as sodium oleate or a sulfosuccinamate were successful.

With respect to the concentration of surfactant, and hence surface coverage, required, Sivamohan and Cases [18] find that shear-flocculation needs lower surface coverages than flotation. On the other hand, Warren [2] concluded that shear-flocculation required nearly monolayer coverage, whereas flotation can proceed with less adsorbed surfactant.

Shear rate

With most systems it has been found necessary to shear the suspension of hydrophobic particles above some critical shear rate in order to initiate aggregation, e.g. see Figure 2. In small stirred tanks, impeller speeds above 500 rpm are often required. This can be explained by the fact that in such systems the hydrophobic particles are also charged and repel one another, and it is necessary to give them additional kinetic energy so that they can approach closely enough to allow the attractive hydrophobic forces to take over.

Shear-flocculation tests have been carried out mainly in stirred tanks. Unfortunately, stirred tank reactors produce complicated turbulent flows with a wide range of shear rates. Camp [19] suggested that an average shear rate may be defined and that it is related directly to the impeller speed. Most authors who have studied the effect of shear rate on the degree of shear-flocculation have merely quoted impeller speeds. These of course are not necessarily comparable in terms of shear rates unless the tank and impeller geometries are identical.

Koh et al. [20] were able to define the critical shear rate more precisely by carrying out the shear-flocculation test in a Couette viscometer (Haake Rotovisco RV3). For a sample of ultrafine scheelite suspended in dilute sodium oleate solution they found that there was a critical shear rate of 138 s^{-1} below which no shear-flocculation occurred. Above this value, the rate constant for the rate of decrease of the mass of particles finer than 2 μm (their measure of the degree of flocculation) increased approximately linearly with shear rate up to $\sim$1000 s^{-1} (Figure 4).

A Couette-flow shear vessel was also used by Dippenaar [15] to study the shear-flocculation of 2 μm galena in potassium amyl xanthate solutions. Slight aggregation was observed at 122 s^{-1}; this increased dramatically at 366 s^{-1}. Dippenaar claimed that shear-flocculation was "more effective" with shear vessels having Couette flow

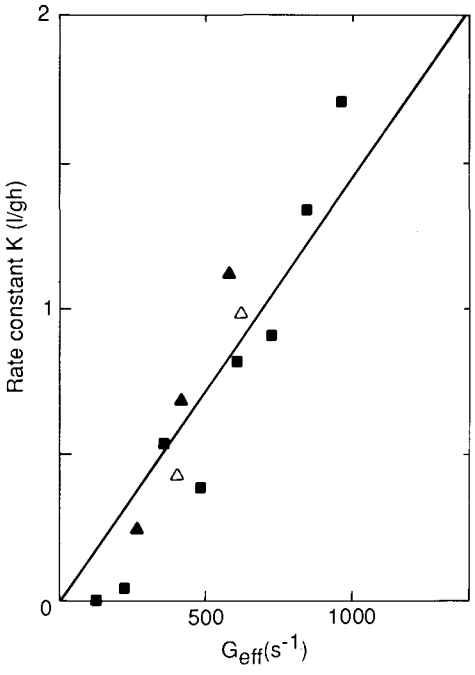

Fig. 4. Experimental flocculation rate constant against effective shear rate for Couette flow (■) and for stirred tanks (▲, $D/T = 0.68$ and △, $D/T = 0.54$). G_{eff} is the "effective" shear rate. (From Koh et al. [20].)

than in stirred tanks. However, the results of Koh et al. [20] suggest that the rate of shear-flocculation is similar at similar "effective shear rates" in either type of vessel (Figure 4).

Tank design

The geometry of the flocculation tank, the number and size of baffles, the type, size and location of the impeller in the tank, all affect the degree of shear-flocculation. However the optimum design of tank is not yet known.

Because a critical shear rate is required to initiate shear-flocculation, it has been assumed that it is the regions of high shear rate in the tank that are most active in causing shear-flocculation [2, 20, 21]. Koh [21] has taken this concept further and defined three zones: an impeller zone of high shear rate, a bulk zone of intermediate shear rate and a "dead space" at the top and bottom of the tank in which the shear rate is below the critical value for aggregation.

The impeller, depending on its design, also acts as a pump and circulates suspension from the impeller zone to the bulk zone and back again to the impeller. The frequency with which particles circulate through the impeller zone and the time

particles spend in each zone thus depend on the impeller pumping rate, and the relative volumes of the three zones.

Maxon and Oldshue [22] pointed out that the energy input by an impeller to the fluid is dissipated through both its pumping action and its shearing action and that it is not known what the optimal split between pumping and shearing should be for flocculation. The "average shear rate D", defined by:

$$D = \left(\frac{\text{power dissipated per unit volume}}{\text{fluid viscosity}} \right)^{1/2} \tag{1}$$

does not distinguish between these two modes of energy dissipation and is not necessarily the best criterion for flocculation tank design.

Despite these qualifications on the interpretation and use of D values they have been used to characterize suitable stirred tank regimes. Good shear-flocculation of ultrafine scheelite in alkaline sodium oleate solutions was obtained by Warren [2] and Koh et al. [20] with D values of the order of 1000 s^{-1}. However, in Couette viscometers where more precise values for shear rate can be calculated, the shear rate to initiate shear-flocculation was much lower, of the order of 100 s^{-1} [15, 23].

Particle charge

The surface charge on the suspended particles, normally measured by their zeta potential, affects the selectivity, the ease and the degree of shear-flocculation and is therefore an important parameter.

In a mixture of minerals, unless all the particles are initially dispersed, it will be difficult subsequently to selectively aggregate the particles of one particular mineral [24]. A convenient way of ensuring initial dispersion is to give all particle surfaces a substantial charge by choosing an appropriate pH value and appropriate dispersing reagents. For example, Hu and Yu [7] found that in order to keep rhodochrosite particles dispersed whilst allowing apatite particles to shear-flocculate it was necessary to keep the pH between 9.5 and 11.5 and in addition to add two dispersants, as well as sodium oleate. Lu et al. [8] used sodium hexametaphosphate to disperse mixtures of siderite–quartz and rhodochrosite–quartz. Warren [2] found that suspensions of 3 μm cassiterite particles required a pH greater than 10 to maintain a dispersed state on stirring (zeta potential approximately −50 mV). However, when the surfactant was added, its adsorption on the cassiterite caused an increase in the magnitude of the zeta potential so that the suspensions were now dispersed even at pH 4–6 (in the absence of stirring). Thus, the surfactant used to make a chosen mineral surface hydrophobic may, in some instances, also act as a dispersant for that mineral, at low shear rates.

The critical shear rate required to force the hydrophobic particles into adhesive contact should decrease with decreasing surface charge. One can imagine an ideal situation in which the surfactant adsorbs selectively on the target mineral both

making it hydrophobic and neutralizing its surface charge, whilst the other minerals retain high surface charges and hydrophilic surfaces. Gentle mixing should then cause hydrophobic aggregation of the target mineral without the need for a critical shear field.

However, in the systems studied so far, in order to achieve selectivity it seems to have been necessary to have *all* particle surfaces relatively highly charged during the shear-flocculation step.

Flocculation time

Generally, shear-flocculation appears to be a slow process, although this does depend on the surface charge, the particle size and the particle concentration. In stirred tanks, residence times of the order of 30 min seem necessary [1, 3, 7, 9, 13, 15, 25]. However, Wei et al. [6] obtained high recoveries of wolframite after only 3 min stirring at 1600 rpm, although it is possible that in their case the particles carried a low surface charge. Dippenaar [15] observed extensive shear-flocculation of galena and chalcocite after only a few minutes in Couette flow; a low charge may again explain this rapid aggregation.

Warren [1] speculated that shear-flocculation was autocatalytic in the sense that the initial aggregates of two or three particles were slow to form, but that once formed, these small aggregates grew more rapidly.

Curve *c* in Figure 1 shows the slow increase in the degree of aggregation with stirring time and the 15 min delay before significant aggregation is observed (autocatalytic effect) while curve *d* shows a great increase in the aggregation rate when the zeta potential is lowered, in this case from about −45 to −25 mV [1].

Particle size

Particles of different sizes will not necessarily be aggregated to the same extent by the shear-flocculation process. In general, smaller particles require higher shear rates than larger particles.

Warren [1] noted that in a small stirred tank, an impeller speed of 850 rpm was too low to cause shear-flocculation of 1 μm scheelite particles in 10^{-4} mol l^{-1} sodium oleate solution. However the same speed caused extensive flocculation of 9 μm particles, slight flocculation of 20 μm particles and no flocculation of 27 μm particles. Thus at 850 rpm, shear-flocculation only occurred with particles in an intermediate size range, 5–20 μm. At 1700 rpm the size range for shear-flocculation shifted to 1–12 μm.

Evidently, although larger particles collide with sufficient energy to cause shear-flocculation they are immediately redispersed. This is consistent with the analysis of Goren [26], who showed that for a doublet of particles in a linear shear field the force tending to separate them is proportional to the square of the particle diameter. In other words, the separating shear increases rapidly with particle size.

Laboratory tests have been carried out on various size particles, either wide size distributions resulting from classifying devices [7, 27] or grinding machines [8, 15], or narrow size distributions from repeated beaker decantation [1, 2, 13, 15]. The average particle size has usually been between 3 and 10 μm. Relatively little work has been carried out on particles finer than 2 μm. These require high shear rates and are the most difficult to deal with in practice [17, 25, 28]. There is evidence that particle inertia and the deviation of particles from streamlines is an important aggregation mechanism even for particles as small as 1 μm [29]. This supports the idea that for particles to undergo shear-flocculation they require a minimum kinetic energy and that for a given shear regime smaller particles will be less likely to have the critical kinetic energy.

Particle concentration

Most of the laboratory tests on shear-flocculation have been carried out at low particle concentrations, usually less than 10 g of solids l^{-1}. In order to measure turbidity changes directly, suspensions have often been less than 1 g l^{-1} [1, 9]. Warren [1] found that increasing the particle concentration from 0.35 to 3.5 g l^{-1} caused a ten-fold increase in the *initial* rate of aggregation, but that after 90 min stirring the degrees of shear-flocculation were similar. Using larger stirred tanks (~3 l) Koh and Warren [25] found that suspensions of 10, 33 and 100 g l^{-1} ultrafine scheelite ore required different reagent additions for acceptable shear-flocculation and flotation and that other effects, such as the generation of voluminous foams during subsequent flotation at 100 g l^{-1}, made comparison of flocculation performance difficult. It appeared that the 33 g l^{-1} suspensions gave better performance overall. More work is required to determine the optimum particle concentration for shear-flocculation.

Suspension composition (head grade)

Investigations of the applicability of shear-flocculation to suspensions of fine particles have usually commenced with studies on single minerals, followed by studies on artificial mixtures with, finally, tests on natural ores. Along the way, the suspension composition changes from 100% of the valuable mineral to about 1% in the natural ore. Unless shear-flocculation gives high recovery on single mineral suspensions and good selectivity on artificial mixtures, it is unlikely to be useful for natural ores.

A loss in performance on going to lower head grades was shown by Jarrett and Warren [13] in their work on 10:90 and 50:50 mixtures of scheelite:garnet. Depending on particle size, the 10% mixtures were upgraded by shear-flocculation and sedimentation to to 20–52% at 68–85% recovery of scheelite. The 50% mixtures were upgraded, depending again on particle size, to 70–93% at 78–95% recovery.

In order to decide whether the performance with 10% mixtures was better or worse than that with 50% mixtures, a logarithmic version of Gaudin's selectivity index was used. This statistic indicated that performance was better with the 50 : 50 mixture.

In the tests performed by Koh and Warren [27] on 1 μm scheelite, about half the particles were converted to fast-floating flocs. Later tests on natural ore, containing only 1.5% scheelite, could only convert one quarter of the 1 μm scheelite particles to fast-floating flocs [25]. The problem of declining performance with decreasing head grade, might not be due to head grade alone but also to, for example, a change in the surface composition of the scheelite particles.

Magnetic fields

Lu et al. [8] found an interesting additional effect by carrying out the shear-flocculation step in a magnetic field. For weakly magnetic minerals such as rhodochrosite and siderite, the degree of aggregation increased over that observed for shear-flocculation alone or magnetic aggregation alone. Higher concentrate grades were obtained in mixtures of these minerals with quartz by using the combined shear and magnetic fields.

Measurement of the degree of shear-flocculation

Ratio of mass of sediment to mass of suspension

When aggregation occurs the aggregates normally settle faster than the remaining dispersed particles, and accumulate preferentially in the sediment. If a settling time is chosen that takes account of the relative settling velocities of discrete particles and aggregates, the supernatant suspension can be decanted or siphoned off after this time, and the sediment weighed and, in the case of mixtures, analyzed for the valuable mineral [6, 8, 13]. The degree of shear-flocculation may then be taken as the ratio of mass of valuable mineral in the sediment to the mass originally in suspension. Note that the sediment will always be contaminated by some discrete particles.

Size distribution of flocculated suspension

During shear-flocculation, the size distribution of a suspension shifts to larger sizes, and a decrease in the turbidity of the suspension occurs. The change will be most clearly seen if the original suspension is narrowly sized, and the flocs are large. Conversely, for a broad initial size distribution, the change may be difficult to detect unless the aggregation is extensive because the size distribution of the aggregates will overlap that of the original discrete particles.

If the particles are highly charged and the initial suspension well dispersed and narrowly sized, shear-flocculation results in a bimodal size distribution [3, 9, 27]. As shear-flocculation proceeds, the peak in the size distribution due to the discrete particles decreases as that due to the flocs increases (Figure 5). Some unflocculated particles will remain unless the surface charge is lowered substantially.

There are difficulties in obtaining accurate size distributions of flocculated suspensions, which have only been solved recently [30]. However, in the papers on shear-flocculation reviewed here, authors have had to contend with the facts that (a) the densities of the flocs were not known, and (b) the degree of breakup of the flocs in suspensions pumped through orifices in the measuring device was unknown.

When using the photosedimentometer method of sizing, in which the turbidity is recorded as a function of the time of settling, Warren [1, 2] and Koh et al. [3] assumed that the flocs had the same relative density as the original discrete particles, an assumption which leads to a significant underestimation of floc sizes as in Figure 5. Li and Fuerstenau [9] used a Microtrac sizer in which light is diffracted by particles in a laser beam. When a flocculated suspension is examined, it must be assumed that the flocs do not breakup, or grow, whilst being pumped and also that the optical properties of the flocs are the same as those of the discrete particles.

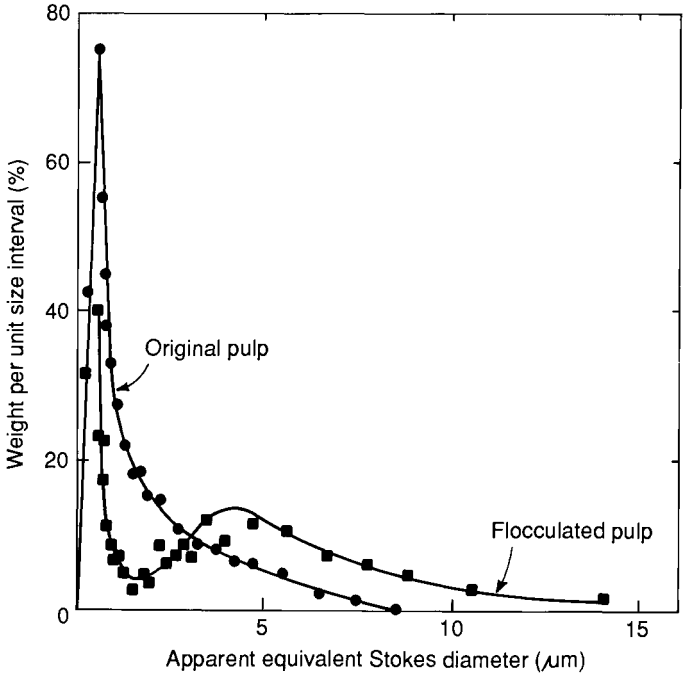

Fig. 5. Size distribution of finely ground scheelite ore before and after shear-flocculation in sodium oleate solution (from Koh and Warren [27]).

Zollars and Ali [17] used a Coulter Counter with a 19-μm aperture; here it must be assumed that there are no changes in floc size on mixing with the prescribed salt solution or in passing through the orifice in the instrument.

Size distributions change significantly on shear-flocculation and the degree of shear-flocculation can be estimated semi-quantitatively from the increase in d_{50}, the size corresponding to 50 w.t.% undersize, or the changes in the proportions of sample mass in different size ranges, e.g. <3, 3–6 and >6 μm for a sample initially finer than 6 μm [2, 9]. It is even more useful to know what the proportions of flocs and discrete particles are in each of these size ranges. This can be done by assuming that the flocs in a given size fraction were formed only from discrete particles in the size fraction below [2, 9].

Use of flotation to measure degree of aggregation

The degree of shear-flocculation may also be obtained indirectly by flotation of the valuable mineral from the flocculated suspension. The flotation recoveries and grades before and after shear-flocculation can then be compared, and any improvement attributed to shear-flocculation [4, 7, 9, 15, 27]. The method is based on the observation that flocs float faster than dispersed particles. For example, Koh and Warren [27] found that flocs of ultrafine scheelite floated ten times faster than the discrete 1 μm particles.

For mixtures of minerals, or natural ore samples, values of recovery and grade generally provide a satisfactory measure of the efficiency of the flocculation process. However, when performance of samples with very different head grades is being compared, it is preferable to use an alternative statistic such as Gaudin's selectivity index [31] or the logarithmic index proposed by Jarrett and Warren [13].

Theory of shear-flocculation

Hydrophobic association

When two particles, made hydrophobic by adsorption of a long-chained surfactant such as sodium oleate or sodium dodecyl sulfate, collide and adhere, part of the interface between the hydrocarbon chains and the aqueous solution will disappear to be replaced by an area of contact between hydrocarbon chains, thereby reducing the surface energy of the system by σ_{HW} units of energy per unit area of contact per particle, where σ = specific surface energy between hydrocarbon layers (H) and water (W). The energy of hydrophobic association thus released will ensure strong binding of the two particles.

There are a number of ways of making an order-of-magnitude estimate of the energy of hydrophobic association. Some of these are given in Figure 6. For 1 μm particles coated with oleate Warren [1] estimated: (a) the energy of the interfacial

energy term σ_{HW}, (b) the energy released in forming a micelle between the particles, and (c) the energy released in various degrees of overlap of the hydrocarbon chains. Vincent, quoted in Warren [1], estimated the free energy of mixing of oleate chains. Lu et al. [8] present a formula for calculating the hydrophobic association energy that is a function of the separation between the particles, the thickness and density of the adsorbed layer and the "association degree".

Whichever method is used to calculate the energy of hydrophobic association, a relatively large value, 1,000 to 10,000 kT, where kT is about 4×10^{-21} J at room temperature, is obtained.

Figure 6 illustrates just how large the hydrophobic association energy is compared with the Van der Waals attraction between similar particles at a similar separation.

Therefore, once contact is made, hydrophobic particles should be strongly bound together, a prediction that is consistent with the observed production of aggregates by the shear-flocculation process, aggregates that are formed under shear and remain stable under shear.

Koh et al. [23] have proposed an additional binding mechanism caused by the capillary condensation of surfactant at the point of contact between particles. They claim that such liquid bridging between particles is more likely to occur in the scheelite–sodium oleate system at lower pH (7.0) when the concentration of oleic acid molecules is greater, and oleic acid can condense, and that this is consistent with an observed higher flocculation rate at pH 7 compared to pH 9.9.

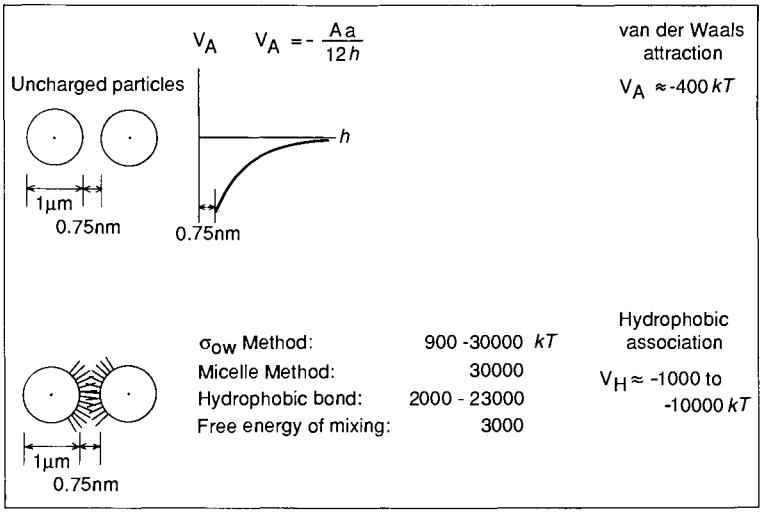

Fig. 6. Comparison of the binding energies due to Van der Waals attraction and hydrophobic association. a = particle radius; h = particle separation; σ_{ow} = interfacial energy between oleate-coated surface (o) and water (w); k = Boltzmann constant; T = absolute temperature; H = Hamaker constant. (From Warren [38].)

Hydrophobic force

The question remains as to how the charged particles approach closely enough, against the force of electrostatic repulsion, to allow the hydrocarbon chains to touch. Lu et al. [8] and Parsonage [32] suggest that the overall hydrophobic interaction can be considered as the sum of (1) a hydrophobic association energy due to overlap of hydrocarbon chains of the surfactant, and (2) a long range essentially entropic interaction, with an exponential decay, of the type measured by Pashley and Israelachvili [33]. The latter has been called a "hydrophobic force" (see also Xu and Yoon [4], Derjaguin [34]).

Kitchener [35] explains hydrophobic forces as follows: water molecules next to a non-polar surface are constrained to conform to the open tetrahedral hydrogen-bonded structure of bulk water on the one side and on the other they are attracted non-specifically to the groups on the substrate. The result is a perturbed water structure and any process which releases some perturbed water, such as the approach and contact of two hydrophobic particles in water, will lower the overall free energy and be spontaneous.

A hydrophobic force was observed by Pashley and Israelachvili [33] in their direct measurements of the forces between two mica plates in aqueous solutions of hexadecyl trimethyl ammonium bromide (HTAB). At 10^{-4} mol l^{-1} HTAB, a packed monolayer of HTA^+ formed on the mica and a hydrophobic surface was exposed to the solution. The attractive force between the two hydrophobic mica surfaces was three times larger than the expected Van der Waals force. The surfaces jumped into contact from a separation of 9 nm rather than the expected 4 nm.

Thus, the hydrophobic force is relatively long range and, according to Israelachvili [36], accounts for the rapid coagulation of hydrophobic particles in water. The calculations of Parsonage [32] and Lu Shouci and Dai Zongfu [37] show that including the hydrophobic force into the calculation of the interaction energy between particles leads to a much deeper primary minimum but only a slight decrease in the height of the energy barrier opposing aggregation (Figure 7).

If the decrease in the energy barrier is small, as predicted in Figure 7, it does not necessarily explain why the particles overcome the barrier and adhere to each other.

Critical shear rate

The experimental results show that for a suspension of charged, hydrophobic particles the shear rate needs to exceed a critical value before shear-flocculation occurs. Qualitatively, this has been explained by the need to give the colliding particles sufficient kinetic energy to allow them to surmount the energy barrier set up by the electrostatic repulsion forces and approach closely enough to allow hydrophobic interactions to dominate [38, 39]. However, this simple explanation pre-supposes:

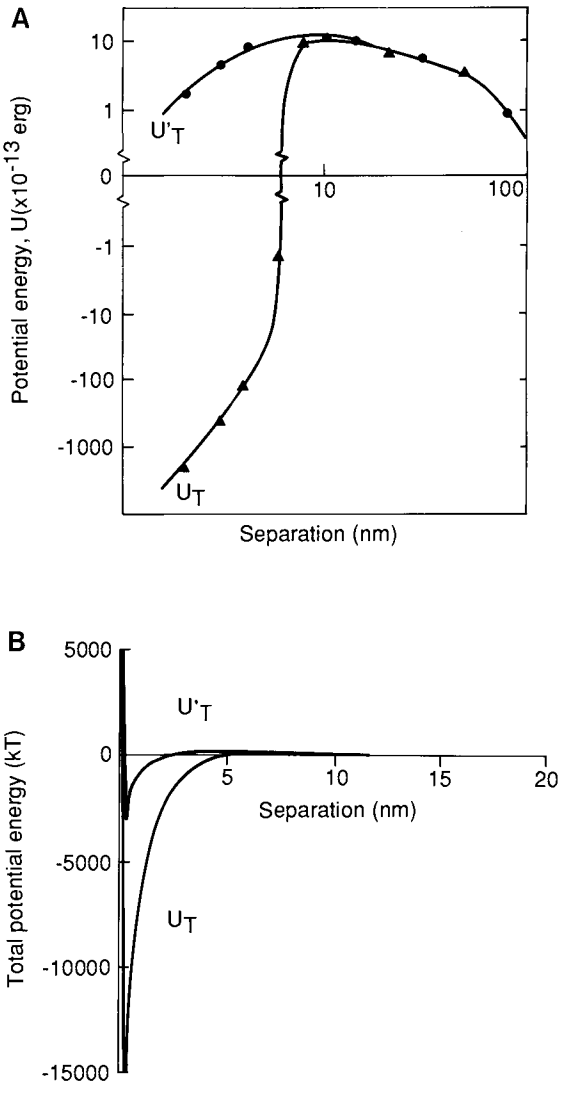

Fig. 7. A. Comparison of potential energy of interaction between 1.8 μm rhodochrosite particles separated by various distances, in the absence (U_T') and presence (U_T) of hydrophobic forces (from Lu and Dai [37]). B. Comparison of potential energy between 1 and 100 μm particles of zeta potentials 45 and 15 mV, respectively, in the absence (U_T') and presence (U_T) of hydrophobic forces (from Parsonage [32]).

(1) that the increased aggregation is not merely the result of an increased rate of collision between particles at higher shear rates; and

(2) that the shear regime would not cause the particles to aggregate if they were not hydrophobic.

Considering first the effect of collision rate, in laminar flow this is propositional to the shear rate D, and in turbulent flow to the energy loss in the flow per second per unit volume [40]. In stirred tanks the energy loss is in turn related to the "average" shear rate D and to the stirrer speed (see section on "Tank design", above). Warren [1], using the relation that the collision rate in the turbulent flow of a stirred tank was approximately proportional to the ½ power of the stirrer speed, estimated that the increase in collision rate was much less than would account for the increased degree of aggregation due to the shear flocculation effect.

Considering now the effect of shear rate on the coagulation of particles not made hydrophobic by an absorbed layer, it is known that such hydrophilic suspensions that are stable at low or intermediate shear rates may nevertheless, coagulate at higher shear rates [41]. This has been called "shear coagulation" and it is important to distinguish it from shear-flocculation. For particles fine enough to have no inertia, and which move with the fluid, the hydrodynamic force during a particle–particle encounter can be large enough to overcome the energy barrier arising from the charge on the particle surfaces. However, shear rates of 100 to 10,000 s^{-1}, which would cover the entire range expected in a stirred tank, are not sufficient for shear coagulation of 1 or 3 μm particles with zeta potentials greater than 30 mV, according to calculations made by Warren [2] using the method of Van de Ven and Mason [41] for inertialess particles. This is consistent with experimental observations on 1 μm scheelite (−45 mV, pH 10) and 3 μm tourmaline (−37 mV, pH 10) but not for 3 μm cassiterite particles (−40 mV, pH 7). It was speculated that inertial effects might be responsible for the anomalous shear coagulation of highly charged 3 μm cassiterite, which has a significantly higher relative density than tourmaline (7 versus 3.1) [2].

Intertial effects were shown by Van Diemen and Stein [42] and Stein et al. [29] to increase coagulation of 5 μm quartz and 0.66 μm zinc oxide particles in a Couette viscometer, whereas for 1.5 μm quartz, intertial effects were not observed in the range of shear rates of 10 to 10,000 s^{-1}. For 3 μm quartz, inertial effects increased the coagulation rate when the shear rate exceeded about 20 s^{-1}.

Since much of the recent work on shear-flocculation has been done using particles of average size 3–10 μm (see section on "Particle size", above), inertial effects may turn out to be more important than currently supposed, whether or not the particle surfaces are made hydrophobic. Particle inertia could well explain how the particles overcome the electrostatic repulsion barrier.

Another effect which may assist the hydrophobic particles to make contact is related to the ease with which the thin layer of liquid separating the approaching particles is removed. Deryagin and Krylov [43] found that the flow rate in 0.1 μm tubes was increased five to ten times by making the surfaces hydrophobic, which suggests that it may be easier to thin the liquid layer separating two hydrophobic particles than that separating two hydrophilic particles [1].

Floc growth and breakage

The first step in the flocculation process is the collision of two primary particles to form a doublet that may then collide with other primary particles or doublets to form larger aggregates and so on. Aggregates do not grow indefinitely but are eventually split into smaller fragments by the shearing forces in the liquid. When this continual process of growth and breakage reaches steady rate, the rate of change in the number of aggregates of any given size will be zero. The rate of formation of aggregates of a certain size by coalescence of smaller fragments or breakage of larger ones will then equal the rate of loss of aggregates of the same size due to their coalescence with other aggregates or their breakage under the action of attrition and shear-redispersion [13].

A number of assumptions have to be made to model the processes of floc growth and breakage. Koh et al. [3, 20] developed a model, with certain assumptions, which predicted, successfully, floc size distributions generated in large stirred tanks from values measured in similar smaller stirred tanks. Their experiments were carried out on particles of ultrafine scheelite, all finer than 10 μm, average size 1 μm, and the rate of disappearance of particles finer than 2 μm was used as a measure of the degree of shear-flocculation. As a reasonable approximation, they proposed that:

$$-\mathrm{d}W/\mathrm{d}t = kW^2 \tag{2}$$

where W is the mass concentration of particles finer than 2 μm, and k is a rate constant. The exponent of 2 for W was an approximation on the basis of tests which gave exponents for W of 1.7 to 3.1. Plots of $1/W$ versus t were found to be approximately linear from 50 to 175 min at average shear rates D of 250 to 1400 s^{-1}. The rate constant k was found to increase linearly with the "effective" shear rate, an average value taking account of the different shear zones in the tank. The size distribution of flocs was self-preserving, i.e. for a given geometry and speed the standard deviation σ of the size distribution did not vary with the time of stirring or the average floc size. The average floc size did change with time depending on the stirrer speed but the changes were said to be small enough after the first 15 min to assume a constant floc diameter d_f for a given geometry and for times greater than 15 min. The shear-flocculation process after the first 15 min could then be described by k, σ and d_f. From correlations of these parameters in small tanks (0.5–2 l), values were predicted in large tanks (4 l) and good agreement with experiment was obtained.

In order to model the rate of shear-flocculation in stirred tanks with various assumed zones of different shear rate, Koh et al. [20] assumed that shear-flocculation occurred by orthokinetic coagulation and that particles or aggregates coalesced into spheres on contact. These assumptions made it possible to use the equation:

$$\frac{N}{N_o} = \exp(-t^*) \tag{3}$$

to describe the rate of change of the number concentration N of particles at time t, where N_o is the initial concentration, $t^* = 4\alpha\phi Dt/\pi$, α = collision efficiency factor, and ϕ = particle volume fraction.

Dippenaar [15] observed that the shear-flocculation of 1.5–5 μm galena produced some flocs of size about 10 μm and a few others, called "superflocs", up to 1 mm diameter. He postulated that dimers and trimers of primary particles form readily, and collisions between them eventually lead to the formation of intermediate flocs. On the other hand, dimers of intermediate flocs are slow to form, but once an embryo superfloc has formed, it consumes single intermediate flocs until its size is limited, probably by the dimensions of the shear vessel.

With respect to the growth of flocs in mixtures of minerals, mixed flocs of particles of the valuable mineral and gangue are inevitably formed. For mixtures of scheelite and garnet, Jarrett and Warren [13] were unable to determine whether garnet particles were entrained within intersitices of existing scheelite flocs or whether garnet co-flocculated with the scheelite. However, they observed that floc grade did not decrease with time of aggregation and suggested that as the scheelite flocs grow, the rate of capture of garnet by the flocs was almost the same as the rate of loss of garnet due to the flexing of the flocs as they moved in the fluid.

Applications

Laboratory tests on ore samples

Mercade [44], in a patent on the froth flotation of low grade scheelite ore, prescribes as part of the method, a 5-minute conditioning of the pulp at 25 horsepower hours per ton before flotation at pH 10 with fatty acid. The agitation was said to form flocs of scheelite and to lead to better flotation performance. Koh and Warren [25] also studied a scheelite ore sample (1.5% scheelite, 8.3% calcite, ~90% garnet) but the sample had been ground till all particles were finer than 11 μm (average size 1.2 μm). Naturally, the rate of flotation of this ultrafine scheelite was low and performance was poor. If the pulp was first treated by shear-flocculation (60 min at 1200 rpm) aggregates of scheelite were formed that floated approximately 20 times faster than the original dispersed particles. The flotation recovery of scheelite was increased from about 30 to 50% without loss of concentrate grade (~8%), in a single rougher flotation step.

Rubio [45] found that deliberate pre-conditioning of an ultrafine malachite ($Cu_2(OH)_2CO_3$) ore at high shear rate led to aggregation of the malachite in preference to the gangue and this in turn gave more efficient flotation. Rubio speculated that the mechanism could have been that of shear-flocculation. Wojcik [5] added 4 kg kerosene t^{-1} of 0.25 mm coal and stirred the mixture at 2000 rpm for 10 min before flotation. This led to more rapid flotation of the coal without the need

for a frother, and better selectivity. Coal aggregates formed with only 1/25 the consumption of kerosene required in the alternative process of oil agglomeration or spherical agglomeration (Capes et al. [46]). Dippenaar [15] obtained significant shear-flocculation of the sulfide minerals, galena and chalcocite, and of galena–quartz mixtures, but only a slight increase in recovery after shear-flocculation of the tailings stream from a pyrite flotation plant. However, the low head grade (3% S), high ionic strength and presence of residual polymeric depressants could have interfered with the shear-flocculation process.

Bulatovich and Slater [47] found that high intensity conditioning of several sulfide ores significantly improved floatability and selectivity of particles less than 10 μm. This was attributed to aggregation of the ultrafines.

Pilot and full scale plant trials

A pilot plant test [28] and a full scale plant trial [48] suggest that under certain circumstances, shear-flocculation is a beneficial pre-treatment of ultrafine ores before flotation.

The pilot plant comprised grinding, classifying, shear-flocculation and rougher flotation (Figure 8). Scheelite ore from King Island was ground to give a high proportion of ultrafine material (up to 70 w.t.% < 15 μm) and its floatability assessed. It was found that under continuous operating conditions 74% of the scheelite could be recovered by rougher flotation. Pre-treatment of the ultrafine pulp by shear-flocculation improved subsequent flotation recovery of scheelite to 83%, concentrate grade was increased from 5 to 6% WO_3. The value of the extra tungsten recovered was as high as four times the incremental running cost of the shear-flocculation tanks.

Grasburg [48] described the modification and reconstruction of the Yxsjoberg scheelite plant in Sweden in which the scheelite ore is conditioned with fatty acid

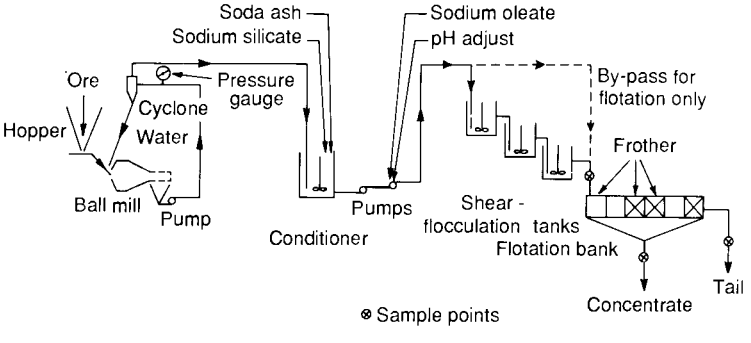

Fig. 8. Pilot plant flow sheet for shear-flocculation and flotation of ultrafine scheelite ore from King Island Tasmania (from Koh and Warren [28]).

and the scheelite is flocculated before flotation. In fact, the flocs were too stable and in the cleaning circuit, special effort was required to liberate entrapped fluorite and calcite, which co-flocculated with the scheelite. A specific comparison of the plant performance with and without the shear-flocculation step was not presented.

Conclusions

Shear-flocculation has been widely tested in the laboratory on single minerals and simple two-component mixtures. Under these conditions it can be an effective method of selectively aggregating ultrafine particles of one mineral from another. Separation of the flocs is then possible by sedimentation or flotation. Critical parameters are the hydrophobicity of the particle surfaces, their charge and the magnitude of the applied shear. The theory is still under development but the key factors are the strength of hydrophobic association between hydrocarbon chains and the hydrophobic force that is relatively long range and acts between hydrophobic surfaces in water. It appears that particle inertia may be the important means by which colliding particles surmount the electrostatic energy barrier between them.

Applications of shear-flocculation to natural ores at the bench-scale, in the pilot plant and in an operating concentrator have not given spectacular improvements but with amenable systems, such as scheelite ores, there have been worthwhile cost benefits. The laboratory tests suggest that further improvement is possible.

References

1 L.J. Warren, J. Colloid Interface Sci., 50 (1975): 307– 318.
2 L.J. Warren, Colloids Surf., 5 (1982): 301–319.
3 P.T.L. Koh, J.R.G. Andrews and P.H.T. Uhlherr, Int. J. Miner. Process., 17 (1986): 45–65.
4 Z. Xu and R.H. Yoon, J. Colloid Interface Sci., 132 (1989): 15
5 W. Wojcik, Powder Technol., 26 (1980): 115–117.
6 Wei Dawei, Wei Kewei Qiu Jicun, Int. J. Miner. Process., 17 (1986): 261–271.
7 Hu Yongping and Yu Mulong, in: A.J. Plumpton (Editor), Production and Processing of Fine Particles, Can. Inst. Min. Metall., 1988, pp. 353–362.
8 Lu Shouci, Song Shaoxian and Dai Zongfu, in: E. Forrsberg (Editor), 16th Int. Miner. Process. Congr., Amsterdam, 1988, pp. 999–1009.
9 C. Li and D.W. Fuerstenau, in: Y.A. Attia (Editor), Flocculation in Biotechnology and Separation Systems, Elsevier, Amsterdam, 1987, pp. 695–706.
10 G.B. Alexander and R.K. Iler, U.S.Patent 2,801,902, 1957
11 E.W. Greene and J.B. Duke , Min. Eng., 14 (1962), 51–55
12 P. Somasundaran, T.W. Healy and D.W. Fuerstenau, J. Colloid Interface Sci., 22 (1966): 599–605
13 R.G. Jarrett and L.J. Warren, Proc. Australas. Inst. Min. Metall., No.262 (1977): 57–66.
14 D.W. Fuerstenau, C. Li and J.S. Hanson, in: A.J. Plumpton (Editor), Production and Processing of Fine Particles, Can. Inst. Min. Metall., 1988, pp. 329–335.
15 A. Dippenaar, Mintek Report No. M230, 6 Dec. 1985, Council for Mineral Technology, Randburg, 19 pp.

16 Wei Dawei, Wei Kewu and Qiu Jicun, Int. J. Miner. Process., 20 (1987): 35–44.
17 R.I. Zollars and S.I. Ali, J. Colloid Interface Sci., 114 (1986): 149–166.
18 R. Sivamohan and J.M. Cases, Int. J. Miner. Process. (in press).
19 T.R. Camp, J. Boston Soc. Civ. Eng., 56 (1969): 1.
20 P.T.L. Koh, J.R.G. Andrews and P.H.T. Uhlherr, Chem. Eng. Sci., 39 (1984): 975–985.
21 P.T.L. Koh, Chem. Eng. Sci., 39 (1984): 1759–1764.
22 J.C. Maxon and J.Y. Oldshue, Proc. Annu. Conf. Am. Water Works Assoc., 1987, Part 2, pp. 1135–1166.
23 P.T.L. Koh, P.H.T. Uhlherr and J.R.G. Andrews, J. Colloid Interface Sci., 108 (1985): 95–103.
24 B. Yarar and J.A. Kitchener, Trans. Inst. Min. Metall., Sect. C: Miner. Process. Extr. Metall., 79 (1970): C23–33.
25 P.T.L. Koh and L.J. Warren, in: J. Laskowski (Editor), Mineral Processing, Proc. 13th Int. Miner. Process. Congr., Warsaw, 4–9 June 1979, Developments in Mineral Processing, 2, Part A, Elsevier, Amsterdam, 1981, pp. 269–293.
26 S.L. Goren, J. Colloid Interface Sci., 36 (1971): 94– 96.
27 P.T.L. Koh and L.J. Warren, Trans. Inst. Min. Metall., Sect. C, Miner. Process. Extr. Metall., 86 (1977): C94–95.
28 P.T.L. Koh and L.J. Warren, in: Chemeca 80: Process Industries in the 80's, 8th Nat. Chem. Eng. Conf., Melbourne, 24– 27 Aug. 1980, R. Austr. Chem. Inst., Parkville, 1980, pp.90–94.
29 H.N. Stein, E.H. Logtenberg, A.J.G. Van Diemen and P.J. Peters, Colloids Surf., 18 (1986): 223–240.
30 J.B. Farrow and L.J. Warren, in: D. McKee (Chair), Dewatering Technology and Practice Conference, 9–11 Oct 1989, Brisbane, Australas. Inst. Min. Metall., Parkville, 1989, pp. 61– 64
31 A.M. Gaudin, Principles of Mineral Dressing, McGraw- Hill, New York, N.Y., 1939, p.235.
32 P. Parsonage, Int. J. Miner. Process, 24 (1988): 269– 293.
33 R.M. Pashley and J.N. Israelachvili, Colloids Surf., 2 (1981): 169–187.
34 B.V. Derjaguin, Theory of the Stability of Colloids and Thin Films, Consultants Bureau, New York, 1989.
35 J.A. Kitchener, in: M.H. Jones and J.T. Woodcock (Editors), Principles of Mineral Flotation, Wark Symposium, Australas. Inst. Min. Metall., Parkville, 1984, pp. 65–72.
36 J.N. Israelachvili, Intramolecular and Surface Forces, Academic Press, London, 1985.
37 Lu Shouci and Dai Zongfu, in: A.J. Plumpton (Editor), Production and Processing of Fine Particles, Can. Inst. Min. Metall., 1988, pp. 317–327.
38 L.J. Warren, Chem. Tech., 11 (1981): 180–185.
39 L.J. Warren, in: M.H. Jones and J.T. Woodcock (Editors), Principles of Mineral Flotation, Wark Symposium, Australas. Inst. Min. Metall., Parkville, Australia, 1984, pp. 185–213.
40 V.G. Levich, Physicochemical Hydrodynamics, Prentice- Hall, Englewood Cliffs, N.J., 1962, p. 207.
41 T.G.M. van de Ven and S.G. Mason, J. Colloid Interface Sci., 57 (1976): 505.
42 A.J.G. Van Diemen and H.N. Stein, J. Colloid Interface Sci., 96 (1983): 150–161.
43 B.V. Deryagin and N.A. Krylov, in: Viscosity of Liquids and Colloidal Solutions, Vol.2, Pap. Acad. Sci. USSR, 1944.
44 V.V. Mercade, U.S. Patent 3,915,391, 1975.
45 J. Rubio, Trans. Inst. Min. Metall., Sect. C, Miner. Process. Extr. Metall., 87 (1978): C284–287.
46 C.E. Capes, A.E. Smith and I.E. Paddington, CIM Bull., July 1974, pp. 115–119
47 M. Bulatovich and R.S. Slater, in: G.S. Dobby and S.R. Rao (Editors), Processing of Complex Ores, Proc. Int. Symp. Process. Complex Ores, 20–24 Aug 1989, Halifax, Canada, Pergamon, New York, N.Y., 1989, p. 169.
48 M. Grasberg, World Min., 32, 3 (1979): 54–58.

Chapter 11

Coating and carrier methods for enhancing magnetic and flotation separations

P. PARSONAGE

Introduction

Amongst the various separation techniques which depend upon surface and colloid chemical phenomena as the basis for selectivity, those involving the addition of solid particles have received surprisingly little attention in the technical literature. Such techniques, which include both coating and carrier methods, rely on the selective aggregation of a target particle with the introduced solid in such a way as to drastically alter some physical property [1]. This in turn alters the response of the particles to some separation method such as flotation or magnetic treatment.

The present article concentrates on two such techniques:

(1) the selective increase in magnetic response by incorporation of a strongly magnetic phase;

(2) modification of froth flotation response. This can either be to *increase* the flotation rate of fine particles by attaching them to coarser particles (carrier flotation), or to *decrease* the flotation rate of coarse particles by coating the surface with fine, hydrophilic particles (slime-coating).

These various techniques are reviewed and the colloid chemical principles underlying the particle adhesion and coating are discussed.

Different types of carrier and coating process

Enhancement of magnetic properties

The magnetic response of weakly magnetic minerals can be increased by incorporating a small proportion of a highly magnetic material into the particles. Commonly, ferromagnetic and ferrimagnetic materials, such as ferrosilicon and magnetite are used; these exhibit magnetisations which are orders of magnitude greater than typical paramagnetic minerals such as wolframite or tourmaline.

TABLE 1

Variation of magnetisation, M, with flux density, B, for paramagnetic materials, and magnetite content of non-magnetic particle for equivalent magnetisation.

Volume susceptibility of paramagnetic mineral, χ (SI units)	Magnetic flux density, B (T)	Magnetisation, M ($A\ m^{-1}$)	Magnetite content of non-magnetic particle to give equal magnetisation (volume %)
5×10^{-3}	0.2	7.96×10^2	0.17
	1	3.98×10^3	0.83
	2	7.96×10^3	1.66
10^{-3}	0.2	1.59×10^2	0.03
	1	7.96×10^2	0.17
	2	1.59×10^3	0.33

The magnetic force on a particle is given by:

$$F_{MAG} = M \cdot V \cdot \left(\frac{dB}{dZ}\right) \tag{1}$$

For paramagnetic minerals:

$$M = \chi \cdot \frac{B}{\mu_o} \tag{2}$$

For particles containing a proportion of a ferromagnetic phase, for $H > DM_{sati}$:

$$M = v_i \cdot M_{sati} \tag{3}$$

Equations (1)–(3) can be used to calculate the amount of magnetite ($M_{sati} = 4.78 \times 10^5\ A\ m^{-1}$) which when incorporated in a particle of non-magnetic material would give rise to a magnetic force similar to that experienced by a paramagnetic mineral particle. Strongly paramagnetic minerals such as garnet, fayalite or siderite which are commonly recovered in conventional magnetic separation have volume magnetic susceptibilities, χ, of about 5×10^{-3} (dimensionless SI units). More weakly paramagnetic minerals, such as monazite and malachite have susceptibilities of around 10^{-3}. The content of magnetite required to produce a magnetisation similar to that of such paramagnetic minerals in a non-magnetic particle have been calculated in Table 1. This shows that the incorporation of as little as 0.1–1% of magnetite by volume gives rise to a magnetic force of the same order as that experienced by the types of mineral readily recovered by conventional high-intensity magnetic separation.

An important difference between the two types of particle is the way the magnetic force changes with the flux density, B. The magnetisation, and hence the magnetic force, for paramagnetic materials increases linearly with flux density. For ferromagnetic materials however, magnetisation reaches a saturation value; further increase

in the flux density has no effect on the magnetic force. Magnetite particles, for example, are magnetically saturated at flux densities of greater than about 0.2 T.

The different techniques for incorporating magnetic material into non-magnetic particles are discussed in the following sections. The general conditioning process is similar for each. The pulp is treated with reagents to optimise the surface properties and the magnetic particles are introduced. The mixture is conditioned to allow coating or flocculation to take place, then treated magnetically using wet high-intensity separators.

Selective magnetic coating

This process relies on the selective adhesion of fine magnetic particles to the surfaces of target minerals. (Figures 1 and 2) Factors controlling the coating formation are the same as those which control slime coating in flotation. Although selectivity is generally improved if the values have a different wettability from the gangue, this is not an essential requirement. Both hydrophobic and hydrophilic mixtures have been successfully separated by this technique [2–4]. Electrical interactions, hydrophobic and hydrophilic interactions, and association between adsorbed surfactant chains are the main parameters controlling selectivity. Fine particles, generally below about 2 μm diameter, are required to form resilient coatings.

The rejection of rutile and anatase from kaolin has been achieved by seeding

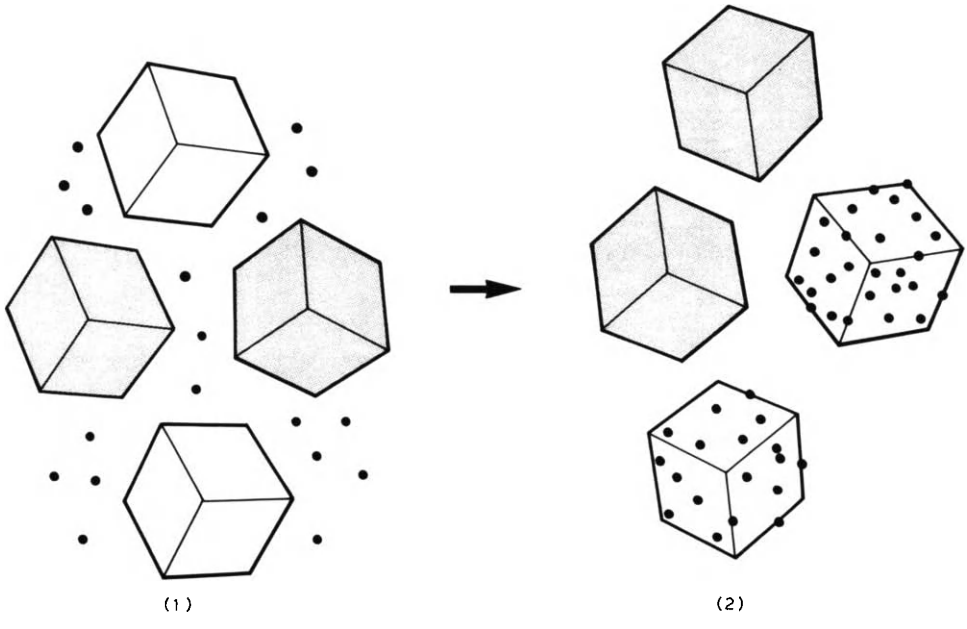

Fig. 1. Selective magnetic coating: (1) mixture of minerals with fine magnetite; (2) selective deposition and adhesion of fine magnetite on the surface of target mineral.

the slurry with fine magnetite [5, 6]. Selective coagulation of the magnetite with the titanium impurities appears to have been involved. Addition of fatty acids was proposed by Cook to improve separation in this system [7]. Presumably hydrophobic flocculation was occurring.

Hubler described the use of fatty acids to improve the magnetic separation of felspathoid ores containing magnetite [8]. A magnetic coating was formed on minerals such as corundum.

Removal of carbonates, such as calcite and dolomite, from mixtures with apatite, barite and scheelite have been demonstrated at laboratory and pilot-plant scale [2–4, 9, 10]. The level and the selectivity of the magnetite coating was strongly pH dependent when used in the presence of sodium oleate. (Figure 3) This was interpreted as being a function of changes in zeta potentials and surfactant adsorption density.

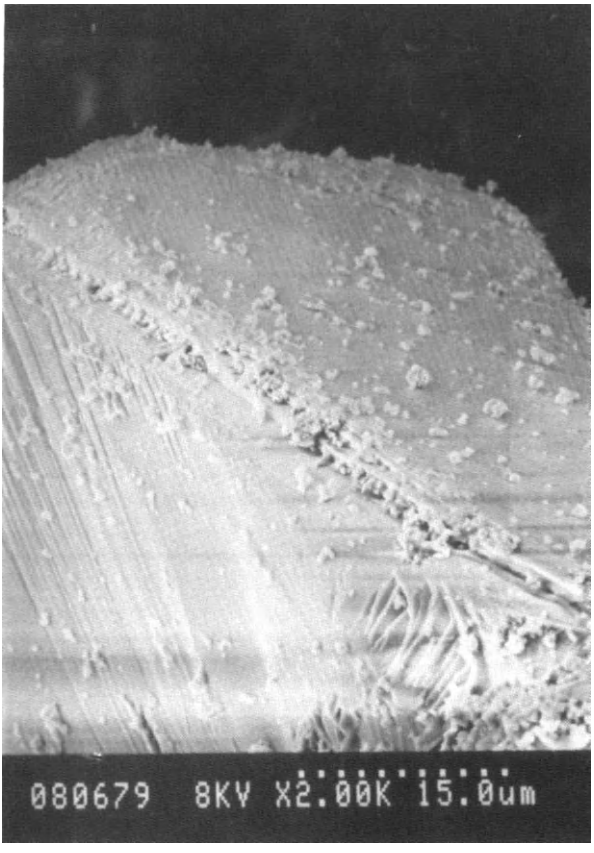

Fig. 2. Particle of fluorite after treatment showing coating of fine magnetite particles. Scale bar = 15 μm.

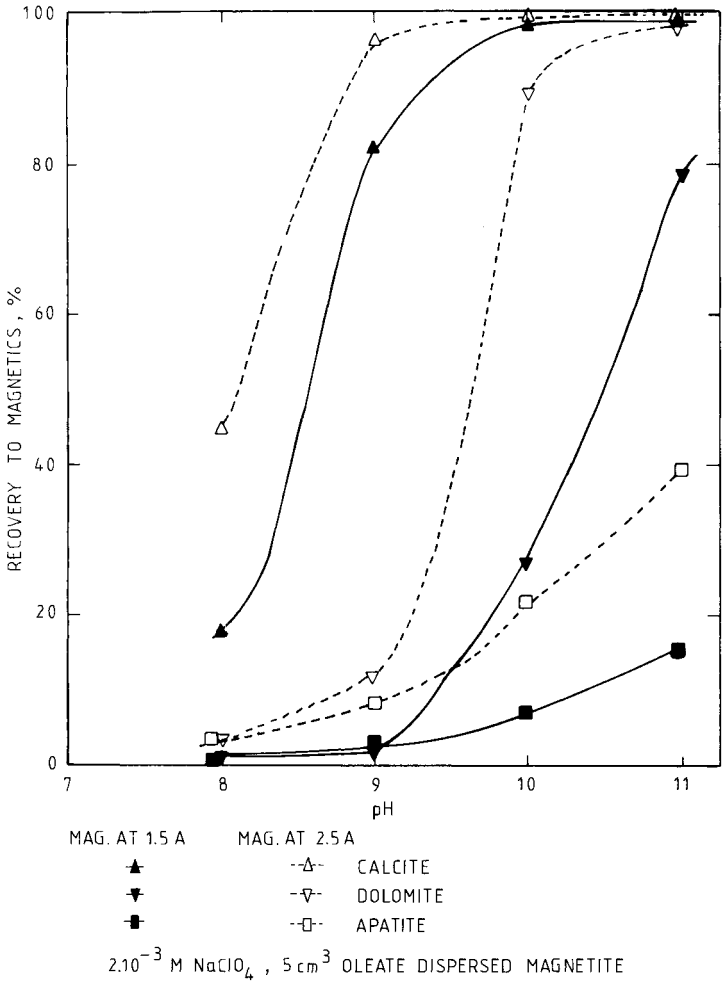

Fig. 3. Effect of pH on recovery of phosphate/carbonates by magnetic separation after treatment with oleate and magnetite (from Parsonage [2]).

Copper metal in the presence of lead was shown to be selectively coated after treatment with dodecylamine to make the surface hydrophobic [2]. Near perfect separation was achieved (Figure 4).

Selective coating with magnetic oil

Pioneering work was carried out by Lockwood for the Murex company and this process is sometimes referred to as the Murex Process [11–13].

Oil droplets will readily attach to, or spread over, the surfaces of particles which have been made hydrophobic or oleophilic. If the oil contains a finely dispersed, magnetic phase then a magnetic coating will form. The magnetic particles may

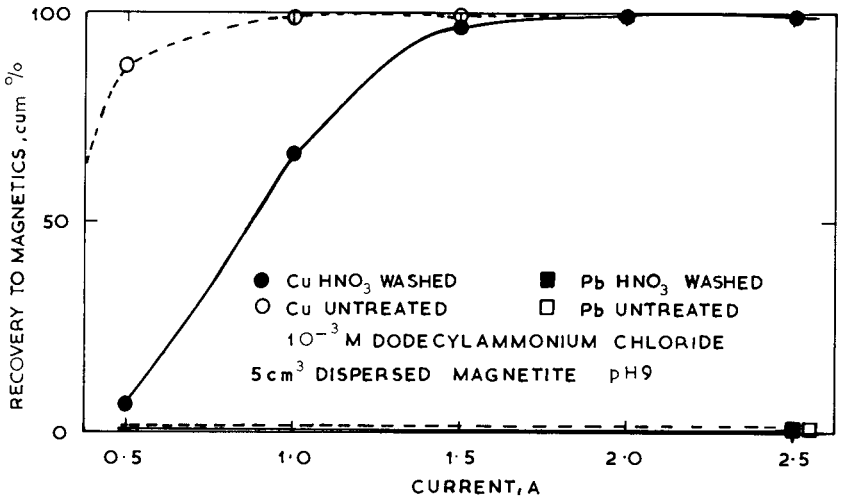

Fig. 4. Separation of metallic copper from lead after selective coating of copper (from Parsonage [2]).

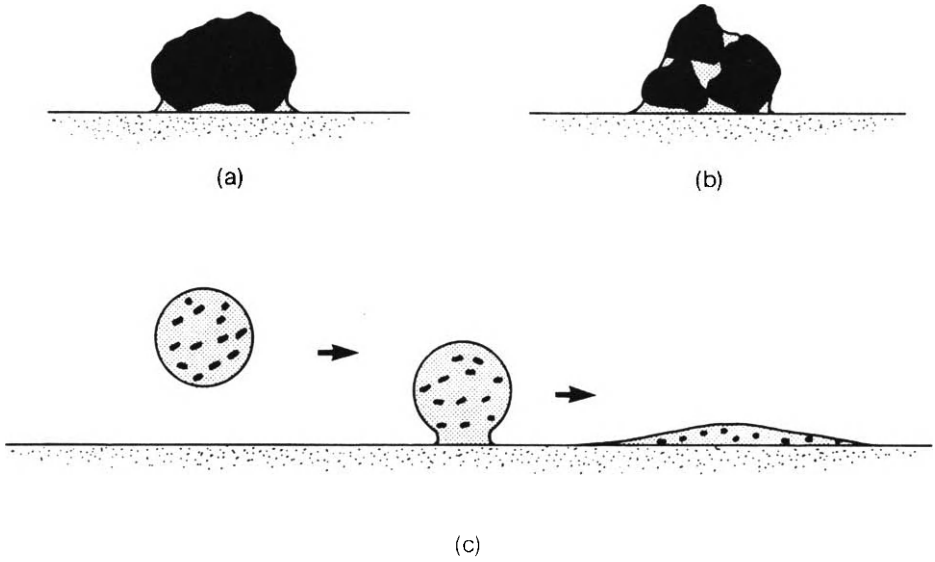

Fig. 5. Selective coating using magnetite and oil: (a) single magnetic particle with oil bridge attached to surface by capillary force; (b) surface attachment of agglomerate; (c) coating by an oil containing dispersed magnetite.

remain mobile within the oil film or may be anchored to the particle surface by the capillary force (Figure 5)

The basis for the selectivity is the same as for froth flotation, i.e. wettability. One advantage of the coating process over flotation is that much coarser particles

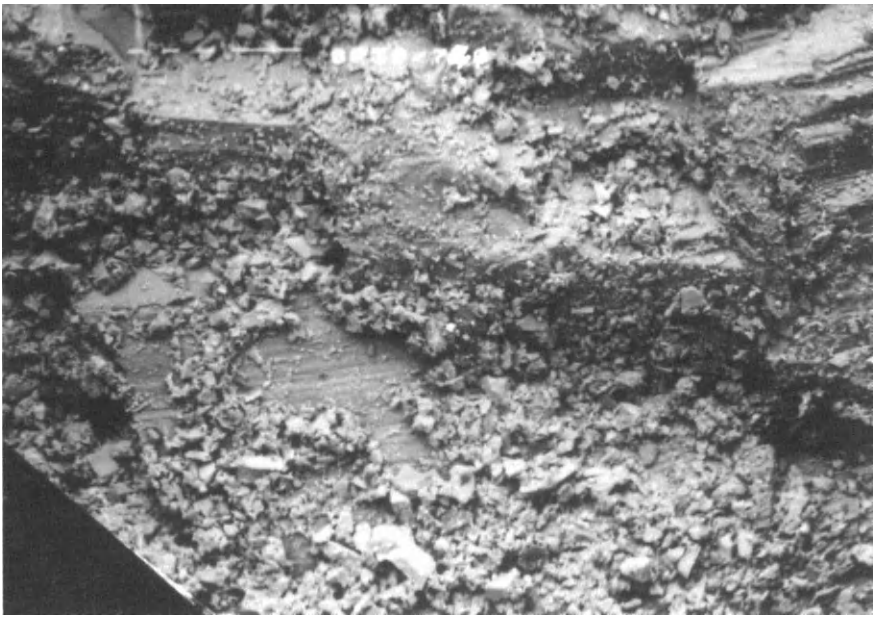

Fig. 6. Surface of coarse (1 cm) fluorite showing adherent coating of particles of magnetite up to 50 μm diameter after treatment with fatty acid and diesel oil. The fluorite was recovered in the magnetic product of a rare-earth roll separator. Width of field of view = 1 mm.

can be treated. A possible limitation for these coarse particles is that although it is possible to selectively coat them with magnetite, there may not be a suitable practical magnetic separator to perform the separation. Recent developments in wet permanent magnet roll separators may be of use in these applications [14]. Particles of up to 1 cm have been separated (Figure 6).

A number of separations based on this process has been described over the years (see Table 2). An important point that has been established is that when used in conjunction with oil, coarser magnetite particles (up to at least 30 μm) are effective as coating materials. This is of significant economic importance since the cost of this material can be an order of magnitude less than the minus 2 μm material which appears necessary when oil is not used.

Selective co-flocculation with magnetic material

Selective flocculation as a method of fine particle separation has received attention over the past two decades [25–28]. The principle of the separation is that by selectively adsorbing a high molecular weight polymer to a selected mineral it can be flocculated, whilst keeping other minerals in a disperse state. Most workers envisage the fractionation of the selectively flocculated mixture as being by sedimentation, using elutriators or thickeners.

TABLE 2

Reported separations using magnetic coatings with oil.

Selective coating of A in the presence of B		Reagents	Size	Ref.
A	B			
Cu + Pb carbonates	Gangue	Oil 6.8 kg t^{-1}, oleic acid 0.36 kg t^{-1}, magnetite 7.7 kg t^{-1}	up to 2–3 mm	[15]
Coarse sulphides Galena	Sn + W minerals Silica, barite			[16]
Hematite		Long chain sulphonates, petroleum sulphonates, fuel oil		[17]
Hematite		Tall oil 2 kg t^{-1}, diesel oil 10 kg t^{-1}		[18]
Chalcocite Sphalerite Coal	Gangue Gangue Ash	Kerosene based ferrofluid		[19]
Quartz	Magnesite	Dialkylquaternary ammonium chloride (ARQUAD-2C) 0.5–0.8 kg t^{-1}, diesel oil 2.8–3.2 l t^{-1}, Flotol B 0.4-0.5 l t^{-1}, magnetite	0.5–8 mm	[20]
Coal	Ash	Magnetite in gas oil		[21]
Coal	Ash			[22]
Weed, seeds	Cultural seeds	"Magnetic powder and oil"		[23]
Fluorite	Quartz	Oleic acid, diesel oil, magnetite	8–9.5 mm	[24]

An alternative process based on this technique is to incorporate magnetic material into the flocs and then use magnetic separation techniques to remove the magnetic flocs from the unflocculated material (Figure 7). A major advantage of this method is that the flocculated material need not be in the form of large, fast settling flocs. This means that high shear conditioning can be used to reduce entrainment of gangue. Also a wider particle size range can be treated because the unflocculated coarse material will go with the non-magnetic tails rather than with the flocs as is the case with sedimentation.

Iwasaki showed that the selective flocculation of hematite from silica can be improved by adding fine magnetite before flocculation, then partitioning using a magnetic trough [29]. Typically he ground the ore with sodium hydroxide and sodium silicate to disperse the silica. Fine magnetite (80% below 30 μm) was added, then

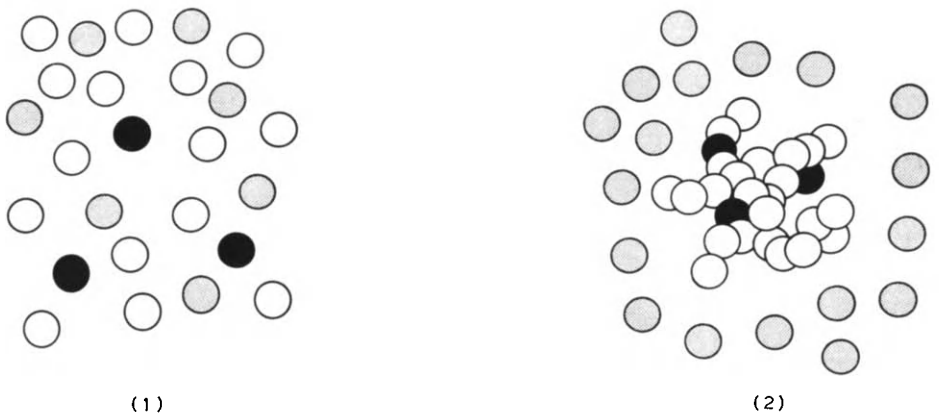

Fig. 7. Selective co-flocculation: (1) mixture of minerals with added magnetite (black); (2) after addition of flocculant, target mineral and magnetite co-flocculate.

causticized starch used as flocculant for the iron minerals. He varied the amount of magnetite in the tests, but typical useful concentrations were 5–10% of the weight of hematite in the ore.

Hwang et al. have described the separation of gibbsite and quartz [30]. The sample (2–20 μm) was dispersed at alkaline pH using Na_2S and NaF. Magnetite (5 μm) was added at 1% and co-flocculated with the gibbsite using 2 ppm of an anionic, very high molecular weight polyacrylamide. The magnetic flocs were recovered by passing the suspension through a plastic tube packed with stainless steel wool in a magnetic field of 0.1 T. As with conventional selective flocculation, redispersion and reflocculation reduced the amount of entrainment in the flocs.

The same workers also reported the separation of alunite ($KAl_3(SO_4)_2(OH)_6$) and quartz [31]. Sodium carbonate and sodium tripolyphosphate dispersants were used. A 1% addition of 5 μm magnetite was made followed by a non-ionic polyacrylamide flocculant. Selective co-flocculation of the magnetite and quartz takes place. Alunite grades of 89% at a recovery of 82% was achieved after recleaning.

The treatment of potash ores by co-flocculation with magnetite has been investigated at both laboratory and pilot-plant scale [32, 33]. The removal of insoluble minerals such as clay, quartz and gypsum, may be achieved by co-flocculating them with magnetite using a non-ionic polyacrylamide with a molecular weight of 20×10^6. Ionic minerals such as sylvite (KCl) and halite (NaCl) remain dispersed. It is believed that the selectivity is due to selective adsorption of polymer on the insoluble minerals and the magnetite by hydrogen bonding through surface oxygen atoms. The sylvite and halite do not possess such a bonding mechanism and remain unflocculated. The important process variables are the dosage and particle size of the magnetite, the flocculant addition, the intensity of mixing and the conditioning time. Magnet current and temperature were less important variables. Long or in-

tense mixing causes breakdown of the flocs and a consequent loss of recovery to the magnetics. On the other hand, too gentle mixing can result in entrainment of the salt minerals in the flocs. For the treatment of a minus 30 μm material it was found that 75 kg t^{-1} of minus 14 μm magnetite and 375 g t^{-1} polyacrylamide enabled the insoluble content to be reduced from 69% to 22% with a salt recovery of greater than 90%. Pilot-plant testing of the process at Boulby Potash Mine, U.K., has been carried out using Boxmag Rapid and Eriez high intensity carousel magnetic separators. Throughputs of up to 100 kg per hour have been achieved. The magnetics product is thickened then attrited to break down the flocs and so release the magnetite for recovery and recycling. Recovering the magnetite may be difficult for heavily flocculated products.

Chemical coating methods

Various chemical techniques for magnetic coating have been exploited as separation methods.

Conversion of a non-magnetic or weakly magnetic iron mineral to a more highly magnetic phase may be achieved by roasting, oxidative alkaline pressure leaching [34] or by the surface decomposition of a gas phase such as iron pentacarbonyl. This latter results in surface deposition of a highly magnetic phase and is known as the Magnex process. It has been explored as a method for treating coal by magnetising the ash and pyrite phases [35–37]. Other investigators have studied its application to chrysocolla–quartz separation [38].

Adhesion of fines to coarse magnetite

Relatively coarse magnetite particles may be carriers for fine non-magnetic particles.

Greene and Duke described the use of minus 45 μm heavy media grade magnetite, treated with tall oil, fuel oil and alkali as a carrier to remove anatase from kaolin [39]. The kaolin was treated separately with reagents. A rejection of 26% of the anatase was achieved in 5.4% of the kaolin feed weight.

WSR Pty Ltd, Australia, have suggested the use of hydrophobic magnetite particles as slime carriers as an alternative to the use of gas bubbles in conventional flotation. Adsorption of minus 20 μm molybdenite particles has been described [40, 41].

A drawback to using coarse carriers is the high weight which must be added to give a useful surface area for adsorbing the fines.

Non-mineral processing applications

The Sirofloc method of water treatment uses ground magnetite to adsorb humic acids and metal ions [42]. An acid pH is used to provide a positive magnetite surface to aid the adsorption of the negative contaminants.

Bacteria can be adsorbed onto magnetite. The use of magnetite in combination

with aluminium has been reported to be effective for the removal of coliform bacteria, algae and viruses [43–45]. In the absence of Al^{3+} the bacterial cells were reduced from 16000 to 400 per 100 ml, whereas in the presence of 3 ppm Al^{3+} the bacteria content was reduced to zero [43]. Calcium ions have also been used as the coagulation aid [46].

Reduction of MNC algal cells in sea water has been achieved by adsorbing them onto magnetite. No coagulant was required [47].

Plankton have been removed from water using polyaluminium chloride as coagulant. High gradient magnetic separation was used. The optimum pH was 9.3 [48].

Other applications of separating biological materials by adsorption onto ferromagnetic material have been reported in the medical and related fields. Poynton et al. for example, have reported the use of fine cobalt to adsorb cells in the treatment of leukaemia [49].

Flotation processes

Fine or "slime" particles can cause problems in froth flotation. They generally have a lower flotation rate than coarser particles. Also they can interfere with the flotation of other particles. One way they do this is by forming slime coatings. Techniques are described in this section whereby a deliberate attachment of fine particles to coarser particles is sought, either in order to increase the flotation rate of the fines or to improve the grade by selectively depressing one phase. It

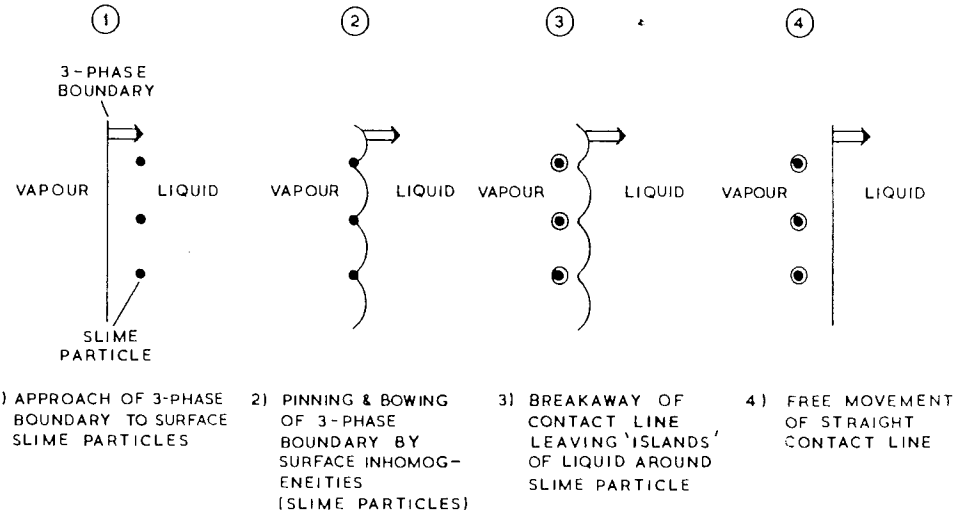

Fig. 8. Mechanism by which a slime coating can impede the movement of the three-phase boundary during bubble pick-up.

is probable that similar beneficial effects occur in many flotation circuits without having been consciously designed.

Selective depression by slime coatings

Hydrophilic slime mineral particles can coat and act as depressants for floatable minerals. Their action is similar to that of hydrophilic colloids such as starches and gums which are used as conventional flotation depressants.

Coatings of *hydrophobic* slime particles produces a lesser effect on flotation [50]. A minor decrease in the efficiency of bubble pick-up may be expected due to the surface roughening effect [51]. It appears that the coatings interfere with flotation by pinning the three-phase boundary as the liquid/air interface moves across the particle surface (Figure 8). The effect can be observed microscopically (Figures 9 and 10).

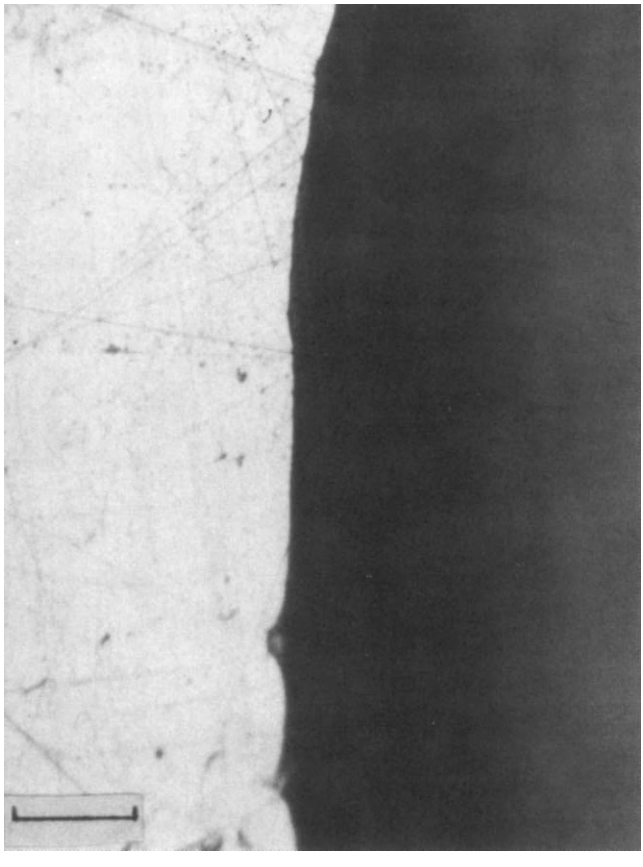

Fig. 9. Three-phase boundary receding across clean, smooth, xanthate coated galena. Note the straight nature of the contact line. Scale bar = 0.1 mm.

The importance of particle charge and zeta potentials on the formation of slime coatings has been highlighted in a number of studies [52–58]. Dense coatings occur when slime and mineral have opposite charges or low charges of the same sign.

It has been observed that sub-micron particles are more effective at coating than are coarser particles [57, 58]. Also surfaces with adsorbed, long chain hydrocarbons have been reported as being more effective at providing adhesion than bare surfaces [54, 58].

The influence of the particle size and coating density of the slime on the decrease in flotation has not been studied in a systematic fashion. Parsonage and Craige [59] have shown recovery of calcite to decrease as a function of size and spacing of limonite slime in Hallimond tube flotation (Figure 11).

Slime particles which selectively coat one mineral species can be exploited as

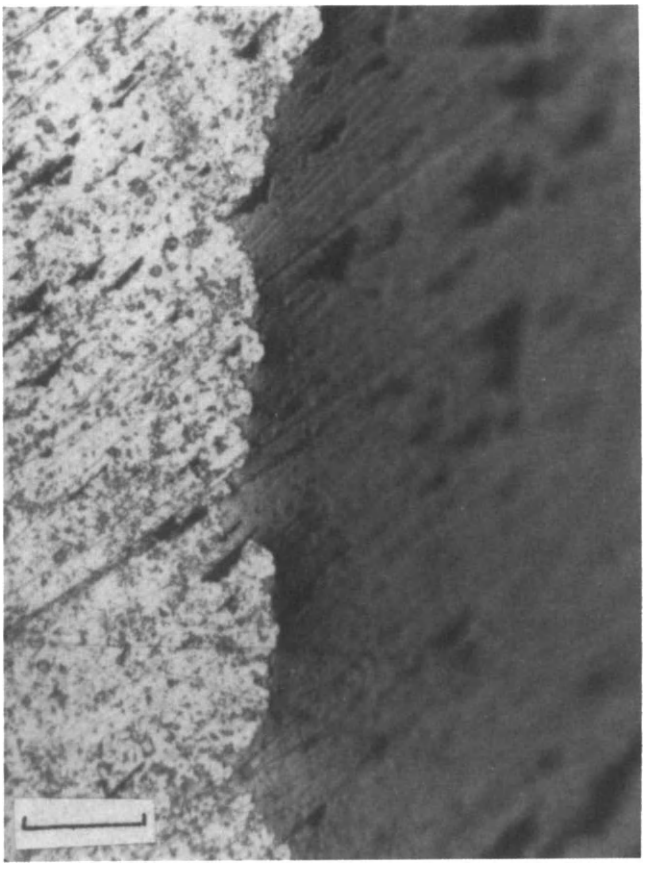

Fig. 10. Three-phase boundary receding across xanthate coated galena surface coated with fine fluorite particles. Note the ragged nature of the contact line as its progress is impeded by the slime particles. Scale bar = 0.1 mm.

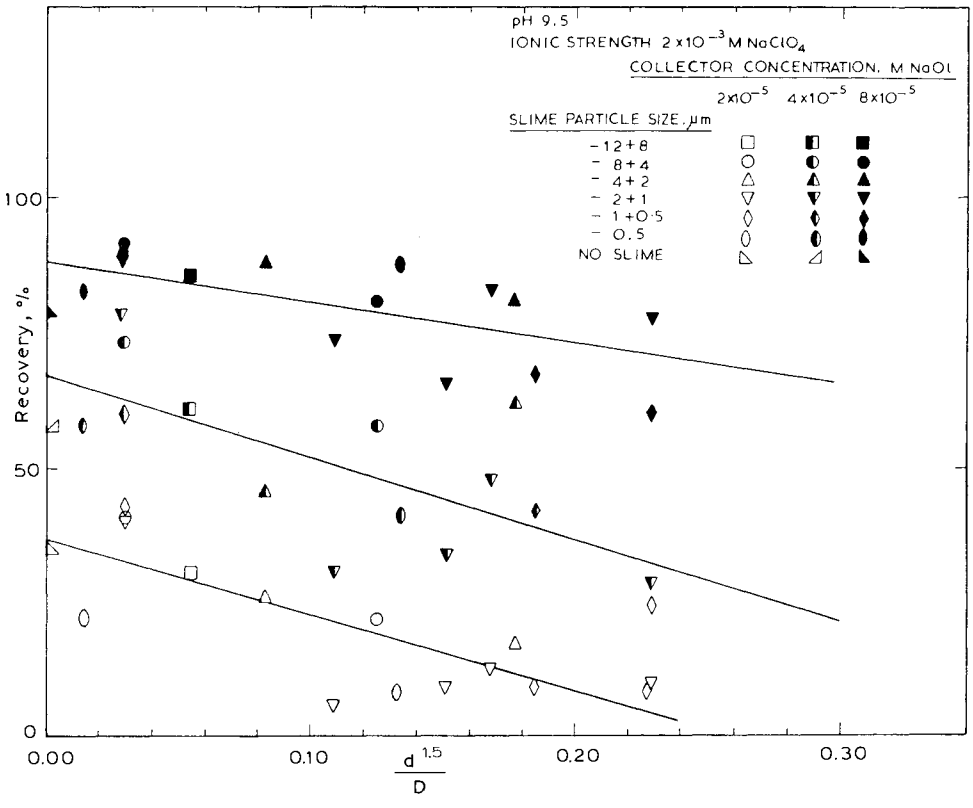

Fig. 11. Relationship between slime particle size (d) and average spacing (D), and flotation recovery for calcite coated with iron oxide slimes. Sodium oleate collector, conditions as shown. (From Parsonage and Craige [59].)

depressants. For example apatite and calcite show a similar flotation with sodium oleate at pH 8 and cannot be separated. However, if hematite slimes are added a slime coating forms on the calcite particles but not on the apatite [51]. Although increasing slime addition resulted in an overall decrease in recovery the apatite grade in the flotation concentrate increased from 58% to 89% as heavier slime coatings formed on the calcite (Figure 12).

Carrier (or piggy-back) flotation

The flotation rate of fine particles can be increased by arranging conditions such that they coat floatable, coarser carrier particle. Flotation of the carrier removes the slime particles into the froth. The carrier particles may have a surface area of 10–15 times that of the air bubbles used and have a higher probability of fruitful collision with a bubble compared with a slime particle. Generally, both carrier and fine particle are made hydrophobic using conventional flotation reagents.

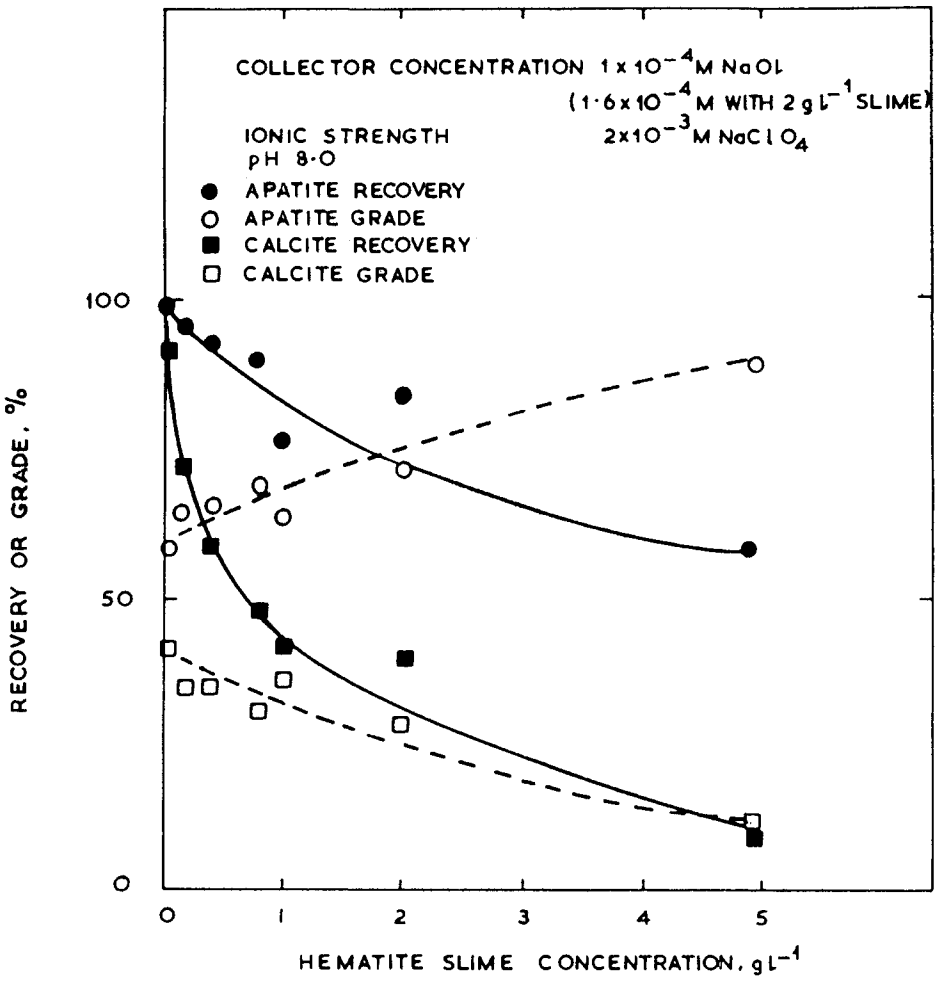

Fig. 12. The effect of hematite slimes on the flotation of a calcite/oleate mixture with Na oleate. A selective, depressant coating forms on calcite leading to increasing apatite grade with increasing slime concentration (from Parsonage et al. [51]).

In the pioneering work on this technique, application to the rejection of anatase from kaolin was investigated [39, 60]. Carrier flotation removed 59.2% of the anatase from a fine kaolin product compared with 10.2% by conventional flotation. The effects of process variables on this particular system have been studied in detail at laboratory scale [61, 62].

Other investigations into carrier flotation are summarized in Table 3. The carrier particle may be either the same mineral as the fine particle to be floated (autogenous carrier flotation) or a different species.

TABLE 3

Carrier flotation separations

Mineral		Carrier	Ref.
Floated	Not floated		
Anatase	Kaolin	Calcite	[39, 60, 67]
Phosphate	Clay	Sulphur	
Anatase	Clay	Calcite	[61, 62]
Phosphate		Sulphur, phosphorite, calcite, quartz	[63]
Apatite		Apatite, sulphur	
Calcite		Calcite, phosphorite	
Quartz		Apatite	
Scheelite		Scheelite	[50]
Wolframite		Wolframite	[64, 65]
Stibnite	Arsenopyrite	Stibnite	[66]
Pb/Zn sulphide		Sulphide	
Hematite		Magnetite	
Cassiterite		Cassiterite	
Hematite	Quartz	Hematite	[68]

According to Samygin et al. the relative rate of collision between coarse and fine particles is dependent on the collision mechanism [63]. Coarser particles move relative to the liquid mass and collide with fines by an inertial mechanism. Fine particles, smaller than the scale of microturbulence, are entrained within the eddies and only collide with each other by diffusion. This results in collisions between fine and coarse particles greatly exceeding those between fines.

Some workers have found that intense agitation is necessary to achieve recovery of the fines [50, 62]. This will be the case if an energy barrier must be overcome for adhesion to occur.

Hu and co-workers have developed autogenous carrier flotation [64, 65]. Feed is classified and the concentrate from the coarse flotation stage is introduced to the slimes feed. This acts as a carrier for the fine particles of the mineral. As has been found with other separations of this type, the stirring conditions can be critical. The optimum size for carrier particles was when their diameter was about equal to the turbulence microscale. Wang et al. have proposed that addition of coarse particles can promote aggregation of fine hydrophobic particles by the effect they have on the turbulent flow regime [66]. The carrier effect is dominant for coarse particles smaller than the microscale of turbulence, whereas for particles larger than this, the aggregation promoting effect is important.

In spite of being patented over a quarter of a century ago [67], the exploitation of carrier flotation has not occurred to any great extent in practice. One drawback

may be the difficulty in separating the fines from the carrier, either for recycling the latter or for recovery of values.

Forces of interaction controlling the adhesion of fines

This section discusses the interparticle forces which control the formation of coatings of fine particles on coarser particles. These determine whether or not adhesion will take place between two colliding particles. The subsequent disrupting forces they experience determine how permanent the attachment will be.

Such particle interactions arise by a number of different mechanisms. Conventionally, the interaction energy from each source is summed to provide a total energy of interaction, V_T. The variation of V_T with distance between two particles is the potential function. Maxima and minima act as barriers and wells tending to aid either repulsion or adhesion of the particles. Adhesion occurs when the energy barrier is insufficient to prevent the particles approaching to the position of the primary potential well.

The most important energies with respect to particle adhesion are those due to:

(a) Born repulsion, V_B;

(b) Van der Waals interaction, V_A;

(c) electrical (Coulombic) interactions, V_R;

(d) association between hydrocarbon chains, V_{assoc}; and

(e) hydrophobic, V_{HPB}, and hydration, V_{HDN}, effects.

The net interaction V_T is assumed to be given by:

$$V_T = V_B + V_A + V_R + V_{assoc} + V_{HDN} + V_{HPB} \quad (4)$$

Other interactions of lesser importance for the processes under consideration include those due to magnetic effects [69–71], steric interactions [72–74] and depletion flocculation [75].

Two other effects are different in kind from the other interactions and are described separately. These are capillary effects due to the presence of oil films between the particles, and bridging flocculation.

Chemical reagents can be used to modify most of these interactions. In practical applications the most useful reagents are hydrocarbon based surfactants, water soluble polymeric flocculants and pH regulators.

Expressions which may be used for evaluating the components of the interaction energy are given below. The values of the critical variables are difficult to estimate for many minerals and in practice the equations are usually used in a semi-quantitative way. These and other equations have been discussed in more detail elsewhere [10, 76].

Born repulsion, V_B

This is the repulsion due to overlapping clouds of electrons at very close range which prevents actual contact of the surfaces. Its magnitude plays a large part in controlling the depth of the primary potential minimum and the adhesive force of contact.

An expression for Born repulsion has been given by Feke et al. [77]. The potential is proportional to the Hamaker constant, A:

$$V_B = 4A\left(\frac{\sigma}{R_1}\right)^{n-6}\frac{(n-8)!}{(n-2)!}\frac{1}{R}\times$$

$$\left\{\frac{-R^2-(n-5)(R_2/R_1-1)R-(n-6)[(R_2/R_1)^2-(n-5)(R_2/R_1)+1]}{(R-1+R_2/R_1)^{n-5}}\right.$$

$$+\frac{-R^2+(n-5)(R_2/R_1-1)R-(n-6)[(R_2/R_1)^2-(n-5)(R_2/R_1)+1]}{(R+1-R_2/R_1)^{n-5}}$$

$$+\frac{R^2+(n-5)(R_2/R_1+1)R+(n-6)[(R_2/R_1)^2+(n-5)(R_2/R_1)+1]}{(R+1+R_2/R_1)^{n-5}}$$

$$\left.\frac{R^2-(n-5)(R_2/R_1+1)R+(n-6)[(R_2/R_1)^2+(n-5)(R_2/R_1)+1]}{(R-1-R_2/R_1)^{n-5}}\right\} \quad (5)$$

where $R = (R_1 + R_2 + h)/R_1$. Equation (5) is valid for all values of n except $n = 7$, 6, 5, 4, 3 or 2; n represents the degree of hardness in the repulsion. In the absence of any information to the contrary, values of $n = 12$ and $\sigma = 5 \times 10^{-10}$ m may be used as standard.

Van der Waals interactions, V_A

Attractive forces between neutral bodies arise due to interactions between permanent dipoles, interaction between a dipole and an induced dipole, or London (dispersion) forces.

The simplest expressions for the interaction [78] need to be modified to take retardation into account. Schenkel and Kitchener have given the following expressions [79].

For $P_o < 0.5$:

$$V_A = -\frac{AR_1R_2}{6(R_1+R_2)h}\left(\frac{1}{1+1.77P_o}\right) \quad (6)$$

For $P_o = 0.5$ to ∞ and $h \ll R_1$ or R_2:

$$V_A = -\frac{AR_1R_2}{6(R_1+R_2)h}12\left(-\frac{2.45}{60P_o}+\frac{2.17}{180P_o^2}-\frac{0.59}{420P_o^3}\right) \quad (7)$$

where $P_o = 2\pi h/\lambda$.

The situation is more complex when adsorbed surface layers are present. The specific effects which adsorbed layers have on the Van der Waals interaction have been described by Vincent [80]. In practical situations the major effect is usually due to steric interactions between the adsorbed layers as the coated surfaces approach.

Values of the Hamaker constant, A, for different minerals are discussed by Visser [81, 82]. Gregory [83], Israelachvili [84] and Hough and White [85] have described methods for estimating Hamaker constants from physical data.

Electrical (Coulombic) interactions, V_R

Forces of attraction or repulsion arise from the overlap of the electrical double layers. The combined influence of the Coulombic and the Van der Waals interactions is described by the well-known DLVO theory [86, 87].

For particles of differing size and potential, the equations of Hogg et al. can be used [88].

For constant potential interaction:

$$V_R = \frac{\pi\epsilon_0\epsilon_r R_1 R_2(\psi_1^2 + \psi_2^2)}{(R_1 + R_2)} \left\{ \frac{2\psi_1\psi_2}{(\psi_1^2 + \psi_2^2)} \ln\left[\frac{1 + \exp(-\kappa h)}{1 - \exp(-\kappa h)}\right] + \ln[1 - \exp(-2\kappa h)] \right\} \quad (8)$$

and for constant charge interaction:

$$V_R = \frac{\pi\epsilon_0\epsilon_r R_1 R_2(\psi_1^2 + \psi_2^2)}{(R_1 + R_2)} \left\{ \frac{2\psi_1\psi_2}{(\psi_1^2 + \psi_2^2)} \ln\left[\frac{1 + \exp(-\kappa h)}{1 - \exp(-\kappa h)}\right] - \ln[1 - \exp(-2\kappa h)] \right\} \quad (9)$$

These interactions can be controlled using reagents and are therefore very important in obtaining selectivity of coatings. In the case of minerals which have similar hydrophobicities, and consequently have similar flotation properties, it is the principal method of achieving selective magnetic coating. The important variables are the zeta potential, ψ, and the double layer thickness, $1/\kappa$. Pugh and Kitchener have discussed the use of zeta potential control to produce selective coagulation as a method for mineral separation [89].

Hydrocarbon chain association, V_{assoc}

An extra attractive force is present between particles bearing adsorbed layers of molecules containing hydrocarbon chains when the layers overlap (Figure 13). It arises from the free-energy decrease in transferring the chains from an aqueous to

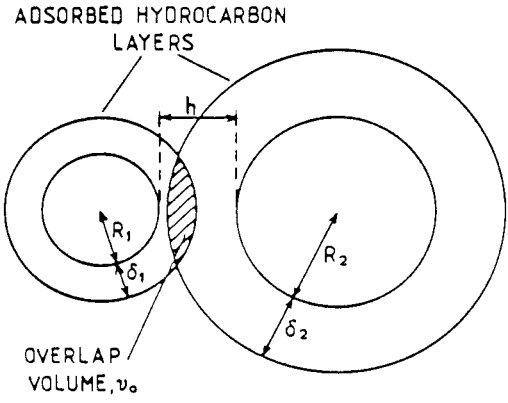

Fig. 13. The adsorbed layer overlap volume, v_o, for two approaching particles.

a hydrocarbon environment. The interaction is in addition to the hydrophobic effect (see section on "Hydrophobic interactions", below).

A model for the interaction has been presented [76]. It was proposed that the free energy decrease as the hydrocarbon chains associate is equal to the product of:

(1) the surface concentration of ($-CH_2-$) groups in the surface layers, $[CH_2^1]$, $[CH_2^2]$;

(2) the overlap volume of the layers, v_o;

(3) the free energy associated with the removal of one ($-CH_2-$) group from the aqueous environment, Φ; and

(4) the fraction of ($-CH_2-$) groups on the surface of the particle with the lower surface concentration which actually associate with groups from the layer of the other particle as overlap takes place, K_f.

This may be expressed:

$$V_{assoc} = 2[CH_2^1] \cdot v_o \cdot \Phi \cdot K_f \tag{10}$$

The surface concentration of hydrocarbon groups on particle 1, i.e. $[CH_2^1]$, may be given by:

$$[CH_2^1] = \frac{4\pi R_1^2 (C_{surf1}) \cdot n_c}{\frac{4}{3}\pi[(R_1 + \delta_1)^3 - R_1^3]}$$

$$= \frac{3R_1^2 (C_{surf1}) \cdot n_c}{[(R_1 + \delta_1)^3 - R_1^3]} \tag{11}$$

where C_{surf1} is the surface concentration of the adsorbed species (mol m^{-2}), n_c is the number of CH_2 groups in the hydrocarbon chain, and δ_1 is the thickness of the adsorbed layer.

The overlap volume can be expressed as:

$$v_o = \left\{ \frac{\pi P^2}{3}[3(R_2 + \delta_2) - P] \right\} + \left\{ \frac{\pi Q^2}{3}[3(R_1 + \delta_1) - Q] \right\} \tag{12}$$

where

$$P = (R_2 + \delta_2) - \left[\frac{(R_2 + \delta_2)^2 + (R_1 + R_2 + h)^2 - (R_1 + \delta_1)^2}{2(R_1 + R_2 + h)} \right]$$

and

$$Q = (R_1 + \delta_1) - \left[\frac{(R_1 + \delta_1)^2 + (R_1 + R_2 + h)^2 - (R_2 + \delta_2)^2}{2(R_1 + R_2 + h)} \right]$$

The free energy change, Φ, associated with the removal of one mole of CH_2 groups from the aqueous environment has been reported as being in the range $-0.71RT$ to $-0.95RT$ for hemi-micellization and should be appropriate to the present case [90].

When the surface coverage is low, the fraction of associating groups, K_f, will be at its highest values. The maximum possible will be if all the groups in the layer with the lower concentration associate with groups in the layer on the other particle.

At higher concentrations, association of the chains within a layer may already occur to some extent before overlap. At monolayer coverage no interpenetration may occur. The value of K_f may thus fall from about 1 at low coverage to near zero at monolayer coverage. Monolayer adsorption densities on mineral surfaces are commonly in the 10^{-6} to 10^{-5} mol m^{-2} range. Higher adsorption densities can occur if bilayers form with reversed orientation of the second layer. This can lead to increased *repulsion* between the approaching surfaces, as a result of electrical and hydration effects caused by the polar groups.

A similar model to that given above was used by Lu and Li in a study of hydrophobic flocculation [91].

Hydration and hydrophobic interactions

Effects on the structuring of water in the vicinity of surfaces can manifest themselves either as a repulsive or an attractive short range force. These forces are not dealt with in conventional DLVO theory but are very important in determining adhesion forces between coating particles and the mineral surface. Over the past decade direct measurements of these forces have been reported. Many of these experiments use the surface force apparatus developed by Tabor and Winterton [92] and Israelachvili and Adams [93]. A useful summary of this work has been given by Israelachvili and McGuiggan [94].

Hydrophobic interactions, V_{HPB}

Israelachvili and Pashley working with mica plates coated with hexadecyl trimethylammonium bromide (CTAB) at pH 9, proposed the hydrophobic force to be a long range attractive force that decayed exponentially with distance [93, 94]. Their proposed equation can be put in the form:

$$V_{HPB} = -\frac{C_{HPB}(R_1 + \delta_1)(R_2 + \delta_2)}{(R_1 + \delta_1) + (R_2 + \delta_2)} l_{HPB} \exp\left[\frac{-[h - (\delta_1 + \delta_2)]}{l_{HPB}}\right] \tag{13}$$

for the interaction between two spheres bearing adsorbed layers of thickness δ_1 and δ_2.

In their original work a value of 0.14 ± 0.02 N m^{-1} for C_{HPB} and of 1.0 nm for the decay length, l_{HPB}, were determined for a monolayer of C_{TAB} on mica [95]. More recent work, has revised the estimate of C_{HPB} to 0.34–0.44 N m^{-1} [97]. Other values for the force constant and decay length have been given in the literature [98, 99]. Estimates for the decay length, l_{HPB}, range from 1.0 nm [95] to 1.4 nm [98]. Some have proposed a double exponential form of decay with a long range decay length from 5.5 nm [99] to about 15 nm [100, 101].

The interaction between a hydrophobic and a hydrophilic surface has not been widely investigated. Claesson et al. have shown that an additional attractive force is present compared with the interaction of two hydrophilic surfaces [102].

Hydration forces, V_{HDN}

Hydrated surfaces or hydrated ions in the vicinity of the surfaces can give rise to a short-range force [103]. The form of the interaction is commonly expressed as a repulsion decaying exponentially with distance.

For unequal spheres with adsorbed layers of thickness δ_1 and δ_2:

$$V_{HDN} = \frac{2\pi(R_1 + \delta_1)(R_2 + \delta_2)}{(R_1 + \delta_1) + (R_2 + \delta_2)} l_{HDN}^2 K_{HDN} \exp\left[\frac{-[h - (\delta_1 + \delta_2)]}{l_{HDN}}\right] \tag{14}$$

Literature values of the hydration force constant, K_{HDN}, for silicates range from 8×10^5 N m^{-2} to 10^7 N m^{-2} with decay lengths of about 1.0 nm [93, 104]. Pashley has discussed the effects of various cations on the magnitude of the hydration force. In some cases a double exponential mode of decay fitted the experimental data more closely [105–109].

The existence of short range repulsive forces due to hydration probably explains the difficulty in adsorbing dense fine particle coatings onto hydrophilic surfaces.

Other types of adhesive forces

Polymer bridging forces

In bridging flocculation, segments of a high molecular weight polymer molecule are attached to the surfaces of two particles. This effectively holds the particles

together and is a different type of force to those previously considered. Provided bridging of the two surfaces occurs, the interaction will be attractive at the equilibrium position. Klein and Luckham have measured this attractive force between mica plates bridged by polyethylene oxide [110]. Discussion of interactions due to adsorbed polymers have been given by Lyklema [111] and Fleer [112].

Capillary forces

Capillary forces are important in those carrier separations where oil is used in addition to surfactants. They arise due to surface tension forces. Maximum forces are achieved if both solids are wetted by the bridging liquid.

For an oil film between two equal oleophilic spheres the maximum force of attraction between the surfaces is:

$$F_{max} = 2\pi R_o \gamma \tag{15}$$

and for sphere–plate geometry:

$$F_{max} = 4\pi R_o \gamma$$

The magnitude of this force may not be much more than the *maximum* attractive force due to DLVO and hydrophobic interactions, but unlike these other forces the particle surfaces do not need to be at very small separation distances for it to be effective. It is also less sensitive to influences of surface roughness. Discussion of the capillary force and its variation with interparticle separation and particle shape have been given by Princen [112], Kitchener [114] and Schubert [115].

Model interaction curves for coating and prevention of coating

The equations given in the previous sections can be used to predict or interpret coating behaviour. Ideally, for coating to take place, the total interaction energy between the target mineral and the magnetic coating particle, or between the carrier and the fine particle, should be attractive without a significant potential energy barrier. An example of this type of interaction is shown in Figure 14. The major contribution to the attraction in this case are the hydrophobic and chain association interactions.

To prevent the magnetic particles from forming a coating, a significant energy barrier should be present. Although this may be achieved by electrical repulsions alone, it is much more effective if repulsive hydration forces operate. These can prevent the fine particles from approaching the mineral surface (Figure 15).

Kinetic aspects

Deposition of colloidal sized particles onto the surface of a rotating disc was studied by Kitchener and co-workers [116, 117]. Deposition rate of negatively charged

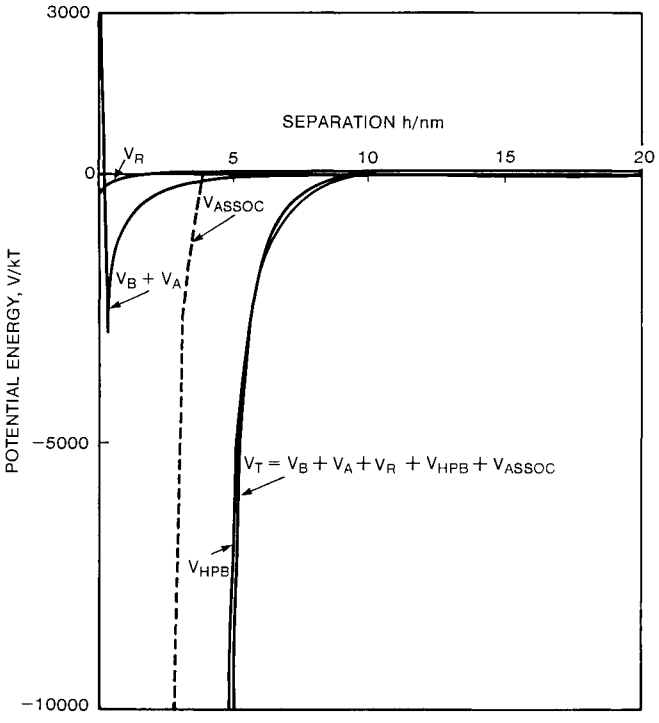

Fig. 14. Example of interactions favouring the formation of a coating. Particle surfaces with adsorbed hydrophobic surfactant. $R_1 = 0.5\ \mu m$, $R_2 = 50\ \mu m$; $\psi_1 = 25$ mV, $\psi_2 = 5$ mV; $A = 5 \times 10^{-20}$ J; $\kappa = 1.5 \times 10^8\ m^{-1}$; $\delta 1 = \delta 2 = 1.9$ nm; $n_c = 16$; $C_{surf1} = C_{surf2} = 5 \times 10^{-7}$ mol m^{-2}; $C_{HPB} = 0.14$ N m^{-1}; $l_{HPB} = 1$ nm; $K_f = 1$; $kT = 4.11 \times 10^{-21}$ J.

particles onto a positive substrate was found to correspond to the theoretical diffusion controlled mass transfer rate. The deposition rate of negative particles on negative surfaces was much reduced but could not be quantitatively accounted for by DLVO theory.

With coarser coating particles, the magnitude of the detachment forces due to fluid drag are of greater significance than the deposition rate. Detailed description of the detachment forces is beyond the scope of the present article but it has been observed that attachment is dramatically less effective for particles with diameters greater than about 2 microns unless oil is used. Increased energy of mixing can result in a higher coating level if conditions for shear flocculation exist [118]. Mixing at high solids concentrations may lead to abrasion of the coating.

Final remarks

Coating and carrier methods of separation have not yet been exploited to any great extent at industrial scale. They have been shown to have potential use in treat-

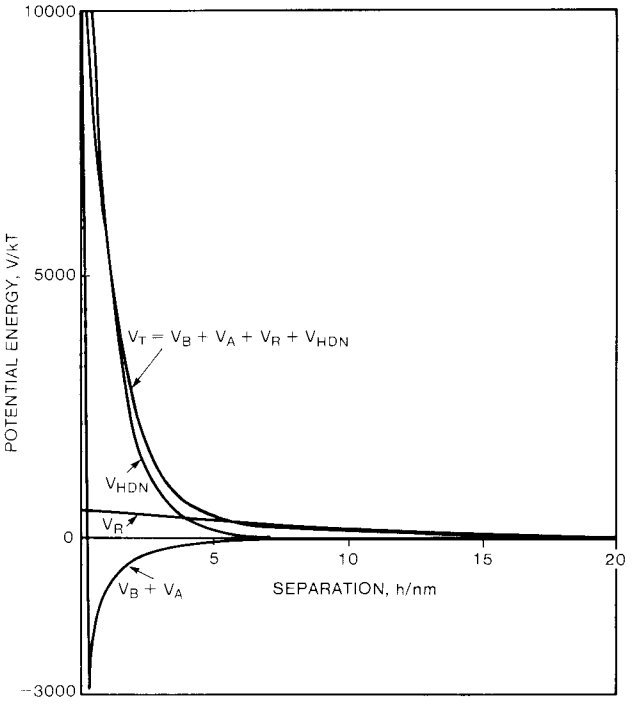

Fig. 15. Example of interactions likely to prevent the formation of a coating. Hydrated surfaces. $R1$ = 0.5 μm, $R2$ = 50 μm; ψ_1 = 25 mV, ψ_2 = 35 mV; $A = 5 \times 10^{-20}$ J; $\kappa = 1.5 \times 10^{8}$ m^{-1}; $K_{HDN} = 10^{6}$ N m^{-2}; l_{HDN} = 1 nm; $kT = 4.11 \times 10^{-21}$ J.

ing a wide range of materials from slime-sized to over 1 cm diameter. They can provide a basis for selective separation of minerals with similar flotation properties and may find application in upgrading flotation concentrates. Further investigations are necessary to optimise the recovery and recycling of the carrier or coating medium as this strongly affects the economics of the process.

Appendix — List of symbols

A	effective Hamaker constant, J
B	magnetic flux density, T
$[CH_2^1]$, $[CH_2^2]$	concentration of CH_2 groups in adsorbed layers on particles 1 and 2, where $[CH_2^1] \leq [CH_2^2]$, mol m^{-2}
C_{HPB}	hydrophobic interaction constant, N m^{-1}
C_{surf1}	surface concentration of surfactant on particle 1, mol m^{-2}.
dB/dZ	magnetic flux gradient, T m^{-1}
D	demagnetising factor
F_{MAG}	magnetic force, N
F_{max}	capillary force maximum, N

H	magnetic field, A m^{-1}
h	minimum separation distance between particle surfaces, m
K_f	fraction of CH_2 groups on particle 1 which associate with groups on particle 2 on overlap
K_{HDN}	hydration force constant, N m^{-2}
kT	thermal energy, J
l_{HDN}	hydration force decay length, m
l_{HPB}	hydrophobic force decay length, m
M	magnetisation, A m-1
M_{sati}	saturation magnetisation, A m^{-1}
n	parameter in Born repulsion equation (5)
n_c	number of CH_2 groups in hydrocarbon chain
P_o	distance parameter in retardation equations (6, 7)
P, Q	parameters in overlap volume equation (12)
R	parameter in Born repulsion equation (5), m
R_1, R_2	radii of particles 1 and 2, m
R_o	particle radius when both the same, m
RT	thermal energy, J mol^{-1}
V	particle volume, m^3
V_A	interaction energy due to Van der Waals interaction, J
V_{assoc}	interaction energy due to association of hydrocarbon chains, J
V_B	interaction energy due to Born repulsion, J
V_{HDN}	interaction energy due to hydration effects, J
V_{HPB}	interaction energy due to hydrophobic effects, J
V_R	interaction energy due to electrical double-layer effects, J
V_T	total interaction energy, J
v_i	fractional volume of ferromagnetic phase
v_o	overlap volume of adsorbed layers, m^3
γ	interfacial tension, N m^{-1}
δ_1, δ_2	adsorbed layer thickness on particles 1 and 2, m
ϵ_0	permittivity of free space = 8.854×10^{-12} F m^{-1}
ϵ_r	relative permittivity
κ	Debye-Huckel parameter, m^{-1}
λ	wavelength of intrinsic oscillations of atoms, m (usually taken as 10^{-7} m)
μ_o	permeability of free space = $4\pi \times 10^{-7}$ H m^{-1}
π	normal usage (3.14159...)
σ	interatomic separation at which E, the atom pair interaction potential, = 0, m
Φ	free energy change for removal of CH_2 groups from aqueous solution, J mol^{-1}
χ	volume magnetic susceptibility (SI units)
ψ_1, ψ_2	zeta potential of particles 1 and 2, V

References

1 J.S. Laskowski, in: E.Matijevic (Editor), Surface and Colloid Science, Vol.12, 1982, pp 315–357.
2 P. Parsonage, Trans. Inst. Min. Metall., Sect. C, Min. Process. Extr. Metall., 93 (1984): C37–C44.
3 P. Parsonage, in: 15th Int. Miner. Process. Congr., Cannes, 1985, edition GEDIM, St. Etienne, 1985, Vol. 3, pp. 345–356.
4 P. Parsonage, U.S. Patent 4,643,822, 1987.
5 A.J. Nott and W.M. Price, U.S. Patent 4,087,004, 1978.

6 A.J. Nott and W.M. Price, U.S. Patent 4,125,460, 1978.
7 J.A. Cook, G.B. Patent 2,092,026A, 1981.
8 W.G. Hubler, U.S. Patent 2,352,324, 1944.
9 P. Parsonage, Trans. Inst. Min. Metall., Sect. A, Min. Ind., 95 (1986): A154–A158.
10 P. Parsonage, Int. J. Miner. Process., 24 (1988): 269–293
11 A.A. Lockwood, U.S. Patent 996,491, 1911.
12 A.A. Lockwood, U.S. Patent 1,043,850, 1912.
13 A.A. Lockwood, U.S. Patent 1,043,851, 1912.
14 J. Svoboda, Magnetic Methods for the Treatment of Minerals, Elsevier, Amsterdam, 1987, p. 155.
15 H.S. Rexworthy, Eng. Min. J., 104 (1917): 58- -60.
16 A.F. Taggart, Handbook of Mineral Dressing, John Wiley, New York, N.Y., 1945.
17 E.C. Herkenhoff, U.S. Patent 2,423,314, 1945.
18 S.F. Schinkorienko and L.G. Bodnarashek, Gorn. Zh, 7 (1968): 58.
19 R.H. Shubert, U.S. Patent 3,926,789, 1975.
20 A.Z. Frangiskos and T. Gambopoulos, Proc. 12th Int. Miner. Process. Congr., 1977, Sao Paulo, Meeting IV — Pap. 2.
21 S.J. Reeson, PCT Patent Application WO84/04701A, 1983
22 T.A. Sladek and C.H. Cox, Paper presented at Int. Conf. on Industrial Applications of Magnetic Separation, Rindge, New Hampshire, July 30–Aug. 4, 1978.
23 J. Gompper, U.S. Patent 2,828,010, 1956.
24 P. Parsonage and J. Singh, 1990, (in prep.).
25 B. Yarar and J.A. Kitchener, Trans. Inst. Min. Metall., Sect. C, Min. Process. Extr. Metall., 79 (1970): C23- -C33.
26 J.P. Friend and J.A. Kitchener, Chem. Eng. Sci., 28 (1973): 1071–1080.
27 A.D. Read and C.T. Hollick, Min. Sci. Eng., 8 (1976): 202–215.
28 Y.A. Attia and D.W. Fuerstenau, Rec. Dev. Sep. Sci., 4 (1976): 51–69.
29 I. Iwasaki, U.S. Patent 4,298,169, 1981.
30 J.Y. Hwang, G. Kullerud, M. Takayasu, F.J. Friedlaender and P.C. Wankat, IEEE Trans. Magnetics, MAG-18, 6 (1982): 1689–1691.
31 J.Y. Hwang, G. Kullerud, F.J. Friedlaender and M. Takayasu, Paper presented at SME-AIME Annu. Meeting, New York, N.Y., Febr. 1985.
32 P. Parsonage, N. Passant and C. Fru, in: A.J. Plumpton (Editor), Production and Processing of Fine Particles, Can. Inst. Min. Metall., 1988, pp 465–474.
33 P. Parsonage, N. Passant, M. Pearl and G. Holyfield, submitted for presentation at 17th Int. Min. Process. Congr. Dresden, 1991.
34 S.T. Hall, J.A. Finch and N. Rowlands. Trans. Inst. Min. Metall., Sect. C, Min. Process. Extr. Metall., 94 (1985): C35–C39.
35 J.K. Kindig, in: Y.A. Liu (Editor), Industrial Applications of Magnetic Separation, Institute of Electrical and Electronic Engineers, 1979, New York, N.Y., IEEE Publ. No. 78CH447-2 MAG, pp. 99–104.
36 J. Kindig and R. Turner, AIME Fall Meeting, Denver, Colo., September 1976, Preprint No. 76-F-306.
37 C. Porter and D. Goens, AIME Fall Meeting, St. Louis, Mo., October 1977, Preprint No.77-F-352.
38 J.A. Meech and J.G. Paterson, Trans. Inst. Min. Metall., Sect. C, Min. Process. Extr. Metall., 89 (1980): C152–C160.
39 E.W. Greene and J.B. Duke, 1962. Min. Eng., 10 (1962): 792.
40 Anon., Austr. Min., Oct. (1983): 52–54.
41 H. Snook and T.C. Hughes, PCT Patent Application WO83/01397, 1983.

42 R.C. Clayton, P.R. Nadebaum, A.J. Priestly and A.H. Truman, in: Solids Separation Processes, IChemE Symp. Ser. No 59, 1980, pp 8:3/1–8:3/28.
43 C. de Latour, IEEE Trans. Magnetics, MAG-9, 3 (1973): 314–316.
44 C. de Latour and H.H. Kolm, J. Am. Water Works Assoc., 68, 6 (1976): 325–327.
45 R. Mitchell, G. Bitton, C. de Latour and E. Maxwell, Progr. Water Technol., 7, 3–4 (1975): 349–355.
46 G. Bitton and R. Mitchell, Water Res., 8 (1974): 549–551.
47 C. de Latour and H. Kolm. IEEE Trans. Magnetics, MAG-11, 15 (1975): 1570–1572.
48 S. Kurinoba, and S. Uchiyama. IEEE Trans. Magnetics, MAG-18, 6 (1982): 1526–1528.
49 C.H. Poynton, K.A. Dicke, S. Culbert, L.S. Frankel, S. Jaganth and C.L. Reading, Lancet, 1 (1983): 524
50 L.J. Warren, Trans. Inst. Min. Metall., Sect. C, Min. Process. Extr. Metall., 84 (1975): C99–C104.
51 P. Parsonage, D. Watson and T.J. Hickey, 1982. In: Preprints, 14th Int. Miner. Process. Congr., Toronto, 1982, Session V, Pap. 5, 22pp.
52 D.W. Fuerstenau, A.M. Gaudin and H.L. Miaw, Trans. AIME, 212 (1958): 792–795.
53 A.M. Gaudin, D.W. Fuerstenau and H.L. Miaw, Can. Inst. Min. Metall. Bull., 63 (1960): 960–963.
54 W.J. Trahar and L.J. Warren, Int. J. Miner. Process., 3 (1976) 103–131.
55 C.E. Hemmings, Int. J. Miner. Process., 5 (1978): 85–92.
56 C.R. Edwards, W.B. Kipkie and G.E. Agar, Int. J. Miner. Process., 7 (1980): 33–42.
57 I. Iwasaki, S.R.B. Cooke, D.H. Harraway and H.S. Choi, AIME Trans., 223 (1962): 97–108.
58 P. Parsonage, in: K.S.E. Forssberg (Editor), Flotation of Sulphide Minerals, Elsevier, Amsterdam, 1985, pp 111–139.
59 P. Parsonage and S.F. Craige, unpublished data.
60 A. Grounds, Mine Quarry Eng., March (1964): 128– 133.
61 Y.C. Wang and P. Somasundaran, in: P. Somasundaran (Editor), Fine Particles Processing, Am. Inst. Min. Metall. Eng., New York, N.Y., Vol. 2, 1980, pp. 1112–1128.
62 Y.H. Chia and P. Somasundaran, Colloids Surf., 8 (1983): 187–202.
63 V.D. Samygin, A.A. Barskii and S.M. Angelova, Colloid J. USSR, 30 (1969): 435–439.
64 W.B. Hu, D.Z. Wang and H. Jin, in: Preprints, 14th Int. Miner. Process. Congr., Toronto, 1982, Session IV, Pap. 10, 14pp.
65 W.B. Hu, D.Z Wang and G.Z. Qu, in: E. Forssberg (Editor), 16th Int. Miner. Process. Congr., Elsevier Science Publishers, Amsterdam, 1988, pp.445–452.
66 D. Wang, G. Qu and W. Hu, in: A.J. Plumpton (Editor), Production and Processing of Fine Particles, Can. Inst. Min. Metall., 1988, pp 309–316.
67 E.W. Greene, J.B. Duke and J.L. Hunter, U.S. Patent 2,990,958, 1961.
68 D.W. Fuerstenau, C. Li and J.S. Hanson, in: A.J. Plumpton (Editor), Production and Processing of Fine Particles, Can. Inst. Min. Metall., 1988, pp. 329–335.
69 J.H.P. Watson, in: Proc. 6th Int. Cryogenic Eng. Conf., Grenoble, 1976, pp. 223–226.
70 J. Svoboda, Int. J. Miner. Process., 8 (1981): 377- -390.
71 M.R. Parker, R.P.A.R. van Kleef, H.W. Myron and P. Wyder, J. Colloid Interface Sci., 101, 2 (1984): 314–319.
72 R.H. Ottewill, J. Colloid Interface Sci., 58, 2 (1977): 357–373.
73 K. Jaeckel, Kolloid Z. Z. Polym. 16 (1964): 143.
74 D. H. Napper, J. Colloid Interface Sci., 58, 2 (1977): 390–407.
75 P.R. Sperry, J. Colloid Interface Sci., 87, 2 (1982): 375–384.
76 P. Parsonage, Particle interactions in colloidal suspensions. Rep. Warren Spring Lab. No. LR 600(MM), 1987, 46 pp.
77 D.L. Feke, N.D. Prabhu and J.A. Mann, J. Phys. Chem., 88 (1984): 5735–5739.
78 H.C. Hamaker, Physica, 4 (1937): 59–82.

79 J.H. Schenkel and J.A. Kitchener, Trans. Faraday Soc., 56, 1 (1960): 161–173.
80 B. Vincent, J. Colloid Interface Sci., 42, 2 (1973): 270–285.
81 J. Visser, Adv. Colloid interface Sci., 3 (1972): 331–363.
82 J. Visser, J. Powder Technol., 58 (1989): 1–10.
83 J. Gregory, Adv. Colloid Interface Sci., 2 (1969): 396–417.
84 J.N. Israelachvili, J. Chem. Soc., Faraday Trans., 2., 39(12 (1973): 1729–38.
85 D.B. Hough and L.R. White, Adv. Colloid Interface Sci., 14 (1980): 3–41.
86 B.V. Derjaguin and L.D. Landau, ACTA Physiochem., 14 (1941): 633–662.
87 E.J.W. Verwey and J.Th.G. Overbeek, Theory of the Stability of Lyophobic Colloids, Elsevier, Amsterdam, 1948.
88 R. Hogg, T.W. Healy and D.W. Fuerstenau, Trans. Faraday Soc., 62 (1966): 1638–1650.
89 R.J. Pugh and J.A. Kitchener, J. Colloid Interface Sci., 35, 4 (1971): 656–664.
90 I.J. Lin and P. Somasundaran, J. Colloid Interface Sci., 37, 4 (1971): 731–734.
91 S. Lu and G. Li, J. Wuhan Iron and Steel University, 4 (1984): 1–9 (in Chinese).
92 D. Tabor and R.H.S. Winterton, Proc. R. Soc. London, Ser. A, 312 (1969): 435–450.
93 J.N. Israelachvili and G.E. Adams, J. Chem. Soc. Faraday Trans. I, 74 (1978): 975–1001.
94 J.N. Israelachvili and P.M. McGuiggan, Science, 241 (1988): 795–800.
95 J.N. Israelachvili and R.M. Pashley, Nature, 300 (1982): 341–342.
96 Israelachvili, J.N. and Pashley, R.M., J. Colloid Interface Sci., 98, 2 (1984): 500–514.
97 R.M. Pashley, P.M. McGuiggan, R.G. Horn and B.W. Ninham, J. Colloid Interface Sci., 126, 2 (1988): 569–578.
98 R.M. Pashley, P.M. McGuiggan, B.W. Ninham and D.F. Evans, Science, 229 (1985): 1088–1089.
99 P.M. Claesson, C.E. Herder, P.C. Blom and B.W. Ninham, J. Colloid Interface Sci., 114, 1 (1986): 234–242.
100 P.M. Claesson and H.K. Christenson 1988. J. Phys. Chem., 92 (1988): 1650–1655.
101 Ya.I. Rabinovich and B.V. Derjaguin, Colloids Surf., 30 (1988): 243–251.
102 P.M. Claesson, C.E. Herder, P.C. Blom and B.W. Ninham, J. Colloid Interface Sci., 118, 1 (1987): 68–79.
103 B.V. Derjaguin and N. Churaev, J. Colloid Interface Sci., 49, 2 (1974): 249–255.
104 N. Churaev and B.V. Derjaguin, J. Colloid Interface Sci., 103, 2 (1985): 542–553.
105 R.M. Pashley, J. Colloid Interface Sci., 80, 1 (1981): 153–162.
106 R.M. Pashley, J. Colloid Interface Sci., 83, 2 (1981): 531–546.
107 R.M. Pashley, Adv. Colloid Interface Sci., 16 (1982): 57–62.
108 R.M. Pashley, J. Colloid Interface Sci., 102, 1 (1984): 23–35.
109 R.M. Pashley and J.N. Israelachvili, J. Colloid Interface Sci., 97, 2 (1984): 446–455.
110 J. Klein and P.F. Luckham, Nature, 308 (1984): 836–837.
111 J. Lyklema, in: B.M. Moudgil and P. Somasundaran (Editors), Flocculation Sedimentation Consolidation, Am. Inst. Chem. Eng., New York, N.Y., 1986, pp. 3–21.
112 G.J. Fleer, in: P. Somasundaran and B.M. Moudgil (Editors), Reagents in Mineral Technology, Marcel Dekker, New York, N.Y., 1988, pp. 105–158.
113 H.M. Princen, in: E. Matijevic (Editor), Surface and Colloid Science, Vol. 2., Plenum Press, New York, N.Y., 1969, pp. 1–84.
114 J.A. Kitchener, 1973. J. Soc. Cosmet. Chem., 24 (1973): 709–725.
115 H. Schubert, Powder Technol., 37 (1984): 105–116.
116 M. Hull and J.A. Kitchener, Trans. Faraday Soc., 65 (1969): 3093–3104.
117 J. K. Marshall and J.A. Kitchener, J. Colloid Interface Sci., 22 (1966): 342–51.
118 L.J. Warren, J. Colloid Interface Sci., 50, 2 (1975): 307–318.

Chapter 12

Oil assisted fine particle processing

J.S. LASKOWSKI

Water/liquid hydrocarbons two phase systems

General considerations

Disperse systems are characterized by a large free energy since there is such huge interfacial area between the particles (or droplets) and the surrounding medium. Such systems tend toward a minimum level of the free energy by interparticle aggregation. Aggregation can be prevented if the dispersed solid particles are electrically charged or are shielded by thick hydration layers. Neutralization of the electrical charge of the dispersed particles, or compression of the double layers shielding the particles to a range shorter than the range of the London-Van der Waals attractive forces, will initiate coagulation. Bridging of particles by long poly-molecules adsorbing with one end onto one particle and another end onto a second brings about flocculation. Shearing the system with an immiscible organic phase that can wet dispersed particles may lead to agglomeration or the bridging of the particles by the oil.

Depending on the quantity of the immiscible liquid, the hydrodynamic conditions and the method used to separate the agglomerates, the final results may be very different as shown in Table 1.

The first process in the table, *extender flotation*, utilizes small doses of an oil (up to a few hundred grams per tonne) to enhance the collector, and/or to reduce its consumption. Extender oils are frequently used to improve flotation of coarse particles.

In *agglomerate flotation*, invented to treat very fine particles which are not recovered efficiently in conventional froth flotation, oil is added to increase the size of particles by agglomerating them. The method involves conditioning at high pulp density with an appropriate collector to render the particles hydrophobic and with an oil to bridge particles together. Pulp dilution and conventional froth flotation follows.

TABLE 1

Characteristics of separation process using oil

Technique	Ionic collector	Oily collector	Oil consumption (kg t^{-1})	Conditioning	Method of separation
Extender flotation	Yes	Yes	0.05–0.5	Regular	Flotation
Agglomeration flotation	Yes	Yes	a few kg t^{-1}	Intense	Flotation
Emulsion flotation	No	Yes	up to a few kg t^{-1}	Regular	Flotation
Oil agglomeration	No[a]	Yes	5–10%	Slow/intense shearing	Sizing
Liquid–liquid extraction	Yes	Yes[b]	N/A	Intense	Phase separation

(From Finkelstein [1] with permission.)

[a] Ionic collector is not required in the oil agglomeration of inherently hydrophobic solids such as coals. It will be required to process hydrophilic material.
[b] Oil is not used as a collector in this process.

Emulsion flotation is applied to treat inherently hydrophobic solids (coals, graphite, sulphur, molybdenite, talc). In this process, water-insoluble oil is used as a collector and the frother, as in all other flotation processes, is a water-soluble surfactant. Both agglomerate flotation and emulsion flotation use larger quantities of oil than extender flotation (up to a few kg t^{-1}).

The first three techniques mentioned belong to a family of flotation processes, the following two do not. *Liquid phase agglomeration*, as the process is termed by Capes [2–4], can be adopted to separate fine solid particles from suspensions. In coal preparation, the process can be utilized to separate hydrophobic coal particles from hydrophilic inorganic gangue [5]. In this process, the consumption of oil may be as high as 10 wt.% or more, based on feed solids.

In *liquid–liquid extraction*, the dosage of oil is several times the volume of the particles to be extracted. Under shearing conditions, the particles, depending on wetting, report either to oil phase when they are very hydrophobic, or to aqueous phase when they are completely wetted by water. Particles with intermediate ranges of hydrophobicity accumulate at the oil/water interface.

In all these processes, the second liquid added under appropriate hydrodynamic conditions must be immiscible with the suspending liquid, and be capable of displacing this liquid from the surface of the particles. Thus, these processes can be evaluated in terms of the principles of selective wetting as will now be discussed.

Emulsions and emulsification

The use of liquid hydrocarbons, commonly referred to as oils, in these processes involves high intensity conditioning with a pulp. Since the oil is insoluble in water, it cannot coat mineral particles via adsorption, and must be dispersed into fine droplets (oil in water emulsion), which collide and become attached to hydrophobic particles.

The emulsification processes which are involved may differ widely. While oil agglomeration of fine coal does not have to include surfactants, in most cases emulsification takes place in the presence of a surfactant. In the emulsion flotation of molybdenite, an emulsifier under the trade name Artic Syntex L (sulphonated coconut oil) is used [6]. Oils used as an extender in the flotation of coarse fractions of potash ore are applied together with long-chained amines [7]. In agglomeration flotation, an oil is usually applied along with a collector (fatty acids). Oil emulsification is, therefore, facilitated by the presence of a collector; emulsification prior to conditioning with the pulp can improve the overall process significantly [8, 9]. Some difficult-to-float coals require, in addition to an oily collector and a frother, a third reagent: the so-called promoter. Its role is to first of all facilitate emulsification of an oily collector in the pulp [10, 11].

In the case of two immiscible liquids such as oil and water, the reversible work (ΔW) needed to disperse one into the other, under isothermal conditions, is equal to the increase in the system free energy:

$$\Delta G = \Delta W = \gamma_{ow} \Delta A \tag{1}$$

where γ_{ow} is the oil–water interfacial tension and A is the surface area of dispersed droplets.

This equation clearly indicates that any amphipatic, surface active agent which lowers oil/water interfacial tension will facilitate emulsification. The presence of such an agent at the oil/water interface may also affect the attachment of oil droplets to mineral particles and its spreading.

In order to increase the affinity of oil droplets towards specific minerals, Ralston et al. [12, 13] used emulsions stabilized by polymers with specific functional groups. Ralston used a copolymer of methacrylic acid with its methyl ester (mole ratio 2:1)

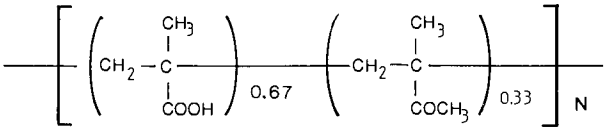

with molecular weight of 10^{-5} to separate calcite from quartz. Cellulose xanthate stabilized emulsions have been used to separate fine chalcopyrite from quartz.

Model systems

Liquid hydrocarbon/water interfacial tension

Molecules located within the bulk of a liquid are subjected to equal forces of attraction in all directions. The molecules in the surface region of the liquid are subject to attractive forces from adjacent molecules which result in a net attraction into the bulk phase in the direction normal to the surface. The attraction tends to reduce the number of molecules in the surface region; the work required to increase the area of a surface isothermally and reversibly by a unit amount is defined as the surface free energy (surface tension).

The intermolecular attractions which cause surface tension, may result from quite different intermolecular forces; while London dispersion forces are universal, always attractive and existing in all types of matter, other forces, such as hydrogen bonding, can exist only if the substance under consideration consists of polar groups capable of hydrogen bonding. Whereas molecules of saturated hydrocarbons can interact only through London dispersion forces:

$$\gamma_h = \gamma_h^d \tag{2}$$

water molecules interact with each other through hydrogen bonding and dispersion forces:

$$\gamma_w = \gamma_w^d + \gamma_w^h \tag{3}$$

where γ_h and γ_w stand for surface tensions of saturated hydrocarbon and water, respectively, while γ_h^d, γ_w^d and γ_w^h are dispersion and hydrogen bonding contributions to surface tension of hydrocarbon and water.

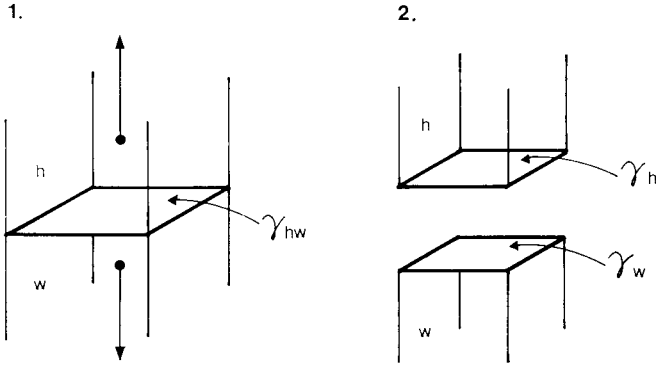

Fig. 1. Definition of the work of adhesion.

At the interface between water and saturated liquid hydrocarbon, London dispersion forces are the only ones operating across the interface.

As shown in Figure 1, the work of adhesion for such a two-phase system is:

$$W_A = \gamma_h + \gamma_w - \gamma_{hw} \tag{4}$$

where W_A is the work of adhesion of water to hydrocarbon, and γ_{hw} is the hydrocarbon–water interfacial tension.

For the water/saturated liquid hydrocarbon interface, across which only dispersion forces operate, the work of adhesion is due entirely to the dispersion forces component, W_A^d, and so for such a case the hydrocarbon/water interfacial tension is:

$$\gamma_{hw} = \gamma_h + \gamma_w - W_A^d \tag{5}$$

According to Fowkes [14]:

$$W_A^d = 2\sqrt{\gamma_h^d \cdot \gamma_w^d} \tag{6}$$

Thus, equation (5) can finally be written in a form [14]:

$$\gamma_{hw} = \gamma_h + \gamma_w - 2\sqrt{\gamma_h^d \cdot \gamma_w^d} \tag{7}$$

Since the liquid/liquid interfacial tension can easily be measured, this equation has been tested for many different systems. For saturated liquid hydrocarbons (n-hexane, n-heptane, n-octane, etc), the experimentally determined interfacial tensions (with water) are in the range 50–52 erg cm^{-2}, and therefore, the calculated value for γ_w^d is 21.8 ± 0.7 erg cm^{-2} [14]. Because equation (7) is true when only dispersion forces operate across the interface, it can be used as a powerful tool to investigate interfacial interactions.

Table 2, taken from Fowkes classic publication [14], indicates that in the case of benzene and toluene, the measured interfacial tension is 15–16 erg cm^{-2} smaller than the value predicted from equation (7) — 51.5 erg cm^{-2}. This difference was ascribed to a pi-bonding interaction between aromatic hydrocarbons and water molecules. Later, this difference was corrected to be in the range from 16 to 22 erg cm^{-2} [15]. Carbon tetrachloride and carbon tetrabromide interaction with water includes the interaction of water dipoles with induced dipoles in the organic phase and amounts to 6 erg cm^{-2}. Butyronitrile–water interaction involves dipole–dipole effects (23 erg cm^{-2}). It is of interest to note that the organic molecules capable of hydrogen bonding have the strongest energy of interaction with water (40–48 erg cm^{-2}).

Electrokinetics of hydrocarbon droplets in aqueous solutions

For any solid/liquid system both the composition of the solid and the concentration and valency of ions in the solution contribute to the sign and value of the electrokinetic potential. In the case of very dilute disperse systems containing a

TABLE 2

Energy of water-organic liquid interaction in excess of dispersion force interaction (in erg cm^{-2} at 20°C)

Liquid No. 2	γ_2	γ_{12}	γ_{12}^d	Excess	$2\sqrt{\gamma_1^d \cdot \gamma_2}$
Benzene	28.9	35.0	51.5	+16.5	50.2
Toluene	28.5	36.1	51.5	+15.4	50.0
Mesitylene	28.8	38.7	51.4	+12.7	50.1
Carbon tetrachloride	26.9	45.0	51.3	+ 6.3	48.4
Carbon tetrabromide	49.7	38.8	56.5	+ 6.8	66.0
Butyronitrile	28.1	10.4	51.3	+23.2	49.6
Aniline	42.9	5.8	53.7	+47.9	62.0
Di-n-butylamine	22.0	10.3	51.0	+40.7	43.8
Octanoid acid	27.5	8.5	51.3	+42.8	49.0
Cyclohexanol	32.7	3.9	51.9	+48.0	53.6
Polydime-thylsilox-anes[a]	15.7	41.3	53.9	+12.6	34.6[b]
Polydime-thylsilox-anes[a]	16.8	41.3	53.6	+12.3	36.0[b]
Polydime-thylsilox-anes[a]	19.4	41.3	53.2	+12.1	39.0[b]

(From Fowkes [14] with permission.)

[a] γ_2^d values estimated as $\gamma_2 - 2$ erg cm^{-2}.
[b] Actually $2\sqrt{\gamma_1^d \cdot \gamma_2^d}$.

small number of individual particles in a large amount of solution, as in a micro-electrophoretic experiment, the contribution from the value of surface potential is more important. The results discussed in this section all pertain to the conditions of the conventional microelectrophoretic experiment conducted at an extremely low concentration of the dispersed phase.

Figure 2, taken from James [16], summarizes the effect of pH on electrokinetic mobility for a non-ionic surface, an ionogenic surface with carboxylic groups, an

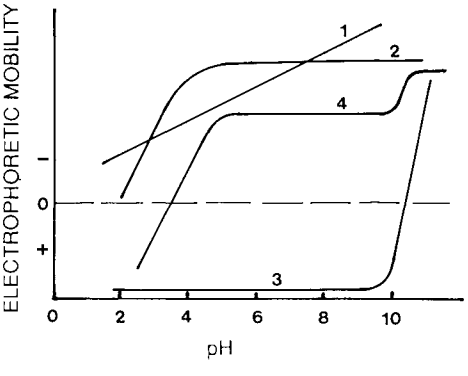

Fig. 2. pH-mobility curves (at constant ionic strength): *1* = nonionic surface; *2* = ionogenic surface with anionic (carboxyl) surface groups; *3* = ionogenic surface with cationic groups; *4* = ionogenic surface with cationic and anionic groups (from James [16] with permission).

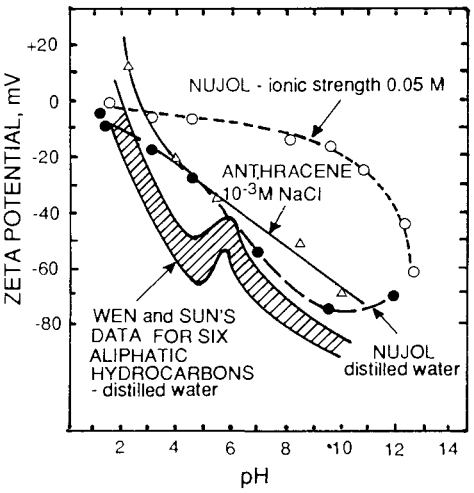

Fig. 3. Zeta potential of Nujol droplets [21], six aliphatic hydrocarbons [19] and anthracene (from Laskowski [18]).

ionogenic surface with amine groups and an ionogenic surface with both acidic and basic functional groups. Fundamental for this section curve *1*, the zeta potential–pH relationship for non-ionic system, is based mainly on Perreira and Schulman [17], who maintain that the negative charge at a hydrocarbon/water interface is due to preferential adsorption of OH^- ions in comparison to that of H_3O^+ ions.

Figure 3 shows a similar relationship as measured for various hydrocarbons [18]. For all the tested paraffinic hydrocarbons (from hexane to octadecane [19]), aromatic hydrocarbon-anthracene, as well as Nujol [20, 21], the zeta potential values are negative over the whole pH range. It is of interest to note that the zeta potential–pH curve for high purity graphite was also found to be negative over the broad pH range [22, 23].

Figure 4, quoted after Wen and Sun [19], shows the effect of a cationic surfactant, dodecylammonium chloride, on the zeta potential of hexadecane droplets in water. Similar effects were found by Mackenzie [21], who used Nujol — a highly refined paraffinic oil. As seen from Figure 4, the iso-electric point of the hexadecane droplets shifts with increasing dodecylammonium chloride concentration towards more alkaline pH values and assumes the value of pH 11; Mackenzie also found that the iso-electric point of Nujol droplets in the presence of dodecylammonium chloride is approximately pH 11. Microbubbles generated in the aqueous solutions of dodecylammonium chloride were found to have iso-electric point around pH 11 as well [24, 25]. Apparently in all these cases the measured iso-electric points are determined by the colloidal precipitate of dodecylamine which i.e.p. is situated at pH 11.

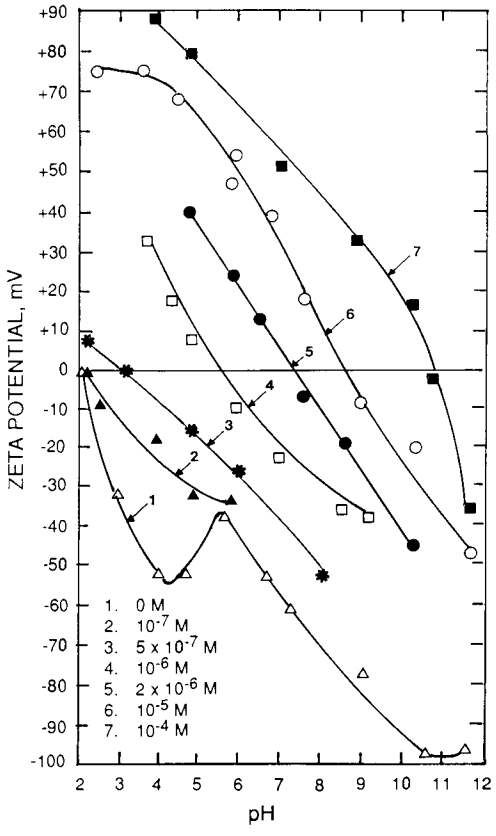

Fig. 4. Effect of dodecylammonium chloride at various concentrations on the electrokinetic potential of hexadecane-in-water emulsion droplets (from Wen and Sun [19] with permission).

Such results reveal that while the effect of ionic groups on the electrokinetic behavior can be satisfactorily predicted, the contribution of the hydrocarbon matrix to the overall particle charge is still not quite clear [26]. For example, it is difficult to understand why the zeta potential–pH curve for the Nujol droplets clearly depends on pH, but is quite flat for the Nujol droplets with pre-adsorbed neutral polysaccharide [20].

Oils in mineral processing

There are two sources of hydrocarbons: crude oils (petroleum) and coal tars. The coal tar distillation products were widely used as collectors in emulsion flotation of coals, but since they contain mostly aromatics with quite a large content of highly toxic phenols and phenol-like compounds their use in coal flotation was abandoned in the 60s. These products have since been replaced by oils produced from crude oil.

According to ASTM D-288, crude petroleum is defined as a naturally occurring mixture, which is removed from the earth in a liquid state, containing predominantly hydrocarbons, and/or sulphur, nitrogen and/or oxygen derivatives of hydrocarbons. In spite of the wide differences in the physical characteristics of crude oils, their ultimate analyses are very consistent as shown in Table 3 [27].

Useful information on the oils used in flotation processes can be found in the book by Glembotski et al. [28] and in the recent publication by Seitz and Kawatra [29].

Table 4 provides information on various types of petroleum products; the table also indicates how major types of hydrocarbons accumulate in various fractions.

The light distillate fractions, intermediate fractions and heavy distillate fractions are characterized by boiling ranges 93–204°, 204–343° and 343–566°C, respectively. The residues, after all the distillates are removed, include residual fuel oils, petrolatum and asphalt. These contain paraffins of very high molecular weight, polycyclic hydrocarbons, condensed polyaromatics and mixed naphteno-aromatics; also, sulphur-, nitrogen- and oxygen-containing compounds. The oxygen content increases with the boiling point of the fraction, the greater portion of oxygen-containing constituents being concentrated in the residual oil where oxygen contents as high as 8% were reported [27].

Two groups of metals appear in crude oil: zinc, titanium, calcium and magnesium in the form of surface active soaps; vanadium and nickel form oil-soluble stable complexes with porphyrins which appear in heavy fractions. Porphyrins are powerful surface active agents promoting the formation of stable emulsions of petroleum in water [27].

Fuel oil No. 2, frequently used in flotation, is one of the products within a boiling range of 204–343°C. It consists of paraffins, iso-paraffins, aromatics, naphtenes, and also sulphur-, nitrogen- and oxygen-containing hydrocarbons not removed by refining. Fuel oils also appear among the products listed under the residues. These are high molecular weight paraffinic and cyclic hydrocarbons along with oxygen, sulphur and nitrogen derivatives. Since these oils are characterized by a high viscosity they are mixed with intermediate distillates. The mixture containing 20–50% of interme-

TABLE 3

Ultimate analysis of crude oils

	% Weight
Carbon	83.90–86.80
Hydrogen	11.40–14.00
Sulphur	0.06– 8.00
Nitrogen	0.11– 1.70
Oxygen	0.50
Metals (Fe, V, Ni, etc.)	0.03

(From King et al. [27] with permission.)

TABLE 4

Chemical composition of various crude oil distillation fractions

Crude oil products	Paraffins C_nH_{2n+2} –C–C–C–C–	Isoparaffins C_nH_{2n+2} –C– | –C–C–C–C–	Naphtenes C_nH_{2n}	Aromatics C_nH_n	Sulphur containing compounds	Nitrogen compounds	Oxygen compounds
Natural gasoline	↑	↑	↓	↑	↓	↓	↓
Light distillates			↑				
Intermediate distillates			↓	↓			
Heavy distillates			↑				
Residues			↓	↓	↓	↓	

Substituted monocyclic naphtenes and polycyclic naphtenes

Condensed polyaromatic molecules

Mercaptans, thio-ethers, cyclic thio-ethers

Basic nitrogen-containing compounds

(Adapted using data from [27].)

diate distillates is referred to as No. 4 and No. 5 fuel oils, the one with only 5–20% of distillate is known as No. 6 fuel oil. No. 6 fuel oil is reported to contain 10–500 ppm vanadium and nickel in the form of porphyrins.

Since all the oil assisted processes discussed in this chapter involve conditioning with oil and eventually its emulsification, the oil/water interfacial tension obviously plays a very important role here. Glembotski [28] quotes after other authors that the water/oil interfacial tension for Russian petroleum products was found to vary from 25–32 erg cm^{-2} to as low as 12 erg cm^{-2}, while well purified petroleum products have interfacial tension above 40 erg cm^{-2}. Comparison of these numbers with Table 2 immediately indicates that while the interfacial tension for purified oils approaches 50, any content of aromatics and especially hydrocarbons with polar groups lowers this value appreciably. Figure 5, taken from Woods and Diamadopoulos [30], shows oil–water interfacial tension as a function of pH for a few crude oils. This relationship reveals that the crudes contain surface active species. An especially strong effect of pH on the water/oil interfacial tension was reported for heavy crude oil fractions, such as asphaltenes [31].

In the final stage of the conditioning with pulp, the oil droplets attach to mineral particles which are hydrophobic to some extent. This state is controlled by coulombic interactions which can be characterized by electrokinetic measurements [32].

As seen from Figure 6 [10], while the zeta potential–pH curve for kerosene resembles the relationships for paraffins, the curve for the No. 2 and No. 6 fuel oil mixture (4:1 ratio) is very different and indicates the presence of heteropolar surface active compounds. Figure 7 [19] points to the presence of surface active

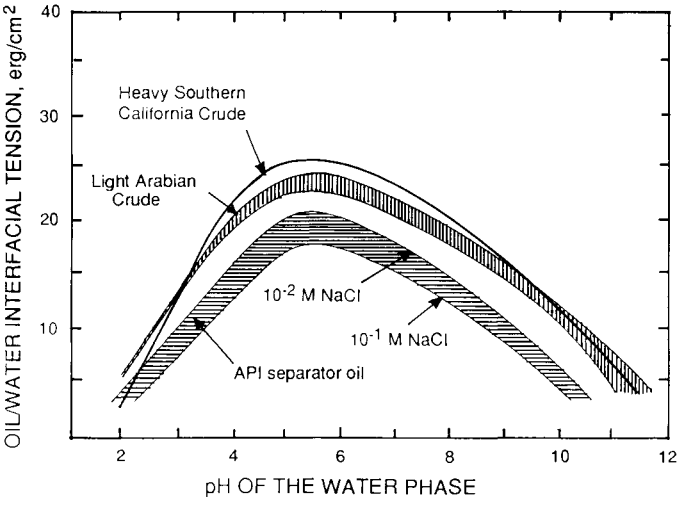

Fig. 5. Oil-water interfacial tension as a function of pH (from Woods and Diamadopoulos [30] with permission).

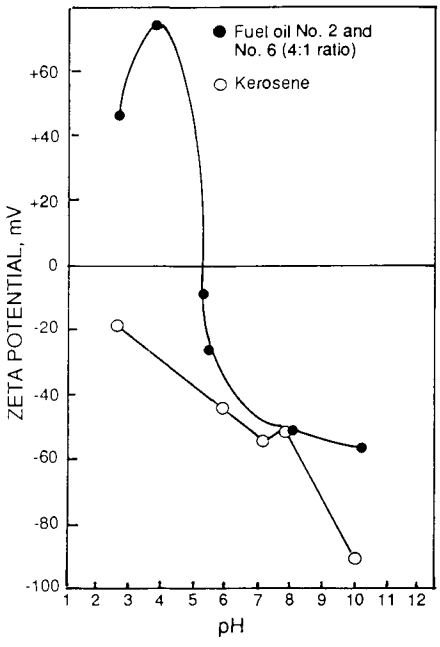

Fig. 6. Zeta potential–pH curves for droplets of kerosene and fuel oils mixture (80% No 2 and 20% No. 6) (from Laskowski and Miller [10]).

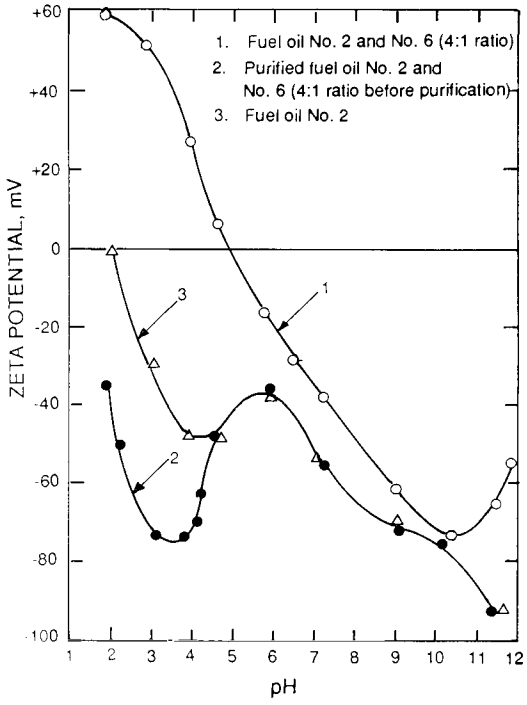

Fig. 7. Electrokinetic potential of oil-in-water emulsion droplets (from Wen and Sun [19] with permission).

"impurities" in the No. 6 fuel oil and indicates that these "impurities" make the electrokinetic properties of the mixture differ from that of other hydrocarbons (see Figure 3). Wen and Sun [19] observed that the i.e.p. shifted towards a more alkaline pH with an increase of the No. 6 to No. 2 ratio in the mixture: it was pH 4.9 at 1:4 ratio, and pH 5.5 for 1:2 ratio, but remained unchanged at pH 4.9 when this ratio was only 1:9. This seems to indicate that what is important here are the surface active compounds in the No. 6 oil.

Both the interfacial tension and electrokinetic measurements provide quite consistent information on the nature of various crude oil products and their "impurities". The presence of such surface active compounds must obviously be very important for the behaviour of the oils in the separation processes.

Competitive wetting of solid particles with immiscible liquids

Particle–oil droplet interactions

In the case of oil-assisted separation processes, the reagent system is more complex than in the case of soluble collectors. There may be both soluble and insoluble components as in the case of extender and agglomerate flotations, where ionizable collectors and frothers are utilized along with oil, and in emulsion flotation, where water-soluble frothers are used together with water-insoluble oily collectors. It should also be pointed out that the oil used in the oil agglomeration process may contain surface active compounds which are soluble in water. In all these processes, the equilibrium changes quickly with conditioning, accompanied by adsorption of surfactants onto mineral particles, adsorption of surfactant onto oil droplets which are formed during conditioning, and extraction of various species from the oil into the aqueous phase. The oil droplets, with or without pre-adsorbed surface active agents, collide with particles either adhering or not, depending on mutual surface chemistry. In line with Arbiter and Williams [9, 29], the following rate-controlling processes can be singled out:

(1) equilibration of mineral particles with the species in solution at a given pH;

(2) equilibration of an oil with species in solution at a given pH;

(3) emulsification of an oil into fine droplets;

(4) adsorption of a collector and other dissolved species onto mineral particles;

(5) hydrophobic flocculation of fine hydrophobic particles;

(6) interaction of oil droplets with mineral particles and the attachment of droplets to hydrophobic particles;

(7) attachment of air bubbles to hydrophobic particles;

(8) spreading of oil lenses on mineral particles and formation of agglomerates containing many particles (and entrained bubbles) held together by bridging oil films;

(9) rearrangement of initially formed aggregates under high shear turbulent conditions;

(10) readjustment of a new, quickly changing "equilibrium" that follows changes in the concentration of dissolved surface active species;

(11) abrasion and desorption of the collector from particles when the collector is adsorbed due to its initially high concentration.

It is of interest to note that while processes 1, 2, 4 and 10 are simple equilibrations and do not require high intensity conditioning, processes 3, 8, 9 and 11 are characterized by high energy requirements.

By all evidence, in all flotation and agglomeration processes involving the use of oil, proper oil pre-emulsification is extremely important [33–37]. The proper drop size should be obtained before rather than during the conditioning step. As indicated by Arbiter and Williams [9], it is more efficient to disperse oil in a concentrated stock solution with small specifically designed equipment. If the droplets are initially coarse, the separation results are poorer and cannot be brought to the same level as those with a pre-emulsified reagent.

In the oil-assisted separation processes, interaction of oil droplets with mineral particles results in attachment when particles are hydrophobic — either hydrophobic by nature or rendered hydrophobic with collectors.

If a particle is forced against an oil droplet (Figure 8) isothermally and in a reversible way, the work performed is identical to the free energy change of the system:

$$\Delta G = G_2^s - G_1^s$$

$$G_1^s = A_{sw}\gamma_{sw} + A_{ow}\gamma_{ow} \tag{8}$$

where A_{sw} and A_{ow} stand for the surface areas of the solid particle and oil droplet, respectively, and γ_{sw} and γ_{ow} are solid/water and oil/water interfacial tensions.

If the attachment area A_{so} is assumed equal to 1 cm^2:

$$G_2^s = (A_{sw} - 1)\gamma_{sw} + (A_{ow} - 1)\gamma_{ow} + 1\gamma_{so} \tag{9}$$

and:

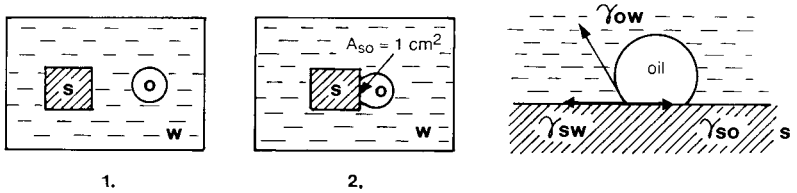

Fig. 8. Attachment of solid particle to oil droplet in water.

$$\Delta G = G_2^s - G_1^s = \gamma_{so} - \gamma_{sw} - \gamma_{ow} \tag{10}$$

Since from Young's equation:

$$\gamma_{sw} = \gamma_{so} + \gamma_{ow} \cos\theta \tag{11}$$

then:

$$\Delta G = \gamma_{ow}(\cos\theta - 1) \tag{12}$$

The result is that the attachment of an oil droplet to a mineral particle is likely to take place only when $\theta > 0$; for $\theta = 0$, $\cos\theta = 1$ and $\Delta G = 0$, the attachment is impossible.

Attachment and spreading — the effect of particle hydrophobicity

Taubman and Janova [38] showed that non-polar oils are better flotation collectors when they are less soluble in water. This again confirms that the mode of action of such flotation agents is quite different from water-soluble collectors which adsorb onto solids from the aqueous environment. Non-polar oils are emulsified and their droplets must attach to the mineral particles in order to improve floatability.

Burkin and Soane [39] proved experimentally that hydrophilic quartz particles could not be floated with oil. The same quartz could, however, be floated when extremely small amounts of dodecylamine were simultaneously added; these amine quantities were not sufficient to cause the flotation of quartz by themselves. These findings can be explained with the results obtained by Schulman and Leja [40], who studied wettability of barite in the presence of the surfactants which adsorb onto $BaSO_4$. The contact angles in aqueous solutions of the surfactants (fatty acids, alkyl sulphonates) were much larger when measured at oil droplets than at air bubbles. The contact angle for these two systems, solid–water–oil and solid–water–air, in accordance with Young's equation is the result of three tensions:

$$\gamma_{wa} \cos\theta_{(air)} = \gamma_{sa} - \gamma_{sw} \tag{13}$$

$$\gamma_{ow} \cos\theta_{(oil)} = \gamma_{so} - \gamma_{sw} \tag{14}$$

where $\theta_{(air)}$ and $\theta_{(oil)}$ are the contact angles measured across the aqueous phase by drops of oil or by air bubbles. While it is seldom that the water/air surface tension can be reduced to values below 30 erg cm^{-2} by addition of surface active agent, the interfacial tension of the oil/water interface can be easily reduced to values of 1 erg cm^{-2} by addition of a suitable surface active agent either to water or to oil. In the presence of a surfactant in oil, the value of γ_{so} must also be much smaller than the value of γ_{sa}, and all this leads to much larger contact angles at the solid–water–oil juncture than at the solid–water–air three phase contact.

It is also interesting to observe that while micelles, formed at surfactant concentration exceeding CMC, depress froth flotation of minerals [41], in emulsion systems the micelles are solubilized by oil phase and the contact angle at the solid–oil–water interface remain unchanged above the critical micelle concentration [40].

In further experiments with attachment of oil droplets to hydrophobic coal particles, Burkin and Bramley [42, 43] measured the zeta potential of the oil droplets and coal particles and used DLVO theory to characterize the interaction. Their results clearly suggest that the collision of the droplet and the particle can lead to attachment only if the kinetic energy of approach between them is larger than the energy of repulsion. Their work revealed that some surface active agents (Lissapol NBD) can drastically improve flotation, and that this effect is accompanied by a decrease in the zeta potential value of the interacting coal and oil droplets.

The beneficial effect of frother on flotation with oily collector was demonstrated and explained by Melik-Gaykazian and co-workers [44]. Frother adsorbs at the oil/water interface, lowers the interfacial tension and improves emulsification. However, it also adsorbs at the coal/water interface [45–47], and provides anchorage for the oil droplets to the coal surface. At higher frother concentration, as shown in Figure 9, an opposite effect can be expected.

A similar approach was adopted by Mackenzie [32], who through electrokinetic measurements explained the effect of ionic surfactants on the interaction of oil droplets with mineral surfaces and on flotation (Figure 10).

As it is known, the DLVO theory takes into account only Van der Waals-London attractive forces and coulombic forces. In the systems typical for mineral process-

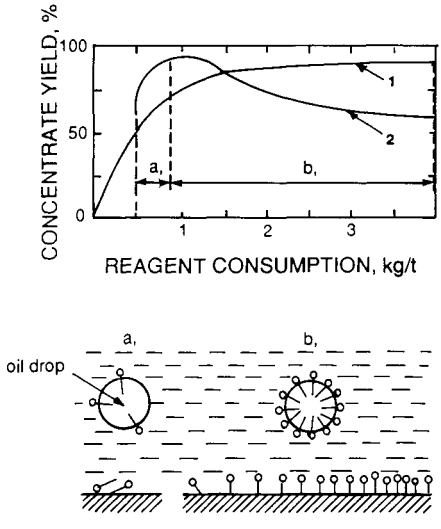

Fig. 9. Flotation of coal under various conditions: *1* = flotation with kerosene only; *2* = flotation with kerosene and n-octyl alcohol (from Melik-Gaikazian and co-workers [44]).

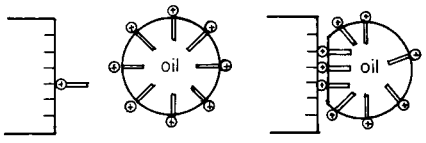

a) Penetration model for low CTAB conc.

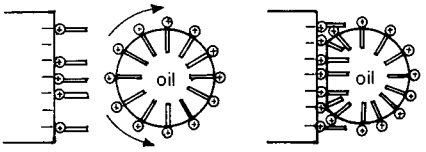

b) Sweeping — penetration model for medium CTAB conc.

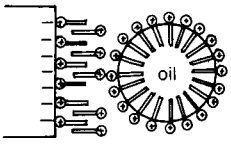

c) No adhesion possible at high CTAB conc.

Fig. 10. Schematic model of oil droplet-mineral particle adhesion. Long-chain ions adsorbed at mineral surface are identical to those at oil/water interface and blacked out to clarify model. (From Mackenzie [32] with permission.)

ing, the hydrophobicity of interacting bodies varies significantly. The hydrophobic interaction term missing in the DLVO theory seems to be a source of problems associated with applying this theory in the mineral processing area. It has recently been shown [48] that inclusion of the hydrophobic interaction term will enable better understanding of the aggregation phenomena. The calculation of the interaction energy between oil droplets and hydrophobic solid particles will definitely be much improved with such corrections.

It is often assumed that after attachment, oil spreads onto the mineral surface and forms a thin film. But is it realistic to assume the existence of such a film?

As shown in Figure 11, the spreading of oil at the solid/water interface will require a change in free energy given by:

$$\Delta G = \gamma_{so} + \gamma_{ow} - \gamma_{sw} \tag{15}$$

Substitution of γ_{sw} from equation (11) gives:

$$\Delta G = \gamma_{ow} - \gamma_{ow} \cos \theta_{(oil)} = \gamma_{ow}(1 - \cos \theta_{(oil)}) \tag{16}$$

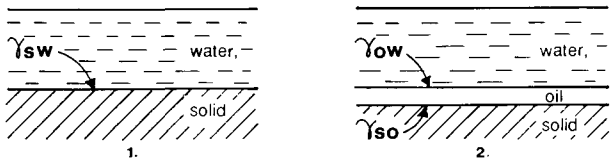

Fig. 11. Schematic model of oil spreading at solid/water interface.

But since $\theta_{(oil)} = 180 - \theta$ (Figure 12):

$$\Delta G = \gamma_{ow}(1 + \cos\theta) \tag{17}$$

and ΔG is always a positive number indicating that thermodynamically the spreading of oil into thin film at the solid/water interface is always unlikely. $\Delta G = 0$ only if $\cos\theta = -1$, that is when $\theta = 180°$, a condition never met in practice.

The spreading process is also analyzed with the use of Harkins spreading coefficient:

$$S = \gamma_{sw} - \gamma_{so} - \gamma_{ow} \tag{18}$$

Since the spreading coefficient represents the energy gained by spreading, the process may occur spontaneously if S is positive. When S is negative, the oil droplet adopts a stable position on the solid surface displaying a contact angle $\theta > 0$.

Applying Young's equation, it can be shown that the spreading coefficient is given by:

$$S = -\gamma_{ow}(\cos\theta + 1) \tag{19}$$

therefore, this expression is always negative for a finite value of θ.

Brown et al. [49] studied wetting of various coals by paraffinic oil in water, also in the presence of surface active agents. Some of their results are given in Figure 13. It is apparent that oils do not spread spontaneously on coal when it is immersed in water. This is true even when the oil/water interfacial tension is reduced by

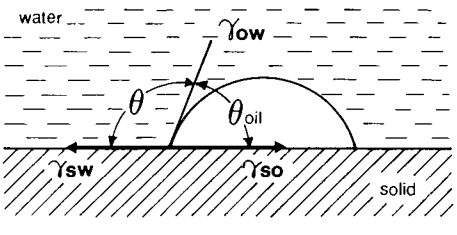

Fig. 12. Contact angles at solid–water–oil three-phase contact.

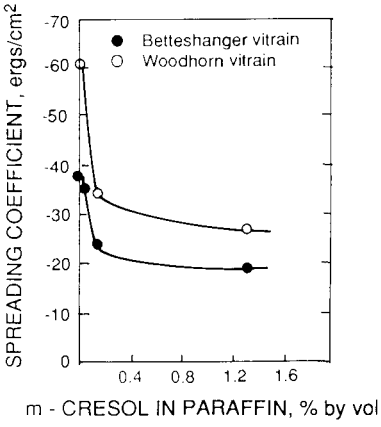

Fig. 13. Spreading coefficient of paraffin with m-cresol added on two different vitrains (from Brown et al. [49] with permission).

the addition of surface active compounds. In accordance with these conclusions, Figure 14 shows oil droplets on a hydrophobic solid (coal), and also on a porous hydrophobic solid in water [50]. The pores on coal surface, as shown in Figure 14, are partially filled with oil since the condition for replacement of water (or air) by oil in a capillary, or crack, or space between the particles is undoubtedly different [49].

Coal is a highly heterogenous solid. It is a mosaic at both the molecular and macroscopic levels in which the hydrophobic organic matrix, that may also contain hydrophilic polar groups, is associated with various hydrophilic inclusions of mineral matter. Our recent observations [51] indicate that the pores on coal surface are also important constituents of such a mosaic. In the case of hydrophobic coal particles immersed in water, the pores may stay filled with air for a very long time, whereas the pores on more hydrophilic particles are quickly filled with water. This increases further the difference in wettability between such particles and sets up conditions under which oil, if added to such a pulp, will easily penetrate into the pores of hydrophobic particles.

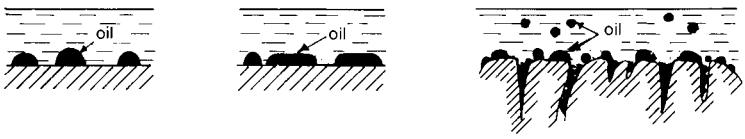

Fig. 14. Oil droplets on coal surface in water (from Klassen [50]).

Emulsion flotation

The thermodynamic criteria such as the spreading coefficient [equations (18) and (19)] are not favorable for displacing water by hydrocarbons even on very hydrophobic teflon [52]. In spite of the negative value of the spreading coefficient which indicates that the oil will not displace water, the oil may, however, displace water if a four-phase teflon/oil/water/air interface is established. Since this situation is relevant to flotation, it is further analyzed in Figure 15 adapted after Zettlemoyer et al. [52], and Klassen [53, 54].

The spreading coefficient of oil (purified white mineral oil, $\gamma_o = 30.4$ erg cm^{-2}) on teflon in contact with water was $S_{o/sw} = -2.42$ erg cm^{-2} and the oil exhibited a finite contact angle of 37°. In Figure 15A, the water film can be thought of as a duplex film which has been mechanically extended over a substrate on which it has a negative spreading coefficient, $S_{w/o} = -94.2$ erg cm^{-2}. The water recedes down the oil drop when the particle approaches a bubble until the water/oil interface is eliminated. After this, the water dewets the teflon plate, receding to the ends. This may either be followed by the film breaking into individual droplets with $\theta_{o/w} = 37°$ or, according to Klassen [53, 54], the oil recedes into a thread along the solid/water/air interface (Figure 15D).

One noticeable effect of the oily collector addition is an increased size of floated particles. As maintained by Melik-Gaykazian [44, 55], the location of oily hydrocarbon at the line of contact at the three phases, and its sudden outflow when the

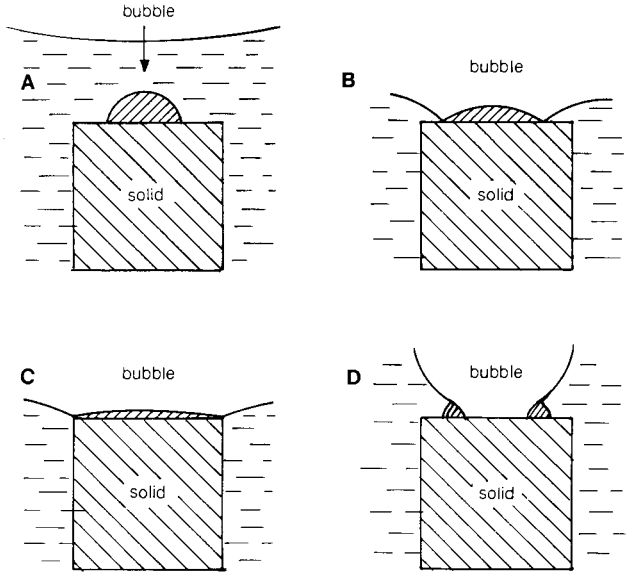

Fig. 15. Attachment of bubble to hydrophobic particle in the presence of oil droplet on the solid particle.

bubble is deformed under shearing forces leads to a sharp increase in the bubble–particle adhesion that prevents detachment.

Since an oily collector can only be used when particles are to some extent hydrophobic, typical examples of emulsion flotation include flotation of molybdenite and flotation of coal.

In the flotation of copper-molybdenum sulphide ores, the bulk concentrate contains both valuable sulphides and is further processed by depressing copper sulphides and floating molybdenite. The former is usually depressed with NaHS (or Na_2S) while the latter is floated with the use of oily collector aided by some amount of emulsifier [6]. The compound under trade name *Syntex*-classified as sulphated coconut oil:

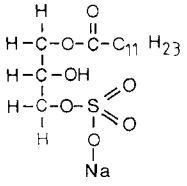

is generally claimed to be the best emulsifier in the flotation of molybdenite.

Smit and Bhasin [56] showed that petroleum hydrocarbons, used as collectors in molybdenite flotation, differ in their effectiveness. Their experiments indicate that a two-component blend of a higher molecular weight naphtenic fractions and No. 2 fuel oil gave superior flotation results.

In the 1960s, the most impressive research program on the flotation of coals was carried out by V.I. Klassen and his co-workers [50, 54, 57]. Flotation activity of simple hydrocarbons, varying in chain length and chemical composition was tested [50, 57]. It was revealed that simple pure hydrocarbons are not very efficient collectors. While they improve the floatability of unoxidized metallurgical coals to some extent, they are not useful in the flotation of lower rank coal particles (see figures 27 and 28, Chapter 4). Compounds containing more than eight carbon atoms (octane) and especially cyclic hydrocarbons such as decalin ($C_{10}H_{18}$), were found to be better than shorter chain homologues [57].

Since the action of these non-polar agents directly results from their immiscibility with water, relatively good solubility and high volatility of lower chain homologues were postulated to be responsible for their poor flotation performance [38]. Glembotski et al. [58] found correlation between viscosity of hydrocarbon homologues and their flotation properties, and claim that all properties of non-polar compounds directly influencing their attachment to mineral surfaces are related to viscosity. Although they were not able to explain differences in flotation activity between various classes of hydrocarbons {paraffins, cycloparaffins, aromatics}, the relationships with viscosity found within these groups were straightforward. Klassen also noticed the effect of viscosity, but he maintained that this results from the effect of the oil

TABLE 5

Flotation of coals varying in rank with the use of different reagents

Coal type	Flotation agents	Concentrate		Tailings	
		Yield (%)	Ash (%)	Yield (%)	Ash (%)
Bituminous medium volatile	tar oil 2.5 kg t^{-1}	71.7	4.5	28.3	63.9
Bituminous high volatile C	tar oil 2.5 kg t^{-1}	38.9	3.9	61.1	23.2
Bituminous high volatile C	kerosene 2 kg t^{-1}, nonyl alcohol 0.62 kg t^{-1}	79.1	4.1	20.9	62.1

(From Klassen [50].)

viscosity on its emulsification [50]. This subject was revitalized recently by Moxon et al. [59], who claim that in the flotation of a porous solid such as coal, the oil not only spreads over the coal surface, but also penetrates the pores. According to these authors, optimum length of twelve carbon atoms in the collector molecule results from these rival effects as they also depend on hydrocarbon viscosity. As already pointed out, only the pores on hydrophobic particles, which are likely to stay filled with air for a long period [51] may be easily penetrated by oils.

Difficult-to-float low rank and/or oxidized coals were shown to require a high consumption of the collectors. If such a process is carried out with the use of the oily collector only, the results are characterized by a clean concentrate, but also by low ash content of the tailings and, consequently, low recovery of combustible matter. While for metallurgical coals the recovery can easily be improved by increasing collector consumption, the low rank coals do not respond well to such a treatment. This, however, can be remarkably improved if two agents, water-insoluble collector and water-soluble frother, are properly selected (Table 5) [50]. This joint effect has already been discussed (Figure 9) [44].

In case of very difficult-to-float coals, a combination of the two reagents, as shown in Table 5, may not be sufficient to provide satisfactory results. The third agent, referred to as promoter, may further enhance the process [11].

As already pointed out, the emulsification of an oily collector increases the number of oil droplets and aids flotation kinetics [33–37, 60, 61]. Since many fine coal flotation circuits do not provide for effective conditioning of the collector, oil dispersion into fine droplets must be aided by chemical means. Emulsification is facilitated by surfactants, referred to as emulsifiers, which reduce the value of oil/water interfacial tension. The promoters belong to this group. The use of such chemical aids in coal flotation was reviewed in 1984 [10].

One of the promoters used by industry is Dowell M-210. It is also known as a froth conditioning agent [62]. It contains imidazoline, or imidazolinium salts of the following formula:

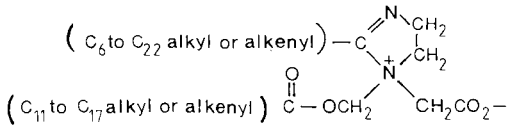

Imidazoline is amphoteric with a point-of-zero charge of approximately pH 8 [63]. It behaves as a cationic surfactant at pH < 7.3 and as an anionic compound at pH > 8.8.

Figure 16 shows the effect of the Dowell M-210 promoter on the flotation of coarse coal (−600 + 212 μm) with kerosene [11]. Whereas metallurgical coal floats very well under such conditions, the surface of the oxidized coal (Oxide 13, Fording mine, British Columbia) requires the addition of promoter. As can be seen, the promoter also enhances the flotation of quartz and, therefore, its concentration must be kept within certain limits.

As shown in Figure 3, the electrokinetic potential of hydrocarbon droplets in water is negative over the entire pH range. So is the zeta potential of kerosene droplets (Figure 6). Since the zeta potential of the oxidized coal particles is also negative (figure 29, Chapter 4), this must seriously hinder the possibility of the oil-to-coal particle attachment [32].

The zeta potential of kerosene droplets in the presence of Dowell M-210 is also shown in Figure 6, and as seen these values can be compared to the zeta potential of

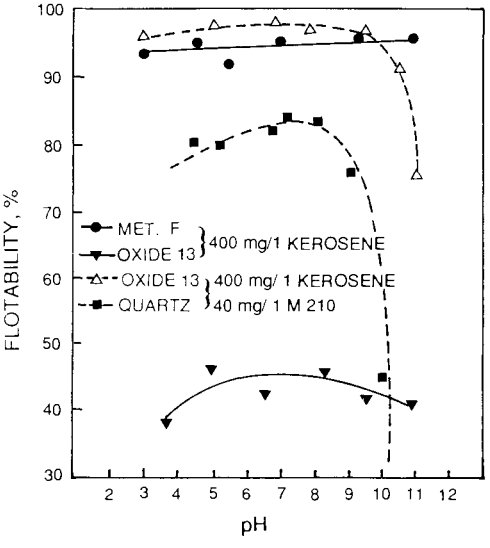

Fig. 16. Hallimond flotation of −600 +212 μm particles of Met. F and Oxide 13 coals, and −212 +105 μm quartz particles. Flotation was carried out either with kerosene only, or with kerosene containing M-210 promoter. (From Laskowski [11].)

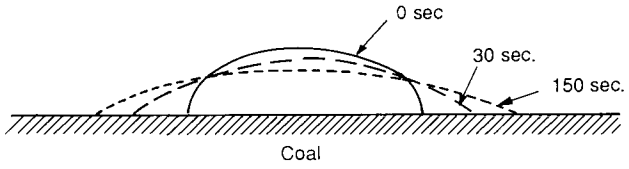

Fig. 17. Dynamic process of spreading of kerosene droplets containing 5% of Dowell M-210 promoter on coal surface in water (from Laskowski [65]).

fuel oil No. 2 with 25% addition of Fuel oil No. 6. Based on this type of experiments, Wen and Sun [19] suggested that the four-to-one mixture of fuel oils No. 2 and No. 6 be used as a better collector for flotation of low rank coals. In line with these findings, Carbini et al. [64] have recently confirmed that mixtures of commercial oils are better collectors for low rank coals.

As our experiments have shown, promoters also reduce the kerosene/water interfacial tension from 50 erg cm^{-2} down to below 1 erg cm^{-2} at 5% addition of Dowell M-210 to kerosene. This leads to improved spreading of kerosene onto the coal surface as shown in Figure 17 [65].

Japanese researchers [66] studied the effect of various promoters on flotation of coal with water-insoluble oily collector. It is noteworthy that they observed nonionic surfactants with low HLB values and high molecular weight produced better flotation results.

Humic acids, whose content may be quite substantial in low rank coals, can be extracted into an aqueous phase. These anionic polyelectrolytes adsorb strongly onto hydrophobic surfaces, make the value of the zeta potential of both coal particles and oil droplets more negative and finally may render the coal surface completely hydrophilic [67, 68]. Flotation of coal under such conditions is obviously depressed [68, 69]. The harmful effect of humic acids may be greatly reduced in the presence of promoters. Figure 18 shows the effect of pH on the contact angle of kerosene droplets on coal in water, measured within water. In an acidic environment, the presence of humic acids reduces the contact angle value from about 80–90 degrees to almost zero (at 20 ppm concentration of humic acids). This means that kerosene does not wet coal surfaces immersed in water under such conditions. Addition of 5% Dowell M-210 to kerosene restores the value of the contact angle remarkably, also in the presence of humic acids, and these findings provide new insight into the role that promoters play in the flotation of low rank coals.

It has also been shown that promoters improve flotation of coarse coal particles [70]. Since coal flotation circuit variations, widely tested in Australia [71], may require separate flotation of coarse particles under appropriate conditions, the use of promoters to aid coarse coal flotation is an important subject. Australian researchers tested polyethylene nonyl phenol [72]. Polyoxy surfactants have also been used in Poland as coal flotation promoters [73–75].

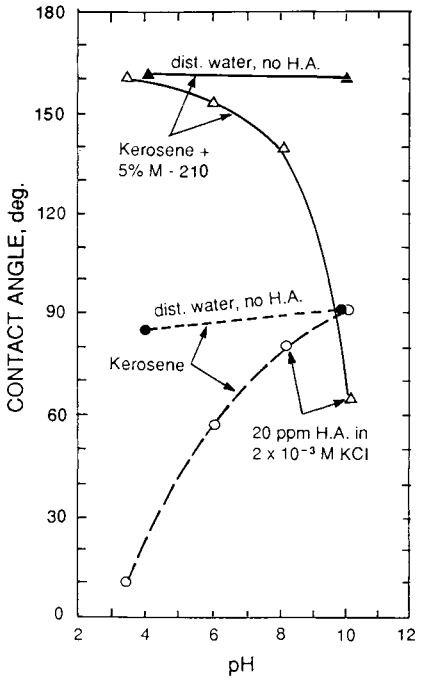

Fig. 18. Contact angles of droplets of kerosene and kerosene containing 5% of Dowell M-210 promoter, measured across the water phase, on metallurgical coal (from Laskowski [65]).

Crude oil distillation products contain not only paraffinic hydrocarbons, but also some polar compounds and heavy fractions. The residues contain also polycyclic hydrocarbons, condensed polyaromatics as well as nitrogen-, sulphur- and oxygen-containing compounds (Table 4). These polar functional groups are apparently able to interact with various mineral surfaces, and while such compounds are much better collectors for lower rank and oxidized coals, their use may also lead to a higher ash content in the final products.

Abundant evidence — both from laboratory testing and plant practice — show that dispersion of an oily collector into fine droplets by mechanical conditioning, or by using admixtures with frothers to provide emulsifying action, or by application of promoters, improves flotation. Oil-in-water emulsions, and the interaction of oily droplets with mineral particles in aqueous phase, are typical subjects of colloid chemistry. The examples illustrating the principles of emulsion flotation have been selected in this section to show how the colloid chemistry experimental methods can be utilized to promote better flotation.

Extender and agglomerate flotations

All flotation methods in which water-insoluble oils are utilized belong to a single class of emulsion flotation processes and the terms: emulsion flotation, extender flotation and agglomerate flotation may be quite arbitrary.

An example of extender flotation is fatty acids flotation of phosphates with simultaneous addition of fuel oil [76]. The process described by Rinelli and Marabini [77] to float zinc–lead oxide–sulphide ores with some chelating collector along with fuel oil is an interesting example of extender flotation. The emulsion flotation process developed by Rosas and Poling [78], in which non-sulphide copper ores containing brochantite, malachite or chrysocolla are floated with a collector — diphenylguanidine — and an emulsified water-insoluble oil, also illustrates well what is here referred to as extender flotation.

The utility of extender flotation to promote better recovery of coarse particles can be illustrated by the industrial flotation of potash ore in Saskatchewan, in which fine sylvite is floated with long chain amines, whereas the flotation of coarse sylvite fractions requires an oil in addition to the long chain amines (Saskatchewan Potash Corporation uses Esso 904 oil [7]).

The process described by Kihlstedt [79] in 1957, in which the Swedish hematite ores were floated with the use of emulsified tall oil (fatty acids) and fuel oil, seems to be different from the examples of extender flotation. First, the consumption of fuel oil, fed as an 4 : 1 mixture with tall oil, was very high (2–3 kg t^{-1}), oil was emulsified with aid of emulsifiers, and a long conditioning time at high solid content after the emulsion addition but prior to flotation was found to be beneficial. Such a flotation process was revealed to provide satisfactory results without desliming the feed. Further details of the process were discussed by Runolinna et al. [80] who studied the same process to float ilmenite ore from Finland. These results entirely corroborated previous findings. With intense conditioning and rather high consumption of oil (about 3 kg t^{-1} at 2 : 1 ratio of fuel oil to tall oil) a desliming stage was unnecessary. Among various tested anionic, cationic and non-ionic emulsifiers, which were shown to accelerate conditioning, non-ionic akyl-phenol-polyethoxy-ethers (Ethoxol P-19) were found to be the best. The tests revealed that the non-polar emulsion agglomerated ilmenite particles. Three percent of Ethoxol P-19 in oil accelerated aggregation of ilmenite particles which were dispersed when only 0.5 to 1.5% of Ethoxol was added. As proved by Karjalahti [8], emulsification of non-polar oil prior to the conditioning with pulp improves significantly the process and reduces energy requirements in the conditioning stage. All these observations point to a quite distinct flotation process, agglomerate flotation. The process is especially suited for very fine feeds.

Since the hydrodynamics of fine particle–bubble collisions is not favourable, flotation of very fine particles is not efficient. Obviously, such flotation could be much improved if the fines could be selectively aggregated into larger entities. In

agglomeration flotation, this is achieved by the conditioning of pulp at high solids content (50–70%) with a collector and fuel oil. The oil droplets bridge the particles, which were rendered hydrophobic by the collector, into larger agglomerates. As pointed out by Lapidot and Mellgren [81], conditioning hydrodynamics in the mixing stage is of primary importance for overall results and for the grade of the final products in particular, i.e. the promotion of selective agglomeration of one mineral from a group.

Recent publications by Al-Taweel and Kasireddy [82] and by Hirajima et al. [83] demonstrate that agglomerate flotation of fine coal can be much improved when flotation columns are used. As discussed in the following section, 5–10% oil additions are required to produce agglomerates large enough to be recovered by screening. Such a high oil addition produces relatively high ash levels in the final clean coal product. Agglomeration at lower oil levels is more selective but yields weaker floc-agglomerates. As pointed out by Capes et al. [84], flotation recovery of such agglomerates leads to better results. It is not then surprising that the use of flotation columns [82, 83] in agglomerate flotation was proven to improve the overall process efficiency.

Liquid phase agglomeration

In the case of agglomerate flotation, some amount of bridging oil is only needed to increase the size of the floated entities. In the presence of larger amounts of oil, and under appropriate hydrodynamic conditions, the agglomerates may reach sizes sufficient to be separated from the slurry by, for instance, screening. This is *oil agglomeration*. It belongs to the group of "size enlargement processes" and is also referred to as "liquid phase agglomeration" [2].

As with emulsion flotation, oil agglomeration of coal relies on differences in the surface properties of coal and inorganic gangue. While flotation becomes less effective for fine sizes of mineral particles, there is no lower size limit on the particles suitable for oil agglomeration.

Three major factors control liquid phase agglomeration [4]: (a) the solid wettability; (b) the amount of bridging oil; and (c) the type and intensity of conditioning.

The amount of agglomerating liquid is critical, as shown in Figure 19. At low liquid levels, discrete lens-shaped rings are formed at the points of contact of the particles (Figure 19a). At higher doses, the liquid rings begin to coalesce and form a continuous network, the funicular state (Figure 19b). The interparticle space becomes filled with liquid when the capillary state prevails (Figure 19c). At higher than 10% oil consumption, the spherical agglomerates may be a few mm in size, whereas at the oil dosages corresponding to the pendular-funicular state more open but smaller flocs are formed.

As pointed out by Keller and Burry [85], Figure 19 does not depict accurately the

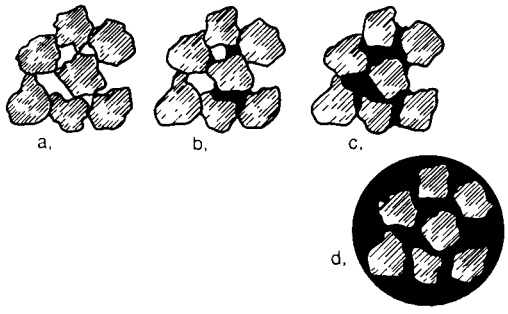

Fig. 19. Oil distribution on moist agglomerates: a. pendular state; b. funicular state; c. capillary state; d. oil droplet with particles inside or at its surface (from Capes [2] with permission).

process of oil agglomeration for such a heterogenous solid as coal. Since the surface of coal is a patchwork assembly [86] which consists of areas of various organic matter, mineral matter and pores, it can display various contact angles with water from zero to over one hundred. The spreading of oil proceeds to the limit of an area in which water is hydrogen-bonded to the particle surface. While hydrocarbon liquid bridges are formed between hydrophobic parts of coal particles, water is attached to the patches on the coal surface at points where exposed mineral matter imbedded in the coal intersects the particle surface, or pore areas filled with water.

In the thermodynamic analysis of the wetting and bridging between individual solid particles by a second liquid phase that preferentially wets the solid particles suspended in liquid 1, Jacques et al. [87] found that formation of the bridges (Figure 20b) is more likely than the formation of films of liquid 2 around particles suspended in liquid 1 (Figure 20a). If so, then water will form similar bridges between hydrophilic spots on coal particles in the agglomerates. This explains why there is always some water in the agglomerates.

According to Keller and Burry [85], the unique trend is observed when bituminous coals are agglomerated with the use of various agglomerants. This is shown in Figure 21, the higher the interfacial tension of the agglomerant with water, the lower the ash content in the product coal. As discussed in the section on "Model Systems", saturated hydrocarbons interact with water only through dispersion forces and their interfacial tensions with water are in the range of 50–52 erg cm^{-2}. Aromatic hydrocarbons interact with water also via pi-bonding and their interfacial tensions with water are 15–16 erg cm^{-2} smaller; hydrocarbon molecules that contain some polar groups and interact with water also through hydrogen bonding are characterized by very small values of interfacial tension. Various types of interactions displayed by aromatic, naphtenic and oxygen-, sulphur- or nitrogen-containing hydrocarbons permit them to adsorb onto various solids. This is consistent with the observations in which heavier fractions from crude oil distillation were

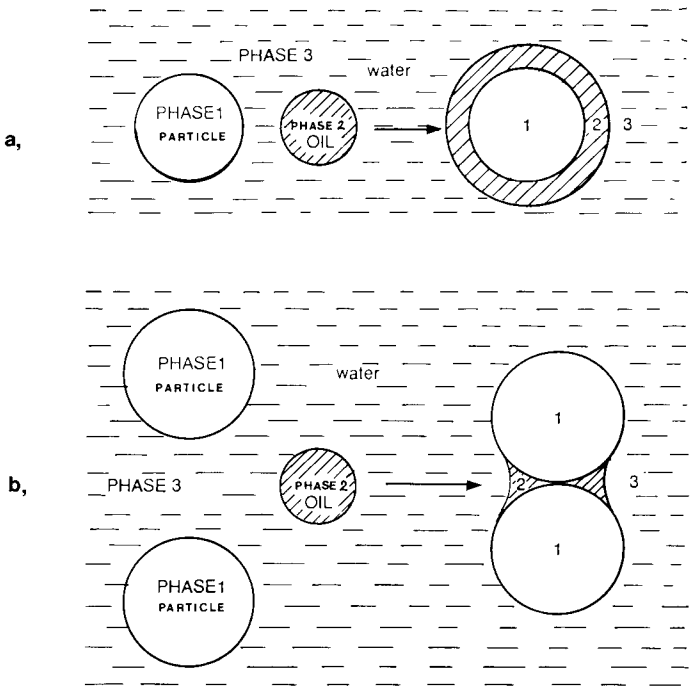

Fig. 20. Schematic model of oil spreading (a) or formation of oil bridges between dispersed in water hydrophobic particles (b) (from Jacques et al. [87] with permission).

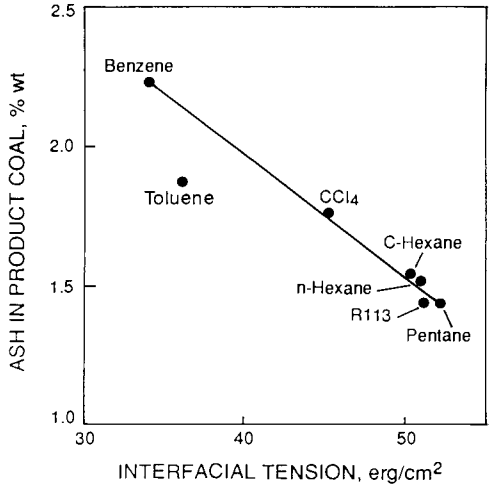

Fig. 21. Variation in product coal ash content after agglomeration with various agglomerants that have different interfacial tension values with water. R-113 is trichloro-trifluoro-ethane. (From Keller and Burry [85] with permission.)

shown to be better collectors in the emulsion flotation of low rank and/or oxidized coals.

Formation of agglomerates requires proper conditioning. Mixing time needed to form adequate agglomerates decreases as agitation is intensified. The importance of agitation time increases as oil density and viscosity increases [5]. Prior emulsification of the oil reduces the energy input [88].

As Capes and Germain [5] pointed out, in fine coal beneficiation, oil characteristics are extremely important for ash rejection. Lower viscosity paraffinic fractions provide cleaner products, but the viscous heavy fractions give larger agglomerates that hold less moisture. These latter products are, however, less selective. Higher ash levels are also characteristic for oils with a higher degree of aromaticity. As it results from what has already been said, the heavier fractions should be better suited for oil agglomeration of lower rank coals. In fact, thermal and subbituminous coals (that is low rank coals characterized by lower hydrophobicity, see figures 27 and 28, Chapter 4) were found to be well agglomerated when the oils containing bitumen or heavy refinery residues were utilized [89]. Perfectly in line with these concepts are Blaschke's results [90]. She has found that while metallurgical coals are well agglomerated by Diesel oil, sub-bituminous coals can be cleaned by oil agglomeration if the oil used contains aromatic hydrocarbons. It is noteworthy that the effect of various oils on emulsion flotation of coals agrees very well with the results on oil agglomeration.

In the model experiments, to study the principle variables that control oil agglomeration process in which fine alumina, sodium dodecyl sulphonate and iso-octane as the bridging liquid were used, the agglomerates were only formed under conditions in which the adsorption of SDS at the alumina/water interface produced contact angles with the bridging liquid of more than 90 degrees [91]. This explains why oil agglomeration is so attractive a technique for fine coal beneficiation.

Liquid–liquid extraction

In the described processes the quantity of oil used is such that no separate oil phase is visible at the end of the separation. In liquid–liquid extraction, also referred to as two-liquid flotation [92], large amounts of aqueous and organic phases are contacted and the particles, depending on their wettability, report either to the aqueous or organic phases. The process is illustrated in Figure 22 which shows that, depending on wettability, the particles are dragged in by capillary forces either in the organic or in aqueous phases (see also [40]).

As in the case of the alumina–water–isooctane system discussed above, fine rutile particles could be extracted into benzene over the small range of collector concentration (sodium tetradecyl sulphate) in the pH range where the collector adsorbs by coulombic attraction and provides an approximately monolayer coverage [92].

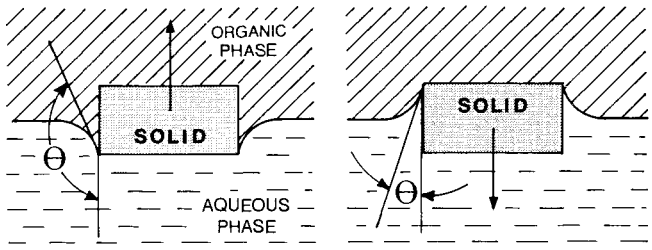

Fig. 22. Schematic model illustrating behaviour of hydrophobic and hydrophilic solid particles at the oil/water interface.

These results agree reasonably well with Zambrana et al. [93] who tested the liquid–liquid extraction method to beneficiate very fine cassiterite. In this early work it was also reported that the extraction of cassiterite into benzene took place only at pH values lower than the p.z.c. of the oxide when an anionic collector (Aerosol-22) was used.

It is worth mentioning that in all the processes discussed in this chapter, oil appears as a separate phase and forms a typical colloidal system when conditioned. Changes of pH and the use of surfactants affect the surface properties of both the solid particles and oil droplets. This facilitates or inhibits interaction between these two. As a result of these interactions, oil droplets may attach to solid particles and thus, depending on the size of the particles and the type of ore, may be utilized in a form of different separation techniques.

Acknowledgements

This chapter was to be written jointly with a very good friend of mine, and one of Dr. Kitchener's previous Ph.D. students, Professor Jorge Rubio, Universidade Federal do Rio Grande do Sul, Porto Alegre, Brazil. Large distances that separate Brazil from Canada made our co-operation so difficult that in a great disappointment to both of us, I have finally written this chapter myself.

Thanks are due to Dr. John Meech for his friendly assistance, and to Mrs. Elizabeth Fedyczkowski and Mrs. Marina Lee for their help in the preparation of figures and typing the text. Also, I wish to thank George Nyamekye, without whose computer touch, this chapter would not have materialized in time.

References

1 N.P. Finkelstein, in: P. Somasundaran and N. Arbiter (Editors), Beneficiation of Mineral Fines, AIME, 1979, pp. 331–340.

2 C.E. Capes, in: M.E. Fayed and L. Otten (Editors), Handbook of Powder Science and Technology, Van Nostrand Reinhold, New York, N.Y., 1982, pp. 230–344.
3 C.E. Capes, Particle Size Enlargement, Elsevier, Amsterdam, 1980.
4 C.E. Capes, in: K.V.S. Sastry and M.C. Fuerstenau (Editors), Challenges in Mineral Processing, Soc. Min. Eng., Littleton, 1989, pp. 237–252.
5 C.E. Capes and R.J. Germain, in: Y.A. Liu (Editor), Fine Coal Beneficiation, Marcel Dekker, New York, N.Y., 1982, pp. 293–351.
6 R.M. Hoover and D. Malhotra, in: M.C. Fuerstenau (Editor), Flotation — A.M. Gaudin Memorial Volume, 1, AIME, New York, N.Y., 1976, pp. 485–505.
7 G.G. Strathdee et al., in: Proc. 14th Int. Min. Process. Congr., Toronto, 1982, Paper V-12.
8 K. Karjalahti, Trans. IMM, Sec.C, 81 (1972): C219.
9 N. Arbiter and E.K.C. Williams, in: P. Somasundaran (Editor), Fine Particles Processing, AIME, New York, N.Y., 1980, Vol. 1, pp. 802–831.
10 J.S. Laskowski and J.D. Miller, in: M.J. Jones and R. Oblatt (Editors), Reagents in the Minerals Industry, IMM, London, 1984, pp. 145–154.
11 J.S. Laskowski, in: Proc. 10th Int. Coal Prep. Congr., Can. Inst. Min. Metall., Edomton, 1986, vol. 1, pp. 122–142.
12 J. Ralston, W. Kent and G. Newcombe, Int. J. Miner. Process., 13 (1984): 167.
13 W. Kent and J. Ralston, Int. J. Miner. Proces., 14 (1985): 217.
14 F.F. Fowkes, Ind. Eng. Chem., 56 (1964): 40.
15 F.F. Foweks, in: S. Ross (Editor), Chemistry and Physics of Interfaces — II, Am. Chem. Soc., Washington, D.C., 1971, pp. 153–168.
16 A.M. James, in: R.J. Good and R.R. Stromberg (Editors), Surface and Colloid Science, Plenum Press, New York, N.Y., 1979, Vol. 11.
17 H.C. Perreira and J.H. Schulman, in: R.F. Gould (Editor), Solid Surfaces Adavances in Chemistry Series, No. 33, Am. Chem. Soc., Washington, D.C., 1961, p. 160.
18 J.S. Laskowski, in: Preprints of Papers, American Chemical Society — Division of Fuel Chemistry, Denver, Colo., Vol. 32, 1 (1987): 367–377.
19 W.W. Wen and S.C. Sun, Sep. Sci., 16 (1981): 1491.
20 H.W. Douglas and D.J. Shaw, Trans. Faraday Soc., 53 (1957): 512.
21 J.M.W. Mackenzie, Trans. AIME, 244 (1969): 393.
22 J. Spurny ands B. Dobias, Collect. Czech. Chem. Commun., 27 (1962): 931.
23 A. Solari, A.C. de Araujo and J.S. Laskowski, Coal Prep., 3 (1986): 15.
24 J.S. Laskowski, J.L. Yordan and R.H. Yoon, Langmuir, 5 (1989): 373.
25 J.S. Laskowski, in: K.V.S. Sastry and M.C. Fuerstenau (Editors), Challenges in Mineral Processing, Soc. Min. Eng., Littleton, Colo., 1989, pp. 15–34.
26 J.S. Laskowski and G.D. Parfitt, in: G.D. Botsaris and Y.M. Glazman (Editors), Interfacial Phenomena in Coal Technology, Marcel Dekker, New York, N.Y., 1989, pp. 279–327.
27 P.J. King, F. Morton and A. Sagarra, in: G.D. Hobson and W. Pohl (Editors), Modern Petroleum Technology, John Wiley, New York, N.Y., 1973, pp. 186–219.
28 V.A. Glembotski, G.M. Dmitrieva and M.M. Sorokin, Nonpolar Flotation Agents (translated from Russian), Israel Program for Scientific Translations, Jerusalem, 1970.
29 R.A. Seitz and S.K. Kawatra, in: D. Malhotra and W.F. Riggs (Editors), Chemical Reagents in the Mineral Processing Industry, Soc. Min. Eng., Littleton, Colo., 1986, pp. 171–179.
30 D.R. Woods and E. Diamadopoulos, in: D.T. Wasan, M.E. Ginn and D.O. Shah (Editors), Surfactants in Chemical Process Engineering, Marcel Dekker, New York, N.Y., 1988, pp. 369–539.
31 P.D. Cratin, in: S. Ross (Editor), Chemistry and Physics of Interfaces — II, Am. Chem. Soc., Washington, D.C., 1971, pp. 35–48.
32 J.M.W. Mackenzie, Trans. AIME, 247 (1970): 202.

33 S.C. Sun, L.Y. Tu and E. Ackerman, Min. Eng., 7 (1955): 656.
34 V.I. Klassen and I.N. Plaksin, Izv. Akad. Nauk SSSR, Otd. Tekh. Nauk, 3 (1954): 62.
35 A.A. Baitsenko, V.I. Melik-Gaykazian and G.G. Livsits, Ugol, No. 11, 1956.
36 C.N. Bensley, A.R. Swanson and S.K. Nicol, Int. J. Miner. Process., 4 (1977): 173.
37 V.I. Tyurnikova and M.E. Naumov, Improving the Effectiveness of Flotation, Technocopy Ltd., Stonehouse, 1981.
38 A.B. Taubman and L.P. Janova, Russ. Colloid J., 24 (1962): 185.
39 A.R. Burkin and S.B. Soane, in: Proc. 3rd Congr. Surface Activity, Cologne, 1960, Vol. 4, p. 430.
40 J.W. Schulman and J. Leja, Trans. Faraday Soc., 50 (1954): 598.
41 B. Dobias, in: J.F. Scamehorn (Editor), Phenomena in Mixed Surfactant Systems, ACS Symp. Series 311, Am. Chem. Soc., Washington D.C., 1986, pp. 216–224.
42 A.R. Burkin and J.V. Bramley, J. Appl. Chem., 11 (1961): 300.
43 A.R. Burkin and J.V. Bramley, J. Appl. Chem., 13 (1963): 417.
44 V.I. Melik-Gaykazian, I.N. Plaksin and V.V. Voronchikhina, Dokl. Akad. Nauk SSSR, 173 (1967): 883.
45 N.Z. Frangiskos, C.C. Harris and A. Jowett, Proc. 3rd Int. Congr. Surface Active Substances, Köln, 1960.
46 D.W. Fuerstenau and Pradip, Colloids Surf., 4 (1982): 229.
47 J.D. Miller, C.L. Lin and S.S. Chang, Colloids Surf., 7 (1983): 351.
48 Zhenghe Xu and R.H. Yoon, J. Colloid Interface Sci. 132 (1989): 15.
49 D.J. Brown, V.R. Gray and A.W. Jackson, J. Appl. Chem., 8 (1958): 752.
50 V.I. Klassen, Coal Flotation, Gosgortiekhizdat, Moscow 1963.
51 Yingbin He and J.S. Laskowski, Contact Angle Measurements on Discs Compressed from Fine Coal, Powder Technology (submitted).
52 A. Zettlemoyer, M.P. Aronson ands J.A. Kavalle, J. Colloid Interface Sci., 34 (1970): 545.
53 V.I. Klassen and S.I. Krokhin, in: A. Roberts (Editor), Mineral Processing, Proc. 6th Int. Min. Process. Congr., Pergamon Press, Oxford, 1965, pp. 397–406.
54 V.I. Klassen, in: I.N. Plaksin (Editor), Physicochemical Bases of the Action of Nonpolar Collectors in Flotation of Ores and Coal, Izdat. Nauka, Moscow, 1965, pp. 3–11 (in Russian).
55 V.I. Melik-Gaykazian, in: I.N. Plaksin (Editor), Physicochemical Bases of the Action of Nonpolar Collectors in Flotation of Ores and Coal, Izdat. Nauka, Moscos, 1965, pp. 22–49 (in Russian).
56 F.J. Smit and A.K. Bhasis, Int. J. Miner. Process., 15 (1985): 19.
57 N.S. Vlasova, V.I. Klassen and I.N. Plaksin, Investigation Into the Action of Reagents in Flotation of Coals. Izdat. Akad. Nauk USSR, Moscow, 1962 (in Russian).
58 V.A. Glembotski, G.M. Dmitrieva and M.M. Sorokin, Nonpolar Flotation Agents (translated from Russian), Israel Program for Scientific Translations, Jerusalem, 1970
59 N.T. Moxon, C.N. Bensley, R. Keast-Jones and S.K. Nicol, Int. J. Miner. Process., 21 (1987): 261.
60 J.H. Bitter, Conditioning of the Pulp and Its Influence Upon the Results of Flotation. 6th Int. Coal Prep. Cong., Pittsburgh, Pa., 1966, Paper A3.
61 I.N. Plaksin and V.I. Klassen, Scientific and Technical Progress in Coal Flotation. 6th Int. Coal Prep. Congr., Pittsburgh, Pa., 1966, Paper A4.
62 K.H. Nimerick, Characetrization of Coals Responding to Froth Conditioning. SME-AIME Fall Meeting, Honolulu, Sept. 1982, Preprint 82-377.
63 A. Watanabe, in: E. Matijevic (Editor), Surface and Colloid Science, Plenum Press, 1984, Vol 13, p. 32.
64 P. Carbini, R. Ciccu, M. Ghiani and F. Satta, in: Proc. 11th Int. Coal Prep. Congr., Mining and Materials Processing Institute of Japan, Tokyo, 1990, pp. 293–298.
65 J.S. Laskowski, Coal Flotation Promoters and Their Mechanism of Action, 191st Am. Chem. Soc. Meet., New York, N.Y., April 1986.

66 Y. Ogura, Y. Mizuno, N. Ueshima and A. Naka, in: 6th Int. Symp. Coal Slurry Combustion and Technology, Orlando, Fla., 1984, pp. 621–638.
67 K. Wong and J.S. Laskowski, Colloids Surf., 12 (1984): 239.
68 J.S. Laskowski, L.L. Sirois and K.S. Moon, Coal Prep., 3 (1986): 133.
69 Q. Liu and J.S. Laskowski, Effect of Humic Acids on Coal Flotation, Part II, The Role of pH. SME Annu. Meet., Phoenix, January, 1988.
70 R.O. Keys, Improvement in Coal Recovery Through Coarse Coal Flotation. 1st Annu. Coal Prep. Conf., Lexington, Ky., March 1984.
71 B.A. Firths, A.R. Swanson and S.K. Nicol, Int. J. Miner. Process., 5 (1979): 321.
72 N.T. Moxon and R. Keast-Jones, Int. J. Miner. Process. 18 (1986): 21.
73 Polish Patent, No. 104,569 (1977).
74 J. Sablik, Int. J. Miner. Process., 9 (1982): 245.
75 J. Sablik, Physicochemical Problems of Mineral Processing, No. 21 (1989): 171 (in Polish).
76 R.E. Boarson, C.L. Ray and H.B. Treweek, in: D.W. Fuerstenau (Editor), Froth Flotation, AIME, New York, N.Y., 1962, pp. 427–453.
77 G. Rinelli and A.M. Marabini, in: M.J. Jones (Editor), Proc. 10th Int. Miner. Process. Congr., Inst. Min. Metall., London, 1974, pp. 493–521.
78 J.E. Rosas and G.W. Poling, in: Proc. 11th Int. Miner. Process. Congr., Universita di Cagliari, Cagliari, 1975, pp. 73–98.
79 P.G. Kihlsteadt, in: Progress in Mineral Processing, Proc. 4th Int. Miner. Process. Congr., Stockholm 1957, Almqvist and Wiksell, Stockholm, 1958, pp. 559–576.
80 U. Runolinna, R. Rinne and S. Kurronen, in: Int. Miner. Process. Congr., Inst. Min. Metall., 1960, pp. 447–475.
81 M. Lapidot and O. Mellgren, Trans. IMM, Sec. C. 77 (1968): 149.
82 A.M. Al-Taweel and V.K. Kasireddy, in: S. Chander and R.R. Klimpel (Editors), Advances in Coal and Mineral Processing Using Flotation, Soc. Min. Metal Explor., Littleton, Colo., 1989, pp. 356–366.
83 T. Hirajima, T. Takamori, M. Tsunekava, N. Wang and H. Tomita, in: Proc. 11th Int. Coal Prep. Congr., Mining and Materials Processing Institute of Japan, Tokyo, 1990, pp. 361–366.
84 C.E. Capes, J.D. Hazlett and B.L. Ignasiak, in: Proc. 11th Int. Coal Prep. Congr., Mining and Materials Processing Institute of Japan, Tokyo, 1990, pp. 355–360.
85 D.V. Keller and W. Burry, Colloids Surf., 22 (1987): 37.
86 D.V. Keller, Colloids Surf., 22 (1987): 21.
87 M.T. Jacques, A.D. Hovarongkura and J.D. Henry, AIChE J., 25 (1979): 160.
88 C.N. Bensley, A.R. Swanson and S.K. Nicol, Int. J. Miner. Process., 4 (1977): 173.
89 W. Pawlak, A. Turak and B. Ignasiak, in: C.E. Capes (Editor), Proc. 4th Int. Symp. on Agglomeration, AIME Iron and Steel Society, Toronto, 1985, pp. 907–916.
90 Z. Blaschke, in: Proc. 11th Int. Coal Prep. Congr., Mining and Materials Processing Institute of Japan, Tokyo, 1990, pp. 257–260.
91 C.B. Kavouridis, H.L. Shergold and P. Ayers, Trans. IMM, Sec. C. 90 (1981): 53.
92 R. Stratton-Crawley, in: P. Somasundaran and N. Arbiter (Editors), Beneficiation of Mineral Fines, AIME, 1979, pp. 317–330.
93 G. Zambrana, R. Medina, G. Gutierrez and R. Vargas, Int. J. Miner. Process., 1 (1974): 335.

Chapter 13

Fundamental aspects of microbubble flotation processes

JAIME A. SOLARI and RODNEY J. GOCHIN

Introduction

Flotation is a process in which a buoyant phase is used to remove particulates dispersed in a solution. Air bubbles are the most commonly used buoyant phase but also oil emulsions and more recently plastic spheres [1], have been used as floating carriers for the dispersed phase. Flotation of the suspended phase may be total, as in solid/liquid separation applications, or partial, as in the froth flotation process where certain minerals are selectively separated from others by air bubbles. With regard to the solids that may be removed by flotation, they can be as varied as metal hydroxide precipitates, wastes of various kind, biological materials, minerals and fossil fuels.

As in many other cases, industrial applications of flotation moved much faster that scientific understanding of the phenomena involved. However, it was soon recognized that the size of the bubbles had an influence on the efficiency of the flotation process [2, 3]. Also, it became apparent that bubble size was dependent on the method used for bubble generation and thus, certain flotation machines were developed for specific applications. While now it is widely accepted that a bubble diameter (d_b) of around 1 mm is optimum for conventional and column flotation of minerals, the main use of microbubbles has been in applications of flotation to solid/liquid separation. In this area, the most important industrial microbubble flotation processes are electroflotation and dissolved air flotation (also referred to as "pressure flotation" or "pressure release flotation" by some authors). For the purpose of this review, microbubbles are defined as bubbles having mean d_b below 100 μm. Bubble size distributions are quoted as mean $d_b \pm$ the standard deviation.

Generation and properties of microbubbles

Microbubble generation

Microbubbles can be generated by several mechanisms, namely, electrochemically, liquid cavitation induced by pressure reduction or high shear rates, and by gas injection through porous devices. Typical size distribution of bubbles generated by various systems are presented in Figure 1.

The method of producing microbubbles by passing gas under pressure through sintered glass discs of adequate porosity has been used mostly for flotation studies at the laboratory scale. Ahmed and Jameson [4] reported that a sintered disc of pore size 5–15 μm (British standard 1752) produced a bubble size distribution of 74.7 $\pm$ 21 μm. This method of bubble generation requires the addition of surface-active agents in order to obtain microbubbles and has been used to float metal precipitates [5–7] and to study the flotation mechanism of fine particles by small bubbles [8, 9].

In the dissolved air flotation (DAF) process, microbubbles are generated by cavitation using an aqueous solution which has been saturated with air at high pressure (300–500 kPa). This solution is forced through a constriction (usually a orifice plate, a nozzle or a needle valve) where pressure reduction occurs, the solution becomes supersaturated and air precipitates out of solution as microbubbles with mean d_b in the range 50–80 μm. Detailed studies on the formation of microbubbles in DAF systems were carried out at Imperial College, London, in the

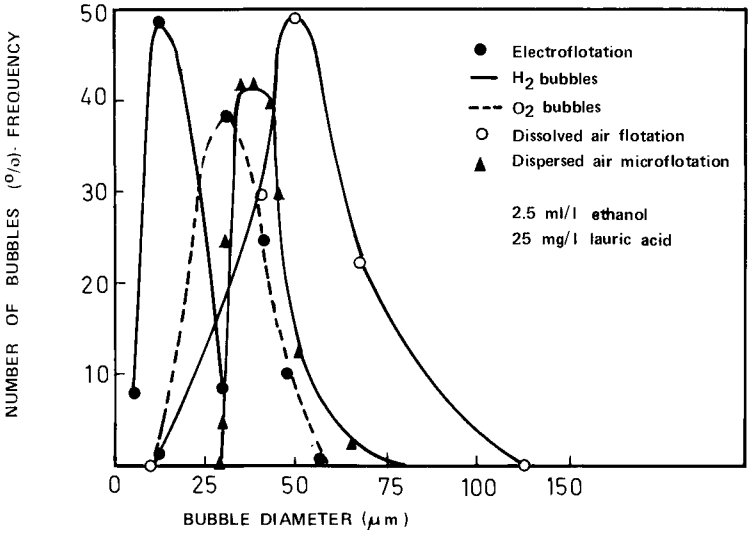

Fig. 1. Size distribution of bubbles generated by various systems (●: from Glembotsky et al. [24]; ○: from Neis and Kiefhaber [13]; ▲: from Cassell et al. [6]; with permission).

late 1970's under the leadership of J.A. Kitchener [10–12]. From this and other work [13, 14], it is known that the size of the bubbles generated in DAF is a function of air saturation pressure, pressure reduction at the constriction, nozzle design and inlet water injection pressure. Also, the performance of the saturator device influences bubble size distribution through its effect on the efficiency of air saturation in water [15].

Another way of generating microbubbles through liquid cavitation has been proposed by Sebba [16]. In this method, a fast moving (10 l min^{-1}) stream of liquid is forced through a venturi to which air is injected at the point of lowest pressure. By repeated cavitation and recirculation of a solution containing about 0.01 M of a surfactant, a "microfoam" consisting of microbubbles of average d_b = 25 μm was obtained [17]. Shea and Barnett [18] used this cavitation technique to generate "microgas dispersions" whose surface area to bulk volume ratios were as large as 5000 cm^2 cm^{-3}. In a later publication [19], the microfoam is described as "colloidal gas aphrons" (CGA). The term *aphron* was applied to a spherical phase which is encapsulated in a shell of a thin soapy film. However, all microbubbles generated by cavitation of surfactant solutions will be referred to as microgas dispersions (MGD) in this work.

Research on the application of microbubble generation to a mineral flotation machine was continued over the past decade by workers at Virginia State University and has been recently summarized [20]. These researchers have designed various microbubble generators based on the cavitation principle but which allow the direct use of mineral slurries in the cavitation device. This has the advantage that no extra water needs to be added to the flotation reactor in order to generate bubbles and therefore, water consumption is reduced and the reactor capacity is maximized.

MGDs may also be generated by a spinning disc that entrains air into a surfactant solution when the stirring rate is above a critical value (>4000 r.p.m., for the conditions described by Sebba in [21]). Szatkowski and Freyberger [22] used a disc rotating at high speed in a small chamber to obtain microbubbles of size distribution 55 $\pm$ 25 μm (8000 r.p.m.) and 75 $\pm$ 35 μm (5000 r.p.m.). Yoon et al [20] described a system which uses an in-line static mixer in conjunction with a centrifugal pump to generate microbubbles. A slurry containing frother is pumped at high speed through the mixer while a controlled amount of air is injected into the line in order to stabilize the microbubbles.

The basis of the electrochemical method of microbubble generation is the electrolysis of dilute aqueous, conducting solutions with production of gas bubbles at both electrodes. The main parameters that control the size and number of electrogenerated micobubbles are current density, pH and electrode material. Mean values for d_b are in the range 20–70 μm but the bubble size distributions generated by electroflotation systems are usually much narrower than in DAF machines (see Figure 1). The growth kinetics of electrogenerated bubbles has been studied by Brandon and Kelsall [23]. These authors reported that the departure diameter

of bubbles generated at microelectrodes is a function of pH in surfactant-free solutions. Hence, hydrogen bubbles were much larger at low pH than at alkaline pH values whereas the opposite behaviour occurred for oxygen and chlorine bubbles. In the presence of surfactant, the influence of pH on the departure diameter of bubbles decreased for both oxygen and hydrogen bubbles. Similar findings have been reported by Glembotsky et al. [24] in a review article which summarized Russian research on electroflotation until the mid 70's.

Among other processes for microbubble or small bubble generation, the bubbler produced by the U.S. Bureau of Mines for column flotation systems is reported to give bubbles as small as 200 μm [25]. Also, Soviet researchers [26] claim that "activated aqueous dispersions of air" increase flotation efficiency. The description of their system is unclear but resembles Sebba's CGA; however, no bubble size distribution was reported in their work. Although some authors mention that vacuum flotation may produce fine bubbles, research on gas nucleation from supersaturated solutions suggests that the equilibrium mean size of these bubbles is larger than 100 μm [10, 11]. Also, some authors [10, 27] have attempted to use gases other than air for microbubble production in dissolved air flotation due to their greater solubility in water. The use of CO_2 did not result in better efficiencies than air and this was attributed to the much larger bubbles that are produced when using this gas, alone or mixed with nitrogen [27].

Interfacial properties of microbubbles

The interfacial properties of microbubbles that are of interest in flotation are the distribution of surface-active agents on the bubble surface and the charge density and electrical potential at the bubble/solution interface as these properties have been shown to affect the mechanism of attachment of bubbles to surfaces.

Experimental results on the motion of bubbles in fluids have shown that below a critical size (around 0.5 mm), bubbles behave as solid spheres. This behaviour has been explained in terms of contamination of the gas/solution interface by adsorbed surface-active agents which retard interfacial motion. Surfactants have a large effect on bubble rise rate and various authors have used this variable as a measure of the cleanliness of a solution. Hence, Figure 2 shows results given by Brandon [28] on the effect of bulk surfactant concentration on the rise rate of a bubble. The rise rate (v) of a single microbubble ($Re < 1, d_b < 100\ \mu$m) in surfactant-free water is given by [29]:

$$v = \tfrac{1}{3}\left[\frac{r^2 g(d - d')}{u}\right] \tag{1}$$

where d is the density of the liquid of viscosity u and d' is the density of a gas bubble of radius r. In the case that an adsorbed layer of surfactant restrains bubble motion, the coefficient (2/9) should replace (1/3) in equation (1) [30].

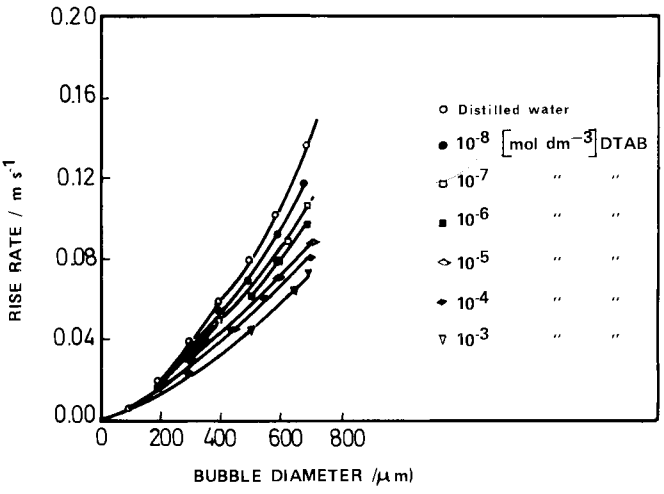

Fig. 2. Influence of the bulk surfactant concentration dodecyl trimethyl ammonium bromide (DTAB) on bubble rise rate (from Brandon [28] with permission).

It is known, however, that the presence of other bubbles may affect the absolute value of v and in the case of real flotation systems the rise rate of bubble swarms (V) has to be considered. Rulev et al. [30] proposed that V depends on the volumetric fraction of dispersed gas (Φ) in the system, and therefore:

$$V = vf(\Phi) \tag{2}$$

The function $f(\Phi)$ has been calculated by these workers and it is presented graphically in Figure 3. It may be observed that for a value of the volumetric fraction of dispersed air of 5%, the rise rate of the swarm is half of that of a single bubble. Also, the correlation proposed by Concha and Almendra [31] for the settling of

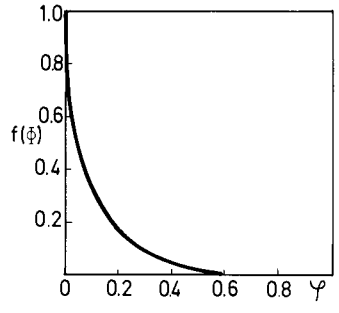

Fig. 3. Effect of volumetric fraction of air on $f(\Phi)$, the factor relating the rise rate of a bubble swarm to that of a single bubble [see equation (2)].

particulate systems has been used to predict the rising velocity of bubble swarms in flotation columns [32].

Brandon [28] and Laskowski et al. [33] have reviewed work carried out to determine the charge density and electric potential at gas–liquid interfaces. The techniques used have involved the measurement of bubble migration velocities under an applied field in horizontal rotating cylinders [34–35] or of rising bubbles in a horizontal electric field [33, 36–39], while other workers have measured the Dorn potential of rising bubble swarms [40–41]. These workers generally report significantly negative electrophoretic mobilities at neutral pH.

Brandon et al. [42] have done detailed electrophoresis measurements on electrogenerated bubbles of hydrogen, oxygen and chlorine rising in a lateral field. In surfactant-free electrolytes, all bubbles showed an isoelectric point in the pH range 2–3. Also, the results indicated that the gas–aqueous solution interface was mobile so that classical electrophoresis theory of solid particles could not be applied. This was evident from the linear dependence of bubble electrophoretic mobility on bubble diameter over the pH range 4–10 in surfactant-free sodium sulphate as shown in Figure 4. Charge separation was attributed to either the hydrodynamic flow produced by the rising bubble, or to the polarization of the surface charge by the horizontal electric field. However, the presence of surfactants modified the apparent bubble charge and led to increased rigidity of the bubble surface so that at monolayer coverage the microbubbles behaved as solid particles.

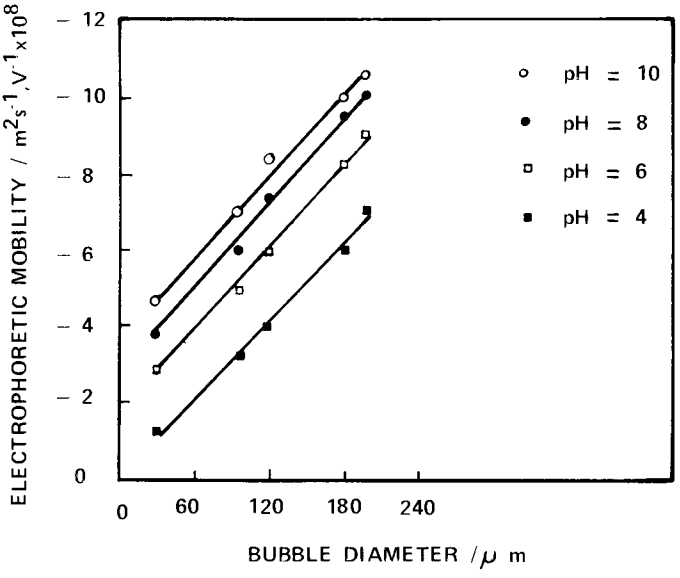

Fig. 4. The influence of bubble diameter on the electrophoretic mobility of bubbles in milli-molar sodium sulphate (from Brandon [28] with permission).

In the presence of ionic surfactants, microbubbles exhibit an electrokinetic potential of the same sign as the charge of the polar group of the reagent, i.e. it is positive in solutions of cationic surfactants and negative in solutions of anionic surfactants. However, some researchers observed that the bubbles in an aqueous solution of dodecylamine (a cationic surfactant) could exhibit a negative electrokinetic potential [39, 43]. This behaviour was investigated by Laskowski and co-workers [33] who showed that in the presence of a weak-type electrolyte surfactant, the sign of the electrokinetic potential of the microbubbles was pH dependent. These workers demonstrated that the isoelectric point of the bubbles correlated well with those of the colloidal precipitate present in the solution when the solubility limit of a free amine, or acid, was exceeded. Thus, for example, the negative sign of the electrokinetic potential of microbubbles measured in alkaline solutions of dodecylamine can be explained in terms of the "armoring" of the bubbles by a colloidal precipitate.

Summarizing, microbubbles may be considered as rigid spheres for hydrodynamic considerations even in the absence of surface-active agents but the gas/liquid interface appears to be mobile. Under these conditions, the microbubbles carry a negative charge and an electrical potential which is pH and size dependent. The precise origin of the unequal charge distribution at the gas/liquid interface is not completely understood. Additions of oppositely charged surface-active agents reverse the electrokinetic potential of the bubbles at a concentration dependent on the bubble surface potential whereas surfactants of like-charge adsorb specifically increasing the electrokinetic potential at the gas/liquid interface. In the presence of ionic surfactants, microbubbles exhibit an electrokinetic potential of the same sign as the charge of the polar group of the surfactant. However, in the presence of weak-type surfactant electrolytes, the electrokinetic potential of microbubbles is pH dependent due to adhesion of colloidal precipitates at the gas/liquid interface.

The theoretical effect of bubble size on the mechanism of flotation

Bubble–particle attachment in flotation

After the pioneering work of Sutherland [44], many authors have studied the various stages involved in the elementary process of flotation with the aim of constructing a unified picture of the bubble–particle attachment process. The reviews of Kitchener [45], Derjaguin and co-workers [46–48], Schulze [49], Hornsby and Leja [50], Ralston [51], Jameson et al. [52], Trahar and Warren [53] and of Yoon and Luttrell [54], provide an excellent background for this discussion on the specific characteristics introduced by the size of the bubbles on the flotation mechanism.

The attachment of a particle to a gas bubble in a flotation system is usually described as the result of a series of consecutive stages, each of which is determined by different properties of the system. Hence, it is generally accepted that for a

particle to be collected and floated by a bubble there must be: (1) a collision between them, (2) an adhesion step where particle and bubble form an aggregate, and (3) the bubble–particle aggregate must be stable enough to resist the action of detachment forces. If probabilities are ascribed to each of these stages, the probability that flotation (P_f) occurs is:

$$P_f = P_c P_a P_d \tag{3}$$

where P_c, P_a and P_d are the probabilities of collision, adhesion and that detachment does not occur, respectively. This review will be mainly concerned with the collision and adhesion stages of flotation as the probability of particle detachment from small bubbles is considered to be very low in flotation systems [49].

As it is difficult sometimes to separate experimentally the collision and adhesion steps, the term "collection" has been used to describe the joint result of these two stages. Also, some authors have employed the term "efficiency" to calculate the value of the above mentioned probabilities. Therefore, the efficiency of collection (E) has been defined as:

$$E = P_c P_a = E_c E_a \tag{4}$$

Some authors [55–57] have arrived at experimental values of E by measuring the absolute rate of capture of hydrophobic particles, i.e. by assuming that the probability of adhesion, for very hydrophobic particles is equal to unity.

Also, assuming that flotation is a first-order kinetics process, Jameson et al. [52] have shown that the flotation rate constant (k) is directly proportional to the collection efficiency and therefore, that the conclusions obtained from a study of E can be related to the rate and recovery of flotation. These authors proposed that:

$$k = 1.5 Q E \frac{h}{d_b} V_c \tag{5}$$

where Q is the gas volumetric flowrate, and h and V_c are the depth and effective cell volume, respectively. Hence, for a given air input and constant particle size, a decrease in bubble diameter leads to a larger number of bubbles with a slower rise velocity and therefore the residence time and flotation rate should increase.

Particle collection by microbubbles

It is customary to begin considering the collision step as the approach of a particle and a bubble of diameters d_p and d_b, respectively, and then to calculate the critical streamline that allows the particle to make grazing contact with the bubble surface. The bubble–particle collision is therefore assumed to be basically determined by the hydrodynamic flow around the bubble which is a function of the particle and bubble sizes. Recent reviews of the hydrodynamics involved in the collision stage have been presented by Schulze [49, 58], Derjaguin and Dukhin [47]

and Yoon and Luttrell [54]. Also, Weber and Paddock [59] proposed an expression for P_c that applies within a wide range of bubble and particle sizes.

Anfruns and Kitchener [55, 56] and Yoon and Luttrell [57] have studied bubble–particle collection experimentally in the case of potential flow and intermediate Reynolds numbers ($1 < Re < 40$) whereas Flint and Howarth [60], Reay and Ratcliff [8, 61], Collins and Jameson [9] and Ahmed and Jameson [4] have carried out studies in the Stokes flow regime ($Re \ll 1$). These authors reported that the probability of collision (P_c) of particles with microbubbles is inversely proportional to the square of the bubble size. Hence:

$$P_c = B\left(\frac{d_p^N}{d_b^2}\right) \tag{6}$$

where B is a constant and N has been found to vary between 1.3 and 1.8 depending on whether the experiments were performed under quiescent or turbulent conditions [4, 9]. If equation (6) is combined with (5), the effect of bubble size on the flotation rate constant in the Stokes regime is obtained. Thus:

$$k \propto d_b^{-3} \tag{7}$$

which indicates that smaller bubbles increase the rate of collision and therefore, that the probability of flotation of fine particles is higher when using microbubbles.

Once particle–bubble collision occurs, the particle slides over the bubble surface for a period of time and it is during this "sliding time" that bubble–particle adhesion proceeds. The adhesion step consists of the thinning and rupture of the wetting film on the solid surface followed by the establishment of a three-phase contact angle. The minimum time required to thin and rupture the wetting film is known as the "induction time". Film collapse occurs at a critical thickness h_c. From this picture of the adhesion stage it is clear that there are two basic prerequisites for flotation, namely, that the induction time be shorter than the sliding time and secondly, that the wetting film be capable of spontaneous rupture. This allows a distinction between kinetic and thermodynamic conditions for bubble–particle adhesion to occur [62].

Following Sutherland [44], the probability of adhesion has been formulated by Dobby and Finch [32] as the fraction of particles in the path of the bubble that remain adhered after collision. These particles are those whose sliding time (t_s) is larger than their induction time (t_i). For a given bubble and particle sizes, the sliding time may be calculated from the distance travelled on the bubble surface and the particle sliding velocity. A limiting angle (θ_o) is defined as the angle of incidence of particles whose $t_s = t_i$. Thus, only those particles which strike the bubble at an angle of incidence (θ_i) smaller than (θ_o) will have $t_s > t_i$ and will remain attached. Calculations of the sliding time using this model were compared with the experimental results of Schulze and Gottschalk [63] and gave a reasonable

fit. Yoon and Luttrell [54] have developed this model further and calculated the probability of adhesion in the Stokes flow regime as:

$$P_a = \sin^2 \left\{ 2 \arctan \exp \left[\frac{-1.5 v t_i}{d_b (d_b/d_p + 1)} \right] \right\} \tag{8}$$

The effect of bubble size on the probability of adhesion may be deduced from equation (8) which has been plotted in Figures 5 and 6 as a function of induction time and particle size. The value of v in equation (8) was taken from (1) considering restrained bubble motion.

Figure 5 shows that for constant hydrophobicity, an increase in particle size decreases the probability of attachment and this effect is more pronounced for the larger microbubbles. Furthermore, for particles below 10 μm, P_a assumes values >0.95 and is practically independent of bubble size. On the other hand, Figure 6 indicates that as the particles become more hydrophilic, i.e. their induction time increases, their probability of attachment decreases and this effect is again more significant as bubble size increases. This trend indicates that selectivity is enhanced as bubble size increases above a critical value and this effect should be more relevant in the flotation of ultrafine particles.

With regard to Figure 5, it should be noted that a 50 μm particle may attach to a 10 μm bubble with high probability but this does not necessarily mean that flotation will occur as the aggregate will not levitate. Therefore, the trends presented should be viewed with caution when considering the probability of flotation of particles larger than the bubbles.

It is important to point out that in this model of the adhesion process it is implicit that the time necessary for the film to spontaneously rupture at the critical thickness h_c is much less than the time required for the film to thin to h_c. Thus, it is assumed

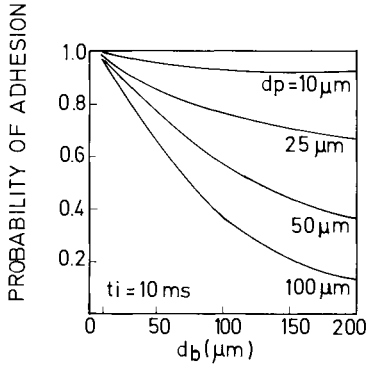

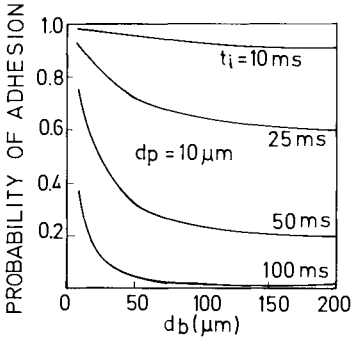

Fig. 5 (left). Effect of bubble diameter on probability of adhesion (P_a) at various particle sizes

Fig. 6 (right). Effect of bubble diameter on probability of adhesion (P_a) at various induction times

that the induction time is basically a function of the time required for film thining and drainage and therefore, it is controlled by the hydrodynamics of the system. Thermodynamics would only determine the value of h_c [57]. The model has not been validated for microbubbles, but it has been shown that for bubbles in the intermediate Reynolds numbers, P_a calculated from induction time measurements follows qualitatively the same trend than flotation recovery [64].

Another approach has been taken by Derjaguin, Dukhin and Rulyov [47, 48]. These authors have simultaneously considered the hydrodynamic interaction between a small particle and a bubble and the action of surface forces in the thinning of the wetting film. They pointed out that the hydrodynamic drag (the short-range hydrodynamic interaction) that presses the particle against the bubble is unable to collapse the film because the resistance increases indefinitely as the wetting film grows thinner and therefore, surface forces or rather, the "disjoining pressure" of the thin film has to be considered in the particle–bubble adhesion step. Two cases were distinguished; attachment with rupture of the wetting film and establishment of a contact angle as the particle attained a critical distance h_c from the bubble, and attachment due to heterocoagulation of bubble and particle through a wetting film, e.g. there is no critical distance for the wetting film to collapse and no three-phase contact angle is formed. This latter mechanism of capture has been named "contactless flotation".

Firstly, they considered the case in which long-range molecular forces are neglected and where h_c has a finite value, e.g. the surface is hydrophobic and electrostatic repulsion is supressed due to high electrolyte concentration. The results of modelling the effect of h_c on E indicated that, under those conditions, the influence was very weak [48], thus corroborating the assumption of Yoon and Luttrell [57] that induction time is determined by the hydrodynamics of film drainage rather than by film rupture. By a similar argument, Rulev [65] derived the following expression by considering the combined effect of hydrodynamic and molecular forces in the case of the Stokes regime:

$$E = 0.11 A^{1/6} \left(\frac{d_p^{1.4}}{d_b^2} \right) \tag{9}$$

This relationship is very similar to equation (6) and shows that the absolute value of the collection efficiency is only weakly dependent on the Hamaker constant A. Nevertheless, it also indicates that particle capture can only occur when $A > 0$, which means that molecular forces essentially decide through their sign whether flotation will proceed or not.

However, the experiments of Collins and Jameson [36] and of Anfruns and Kitchener [55] showed that electrostatic interactions through overlapping of diffuse double layers between microbubbles and particles affected the rate of flotation and therefore particle collection. This has been interpreted as an influence of surface

forces on particle trajectory by Ralston [51], but it also may be viewed as the effect of thick wetting films stabilized on hydrophobic surfaces by long-range electrostatic forces. The experiments of Laskowski and Kitchener [66] and of Blake and Kitchener [67] showed that a hydrophobized surface (methylated silica) retains its negative electrokinetic potential and stabilizes wetting films which resist rupture unless electrolytes are added to weaken the electrical double-layer forces. These results indicated that the mere existence of a hydrophobic surface may not necessarily result in particle collection by a bubble as other surface forces may prevent film thinning. In these cases, the time taken to collapse the film at h_c is rate-limiting and induction time is no longer determined by the hydrodynamic conditions. There is a good deal of experimental data in the literature showing that the flotation rate is maximum at the isoelectric point of the solids [48, 52].

The second possibility of particle–bubble adhesion proposed by Derjaguin and co-workers is contactless flotation. These authors suggested that for very fine particles the detachment forces are very small and therefore the absence of a wetting perimeter may be balanced by attractive surface forces between bubble and particle

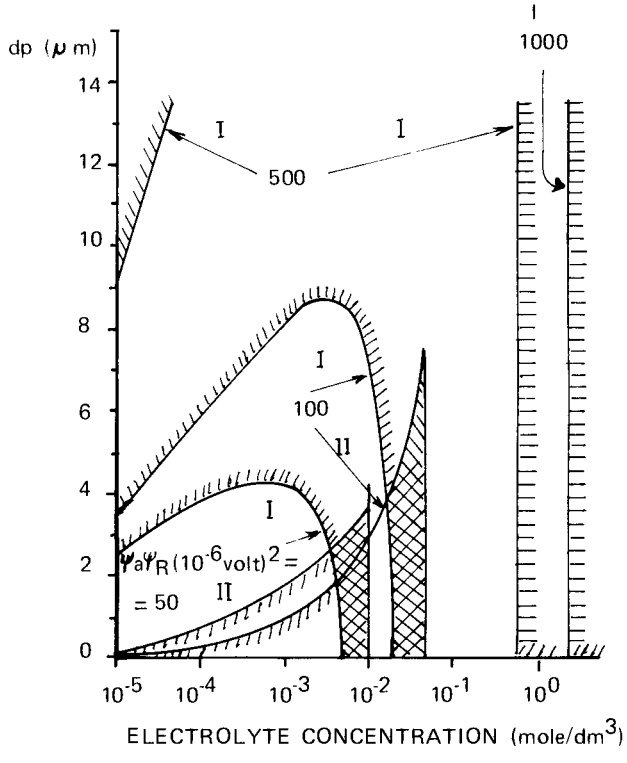

Fig. 7. Regions of floatability in the case of Stokes flow (shaded). *I* = the lower boundary of flotation in the primary minimum; *II* = the upper boundary of flotation in the secondary minimum (from Derjaguin and Dukhin [47] with permission).

[48]. The argument goes that under certain conditions the hydrodynamic drag may exceed the energy barrier imposed by the disjoining pressure of the wetting film and flotation may occur in the primary minimum. Also, provided that the bubbles and particles are small enough, flotation also occurs as the result of heterocoagulation in the secondary minimum. Using DLVO heterocoagulation theory [48, 49], the floatability limits of fine particles by microbubbles of like charge in the primary and secondary minimum may be calculated. The results of these calculations are presented in Figure 7 for the Stokes flow regime as a function of the Stern potentials of the bubble and the particle and of the electrolyte concentration.

Kitchener [45] considered this proposition to be hypothetical as no examples of contactless flotation had been reported. He also viewed with skepticism the possibility of flotation proceeding as a case of heterocoagulation theory, i.e. flotation due to electrostatic attraction between oppositely charged particles and bubbles. According to Figure 7, a qualitative analysis would indicate that the flotation of 10 um quartz particles by microbubbles should be possible in the pH range 2–3 considering that at this pH both quartz and microbubbles have a very low (if any) electrokinetic potential. Solari [11] found absence of floatability of fine quartz particles by microbubbles generated by dissolved air flotation techniques at pH 2.4, with and without frother. However, Drzymala and Lekki [68] have recently claimed contactless flotation of quartz and magnetite particles in a modified Hallimond tube in the presence of 20% ethanol. It is unfortunate that there is no chance of correlating the results obtained by these workers with the calculations of Derjaguin et al. [48] for contactless flotation in the potential regime as the studies were carried out in turbulent flow (d_b = 5 mm). The possibility of "floating" particles by the wake volume of rising bubbles has been pointed out by Yoon [69] and this effect would increase with bubble size.

Experimental studies on flotation by microbubbles

It appears from the discussion on the mechanism of bubble–particle attachment in flotation that there are several advantages in reducing the size of the bubbles. For a constant particle size, the use of smaller bubbles would increase the probability of collision, the probability of adhesion and also the rate of flotation, as k is inversely proportional to the cube of the bubble size [equation (7)]. On the other hand, from a theoretical point of view, given the right conditions, microbubbles would be able to capture particles through a heterocoagulation mechanism, i.e. without the need to establish a contact angle. With this theoretical background in mind, various researchers set out to investigate microbubble flotation applied to the recovery of fine mineral particles using some of the methods of microbubble generation described previously. As it will be shown in this section, the experimental results confirmed the theoretical predictions about the effect of bubble size on flotation

but also showed that there were some constraints to the possible applications of microbubble flotation.

The flotation of hydrophilic metal hydroxides would be the most obvious case of contactless flotation with microbubbles. Reviews [70, 71] on the microflotation of solids coagulated by hydrolyzing metal ions showed that: (a) the region of floatability corresponded closely with the precipitation regions of the ion, (b) large bubbles were inefficient to float precipitates, and (c) the role of hydrophobicity was unclear, some studies reporting the need of a collector while there were examples in the industrial practice of microbubble flotation where particle aggregation was reported to be more critical.

The question whether hydrophobicity was a prerequisite in dissolved air flotation (DAF) systems has been addressed by Gochin and Solari [72]. It should be mentioned that it is unusual in the industrial practice of this process to add surface-active reagents to the suspension in order to increase the efficiency of flotation. This led some researchers in this field to postulate that microbubble flotation of

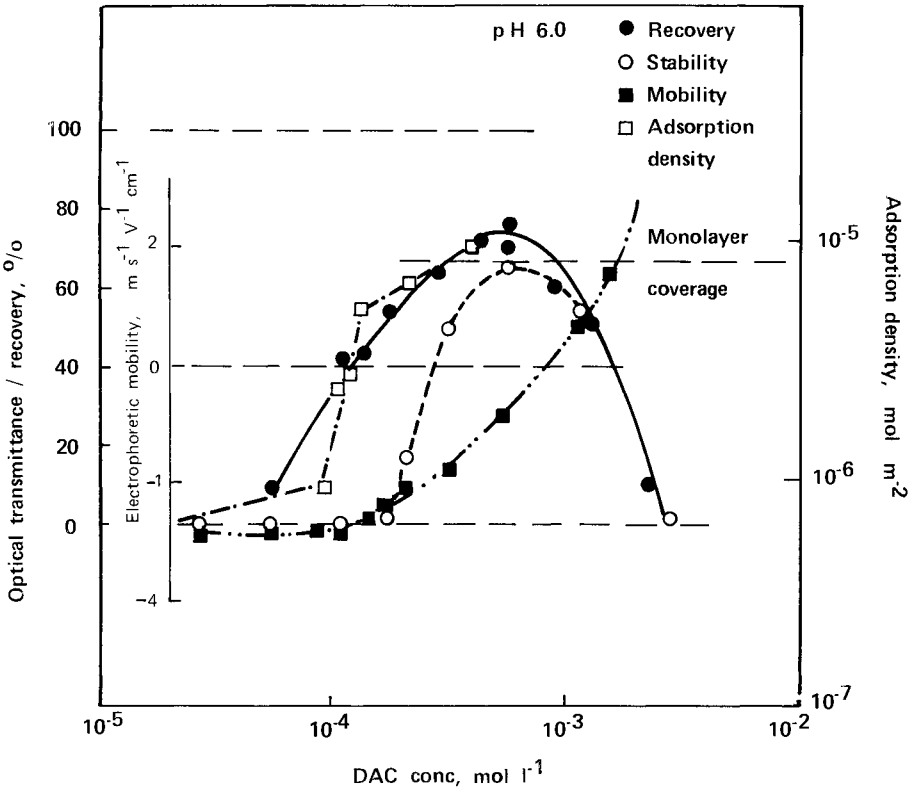

Fig. 8. Correlation of dissolved air flotation recovery of quartz with surface chemistry at pH 6.0 (from [72]).

hydrophilic solids was possible through entrapment in floc structures and therefore that particle aggregation was the key factor in DAF applied to solid–liquid separation [73]. Studies conducted with quartz and silica in the presence of surfactants and various polymeric flocculants indicated that flotation by microbubbles was possible only when there was surfactant adsorption at the quartz–solution interface. This is shown graphically in Figure 8 where the microbubble flotation of quartz at pH 6.0 is correlated with electrophoretic, suspension stability and adsorption density measurements as a function of surfactant concentration. The classical correlation first observed by Fuerstenau [74] for the dodecylamine–quartz system is also obtained when microbubbles are used as the gaseous phase. In another work, the DAF of cassiterite slimes in the presence of anionic collectors was studied and a broadly similar correlation was obtained between flotation recovery, particle aggregation and surfactant adsorption [75]. Also, it was shown [72] that silica and quartz flocculated with polymeric macromolecules leading to the formation of hydrophilic flocs of various physical structures could not be floated by the microbubbles through an "entrapment" mechanism unless an adequate "collector" was added.

Nevertheless, when a hydrophilic solid such as quartz was coagulated with hydrolyzing metal ions like iron and aluminium, various degrees of floatability were obtained with microbubbles generated by DAF and electrolysis [11, 12]. This observation has been reported by many authors and Figure 9 shows a recently published example of the precipitate flotation of metal hydroxides by dissolved air flotation in the absence of collector and frother [76]. However, the experiments of Kitchener

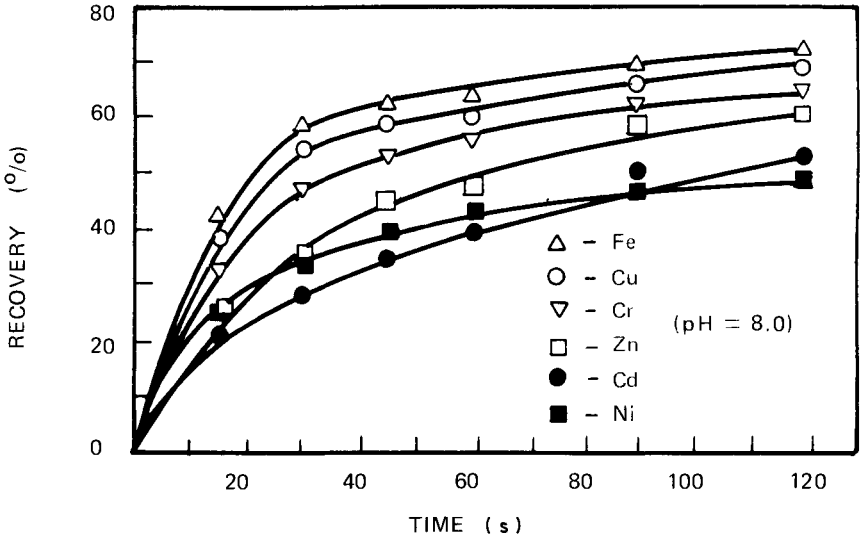

Fig. 9. Kinetics of recovery of metal hydroxides in the absence of surfactant and frother (from Miskovic et al. [76] with permission).

and Gochin [12] showed that floatability of metal hydroxide precipitates was very sensitive to the presence of organic impurities in the system. These authors postulated that natural waters contain surface active compounds which are adsorbed onto precipitated hydroxides forming insoluble hydrophobic soaps that provide sites for bubble adhesion. Due to the low density of these flocs, microbubble attachement to a few hydrophobic spots would ensure precipitate flotation. This has been demonstrated by experiments in thoroughly cleaned systems where it was shown that a few mg l^{-1} of an appropiate collector was sufficient to float an otherwise non-floating suspension of ferric hydroxide flocs [12]. The fact that biologically derived surfactants present in natural waters stabilize long-lived gas microbubbles is well documented [77, 78] and gives support to the hypothesis that natural organic compounds may be responsible for particle hydrophobicity in some industrial DAF operations.

The role of particle aggregation in microbubble flotation is another aspect that has been the subject of study. It is a common industrial practice to add coagulants and flocculating reagents in dissolved air flotation and electroflotation applied to solid–liquid separation [73, 79, 80]. The experiments of Gochin and Solari [72, 75] on fine mineral flotation by microbubbles showed that there was a very clear correlation between maximum aggregation and flotation recovery (see Figure 8). The action of polymeric flocculants in DAF applied to solid–liquid separation has been studied by Solari and Rubio [81]. These authors studied the effect of various hydrophilic polymeric flocculants on the settling and flotation characteristics of chromium hydroxide precipitates formed from Cr (III) and reduced Cr (VI). It was reported that the addition of these macromolecular reagents increased the rate of flotation and allowed the treatment of higher feed solids concentrations. It was also reported that in continuous DAF tests of chromium hydroxide in a column cell, a flotation collector only performed better than a polymeric flocculant at high solids loading rates.

These results were explained in terms of the two-fold effect of adding particle-aggregating reagents, namely, they simultaneously decrease the total number of particles to be collected and increase the "effective" particle size. In this way, it is possible to treat higher concentrations of solids by concentrating them in less units having higher probability of bubble capture. Secondly, as demonstrated in the preceeding section, an increase in particle size improves the probability of particle–bubble collision and thus the flotation rate (but not the probability of attachment, see Figure 5). However, an increase in the effective size of the particle to be removed would also result in an increase in the inertial and detachment forces on the floc–bubble aggregate. Rulev et al. [82] have carried out a mathematical analysis of the effect of particle aggregation on the efficiency of capture by single bubbles rising in the Stokes flow regime. These authors show that for a given bubble size, there is an optimum aggregate size that maximizes flotation rate and recovery. The use of larger bubbles leads to a decrease in the optimum size of the aggregate in order to

diminish the detachment forces as the bubble rising velocity increases. Conversely, a considerable decrease in bubble size will lead to a sharp decrease in the rising velocity of the bubble–floc aggregate and would decrease the flotation rate. Theoretical evaluation of the optimum bubble size for collection of particle aggregates of a given size is complicated by the need to account for the rheological properties of the flocs.

The effect of the size of individual particles on flotation by microbubbles is of interest in order to separate the effect of aggregation from the effect of an increase in "effective" particle size. It has been shown from capture measurements with fine coal particles that the probability of collection increases with particle size in the range 11–40 μm [54, 57]. A similar effect has been shown by Ahmed and Jameson [4] in the 5–40 μm size range through flotation rate measurements of mineral particles with microbubbles generated by air dispersion in a turbulent hydrodynamic regime. Under these experimental conditions, the flotation rate constant was a complex function of particle size, density and stirring rate.

A series of experiments on microbubble flotation over a wide range of particle sizes (2–355 μm) were carried out by Solari and Laskowski [83] in a modified Hallimond tube, where a constant volume of microbubbles generated at a constant rate by a dissolved air flotation system was used to float sized, low-ash hydrophobic coal particles. The results shown in Figure 10 indicated that for a constant mass of added solids, higher recoveries were obtained for the larger particles than for the slimes. It is likely that the collection of the larger particles occurred by attachment of more than a single bubble as mean bubble size was in the range 40–60 μm. Figure 10 also shows that the eventual suppression of electrostatic repulsion forces by an increase in the ionic strength of the solution does not modify the trend. If it is assumed that hydrophobicity was constant over the particle size range studied, it is clear that particle aggregation of ultrafine particles is a necessary condition to increase the probability of bubble–particle collision. A second conclusion that

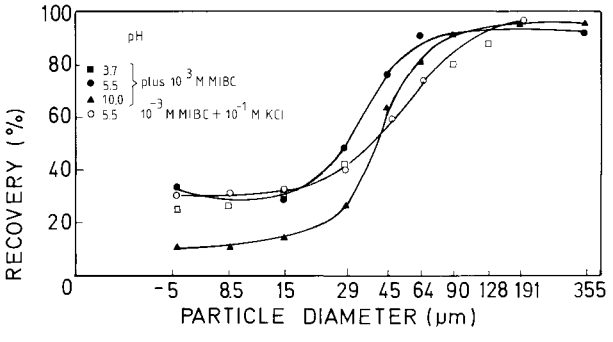

Fig. 10. Effect of particle size on ultrafine coal flotation by microbubbles (from [83]).

may be derived from these results is that, for constant hydrophobicity, there is no apparent decrease in the probability of attachment with an increase in particle size as predicted by the model of Yoon and Luttrell [54] in the Stokes regime (see Figure 5).

The kinetics of flotation with microbubbles in a bubble swarm has received mathematical analysis by Rulev et al. [30]. These authors derived equations to describe flotation in terms of the capture efficiency of rising microbubbles in mono and polydispersed systems. Of particular interest is the incorporation of the effect of Φ, the volumetric fraction of dispersed air in the cell, and of Q, the gas flowrate on the rate of flotation. It is deduced that an optimum value of Φ exists which may be controlled by Q in such a way that the flotation rate is maximized. This proposition has received experimental corroboration by the experiments of Szatowski and Freyberger [22], who showed that the maximum flotation rate of quartz with dispersed air microbubbles depended on bubble size and air flowrate. These authors went as far as to propose that for microbubbles the rate constant, k, should be changed by a "flotation air factor" which represented flotation rate in terms of the volume of air introduced into the pulp rather than by time. A critical bubble size that maximized flotation was reported and the flotation air factor was inversely proportional to bubble diameter. Also, the experiments of Ahmed and Jameson [4] with air dispersed microbubbles in a turbulent regime showed that the rate of flotation of mineral fines increased with decreasing bubble size but k was not as strongly dependent on d_b as suggested by equation (7).

An interesting point raised by the research of Szatowski and Freyberger [22] was the dependence of their flotation rate constant (or air factor) on solids concentration in the pulp. Thus, the flotation air factor decreased with an increase in the concentration of solids and this effect was slightly dependent on particle size. This was explained in terms of the effect of limiting buoyancy that must be taken into account when considering flotation with microbubbles. This observation may explain why a strong dependence of flotation recovery on solids concentration is usually reported. Figure 11 illustrates this effect for the microbubble flotation of ultrafine coal carried out by several authors in various microbubble generation systems.

Reports of contactless flotation occurring would imply that there would be no gain in selectivity by using microbubbles as both hydrophobic and hydrophilic particles might be collected. This is not usually the case and the lack of selectivity that some authors have found in some systems has arisen from inadequate surface chemistry control of the solution–mineral interface rather than from using microbubbles. In fact, Yoon [69] reports that less entrainment of gangue particles should be expected in microbubble flotation systems due to hydrodynamic considerations. Nevertheless, Szatowski and Freyberger [84] investigated the effect of bubble size distribution on the selectivity of mineral flotation. A mathematical model was formulated which allowed the effect of bubble size distribution on the selectivity of flotation to be simulated. The model was tested with hematite ore and bubbles

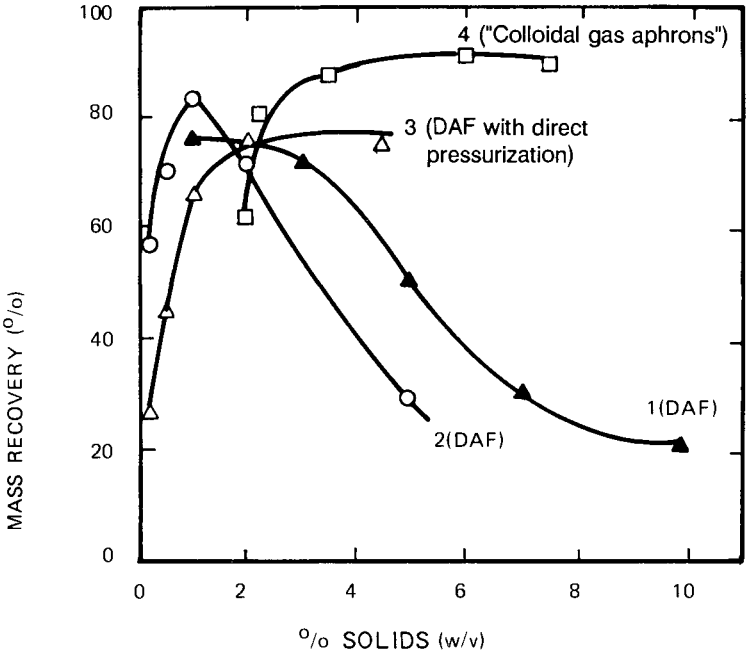

Fig. 11. Effect of solids content on ultrafine coal flotation with microbubbles generated by various processes (*1* from [92]; *2* and *3* from Shimoiizaka and Matsuoka [90]; *4* from Yoon [91]; with permission).

generated in different flotation machines to give a 55–725 μm mean bubble diameter range. The results showed that selectivity was maximum for the intermediate range of bubble diameters which was in qualitative agreement with the theoretical predictions of this model. This observation is also in qualitative agreement with the prediction of Yoon and Luttrell [54] that the probability of attachment goes through a maximum at intermediate values of bubble size (around 400 μm).

Applications of microbubble flotation processes

The microbubble flotation processes that are applied on an industrial scale are dissolved air flotation and electroflotation, both of them in the field of solid–liquid separation. Microbubbles generated as microgas dispersions [18] or colloidal gas aphrons [19] have not attained commercial application yet. Applications of dissolved air flotation and electroflotation in solid–liquid separation have been extensively reviewed in the literature and therefore, the aim of this section is to point out relevant articles where more detailed information may be found.

Bratby and Marais [14] have given extensive details about the principles and operation of DAF and electroflotation units, described experimental testing proce-

dures for obtaining design parameters, and proposed design methods that incorporate economic criteria. Solari [11, 85] and Gochin [79] have critically reviewed the literature on principles and applications of DAF to effluent treatment. Roe [86] presented an informative account of industrial waste flotation which covers flotation machines and processes, a list of the wastes floated, descriptions of "zero-discharge" plants, and economic data. Zabel [87] has carried out a good deal of research and development into the industrial application of DAF to the production of potable water. Matis and Gallios [88] have reviewed DAF and electroflotation in connection with effluent treatment and with the application of these processes to mineral flotation. Finally, Mouchet [89] describes in detail principles, equipment and plants that use DAF technology for solid–liquid separation in France.

With regard to selective flotation of minerals by microbubbles, Solari [11] reported that despite some early attempts no succesful separations had been carried out by dissolved air flotation systems until 1980. The first published works on the microbubble flotation of fine coal appeared in 1982 [90, 91]. Later, the selective separation of fine cassiterite particles from synthetic cassiterite/quartz mixtures was reported by Gochin and Solari [75]. Guerra et al. [92] compared the performance of dissolved air flotation with that of conventional flotation, floc flotation and oil agglomeration for ultrafine coal. Matis et al. [93] have recently studied the application of DAF to the selective recovery of salt-type minerals with promising results.

Electroflotation of minerals has been reviewed by Glembotsky et al. [24], Hogan et al. [94] and by Matis and Gallios [88]. A paper has been published on the electroflotation of cassiterite slimes [95] where some degree of selectivity is reported. However, these authors do not mention the recoveries obtained making it difficult to evaluate their results. On the other hand, the studies carried out by Sebba and Yoon [19] and by Yoon [69, 91] showed that MGD may selectively float fine coal particles. Auten and Sebba [17] and Gregory and co-workers [96] have studied the use of MGD for solid–liquid separation applied to the removal of phosphate slimes and precipitated manganese dioxide, respectively. Yoon and co-workers [20] have recently reported succesful pilot-scale and field tests of a flotation column fitted with a MGD microbubble generator to produce clean coal from high clay-content refuse streams from the coal industry. At present, this appears to be the application with most potential for commercial development.

The potential and future of microbubble flotation

The processes that have achieved most industrial development are dissolved air flotation (DAF) and electroflotation, both applied to solid–liquid separation. Thus, it has not been surprising that more research has been directed to the use of these two processes to mineral separations than to any other microbubble generation processes. A process based on the generation of microbubbles by forcing air through

rigid porous devices is unlikely to attain industrial application given the experience gained in column flotation operations when those kind of spargers are located inside the flotation cell. On the other hand, microgas dispersions (MGD) have only been investigated in relation to coal flotation so that it is not known how these microbubbles generated at high concentrations of frother and surface active agents would behave in a system involving a more complex surface chemistry.

It appears from this review that although microbubbles would improve certain aspects of fine particle flotation, they are not a magic recipe for increasing the overall performance of a particular flotation system. The range of their application seems to be very specific and is still far from being wholly defined. In order to obtain a better picture of the field of application of microbubbles in mineral processing, it is necessary to carry out doing further research into basic mechanisms and applied studies on potential applications of economic interest.

It has been concluded from some recent publications in flotation that separately treating the coarse and the fine particle size ranges could improve the overall performance of a flotation circuit. If an economic evaluation proves this to be a feasible idea, then microbubble flotation of the slime fraction may be an application that deserves experimental testing. In this connection, an investigation into the application of DAF and MGD to the particular system would have priority. Electroflotation is not cost effective for a system involving a mineral pulp because of the energy and electrode costs. The main advantage of DAF over other systems is the industrial experience already gained on the process. MGDs have the advantage of being microbubbles of a large surface area to volume ratio and of being generated at higher volumetric fractions than DAF-generated microbubbles. The lack of any industrial experience with MGDs is their main disadvantage. At present, it seems that the use of a MGD generator in a flotation column has the greatest potential for becoming an industrial application in the field of fine coal processing.

With regard to the basis of microbubble flotation, it seems clear that some degree of particle aggregation is necessary for ultrafine particles to be recovered at an economic rate. Whether MGDs also require particle aggregation is not known. Selective hydrophobicity is a prerequisite for microbubble flotation applied to fine mineral particles. If heterocoagulation is possible in industrial cells, the non-selective nature of this process would be a distinct disadvantage in mineral separations. In solid–liquid separations, where flocculated structures are near their isoelectric point, it is recognized that minute degrees of hydrophobicity are sufficient to ensure stable microbubble–floc adhesion. However, surfactants perform better than polymeric flocculants at high concentrations of metal hydroxide precipitates as higher levels of surface hydrophobicity increase the strength of microbubble–floc attachment and save air consumption. For each specific application, there exits an optimum bubble and particle size that maximizes the recovery and rate of flotation. Theoretical equations exist that may predict these values but experimental confirmation has not been carried out for microbubbles yet. Nor has the concept of con-

tactless flotation been verified experimentally. Thus, more basic research into the mechanisms of microbubble flotation would help the understanding of and develop further, the technology of microbubble flotation processes.

References

1 J. Rubio, personal communication, 1990.
2 A.M. Gaudin, Flotation, 2nd edition., McGraw Hill, New York, N.Y., 1977.
3 V.I. Klassen and V.A. Mokrousov, An Introduction to the Theory of Flotation, Butterworths, London, 1963.
4 N. Ahmed and G.J. Jameson, Int. J. Miner. Process., 14 (1985): 195–215.
5 D.G.De Vivo and B.L.Karger, Sep. Sci., 5 (1970): 145–167.
6 E.A. Casell, K.M. Kaufman and E. Matijevic, Water Res., 9 (1974): 1017–1024.
7 J.B. Melville and E. Matijevic, in: R.J. Akers (Editor), Foams, Academic Press, London, 1977, pp. 217–234.
8 D. Reay and G.A. Ratcliff, Can. J. Chem. Eng., 53 (1975): 481–486.
9 G.L. Collins and G.J. Jameson, Chem. Eng. Sci., 31 (1976): 985–991.
10 M.R. Urban, Ph.D. Thesis, University of London, London, 1978.
11 J.A. Solari, Ph.D. Thesis, University of London, London, 1980.
12 J.A. Kitchener and R.J. Gochin, Water Res., 15 (1981): 585–590.
13 U. Neis and K.P. Kiefhaber, in: P.Somasundaram (Editor), Fine Particles Processing, AIME, New York, N.Y., 1980, pp. 755–766.
14 J. Bratby and G.V.R. Marais, in: D.B. Purchas (Editor), Solid/Liquid Separation Scale-Up, Upland Press, Croydon, 1977, pp. 155–198.
15 J. Bratby and G.V.R. Marais, Water Res., 9 (1975): 929–936.
16 F. Sebba, J. Colloid Interface Sci., 35 (1971): 643–646.
17 W.L. Auten and F. Sebba, in: J. Gregory (Editor), Solid and Liquid Separations, Ellis Horwood, Chichester, 1984, pp. 41–52.
18 P.T. Shea and S.M. Barnett, Sep. Sci. Technol., 14 (1979): 757
19 F. Sebba and R.H. Yoon, in: B. Yarar and D.J. Spottiswood (Editors), Interfacial Phenomena in Mineral Processing, Engineering Foundation, New York, N.Y., 1982, pp. 161–172.
20 R.H. Yoon, G.H. Luttrell, G.T. Adel and M.J. Mankosa, in S. Chander and R.R. Klimpel (Editors), Advances in Coal and Mineral Processing Using Flotation, SME/AIME, Littleton, 1989, pp. 211–218.
21 F. Sebba, Chem. Ind., Feb. (1985): 91–92.
22 M. Szatowski and W.L. Freyberger, Trans. Inst. Min. Metall., Sect.C, 94 (1985): C61–70.
23 N.P. Brandon and G.H. Kelsall, J. Appl. Electrochem., 15 (1985): 475–484.
24 V.A. Glembotsky, A.A. Mamakov, A.M. Romanov and V.E. Nenno, in: Proc. XI Inter. Mineral Process. Congress, Arte Mineraria, Cagliari, 1975, pp. 1–22.
25 G.R. Hyde and A. Stojsic, Min. Eng., July 1987, pp. 481–484.
26 P.M. Solozhenkin, V.P. Ostapenko and S.S. Shakhmatov, in E. Forssberg (Editor), XVI Int. Miner. Process. Congr., Elsevier, Amsterdam, 1988, pp. 763–773.
27 S.M. Travers and D.A. Lovett, Water Res., 19 (1985): 1479–1482.
28 N.P. Brandon, Ph.D. Thesis, University of London, London, 1985.
29 V.G. Levich, Physicochemical Hydrodynamics, Prentice-Hall, New Jersey, 1962, pp. 395–471.
30 N.N. Rulev, B.V. Derjaguin and S.S. Dukhin, Colloid J. USSR, 39 (1977): 267–274 (English translation).

31 F. Concha and E.R. Almendra, Int. J. Miner. Process., 5 (1979): 349–367.
32 G.S. Dobby and J.A. Finch, Int. J. Miner. Process., 21 (1986): 241–260.
33 J.S. Laskowski, J.L. Yordan and R.H. Yoon, Langmuir, 5 (1989): 373–376.
34 R.W. Huddleston and A.L. Smith, in: A.J. Akers (Editor), Foams, Academic Press, London, 1976, pp. 147–160.
35 J.A. McShea and I.C. Callaghan, Colloid Polym. Sci., 261 (1983): 757.
36 G.L. Collins and G.J. Jameson, Chem. Eng. Sci., 32 (1977): 239–246.
37 G.L. Collins, M. Motarjemi and G.J. Jameson, J. Colloid Interface Sci., 68 (1978): 69.
38 Y. Fukui and S. Yuu, AICHE J., 28 (1982): 866.
39 R.H. Yoon and J.L. Yordan, J. Colloid Interface Sci., 113 (1986): 430.
40 S. Usui and H. Sasaki, J. Colloid Interface Sci., 65 (1978): 36–45.
41 S. Usui, H. Sasaki and H. Matsukawa, J. Colloid Interface Sci., 81 (1981): 80–84.
42 N.P. Brandon, G.H. Kelsall, S. Levine and A.L. Smith, J. Appl. Electrochem., 15 (1985): 485–493.
43 H.P. Dibbs, L.L. Sirois and R. Bredin, Can. Met. Quart., 13 (1974): 395.
44 K.L. Sutherland, J. Phys. Chem., 52 (1948): 394–425.
45 J.A. Kitchener, in: M.H. Jones and J.T. Woodcock (Editors), Principles of Mineral Flotation, The Wark Symposium, Symp. Ser. No 40, Austr. Inst. Min. Metall., Victoria, 1984, pp. 65–71.
46 B.V. Derjaguin and S.S. Dukhin, Trans. Inst. Min. Metall., 70 (1960–61): 221–245.
47 B.V. Derjaguin and S.S. Dukhin, in: J.S. Laskowski (Editor), Mineral Processing, Proc. 13th Int. Mineral Processing Congress, Elsevier, Amsterdam, Part A, 1981, pp. 21–62.
48 B.V. Derjaguin, S.S. Dukhin and N.N. Rulyov, in: E. Matijevic (Editor), Surface and Colloid Science, Plenum Press, New York, N.Y., 13 (1984): 71–113.
49 H.J. Schulze, Physico-chemical Elementary Processes in Flotation, Elsevier, Amsterdam, 1984, 348 pp.
50 D. Hornsby and J. Leja, in: E. Matijevic (Editor), Surface and Colloid Science, Plenum Press, New York, N.Y., 12 (1982): 217–313.
51 J. Ralston, Adv. Colloid Interface Sci., 19 (1983): 1–26.
52 G.J. Jameson, S. Nam and M.M. Young, Minerals Sci. Eng., 9 (1977): 103–118.
53 W.J. Trahar and L.J. Warren, Int. J. Miner. Process., 3 (1976): 103–131.
54 R.H. Yoon and G.H. Luttrell, Miner. Process. Technol. Rev., 5 (1988): 101–122.
55 J.P. Anfruns and J.A. Kitchener, Trans. Inst. Min. Metall., Sect. C, 86 (1977): C9–15.
56 J.P. Anfruns and J.A. Kitchener, in: M.C. Fuerstenau (Editor), Flotation, A.M. Gaudin Memorial, AIME, New York, N.Y., 2 (1976): 625–637.
57 R.H. Yoon and G.H. Luttrell, Coal Prep., 2 (1986): 179–192.
58 H.J. Schulze, in: J.S. Laskowski (Editor), Frothing in Flotation, Gordon and Breach, New York, N.Y., 1989, pp. 43–76.
59 M.E. Weber and D. Paddock, J. Colloid Interface Sci., 94 (1983): 328–335.
60 L.R. Flint and W.J. Howarth, Chem. Eng. Sci., 26 (1971): 1155–1168.
61 D. Reay and G.A. Ratcliff, Can. J. Chem. Eng., 51 (1973): 178–185.
62 J.S. Laskowski, in: J.S. Laskowski (Editor), Frothing in Flotation, Gordon and Breach, New York, N.Y., 1989, pp. 25–41.
63 H.J. Schulze and G. Gottschalk, in: J.S. Laskowski (Editor), Mineral Processing, Part A, Elsevier, Amsterdam, 1981, pp. 63–84.
64 J.L. Yordan and R.H. Yoon, in: Y.A. Attia, B.M. Moudgil and S. Chander (Editors), Interfacial Phenomena in Biotechnology and Materials Processing, Elsevier, Amsterdam, 1988, p. 333.
65 N.N. Rulev, Colloid J. USSR, 40 (1979): 747–756 (English translation).
66 J. Laskowski and J.A. Kitchener, J. Colloid Interface Sci., 29 (1969): 670–679.
67 T.D. Blake and J.A. Kitchener, J. Chem. Soc., Faraday Trans. I, 68 (1972): 1435–1442.
68 J. Drzymala and J. Lekki, J. Colloid Interface Sci., 130 (1989): 197–204.

69 R.H. Yoon, Microbubble Flotation of Fine Coal, U.S. Department of Energy, Report DOE/PC/30234-T3, 1984.
70 P. Somasundaran, in: E.S. Perry and C.J. van Oss (Editors), Separation and Purification Methods, 1, 1973, pp. 117–198.
71 A.J. Rubin, in: R. Lemlich (Editor), Adsorptive Bubble Separation Techniques, Academic Press, New York, N.Y., 1972, pp. 199–217.
72 R.J. Gochin and J.A.Solari, Water Res., 17 (1983): 651–657.
73 H. Lundgren, Filtr. Sep., 13 (1976): 24–28.
74 D.W. Fuerstenau, Trans. AIME, 208 (1957): 1365–1367.
75 R.J. Gochin and J.A.Solari, Trans. Inst. Min. Metall., Sect.C, 92 (1983): C52–58.
76 D. Miskovic, E. Karlovic and B. Dalmacija, in: L.Pawlowski, A.T. Verdier and W.J. Lacy (Editors), Chemistry of Protection of the Environment, Elsevier, Amsterdam, 1984, pp. 245–252.
77 J.S.D'Arrigo, C. Saiz-Jimenez and N.S. Reimer, J. Colloid Interface Sci., 100 (1984): 96–105.
78 J.S. D'Arrigo, J. Colloid Interface Sci., 100 (1984): 106–111.
79 R.J. Gochin, in: L. Svarovsky (Editor), Solid–Liquid Separation, Butterworths, London, 1981, pp. 503–524.
80 J.R. Backhurst and K.A. Matis, J. Chem. Tech. Biotechnol., 31 (1981): 431–434.
81 J.A. Solari and J. Rubio, in: M.J. Jones and R. Oblatt (Editors), Reagents in the Minerals Industry, The Institution of Mining and Metallurgy, London, 1984, pp. 271–276.
82 N.N. Rulev, S.S. Dukhin and V.P. Semenov, Colloid J. USSR, 41 (1975): 208–215 (English translation).
83 J.A. Solari and J.S. Laskowski, (in preparation).
84 M. Szatowski and W.L. Freyberger, Int. J. Miner. Process., 23 (1988): 213–227.
85 J.A. Solari, Eng. Sanitaria, 20 (1981): 332–335.
86 L.A. Roe, Industrial Waste Flotation, ROECO Inc., Illinois, 1983, 228 pp.
87 T. Zabel, J. Am. Water Works Assoc., May 1985, pp. 42–46.
88 K.A. Matis and G.P. Gallios, in: B.A. Wills and R.W. Barley (Editors), Mineral Processing at a Crossroads — Problems and Prospects, NATO Advanced Science Institute, Martinus Nijhoff, Dordrecht, 1986, pp. 37–69.
89 P. Mouchet, Industrie Minérale — Les Techniques, Juin 1983, pp. 312–330.
90 J. Shimoiizaka and I. Matsuoka, in: Proc. XIV Int. Miner. Process. Congress, Can. Inst. Metall., 1982, Paper No IV-11, pp. 1–15.
91 R.H. Yoon, Min. Congr. J., 68(12) (1982): 76–80.
92 E.A. Guerra, J. Rubio and J.A. Solari, in: Proc. 10th Int. Coal Prep. Congr, Can. Inst. Metall., 1 (1986): 105–121.
93 K.A. Matis, Th.N. Balabanidis and G.P. Gallios, Colls. Surfs., 29 (1988): 191–203.
94 P.Hogan, A.T. Khun and B.A. Wills, J. Camborne School Mines, 76 (1976): 48–54.
95 P.Hogan, A.T. Khun and J.F. Turner, Trans. Inst. Min. Metall., 88 (1979): C83–87.
96 O.J. Gregory, S.M. Barnett and F.J. DeLuise, Sep. Sci. Technol., 15 (1980): 1499–1512.

Subject Index

adsorption, 10, 37, 77, 116, 235
—, affinity constant, 49, 68, 85
—, BET theory, 11
—, binary system, 51
—, bilayer, 86
—, bridging attraction, 75, 83
—, chemisorption, 10
—, collector, 235
—, density, 177, 178
—, dispersing agents, 138–148
—, effect on wettability, 147, 232, 233
—, forces in adsorption of polymers, 295, 296
—, frothers, 376
—, Frumkin-Fowler-Guggenheim (FFG) equation, 52, 69, 70, 84
—, gases, 37
—, Gibbs convention, 42
—, Gibbs dividing plane, 41
—, Gibbs isotherm, 10, 43, 45, 177
—, homopolymers, 73
—, in diffuse layer, 54
—, inorganic dispersants, 138, 139
—, inorganic ions, 53
—, ion-exchange, 12
—, ions, 53
—, Langmuir isotherm, 67
—, modelling, 37
—, monolayer, 46, 48
—, one-p*K* model, 63–65
—, one-p*K*-SGC models, 65
—, organic ions, 69
—, organic molecules, 68
—, orientation of collector molecules, 181
—, physisorption, 10
—, polyelectrolytes, 73, 79–84
—, polymers, 12, 19, 73–75, 78, 279, 295
—, polymers adsorption segmental energy, 78
—, poly-oxy surfactants, 146
—, —, effect on colloid stability, 147
—, —, effect on coal–water slurries, 165, 166
—, polysaccharides, 140–145
—, polyvalent ions, 67
—, potential determining ions, 182, 183, 232, 233
—, protons, 59, 61, 63
—, rate of polymer adsorption, 279
—, real monolayer, 48
—, selective adsorption of polymers, 296–300
—, selectivity coefficient, 49, 52, 60, 71
—, site binding models, 58
—, specific adsorption, 55, 56, 58, 65
—, spreading pressure, 46, 176
—, strong, 80
—, surface charge determining ions, 58
—, surface complexation, 58, 66
—, surface excess, 42
—, surface heterogeneity, 84
—, surface pressure, 46, 52, 176
—, surfactants, 73, 84–90
—, thermodynamics, 37
—, two-p*K* model, 62–65
—, weak, 80
adhesion, work of, 231, 364
agglomeration, 362, 387
aliphatic hydrocarbons, 367
alizarin, 298
alumina, 22, 145, 311, 390
aluminium, 341
amino acid, 147
aminopolyphosphate, 139
ammonium lignosulphonate, 166, 274
amosite, 32
amphoteric surfaces, 59

anatase, 273, 311, 345, 346
Andreasen pipette, 153
anglesite, 32
anhydrite, 306
aniline, 366
anthracene, 367
apatite, 26, 312, 315, 346
aromatics, 370, 381, 388

Bangham's equation, 11
barite, 31, 375
beidellite, 262, 263
benzene, 366, 391
benzyl arsonic acid, 313
Bingham equation, 151
Boltzmann's equation, 53
bridging
—, by immiscible liquid, 236, 277–279, 387–390
—, by polyelectrolytes (flocculation), 239, 277–279, 352
British gum, 119
brochantite, 386
Brownian motion, 123
brucite, 32
bubble, 205, 210
—, bubble–particle aggregate, 212–216, 402
—, bubble–particle attachment, 401–407
—, bubble–particle collection, 402–405
—, bubble–particle collision, 212, 221
—, bubble–particle interaction kinetics, 204–212
—, electrogenerated, 397
—, energy of bubble detachment from particle, 214, 215
—, microbubble generation, 396–398
—, microbubbles interfacial properties, 398–401
—, rise rate, 398, 399
—, size, 395, 403, 404, 407, 410–413
—, size effect on flotation, 407–413
—, surface, 210, 211
—, swarms, 399, 400, 412
—, zeta potential, 400
butyronitryle, 366

calcite, 12, 33
calcium oleate, 12
Calgon, 139
callulose, 119, 166, 303
Camp-Stein's equation, 283, 284
capilary force, 213
carbon tetrabromide, 366
carbon tetreachloride, 366
carboxymethyl cellulose, 119, 140
Cassie's equation, 191
cassiterite, 296, 313, 315, 324, 346, 391, 409
Cataflot, 122
cellulose xanthate, 363
chalcocite, 312, 316, 338
chalcopyrite, 26, 303, 363
chelating collector, 386
chlorite, 269, 306
chromium hydroxide, 410
chrysocolla, 303, 304, 340, 386
chrysolite, 30
clay minerals, 259–263, 274, 306, 346
coagulation, 30, 98, 125, 127, 239, 361
—, adagulation, 34
—, critical concentration, 261
—, edge-face, 262
—, effect on rheology, 152
—, fast, 243
—, heterocoagulation, 115, 407
—, into primary minimum, 131
—, into secondary minimum, 131, 247
—, mutual, 243
—, orthokinetic, 128, 129, 244, 265
—, perikinetic, 124, 244
—, rate, 127, 245, 246
—, selective, 228, 239, 243, 252, 272
—, slow, 243, 274
—, stability factor, 159, 228, 249, 291, 337
—, steric stabilization, 134
—, time, 245
—, under turbulent flow conditions, 132
—, weak, 126
coal, 25, 140, 161, 162, 299, 301, 302, 326, 338, 376, 381, 382, 390, 411, 412, 413, 414
—, beneficiation, 390
—, coal–water slurries, 164–166
—, difficult-to-float low rank, 382
—, emulsion flotation, 376, 379, 382–385
—, hydrophobicity, 158
—, oil agglomeration, 387–390
—, oxidized, 382
—, rank, 161, 300
—, selective flocculation, 301, 302
—, surface properties, 161–163
—, ultrafine, 411, 412
coal tar, 368

coal–water slurries, 163–166
coating,
—, armouring of bubbles by colloidal precipitate, 401
—, selective coating, 335, 336
—, slime coatings, 115, 158, 159, 343, 344
—, —, effect on flotation, 341–344
cobalt, 341
colloids,
—, colloid separation methods, 238, 239
—, colloidal mineral particles, 243
—, DLVO theory of stability, 23, 98, 106, 124, 128, 239, 243, 244, 348, 361, 376, 407
—, lyophilic, 2, 98
—, lyophobic, 2, 98
—, stability, 3, 74, 75, 78, 82, 84, 90, 116
contact angle, 8, 173, 188, 189, 204, 213, 232, 375
—, adsorption effect on, 178, 181, 235, 390, 391
—, advancing, 174, 192, 217–219
—, capillary rise, 195
—, Cassie's equation, 191
—, condition of hydrophobicity, 230, 231
—, dispersion, electrical and hydrogen bonding forces effect, 231
—, drop dimensions, 194
—, drop profile, 194
—, dynamic, 173, 197, 199, 213
—, effect on flotation, 228, 229, 239
—, effect on oil droplet–mineral particle attachment, 375
—, effect on spreading, 378
—, flat plates, 194
—, heterogeneity effect, 190–194
—, hysteresis, 8, 190, 191
—, macroscopic, 178
—, measurement of, 194–197
—, microscopic, 178, 193
—, non-ideal surfaces, 190
—, powders, 196
—, receding, 174
—, solid electrical charge effect on, 182–186, 232, 233
—, spherical particle, 212
—, static, 173
—, surface charge effect on, 182, 231–233
—, thermodynamic significance of, 180, 234
—, Wenzel's equation, 191
—, Wilhelmy plate, 195
—, work of liquid cohesion effect, 230
—, work of liquid-to-solid adhesion effect, 230
—, Young's equation, 8, 175, 177, 182, 189, 229
copper minerals, 296, 299, 304
copper–molybdenum ore, 381
corundum, 26
m-cresol, 379
critical micelle concentration, 86, 87, 147, 376
—, hemimicellization, 18
—, micellization, 18
crude oil, 368, 369, 370, 385
—, distillation products, 385
—, heavy distillation products, 369
—, —, in emulsion flotation, 373, 384–386
—, —, in oil agglomeration, 390
—, intermediate fractions, 369
—, light distillate fractions, 369
cyclic hydrocarbons, 369
cyclohexanol, 366

Debye-Hückel reciprocal length, 55, 100, 128, 245
decalin, 381
depressant, 116
Derjaguin's approximation, 102
desorption
—, by dilution, 78
—, by displacement, 78
dextrin, 118–120, 141
Di-n-butylamine, 366
diamond, 26
Diesel oil, 312, 338
diphenylguanidine, 386
disjoining pressure, 24, 101, 200–210, 234
dispersants, 115, 122, 159, 293
—, adsorption, 138–148
—, classification of, 117
—, dextrin, 118–120, 141
—, effect on suspension stability, 148–158
—, hexametaphosphate, 118
—, inorganic dispersants, 117
—, lignosulphonates, 121, 145, 166
—, mechanism of action, 123–138
—, phosphates, 117, 118, 158
—, polymeric dispersants, 118–122
—, selective, 293, 294, 302
—, sodium silicate, 117, 159
—, tripolyphosphate, 339
dispersions, 115, 148, 243, 341
—, stability measurements, 148–158

Dispex, 122
DLVO theory, 23, 98, 106, 124, 128, 239, 243, 244, 348, 355, 361, 376, 407
—, Debye-Hückel length, 100, 101, 125, 243, 245, 349
—, disjoining pressure, 24, 181, 208–210, 234
—, electrostatic double-layer forces, 99, 123, 347, 361
—, energy barrier, 126, 234, 246
—, Hamaker constant, 125, 208, 244
—, hydration forces, 137, 351
—, primary minimum, 125, 131, 245
—, retardation, 247
—, secondary minimum, 125, 131, 245
—, steric stabilization, 134
—, structural forces, 104, 128, 136, 350
—, Van der Waals forces, 98, 123, 244, 347, 361
dodecyl sulphonate, 309, 311
dodecylammonium chloride, 367, 409
dolomite, 32, 154, 155, 297, 304, 306, 334
Dowell M-210, 382–385, 384

electrical double layer, 20, 22, 23, 53–60, 97, 99, 128, 183–186, 234, 243–245, 349
—, capacitance of diffuse layer (differential), 54
—, capacitance of double layer (integral), 57
—, Debye-Hückel model, 55
—, Debye-Hückel reciprocal length, 55, 101, 125, 128, 245, 263, 349
—, diffuse layer, 53
—, free energy of double layer formation, 184, 233
—, Gouy-Chapman (GC) model, 22, 54, 100
—, Helmholtz layer
—, —, inner, 63
—, —, outer, 63
—, Helmholtz plane
—, —, inner, 57
—, —, outer, 58
—, interaction of, 22–24, 405
—, SGC model, 55, 56
—, Stern layer, 55, 149
—, —, capacitance, 57–60
—, Stern plane, 55
—, surface potential, 54, 56, 125, 132, 349
electrokinetic phenomena, 20, 150
—, acoustophoresis, 150, 151
—, coal–water slurries, 161–166
—, electrokinetic potential (zeta potential), 21, 59, 67, 69, 97, 139, 149, 159, 163, 251–253, 258, 334, 349, 383, 401
—, —, bubbles, 400, 401
—, —, critical, 97
—, —, hydrocarbon droplets, 365–368, 372, 376
—, —, measurements, 149–151
—, electroosmosis, 20, 150
—, electrophoresis, 20, 150, 400
—, —, mass transfer, 150
—, electrophoretic mobility, 21, 165, 366
—, sedimentation potential (Dorn effect), 20, 159, 400
—, streaming potential, 20, 150
electrolytes,
—, indifferent, 185, 186
—, polyelectrolyte, 19, 122
—, weak or strong, 235
emulsions, 236, 363, 368, 385
—, emulsion flotation, 228, 235, 362, 387
—, emulsification, 235, 363, 371, 374, 382, 385, 386
—, —, effect on emulsion flotation, 374
—, —, effect on oil agglomeration, 390
—, emulsifier, 381, 382, 386
—, oil droplet–solid particle interactions, 373, 375–379, 386
—, —, Murex process, 335
Ethoxol P-19, 386
ethoxylated alkylamine alkylguanidine, 306
2, ethylhexylmethacrylate, 119, 302
fatty acid, 327
feldspar, 297, 303, 304
ferric oxide, 34
films, 209–211, 234, 235
—, disjoining pressure, 24, 181, 208–210, 234
—, film drainage, 209
—, —, drainage rate, 210
—, induction time, 209–211, 403–406
—, spreading pressure, 176
flocculation, 227, 239, 277, 285, 361
—, applications in mineral processing, 288–290
—, bridging, 239, 277–279, 352
—, co-flocculation, 337–340
—, effect of hydrodynamics on, 283
—, effect of microturbulences on, 285
—, effect on rheology, 152
—, effect on settling, 288
—, floc breakage, 282, 325

flocculation (continued)
—, floc growth, 282, 325
—, floc size, 157
—, flocculants, 278, 294
—, —, selective flocculants, 296–301
—, hydrodynamic effects, 283–288
—, hydrophobic flocculation, 309, 334
—, hydrophobic polymers, 298, 299, 302
—, kinetics of, 279
—, latex, 302
—, polyelectrolytes, 19
—, polymer adsorption, 73, 80, 295
—, polymeric flocculants, 278, 279, 409, 415
—, rate, 280, 282
—, selective, 159, 228, 239, 291–295, 301–306, 337
—, —, flocculants selective adsorption, 296
—, shear flocculation, 236, 275, 309
—, —, applications, 326–328
—, —, theory of, 320–326
—, stereoselective flocculant, 298
—, use of selective dispersants in, 293
Flory-Higgins interaction parameter, 50, 68, 85
flotation, 374, 395, 401, 406
—, aggregation flotation, 225, 226
—, agglomeration flotation, 237, 361, 386, 387
—, bubble–particle aggregate, 212–217
—, bubble–particle attachment, 234, 401
—, bubble size effect on, 410-412
—, carrier flotation, 220, 236, 237, 311, 344
—, collectors, 116, 235
—, collectorless, 183
—, column, 238, 414
—, contactless, 406, 412
—, depressants, 116
—, dissolved air flotation, 302, 395, 413
—, effect of slimes on, 341
—, electroflotation, 395–397, 413, 414
—, emulsion flotation, 228, 235, 362, 380, 390
—, energy barrier effect on, 234
—, extender flotation, 361, 386
—, floatability, 406
—, floc flotation, 238
—, flocculants use in flotation, 290
—, froth flotation, 228
—, frothers, 235, 376, 382
—, induction time, 209, 211, 212, 234, 403–406
—, kinetics of, 220, 221, 402, 412
—, limits for coarse particles, 217
—, limits for fine particles, 216, 407
—, maximum floatable diameter, 216
—, mechanical machine, 237
—, methods, 227, 235, 331, 341, 374
—, microbubble flotation, 395, 408, 410, 412, 414, 415
—, microbubble generation, 396–398
—, modifiers, 234
—, native floatability, 9, 230
—, particle collection, 402
—, particle size effect on, 203, 302
—, probability of flotation, 205, 402
—, probability of particle-to-bubble attachment, 404
—, promoter, 382–384
—, rate, 234, 406, 410–412
—, rate constant, 206, 402
—, reagents, 230, 235
—, recovery, 204
—, shear-flocculation in flotation, 320
—, slimes effect on, 115, 158, 159, 333, 341
—, thermodynamic criterion of, 229
—, under starvation collector conditions, 222
—, vacuum, 398
fluorite, 297, 338
forsterite, 29
Fowkes equation, 187
free energy, 38, 39
free energy change during oil droplet-to-particle attachment, 375
free energy change during particle-to-bubble attachment, 228
free energy of double layer formation, 183–185, 233
Frumkin-Fowler-Guggenheim equation, 52
Fuchs theory, 246
fuel oil, 340, 369, 372, 383, 384, 386

galactomannan, 119, 144
galena, 26, 275, 303, 312, 313, 316, 326, 338
gangue, 25, 234, 306, 412
garnet, 317, 326
gasoline, 370
Gibbs adsorption equation, 10, 43, 44, 177
Gibbs-Duhem equation, 39, 177
Gibbs free energy, 39, 176, 228, 363, 374
gibbsite, 339
glass (sodium silicate), 138
goethite, 65, 305

gold, 26, 27, 267, 271
Gouy-Chapman theory, 21, 22, 56, 58, 61–64, 97–100
graphite, 26, 140, 141, 367
guar gum, 166
gum karaya, 166
gum tragacanth, 119, 145

halite, 339
Hamaker constant, 98, 244, 348, 349
heavy distillates, 370, 388, 390
Helmholtz free energy, 38, 39, 176, 198
Helmholtz-Grahame model, 57
hematite, 26, 65, 140, 252, 254, 258, 268, 272, 305, 306, 309, 312, 338, 344, 345, 346, 386, 412
Herschel-Bulkley equation, 152
hexadecane, 367
hexadecyl trimethyl ammonium bromide, 322
hexamethaphosphate, 118, 315
HLB, 16, 384
humic acid, 121, 145, 340, 384
hydrogen bonding, 143, 231
hydrophobicity, 143, 230, 231, 311, 312, 411
—, coating of hydrophobic particles, 335
—, condition of, 230, 231
—, effects on shear flocculation, 311–313
—, hydrogen bonding, dispersion and electrical forces, contribution to, 231
—, hydrophobic aggregation, 309
—, hydrophobic association, 17, 322, 349
—, hydrophobic force, 272, 273, 322
—, hydrophobic interactions, 111, 143, 352
—, hydrophobic polymers, 298
—, oil spreading on hydrophobic solids, 375–380
—, —, Murex process, 335

illite, 265, 267, 306
ilmenite, 26, 386
imidazoline, 382–383
interface model, 3–5
intermolecular forces, 13, 14, 97–100, 124–127, 244, 347
interfacial tension, 187–189, 364, 371, 398
iron ore, 305
iron oxide, 65
—, α-Fe_2O_3, 259, 272
iso-electric-point, 150, 155, 255, 258, 268, 274, 367
isooctane, 390
isoparaffinis, 370

kaolin, 156, 274, 340, 345
kaolinite, 26, 30, 265, 267, 298, 303, 306
Kelvin equation, 4
kerosene, 326, 338, 383, 384
Kolmogorov length microscale, 285

Langmuir adsorption equation,
Langmuir isotherm,
Laplace equation, 214
Laplace pressure, 196
Laplace-White equation, 196
latex, 257, 302
liberation, 225
Lifshitz theory, 189
light distillates, 370
lignin, 119, 120
lignosulphonate, 121, 145, 166
Lippmann equation, 182, 232

magnesite, 32
magnetic aggregation, 267–270, 318, 331, 335
magnetic coating, 333–337
magnetic force, 332
magnetite, 155, 273, 333, 334, 338, 339–341, 407
Magnex process, 340
malachite, 304, 326, 386
mesitylene, 366
metacrylic acid–methyl ester copolymer, 363
metal hydroxides, 408, 410
MIBC, 302
mica, 106, 269
micellization, 18, 86, 89
—, critical micelle concentration, 86, 87, 147, 376
—, hemimicellization, 18
Mie equation, 13
mineral surfaces, 25–35
—, amphoteric, 59
—, coal, 140, 158, 162, 163, 301, 302, 338, 379, 411
—, gold, 271
—, heterogeneity, 32, 33, 388
—, ideal surface, 173
—, iron oxide, amorphous, 65
—, α-F_2O_3, 272

mineral surfaces (continued)
—, methylated quartz, 182, 184, 185, 217–219, 234
—, mica crystals, 106–108
—, minerals crystal-chemical classification, 26
—, minerals in water, 26–34
—, —, noble metals, 27
—, —, oxides, 28, 29
—, —, real mineral surfaces, 31–34
—, —, silicates, alumino-silicates, 29–31
—, —, sulphides, 27, 28
—, model clay colloids, 261
—, molecularly smooth crystals, 105, 106
—, non-ideal surfaces, 190–193
—, oxides, 61
—, —, exchange reaction, 66
—, —, intrinsic affinity constants, 65
—, —, metal ion adsorption, 65
—, —, metal ions complexation, 67
—, —, one-p*K* model, 63, 64
—, —, one-p*K* SGC model, 65
—, —, oxyanion adsorption, 65
—, —, proton adsorption, 61
—, —, site binding, 63
—, —, specific adsorption, 63
—, —, surface complexation, 66
—, —, surface groups, 63, 65
—, —, two-p*K* model, 61, 62
—, real minerals, 21–23
minerals,
—, alumina, 22, 145, 311, 390
—, alunite, 339, 390
—, amosite, 32
—, anatase, 273, 311, 345, 346
—, anglesite, 32
—, anhydrite, 306
—, apatite, 26, 312, 315, 346
—, barite, 31, 375
—, beidellite, 262, 263
—, brochantite, 386
—, brucite, 32
—, calcite, 12, 33, 152, 155, 311, 334, 343, 346
—, cassiterite, 296, 313, 315, 324, 346, 391, 409
—, chalcocite, 312, 316, 338
—, chalcopyrite, 26, 303, 363
—, chlorite, 269, 306
—, chrysocolla, 303, 304, 340, 386
—, chrysolite, 30
—, clay minerals, 259–263, 274, 306, 346
—, coal, 25, 140, 161, 162, 299, 301, 302, 326, 338, 376, 381, 382, 390, 411, 412, 413, 414
—, copper minerals, 296, 299, 304
—, copper–molybdenum ore, 381
—, copper ore, 303, 304
—, corundum, 26
—, diamond, 26
—, dolomite, 32, 154, 155, 297, 304, 306, 334
—, feldspar, 297, 303, 304
—, fluorite, 297, 338
—, forsterite, 29
—, galena, 26, 275, 303, 312, 313, 316, 326, 338
—, garnet, 317, 326
—, gibbsite, 339
—, goethite, 65, 305
—, gold, 26, 27, 267, 271
—, graphite, 140, 141
—, halite, 339
—, hematite, 26, 65, 140, 252, 254, 258, 268, 272, 305, 306, 309, 312, 338, 344, 345, 346, 386, 412
—, illite, 265, 267, 306
—, ilmenite, 26, 386
—, iron ore, 305
—, kaolin, 156, 274, 340, 345
—, kaolinite, 26, 30, 265, 267, 298, 303, 306
—, magnesite, 155, 334, 339, 340, 341
—, magnetite, 155, 273, 333, 334, 338, 339–341, 407
—, malachite, 304, 326, 386
—, mica, 106, 269
—, molybdenite, 340
—, montmorillonite, 262, 263, 265, 266
—, oil shale, 299
—, orthoclase, 26
—, oxides, 28, 61
—, periclase, 26
—, phosphate, 346
—, potash ore, 308, 339, 386
—, pyrite, 26, 28, 301, 302, 303
—, pyrophyllite, 269
—, quartz, 26, 28, 33, 140, 145, 217, 252, 253, 254, 257, 269, 296, 303, 304, 305, 306, 338, 339, 346, 363, 407, 408, 409
—, —, methylated quartz, 142, 147
—, rhodochrosite, 312, 315, 318
—, rutile, 65, 253, 273, 311
—, scheelite, 26, 275, 310, 313, 316–318, 324, 325, 327, 346

minerals (continued)
—, siderite, 32, 312, 315, 318
—, silica, 24, 65, 305, 311, 409
—, smectite, 261, 267
—, sodium smectite, 261
—, sparingly soluble salts, 31
—, sphalerite, 26, 338
—, stibnite, 346
—, sylvite, 305, 339, 386
—, tourmaline, 296, 324
—, wolframite, 312, 346
—, zinc–lead oxide-sulphide ores, 386
—, zircon, 26
molybdenite, 340
montmorillonite, 262, 263, 265, 266

naphtenes, 370, 388
Nerstian surface, 184
nickel, 371
nonyl alcohol, 382
Nujol, 367, 368

octanoic acid, 366
octyl alcohol, 376
oil shale, 299
oleate, 310, 312
oleic acid, 338
orthoclase, 26
oxides, 28, 61

paraffinic oil, 367
paraffins, 370, 381, 390
particles
—, effect of charge on particles aggregation, 160, 161
—, fines, 227
—, fines aggregation in flotation, 226, 311, 320
—, particle size effect, on shear flocculation, 316
—, —, on flotation, 212–230
—, particle size measurement, 148, 149, 153–157, 318
—, particle–oil droplet interactions, 373–375
—, particle-to-bubble collision and attachment, 205–209, 401–407
—, slimes, effect on flotation, 158, 159, 333, 341–344, 411
pentacarbonyl, 340
perfect solutions, 40
periclase, 26
petroleum, 369, 381
phenol, 368
phosphate, 65, 346
point-of-zero charge, 22, 182, 183, 232, 391
Poisson-Boltzmann equation, 100, 185
polyacrylamide, 166, 298, 339, 340
polyacrylamide-glyoxal-bis-2-hydroxyanil (PAMG), 296, 304
polyacrylate–acrylodithiocarbonate, 302
polyacrylic acid xanthate (PAAX), 298, 302
polyaluminium chloride, 341
polyaromatics, 369
polycarboxylate, 166
polycyclic hydrocarbons, 369
polyethylene nonyl phenol, 384
polyethylene oxide, 143
polygalactronic acid (PGUA), 119
polyglycol ether, 122
polymers,
—, adsorption, 70, 139–147, 279, 295, 296
—, copolymers, 77
—, grafted, 77
—, latex, 257, 258, 302
—, PAMG, 296, 304
—, polyelectrolytes, 19, 122, 278
—, polycarboxylates, 166
—, polyethoxysulphonates, 166
—, polyethylene oxide, 143
—, polygalactyronic acid (PGUA), 119
—, polyglycol ethers, 122
—, polymeric dispersants, 118–122
—, —, adsorption, 139–147
—, polymeric flocculants, 278, 279, 409, 410, 415
—, —, adsorption, 279, 295, 296
—, —, selective, 291–306
—, polymethylvinyloxime, 296, 297
—, polyoximes, 296
—, polyoxysurfactants, 147, 384
—, polyphosphates, 138, 139, 339
—, polysaccharides, 118–121, 139, 305
—, —, adsorption, 139–144, 166
—, polysilicic acid, 138
—, polyxanthate, 296
polymethylvinyloxime (PMVOX), 296, 297, 298
polyoxime, 296
polyphenol, 119
polyphosphate, 138, 139, 339
polysaccharide, 118–121, 139, 144, 166, 305
polysilicic acid, 138

polytetrafluoroethylene (PTFE), 258
polyxanthate, 296, 304
porphyrins, 369, 371
potash ore, 308, 339, 386
potassium amyl xanthate, 312, 313
potential determining ions, 58, 233
protein, 17
pseudo-Nerstian behaviour,
PVA xanthate, 303
pyrite, 26, 28, 301, 302, 303
pyrophosphate, 117
pyrophyllite, 269

quartz, 26, 28, 33, 140, 145, 217, 252, 253, 254, 257, 269, 296, 303, 304, 305, 306, 338, 339, 346, 363, 407, 408, 409
quebracho, 119

Reynold's equation, 209
rheology, 151, 164
—, shear rate, 151
—, shear stress, 151
rhodochrosite, 312, 315, 318
Richardson-Zaki equation, 156
ruthenium oxide, 65
rutile, 65, 253, 273, 311

scheelite, 26, 275, 310, 313, 316–318, 324, 325, 327, 346
Schulze-Hardy rule, 103
sedimentation
—, balance, 153
—, bed volume, 153
—, hindered settling, 153, 156
—, potential, 20, 150
—, rate, 153, 156
—, Steinour's equation, 156
—, Stokes' equation, 153
separation methods, 225, 226
—, aggregate flotation, 228
—, agglomerate flotation, 237, 361, 386
—, carrier flotation, 228, 236, 237, 344
—, carrier separation, 239, 331
—, colloidal methods, 227, 238
—, dissolved air flotation, 395, 413
—, electric separation, 226
—, electroflotation, 395, 413
—, electrophoresis, 228
—, emulsion flotation, 228, 235, 362
—, extender flotation, 362, 386
—, floc flotation, 228
—, flotation methods, 227, 235, 331, 341, 374
—, gravity concentration, 226
—, liquid–liquid extraction, 362, 390
—, magnetic separation, 226, 267, 269, 331
—, microbubble flotation, 395, 407
—, oil agglomeration (liquid phase agglomeration), 228, 362, 387
—, physicochemical separation methods, 226, 227
—, selective coagulation, 228, 239, 243, 272
—, selective flocculation, 159, 228, 291, 337
—, shear flocculation, 236, 275, 309
siderite, 32, 312, 315, 318
silica, 24, 65, 305, 311, 409
silver iodide, 22, 31, 62, 186, 232
Sirofloc method, 340
slimes, 34, 203, 267
—, coating, 158, 341–344
smectite, 261, 267
Smoluchowski's equation, 130
Smoluchowski-Miller theory, 127
sodium hydrogen phosphate, 158
sodium lignoisulphonate, 145
sodium oleate, 139, 275, 310, 312, 313, 315, 345
sodium phosphate, 117, 159
sodium poly(acrylate–acrylodtihiocarbonate), 297, 302
sodium polyphosphate, 117
sodium silicate (water glass), 117, 159, 338
sodium smectite, 261
sodium tetradecyl sulphonate, 390
sphalerite, 26, 338
spinel, 26
spreading, 8, 375–379, 382
starch, 118, 119, 305
Steinour's equation, 156
stibnite, 346
Stokes' equation, 153
Stokes flow regime, 404, 405
styryl phosphonic acid, 313
sulphated coconut oil, 381
sulphosuccinate, 313
sulphur, 26
surface activity in water, 15–17
surface excess Helmholtz free energy, 43, 176
surface forces, 24, 98, 106, 123, 234, 244, 272, 273, 322, 347, 405
—, Born repulsion, 348

surface forces (continued)
—, capillary forces, 213, 352–354
—, Coulombic electrical, 100, 101, 126, 244, 245, 349
—, hydration forces, 136–138, 352
—, hydrocarbon chain association, 320, 321, 349, 350
—, hydrophobic interaction, 322, 351, 352
—, measurement of, 106–110
—, polymer bridging forces, 277, 278, 352
—, structural forces, 104, 105, 134–136
—, Van der Waals-London attractive, 98, 99, 125, 244, 245, 348
surface free energy, 4, 5
surface Gibbs energy, 43
surface tension, 17, 41, 176, 364
—, critical, 189
—, dispersion forces contribution, 187–189, 364
—, dynamic, 176
—, surfactants, 84–90
—, —, poly-oxy, 166, 384
sylvite, 305, 339, 386
Syntex, 381
Szyszkowski's equation, 49, 53

Talc, 26
tall oil, 386
tannic acid, 274
tannin, 119
thermodynamics of adsorption, 37–46
toluene, 366
tourmaline, 296, 324
trichloro-trifluoro-ethane, 389
tripolyphosphate, 339

uranium, 269, 271

vanadium, 371
viscosity, 164, 381

wattle bark, 119
Weissenberg rheogoniometer, 152
Wenzel's equation, 191
wetting, 8, 84, 180–182, 373
—, coal surface wettability, 162
—, effect of collector on, 178
—, effect of electrical charge on, 182–186, 231–233
—, effect on flotation, 233, 234
—, effect on flotation limits of coarse particles, 212–216, 218, 219
—, effect of surfactants on, 147
—, films, 23, 210, 230, 234
—, thermodynamic criterion of flotation, 229
wolframite, 312, 346

xantham gum, 166
xanthate, 275, 303

Young's equation, 8, 175, 178, 228

zeta potential, 21, 59, 67, 69, 97, 139, 149, 159, 163, 165, 251–253, 258, 270, 274, 315, 334, 349, 368, 372, 383, 401
zinc–lead oxide-sulphide ores, 386
zinc oxide, 324
zircon, 26